NASA Reference Publication 1258, Vol. 2
WRDC Technical Report 90-3052

August 1991

Aeroacoustics of Flight Vehicles: Theory and Practice

Volume 2: Noise Control

NASA

NASA Reference Publication 1258, Vol. 2
WRDC Technical Report 90-3052

1991

Aeroacoustics of Flight Vehicles: Theory and Practice

Volume 2: Noise Control

Edited by
Harvey H. Hubbard
NASA Langley Research Center
Hampton, Virginia

NASA
National Aeronautics and Space Administration
Office of Management
Scientific and Technical Information Program

Errata

NASA Reference Publication 1258, Vol. 2

Aeroacoustics of Flight Vehicles:
Theory and Practice
Volume 2: Noise Control

Harvey H. Hubbard, Editor
August 1991

The authorship of chapter 17, pp. 357–382, should be as follows:

Lead Author: Noel A. Peart, The Boeing Co., Seattle, Washington

Contributing Authors: Boeing Noise Organization, The Boeing Co., Seattle, Washington

M. J. T. Smith, Rolls-Royce, Derby, England

B. Magliozzi, United Technologies, Windsor Locks, Connecticut

Harry Sternfeld, Boeing Vertol Co., Philadelphia, Pennsylvania

Issue Date: March 1992

Contents

Preface

The field of aeroacoustics has matured dramatically in the past two decades. Researchers have gained significant theoretical and experimental understanding of the noise generated by aircraft power plants and their components. In addition, airframe noise and interior noise have been investigated extensively. The physical understanding obtained from these efforts has resulted in the development of hardware capable of reducing community noise and of meeting strict noise certification requirements. Reductions in overall sound pressure level of 20 to 30 dB have been obtained for some types of power plants, while in the same period their installed power has increased significantly.

Current quiet flight vehicle designs are based on information reported in a multitude of journals, conference proceedings, research reports, and specialized books. Each of these scientific publications represents only incremental steps in the evolution of our present understanding of the various aeroacoustic noise generation and propagation mechanisms and procedures for noise control. There is thus a need for a reference document summarizing the current status of aeroacoustics. It is recognized that some other fine books on aeroacoustics are already available. The reader is referred to the classic handbooks by Harris on noise and vibration control, to Goldstein's "Aeroacoustics," which provides a general theoretical treatment of most aeroacoustic noise sources, to the text "Noise and Acoustic Fatigue in Aeronautics" by Richards and Mead, and to the AIAA Reprint Series volume entitled "Aerodynamic Noise." The current book represents an attempt to integrate and update the information in previous related publications, to provide a balanced viewpoint with both fundamental and applied aspects being considered, and to focus on those topics that are significant for the design and operation of quiet flight vehicles.

In July 1982, the Continuing Education Subcommittee of the Institute of Aeronautics and Astronautics (AIAA) Aeroacoustics Technical Committee identified a critical need for a reference book summarizing and interpreting the status of research in aeroacoustics. The full Aeroacoustics Technical Committee agreed with this conclusion and enthusiastically supported the concept of publishing such a book. The book would have a scope consistent with that of the Technical Committee and would include physics of noise produced by motion of fluids and bodies through the atmosphere and by chemical reaction processes; it would also include the responses of human beings, structures, and the atmosphere to aerodynamic noise. The subcommittee was then instructed to prepare an initial outline of the book for planning purposes and to procure financial support for its printing. This effort has been given

generous support by NASA (Langley, Lewis, and Ames Research Centers), the U.S. Air Force Wright Research and Development Center, and the U.S. Army Aviation Systems Command.

This book is planned as a reference publication, easily readable by persons with scientific or engineering training who have completed a bachelor degree study program. It serves as an authoritative resource book for teachers, students, and researchers, but it is not designed for use directly as a textbook. It provides recommended methodology to evaluate aeroacoustics-related problems and suggests approaches to their solutions, without extensive tables, nomographs, and derivations. It is oriented toward flight vehicles and emphasizes underlying physical concepts. Theoretical, experimental, and applied aspects are covered, including the main formulations and comparisons of theory and experiment.

The preparation of the material for this book has been carried out under the general supervision of the AIAA Technical Committee on Aeroacoustics. The Committee elected the editor (Harvey H. Hubbard), two associate editors (Christopher K. W. Tam and Robert H. Schlinker), and six additional editors (Charles E. Feiler, James C. Yu, Walter K. Eversman, Marvin E. Goldstein, Robert E. Kraft, and Yung H. Yu). Donald L. Lansing and John Laufer (until his untimely death) also served for short terms. They functioned as an editorial board to establish the overall policy for the organizing, reviewing, and editing of the book. Each was selected because of his expert knowledge of at least one of the specialty areas covered in the book. They collectively comprise a team of experts who represent industry, government, and academia viewpoints.

The editorial board members chose by vote the lead authors for each chapter based on their stature and expertise in particular technical areas and on their proven ability to communicate. In all cases, contributing authors were selected and enlisted by the lead authors on the basis of the same criteria. An outline of each chapter was first approved by the editorial board as a means of defining the overall scope of that chapter. Technical reviewers were chosen by vote of the editorial board based on their expertise of subject matter and the nature of their experience. Two to four persons were selected to provide technical reviews for each manuscript. These technical reviews were then provided to the appropriate authors as a basis for the preparation of their final manuscripts. Final editing was accomplished by Mary K. McCaskill and Thomas H. Brinkley of the NASA Langley Research Center Technical Editing Branch. This latter effort involved skilled technical editors closely associated with the publication profession. Their work included checking for accuracy, grammar, consistency of style, compliance with editorial instructions, and assembly for printing.

Authors and reviewers contributed their time for this project without receiving compensation. Draft manuscript preparation, typing, and graphics were supported partially or wholly by the participant's employer. All these contributions were vital to the success of this project and are greatly appreciated.

Supporting reference information cited in this book is limited to publications available at the time of the text preparation. No proprietary or classified information is included in order to protect the interests of authors' companies and governments. In order to enhance its utility, this book is divided into two volumes, each of which has a list of symbols, an index, and a separate glossary of terms. Reference lists for each chapter contain the key available supporting documents.

Volume 1 includes all the chapters that relate directly to the sources of flight vehicle noise: Propeller and Propfan Noise; Rotor Noise; Turbomachinery Noise; Jet Noise Classical Theory and Experiments; Noise From Turbulent Shear Flows; Jet Noise Generated by Large-Scale Coherent Motion; Airframe Noise; Propulsive Lift Noise; Combustion and Core Noise; and Sonic Boom. Volume II includes those chapters that relate to flight vehicle noise control and/or operations: Human Response to Aircraft Noise; Atmospheric Propagation; Theoretical Models for Duct Acoustic Propagation and Radiation; Design and Performance of Duct Acoustic Treatment; Jet Noise Suppression; Interior Noise; Flyover-Noise Measurement and Prediction; and Quiet Aircraft Design and Operational Characteristics.

Technical Reviewers

Anders O. Andersson
Boeing Commercial Airplane Co.
Seattle, Washington

Frank J. Balena
Lockheed California Co.
Burbank, California

Henry E. Bass
National Center for Physical Acoustics
University, Mississippi

Earl H. Dowell
Duke University
Durham, North Carolina

Norris L. Haight
McDonnell Douglas Corp.
Long Beach, California

Alan S. Hersh
Hersh Acoustical Engineering, Inc.
Chatsworth, California

Karl D. Kryter
Stanford Research Institute
Menlo Park, California

Alan H. Marsh
Dytec Engineering, Inc.
Huntington Beach, California

John C. McCann
United Technologies Corp.
Pratt & Whitney
East Hartford, Connecticut

Michael K. Meyers
George Washington University
NASA Langley Research Center
Hampton, Virginia

Jack V. O'keefe
Boeing Commerical Airplane Co.
Seattle, Washington

Karl S. Pearsons
Bolt Bernaek & Newman Labs
Canoga Park, California

Robert E. Pendley
McDonnell Douglas Corp.
Long Beach, California

Allan D. Pierce
Georgia Institute of Technology
Atlanta, Georgia

Roland A. Prydz
Lockheed California Co.
Burbank, California

James D. Revell
Lockheed California Co.
Burbank, California

Edward J. Rice
NASA Lewis Research Center
Cleveland, Ohio

C. G. Rice
ISVR
University of Southampton
Southampton, England

Kevin P. Shepherd
NASA Langley Research Center
Hampton, Virginia

M. J. T. Smith
Rolls Royce
Derby, England

James R. Stone
NASA Lewis Research Center
Cleveland, Ohio

Rimas Vaicaitis
Columbia University
New York, New York

John E. Wessler
Wyle Labs
Arlington, Virginia

Symbols

A	cross-sectional area; acoustic admittance
b	chord
C_D	drag coefficient
C_L	lift coefficient
C_p, c_p	specific heat at constant pressure
C_v	specific heat at constant volume
c	speed of sound
D, d	diameter
d	distance, e.g., from source to receiver
F	fuel-air ratio; force
f	frequency
G_p	cross spectral density of acoustic pressure
H, h	height
h	enthalpy
I	intensity
i	imaginary number, $\sqrt{-1}$
k	wave number
L_A	A-weighted sound level
L_D	D-weighted sound level
L_{dn}	day-night average sound level
L_{EPN}	effective perceived noise level
L_{eq}	equivalent continuous sound level

L_{PN}	perceived noise level
l, ℓ	length
M	Mach number
m	mass
$\dot{m}$	mass flow ratio
N_{Pr}	Prandtl number
N_{Re}	Reynolds number
N_{St}	Strouhal number
P	power
p	sound pressure
R	reflection coefficient; acoustic resistance; gas constant; duct radius; jet radius
$\Re$	distance from arbitrary point on rotating rotor blade to observer
r	rotor radial position
S	wing area
$S(\sigma)$	Sears function
T	temperature
t	time; wing thickness
U	flight velocity
u	particle velocity; mean velocity; axial velocity
V	velocity
V_e	exit velocity of jet
X	acoustic reactance
x, r, θ	cylindrical coordinates
Z	impedance
α	sound absorption
β	$= \sqrt{M^2 - 1}$
γ	ratio of specific heats
δ_f	flap deflection

δ_{ij}	Kronecker delta
ζ	ratio of characteristic impedances
λ	wavelength
ν	viscosity
ξ	cutoff ratio
ρ	density
σ	reduced frequency of gust
ϕ	phase angle
Ω	rotor rotational rate
ω	circular frequency, $2\pi f$

Abbreviations:

BPF	blade-passage frequency
BVI	blade-vortex interaction
DNL	day-night average sound level
EPNL	effective perceived noise level
FAR	Federal Aviation Regulations
HSI	high-speed impulsive
ICAO	International Civil Aviation Organization
LEQ	equivalent continuous sound level
LL_S	Stevens loudness level
LL_Z	Zwicker loudness level
NR	noise reduction
OASPL	overall sound pressure level
PNL	perceived noise level
PWL	power level
rms	root-mean-square
SLA	A-weighted sound level
SLD	D-weighted sound level
SLE	E-weighted sound level

SPL	sound pressure level
SWR	standing wave ratio
TL	transmission loss

11 Human Response to Aircraft Noise

Lead author

Clemans A. Powell
NASA Langley Research Center
Hampton, Virginia

Contributing author

James M. Fields
Government Accounting Office
Washington, D.C.

Introduction

If noise is defined as sound that produces adverse effects, then aircraft are a major source of noise affecting, at least to some extent, the work and leisure activities of a large proportion of people in nearly all developed countries. Although only a small percentage of the propulsion energy of an aircraft is converted into sound, that percentage represents a large power source. The sources of aircraft noise most responsible for community and ground crew effects are the high-velocity jet exhausts, fans, internal turbomachinery, propellers, rotors, internal combustion engine exhausts, and, for supersonic aircraft, sonic booms. Those sources most responsible for passenger or flight crew effects are turbulent boundary layers, propellers, helicopter gear boxes, jet exhausts, internal combustion engine exhausts, and structureborne vibration from unbalanced rotational forces. However, there is not a one-to-one relationship between sound energy and any given noise effect. To effectively control the noise, that is, reduce those components that are most responsible for adverse human effects, it is necessary to thoroughly understand the physical characteristics of the sound and how each of those characteristics can affect human response.

Adverse effects of aircraft noise include hearing loss, task performance degradation, speech intelligibility reduction, sleep interruption, and general feelings of annoyance. A number of nonauditory physiological effects that may adversely affect health are claimed to result from noise exposure. It is not possible in the limited space of this chapter to examine all the potential effects of aircraft noise in great

detail. Since nearly all effects of noise on humans rely on the perception of sound by the hearing mechanism, the human auditory system and the general perception of sound are discussed. However, the major concentration of this chapter is on annoyance response and methods for relating physical characteristics of sound to those psychosociological attributes associated with human response. Results selected from the extensive laboratory and field research conducted on human response to aircraft noise over the past several decades are presented along with discussions of the methodology commonly used in conducting that research. Finally, some of the more common criteria, regulations, and recommended practices for the control or limitation of aircraft noise are examined in light of the research findings on human response.

Those readers with particular interest in the effects of noise on task performance, sleep interruption, health, or other nonauditory physiological functions are referred to the general reference texts of references 1 to 3.

Perception of Sound

The human auditory system is capable of sensing, analyzing, or interpreting fluctuations in air pressure over an extremely wide range. The interested reader can find more details of this fascinating sensory system in many modern textbooks such as reference 4. The following sections, however, provide a brief overview of hearing anatomy and theory and those attributes which are considered most critical to human response to aeroacoustic noise sources.

Anatomy of the Ear and Hearing Theory

The auditory system consists of the outer (pinna and ear canal, or external meatus), middle (ossicular chain), and inner (cochlea) ears and the associated pathways to the brain. A diagram of the internal hearing organs is shown in figure 1. Air pressure fluctuations in the external meatus vibrate the tympanic membrane, or eardrum, which is coupled mechanically to the fluid-filled inner ear through the bones (malleus, incus, and stapes), tendons, ligaments, and muscles which make up the ossicular chain located in the middle ear. The mechanical linkage forms the impedance-matching interface between air and the fluid-filled cochlea.

The tensor tympani and stapedius muscles in the middle ear are capable of impeding the motion of the ossicular chain and are responsible for the acoustic, or aural, reflex. This reflex, which is involuntary in most people, attenuates intense sounds and thereby offers some protection to the sensory organs in the inner ear.

The vibratory motion of the stapes is coupled to the fluid-filled cavity of the cochlea through the oval window. Pressure fluctuations cause a traveling wave to pass along the cochlear partition, or basilar membrane, with the ultimate excitation of the hair cells situated on the basilar membrane within the organ of Corti. The mechanisms of nerve cell excitation and transmittal of neural signals to the brain are beyond the scope of this review but can be found in most texts on hearing such as reference 4.

Since the cochlear partition decreases in stiffness from the stapes, it acts as a low-pass filter, with the result that the end further from the stapes is more responsive

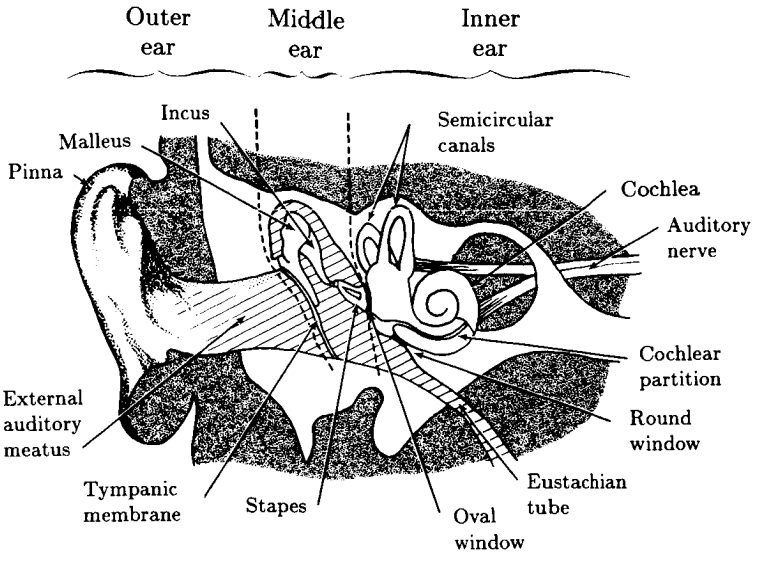

Figure 1. Cross section of the human ear.

to low frequencies. This mechanism facilitates the frequency analysis capabilities of the auditory system, particularly at higher frequencies, and forms the basis of the "place" theory of hearing. In addition, the "volley" theory proposes that analysis is performed by the central auditory nervous system, particularly at low frequencies, and that frequency information is transmitted in volleys of neural discharges which are phase locked to the pressure fluctuations. It is now generally accepted that neither theory can fully explain the sensitivity and selectivity of the auditory system over the total frequency range and that a better explanation is found in an interaction of both mechanisms.

Because of the complexity of the auditory system and the interfaces between the acoustical, mechanical, and neurological systems, it is not surprising that the response of the auditory system to sounds with differing spectral and temporal characteristics is not easy to predict or measure. However, several generalities can be stated:

1. The human auditory system is sensitive to a very wide range of air pressure fluctuation. The pressure ratio of the threshold of pain to the threshold of audibility is approximately 1 million.

2. The audible frequency range of hearing is normally considered to be 20 Hz to 20 kHz. However, the sensitivity is not uniform across the frequency range; lower sensitivity occurs at both the high- and the low-frequency end of the range.

3. One sound can mask the perception of another sound of lower intensity. In general, although the masking is most efficient if the frequency contents of the two sounds are similar, a sound with lower frequency content than a given sound is more efficient at masking the given sound than is a sound with higher frequency content.

4. Sound at high sound pressure levels can cause both temporary and permanent threshold shifts in hearing ability. Levels greater than about 180 dB can rupture the tympanic membrane, and levels greater than about 85 dB can cause significant temporary or permanent loss of hearing acuity depending on the duration of the noise exposure.

Auditory Phenomena Affecting Perception of Sound

The following sections consider those auditory phenomena that have been found to be important in predicting how people perceive and respond to a given sound in a given situation. The scope of this discussion does not allow a complete treatment of any of these important topics. The reader can find more information in a number of general references including references 2 and 4.

Loudness

Loudness is traditionally defined as the perceived intensity of a sound. Considerable research has been conducted over the last 75 years to investigate how the human auditory system integrates the temporal and spectral information contained in sound waves arriving at the ear so that it may be quantified subjectively in terms of a single overall intensity measure. The basic mechanisms and important parameters have been known and studied for many years (ref. 5); however, the advent of modern electronic and audio systems has resulted in improvements in and refinements to loudness prediction models.

The curves of figure 2 represent the sound pressure levels of octave bands of noise which produce the sensation of equal loudness (ref. 6). As can be seen, the auditory system is neither uniform across frequency nor completely linear with amplitude. Similar equal-loudness curves have been defined for sounds consisting of pure tones. The basic shapes of the equal-loudness curves are similar, with the region of greatest sensitivity occurring at about 3 kHz.

The question of how the auditory system sums the loudness of sounds comprised of more than a single component has also been the subject of much research. The model of loudness summation in reference 7 considers not only the loudness of the individual components but also the concepts of critical bandwidths and mutual masking, or inhibition, between the various sound components. Again the more interested reader is referred to a more complete text (refs. 2–4).

The loudness of a sound has also been found to depend on its duration. The loudness of a constant-amplitude tone increases with increasing duration up to a duration of approximately 200 msec. This duration is commonly referred to as the "integration time of the ear." This temporal summation is believed to take place in the central nervous system rather than in the ear itself (ref. 8). Most research in this area indicates that the loudness increases about 10 dB for a factor-of-10 increase in duration up to the integration time. This type of loudness increase is very important for sounds of short duration such as impulses and is discussed at more length in subsequent sections. There have also been studies that indicate a type of loudness adaptation, or decrease in loudness, with increasing durations beyond the integration time; however, the study of reference 9 suggests that the previously measured adaptation may be an artifact of the test methods used.

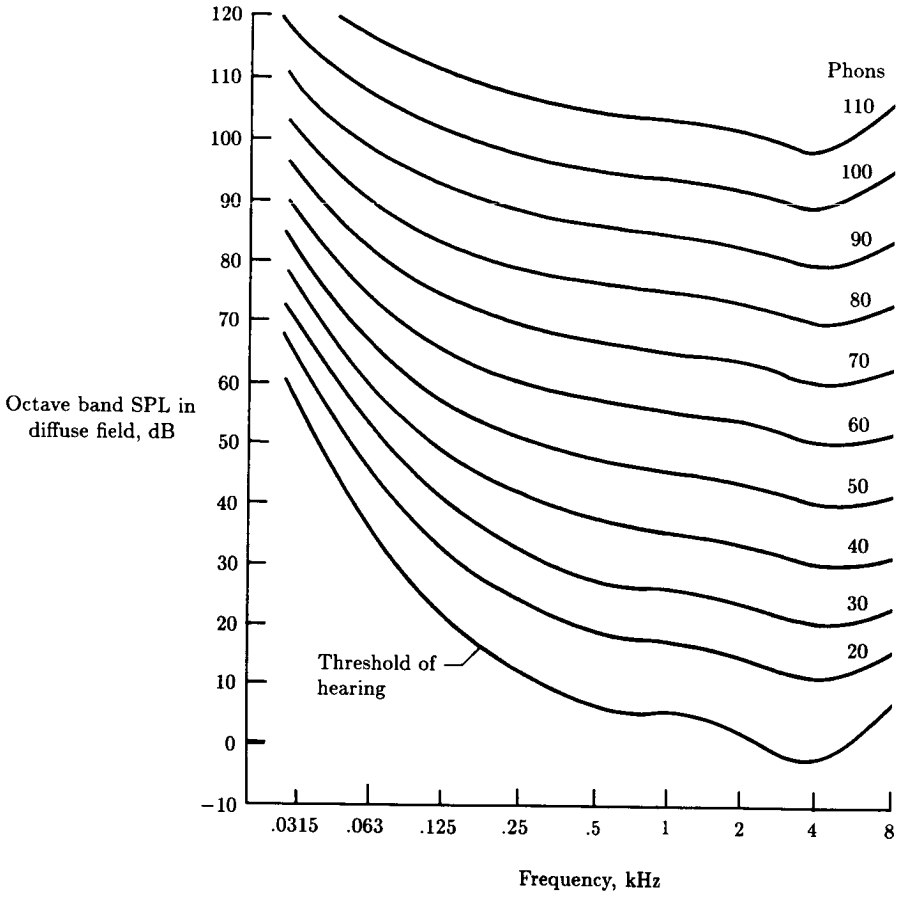

Figure 2. Equal-loudness contours. (From ref. 6.)

Pitch

Pitch can be defined as the perceived frequency of sound. High-frequency tones or narrow bands of noise are heard as being "high" in pitch, and low-frequency tones or narrow bands as being "low" in pitch. Although there has been much research into the perception of pitch, there has been very little consideration of pitch and some related phenomena, other than simple frequency content, in explaining reaction of people to the noise of aircraft or other aeroacoustic noise sources. The potential relevance of these phenomena may be of increasing importance for some configurations of advanced turboprop aircraft which may have counterrotating propellers with unequal numbers of blades.

The relationship of pitch and consonance or dissonance of multiple tones is described in the model of reference 10. A concept of virtual pitch is described which accounts for many psychoacoustic and musical phenomena related to combination and residue tones. A historical review and the determination of the detectability of combination tones which result when two (or more) tones at different frequencies, f_1 and f_2, are heard simultaneously are presented in reference 11. These combination

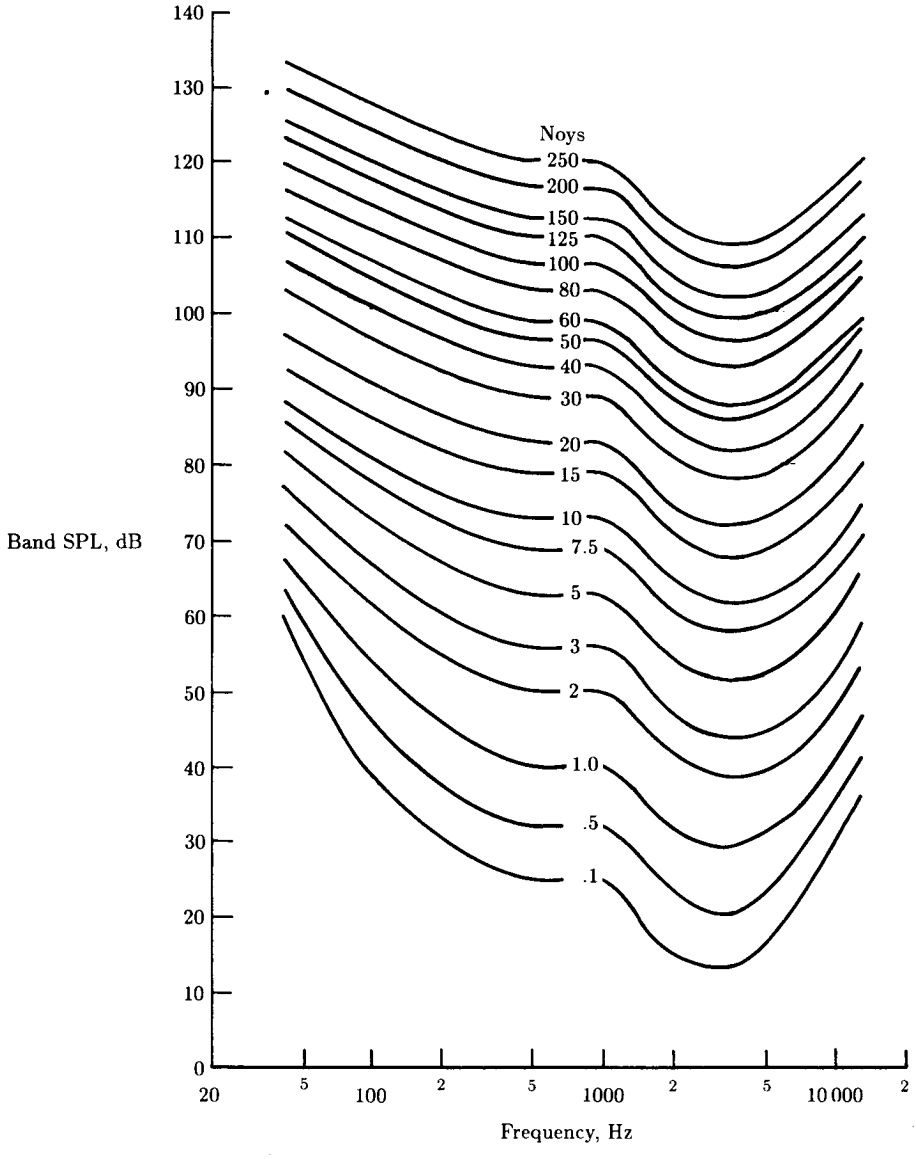

Figure 3. Equal-noisiness contours. (From ref. 14.)

tones include not only the summation $(f_1 + f_2)$ and difference $(f_2 - f_1)$ tones but also the cubic difference $(2f_1 - f_2)$ tone and higher order tones. The "residue" is the pitch produced by a set of frequency components rather than by any of the single components (ref. 12). The low pitch tone associated with large high-bypass-ratio turbofan aircraft engines, commonly called "buzz saw," is one such example. This pitch results from the difference in frequency of the many harmonically related components of the fan shaft frequency rather than from the fundamental itself.

Noisiness

Noisiness was suggested in reference 13 to refer to the characteristic or attribute of a sound which makes it unwanted, unacceptable, disturbing, objectionable, or annoying and which may be distinguishable from loudness. Through extensive laboratory tests a set of equal-noisiness contours were determined (ref. 14). As indicated in figure 3, these curves have the same general shape as the equal-loudness contours of figure 2 although there are some differences particularly at high frequencies.

The temporal summation of noisiness has been shown to be very similar to that of loudness for durations less than the integration time of the ear. However, the summation for noisiness continues for durations considerably in excess of that time. Based on analysis of data from many studies, 3 dB per doubling of duration, or 10 dB for a factor-of-10 change in duration, seems appropriate as a temporal summation factor for noisiness.

Localization and Precedence

The ability to determine the location of sound sources is one of the major benefits of having a binaural hearing system. Localization has been studied nearly as long as has loudness. It is generally recognized that the human auditory system uses both interaural intensity and interaural temporal differences between the ears as cues which are processed in the central auditory nervous system. At low frequencies, temporal or phase differences at the ears are thought to provide the dominant cues, whereas at higher frequencies, intensity differences are thought to provide more useful information. Typical examples from the work of reference 15 on the error in ability to locate a sound source are shown in figure 4. As indicated, the error is greatest in the frequency region about 3 kHz where the localization cues are more ambiguous. The localization errors are minimal directly in front of the head, and with head movement most people can locate the origin of a sound within 1° or 2°.

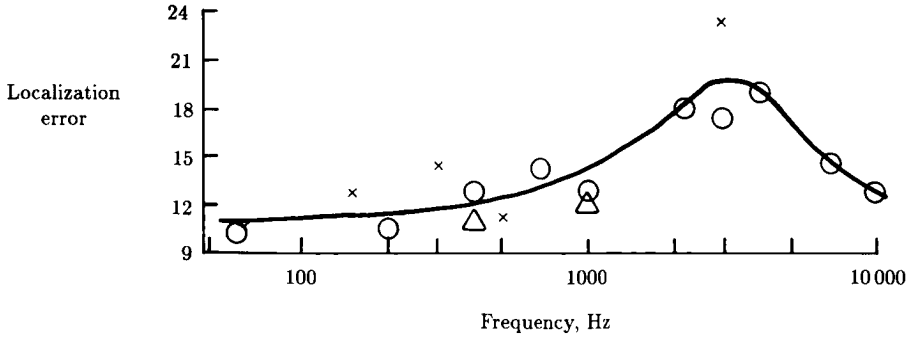

Figure 4. Error in localization as a function of frequency. (From ref. 15.)

Another phenomenon related to binaural hearing is commonly called the Haas, or precedence, effect (ref. 16). This refers to the ability to hear as a single acoustic event the sound from two or more sources radiating nearly identical acoustic signals provided that the signals arrive at the listener's ears with a delay not exceeding

50 msec. In addition the sound appears to originate at the nearer source or that source from which the first signal arrives. Although neither localization nor the precedence effect is as significant in determining human response to aeroacoustic sources as is loudness or noisiness, they may be significant modifiers to that response if the sound is perceived to be too close or in some location where safety is compromised.

Noise Metrics for Predicting Human Response

Considerable research has gone into developing methods to predict the loudness, noisiness, and annoyance of sounds on the basis of measurable physical characteristics of the sounds. In the following sections some of the procedures developed to predict human response to noise from aeroacoustic sources are discussed. Complete details of the calculation procedures can be found in a number of references (e.g., refs. 17 and 18).

Single Events

Loudness Level

Metrics developed to predict loudness have, in general, incorporated various means to account for the human sensitivity to frequency and sound level and the summation of the different frequency components of sound. The most commonly used metric is based on a simple frequency filter (defined as the A-weighting filter) for weighting the spectral content of a possibly complex sound. Although originally intended to approximate the loudness level of sounds with sound pressure level (SPL) between 24 and 55 dB, the A-weighted sound level (SLA) has been found to correlate very well with noisiness and loudness of many sounds with broadband spectra regardless of level. The relative response of the A-weighting filter is indicated in figure 5. The summation of different frequency components is a simple energy

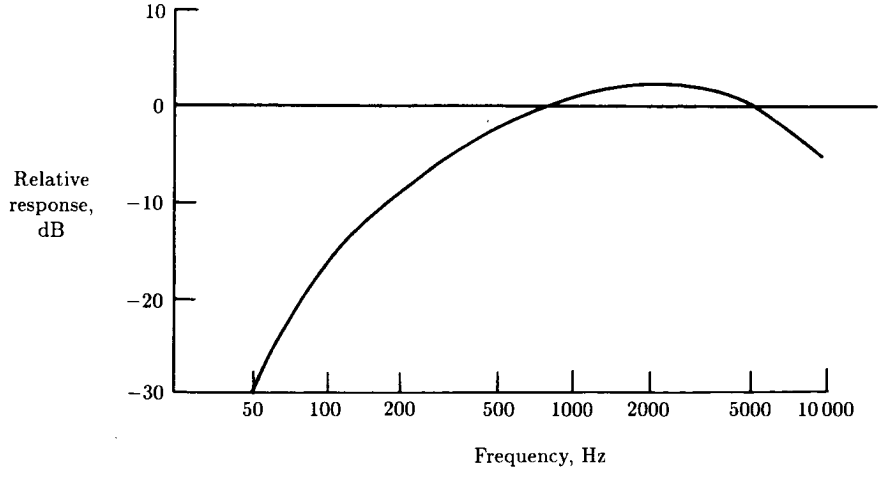

Figure 5. Relative response of the A-weighting filter.

summation after frequency weighting. If the weighting is incorporated in a sound level meter, the root-mean-square (rms) circuitry in the meter performs the necessary summation. If the A-weighting is applied to octave or 1/3-octave band SPL's, the resulting weighted SPL's are summed on an energy basis:

$$L_A = 10 \log_{10} \left[\sum_{i=1}^{n} 10^{L_A(i)/10} \right] \tag{1}$$

where $L_A(i)$ are the weighted SPL's of the frequency bands.

A somewhat more complicated procedure for predicting loudness level (LL_S) was developed by Stevens (ref. 19) and called Mark VI. It accounts for frequency characteristics including nonlinear level effects and in a simplified way for masking and inhibition between frequency components. The unit of loudness, sone, is defined as the loudness of a 1-kHz pure tone with a sound pressure level of 40 dB. The loudness in sones thereby represents a ratio scale with the property that twice as many sones indicate twice the loudness.

The frequency and level characteristics of the Mark VI loudness procedure are shown in figure 6. The loudness in sones $S(i)$ of each octave or 1/3-octave band is determined from the figure or a calculation algorithm. The total loudness is then found from the summation

$$S_t = S_m + F \left[\sum_{i=1}^{n} S(i) - S_m \right] \tag{2}$$

where S_m is the loudness of the loudest band and F is a masking factor, 0.15 for 1/3-octave band data or 0.30 for octave band data. The loudness level in phons is then calculated by

$$L_L = 40 + 10 \log_2 S_t \tag{3}$$

The phon scale has decibel-like properties and a factor of 10 phons represents an approximate doubling of loudness.

Another prediction scheme for loudness level (LL_Z) has been developed by Zwicker (ref. 20) and accounts for more of the complexities of the human auditory system, such as widening of "critical bandwidth" at low frequencies, "remote masking," and different sensitivities to different types of sound fields. In the original formulation of the method, only loudness of stationary sound fields or of time-varying sound fields at a limited number of instants was easily calculated because the method relied on the plotting of 1/3-octave band sound levels and integration under the curve with a planimeter. The development of relatively inexpensive computer systems, however, allows this method to be easily applied to nonstationary sounds. After calculation of the total loudness of the sound in sones S_t using the graphical or computer method, the loudness level LL_Z, in phons, is calculated using the same type of relationship as equation (3).

Perceived Noisiness

The noise metric which is most commonly used to predict the noisiness level of sounds is the perceived noise level (PNL). This metric, which was developed to predict the reported annoying quality of jet aircraft sounds (ref. 13), is calculated

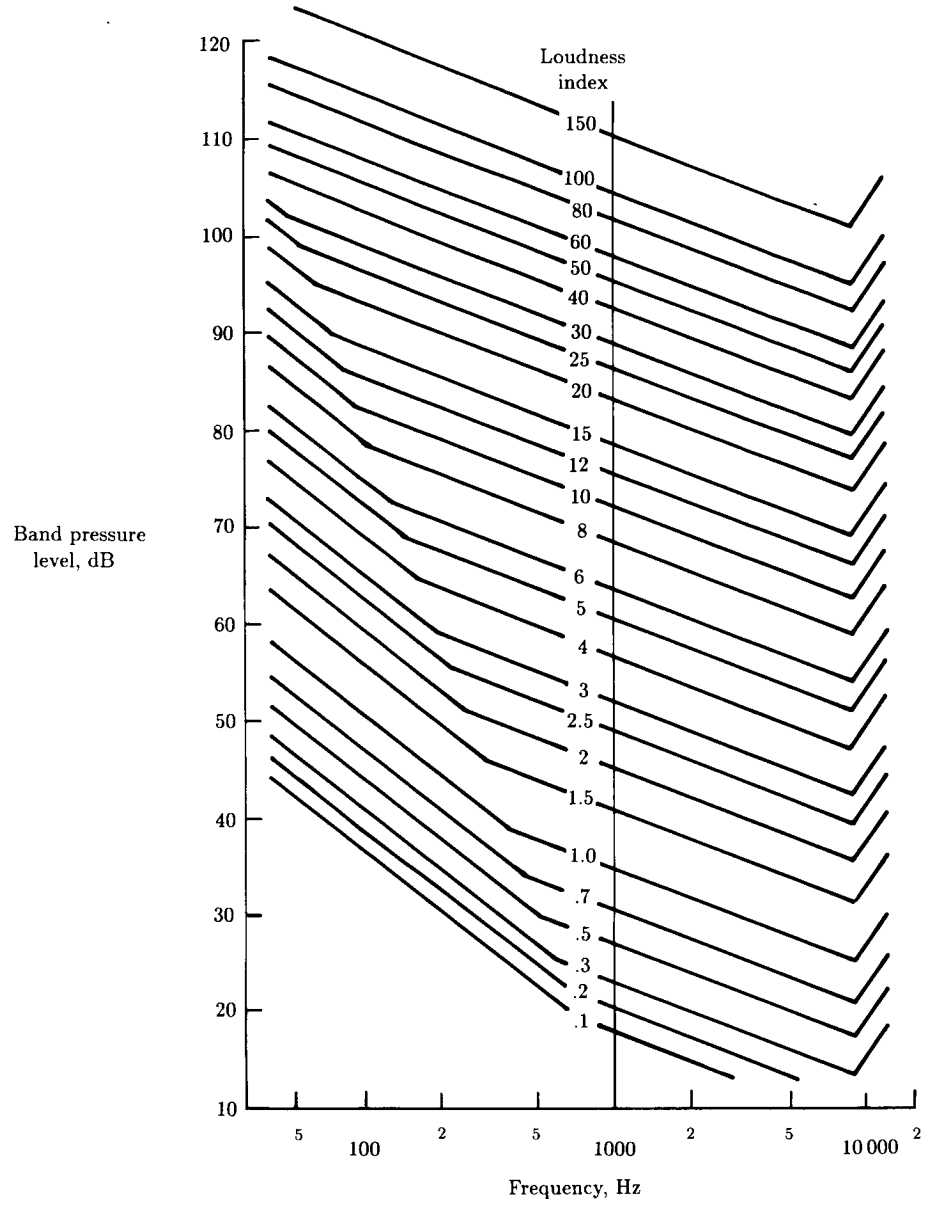

Figure 6. Frequency characteristics for the Mark VI loudness procedure. (From ref. 19.)

very similarly to the loudness level LL_S (ref. 19). The unit of perceived noisiness, noy, is defined as the noisiness of an octave band of noise centered at 1 kHz with a sound pressure level of 40 dB. A sound which is subjectively twice as noisy as the reference sound has therefore a perceived noisiness of 2 noys.

The noisiness of each 1/3-octave band $N(i)$, expressed in noys, is determined by using curves such as those in figure 3, by using a set of tables based on those curves, or by using a computerized algorithm. The noisiness of the total sound at any instant

is given by

$$N_t = N_m + F\left[\sum_{i=1}^{n} N(i) - N_m\right] \tag{4}$$

where N_m is the noisiness of the noisiest band and F is the masking factor in equation (2) for the Stevens loudness calculation. The PNL is then given by

$$L_{\mathrm{PN}} = 40 + 10\log_2 N_t \tag{5}$$

The PNL scale is thereby similar to the phon scale for loudness in that it has decibel-like properties, and a factor of 10 in PNL represents an approximate doubling of noisiness.

In much the same way that SLA has been used as a simplified method to approximate the loudness of sounds, another frequency-weighted metric has been used to approximate the noisiness of sounds. The D-weighted sound level (SLD) uses the frequency weighting shown in figure 7, which is comparable to the inverse of the 40-noy contour of equal noisiness (fig. 3). The summation of different frequency components is an energy summation after frequency weighting. The D-weighting filter is also incorporated in some sound level meters which provide the necessary rms circuitry for the summation. If the D-weighting is applied to octave or 1/3-octave SPL's, the resulting weighted SPL's $L_D(i)$ are summed on an energy basis:

$$L_D = 10\log_{10}\left[\sum_{i=1}^{n} 10^{L_D(i)/10}\right] \tag{6}$$

The similarity of the equal-noisiness and equal-loudness contours is obvious by comparing figures 2 and 3. Because of the similarity and reanalysis of data of many

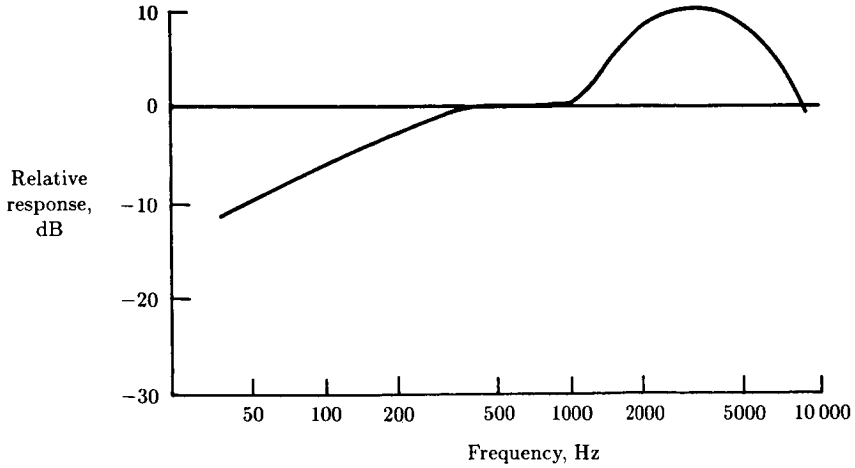

Figure 7. Relative response of the D-weighting filter.

noisiness and loudness experiments, it was proposed in reference 21 that loudness and noisiness were actually manifestations of the same auditory response and could be predicted using a slightly modified set of response curves. This calculation procedure was called Mark VII, perceived level (PL). The unit of perception for PL is based, however, on the perception of a 1/3-octave band of noise centered at 3.15 kHz with a sound pressure level of 32 dB as a reference sound. The frequency weighting for this procedure is given in figure 8. The magnitude of each octave or 1/3-octave band $S(i)$ is determined from the curves in the figure or from a calculation algorithm. The total perceived level of a sound is then calculated using the summation relationship of equation (2). The masking factor F for this newer procedure was proposed to be a function of S_m as indicated in figure 9. The perceived level of the sound is given by the relation

$$L_P = 32 + 9 \log_2 S_t \tag{7}$$

which is based on a doubling of perceived magnitude being equivalent to a 9-dB change in sound level.

A simplified method of approximating the perceived level of a sound was also proposed in reference 21. This metric, analogous to the A-weighted and D-weighted sound levels, is called the E-weighted sound level (SLE) and is computed using the frequency weighting of figure 10.

Tone and Duration Corrections

The advent of fan-jet engines on commercial airplanes was accompanied by a concern of whether the tonal nature of the sound was adequately accounted for by the PNL metric. A number of tone correction procedures were developed and one procedure was incorporated into the noise metric for noise certification of new transport aircraft. It was also proposed that sounds of longer duration were more annoying than those of shorter duration. Therefore a duration correction procedure was also incorporated into the certification noise metric. The certification noise metric developed for large jet airplanes was based on the PNL metric (ref. 13) to account for the basic frequency characteristics and sound pressure levels of the noise which the airplanes made in airport communities. The certification noise metric, effective perceived noise level (EPNL), requires that the PNL be calculated and corrected for significant tones every 0.5 sec and energy summed over the effective duration of the flyover noise (ref. 22). The tone correction procedure consists of identifying tones contained in the spectra, estimating the level differences between the tones and the broadband noise in the 1/3-octave bands containing the tones, determining the value of the tone correction, and adding that value to the PNL to obtain the tone-corrected perceived noise level (TPNL) for each 0.5-sec interval. If the frequency of the tone is less than 500 Hz or greater than 5000 Hz, the correction for that band is one-sixth the level difference (in dB) between the tone and broadband noise; if between 500 Hz and 5000 Hz, the correction is one-third the level difference. The corrections for the bands, however, are limited to 3.3 dB and 6.7 dB, respectively. The overall correction for the time interval is the maximum of the corrections for the individual bands. The EPNL for the flyover is then given by

$$L_{\mathrm{EPN}} = 10 \log_{10} \left[\sum_{i=1}^{n} 10^{L_{\mathrm{TPN}}(i)/10} \right] - 13 \tag{8}$$

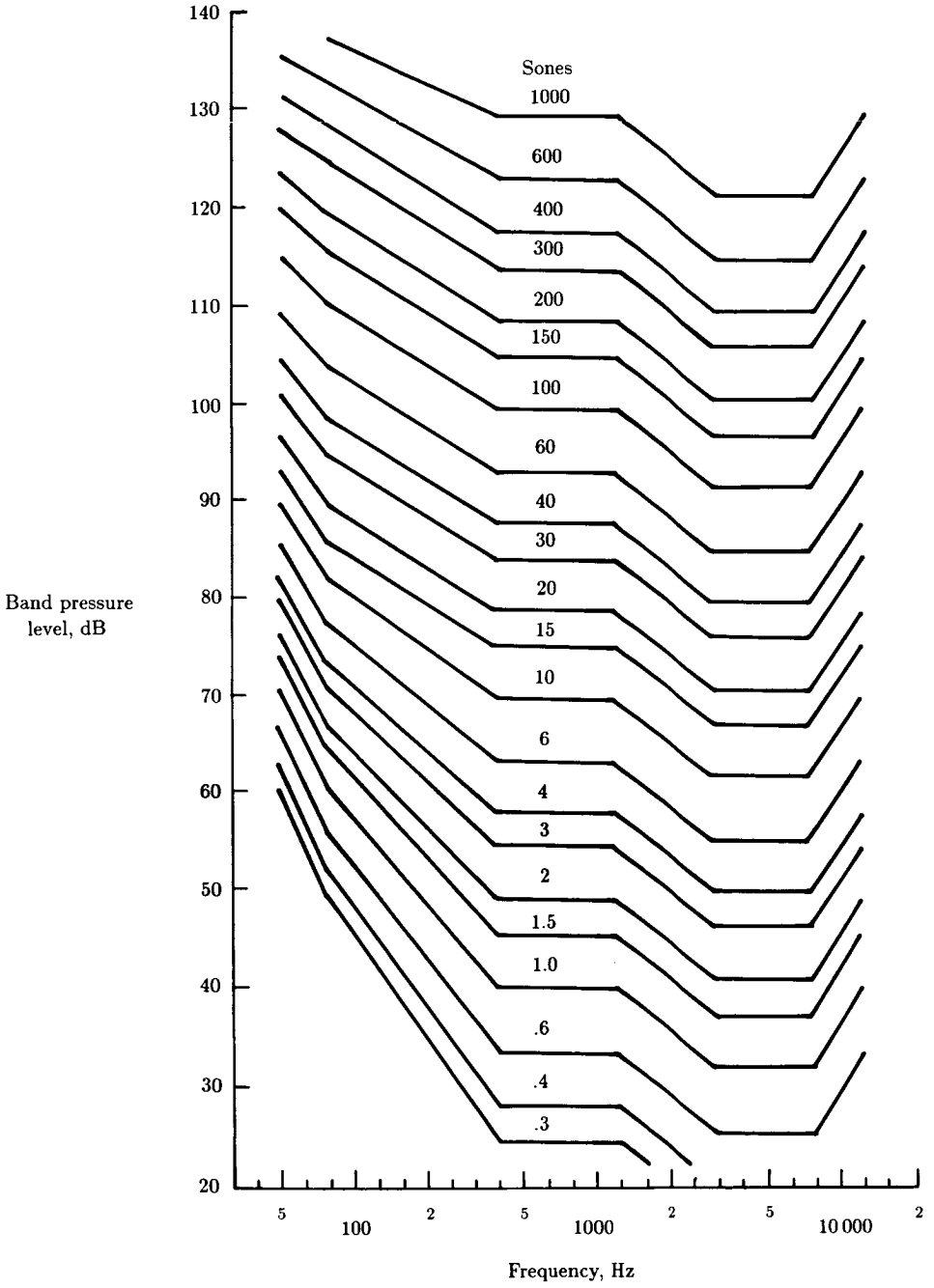

Figure 8. Frequency characteristics for the Mark VII loudness or noisiness procedures. (From ref. 21.)

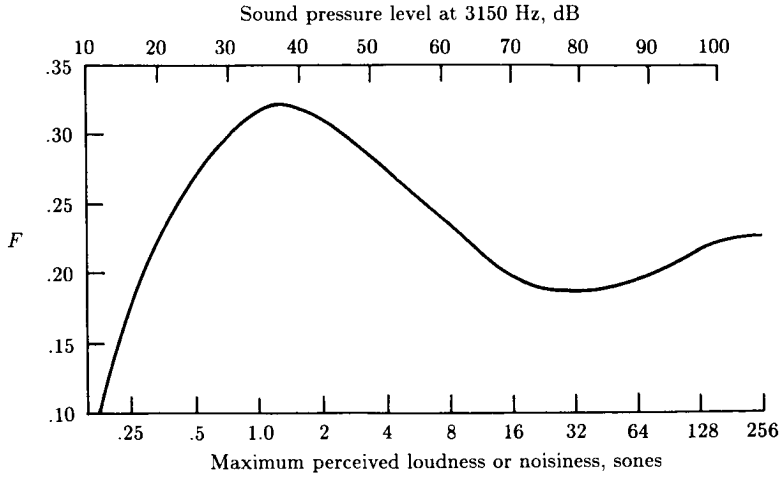

Figure 9. Masking factor F for the Mark VII loudness or noisiness procedure. (From ref. 21.)

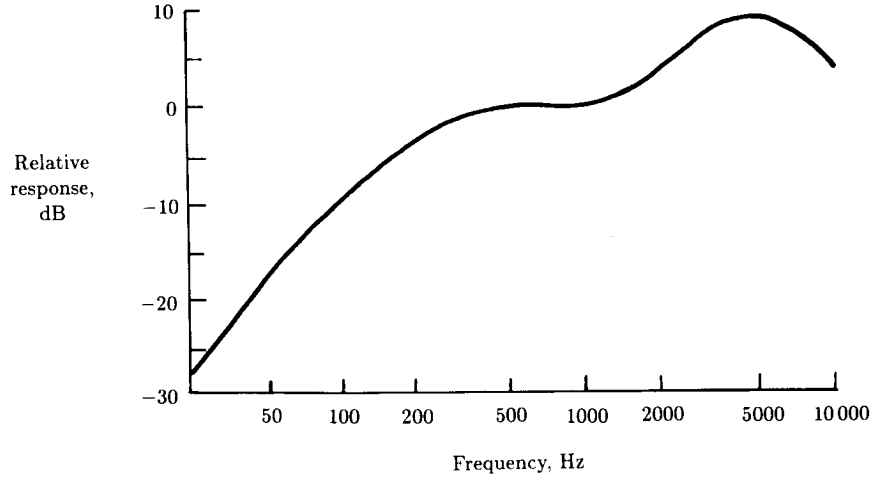

Figure 10. Relative response of the E-weighting filter. (From ref. 21.)

where $L_{\mathrm{TPN}}(i)$ is the value of the TPNL in the ith 0.5-sec interval of the flyover. The summation is over the duration when the $L_{\mathrm{TPN}}(i)$ are within 10 dB of the maximum TPNL of the flyover. The factor of 13 dB is subtracted to account for the difference in the 0.5-sec time increments and a reference duration of 10 sec.

Another duration-corrected noise metric commonly used to predict the annoyance of single aircraft and other noise events is the sound exposure level (SEL). This metric is the energy average over the duration of a noise event referenced to a duration of 1 sec. If the noise level is sampled with period t between samples, the calculation

formula is

$$L_{AE} = 10 \log_{10} \left[\sum_{i=1}^{n} 10^{L_A(i)/10} t \right] \tag{9}$$

where $L_A(i)$ is the instantaneous A-weighted sound level for the ith sample. For practical purposes the summation is normally limited to the duration for which the instantaneous level exceeds a level 10 dB below the maximum level.

Speech Interference

A number of metrics have been developed to predict the effect that a given noise environment will have on the intelligibility of speech. Several of the methods, including articulation index (AI) and speech transmission index (STI), require more detail to adequately describe the calculation procedures than can be given in this review. The more interested reader is referred to the original work in reference 23 and the suggested modifications in reference 24 for the procedures involved in calculating AI, which predicts how much of the speech spectrum is masked by the noise signal. Because of its wide acceptance and usage, the calculation procedure is covered by ANSI standard S3.5-1969(R1971) (ref. 25). The newer STI method of reference 26 considers the effective signal-to-noise ratio produced by the modulated speech signal and includes the effects of reverberation.

The speech interference level (SIL) is a simpler method for predicting speech interference effects of noise of essentially constant level and is frequently used to quantify aircraft interior noise (ref. 27). The calculation of SIL is the simple numerical average of the unweighted SPL in the four octave bands from 500 Hz to 4000 Hz as defined in ANSI standard S3.14-1977 (ref. 28). Initially the average was defined over the three octave bands which encompassed the frequency range from 600 Hz to 4800 Hz. After the introduction of the "preferred" frequencies for octave bands, the range was modified to include the three newly defined octave bands centered at 500 Hz, 1000 Hz, and 2000 Hz, and the procedure was called preferred speech interference level for a short period. The method has its greatest applicability if the noise is relatively steady, has a smooth spectrum, and is in an environment which is not highly reverberant.

Multiple Events and Total Noise Exposure

Many different noise indices have been suggested to quantify the annoyance potential of time-varying continuous and multiple-discrete-event noises. Those most commonly used for aircraft noise have been based either on the A-weighted level or on the perceived noise level to account for the basic frequency characteristics. The following sections describe several of the more commonly used indices.

A-Weighted Indices

The continuous or multiple-event character of noise is accounted for in the A-weighted indices through energy averaging or summation. The basic index is called the equivalent continuous sound level (LEQ) and is defined as the level of the time-averaged A-weighted sound energy for a specified period of time. The most

common periods for averaging are 1 hour, 8 hours, and 24 hours. The LEQ for a given period can be calculated from temporal samples of the A-weighted sound level by

$$L_{eq} = 10 \log_{10} \frac{1}{n} \left[\sum_{i=1}^{n} 10^{L_A(i)/10} \right] \tag{10}$$

where n is the number of samples and $L_A(i)$ is the level of the ith sample. In addition to its wide use to assess people's reaction to aircraft community noise, LEQ is widely and effectively used to assess reaction to other community noises and to predict hearing loss for long-term noise exposure.

In an effort to account for the possibility that noise occurring when most people are asleep is more annoying than during the day, the U.S. Environmental Protection Agency (EPA) developed noise criteria based on a modified LEQ with a 10-dB penalty for the period between 10:00 p.m. and 7:00 a.m. The index is called the day-night average sound level (DNL) and can be calculated in a number of ways depending on the sound level information available for the day and night periods. If the LEQ is known for both periods, DNL is given by

$$L_{dn} = 10 \log_{10} \left\{ \frac{1}{24} \left[15(10^{L_d/10}) + 9(10^{L_n/10}) \right] \right\} \tag{11}$$

where L_d is the LEQ for the day period (7:00 a.m. to 10:00 p.m.) and L_n is the LEQ for the night period (10:00 p.m. to 7:00 a.m.).

Another variant on the equivalent continuous sound level applies not only the 10-dB night penalty but also a 5-dB evening penalty. This index is primarily used in California for airport community noise. The community noise equivalent level (CNEL) is calculated by

$$L_{den} = 10 \log_{10} \left\{ \frac{1}{24} \left[12(10^{L_d/10}) + 3(10^{L_e/10}) + 9(10^{L_n/10}) \right] \right\} \tag{12}$$

where L_d is the LEQ for the day period (7:00 a.m. to 7:00 p.m.), L_e is the LEQ for the evening period (7:00 a.m. to 10:00 p.m.), and L_n is the LEQ for the night period (10:00 p.m. to 7:00 a.m.).

PNL-Based Indices

Before the EPA adopted DNL for assessment of all community noise, the most widely used index for assessing airport community noise was the noise exposure forecast (NEF). This index was based on EPNL for assessing the impact of each aircraft operation with adjustments for the time and number of occurrences during the 24-hour period. The nighttime adjustment was based on a 10-dB penalty if the average number of aircraft operations per hour during the day and night were the same. If, however, EPNL is known for each event ($L_{EPN}(i)$) at some location, the NEF is given by

$$L_{NEF} = 10 \log_{10} \left[\sum_{i=1}^{n} 10^{L_{EPN}(i)/10} + 16.67 \sum_{i=1}^{m} 10^{L_{EPN}(i)/10} \right] - 88 \tag{13}$$

where n is the number of events occurring during the day (7:00 a.m. to 10:00 p.m.) and m is the number occurring during the night (10:00 p.m. to 7:00 a.m.). The factor of 16.67 is the night correction factor which applies an effective penalty of 12.2 dB to each event occurring during the night period.

Another PNL-based index is frequently used in the United Kingdom to assess the effects of aircraft noises on communities. The noise and number index (NNI) is based on the average (energy basis) PNL of aircraft noise events "heard" at a location in the community and an adjustment for the number of events occurring during a given period. The calculation formula is

$$L_{\mathrm{NNI}} = \overline{L_{\mathrm{PN,\,peak}}} + 15 \log_{10} N - 80 \tag{14}$$

where $\overline{L_{\mathrm{PN,\,peak}}}$ is the energy average of the peak PNL's of all events which exceed 80 dB during the period, and N is the number of those events. It is interesting to note that the number correction, 15, is greater than a correction based on equivalent energy principles, 10. This results in a correction of 4.5 dB for a doubling or halving of the number of operations rather than the correction of 3 dB for indices such as LEQ or NEF.

Laboratory Assessment of Human Response

Many laboratory experiments have been conducted over the last three decades to determine various aspects of human response to aircraft noise as heard in the airport community and within the aircraft. In most of these experiments, test subjects have judged or rated the annoyance of noise stimuli that the experimenter reproduced in the laboratory. Since the noise stimuli rarely interfere with an activity that the subject prefers or has to do, it is questionable whether true annoyance is involved in the laboratory situation. There has been, however, limited validation of laboratory findings through carefully controlled field studies of response to specific physical characteristics of aircraft noise. Thus it is generally accepted that laboratory testing can play a major role in the assessment of the physical characteristics of noise that can cause true annoyance in real-life situations. The major advantages of laboratory experimentation are the cost savings and experimental control relative to field experimentation. The following sections present some aspects of methodology and findings of laboratory experiments of aircraft community and interior noise which deal with noisiness or the potential for causing annoyance in a real-life situation.

Methodology

Facilities and Stimuli Presentation Systems

The use of modern high-quality headphones to reproduce aircraft or other noises that are used as stimuli in psychophysical tests circumvents several potential problems of facilities and stimuli presentation systems. First, very little consideration need be given to the facility other than providing a measure of creature comfort and a relatively low background noise condition. Normal office or home environments are generally satisfactory. Second, headphones are generally capable of reproducing

aircraft-type noises with lower distortion, over a wider frequency range, and at higher intensity levels than are most normal loudspeaker systems. Their major disadvantages are slight discomfort over long periods of time, difficulty of calibration, and variability in stimuli between subjects and tests due to variations in placement on the head. A direct comparison of results of noisiness tests conducted under headphone, anechoic, and semireverberant listening conditions is reported in reference 29. Very little difference in subjective results was found between the three methods.

Although loudspeaker systems suffer from a number of shortcomings, they have been used extensively to reproduce noise stimuli for most subjective tests involving aircraft noise. Loudspeaker systems of all levels of sophistication have been used. Since the efficient response range of a loudspeaker system is related to the physical size of the drivers, most modern systems use multiple drivers of different sizes. As a consequence some reinforcement and cancellation occur at various locations for some frequencies. This can result in less than ideal or flat frequency response in the direct field of even the most expensive and reportedly smooth response systems. Another problem which plagues loudspeaker systems is harmonic distortion at high intensity levels. Loudspeaker systems are, at best, low-efficiency devices; therefore, aircraft noises at realistic outdoor levels are difficult to reproduce, particularly if they contain much low-frequency energy. Loudspeaker systems also have considerable phase distortion. While such distortion is not normally considered important for most broadband noises, it does prevent the realistic reproduction of the time signature of impulsive noises such as blade slap produced by some helicopter operations. It is possible, in some cases, to electronically predistort the phase of different frequency components so that the pressure field at the listener location has the proper phase relationships (ref. 30).

In order to better control loudspeaker-reproduced stimuli and to simulate outdoor listening conditions, many subjective listening tests have been conducted in anechoic chambers. In addition, a limited number of tests have been conducted in progressive wave facilities (ref. 31). These types of facilities have the obvious advantages of reducing the effects of reflected sound and of generally having low background noise levels. However, such facilities have a potential disadvantage of poor visual realism and may cause anxiety in some subjects during tests of long duration.

Many subjective aircraft noise tests have been conducted under semireverberant conditions such as in normal office environments or in special quiet facilities such as audiometric booths. As indicated in reference 29, little difference in results of noisiness tests is anticipated provided that the frequency response characteristics and room acoustics effects on those characteristics are accounted for in the analysis of results or, better yet, by the electronic filtering of the input signals to the sound reproduction system.

A number of special purpose facilities have been built to provide a realistic visual environment in addition to the required acoustic environment (refs. 32–34). The Interior Effects Room located at the NASA Langley Research Center (ref. 35) produced the visual simulation of a living room as well as the acoustic simulation of a typical house structure. Multiple loudspeaker systems were located outside the room structure, and realistic aircraft and other environmental noises were transmitted through the structure. While such attention to detail is most probably unwarranted on purely acoustic grounds, numerous tests were conducted in the facility where both visual and acoustic simulation was required for long-duration, multiple-event, and

multiple-noise-source studies. The Passenger Ride Quality Apparatus also located at the NASA Langley Research Center (ref. 36) provided both the visual simulation and the vibration simulation of an aircraft interior as well as acoustic simulation for many passenger annoyance studies.

Psychoacoustic Procedures

The purposes of most laboratory aircraft annoyance studies have been to determine how different physical characteristics of aircraft sounds affect reported annoyance response, how the sounds of different aircraft types will be accepted in communities, or how well different noise metrics predict annoyance or noisiness. Since it is generally recognized that these types of laboratory assessments are not absolute but rather are relative to either the whole set of sounds or to a specific sound used in the tests, comparative types of psychoacoustic test procedures and/or analyses are most often used. Frequently the goal of the tests is to determine noise levels for a set of stimuli which produce equal annoyance or noisiness response. The most commonly used procedures are described in the following paragraphs. Additional information on the various psychometric methods and analysis of data obtained can be found in references 37 and 38. In reference 39 the different procedures for determining human response to aircraft noise were evaluated using a standardized set of test conditions and noise stimuli.

In the method of adjustment (MOA), or method of average error as it is sometimes called, the task of the test subjects is to adjust the intensity of one of a pair of sound stimuli so that each has equal noisiness or some other attribute. Subjects are typically instructed (ref. 14)

> Your job is to listen to the standard noise ... then ... the comparison noise ... and adjust the intensity of the comparison noise until it sounds as acceptable to you as the standard.

Subjects can usually make the adjustment and comparison as many times as necessary for convergence. The experimenter then records the sound level of the variable stimulus for comparison with the level of the fixed stimulus. Both orders of presentation of the fixed and variable stimuli are usually given in the tests to prevent an order bias. By averaging over the reported points of equality for all test subjects or repeated trials for single subjects, the experimenter obtains a statistical estimate of sound levels which produce responses of equal noisiness (or some other attribute) for the two stimuli. These noise levels will be referred to as "levels of subjective equality" (LSE) in subsequent discussions. The exact application of this methodology has been varied between different laboratories and experimenters. In some cases the level of the standard sound is varied and in others the level of the comparison sound is varied. While intuitively MOA has many virtues, it is perhaps the most time-consuming and difficult test procedure for the subject and is therefore rarely used for tests involving many stimuli.

Another frequently used psychometric test method is also based on direct comparisons of pairs of sounds. This method has been called paired comparisons by some experimenters but is more properly called the method of constant stimulus differences (CSD). In this procedure many pairs of noise stimuli, comprised of a standard and a comparison stimulus, are presented to the test subjects who judge

which member of each pair is more annoying or noisy. The subjects are typically instructed (ref. 14)

> You are to judge which of the sounds you think would be more disturbing to you if heard regularly ... 20 to 30 times per day in your home.

Each comparison stimulus is presented at a number of levels greater than and less than the standard stimulus. In the course of a test the order of presentation of the standard and comparison stimuli is varied to prevent order bias, and frequently the overall order of presentation of the pairs is varied between different subject groups to minimize learning or other temporal effects. Psychometric functions of the proportion of responses, versus noise level, for which the comparison stimulus is more annoying than the standard are determined using appropriate statistical methods (refs. 37 and 38). Levels of subjective equality (LSE) for all comparison stimuli are then based on estimates of levels which would produce an equal number of positive and negative responses. The CSD procedure generally requires less time for the test subject than does the MOA procedure since the number of comparisons is fixed. However, a comparison of the two methods (ref. 39) indicates that MOA provides somewhat smaller standard deviations in LSE than does CSD and therefore may have slightly better reliability.

The method of magnitude estimation (ME), or fractionation, has been extensively used in experiments concerned with aircraft flyover and interior noise. The task of the subject is to assign a numerical value to each test stimulus, the magnitude of the value being proportional to the perceived magnitude of the stimulus. A reference or standard stimulus is presented and is assigned a convenient numerical value, such as 10, and the subject assigns to a test stimulus a value twice as great (i.e., 20) if it is twice as noisy or annoying, etc. Since the relationship between the magnitude of many types of sensations and a physical measure of their intensity is generally found to be a power function, a plot of the logarithm of the subjective magnitude as a function of the level of a sound is usually found to be linear. The ME procedure thus provides much more information than does the MOA or CSD procedures about response to the noise stimuli. The LSE for each test stimulus can be found by graphical interpolation or regression analysis to estimate the level which produces the same noisiness or annoyance response as the standard. The functional relationship of response to noise level provides estimates of the growth of noisiness with level and convenient comparisons between test stimuli. The subjective responses can be converted into numerical values having properties like decibels from prediction equations based on regressions of noise level on subjective responses for a standard or reference sound presented over a range of sound levels. The total amount of time required by each test subject is approximately one-half that required for a CSD test with the same number of test stimuli. Based on comparisons of results of ME with those of MOA and CSD (refs. 29 and 39), ME provides reliability at least as good as, if not better than, the other comparative procedures.

Another test procedure, numerical category scaling (NCS), has also been used in many aircraft flyover and interior noise subjective studies. This procedure more closely parallels the procedure used in many community noise surveys and has been almost exclusively used in laboratory studies concerned with multiple noise events or multiple noise sources. The task of the subject is to assign a numerical value

or a category to each test stimulus which is related to the subject's assessment of annoyance or other attribute of the stimulus. There has perhaps been more variability in the specific application of this procedure than in the other procedures. Different experimenters have used different numbers of categories (4 to 11 is typical), different labeling of categories, and in some cases only labeling of the end points of the scale. Typical analyses and comparisons of the noisiness of the different stimuli are based on linear regression of the subjective responses on measured or computed noise levels or are based on analysis of variance of the responses. Like the responses from the ME procedure, the NCS responses can be converted to a scale having decibel-like properties. Based on the evaluations of reference 39, the reliability of NCS is comparable to that of CSD but not quite as good as that of ME or MOA for determining levels of subjective equality. For comparison of different noise stimuli using the decibel-like computed scale values, the NCS procedure provides reliability very comparable to the ME procedure.

Findings Related to Aircraft Noise Annoyance in the Community

Most laboratory studies of aircraft noise have concentrated on various physical characteristics of the sounds which can affect the noisiness or annoyance of the sounds as heard in the community. Although laboratory settings have also been used to study other effects such as sleep interference, there is considerable concern whether results are directly applicable to the normal environment (ref. 3). In addition it is very difficult to obtain enough data for statistically meaningful interpretation of those results. The reader particularly interested in effects of aircraft noise on sleep is referred to the review in reference 40. The following sections therefore consider only annoyance studies (and some appropriate loudness research) related to those physical characteristics which are considered most influential in determining human response. Additional information on studies of human response to aircraft noise prior to about 1975 can be found in reference 41.

Spectral Content

Very few studies using real aircraft noise have been specifically designed to study the most appropriate frequency weighting and component summation for predicting human annoyance response. Fundamental studies that led to the development of the PNL metric for aircraft noise assessment were conducted using filtered bands of noise of various bandwidths. The problem with using actual aircraft sounds is that most of the other variables, such as duration, tonal content, and Doppler shift, are highly correlated with frequency content through their individual dependencies on distance. Many studies using real or recorded aircraft sounds, however, have examined the subjective results for clues as to which metric or frequency weighting procedure is most highly correlated with reported annoyance. A series of MOA and CSD studies using eight jet and propeller aircraft recordings (ref. 13) indicated that an early version of PNL was less variable in predicting the judged noisiness of the flyover noises than were various loudness measures or simple frequency weighting schemes. In a later field test, using real aircraft overflight noises in outdoor and indoor settings, PNL and LL_S were found superior to SLA and SLD (ref. 42).

An extensive set of CSD tests were conducted (ref. 31) under closely controlled acoustical conditions in a traveling wave facility. Subjects compared a reference octave band of noise centered at 1000 Hz with the noisiness of 120 recorded jet airplane, propeller airplane, and helicopter flyover sounds. Because of the great number of different sounds, the intercorrelation between the various acoustic variables such as duration, Doppler shift, and frequency content was reduced. Some data from this study are plotted in figure 11. The standard deviation of the prediction error, the difference between the judged (or subjective) level and measured noise level for the different metrics, is plotted for all aircraft—jets, turboprops, piston-engine propeller aircraft, and helicopters. In general, LL_Z followed by LL_S and PNL produced less error than SLD and SLA. The noisiness of jet and piston-engine aircraft was predicted better by all metrics than was the noisiness of turboprops and helicopters. It was postulated that the combination of high-frequency (compressor) and low-frequency (propeller) tones of the turboprops and the low-frequency pulsatile nature of the helicopters may have been responsible for the poor performance of the metrics. A subsequent propeller and jet aircraft annoyance study (ref. 43) using NCS methodology reported similar findings that the band summation metrics PNL, PL, and LL_S were somewhat superior to the weighted metrics SLD and SLA. A reanalysis (ref. 44) of data from 23 studies of environmental noises indicated that the more complicated summation metrics LL_S, PL, PNL, and LL_Z in general better predicted loudness and acceptability than the weighted metrics SLA, SLD, and SLE. In addition the weighted metrics SLE and SLD were slightly, but significantly, better predictors than SLA.

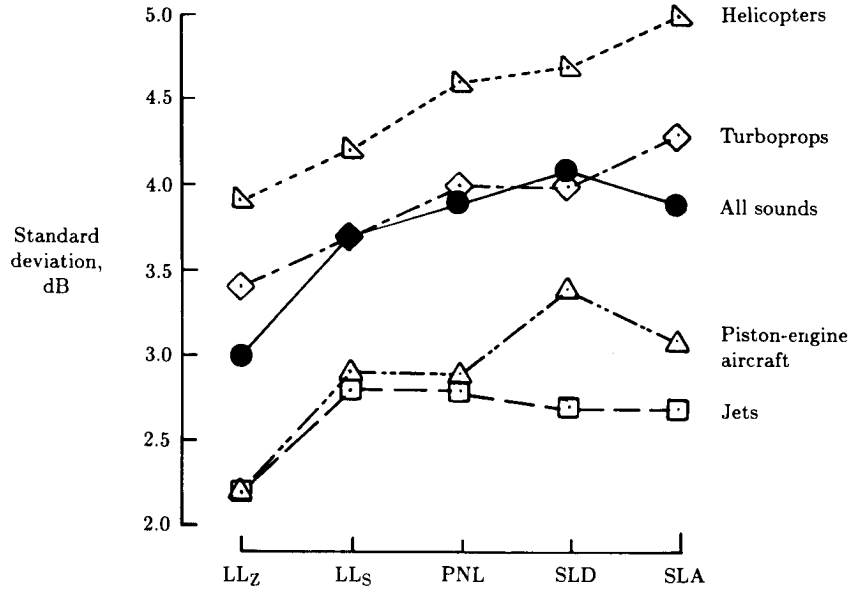

Figure 11. Prediction error for different noise metrics. (Based on ref. 31.)

It is perhaps not surprising that the majority of laboratory noise annoyance studies indicate that the more complicated computed or band summation metrics

perform better at their intended tasks than the more simple frequency-weighted metrics. Their summation procedures are empirically based on response to complex sounds. Another finding from most studies, based solely on the spectra of aircraft sounds (i.e., keeping duration constant or the same), is that there seems to be very little difference between annoyance and loudness. The loudness-derived metrics LL_S and LL_Z predict noisiness as well as does PNL, the noisiness-derived metric.

Duration

It is logical to assume that the longer an intense sound is present in the environment, the more annoyance it can cause. The question then arises, how much more annoying? Loudness has been shown not to increase with duration after a few tenths of a second, the integration time of the human hearing system. Thus the effect of duration is potentially different for annoyance and loudness and has been studied extensively for aircraft noise assessment purposes.

In a series of CSD tests (ref. 14) using shaped time histories of recorded helicopter and simulated jet and propeller noise with 1.5- to 12-sec duration, it was found that the judged annoyance of the sounds increased about 4.5 dB for a doubling of duration. An extension of these tests to longer durations (ref. 45) indicated that the duration effect decreased with longer durations. Figure 12 presents the results of both these studies. Based on these results and other laboratory confirmations, a penalty of 3 dB per doubling of duration was incorporated in the noise metric used by the Federal Aviation Administration (FAA) for noise certification of new jet aircraft. This penalty was tested in a laboratory-type field study (ref. 42) and in the extensive laboratory tests (ref. 31) with the general conclusion that the 3 dB per doubling penalty did reduce the scatter and improve the correlation between subjective response and various noise metrics. The necessity of a duration correction was refuted in reference 46 based on results of laboratory tests and examination of previous work. Reference 46 suggested that all studies that showed a significant and large effect of duration used strong duration cues in the instructions to the test subjects and that the subjects actually used a form of cross-modality judgment in which they rated intensity in terms of duration. The lack of an apparent duration effect in some studies was suggested in reference 47 to be the result of cues within the aircraft sounds. Cues, such as Doppler shift, could provide distance and speed information which would result in the listener rating a sound by what he expects to hear rather than by what he actually hears.

A number of the postulates were investigated in the study of reference 48 using computer synthesized flyovers in which spectra, flyover velocity, and altitude could be independently controlled. Thus duration, spectra, and Doppler shift could be uncoupled in the experimental design. The instruction to the test subjects used no duration cue, but rather the subjects were simply instructed to make their NCS judgments when they heard a beep, which occurred at the end of each flyover. Results from the study indicated that the duration correction of 3 dB per doubling was very nearly optimum and that Doppler shift was not significantly correlated with the annoyance judgments. These findings were further substantiated in the study of reference 49, in which recorded aircraft flyovers were modified by playback at higher or lower speeds to change the apparent Doppler shift, by spectral filtering to correct for spectral changes resulting from the playback speed changes, and by shaping the flyover time histories to produce changes in the duration of the flyovers.

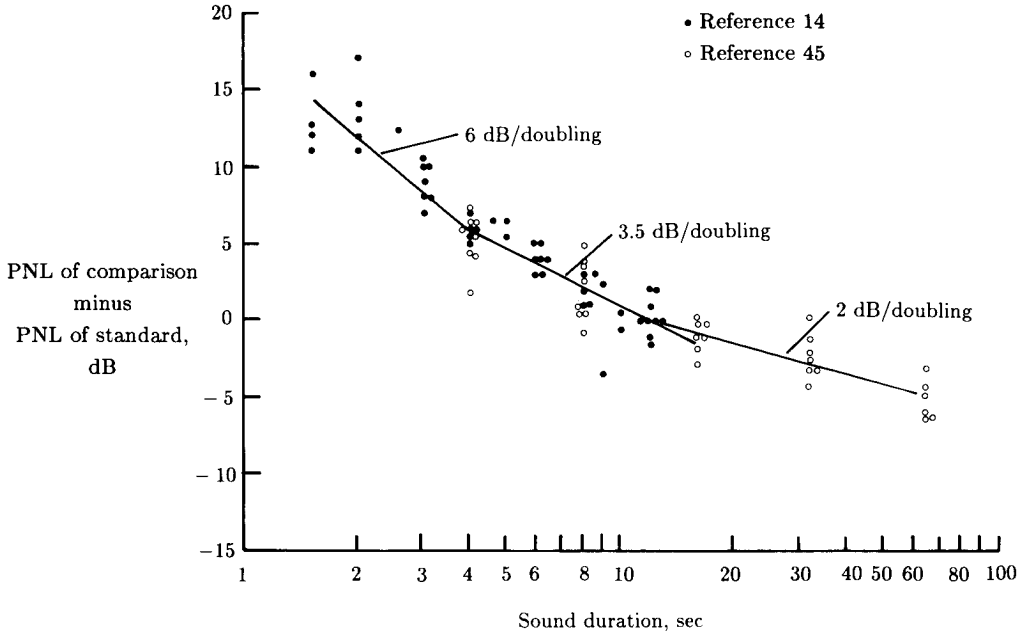

Figure 12. Effect of duration on annoyance. (From ref. 45.)

Tones

The question of whether or not a tone correction or penalty is needed to assess the human response to aircraft noise has been hotly debated since the advent of turbofan jet engines in the early 1960's. As pointed out in a review of research results (ref. 50), most studies that indicated the need for tone corrections used artificial sounds, such as pure tones in shaped bands of random noise, whereas studies that indicated no need for corrections most often used actual aircraft overflights or recorded aircraft sounds.

A typical example of results indicating the need for a tone penalty is shown in figure 13. These summary results, from references 51 and 52, indicate that in order to produce equal noisiness, the sound pressure level of a tone in an octave band of noise must be reduced by as much as 15 dB relative to the same octave band of noise without the tone component. The tone effect increases with tone-to-noise ratio up to 30 dB and increases with frequency up to 4000 Hz. Later results (ref. 53) indicated that modulation of the tones had little effect on judged noisiness of the tone-in-noise complexes, that multiple tones within the noise bands increased the effect by up to 5 dB, but that it made very little difference whether the multiple tones were harmonically related or not. Primarily because of this type of data, the Federal Aviation Administration included a tone correction in the noise certification metric for jet aircraft.

In field and laboratory studies using actual or recorded aircraft sounds, the results have not indicated so conclusively that a tone correction is necessary to assess aircraft noise impact. In a controlled flyover field study (ref. 42), both the FAA and another tone correction procedure gave inconsistent results and offered no significant

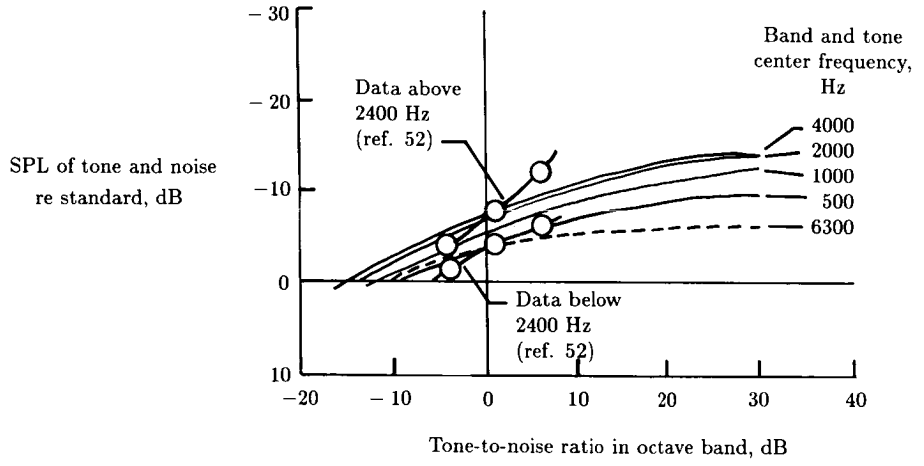

Figure 13. Effect of tone-to-noise ratio on noisiness. (From ref. 51.)

improvement over the non-tone-corrected metrics. Similar results were found in the large-scale laboratory study of reference 31. As indicated by the summary of these results in figure 14, the standard deviation in annoyance prediction error was reduced by the addition of a tone correction only for EPNL for jet aircraft. In all other cases the addition of tone corrections increased or did not change the standard deviation. In a reanalysis (ref. 54) of over 500 aircraft and other spectra with and without tonal components and responses to those spectra, very little evidence could be found to support either the FAA or several other tone corrections.

Repeated Impulses

A characteristic of some helicopter noise which has been reported to cause increased annoyance without an equivalent increase in level, as measured by most of the common noise metrics, is the repetitious impulses called blade slap. Although blade slap can be attributed to several mechanisms, it is generally characterized by a popping or banging sound with a repetition frequency equal to the main-rotor blade passage frequency. In terms of human response and the need to apply a correction to the common aircraft noise metrics to account for increased adverse responses, research studies have been about as inconclusive as they have been for tone corrections. In a review of 34 psychoacoustic studies (ref. 55), the conclusion was reached that helicopter noise should be measured in the same way as other aircraft noise and that no impulse correction was necessary to account for blade slap. Although many studies indicated the need for an impulse correction, nearly all utilized electronically synthesized or modified examples of helicopter noise. Conversely, most of those that indicated no need for corrections used natural live or tape-recorded helicopter sounds. A typical example of the type of mixed results is illustrated in figure 15, which is based on data from a CSD method study of reference 56. In the tests the subjects compared the annoyance of sounds with and without repetitive impulses. For stationary sounds with various levels of added impulses, there was a rather strong trend for increased annoyance without a corresponding increase in PNL as the level of the impulses was increased. For

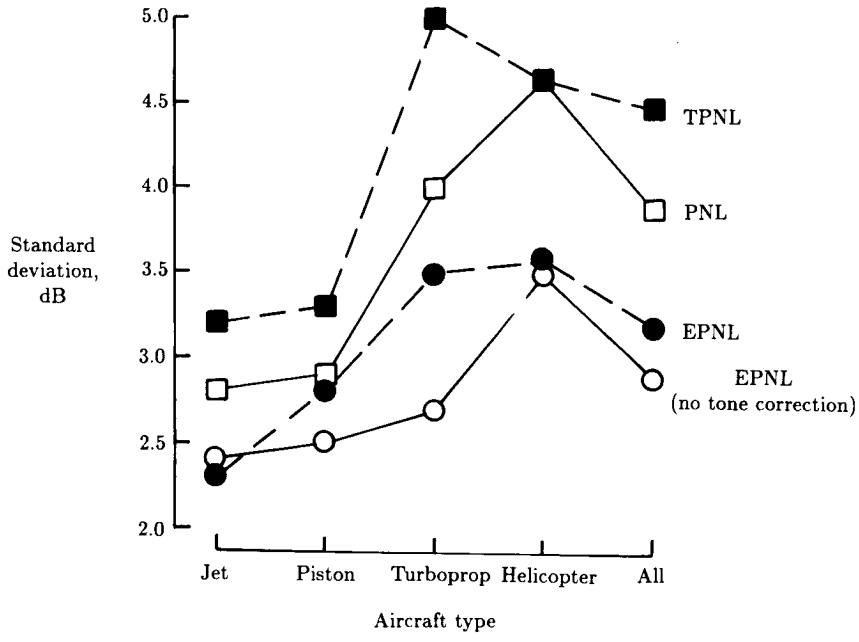

Figure 14. Effect of a tone correction on annoyance prediction error for different aircraft types. (Based on ref. 31.)

transient noises that were recordings of helicopter flyovers, no such clear trend was indicated. Similar results were reported in reference 57. In these tests no significant effects of impulsiveness were found for a limited number of recorded helicopter flyovers, but a significant effect was found for fabricated noises with added pulses.

In a study (ref. 58) in which subjects located indoors and outdoors judged the annoyance of actual helicopter operations using the NCS method, EPNL without any impulse correction was most highly correlated with the reported annoyance. The biggest drawback to this study was that only two helicopter types were used, although one type was flown in such a manner that various levels of impulsiveness were generated for different flyovers. In order to overcome this drawback, an extensive set of tests were conducted (ref. 59) using recordings of 89 different helicopter flights (22 different types) and 30 conventional aircraft flights. These tests utilized both headphone and loudspeaker presentations and compared the NCS and MOA techniques. Results of these tests also indicated no significant need for an impulse correction and in fact indicated that the helicopter sounds were no more annoying than conventional aircraft sounds for the same EPNL.

Sonic Boom

The concern about adverse effects of sonic boom has resulted in the prohibition of commercial supersonic flight over land within the United States. A recent bibliography (ref. 60) includes a very extensive listing of physical and psychological studies of sonic boom. In addition to annoyance due to the actual noise levels produced by a sonic boom, there is perhaps a more important startle reaction due to

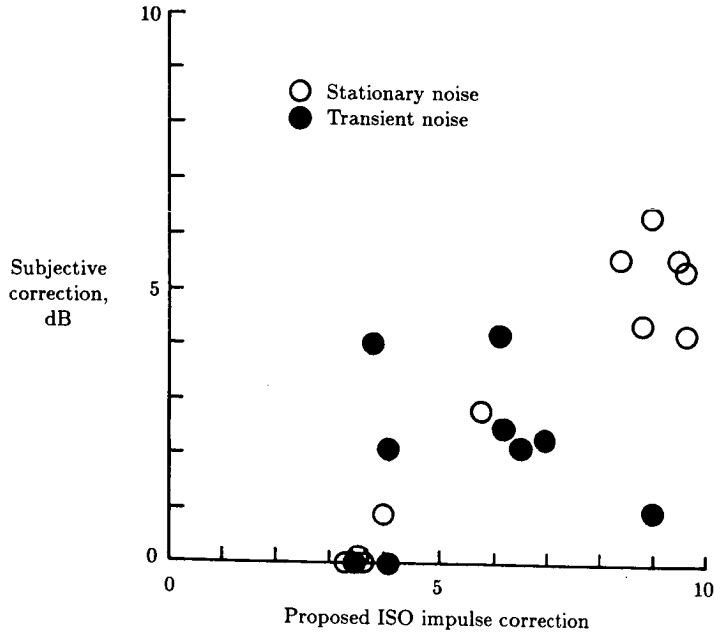

Figure 15. Effect of impulsiveness on subjective response to helicopter-type sounds. (Based on ref. 56.)

the suddenness of the sonic boom sound. The sonic boom noise characteristics result from the N-shaped pressure pulse caused by the compression and rarefaction of air as an aircraft flies at a speed greater than the speed of sound. A Fourier transform of the pressure time history into the frequency domain indicates that the acoustic energy covers a wide frequency range and that the low-frequency cutoff is determined by the duration between the positive and negative pressure peaks. The amount of high-frequency acoustic energy is inversely related to the rise time of the pulse. A series of CSD tests (ref. 61) on simulated and idealized sonic-boom-type N-waves and sawtooth pressure pulses indicated that the duration between the positive and negative pulses was not a major factor of loudness, that loudness increased with a decrease in rise time, and that loudness and annoyance were not very different for sonic-boom-type noises.

Fourier transformation of the pressure time history into the frequency domain serves as the basis of several loudness and annoyance prediction procedures. The method described in reference 62 basically converts the spectral information into 1/3-octave band pressures, corrects for the integration time of the ear, corrects for the large amount of energy at very low frequencies, and then uses the Stevens loudness calculation procedure to predict a composite loudness level. A simplified method of loudness prediction for sonic booms has been suggested in reference 63. Based on analysis of subjective data from outdoor judgments of sonic booms from a test conducted in Meppen, W. Germany, an empirical relationship for determining the loudness of the booms was developed. The loudness in terms of phons is approximated by

$$L = 20 \log_{10}(p/p_o) - t - 12 \tag{15}$$

where p is the peak overpressure of the boom, p_o is the reference acoustic pressure, 2×10^{-5} Pa, and t is the rise time in msec. In a later report (ref. 64), also based on results of the Meppen tests, startle reactions were investigated and could be related to a similar function of p and t.

An investigation of sonic boom reaction is presented in reference 65. Some results of these CSD tests are shown in figure 16. The boom signatures were produced using computer-generated electrical signals and special filtering. Effects of rise time and peak overpressure agreed well with previous studies (refs. 61, 62, and 66). Although little effect of duration was found for short durations, a significant increase in loudness was found for durations exceeding 200 msec. Since this duration exceeds the integration time of the ear, it is suspected that the subjects were reacting to both the positive and the negative portions of the simulated N-waves.

Multiple Noise Exposures and Other Effects

Community annoyance due to aircraft noise exposure is generally considered to depend on the number of flight operations in the community as well as the noise levels of the operations. Although numerous social survey studies have been conducted to determine the relationship of annoyance to noise exposure, the relationship of annoyance to the number of events has remained relatively unresolved. The first major laboratory study to investigate the effects of the number of aircraft events on annoyance was reported in reference 34. In the study, subjects in a living-room-type environment who were engaged in quiet activities, such as reading, made NCS-type judgments on 1-hour-long sessions of aircraft noise exposure. The sessions contained from 4 to 64 aircraft flyover noises of various types. Based on results of the study, the best fit for number of events was about $7 \log_{10} N$ or $N/6$, where N was the number of flyover events per hour. A series of similar tests (refs. 67 and 68) indicated a somewhat larger number effect, $15 \log_{10} N$. However, this effect did not significantly differ from the number effect, $10 \log_{10} N$, implied in the energy-averaging-type metrics, such as LEQ or DNL. Some other findings of the study of reference 68 were as follows. The time of occurrence of the flyovers in the session was not a significant factor; thus annoyance does not decrease significantly after exposure at least for relatively short periods of time (minutes and hours). In addition annoyance decreased with increases in session duration for a fixed number of flyovers in the session; thus the subjects make an averaging-type judgment over time rather than a simple summation. Thus an energy-averaging noise exposure metric may be very appropriate for assessing total community noise exposure.

Another factor that has been considered to affect human response to aircraft noise is the level of the ambient or background noise in which the aircraft noise is heard. Most studies that investigated background noise effects have used NCS procedures in which aircraft noises with different noise levels were heard in a session with a constant background noise. The background noise effects were determined by having the subjects judge the same aircraft flyovers in a number of sessions with different background noise levels. A summary of three different studies (refs. 69–71) is shown in figure 17. A significant reduction in subjective noise level for increasing background noise level was found in each study, and the magnitudes of the effects were very similar as indicated by the high correlation of the pooled data. Although these effects are consistent and significant, the effect is rather small at typical

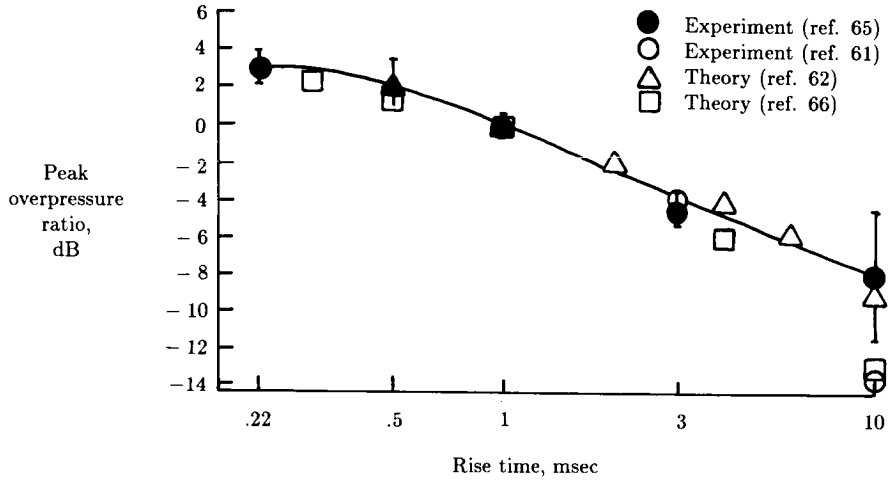

(a) Equal loudness as a function of rise time.

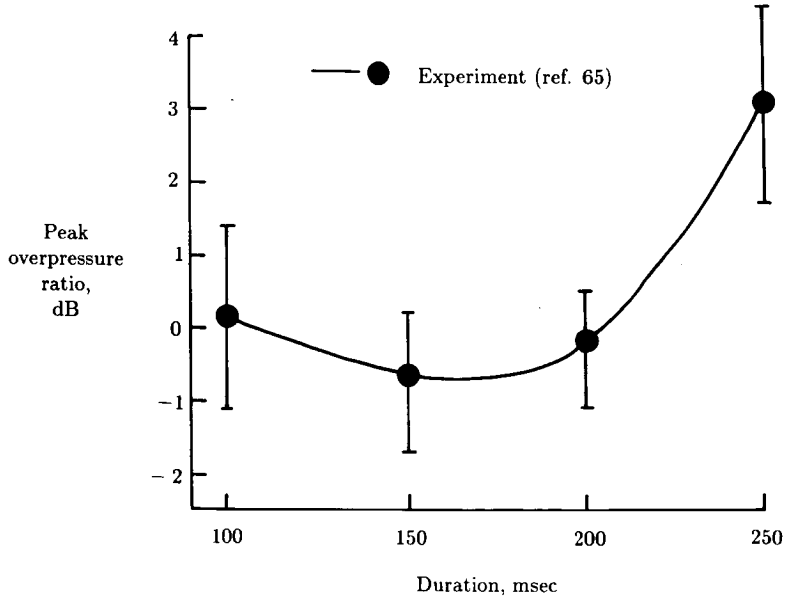

(b) Equal loudness as a function of duration.

Figure 16. Effect of rise time and duration on response to simulated sonic booms. (From ref. 65.)

aircraft-to-background noise ratios (>20 dB); therefore it is not expected that background noise is a major factor in determining community annoyance to aircraft noise.

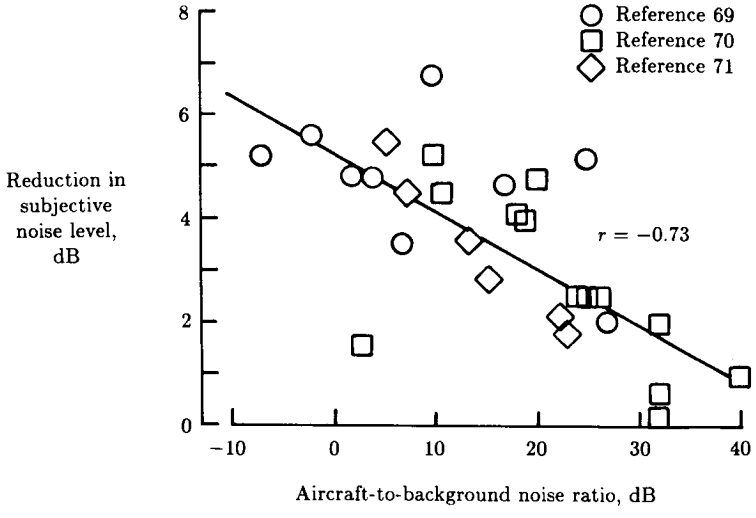

Figure 17. Effect of background noise on aircraft noise annoyance judgments.

Findings Related to Aircraft Interior Noise

The effects of aircraft interior noise on people have received much less specific attention as a research topic than has aircraft community noise. Many reasons may contribute to the apparent lack of interest in aircraft interior noise as a research topic. First, the people exposed to aircraft interior noise normally are willing participants and benefit directly from flying. They have some control over their overall exposure and level of annoyance by simply not flying or by flying in aircraft that provide an acceptable interior noise environment. Second, the airlines tend toward buying aircraft with acceptable interior noise levels as much as economically possible so that the passengers will continue to fly with their airline. Third, the aircraft industry takes whatever noise control measures are necessary and economically feasible to maximize passenger acceptance and sales to the airlines or private operators. And finally, the nature of the noise itself allows application of findings from basic or generic research on human response to noise to guide noise control methods.

Aircraft interior noise environments vary significantly with the type of aircraft and operation. For most flights, however, the cruise phase lasts much longer than takeoff or landing phases or other phases with significant maneuvers which cause variations in noise level or spectrum. Typical cruise noise levels for the interiors of a number of different classes of aircraft are indicated in figure 18 and are compared with the noise levels typically measured in ground transportation systems (ref. 72). Typical interior noise levels in commercial jet aircraft range from 80 dB

to 85 dB (A-weighted). Typical general aviation airplanes and helicopters have significantly higher interior noise levels and can create the possibility of hearing damage with long and unprotected exposures. Private business jets are frequently quieter than commercial jets so that better verbal communication is possible between the passengers. The noise levels for large commercial jets are actually optimized so that communication is possible between adjacent seats but a measure of privacy is provided from other passengers.

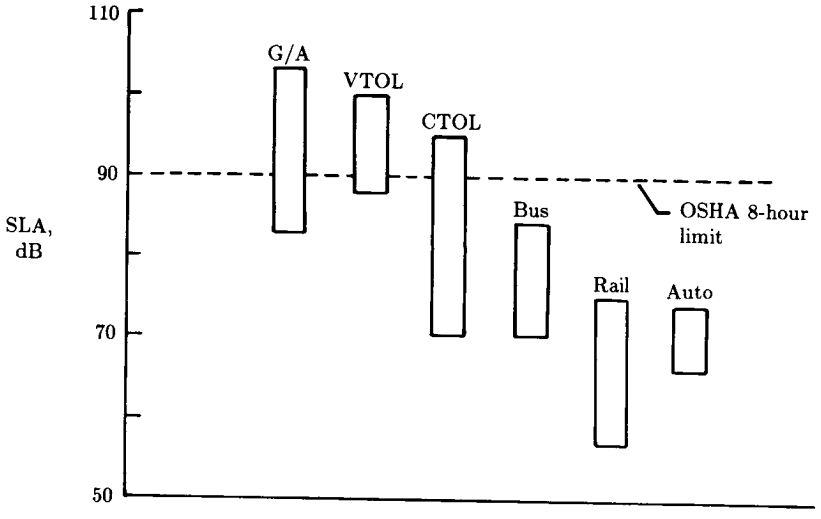

Figure 18. Comparative interior noise levels for different aircraft and ground transportation systems. (From ref. 72.)

The three most important effects of aircraft interior noise on passengers and crew are the potential for permanent hearing loss, speech interference, and general annoyance. Since for the most part aircraft interior noise has constant level and spectrum, generic hearing damage and speech intelligibility research is directly applicable for predicting those effects of the aircraft interior noise environment. A possible exception would be for speech intelligibility in some helicopters where the noise environment is dominated by high-frequency tones. In reference 73 it was found that the commonly used articulation index procedure tended to underestimate the intelligibility scores (percent correct) for a helicopter interior noise environment with very strong pure tone components. The following sections therefore present some research results of factors related specifically to aircraft interior noise annoyance.

Interaction of Speech Interference and Annoyance

Aircraft crew and passengers can suffer from fatigue as the result of the increased vocal effort required to communicate effectively inside aircraft with high noise levels. Thus in addition to the direct effects on general annoyance and speech intelligibility, aircraft interior noise can be the source of increased annoyance which results from the increase in fatigue level.

In reference 74, subjects were asked to rate recorded aircraft interior noises for general annoyance and "communication annoyance," assuming they would want to be able to converse in the noise. Recorded speech noises were presented simultaneously with the aircraft interior noise, and speech intelligibility tests were administered during part of the study. Results of the study are presented in figure 19. The percentage of the subjects who reported that they were highly annoyed by aircraft interior noises was in general greater when the subjects considered verbal communication, particularly in the middle range of the noise levels presented. The communication noise ratings were also found to be significantly correlated with speech intelligibility. Figure 20 presents the communication annoyance ratings grouped according to speech intelligibility and related to noise level. An interaction of noise level and speech intelligibility is clearly indicated. Since speech communication is a common and important activity in aircraft, it must be concluded that speech intelligibility as well as noise level should be considered in determining appropriate noise environments inside aircraft.

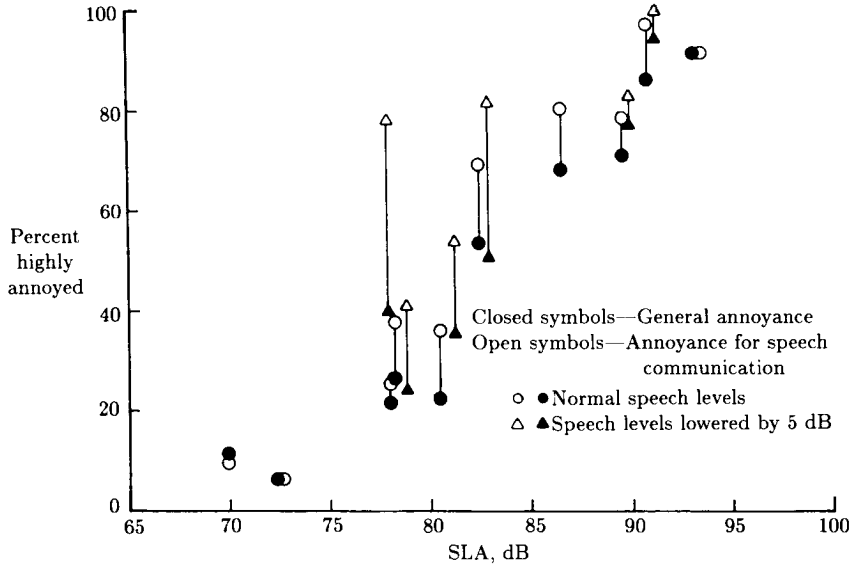

Figure 19. Effects of aircraft interior noise levels on general annoyance and communication annoyance. (From ref. 74.)

Interaction of Noise and Vibration

Aircraft interior noise is usually accompanied by vibration over a wide frequency range. Depending on the level and frequency, the vibration may be sensed through whole-body motion or tactile sensation through the hands or feet or other body members. In 1975 a research program was instituted at the NASA Langley Research Center to develop a ride quality model that would be applicable for predicting human response to the wide range of vibration inputs possible from all types of aircraft. During the research for development of the model, it was found that the effects

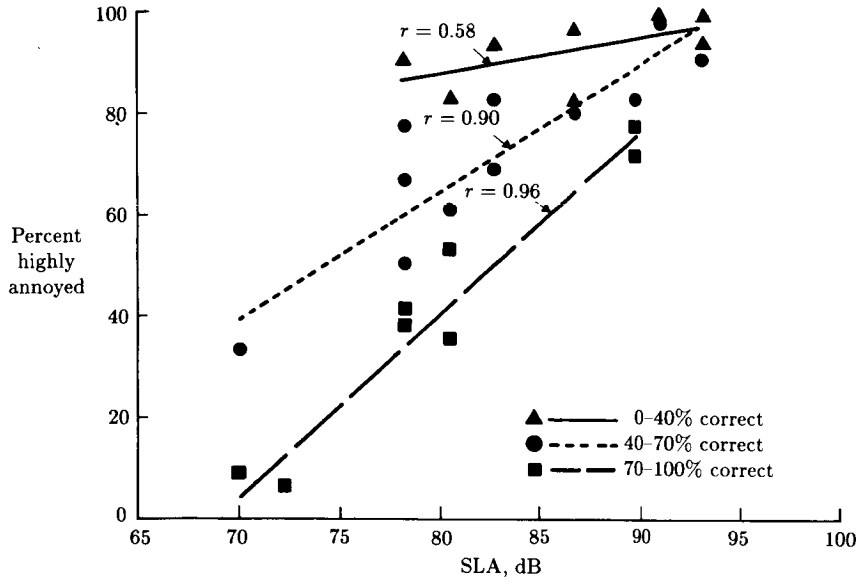

Figure 20. Effects of noise level and speech intelligibility on communication annoyance. r is the product moment correlation coefficient. (From ref. 74.)

of noise and vibration were interactive in determining the acceptability of a given aircraft interior environment.

The ride quality model involves transforming the physical noise and vibration characteristics into subjective discomfort units of noise and vibration using a common scale which can be combined into a single discomfort index (ref. 75). The model was validated in a simulator study using the Passenger Ride Quality Apparatus mentioned previously with recorded helicopter interior noise and vibration (ref. 76). Experienced military helicopter pilots served as test subjects. Typical results from the study are shown in figure 21. The open symbols represent the mean discomfort ratings given by the pilots; the closed symbols are the predicted discomfort ratings from the model. The agreement is good over the range of conditions, and the data illustrate the interaction between noise and vibration in determining total discomfort.

Field Assessment of Human Response[1]

Community noise annoyance surveys are the major source of information about the effects of noise on people in the community. Over 200 social surveys of community response to noise have been performed and over 90 of those surveys have specifically addressed aircraft noise (ref. 77). The reader interested in a more detailed discussion of the findings from field studies of aircraft and other types of transportation noise sources is referred to reference 78. Such studies consist of two main parts: a social survey in which residents in the studied community answer questions about their reactions to aircraft noise and/or other community environmental factors and a noise

[1] Section authored by James M. Fields.

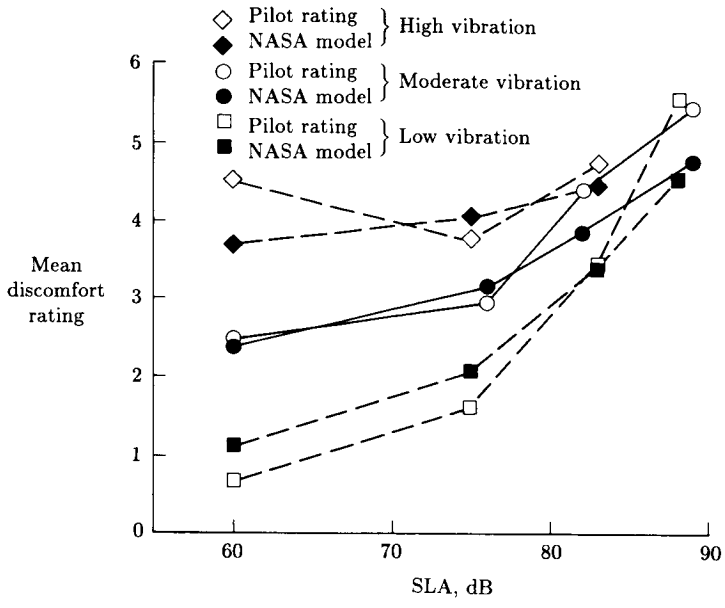

Figure 21. Comparison of pilot discomfort judgments with predictions of the NASA Ride Quality Model showing the interaction of noise and vibration. (From ref. 76.)

measurement survey which provides estimates of the residents' noise exposures. The major advantages of field assessment of the effects of noise are that community residents are exposed to the actual noise environment which can interact with other environmental factors and their personal living conditions to produce feelings of annoyance or dissatisfaction with the environment. The major disadvantages are that a carefully conducted social and physical survey of aircraft noise is expensive and time-consuming but still may not provide the necessary statistical accuracy to test hypotheses of the effects of some acoustical variables. The following sections present some of the methodological considerations and findings of aircraft noise surveys which relate to both individual noise annoyance and community complaint activity.

Methodology

Activity Disturbance and Annoyance Scaling

Activity disturbances are normally studied in a natural community setting by asking retrospective questions in surveys rather than by directly observing specific instances of activity interference as is done in the laboratory. Respondents are asked a series of questions such as the following from the 1967 Heathrow aircraft noise survey (ref. 79):

Do aircraft ever . . .

i. Startle you?

ii. Wake you up?

iii. Interfere with listening to radio or TV?

iv. Make the TV picture flicker?

v. Make the house vibrate or shake?

vi. Interfere with conversation?

vii. Interfere with or disturb any other activity?

Respondents are also frequently asked how annoying they find the disturbance (e.g., "very, moderately, a little") or how often they are disturbed (e.g., "very often, fairly often, occasionally"). In spite of the diverse exposure conditions and the use of self-reports rather than laboratory observations, the surveys consistently show that activity interference consistently increases with increasing noise exposure. A typical example is shown in figure 22, which is from data collected in a survey around the Geneva, Switzerland, airport (ref. 80). These results indicate that communication interference (conversation, radio, TV) is the most frequently mentioned type of activity interference.

Although there is consistency in the qualitative results of activity interference across different surveys, the level of reported activity interference varies widely between surveys (ref. 81). The exact wording of the questions has been found to result in large differences in reported disturbance even within the same survey. Therefore attempts to summarize interference results across studies or to compare results from different studies need to take into account the specific questions asked in the surveys.

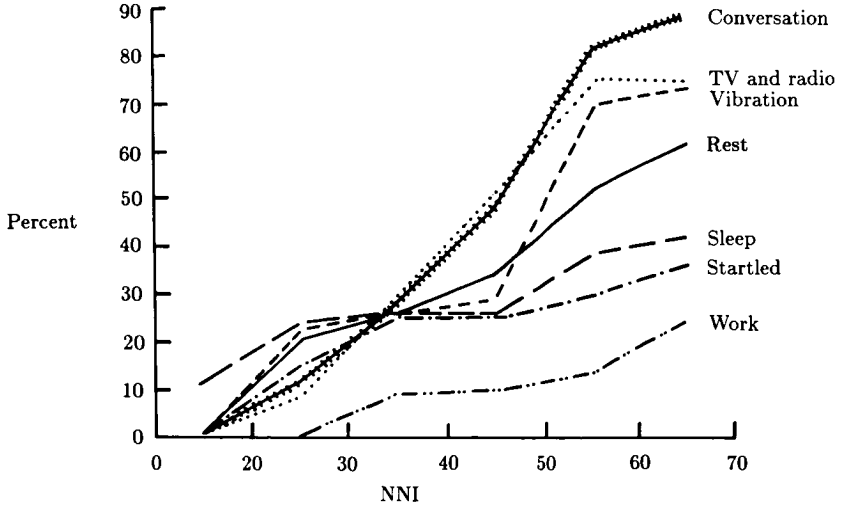

Figure 22. Reported activity interference (percent) as related to aircraft noise exposure around Geneva airport. (From ref. 80.)

Social surveys typically measure annoyance by asking whether specific noises "annoy" or "bother." Since the respondents hear only these questions rather than a philosophical treatise on the "true meaning of annoyance," the annoyance which is

measured is nothing more than whatever dimensions are tapped by the particular wording of the survey questions. Questions which are typically used are as follows:

> Please look at this scale and tell me how much the noise of the aircraft bothers or annoys you.
>
> Very much
> Moderately
> A little
> Not at all (From the 1967 Heathrow survey, ref. 79)

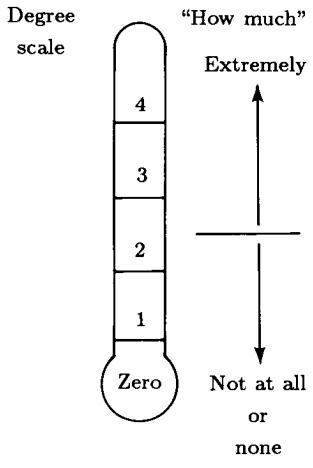

> I will now read a number of noises heard in different neighborhoods.
>
> Which ones do you hear in this neighborhood?
>
> Of those that you hear, how much are you bothered or annoyed? Use the Opinion Thermometer. (From a U.S. survey, ref. 82)

Individual responses to these types of questions can be scored numerically and used to obtain group averages as a function of noise exposure, or they can be scored categorically and used to determine percentages of the population in each category as a function of noise exposure. In an effort to compare results across a large number of surveys for a number of noise sources, the upper 27 to 29 percent of any annoyance scale was used in reference 81 to represent "high" annoyance. Therefore most subsequent studies of community noise annoyance have presented results in terms of the "highly annoyed" dichotomy. There is, however, no scientific reason for choosing a particular dichotomization of the annoyance scale. It may be argued that a "high" annoyance point should be less influenced by personal characteristics and more related to noise level. The only empirical data that compare different annoyance cutting points show that the high annoyance dichotomization is no more closely related to noise level than less severe dichotomizations (ref. 83).

Validity and Reliability

In order to correctly interpret the meaning of annoyance measurements from social surveys, it is important to consider both the validity and the reliability of the annoyance measurements. Validity is defined as the extent to which a question actually measures some "true" underlying annoyance. Reliability is the extent to which repeated measures of some individuals' annoyance are consistent.

The subjective nature of the response of the residents and the possibility that the responses might be biased by the interview procedure have led to carefully designed and tested social survey research procedures for community noise studies. General guidelines for the design and conduct of social surveys can be found in specialized texts (ref. 84). The following practices reduce or eliminate some of the potential biases. Survey questionnaires conceal the focus on noise as long as possible by being presented as studies of general environmental problems. The primary noise annoyance question is presented early in the questionnaire in the context of a list

of environmental disturbances. Interviewers are trained to ask all questions exactly as printed so that they do not bias the respondents' answers. Questions are stated in a simple, unbiased manner. And finally, the selection of respondents is based on sampling techniques which ensure that the sampled respondents represent the community as a whole.

Methodological studies of the annoyance measures have given further confidence that other characteristics of the surveys do not bias the results if the guidelines are followed (ref. 78). In general it has been found that answers are not affected by variations in the order of questions or the order in which the alternatives are presented. Studies have found that responses are not distorted by the length of the questionnaire or deliberate falsification on the part of the respondents. Other support for the validity of the annoyance measures comes from the fact that annoyance responses correlate with other variables in a meaningful manner (ref. 85) and are highly correlated with one another as well as with more objective measures such as activity interference, private behavior, and public complaint reports. Annoyance responses also correlate with noise exposures.

Whereas the available research indicates that annoyance responses obtained in surveys are valid, unbiased measures of annoyance, the responses to any single noise environment are highly variable and affected by the exact wording of questions. The reliability of annoyance indices consisting of several questionnaire items has generally met the standard, accepted social science reliability criterion (in terms of product moment correlation), $r \geq 0.80$, although there is still a great deal of variability. When the same individuals were asked about their unchanged noise environments at an interval of about 1 year (ref. 86) only about 35 percent of the variance in response ratings could be explained by their answer on the previous questionnaire. Since respondents in surveys in general must consolidate all their experiences and feelings about noise into a single response and must make a somewhat arbitrary choice between the words or numbers that the interviewer offers, the low level of reliability is not surprising.

Findings Related to Aircraft Noise Annoyance in the Community

Community aircraft noise annoyance is related to noise exposure and other environmental factors as well as to attitudes and other personal factors. The next sections examine results of selected aircraft noise surveys for information related to those factors that can affect community response.

Extent of Aircraft Noise Annoyance

Large numbers of people in nationally representative surveys have reported that they are annoyed by aircraft noise. In the United States an annual national housing survey found that about 8 percent of the population is bothered by aircraft noise in contrast to about 18 percent bothered by road traffic noise (ref. 87). Although aircraft noise was found to be the second most widely heard noise source in England (road traffic noise was the most widely heard source), it was rated as annoying less often than were the noises from children and animals (ref. 88).

It has been generally found in airport community surveys that individual annoyance and the percentage of people highly annoyed increase with increasing aircraft

noise exposure. Figure 23 presents the percentage of people highly annoyed (dichotomized according to the top 27 to 29 percent of an annoyance scale after ref. 81) in five European and one U.S. survey as related to their noise exposure in L_{dn} (ref. 3). Using these data and estimates made in 1974 (ref. 89) of the numbers of people living in urban areas of the United States exposed to various levels of aircraft noise, it can be estimated that between 3 million and 5 million people are highly annoyed by aircraft noise in urban areas of the United States alone.

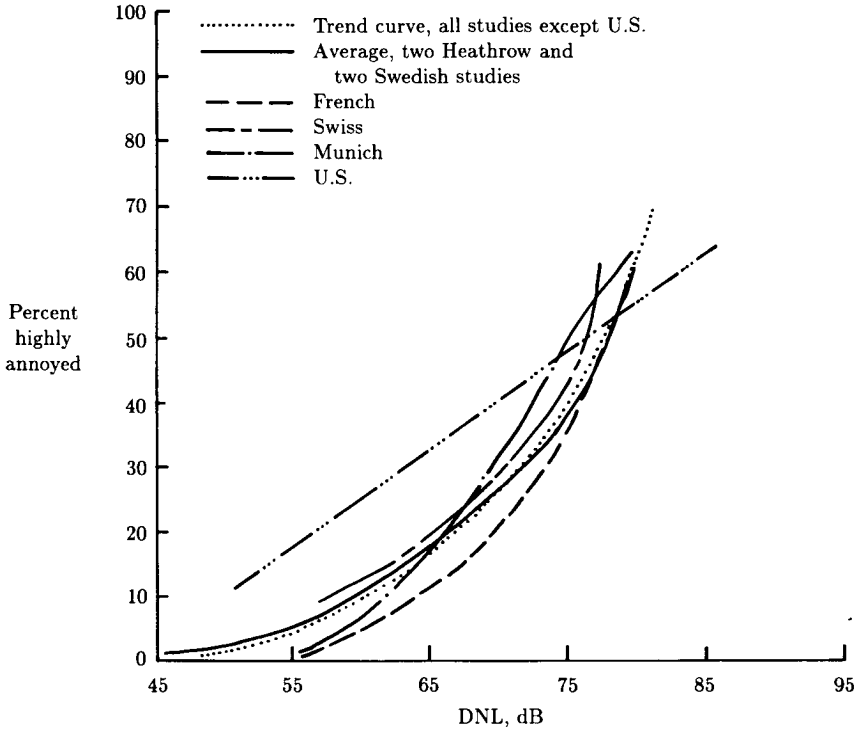

Figure 23. Percentage of respondents highly annoyed in several surveys. (From ref. 3.)

Acoustical and Situational Factors

Community aircraft noise annoyance has been found to be systematically related to noise exposure. The total noise exposure is made up of many single events which result from different aircraft types, occur at different times of day or night in combination with other noises, and vary in noise level, spectral content, and duration. Most information on spectral, duration, and aircraft-type effects has come from laboratory studies. The general findings are that duration affects annoyance and that an energy summation procedure such as used in EPNL or SEL is appropriate. The commonly used A-weighted scale appears to be as useful as the more complex metrics for rating aircraft noise in most environments.

The importance of the number of noise events relative to the noise level of the events has been a major issue in aircraft noise evaluation. The most common method

of describing the number effect is the "decibel equivalent" of a tenfold increase in the number of events (ref. 79). The 1961 Heathrow study (refs. 90 and 91) estimated the decibel equivalent to be either 24 $\log_{10} N$ or 15 $\log_{10} N$ depending on the type of analysis used. The 1967 Heathrow study (ref. 79) was specifically designed to estimate the number weighting and reported a value of 4. In a review and analysis of available survey data (ref. 92), it was concluded that the balance of evidence suggests that the number weighting is no more than, and is perhaps somewhat less than, the weighting of 10 $\log_{10} N$ which is implicit in equivalent energy indices such as LEQ.

It is generally assumed that the same noise levels cause more annoyance in residential areas if they occur during the evening or night than if they occur during the day, because more residents are at home and are engaged in more noise sensitive activities (TV viewing, conversation, etc.) and because the noise may be more intrusive given the lowered nighttime ambient noise level. It has been found that after adjusting for the difference in noise levels, people rate their nighttime and evening environments as more annoying than their daytime environments (ref. 93). On the other hand, the study of reference 94 found that people were not sensitive to a change in late-night noise exposure. In this study, conducted around the Los Angeles International Airport, people did not report a reduction in nighttime annoyance after an almost total elimination of nighttime (11:00 p.m. to 6:00 a.m.) flights over the study area. A review of surveys providing information on time-of-day effects (ref. 93) found that good numerical estimates of the relative importance of daytime, nighttime, or evening noises are not available and the results are highly variable. Some studies have reported that the nighttime weighted indices, such as DNL, are more closely related to annoyance than simple unweighted 24-hour indices, such as LEQ; other studies have reported the opposite. The lack of consistency of the survey results may be due in part to high correlation between the daytime and nighttime noise levels at individual airports. As a consequence, it may not be possible to adequately determine the most appropriate time-of-day weightings from conventional surveys.

The reactions of people to aircraft noise in the presence of ambient noise have been addressed with two alternative hypotheses. It is frequently hypothesized that annoyance to a specific noise would be greater when experienced along with a low ambient noise than when experienced along with a high ambient noise. It has also been hypothesized (ref. 95) that an intrusive sound may be more annoying in a high ambient noise because people can become sensitized in general to noise. Early attempts to investigate ambient noise effects in surveys were hampered by inadequate ambient noise level data (ref. 79) or unacceptably small numbers of study sites for each ambient noise category (ref. 96). Results were inconsistent for the magnitude or direction of an ambient noise effect. A large-scale survey (ref. 97) that was specifically designed to study ambient noise effects found that aircraft noise annoyance was not affected by the level of road traffic ambient noise. These findings along with the small ambient noise effects found in laboratory studies suggest that most normally occurring ranges of ambient noise do not strongly affect, if at all, community annoyance to aircraft noise.

Another issue concerning multiple noise sources that has been investigated using data from community noise surveys is the relationship between total noise annoyance and the levels of the individual noise sources. The analyses of reference 98, which

examined five alternative models for evaluating annoyance reactions in mixed noise environments, indicated that annoyance reactions were more accurately predicted by any of the more complex models than by the simple measurement of the LEQ of the total environment. Although it was not possible to identify the correct model with the analyses, the findings do suggest that it may ultimately be possible to identify a model for general community noise annoyance that is better than the equivalent energy models LEQ or DNL.

Findings on differences in annoyance between different classes of aircraft have often been contradictory. A study in Australia (ref. 99) found that annoyance around a military airfield was similar or less than that around civilian airports, whereas a study in the Netherlands (ref. 100) concluded that noise annoyance around military airfields was probably greater than around civilian airports at the same noise level. A West German survey (ref. 101) found general aviation noise to be more annoying than commercial aviation noise, but a Canadian survey (ref. 102) found that annoyance differentials varied between questions in ways that were related to differences between the acoustical environments at the general aviation and commercial airports.

Most aircraft noise surveys have been conducted in areas where the noise environments have been largely unchanged for several years. When a noise environment changes significantly over a short time span, however, reactions to the change might differ from the reactions predicted from the relationship between noise exposure and response obtained from the static data. One such example was the lack of change in general and sleep activity annoyance when nighttime operations were severely cutback over certain areas near Los Angeles International Airport (ref. 94). Although there was only a small change in total noise exposure as measured with the DNL index, thus explaining the lack of effect on general aircraft noise annoyance, the lack of effect on sleep-related annoyance is not easily explained. A study of reactions to temporary changes in noise levels around an airport in Burbank, California (ref. 103), found that reactions followed the changes in noise levels; 2 months after the change, reactions were similar to those predicted from the originally collected static data. Studies conducted 1 and 4 years after the opening of Charles de Gaulle Airport near Paris (ref. 104) were consistent with each other and with relationships observed earlier in a static noise situation around the Orly Airport also near Paris. These latter studies suggest that changes in noise exposure do lead to changes in annoyance which, at least after a period of time, would be predicted from static data.

A number of other environmental and situational factors have been hypothesized to affect airport community annoyance. Based on data from a number of surveys, it has been found that double glazing, locations of bedrooms, and other factors related to individualized noise exposure affect annoyance (ref. 78). However, good estimates are not available on the relative effect of a decibel of localized reduction (at the receiver) as opposed to the same reduction at the source. Many studies have found that there are unexplained differences between the reactions found in different study areas (ref. 105). These are sometimes assumed to be due to differences between reactions of people in different countries or different cities. The explanation of such differences is not known, and the possibility clearly exists that there are other important acoustical or situational factors which have not yet been investigated. Given the presence of correlated neighborhood characteristics, knowledge about the effects of these variables is not likely to be obtained except through large-scale, carefully designed surveys that include large numbers of fully described study areas.

Attitudinal and Personal Factors

The large variance in annoyance found in surveys which is not associated with noise exposure factors has led to a number of hypotheses about attitudinal and personal factors that may be associated with annoyance. References 82, 90, and 106 in particular discuss a wide range of variables and their effects on reported aircraft annoyance. The six most consistently reported attitudes that have been hypothesized to affect aircraft noise annoyance, when the actual noise exposure has been held constant or otherwise accounted for, are fearfulness, preventability, noise sensitivity, perceived neighborhood quality, health effects, and non-noise impact of the source.

Respondents who express fear that aircraft may crash in the neighborhood are generally more annoyed than those who express little or no fear of crashes (ref. 79). Similarly, respondents who believe that authorities could do something to reduce the aircraft noise exposure are also generally more annoyed than those who believe that authorities do all that is possible (ref. 107). Those respondents who report that they are sensitive to other noises or to noise in general have also been found to be more annoyed with aircraft noise (ref. 90). The level of sensitivity, however, has never been found to be related to their actual environmental noise level. Increased aircraft noise annoyance has also been found to be related to general negative evaluations of other neighborhood characteristics (ref. 108). The few people who believe that their health is affected by aircraft noise are also likely to be more annoyed by a given noise environment (ref. 90). Finally, people who are annoyed by other intrusive aspects of aircraft, such as lights and odors, are also generally more annoyed by the noise of aircraft (ref. 92).

It is sometimes argued that the above findings indicate that annoyance is caused by these attitudes (refs. 107 and 109). However, the difficulties in providing firm evidence for the nature of the causal relationships have led other investigators to state that although the variables are interrelated, conclusions cannot be drawn about the direction of causation (ref. 110).

Many studies have examined the standard demographic variables of age, sex, marital status, size of household, education level, social status, income, length of residence, type of dwelling, and type of tenure (own or rent). None of the variables, however, have consistently been found to be related to aircraft annoyance response.

Complaint Activity

Individual and group complaint activities, in the absence of social surveys, are indicators of noise impact which are likely to be used by public authorities. Whether or not such actions are good indicators of aircraft noise impact is open to discussion and is examined in the following sections.

Conditions That Affect Public Action

The first condition that affects the amount of public action is that there is a basic underlying dissatisfaction with the existing aircraft noise situation. The consistent relationship between aircraft annoyance and noise level means that there is dissatisfaction in virtually all high aircraft noise areas. The second condition is that there is an identifiable object or authority responsible for the control of

noise. The existence of a highly visible and centralized airport authority could help explain why airport noise has been the focus of more public attention relative to the total number of people impacted than has road traffic noise. The third condition is that the group or individual believes that action can lead to a change in the noise situation. Thus beliefs about preventability of aircraft noise could have even more impact on complaints than on annoyance (ref. 90). The fourth condition is that people must be aware of a means of contacting the appropriate authority; when the availability of a telephone complaint service is publicized, the number of complaints rises (ref. 111). The fifth condition required, for group action in particular, is that the social structure of the area and society as a whole facilitate public action. It is obvious that complaints and group actions are much more likely to occur in a democratic society than in a totalitarian society. A sixth condition that can increase the amount of action is a new focal point. The introduction of the Concorde supersonic transport into service at New York and Washington, D.C., in the mid-1970's is an example of a relatively small change in noise exposure causing a major public action.

Complaints as Noise Effect Indicators

Superficially, centrally collected reports of complaint activity have attractive characteristics for monitoring responses to aircraft noise. They are relatively economical to obtain and seem to indicate an important type of disturbance since the complainant must usually go to some trouble to make the complaint. No evidence was found in a survey around Heathrow that complainants have unusual psychological traits such as neuroticism (ref. 90). Although complainants were more annoyed than the average resident around Heathrow, there was no indication that they were a tiny hypersensitive minority; many more equally annoyed residents did not complain. In the Heathrow survey and in the major survey around U.S. airports (ref. 107), complainants were no more likely than the remainder of the population to be sensitive to other noise sources. In the U.S. airport survey, complaint activity was found to be related to the noise exposure but not as strongly as annoyance.

In spite of the fact that complaints seem to be genuine expressions of annoyance, the conclusion has been reached by many researchers (e.g., refs. 112 and 113) that complaint records are misleading indicators of the extent or causes of noise effects in populations. Complaint records seriously underestimate the extent of aircraft noise effects. In a survey around Heathrow, 62 percent of the population were annoyed by aircraft noise, 15 percent were very annoyed, but only 1 percent reported making a complaint (ref. 90).

Complainants differ from the rest of the impacted population in several respects. They are typically articulate and have greater confidence that they can deal with authorities. Consequently, unlike annoyance response, complaint action is affected by social class indicators such as occupation, education, income, and property value (refs. 90 and 107). Complaint activity, unlike annoyance, has also been found to be affected by the individual's attitude toward the noise source (ref. 107). It has also been frequently observed that more affluent neighborhoods complain more about aircraft noise.

Most complaint data are collected by various authorities for nonresearch purposes. The incidence of recorded complaints and how they are categorized,

tabulated, and reported could depend heavily on the agency recording the data. It has also been frequently noted that only a few individuals may be the source of a substantial proportion of the complaints. Thus, one might erroneously conclude that aircraft noise bothers only a few well-to-do people who are hostile toward aircraft and that noise impact varies widely in ways which are only loosely related to the aircraft noise exposure.

Noise Regulations, Criteria, and Recommended Practices

With the increasing awareness of the need to protect the overall environment in the late 1960's and early 1970's, there was increased concern with the community noise environment. The increasing popularity of commercial air transportation and the increasing numbers of large jet transports with high noise levels created adverse environmental conditions affecting an ever-increasing number of residents near commercial airports. As a result of the pressure exerted on the U.S. Congress and the governments of other countries, a number of legislative actions and resulting noise regulations were enacted to reduce or at least limit the growth of the community noise problem. A few of the major actions in the United States affecting aircraft noise in particular are discussed in the final sections of this chapter.

Aircraft Noise Certification

In 1969 the U.S. Federal Aviation Administration issued a noise certification regulation, Federal Air Regulation, Part 36 (ref. 22). This regulation, which is commonly referred to as "FAR 36," was issued with the objective of preventing the escalation of noise levels of civil turbojet and transport categories of aircraft. In order to be given a type certification for operation within the United States, new aircraft were required to be significantly quieter than the turbojet aircraft developed in the late 1950's and early 1960's.

In order to best reflect the annoyance response of people to aircraft noise, the metric selected for use in the noise certification procedure was the effective perceived noise level (EPNL), which considers frequency content, duration, and tone content in addition to overall sound pressure level. The tone corrections were considered particularly important to account for the strong tonal components of the new generation of turbofan engines. The new aircraft were required not to exceed prescribed noise levels at three locations: (1) 3.5 n.mi. (6500 m) from brake release on the runway centerline during takeoff, (2) 0.25 n.mi. (450 m) to the side of the runway centerline at the point of maximum noise level after lift-off during takeoff (later modified to 650 m if more than three engines), and (3) 1.0 n.mi. (2000 m) from touchdown during landing. The noise level limits varied as a function of gross weight of the aircraft as shown by the upper lines in figure 24. For both takeoff and landing, closely prescribed operational procedures had to be followed.

The basic FAR 36 standards have been modified over the years to account for improved technology and reduced noise levels for new generation aircraft (ref. 114). The additional lines in figure 24 represent the current noise limits for newly certified aircraft. The noise limit for a particular transport aircraft, turbojet or propeller, depends not only on the weight of the aircraft but also on the date of application for

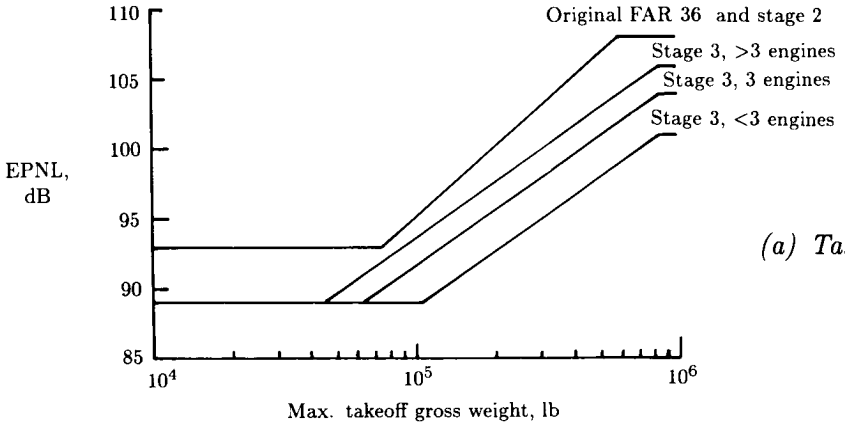

(a) Takeoff limits.

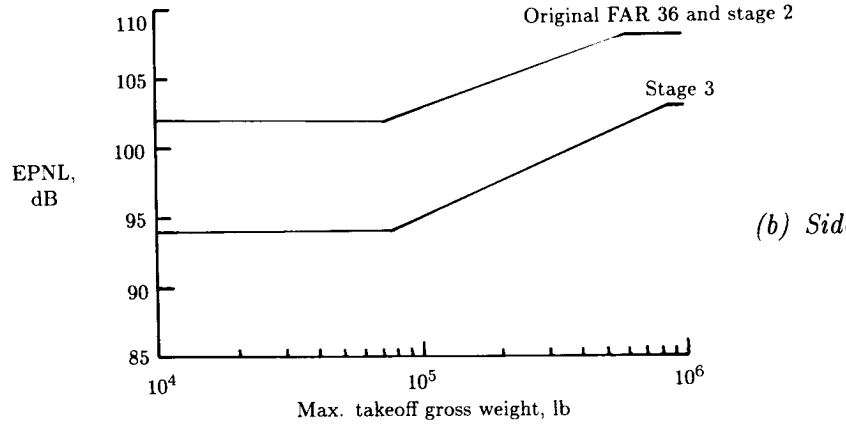

(b) Sideline limits.

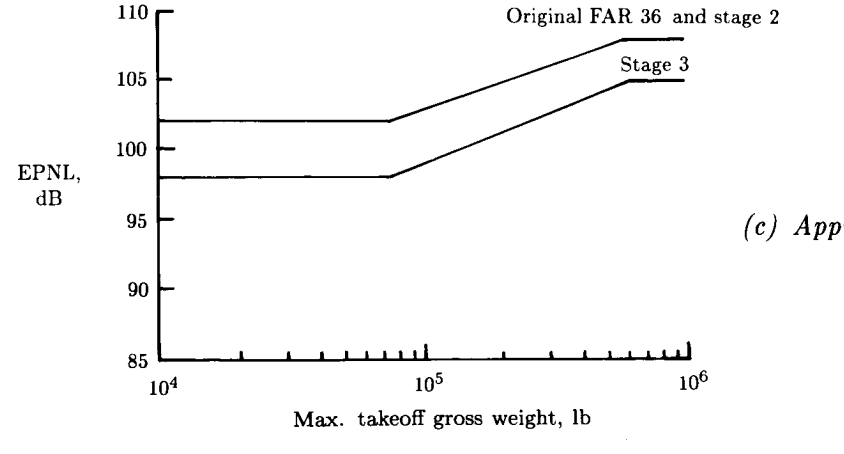

(c) Approach limits.

Figure 24. FAR 36 noise limits for transport aircraft.

type certification. If application was made prior to January 1, 1967 (stage 1), the aircraft must meet the stage 2 limits in figure 24 or be granted special exception. If application was made after January 1, 1967, but before November 5, 1975 (stage 2), the aircraft must meet the stage 2 limits without exception. If application is made on or after November 5, 1975 (stage 3), the aircraft must meet the stage 3 limits. Through the application of the stage 1 and stage 2 requirements, a number of older and noisier aircraft were forced out of service or had to be upgraded to meet the more stringent rules.

The FAR 36 regulation also covers propeller-driven small airplanes. For this type of aircraft a different noise metric, different operational procedures, and different noise limits are prescribed. These differences were prescribed to reduce the cost of certification for the smaller manufacturer and to reduce the noise for one of the most common and frequently annoying flight operations for small propeller airplanes, low-altitude flights around or near small airports with frequent touch-and-go landings. The metric prescribed for this type of airplane is the simple A-weighted sound level (SLA). The prescribed flight procedure is a constant-altitude flyover at 1000 ft (305 m) at highest normal operating power. The noise limits depend on the weight of the airplane as indicated in figure 25. If certification was applied for after January 1, 1975, the slightly lower maximum limit applies.

The International Civil Aviation Organization, to which most developed nations belong, also issues noise regulations, commonly called Annex 16 (ref. 115), which cover the aircraft categories covered by the FAR 36 and in addition, helicopters. The procedures and noise limits, with only minor exception, are the same as those in FAR 36. Thus, aircraft manufactured in and meeting certification requirements in any member nation can be operated in all member nations.

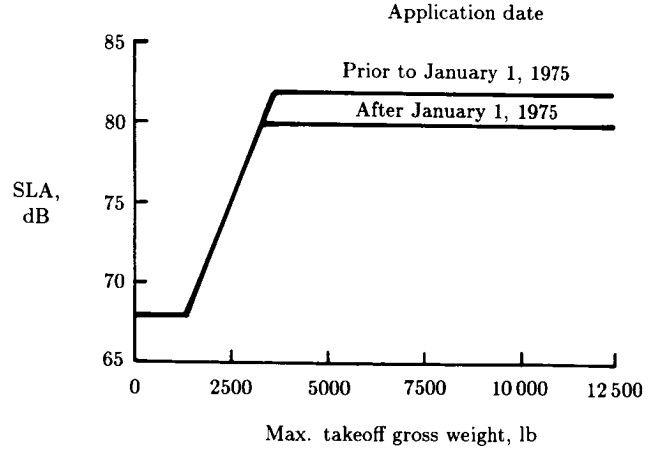

Figure 25. FAR 36 noise limits for small propeller-driven aircraft.

Community Noise Criteria

In the Noise Control Act of 1972 the U.S. Congress directed the Environmental Protection Agency (EPA) to "develop and publish criteria with respect to noise"

and "publish information on the levels of environmental noise the attainment and maintenance of which in defined areas under various conditions are requisite to protect the public health and welfare with an adequate margin of safety." To accomplish this goal, the EPA established an august working group of experts in all aspects of human response to noise, including noise-induced hearing loss, other health effects, and activity interference. As a result of this committee's actions and several review meetings, the EPA published what has come to be known as the "Levels Document" (ref. 116). In the document the A-weighted sound level SLA and the day-night average sound level DNL were recommended as a "simple, uniform and appropriate way" for describing the effects of environmental noise. The effects, levels, and appropriate areas for application of the criteria are given in table 1.

These levels are not to be construed as levels that should never be exceeded but rather as a total "dose," or exposure, summed over a period of time. In establishing the activity interference and annoyance criteria, a large amount of consideration was given to aircraft community noise. A summary figure of aircraft annoyance survey and community reaction results was presented which provides relationships between percentage of people highly annoyed, percentage of people who could be expected to

Table 1. Summary of Noise Levels Identified as Requisite To Protect Public Health and Welfare With an Adequate Margin of Safety

Effect	Level	Area
Hearing loss	$L_{eq(24)} \leq 70$ dB	All areas
Outdoor activity interference and annoyance	$L_{dn} \leq 55$ dB	Outdoors in residential areas and farms and other outdoor areas where people spend widely varying amounts of time and other places in which quiet is a basis for use
	$L_{eq(24)} \leq 55$ dB	Outdoor areas where people spend limited amounts of time, such as school yards, playgrounds, etc.
Indoor activity interference and annoyance	$L_{dn} \leq 45$ dB	Indoor residential areas
	$L_{eq(24)} \leq 45$ dB	Other indoor areas with human activities, such as schools, etc.

complain, the severity of community reaction, and noise level in DNL. This summary is given in figure 26. The recommended outdoor noise level of $L_{dn} \leq 55$ dB would thereby be expected to cause no adverse community reaction, would cause only a few complaints, but would still cause about 20 percent of the exposed population to be highly annoyed. The percentage of people highly annoyed in this figure, however, is

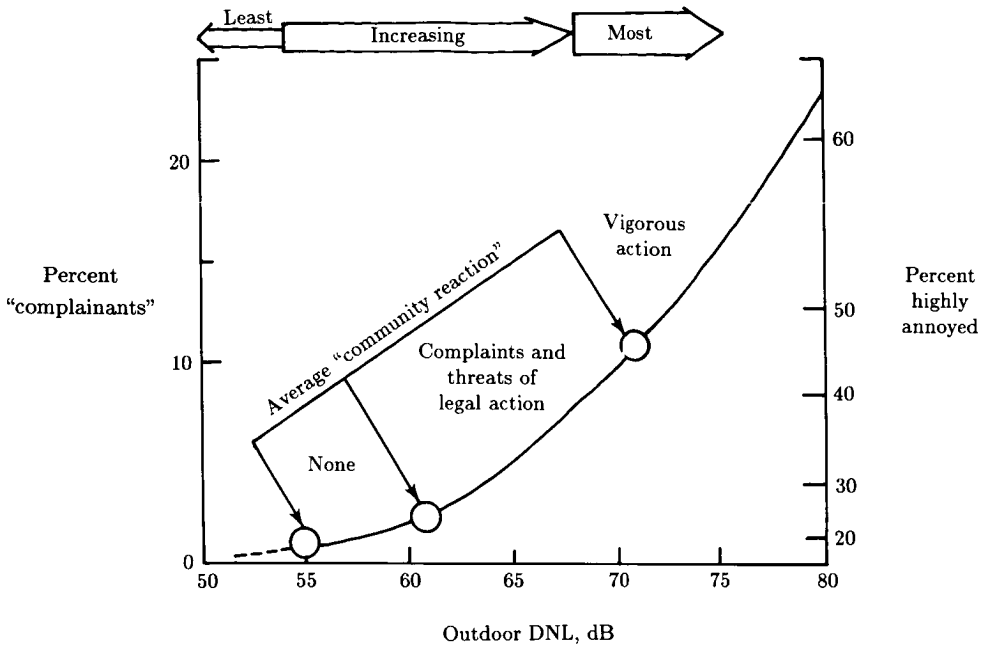

Figure 26. Summary of expected annoyance and community reactions as related to aircraft noise exposure. (From ref. 116.)

greater than the 5 to 10 percent reported in other attempts to summarize community reaction to aircraft noise (refs. 81 and 117).

Land Use Planning

To reduce the adverse impact of aircraft noise on the airport community, it is not always necessary that noise limits be placed on individual aircraft or that operational limits be placed on the air carriers. An equally effective measure is appropriate use of the land around the airport. In 1980 a U.S. Government interagency committee comprised of members from the Environmental Protection Agency, Department of Housing and Urban Development, Department of Defense, Veterans Administration, and Department of Transportation issued noise guidelines for land use planning and control (ref. 118). The stated purpose for land use planning is not to limit development but to encourage noise compatible development, guiding noise sensitive land uses away from the noise, and encouraging nonsensitive land uses where there is noise. The report provides the classification of seven noise zones with a wide range of noise exposure in terms of SLA, DNL, and NEF. Approximately 100 different land uses are then categorized for compatibility with the noise zones.

To obtain Federal financial aid for implementing a noise compatibility program, airports in the United States must comply with the Federal Aviation Regulation, Part 150 (ref. 119). This regulation prescribes the noise metric DNL for measuring the noise and determining the exposure of individuals to noise that results from operations at the airport and the land uses which are normally compatible with the noise exposure. The noise exposure is classified into 6 zones, which are the

same as the highest zones of the previously described land use guidelines, and 24 land uses are identified and categorized for compatibility with the exposure zones. The compatibility guidelines are essentially the same as those in the previously described general noise guidelines. The distinction between FAR Part 150 and the previously described general land use guidelines is that an airport must comply with Part 150 in applying for Federal aid for implementing a program which seeks to ensure land compatibility established by the guidelines. Thus, while FAR Part 150 does not directly force land use compatibility, it provides some insurance that airports uniformly assess their problems and that if a noise compatibility program is implemented, it is expected to make a measurable reduction in adverse human response.

References

1. Burns, William: *Noise and Man.* J B Lippincott Co., c.1973.
2. Kryter, Karl D.: *The Effects of Noise on Man.* Academic Press, Inc., 1970.
3. Kryter, Karl D.: *Physiological, Psychological, and Social Effects of Noise.* NASA RP-1115, 1984.
4. Gelfand, Stanley A.: *Hearing—An Introduction to Psychological and Physiological Acoustics.* Marcel Dekker, Inc., c.1981.
5. Fletcher, Harvey; and Munson, W. A.: Loudness, Its Definition, Measurement and Calculation. *J. Acoust. Soc. America,* vol. 5, no. 2, Oct. 1933, pp. 82–108.
6. Robinson, D. W.; and Whittle, L. S.: The Loudness of Octave-Bands of Noise. *Acustica,* vol. 14, no. 1, 1964, pp. 24–35.
7. Zwicker, Eberhard; and Scharf, Bertram: A Model of Loudness Summation. *Psychol. Rev.,* vol. 72, no. 1, 1965, pp. 3–26.
8. Zwislocki, J. J.: Temporal Summation of Loudness: An Analysis. *J. Acoust. Soc. America,* vol. 46, no. 2, pt. 2, Aug. 1969, pp. 431–441.
9. Morgan, Donald E.; and Dirks, Donald D.: Suprathreshold Loudness Adaptation. *J. Acoustic. Soc. America,* vol. 53, no. 6, June 1973, pp. 1560–1564.
10. Terhardt, Ernst: Pitch, Consonance, and Harmony. *J. Acoust. Soc. America,* vol. 55, no. 5, May 1974, pp. 1061–1069.
11. Plomp, R.: Detectability Threshold for Combination Tones. *J. Acoust. Soc. America,* vol. 37, no. 6, June 1965, pp. 1110–1123.
12. Patterson, R. D.: The Effects of Relative Phase and the Number of Components on Residue Pitch. *J. Acoust. Soc. America,* vol. 53, no. 6, June 1973, pp. 1565–1572.
13. Kryter, Karl D.: Scaling Human Reactions to the Sound From Aircraft. *J. Acoust. Soc. America,* vol. 31, no. 11, Nov. 1959, pp. 1415–1429.
14. Kryter, Karl D.; and Pearsons, Karl S.: Some Effects of Spectral Content and Duration on Perceived Noise Level. *J. Acoust. Soc. America,* vol. 35, no. 6, June 1963, pp. 866–883.
15. Stevens, S. S.; and Newman, E. B.: The Localization of Actual Sources of Sound. *American J. Psychol.,* vol. 48, 1936, pp. 297–306.
16. Gardner, Mark B.: Historical Background of the Haas and/or Precedence Effect. *J. Acoust. Soc. America,* vol. 43, no. 6, June 1968, pp. 1243–1248.
17. Pearsons, Karl S.; and Bennett, Ricarda L.: *Handbook of Noise Ratings.* NASA CR-2376, 1974.
18. Bennett, Ricarda L.; and Pearsons, Karl S.: *Handbook of Aircraft Noise Metrics.* NASA CR-3406, 1981.
19. Stevens, S. S.: Procedure for Calculating Loudness: Mark VI. *J. Acoust. Soc. America,* vol. 33, no. 11, Nov. 1961, pp. 1577–1585.
20. Zwicker, E.: A Comparison of Methods for Calculating the Loudness Level. *Acustica,* vol. 17, no. 5, 1966, pp. 278–284.
21. Stevens, S. S.: Perceived Level of Noise by Mark VII and Decibels (E). *J. Acoust. Soc. America,* vol. 51, no. 2, pt. 2, Feb. 1972, pp. 575–601.
22. Noise Standards: Aircraft Type Certification. *Fed. Regist.,* vol. 34, no. 221, Nov. 18, 1969, pp. 18364–18379.
23. French, N. R.; and Steinberg, J. C.: Factors Governing the Intelligibility of Speech Sounds. *J. Acoust. Soc. America,* vol. 19, no. 1, Jan. 1947, pp. 90–119.

24. Kryter, Karl D.: Methods for the Calculation and Use of the Articulation Index. *J. Acoust. Soc. America,* vol. 34, no. 11, Nov. 1962, pp. 1689–1697.
25. *American National Standard Methods for the Calculation of the Articulation Index.* ANSI S3.5-1969, American National Standards Inst., Inc., Jan. 16, 1969.
26. Houtgast, T.; and Steeneken, H. J. M.: A Review of the MTF Concept in Room Acoustics and Its Use for Estimating Speech Intelligibility in Auditoria. *J. Acoust. Soc. America,* vol. 77, no. 3, Mar. 1985, pp. 1069–1077.
27. Beranek, Leo L.; and Rudmose, H. Wayne: Sound Control in Airplanes. *J. Acoust. Soc. America,* vol. 19, no. 2, Mar. 1947, pp. 357–364.
28. *American National Standard for Rating Noise With Respect to Speech Interference.* ANSI S3.14-1977, Acoust. Soc. of America, 1977.
29. Clarke, Frank R.; and Kryter, Karl D.: *Perceived Noisiness Under Anechoic, Semi-Reverberant and Earphone Listening Conditions.* NASA CR-2108, 1972.
30. Powell, Clemans A.; and McCurdy, David A.: *Effects of Repetition Rate and Impulsiveness of Simulated Helicopter Rotor Noise on Annoyance.* NASA TP-1969, 1982.
31. Ollerhead, J. B.: *An Evaluation of Methods for Scaling Aircraft Noise Perception.* NASA CR-1883, 1971.
32. Borsky, Paul N.: *A New Field-Laboratory Methodology for Assessing Human Response to Noise.* NASA CR-2221, 1973.
33. Sternfeld, Harry, Jr.; Hinterkeuser, Ernest G.; Hackman, Roy B.; and Davis, Jerry: *A Study of the Effect of Flight Density and Background Noise on V/STOL Acceptability.* NASA CR-2197, 1974.
34. Rice, C. G.: Investigation of the Trade-Off Effects of Aircraft Noise and Number. *J. Sound & Vib.,* vol. 52, no. 3, June 8, 1977, pp. 325–344.
35. Hubbard, Harvey H.; and Powell, Clemans A.: *Acoustic Facilities for Human Factors Research at NASA Langley Research Center—Description and Operational Capabilities.* NASA TM-81975, 1981.
36. Stephens, David G.; and Clevenson, Sherman A.: The Measurement and Simulation of Vibration for Passenger Ride Quality Studies. *Proceedings of the Technical Program, NOISEXPO—National Noise and Vibration Control Conference,* c.1974, pp. 86–92.
37. Guilford, J. P.: *Psychometric Methods,* Second ed. McGraw-Hill Book Co., Inc., 1954.
38. Torgerson, Warren S: *Theory and Methods of Scaling.* John Wiley & Sons, Inc., 1958.
39. Mabry, J. E.; and Parry, H. J.: *An Evaluation of Psychoacoustic Procedures for Determining Human Response to Aircraft Noise. Volume II—Demonstrated Examples.* FAA-RD-72-51, II, Oct. 1973.
40. Lukas, Jerome S.: *Measures of Noise Level: Their Relative Accuracy in Predicting Objective and Subjective Responses to Noise During Sleep.* EPA-600/1-77-010, Feb. 1977.
41. MAN-Acoustics and Noise, Inc.: *Review of Studies Investigating Human Response to Commercial Aircraft Noise.* FAA-RD-75-182, Nov. 1975. (Available from DTIC as AD A022 356 0.)
42. Kryter, K. D.; Johnson, P. J.; and Young, J. R.: *Judgment Tests of Flyover Noise From Various Aircraft.* NASA CR-1635, 1970.
43. McCurdy, David A.; and Powell, Clemans A.: *Annoyance Caused by Propeller Airplane Flyover Noise.* NASA TP-2356, 1984.
44. Scharf, B.; Hellman, R.; and Bauer, J.: *Comparison of Various Methods for Predicting the Loudness and Acceptability of Noise.* EPA 550/9-77-101, Aug. 1977.
45. Pearsons, Karl S.: *The Effects of Duration and Background Noise Level on Perceived Noisiness.* FAA-ADS-78, Apr. 1966.
46. Parry, H. J.; and Parry, J. K.: The Interpretation and Meaning of Laboratory Determinations of the Effect of Duration on the Judged Acceptability of Noise. *J. Sound & Vib.,* vol. 20, no. 1, Jan. 8, 1972, pp. 51–57.
47. Robinson, D. W.: The Subjective Basis for Aircraft Noise Limitation. *J. Royal Aeronaut. Soc.,* vol. 71, no. 678, June 1967, pp. 396–400.
48. McCurdy, David A.; and Powell, Clemans A.: *Effects of Duration and Other Noise Characteristics on the Annoyance Caused by Aircraft Flyover Noise.* NASA TP-1386, 1979.
49. Shepherd, Kevin P.: *The Effect of the Duration of Jet Aircraft Flyover Sounds on Judged Annoyance.* NASA CR-159132, 1979.
50. Sullivan, B. M.; and Mabry, J. E.: *A Study of Noise Metric and Tone Correction Accuracy.* NASA CR-165910, 1982.
51. Kryter, K. D.; and Pearsons, K. S.: Judged Noisiness of a Band of Random Noise Containing an Audible Pure Tone. *J. Acoust. Soc. America,* vol. 38, no. 1, July 1965, pp. 106–112.

52. Little, John W.: Human Response to Jet Engine Noises. *Noise Control, Shock & Vibration,* vol. 7, no. 3, May–June 1961, pp. 11–13.
53. Pearsons, Karl S.; Horonjeff, Richard D.; and Bishop, Dwight E.: *The Noisiness of Tones Plus Noise.* NASA CR-1117, 1968.
54. Scharf, B.; and Hellman, R.: *Comparison of Various Methods for Predicting the Loudness and Acceptability of Noise. Part 2: Effects of Spectral Pattern and Tonal Components.* EPA-550/9-79-102, Nov. 1979. (Available from NTIS as PB82 138 702.)
55. Molino, John A.: *Should Helicopter Noise Be Measured Differently From Other Aircraft Noise? A Review of the Psychoacoustic Literature.* NASA CR-3609, 1982.
56. d'Ambra, F.; and Damongeot, A.: Annoyance of Helicopter Impulsive Noise. *Helicopter Acoustics,* NASA CP-2052, Part II, 1978, pp. 439–462.
57. Berry, B. F.; Fuller, H. C.; John, A. J.; and Robinson, D. W.: *The Rating of Helicopter Noise: Development of a Proposed Impulse Correction.* NPL Acoustics Rep. Ac 93, British A.R.C., Dec. 1979.
58. Powell, Clemans A.: *Subjective Field Study of Response to Impulsive Helicopter Noise.* NASA TP-1833, 1981.
59. Ollerhead, J. B.: *Laboratory Studies of Scales for Measuring Helicopter Noise.* NASA CR-3610, 1982.
60. Hubbard, Harvey H.; Maglieri, Domenic J.; and Stephens, David G.: *Sonic-Boom Research—Selected Bibliography With Annotation.* NASA TM-87685, 1986.
61. Shepherd, L. J.; and Sutherland, W. W.: *Relative Annoyance and Loudness Judgments of Various Simulated Sonic Boom Waveforms.* NASA CR-1192, 1968.
62. Johnson, D. R.; and Robinson, D. W.: Procedure for Calculating the Loudness of Sonic Bangs. *Acustica,* vol. 21, no. 6, 1969, pp. 307–318.
63. May, D. N.: The Loudness of Sonic Booms Heard Outdoors as Simple Functions of Overpressure and Rise Time. *J. Sound & Vib.,* vol. 18, no. 1, Sept. 8, 1971, pp. 31–43.
64. May, D. N.: Sonic Boom Startle: A Field Study in Meppen, West Germany. *J. Sound & Vib.,* vol. 24, no. 3, Oct. 8, 1972, pp. 337–347.
65. Niedzwiecki, A.; and Ribner, H. S.: Subjective Loudness of N-Wave Sonic Booms. *J. Acoust. Soc. America,* vol. 64, no. 6, Dec. 1978, pp. 1617–1621.
66. Zepler, E. E.; and Harel, J. R. P.: The Loudness of Sonic Booms and Other Impulsive Sounds. *J. Sound & Vib.,* vol. 2, no. 3, July 1965, pp. 249–256.
67. Powell, Clemans A.: *Annoyance Due to Multiple Airplane Noise Exposure.* NASA TP-1706, 1980.
68. Powell, Clemans A.: *Multiple-Event Airplane Noise Annoyance.* NASA TP-2101, 1983.
69. Pearsons, Karl S.: *The Effects of Duration and Background Noise Level on Perceived Noisiness.* FAA-ADS-78, Apr. 1966.
70. Powell, Clemans A.: *Effects of Road-Traffic Background Noise on Judgments of Individual Airplane Noises.* NASA TP-1433, 1979.
71. Johnston, G. W.; and Haasz, A. A.: Traffic Background Level and Signal Duration Effects on Aircraft Noise Judgment. *J. Sound & Vib.,* vol. 63, no. 4, Apr. 22, 1979, pp. 543–560.
72. Stephens, David G.: Review of Measured Vibration and Noise Environments Experienced by Passengers in Aircraft and in Ground Transportation Systems. *1975 Ride Quality Symposium,* NASA TM X-3295, DOT-TSC-OST-75-40, 1975, pp. 65–85.
73. Sternfeld, Harry, Jr.; and Doyle, Linda Bukowski: A Method for Determining Internal Noise Criteria Based on Practical Speech Communication Applied to Helicopters. *Helicopter Acoustics,* NASA CP-2052, Pt. II, 1978, pp. 493–511.
74. Pearsons, Karl S.; and Bennett, Ricarda L.: *Effects of Interior Aircraft Noise on Speech Intelligibility and Annoyance.* NASA CR-145203, 1977.
75. Leatherwood, Jack D.; and Barker, Linda M.: *A User-Oriented and Computerized Model for Estimating Vehicle Ride Quality.* NASA TP-2299, 1984.
76. Leatherwood, Jack D.; Clevenson, Sherman A.; and Hollenbaugh, Daniel D.: *Evaluation of Ride Quality Prediction Methods for Helicopter Interior Noise and Vibration Environments.* NASA TP-2261, AVSCOM TR 84-D-2, 1984.
77. Fields, James M.: *A Catalog of Social Surveys of Residents' Reactions to Environmental Noise, 1943–1980.* NASA TM-83187, 1981.
78. Fields, James M.; and Hall, Frederick L.: Community Effects of Noise. *Transportation Noise Reference Book,* P. M. Nelson, ed., Butterworth & Co. (Publ.) Ltd., 1987, Chapter 3.

79. MIL Research Ltd.: *Second Survey of Aircraft Noise Annoyance Around London (Heathrow) Airport. Second International Conference on the Reduction of Noise and Disturbance Caused by Civil Aircraft,* Her Majesty's Stationery Off. (London), 1967.
80. Grandjean, Etienne; Graf, Peter; Lauber, Anselm; Meier, Hans Peter; and Muller, Richard: A Survey of Aircraft Noise in Switzerland. *Proceedings of the International Congress on Noise as a Public Health Problem,* W. Dixon Ward, ed., EPA-550/9-73-008, May 1973, pp. 645–659.
81. Schultz, Theodore J.: Synthesis of Social Surveys on Noise Annoyance. *J. Acoust. Soc. America,* vol. 64, no. 2, Aug. 1978, pp. 377–405. (Erratum, vol. 65, no. 3, Mar. 1979, p. 849.)
82. Connor, William K.; and Patterson, Harrold P.: *Community Reaction to Aircraft Noise Around Smaller City Airports.* NASA CR-2104, 1972.
83. Fields, James M.: A Program To Support the Full Utilization of Data From Existing Social Surveys of Environmental Noise. *Noise Control for the 80's, Proceedings—Inter-Noise 80,* George C. Mailing, Jr., ed., Volume II, Noise Control Foundation, c.1980, pp. 937–940.
84. Rossi, Peter Henry; Wright, James D.; and Anderson, Andy B.: *Handbook of Survey Research.* Academic Press, Inc., c.1983.
85. McKennell, A. C.: Methodological Problems in Survey of Aircraft Noise Annoyance. *Statistician,* vol. 19, no. 1, 1969, pp. 1–19.
86. Hall, Fred L.; and Taylor, S. Martin: Reliability of Social Survey Data on Noise Effects. *J. Acoust. Soc. America,* vol. 72, no. 4, Oct. 1982, pp. 1212–1221.
87. *Annual Housing Survey: 1977—Financial Characteristics by Indicators of Housing and Neighborhood Quality.* Current Housing Rep. Ser. H-150-77, Part F, U.S. Dep. of Commerce, June 1979.
88. Morton-Williams, Jean; Hedges, Barry; and Fernando, Evelyn: *Road Traffic and the Environment.* Social & Community Planning Research (London), c.1978.
89. Galloway, W. J.; Eldred, K. McK.; and Simpson, M. A.: *Population Distribution of the United States as a Function of Outdoor Noise Level.* EPA-550/9-74-009, June 1974. (Available from NTIS as PB 235 022.)
90. McKennell, A. C.: *Aircraft Noise Annoyance Around London (Heathrow) Airport.* S.S. 337, Central Off. of Information (British), Apr. 1963.
91. Committee on the Problem of Noise: *Noise—Final Report.* Her Majesty's Stationery Off. (London), Reprinted 1976.
92. Fields, James M.: The Effect of Numbers of Noise Events on People's Reactions to Noise: An Analysis of Existing Survey Data. *J. Acoust. Soc. America,* vol. 75, no. 2, Feb. 1984, pp. 447–467.
93. Fidell, S.; and Jones, G.: Effects of Cessation of Late-Night Flights on an Airport Community. *J. Sound & Vib.,* vol. 42, no. 4, Oct. 22, 1975, pp. 411–427.
94. Fields, James M.: *The Relative Effect of Noise at Different Times of Day—An Analysis of Existing Survey Data.* NASA CR-3965, 1986.
95. Schultz, Theodore J.: Social Surveys on Noise Annoyance—Further Considerations. *Proceedings of the Third International Congress on Noise as a Public Health Problem,* Jerry V. Tobias, Gerd Jansen, and W. Dixon Ward, eds., ASHA Rep. 10, American Speech-Language-Hearing Assoc., Apr. 1980, pp. 529–540.
96. Bottom, C. G.: A Social Survey Into Annoyance Caused by the Interaction of Aircraft Noise and Traffic Noise. *J. Sound & Vib.,* vol. 19, no. 4, Dec. 22, 1971, pp. 473–476.
97. Taylor, S. M.; Hall, F. L.; and Birnie, S. E.: Effect of Background Levels on Community Responses to Aircraft Noise. *J. Sound & Vib.,* vol. 71, no. 2, July 22, 1980, pp. 261–270.
98. Taylor, S. M.: A Comparison of Models To Predict Annoyance Reactions to Noise From Mixed Sources. *J. Sound & Vib.,* vol. 81, no. 1, Mar. 8, 1982, pp. 123–138.
99. Hede, A. J.; and Bullen, R. B.: *Aircraft Noise in Australia: A Survey of Community Reaction.* N.A.L. Rep. No. 88, Commonwealth Dep. of Health (Australia), 1982.
100. De Jong, Ronald G.: Community Response Surveys and the Dutch Noise Abatement. *Practice of Noise Control Engineering, Proceedings—Inter-Noise 81,* V. M. A. Peutz and A. de Bruijn, eds., Volume 2, Noise Control Foundation, c.1981, pp. 787–792.
101. Rohrmann, Bernd: Community Reaction on Non-Commercial and Sporting Aviation. *Inter-Noise 76—Proceedings,* Roger L. Kerlin, ed., Inst. of Noise Control Engineering, c.1976, pp. 427–430.
102. Taylor, S. M.; Hall, F. L.; and Birnie, S. E.: A Comparison of Community Response to Aircraft Noise at Toronto International and Oshawa Municipal Airports. *J. Sound & Vib.,* vol. 77, no. 2, July 22, 1981, pp. 233–244.

103. Fidell, S.; Horonjeff, R.; Teffeteller, S.; and Pearsons, K.: *Community Sensitivity to Changes in Aircraft Noise Exposure.* NASA CR-3490, 1981.
104. Francois, Jacques (SCITRAN, transl.): *Effect of Aircraft Noise on the Equilibrium of Aircraft Residents: Longitudinal Study Around Roissy—Phase III.* NASA TM-75906, 1981.
105. Fields, James M.: Variability in Individuals' Responses to Noise: Community Differences. *Noise Control: The International Scene, Proceedings—Inter-Noise 83,* Volume II, Inst. of Acoustics (Edinburgh, U.K.), c.1983, pp. 965–968.
106. Rohrmann, B.; Finke, H.-O.; Guski, R.; Schuemer, R.; and Schuemer-Kohrs, A.: *Aircraft Noise and Its Effect on Man: Methods and Results of Research, Consequences for Environmental Protection.* Verlag Hans Huber (Berne, Switzerland), 1978.
107. TRACOR, Inc.: *Community Reaction to Airport Noise,*
Volume I. NASA CR-1761, 1971.
Volume II. NASA CR-111316, 1970.
108. Fields, James M.; and Powell, Clemans A.: *A Community Survey of Helicopter Noise Annoyance Conducted Under Controlled Noise Exposure Conditions.* NASA TM-86400, 1985.
109. Leonard, Skipton; and Borsky, Paul N.: A Causal Model for Relating Noise Exposure, Psychosocial Variables and Aircraft Noise Annoyance. *Proceedings of the International Congress on Noise as a Public Health Problem,* W. Dixon Ward, ed., EPA-550/9-73-008, May 1973, pp. 691–705.
110. Alexandre, A.: An Assessment of Certain Causal Models Used in Surveys on Aircraft Noise Annoyance. *J. Sound & Vib.,* vol. 44, no. 1, Jan. 8, 1976, pp. 119–125.
111. Guski, Rainer: An Analysis of Spontaneous Noise Complaints. *Environ. Res.,* vol. 13, 1977, pp. 229–236.
112. Lindvall, Thomas; and Radford, Edward P., eds.: Measurement of Annoyance Due to Exposure to Environmental Factors—The Fourth Karolinska Institute Symposium on Environmental Health. *Environ. Res.,* vol. 6, 1973, pp. 1–36.
113. Borsky, Paul N.: Review of Community Response to Noise. *Noise as a Public Health Problem,* Jerry V. Tobias, Gerd Jansen, and W. Dixon Ward, eds., ASHA Rep. 10, American Speech-Language-Hearing Assoc., Apr. 1980, pp. 453–474.
114. Noise Standards: Aircraft Type and Airworthiness Certification. FAR Pt. 36, Federal Aviation Admin., June 1974. (Consolidated Reprint Aug. 12, 1985.)
115. *Annex 16—Environmental Protection.* International Civil Aviation Organization, Oct. 1981.
116. *Information on Levels of Environmental Noise Requisite To Protect Public Health and Welfare With an Adequate Margin of Safety.* EPA-550/9-74-004, Mar. 1974. (Available from NTIS as PB 239 429.)
117. Kryter, Karl D.: Community Annoyance From Aircraft and Ground Vehicle Noise. *J. Acoust. Soc. America,* vol. 72, no. 4, Oct. 1982, pp. 1222–1242.
118. *Guidelines for Considering Noise in Land Use Planning and Control.* Federal Interagency Committee on Urban Noise, June 1980.
119. Airport Noise Compatibility Planning. FAR Pt. 150, Federal Aviation Admin., Jan. 1985.

12 Atmospheric Propagation

Lead authors

Tony F. W. Embleton
National Research Council
Ottawa, Ontario, Canada

Gilles A. Daigle
National Research Council
Ottawa, Ontario, Canada

Introduction

How sound propagates from a source to a receiver outdoors is a complicated problem because there are several wave propagation and meteorological mechanisms that can affect the result. The shape and type of ground surface also play a part. The received signal is influenced by each mechanism in a different way and to an extent that depends on range, source and receiver heights, and sound frequency.

The study of sound propagation in the atmosphere has a long and interesting history (refs. 1 and 2). As early as 1636, Mersenne (1588–1648) measured the speed of sound by timing the interval between the flash and sound of a gun blast. He obtained a value of 230 toises per second, equivalent to about 448 m/sec. A contemporary, Gassendi (1592–1655) noted that the speed of sound was independent of its intensity, since the speed was the same whether the sound was made by a large weapon, such as a cannon, or a smaller one, such as a musket. Derham in 1708 concluded that favorable winds speeded sound propagation while adverse winds retarded it: he did not measure temperature but concluded that the speed of sound was the same in summer as in winter. In 1740, Bianconi in Bologna showed that the speed of sound definitely increased with increasing air temperature. The first precise measurements of the speed of sound were probably those made in 1738 under the direction of the Academy of Paris. When corrected to 0°C, the value obtained was 332 m/sec—within about 0.3 percent of the best modern value—and it was obtained two and a half centuries ago.

From about 1860 onward, there was considerable interest in fog signaling for ships—Joseph Henry in the United States and Tyndall in Britain investigated what we would today call absorption or scattering by water vapor. Stokes at that time in a private letter to Tyndall wrote that scattering was more likely caused by temperature differences in the air. Knowledge of sound propagation in the atmosphere has usually developed in response to the needs of practical problems. During the first World War there was the problem of locating artillery; in the 1930's, the need to understand the loss of brilliance of music in concert halls; in the 1960's, the concern over noise produced by many forms of new technology—intense like commercial jet aircraft or widespread like powered lawn mowers and air conditioning. Since then the increasing

numbers of noise sources, and often their greater intensity, have increased the social and political pressures on acousticians to yet again advance their knowledge of sound propagation outdoors. Significant progress has been made in recent years (refs. 3 and 4).

This chapter reviews the current state of knowledge of each basic mechanism and how each changes the spectral or temporal characteristics of the sound received at a distance from the source. An understanding of these mechanisms is important since some affect even short-range measurements, when one is often attempting to characterize the source. Long-range measurements or predictions, such as when one is attempting to predict the influence of a source on a neighboring community or to detect the source at the greatest possible range, are affected in different ways and by other mechanisms.

Some of the basic processes affecting sound wave propagation are present in any situation. These are

1. Geometrical spreading—Sound levels decrease with increasing distance from the source; there is no frequency dependence.
2. Molecular absorption—Sound energy is converted into heat as the sound wave propagates through the air; there is a strong dependence on frequency.
3. Turbulent scattering—Local variations in wind velocity and temperature induce fluctuations in phase and amplitude of the sound waves as they propagate through an inhomogeneous medium; there is a moderate dependence on frequency.

Other phenomena occur only because of the presence of the ground and are usually most significant near the ground. These phenomena and the features that cause them are

1. Reflection at the ground surface—The sound field reflected at the ground interferes with the direct sound field; interference is a repetitive function of frequency; height of source and receiver, their distance apart, and the type of ground surface are important parameters.
2. Type of ground surface—Surfaces have a finite and complex acoustic impedance that results in a phase change on reflection of a sound field and a reflection coefficient that is a function of angle of incidence; this in turn leads to the existence of a ground wave in addition to a plane reflected wave and under some circumstances, to a trapped surface wave.
3. Shape of ground surface—Concave ground surfaces can result in multiple ray paths between source and receiver and hence increased sound levels; convex ground surfaces such as berms or low hills can act as sound barriers and lead to an acoustical shadow that is penetrated by diffracted and scattered waves.
4. Near-surface micrometeorology—The ground surface heats (usually daytime) or cools (nighttime) relative to the atmosphere leading to vertical gradients in temperature; viscous drag of the surface on wind produces similar vertical gradients in wind speed; as a result, sound fields are refracted upward (warmer ground or upwind) or downward (cooler ground or downwind).

Finally, these phenomena depend for the most part on different parameters, and so each can be strong or weak depending on the particular circumstances. Furthermore the phenomena coexist, and a given sound field may be influenced by different

mechanisms at different frequencies, at different heights, or at different distances. These coexisting mechanisms sometimes reinforce, and sometimes nullify, each other.

Geometrical Spreading

Some energy spreads out as it propagates away from its source. At distances that are large compared with the effective size of the sound source, the sound wave fronts spread spherically in three dimensions provided that the atmosphere is isotropic. Note that sound does not necessarily radiate equally in all directions as it would from a true point source. However, if the point source approximation is applicable, the sound level decreases at the rate of 6 dB per doubling of distance. This situation exists once the directionality pattern of the source does not change as a function of distance. For coherent sources (those for which unique phase relationships exist between all the radiating elements), the Fresnel region near the source extends to a distance somewhat greater than the square of the source diameter, or square of its length, divided by the wavelength of the sound. Within this near-field region there is interference between coherent elements of the source and there are no simple relations between sound levels and position.

One should take care in defining the effective size of the source. For example, noise from an axial flow compressor is generated by flow past individual blades, but the pure-tone components of this noise are generated coherently by the complete annular ring of blades and are radiated from the inlet duct of the compressor (in some engines also from the fan outlet). The effective size of the source is the diameter of the inlet duct (or the distance between the inlet orifice and the fan outlet). When the noise source is a turbulent jet, the effective size of the source can be the whole mixing region, which is much larger than any dimension of the mechanical hardware.

The 6-dB decrease per doubling of distance relationship applies either to the instantaneous sound pressure level (or time-averaged sound level of a stationary source) or to the maximum sound pressure level reached during a passby of a moving source.

One must be careful to distinguish these from certain measures of total sound exposure received from a moving source during a passby event. Such measures as single event noise exposure level (SENEL) represent the total value of sound pressure squared when integrated throughout the passby event. In these cases, although the maximum sound pressure level decreases by 6 dB per doubling of the closest distance of approach, the length of time during which the sound pressure level is within a given difference from the maximum value also doubles, and the net result for any such time-and-intensity measures is that the level decreases at the rate of 3 dB per doubling of distance from the source. Three decibels per doubling of distance also represents cylindrical spreading of sound energy propagating away from a line source. Such a sound is that from the traffic flow along a busy road, where the individual vehicles are a line of discrete point sources each radiating sound incoherently with respect to the others.

The phenomenon of geometrical spreading, and the corresponding decrease in sound level with increasing distance from the source, is the same for all acoustic frequencies or wavelengths. Certain parameters of the atmosphere directly affect sound levels calculated from geometrical spreading, but these effects are very small and rarely, if ever, detectable. For example, gross changes in temperature (not to be

confused with transverse temperature gradients that produce refraction) change the speed of sound and hence the sound energy density and measured sound pressure levels. The sound level measured at the ground (temperature of 20°C) directly below an aircraft flying at an altitude where the temperature is −40°C is 0.5 dB less because of this 60°C temperature change than it would be if there were no temperature change. In addition, if the relative humidity was 100 percent, the sound pressure level at the ground would be decreased by a further 0.2 dB because of air density changes alone.

Molecular Absorption

In contrast to geometrical spreading, the absorption of sound energy by the atmosphere is a significant function of frequency, temperature, pressure, and humidity. Studies of molecular absorption have a history going back to the 19th century and continue even today. In this section we summarize the basic mechanisms by which acoustic energy is absorbed by the atmosphere, we discuss the current ANSI Standard for calculating atmospheric absorption (ref. 5), and finally we mention current research to improve the accuracy of the calculations.

The absorption of acoustic energy by a mixture of gases occurs through two basic physical mechanisms (ref. 6). The first involves the direct transfer of acoustic energy (ordered motion) into heat energy (random motion) through processes involving viscous effects and heat conduction. These two loss processes have been known since the 19th century and are known today as classical absorption. The second basic physical mechanism of absorption is molecular relaxation. The compressional energy of the acoustic wave is redistributed into rotational and vibrational modes of the molecules through binary collisions. The time lag associated with this transfer leads to absorption of sound energy, with maximum absorption (per wavelength) being reached at the relaxation frequency. For frequencies below 10 MHz, absorptions due to classical losses and molecular relaxation are additive. Current theory assumes that the total molecular absorption of acoustic energy by the atmosphere is the sum of four terms:

$$\alpha = \alpha_{cl} + \alpha_{rot} + \alpha_O + \alpha_N \tag{1}$$

where α_{cl} is the classical absorption, α_{rot} the absorption due to rotational relaxation, and α_O and α_N are, respectively, the absorption due to vibrational relaxations of oxygen and nitrogen.

The classical absorption is a function of temperature, pressure, and frequency. It is the dominant absorption mechanism for acoustic energy at high frequencies. The absorption due to rotational relaxation is also a function of temperature, pressure, and frequency. Furthermore, the rotational relaxation frequency in the atmosphere is well above 10 MHz. This permits the rotational absorption constant to be combined with the classical absorption constant into one expression for practical purposes. The combined expression yields the curve labeled "α_{cl+rot}" in figure 1. These two absorptions provide the dominant losses at frequencies above approximately 30 kHz.

Historically, classical absorption and rotational relaxation were by themselves unable to account for the loss of brilliance long observed in concert halls in the frequency range above about 2 kHz. In response to this, theory was developed in the early 1930's which included the contribution of the vibrational relaxation of oxygen.

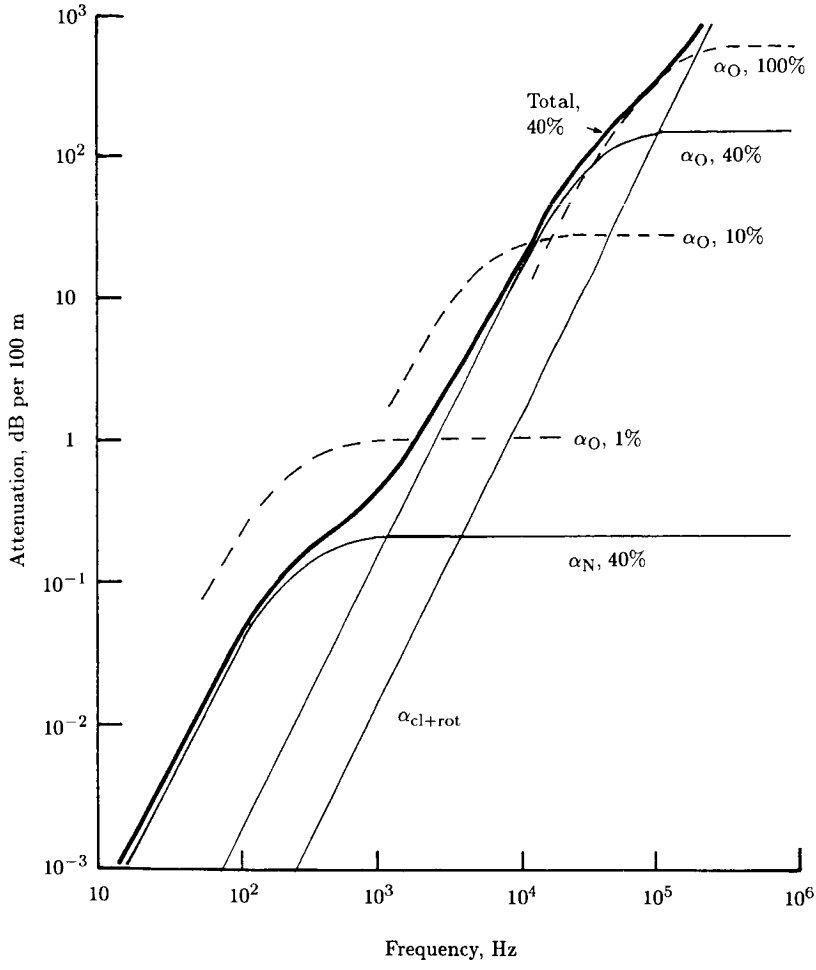

Figure 1. Decrease in sound pressure level with distance as a function of frequency due to four molecular processes in equation (1). Temperature, 20° C; pressure, 1 atm; relative humidity indicated in percent.

In addition to frequency, temperature, and pressure, the vibrational relaxation absorption depends strongly on the concentration of water vapor. Collisions with water vapor molecules speed the energy transfer process and hence influence the frequency of maximum absorption. The dashed curves labeled "α_O" in figure 1 indicate how the relaxation frequency, and hence the absorption due to the oxygen relaxation, changes at 20°C when the relative humidity increases from 1 to 100 percent. At normal temperatures and relative humidities, the oxygen relaxation provides maximum absorption at frequencies above about 2 kHz.

In the 1960's and early 1970's, increasing activity was devoted to predicting environmental noise in urban areas for community planning, including the control of aircraft noise. Measurements began to show deviations from the theory for molecular absorption at low frequencies, where most of the sound energy of environmental noise

is found. Initially empirical procedures (ref. 7) were developed to account for the discrepancies below 2 kHz. Later it was realized that the vibrational relaxation of nitrogen is the main absorption mechanism at low frequencies. The contribution to absorption of the nitrogen relaxation is illustrated by the curve labeled "α_N" in figure 1.

The total molecular absorption due to the four contributions in equation (1) is shown by the curve labeled "Total" in figure 1. The absorption is predicted for a pressure of 1 atm, temperature of 20°C, and relative humidity of 40 percent and is expressed in decibels per 100 m. For example, the total absorption under these conditions is about 1 dB/100 m at 2 kHz. A set of fairly simple equations for practical calculations of the four terms in equation (1) form the basis of an ANSI standard (1978) for atmospheric absorption (ref. 5). The scientific support and experimental evidence for this standard are found in reference 6. The accuracy of the atmospheric absorption calculated from this standard (ref. 5) is approximately 10 percent for temperature from 0° to 40°C, relative humidity from 10 to 100 percent, frequency from 50 Hz to 10 MHz, and atmospheric pressure less than 2 atm. The calculations can have an accuracy of 5 percent over a more limited range of variables within the ones quoted above. On the other hand, outside this quoted range, for example, at low frequencies and low humidities, the accuracy of the calculation is usually worse than 10 percent. There is still a need for more fundamental work, especially at the more extreme conditions, to increase the understanding of these processes. Some recent work (ref. 8) aimed at extending the measurements at low frequencies has revealed discrepancies in the accepted relaxation frequencies of oxygen. It is expected that this and other new knowledge will result in a revision of the current ANSI standard (1978).

Effects Due to the Presence of the Ground

In this section, we consider only the direct effects on sound propagation caused by the ground. These effects are additional to those of geometrical spreading and molecular absorption already discussed. We postpone until later any discussion of near-surface micrometeorological effects such as those caused by heating or cooling. Propagation effects caused by the ground are most significant within a few wavelengths, that is, only a few meters above the ground surface. Furthermore, the ground has a greater effect on sound waves traveling essentially horizontally just above the ground than it does on sound waves impinging from nearly vertical directions.

When the sound source and receiver are above a large flat ground, sound reaches the receiver via two paths: directly from the source to the receiver, the direct field, and after being reflected from the ground surface between the source and receiver, the reflected field (fig. 2). Most ground surfaces are porous to some degree and therefore their acoustic impedance is complex. In simple terms, one may think of a resistive component of impedance that describes the losses of sound energy due to thermal and viscous effects in the interstices of the ground material; there is also a reactive component due to flow into and out of the porous ground in response to the alternating acoustic pressure in the air just above the surface that results in compression either of gas in the interstices or of the solid itself. The complex acoustic impedance of the ground is associated with a complex reflection coefficient

that is rarely as large as unity and is a function of angle of incidence. The sound field reflected from the surface therefore suffers (1) a reduction in amplitude and (2) a phase change between zero and π radians (0° to 180°). There is another more subtle, but very important, effect on the sound field: if the incident waves are plane, the reflected waves are also plane because all parts arrive with the same angle of incidence; but if the incident field is of some other shape (e.g., spherical), then different parts of the wave front meet the plane surface with different angles of incidence and are subjected to reflection coefficients that differ in magnitude and phase. Thus the reflected field has a different shape; for example, a spherical field no longer appears to come from a point source below the surface. Instead the source region becomes blurred and theoretically stretches to infinity.

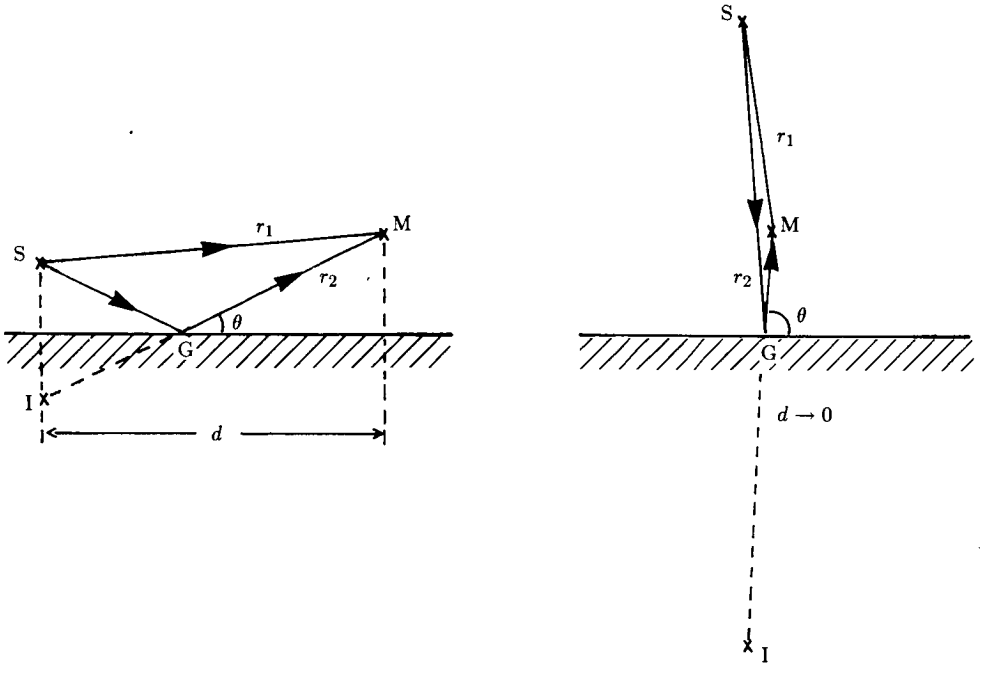

(a) Source near the ground. *(b) Source nearly overhead.*

Figure 2. Schematic of the direct sound field by the ray path SM and that reflected at the ground surface by the path SGM. (I is the location of the geometric image of the source in the ground.)

Plane Waves

The reflection coefficient R_p for plane waves incident on a plane surface is given in its simplest form by

$$R_p = \frac{\sin\theta - Z_1/Z_2}{\sin\theta + Z_1/Z_2} \tag{2}$$

where θ is the angle of incidence (fig. 2) and Z_1/Z_2 is the ratio of the characteristic impedance of air at ground level to the specific normal acoustic impedance of the

ground surface. The impedance Z_2 is complex. This simple form of the equation for the complex reflection coefficient R_p is for a ground surface of local reaction, that is, a surface whose reflection coefficient at any point is not significantly affected by the sound field incident at neighboring points. If the ground can support a significant amount of wave propagation, either in the solid material or in the air of the pores, then the expression for the reflection coefficient becomes more complicated, but its properties remain almost the same. In practice the impedance Z_2 must always remain finite, even though it is very large for hard surfaces such as concrete, so that for θ small enough to make $\sin\theta << |Z_1/Z_2|$, R_p always approaches -1 at grazing incidence. Figure 3 shows the magnitude $|R_p|$ and phase change ϕ of the complex reflection coefficient $R_p = |R_p|e^{i\phi}$ for plane waves incident on a typical grass-covered surface such as an airport or field. Only at grazing incidence does the magnitude of the reflection coefficient reach unity, and this is accompanied by a phase change on reflection of π radians (180°). For most angles of incidence that are not close to grazing, the magnitude of the reflection coefficient is between 0.5 and 1.0, and the phase change on reflection of the sound waves is less than about $\pi/4$ radians (45°) and can often be ignored. The general features shown in figure 3 apply for all ground surfaces although the angle of incidence scale (abscissa) and the magnitude of the reflection coefficient scale (ordinate) change depending on the acoustic impedance of the ground surface. For example, the magnitude of the reflection coefficient $|R_p|$ always has a minimum when its phase change is $\pi/2$ radians (90°). The angle of incidence for which this occurs becomes more nearly grazing as the acoustic impedance of the ground increases, for surfaces like concrete, asphalt, or packed earth, and becomes more oblique as impedance decreases, for softer ground surfaces like snow or the ground in a forest.

Ground and Surface Waves

Because the magnitude and phase of the reflection coefficient R_p vary with angle of incidence, as shown in figure 3, the total sound field near the ground cannot usually be described mathematically by the simple addition of two terms, the incident sound field and the reflected sound field multiplied by the plane-wave reflection coefficient of equation (2). An additional term is required that allows, in effect, for the fact that each curve in figure 3 is not a horizontal straight line. A more complete expression for the sound pressure p, borrowed from electromagnetic theory and known as the Weyl–Van der Pol solution is

$$\frac{p}{p_o} = \frac{e^{ikr_1}}{kr_1} + R_p\frac{e^{ikr_2}}{kr_2} + (1 - R_p)F\frac{e^{ikr_2}}{kr_2} \tag{3}$$

In equation (3), p_o is a constant, k is the wave number of the sound field (the number of wavelengths in a length of 2π meters), r_1 and r_2 are the ray paths in figure 2, and F is a complex amplitude function (ref. 9) that allows for the curvature of the incident sound field and, under some circumstances, the possible existence of a surface wave. Mathematically F is related to the complex error function of a parameter w, known

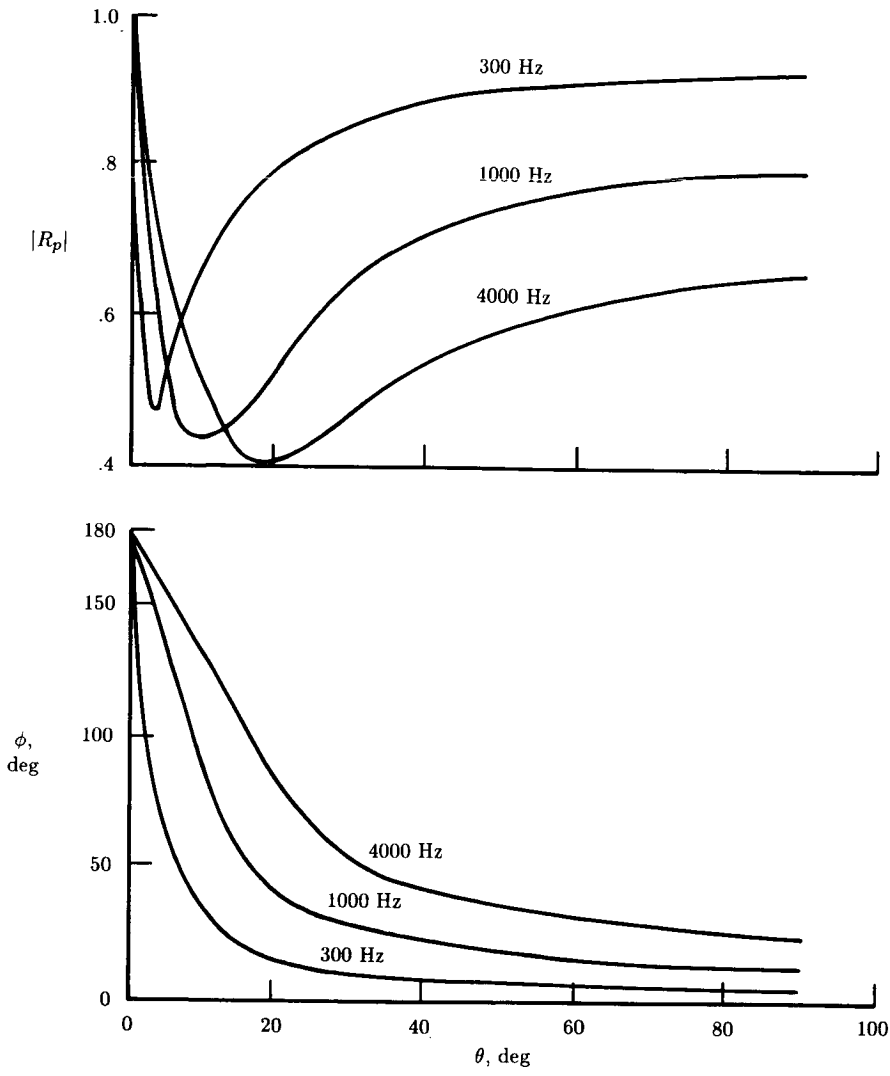

Figure 3. The magnitude $|R_p|$ and phase change ϕ of the plane-wave reflection coefficient as a function of angle of incidence θ at three typical frequencies for a grass-covered surface.

in this context as the numerical distance, and given by

$$w = \left(\frac{1}{2}ikr_2\right)\left(\sin\theta + \frac{Z_1}{Z_2}\right)^2 \tag{4}$$

The first term on the right side of equation (3) clearly represents the direct sound field in both phase and amplitude, the second term represents the field reflected at the ground surface but assuming the plane-wave reflection coefficient at the angle of specular reflection, and the third term corrects the reflected field to account for

the angle of reflection systematically varying with position along the surface. This third term in equation (3) is called a ground wave in acoustics but may also include a surface wave under some circumstances (beware that the term "ground wave" in electromagnetic propagation applies to the whole right side of eq. (3)).

When the source and receiver are both relatively near the ground and are a large distance apart, the direct and reflected fields (the ray paths r_1 and r_2 in fig. 2(a)) become nearly equal and the grazing angle θ tends to zero. The direct and reflected sound fields then cancel each other because $R_p \rightarrow -1$, and any sound reaching the receiver (apart from mechanisms to be described later) is explained theoretically by this third term of equation (3).

The amplitude factor F is shown in figure 4 vs. the numerical distance w described by equation (4). The factor F is complex and is shown for several values of the phase angle ψ of the ground impedance,

$$\psi = \tan^{-1}\left(\frac{\text{Im } Z_2}{\text{Re } Z_2}\right) \tag{5}$$

It is intuitively useful to consider the abscissa of figure 4, the numerical distance w, as the propagation distance between source and receiver but scaled for the value of frequency (proportional to k), for impedance Z_1/Z_2, and for angle of incidence θ. The behavior of the ground wave during propagation is best described by assuming for the moment that the ground surface is purely resistive, that is, the curve for $\psi = 0°$ in figure 4. This curve cannot contain any surface waves (see below). Then at short distances $w << 1$, the ground wave suffers no excess attenuation, $|F|$ is essentially unity, and the second and third terms of equation (3) combine to describe a sound field as if it were reflected from an infinitely hard surface. At greater distances $w >> 1$, or equivalently at higher frequencies, the ground wave decreases at a rate that is 6 dB per doubling of distance faster than that due to geometrical spreading alone.

In reality the phase angle ψ of the ground impedance is about 45° for grass-covered and most other ground surfaces at least up to frequencies of a few kilohertz. The curve for $\psi = 45°$ in figure 4 shows a substantial increase in $|F|$, especially for numerical distances slightly greater than unity. This increase in $|F|$ occurs only for positive values of ψ, which in turn are related to the porous or capacitive behavior of ground surfaces for acoustic waves. The increase is due to the existence of a surface wave which is coupled to the ground but propagates in the air with an amplitude that has a maximum at the ground surface and decreases exponentially with height. For those whose experience and intuition are more mathematical than experimental, the ground wave corresponds to a branch line integral, and the surface wave to a pole. Thus, for certain values of complex impedance, the third term in equation (3) is given completely by a branch line integral, but as impedance is varied, it may become necessary to allow for the contribution from a pole. In these cases the pole contribution effectively appears to grow out of the contribution from the branch line integral, just as the surface wave appears out of the ground wave when the values of complex surface impedance allow.

Obviously ground and surface waves are closely related but their fundamental origins differ, as does their behavior during propagation. Ground waves exist because curved wave fronts strike different parts of the ground at different angles of incidence

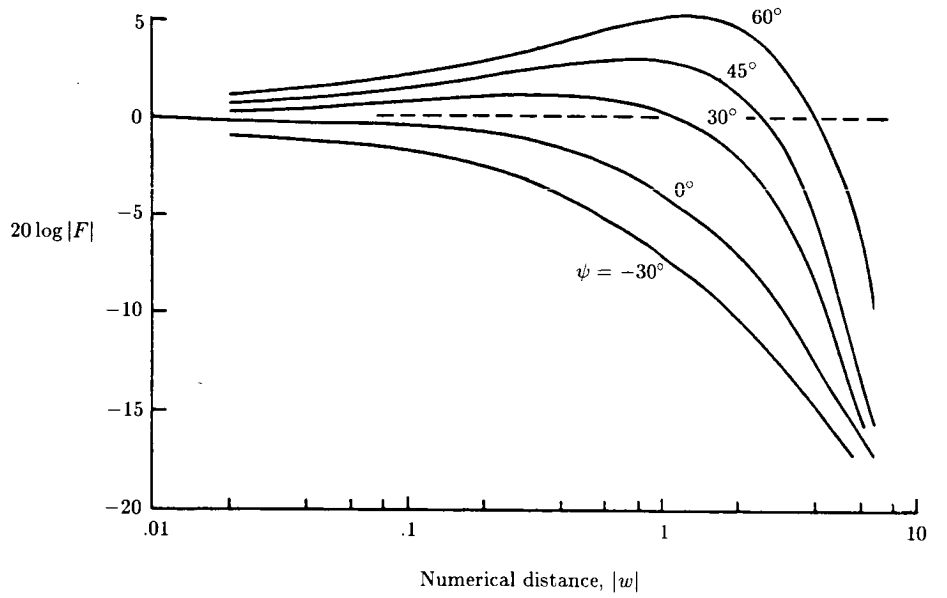

Figure 4. The magnitude of the complex amplitude factor F in decibels as a function of numerical distance w (eq. (4)). (From ref. 3; see also ref. 9.)

and because the reflection coefficient of finite-impedance ground is also a function of angle of incidence. Ground waves exist unless the ground is infinitely hard or infinitely soft or unless the incident wave fronts are plane, that is, the source can be considered infinitely far away. Surface waves exist when the ground surface is sufficiently porous, relative to its acoustical resistance, that it can influence the airborne particle velocity near the surface and reduce the phase velocity of sound waves in air at the surface. This traps some of the sound energy in the air, regardless of the shape of the incident sound field, to remain near the surface as it propagates from the source to the receiver. This latter point may be significant because surface waves, which spread cylindrically (in horizontal directions only), decrease at 3 dB per doubling of distance, whereas all other components of the sound field, including the ground wave component of the reflected sound field, decrease by at least 6 dB per doubling of distance. Though surface waves may initially decrease more slowly with distance, they eventually decay rapidly relative to other components of the total sound field because they are closely coupled to the ground surface and lose energy exponentially with distance through viscous and thermal processes in the pores of the ground.

Acoustic Impedance of Ground Surfaces

Sound waves incident on a ground surface are reflected and interfere with the incident field. This interference field can be probed within a few wavelengths of the ground to measure sound pressure and phase, or equivalently the position of maxima and minima of pressure, or to measure the distribution of phase gradient or of phase, in order to determine the reflection coefficient R_p. Alternatively the ground

impedance can be found directly by determining the pressure and the particle velocity at the surface. All these measurements are difficult to make with the necessary accuracy for most ground surfaces, and so various techniques have been used, each of which provides results of sufficient accuracy over a different but limited range of frequencies or values of ground impedance. Anybody planning to undertake such measurements is strongly advised to read the original papers so as to be aware of the subtleties of the various techniques and precautions that are important to obtaining valid results. We shall do no more than outline each of the measurement techniques and indicate their principal strengths and limitations.

Some early values of ground impedance were measured in reference 10 with an impedance tube "screwed" into the ground in situ to a depth of about 0.2 m. Like several of the other techniques to be mentioned, these measurements are restricted to normal incidence, suffer from the uncertainty of knowing exactly where the theoretical ground surface is located, and can change the flow resistivity, porosity, or other parameters of the microstructure of the ground surface. To avoid some of these limitations, Dickinson and Doak developed a technique based on measuring the pressure profile along a line perpendicular to the surface below a loudspeaker suspended several meters above the surface—the ground surface remained undisturbed and the sound field was unconfined. Later the interference between the direct and reflected sound fields was measured (ref. 11) by moving a microphone along an inclined path, GM in figure 2(a). This method allowed measurements at oblique angles of incidence more appropriate to sound sources near the ground but were restricted to frequencies greater than about 400 Hz, that is, to wavelengths less than about 0.8 m, because the distance between interference minima is increased (inversely as $\sin\theta$) and becomes very large near grazing angles of incidence. More recently, a direct pressure vs. velocity, and hence impedance, measurement (ref. 12) has been obtained with a Helmholtz resonator, one side of the volume of the resonator being open and capable of being pushed into the ground surface. A motor-driven mechanical source provides a known volume velocity source and a microphone measures the resulting pressure. This technique is restricted to frequencies below about 300 Hz both by the capabilities of the sound source and by the requirement that the sound wavelength be large compared with the dimensions of the resonator. Another technique that measures both pressure and pressure difference near the surface, and hence by calculation the impedance at the surface, has been used in reference 13 for small areas of sound absorbent materials. Because of instrumental limitations and finite difference approximations, this technique allows sufficiently precise measurements only for frequencies greater than about 500 Hz. Still more recently, a two-microphone technique (ref. 14) has been used to measure pressure, phase, and phase difference along a vertical line in the spherically spreading interference field below a source suspended several meters above the ground. Measurements have been made down to 30 Hz over grass-covered ground.

A limited selection of measured values of the resistive and reactive components of normalized specific normal impedance for grass-covered ground at different sites is shown by the dashed curves in figure 5.

For many practical purposes our interest in the ground surface is merely the effect it has on the sound field in the air above it. The direct effect is through the reflection coefficient R_p that varies in the complicated way illustrated in figure 3 as a function

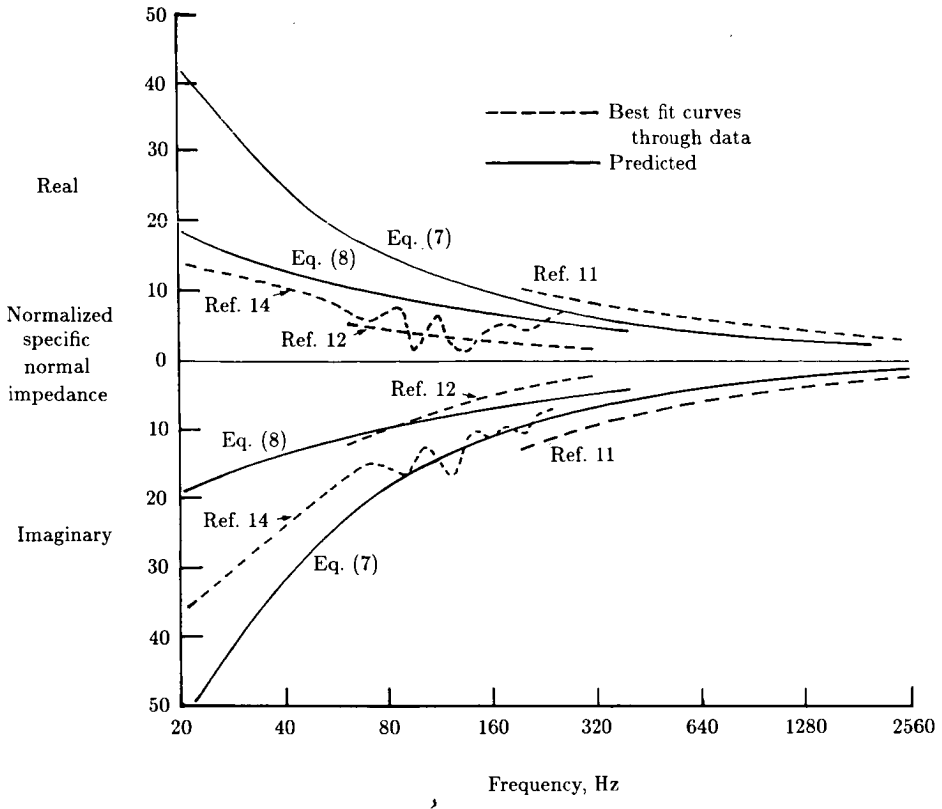

Figure 5. Normalized resistive (real) and reactive (imaginary) components of specific normal impedance for grass-covered grounds as a function of frequency. $\sigma_e = 150 \times 10^3$ Pa-sec/m^2 assumed in equations (7) and (8).

of angle of incidence and frequency. A simpler characterization of the ground is its specific normal acoustic impedance, Z_2 in equation (2). The impedance Z_2 is complex:

$$Z_2 = R_2 + iX_2 \tag{6}$$

where R_2 is the resistive component of the ground impedance, and X_2 its reactive component. Most ground materials are porous, and thus for nonlayered grounds the specific normal acoustic reactance of the surface is capacitive, or springlike in electrical or mechanical analogs. The impedance Z_2 is a function of frequency and its two components for typical grass surfaces are shown in figure 5. Such impedance curves were shown in reference 15 to be described for most porous ground surfaces by a single parameter, the effective flow resistivity σ_e of the ground. In reference 15 the empirical expressions earlier given in reference 16 were used for the specific acoustic impedance of fibrous porous materials. When the implied time dependence is $\exp(-i\omega t)$, these equations become

$$\frac{Z_2}{Z_1} = 1 + 0.051\left(\frac{f}{\sigma_e}\right)^{-0.75} + i0.0769\left(\frac{f}{\sigma_e}\right)^{-0.73} \tag{7}$$

Table 1. Ranges of Effective Flow Resistivity for Various Ground Surfaces

Type of surface	Flow resistivity, Pa-sec/m^2
0.1 m of new fallen, dry snow	7 to 30 $\times$ 10^3
Sugar snow	25 to 50 $\times$ 10^3
Forest floor, pine or hemlock	20 to 80 $\times$ 10^3
Grass on airfield, rough pasture	150 to 300 $\times$ 10^3
Rough roadside dirt, assorted particle sizes	300 to 800 $\times$ 10^3
Sandy silt, packed	0.8 to 2.5 $\times$ 10^6
Limestone chips, thick layer (0.01 to 0.025 m mesh)	1.5 to 4 $\times$ 10^6
Old dirt roadway, stones (0.05 m mesh), interstices filled	2 to 4 $\times$ 10^6
Earth, little vegetation and rain-packed	4 to 8 $\times$ 10^6
New asphalt, depending on particle size	5 to 15 $\times$ 10^6
Quarry dust, packed by vehicles	5 to 20 $\times$ 10^6
Old asphalt, sealed by dust and use	25 to 30 $\times$ 10^6
Concrete, depending on surface finish	30 to 100 $\times$ 10^6

where f is the frequency in hertz, $\omega = 2\pi f$, and σ_e is the effective flow resistivity of the ground in Pa-sec/m^2. Equation (7) is valid for a wide range of ground surfaces but tends to overestimate both components of the impedance below about 200 Hz. Table 1 gives the values of effective flow resistivity for various ground surfaces (ref. 17) that can be used in equation (7) to provide the specific normal acoustic impedance Z_2. This in turn can be used in equation (2) to provide the complex reflection coefficient R_p and, with figure 4, a complete description of the effect of the ground on the sound field above it.

The predicted effect of four ground surfaces on the spectrum of a sound wave measured 1.22 m above the ground at a distance of 500 m is shown in figure 6. In figure 6(a) the source is 2 m above the ground (i.e., nearly horizontal propagation) as in figure 2(a) and in figure 6(b) the source is essentially overhead as in figure 2(b). The flow resistivity parameters of the four curves correspond roughly to snow, grass-covered earth, packed earth, and concrete. The predominant feature of each curve in figure 6(a) is the broad minimum of sound pressure level in the range of frequencies from about 100 to 400 Hz over snow to around 4000 Hz over concrete. The shape is determined by the large phase changes on reflection at nearly grazing incidence, illustrated in figure 3, interacting with the phase differences as a function of frequency that occur because of path length differences between the direct and ground-reflected sound fields (fig. 2). In figure 6(b) for nearly perpendicular reflection at the ground surface, there is almost no phase change on reflection regardless of the effective flow

resistivity of the ground surface. The shape of the curves therefore differs very little between surfaces and is determined almost entirely by path length differences. The first minimum occurs at about 70 Hz, for which the receiver is at a height of one-quarter wavelength above the ground (i.e., the reflected field travels an extra half-wavelength compared with the direct field). Subsequent minima occur at 3, 5, 7, ... times 70 Hz.

It is convenient to be able to characterize a wide range of common ground surfaces by the value of one parameter, whether selected from table 1 or measured for a specific surface of interest. When the one-parameter model is not sufficiently precise, for example, at frequencies below about 200 Hz, or when the ground changes significantly near its surface or is noticeably layered, then more elaborate theory can be invoked. In reference 18 the acoustical properties of homogeneous and isotropic porous soils were shown to depend on four material parameters: flow resistivity, porosity, grain shape factor, and pore shape factor ratio. Of these parameters, the flow resistivity σ and porosity Ω are the two most important; furthermore, the empirically determined effective flow resistivity σ_e of the one-parameter model (eq. (7) and table 1) is essentially given by the product $\sigma\Omega$. Though in general more complicated, the four-parameter model yields a low-frequency and high-flow-resistivity approximation that provides better agreement with measured impedances at frequencies below 200 Hz than does the one-parameter model (eq. (7)). The normalized surface impedance derived from the four-parameter theory but limited to large values of the effective flow resistivity σ_e and low frequencies is (eq. (14) of ref. 18):

$$\frac{Z_2}{Z_1} = 0.218\left(\frac{\sigma_e}{f}\right)^{1/2}(1+i) \tag{8}$$

Equation (8) is an alternative to equation (7) and differs from equation (7) by predicting that the resistive and reactive components of the ground impedance are equal and vary as the inverse square root of the frequency. (Equation (7) predicts a variation close to the inverse three-quarter power of frequency.)

This same low-frequency, high-flow-resistivity approximation also provides an expression for the normalized surface impedance of a ground whose porosity decreases with depth (eq. (31) of ref. 18):

$$\frac{Z_2}{Z_1} = 0.218\left(\frac{\sigma_e}{f}\right)^{1/2} + i\left[0.218\left(\frac{\sigma_e}{f}\right)^{1/2} + 9.74\left(\frac{\alpha_e}{f}\right)\right] \tag{9}$$

Note that equation (9) is the same as equation (8) with the addition to the reactance of a term in α_e/f, where α_e is an effective rate of decrease in porosity with depth. It is predicted that the resistive component of the ground impedance is unchanged by the rate of change of porosity below the surface.

When the ground consists of a porous layer backed by an essentially rigid impervious base, the obvious additional parameter needed to describe the normal surface impedance is the layer thickness ℓ. The impedance of the surface layer Z/ℓ is then calculated by

$$\frac{Z_\ell}{Z_1} = \frac{Z_2}{Z_1}\coth\left(-ik_2\frac{\omega}{c_o}\ell\right) \tag{10}$$

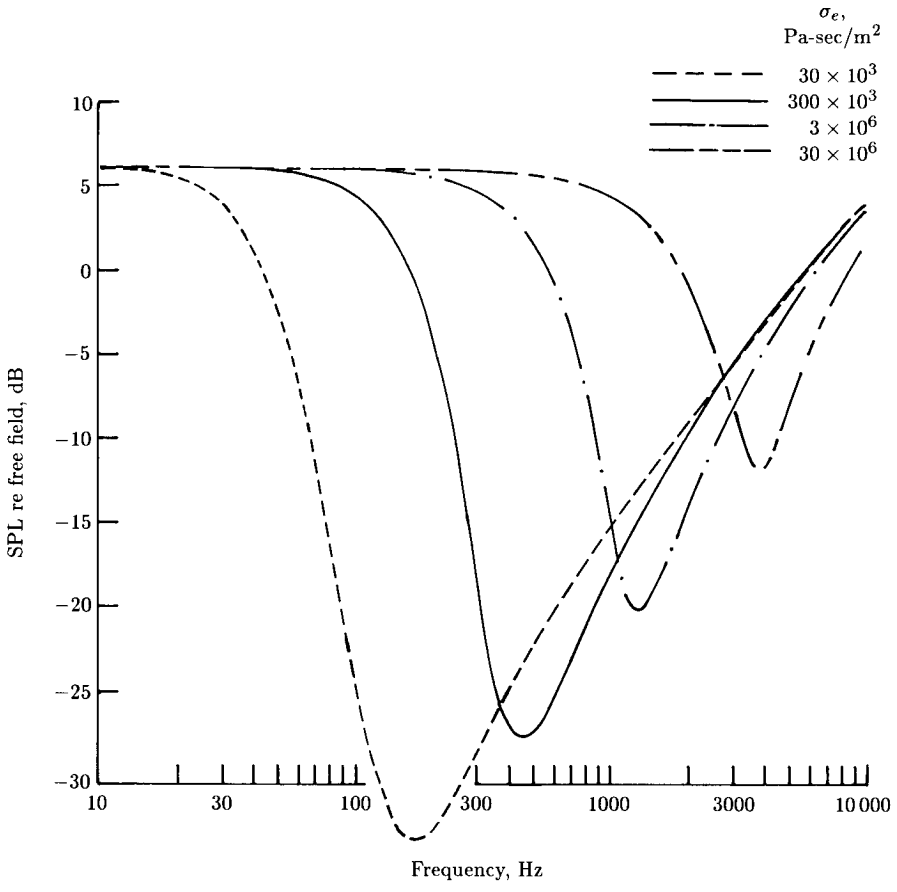

(a) Source 2 m above ground.

Figure 6. Predicted transmission spectrum measured 1.22 m above the ground for a source 500 m away.

where c_o is the sound speed at the surface of the ground and the normalized wave number k_2 is given by

$$k_2 = 1 + 0.0978 \left(\frac{f}{\sigma_e}\right)^{-0.693} + i0.189 \left(\frac{f}{\sigma_e}\right)^{-0.62} \tag{11}$$

and Z_2/Z_1 is given by equation (7), or equation (8) if appropriate.

The low-frequency, high-flow-resistivity approximation allows simplification of the expression for the surface impedance of a layered surface (ref. 18). At low frequencies, for many ground surfaces but not for a layer of snow because its flow resistivity is too small, equations (10) and (11) can be replaced by (eq. (33) of ref. 18):

$$\frac{Z_\ell}{Z_1} = 0.00082\, \sigma_e \ell_e + \frac{i38.99}{f\ell_e} \tag{12}$$

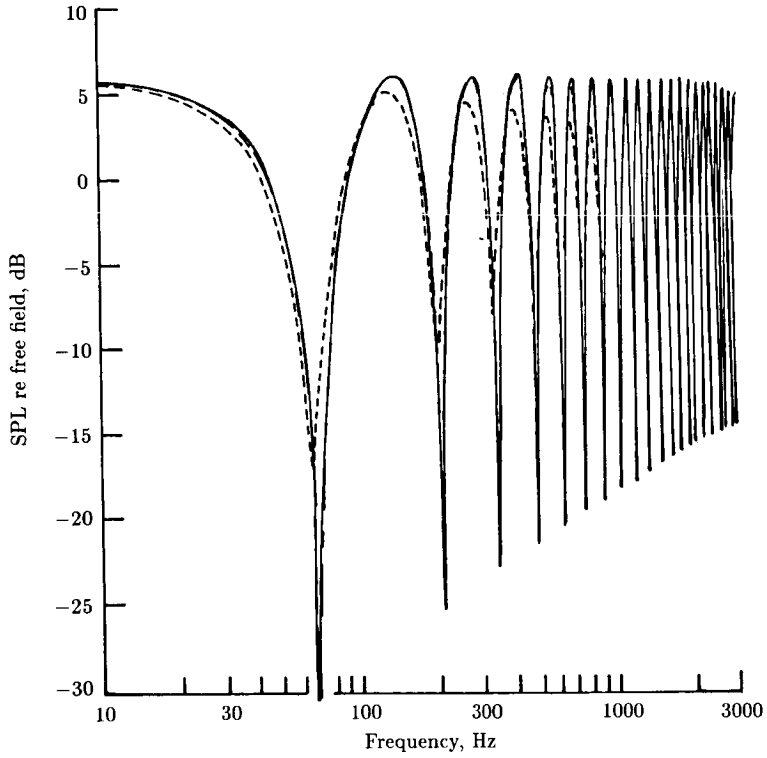

(b) Source directly overhead.

Figure 6. Concluded.

where ℓ_e represents the effective thickness of the layer given by $\Omega\ell$. The porosity for many ground materials lies in the range $0.3 < \Omega < 0.6$. Equation (12) shows that the normalized resistance of a surface layer backed by a hard rigid material is independent of frequency and that its normalized reactance increases rapidly with decreasing frequency.

The general effects on the sound field resulting from reflection at a layered surface for nearly grazing angles of incidence are illustrated in figure 7 (ref. 19). These sound pressure levels were measured at short range over a layered ground model of reticulated foam backed by a hard concrete floor. The principal effect is to deepen the minimum in sound pressure level in the so-called ground effect dip, in the region from 300 to 2000 Hz, compared with propagation over an infinitely thick layer of the same surface material. Although shown in these results, the minimum in sound pressure level does not necessarily occur at a higher frequency above a layered medium than above an infinitely thick ground.

Ground Surfaces With a Discontinuity of Impedance

As is apparent in figure 6(b), all types of ground have essentially the same effect on sound fields reflected almost perpendicularly to the surface. Different types of ground do however have different effects (fig. 6(a)) on sound traveling at nearly grazing angles

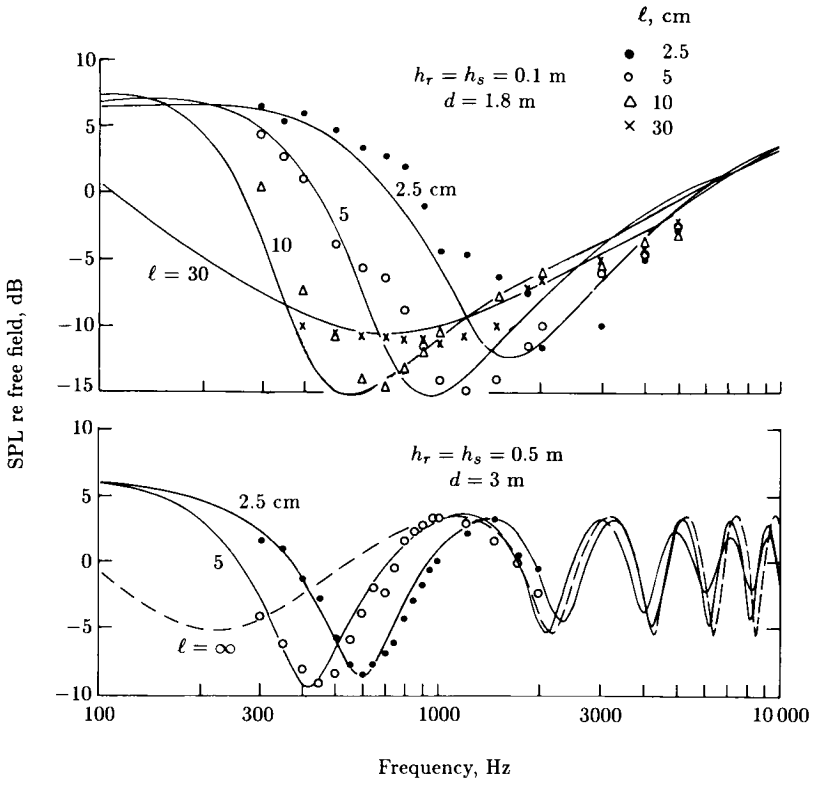

Figure 7. Comparison of sound pressure levels measured above layers of reticulated foam (data points) with predictions from equation (10)(curves).

of incidence. This latter configuration is of importance in many practical situations, for example, sound from an aircraft on the runway or from vehicle traffic on the highway, which propagates horizontally initially above an acoustically hard concrete or asphalt surface and subsequently above a softer grass-covered surface. Several authors (refs. 20–23) have developed theoretical solutions to the problem of nearly horizontal sound propagation across an impedance discontinuity, and measurements both indoors and outdoors up to horizontal distances of a few meters have been made (ref. 24) for various types and distance ratios of hard and soft ground. In general there is good agreement between predictions and measurements, and in all cases the measured sound spectra are significantly different from what they would be for homogeneous ground, whether all hard or all soft. A typical example of a measured spectrum (ref. 24) is illustrated in figure 8 for a source 0.1 m high over asphalt and receiver 0.5 m high over grass where the propagation distances are 2 m and 6 m over the respective surfaces. Predicted spectra for a ground consisting of all asphalt or all grass are also shown, as well as the predictions of the spectra using the theories of references 21 to 23.

In the absence of specific calculations, which are time-consuming in many cases, one can postulate from the variety of measurement configurations shown in the figures of reference 24 that a good rule of thumb is to calculate the spectra by assuming first

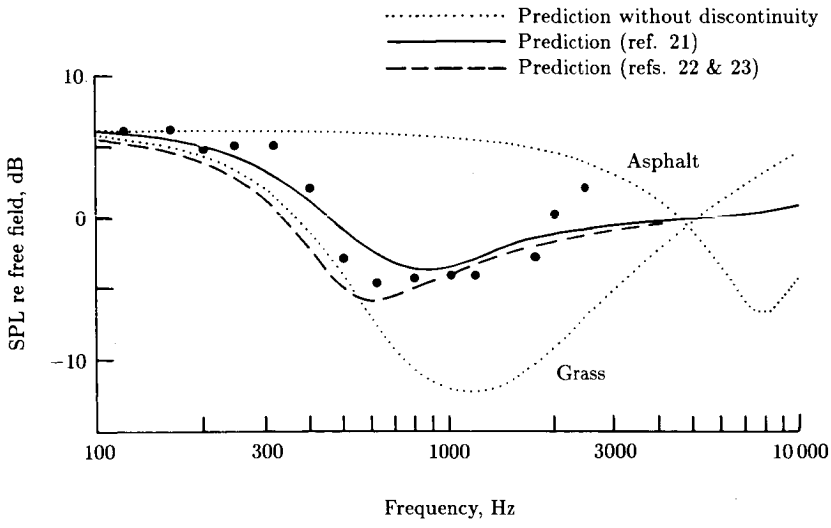

Figure 8. Measured changes in a sound field propagated across the impedance discontinuity between asphalt and grass. Source height 0.1 m above asphalt ($\sigma_e = 30 \times 10^6$ Pa-sec/m^{-2}) and receiver height 0.5 m above grass ($\sigma_e = 85 \times 10^3$ Pa-sec/m^{-2}); distances over surfaces were 2 m and 6 m, respectively. (From ref. 24.)

that the ground is all hard and second that it is all soft acoustically. A reasonably correct spectrum (within about 5 dB) can then be obtained by weighting the hard and soft spectra in proportion to the distances propagated over the hard and soft grounds.

Refraction by Vertical Gradients of Wind and Temperature

Under most weather conditions both the temperature and the wind vary with height above the ground. The velocity of sound relative to the ground is a function of temperature and wind velocity, and hence it also varies with height, causing the sound waves to propagate along curved paths. During the day solar radiation heats the earth surface resulting in warmer air near the ground. This condition, called a temperature lapse, is most pronounced on sunny days but can also exist under overcast skies. A temperature lapse is the common daytime condition during most of the year and ray paths curve upward.

After sunset there is often radiation cooling of the ground which produces cooler air near the surface. In summer under clear skies such temperature inversions begin to form about 2 hours after sunset, when they may extend to less than a meter above the ground; as the night progresses, they extend to increasing heights and can reach altitudes of the order of a hundred meters by sunrise. Throughout this period a temperature lapse exists above the top of the growing temperature inversion. Within the temperature inversion, the temperature increases with height and ray paths curve downward.

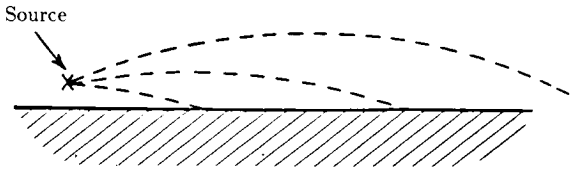

(a) Sound speed increasing with altitude.

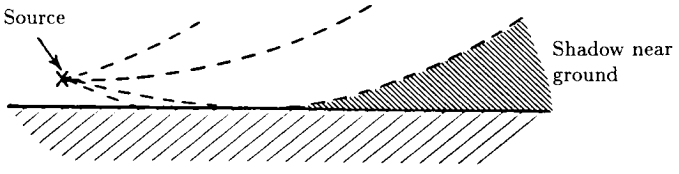

(b) Sound speed decreasing with altitude.

Figure 9. Schematic showing the bending of ray paths.

When there is wind, its speed decreases with decreasing height because of drag on the moving air at the ground. Therefore the speed of sound relative to the ground increases with height during downwind propagation and ray paths curve downward. For propagation upwind the sound speed decreases with height and ray paths curve upward. There is no refraction in the vertical direction produced by wind when the sound propagates directly crosswind. An illustration of the ray paths is shown in figure 9. In a temperature inversion or for propagation downward, the ray paths curve downward as in figure 9(a). Under specific conditions which depend on source and receiver heights, horizontal range, and the strength of the inversion, additional ray paths are possible that involve one or more reflections at the ground. In a temperature lapse or for propagation upwind, ray paths curve upward away from the ground as in figure 9(b). If the relation between sound speed and height is linear, there is a limiting ray that just grazes the ground and beyond which no direct sound energy can penetrate. This causes an acoustical shadow region. If, on the other hand, the sound speed profile is not linear, the limiting ray is replaced by a caustic because sound energy (rays) from various regions of the irradiated sound field can reach the same region along the shadow boundary. The effects of the temperature and wind profiles on the sound speed profile are additive. Rays curve upward or downward in the real atmosphere depending on the relative strength of the vertical gradients of temperature and wind speed. For example, an acoustic shadow can exist even downwind if the temperature lapse dominates the wind speed gradient to produce a sound speed that decreases with height. In what follows we shall distinguish between downward and upward refraction irrespective of which meteorological condition produces the effect.

Downward Refraction

The propagation of sound in a temperature inversion has been studied previously (ref. 25), but the principal results would be qualitatively similar for sound

propagation downwind. We shall therefore discuss here the more general case of a sound velocity profile that increases with height. The form of profile which is most convenient for physical interpretation and mathematical computation is one where the sound velocity increases linearly with height:

$$c = c_o(1 + \gamma h) \tag{13}$$

In equation (13), h is the height above the surface and γ is the coefficient of increase in velocity with height. We note that a linear variation with height is a good approximation for most cases although it is not necessarily achieved in practice. The sound rays between source and receiver are then circular arcs. When either the sound source or the receiver is above the ground, in addition to the direct ray there are reflected rays which also follow circular paths (fig. 10).

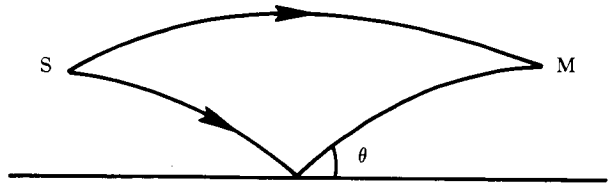

(a) At short or moderate source-to-receiver distances.

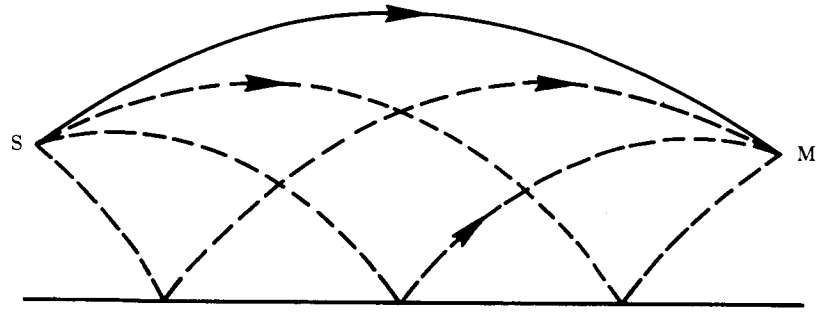

(b) At longer source-to-receiver distances.

Figure 10. Bending of ray paths in downward refraction.

If source and receiver are separated by moderate distances of the order of $d = 100$ m and are a few meters above the ground, there is only one reflected ray, providing that we also assume average atmospheric refraction. The direct and reflected ray paths are illustrated in figure 10(a). Note that the angle θ for the reflected ray is greater than for an unstratified atmosphere. The magnitude of the reflection coefficient therefore deviates further from -1 and the destructive interference between direct and reflected waves becomes less complete. The result is less attenuation for frequencies around 500 Hz. This is illustrated by the measurements (ref. 26) in figure 11. The curve labeled "0" represents sound levels measured in the absence of stratification or crosswind while the curve labeled "+5" represents results for downwind propagation. There is essentially no difference between those two curves below 400 Hz at 110 m or below 300 Hz at 615 m from

the source. At higher frequencies, however, the reduced attenuation for downwind propagation is evident.

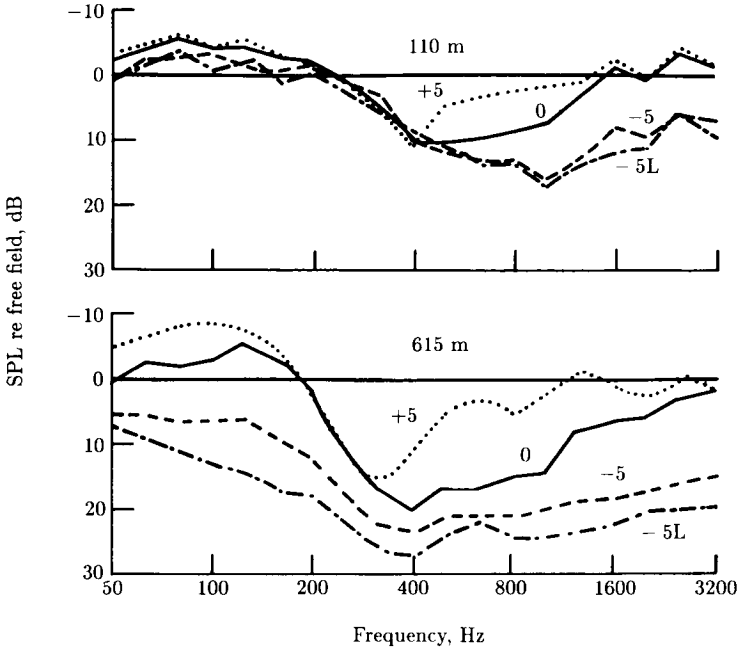

Figure 11. Sound pressure levels relative to free field in 1/3-octave bands of noise measured at 110 and 615 m from a jet engine (ref. 26). Numbers on curves indicate wind velocity, in m/sec, in the direction of propagation; curves marked "L" are for a temperature lapse. (From ref. 3.)

In general at longer distances d there are more than one reflected ray path (refs. 25 and 27). The existence of these additional ray paths is easily predicted (ref. 25) from elementary analytical geometry. Further, a particular ray may be reflected several times between source and receiver. When there is one reflection at the ground for any ray, there are three possible reflected ray paths. These are illustrated in figure 10(b) by the dashed curves. There is the ray reflected at the midpoint between source and receiver, assuming for the moment that the source and the receiver are at equal heights. The two other rays have a point of reflection displaced from this midpoint, one striking the surface relatively near the source and the other near the receiver. These additional paths further degrade the ground effect attenuation as shown in figure 11, at 615 m for frequencies above 400 Hz.

In the general case of finite source and receiver heights h_s and h_r, there are a total of four reflected ray paths for each number of reflections per ray greater than one. There is, however, an upper limit to the number of reflections at the surface, unless $h_s = h_r = 0$. It is not difficult to develop a simple criterion to determine the existence or absence of the higher order paths with multiple reflections. Let H_1 be the height of a ray path at its zenith (fig. 12). One can show for h_s and $h_r << d$, that

$$H_1 \approx \frac{\gamma d^2}{8} \tag{14}$$

where equality occurs when $h_s = h_r = 0$. Further, rays are realizable provided that

$$H_n \approx \frac{H_1}{n^2} \geq h_s \text{ and } h_r \tag{15}$$

Thus when n is sufficiently large that $H_n < h_s$ or h_r then the corresponding ray paths do not exist. To take specific examples, we assume that $h_s = h_r = 1.2$ m and $\gamma = 3 \times 10^{-5}$ m^{-1}, typical for a temperature inversion. Then, from equation (14), $H_1 = 0.04$ m for $d = 100$ m. Thus there is only one reflected ray path as shown in figure 10(a). Next, for $d = 800$ m, we find that $H_1 = 2.4$ m and $H_2 = 0.6$ m. This example corresponds to the illustration in figure 10(b). Finally at a much larger distance, for example, $d = 4$ km, equations (14) and (15) yield $H_1 \approx 60$ m and hence $H_7 \approx 1.2$ m and $H_8 \approx 0.9$ m. Thus, theoretically at least, there should be no ray paths having more than about seven reflections between source and receiver when both are 1.2 m above the surface.

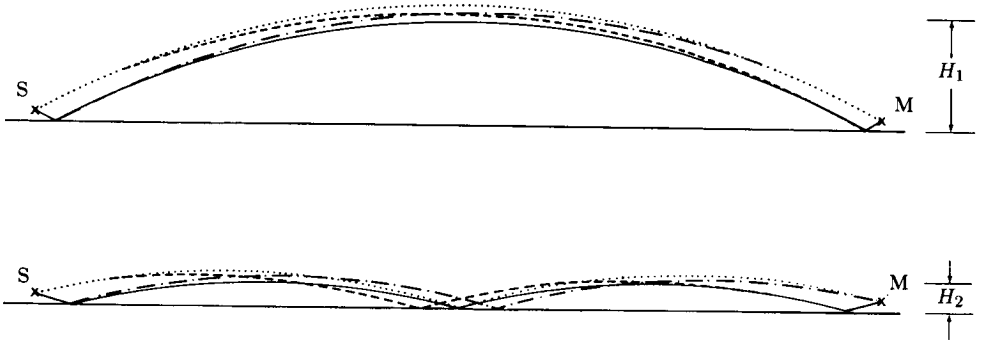

Figure 12. Schematic showing groups of ray paths in downward refraction that have approximately the same heights at zenith. (From ref. 25.)

At these larger distances, when the ultimate goal is to estimate the sound levels at a distant point as a result of sound traveling via the numerous ray paths, it is useful to group them differently from the number of reflections a ray suffered between source and receiver. A convenient grouping is according to the maximum height above the surface reached by the path as shown in figure 12. Thus the four rays having zenith heights of approximately H_1 have different numbers of surface reflections m; one has $m = 0$, two have $m = 1$, and one has $m = 2$. These rays follow almost the same path through the atmosphere and maintain partial coherence between themselves to a much greater extent than between other similar groups of ray paths. Under such conditions a method has been suggested (ref. 25) to estimate the sound levels at distant receivers. The interference between the direct ray from the source and the rays reflected at the surface are first calculated for the first grouping of individual rays in the bundle having zenith H_1. The amplitude and phase of the waves reflected near the source are calculated from the impedance of the surface, assuming that this is known, and added coherently to the direct ray, in effect assuming a composite source (see ref. 25 for the details of the calculations). Because the ground surface in the vicinity of the receiver can vary from one location to another, the sound rays reaching the receiver after a last reflection in the vicinity of the receiver should, on

average, be taken into account by adding their intensity to that of rays not suffering this reflection. If the reflection coefficient of the surface near the receiver is known to be unity, this implies adding 3 dB to the level given by the rays not reflected in this region. However a more typical magnitude for the reflection coefficient is less than unity and an average correction of 2 dB is suggested. The roles of sound source and receiver are reciprocal, so this discussion is valid also when the ground impedance near the receiver is known, but that near the source is not known or may vary from one source location to another. The sound energy traveling via the other groups of ray paths with zenith H_2, H_3, etc., experience different local turbulence (see the next section) and hence are expected to add incoherently to the energy via the primary group. The maximum correction to be added to the results calculated for the primary group is about 2.2 dB when there are an infinite number of possible paths (see ref. 25). In more realistic cases, when only a few of these paths exist, the correction to be added is about 0.5 dB. In most outdoor sound propagation problems this correction for multiple paths in downward refraction is therefore negligible.

The factors just discussed lead to the qualitative conclusion that downward refraction can nullify the reduction in sound pressure levels caused by ground effects. Sound levels therefore increase to the levels predicted by geometrical spreading and molecular absorption alone, but in general not above such levels. Increases above such levels are due to focusing caused by curved, that is, nonlinear, sound speed gradients and are inevitably accompanied by decreases caused by defocusing elsewhere in the sound field.

Upward Refraction

When the sound speed decreases with height, the sound rays are bent upwards, away from the ground. For realistic sound speed profiles, there is a limiting ray leaving the source which just grazes the ground. This limiting ray is shown in figure 13, and when the sound speed decreases linearly with height, the ray is an arc of a circle. Above this limiting ray the sound field is composed of direct and ground-reflected waves. Below the limiting ray there is an acoustical shadow region in which these waves theoretically do not exist; sound energy does however penetrate this shadow region due to other, diffractive propagation mechanisms.

It is perhaps useful to remind ourselves that rays do not represent any real physical entity. Rays are a convenient way of understanding various features of a sound field. For example, interference is a wave phenomenon that depends on phase differences between sound fields; rays provide a convenient set of geometrical lines from which path length differences, and hence phase differences, can be calculated. Similarly in figure 13 the limiting ray is a geometrical line whose trajectory can be calculated and which divides the sound field into two regions; the sound field is however continuous across the limiting ray, although it changes across a broad band of space near the limiting ray at a rate which depends on the wavelength of the sound and often on other geometrical factors—again, affirmation that what occurs in a sound field is governed by wave mechanisms.

Above the shadow region, the sound field can be described by the same arguments as before. A typical pair of direct and reflected waves is shown by the dotted curves in figure 13 to the point M_1. There is always only one ground-reflected wave and the incidence angle θ is smaller than for the unstratified atmosphere. The magnitude

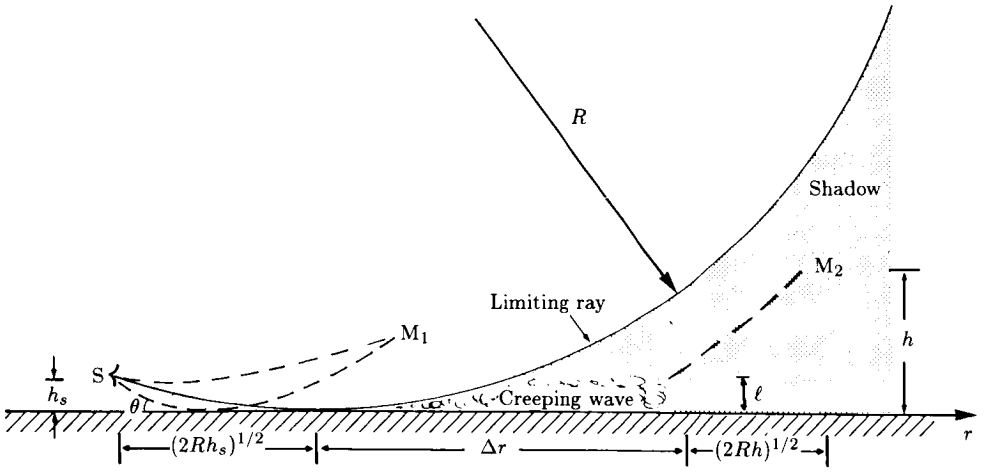

Figure 13. Schematic illustrating the main features of upward refraction. (From ref. 31.)

the reflection coefficient is now closer to −1 and the destructive interference between direct and reflected waves is enhanced. This increases the attenuation for frequencies above about 500 Hz (see the curves in fig. 11 at 110 m, labeled "−5" for upwind propagation and "−5L" for lapse conditions). These results were probably measured just beyond the limiting ray into the fringe of the shadow; however the results still show the effect described above. Theory to account for the changing incidence angle due to the curved ray path has been described in reference 27, where calculated curves predicted well the changes in the spectra of figure 11 at high frequencies.

At 615 m from the source the results labeled "−5" and "−5L" in figure 11 were measured farther into the shadow region (M_2 in fig. 13) and the description of these results requires a very different analysis. A number of numerical methods are available to compute accurate quantitative results (refs. 28 and 29). These reconstruct the sound field allowing for the effects of diffraction, changes in sound velocity with height, or other relevant factors. However to provide a better understanding of the features involved, we shall describe the process in an alternative and more intuitive way. The sound levels, in the absence of turbulence, can be determined from diffraction theory (ref. 30), which suggests that the energy received at M_2 initially leaves the source and travels along the limiting ray to the ground. Then it propagates in the air along the surface in a creeping wave. At an appropriate distance, the energy is then shed from the creeping wave and travels to M_2 along the ordinary geometrical acoustics ray shown by the dashed curve in figure 13. An example of an acoustical shadow governed by this mechanism is shown in figure 14. The points are measurements made above an asphalt surface at a distance of 200 m from a point source (ref. 31), at locations well within the shadow region. Predictions obtained from creeping-wave theory, the solid curves, are in reasonable agreement with the measured values except at the two highest frequencies close to the ground and upwind, that is, where the sound pressure levels are lowest. This discrepancy

is probably due to yet another mechanism, scattering by turbulence, whereby sound energy is redistributed between various regions of otherwise coherently determined sound fields.

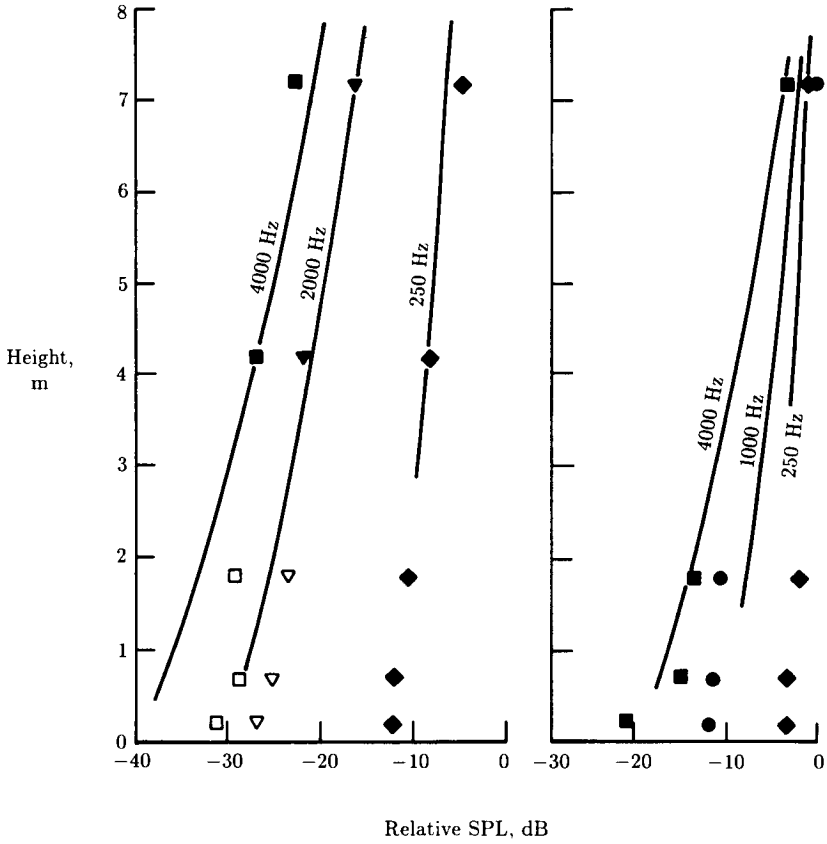

(a) Upwind. *(b) Downwind.*

Figure 14. Comparison of predicted and measured sound pressure levels within shadow region at a distance of 200 m from the source over an asphalt surface. Sound pressure levels marked by open symbols may be perturbed by turbulence. (From ref. 31.)

Atmospheric Turbulence

The atmosphere is an unsteady medium (ref. 32) with random variations in temperature, wind velocity, pressure, and density. In practice only the temperature and wind velocity variations significantly affect acoustic waves over a short time period. During the daytime these inhomogeneities are normally much larger than is generally appreciated. Shown in figure 15 is a typical record of the temperature measured 1 m above a flat ground surface on a sunny day. The measurement was made with a fast response (<1 msec) thermometer. Fluctuations in temperature of

5°C which last several seconds are common and 10°C fluctuations not uncommon. The wind velocity fluctuates in a similar manner and has a standard deviation about its mean value that is commonly one-third of the average value. When waves propagate through the atmosphere, these random fluctuations scatter the sound energy. The total field is then the sum, in amplitude and phase, of these scattered waves and the direct line-of-sight wave, resulting in random fluctuations in amplitude and phase. The acoustical fluctuations are in some respects analogous to more familiar optical phenomena such as the twinkling of light from a star.

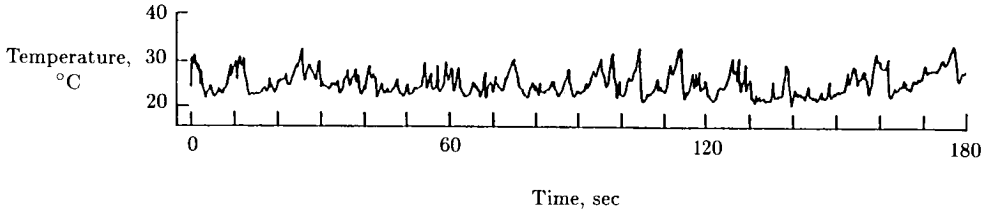

Figure 15. Typical recording of the temperature measured about 1 m above the ground on a sunny summer day. The response time of the thermometer was less than 1 msec.

Large eddies are formed in the atmosphere as energy is injected into the turbulence as a result of instabilities in the thermal and viscous boundary layers near the ground. For example, we have seen in the section on refraction that the average horizontal wind velocity varies as a function of height, being essentially zero at the ground surface, and this variation creates turbulence of a size approximately equal to the height. This is illustrated very clearly in reference 33. The size at which the energy enters into the turbulence is called the outer scale of turbulence and is designated by L_o. The eddies of sizes greater than L_o are generally anisotropic. The spectrum in this range, called the input range, depends on how the turbulence is created in the particular circumstances, and thus there is no general formula describing the turbulence characteristics in this range.

In the range of the spectrum where the eddy size is smaller than L_o, the kinetic energy of the turbulence is very much greater than the amount of kinetic energy that can be dissipated due to viscosity in the time required for a large eddy to break down into smaller eddies. Since the dissipation is negligible, almost all the kinetic energy can be transferred to eddies of smaller size. Thus, the energy transfer can be visualized as a process of eddy fragmentation where large-scale eddies cascade into eddies of ever-decreasing size. The characteristics of the initial conditions disappear, the fluid motion is almost completely random and irregular, and its features can be described in statistical terms. This part of the turbulence spectrum is called the inertial or Kolmogorov range.

However, as the eddy size becomes smaller, the fraction of available kinetic energy being dissipated by viscosity increases. Eventually the smallest size ℓ_o of the eddies is reached where their kinetic energy is of the same order as the kinetic energy being dissipated. At this size ℓ_o, virtually all the energy is dissipated into heat and almost no energy is left for eddies of size smaller than ℓ_o. This size ℓ_o is called the inner scale of turbulence and is typically of the order of 1 mm. The spectrum range of eddy size smaller than ℓ_o is called the viscous range.

The three characteristic ranges of the spectral density of the turbulent atmosphere are illustrated in figure 16. The points are an example of a measured spectrum of wind velocity fluctuations. Essentially, the points represent the fast Fourier transform (FFT) of the time-varying signal recorded by the anemometer. The measurements were made about 1 m above the ground and, as expected, the outer scale is about 1 m.

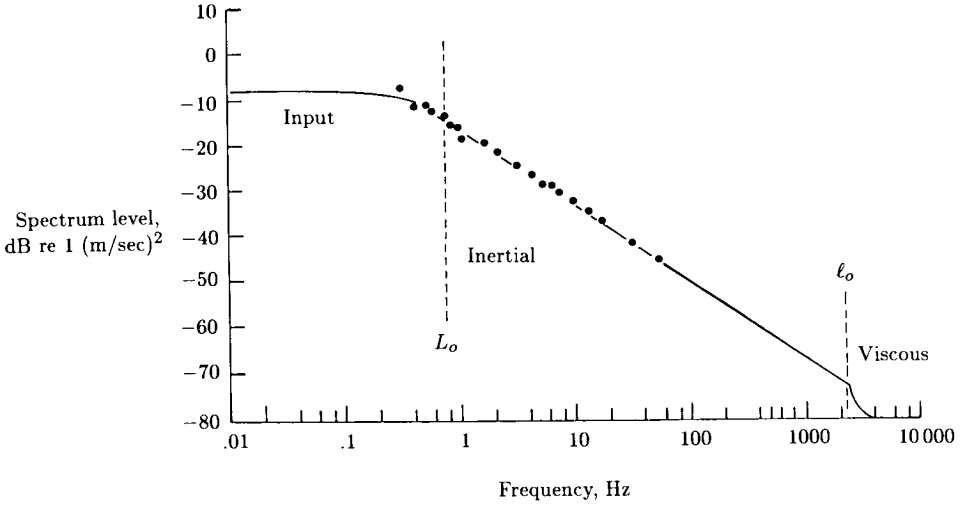

Figure 16. The three ranges of the atmospheric turbulence spectrum. The points are the result of an FFT analysis of a wind velocity recording.

For horizontal sound propagation near the ground in the range of frequencies from a few hundred to a few thousand hertz and distances of hundreds of meters, the propagation is most influenced by eddies having sizes greater than 1 m and hence in the input region of the turbulence spectrum. As explained above, there is no general formula describing the turbulence in this range. Measurements and some simple theory, although still tentative, are beginning to provide information on the mechanism governing the propagation through turbulence in this range (refs. 31 and 34). On the other hand, for air-to-ground propagation from an elevated source, the outer scale is much greater than 1 m and the propagation is most influenced by eddies in the inertial range of turbulence. Our understanding of the mechanism in this case is much better, mainly because of the large body of knowledge accumulated through work on atmospheric sounders (ref. 35).

Regardless of whether the significant turbulence is larger or smaller than the outer scale, the scattering of sound by turbulence produces fluctuations in the phase and amplitude of the received signal. The magnitude of the fluctuations increases with increasing distance of propagation, sound frequency, and strength of turbulence. Shown in figure 17 are measured phase (open points) and amplitude (solid points) fluctuations plotted as a function of the calculated fluctuations (ref. 34). The measured fluctuations are for a variety of frequencies, distances of propagation, and strengths of turbulence. The calculated values are obtained from simultaneous meteorological measurements. The graph shows that the phase fluctuations increase without bound, as predicted, for increasing values of the variables. The amplitude

fluctuations on the other hand, in addition to being systematically lower than the phase fluctuations, clearly show saturation.

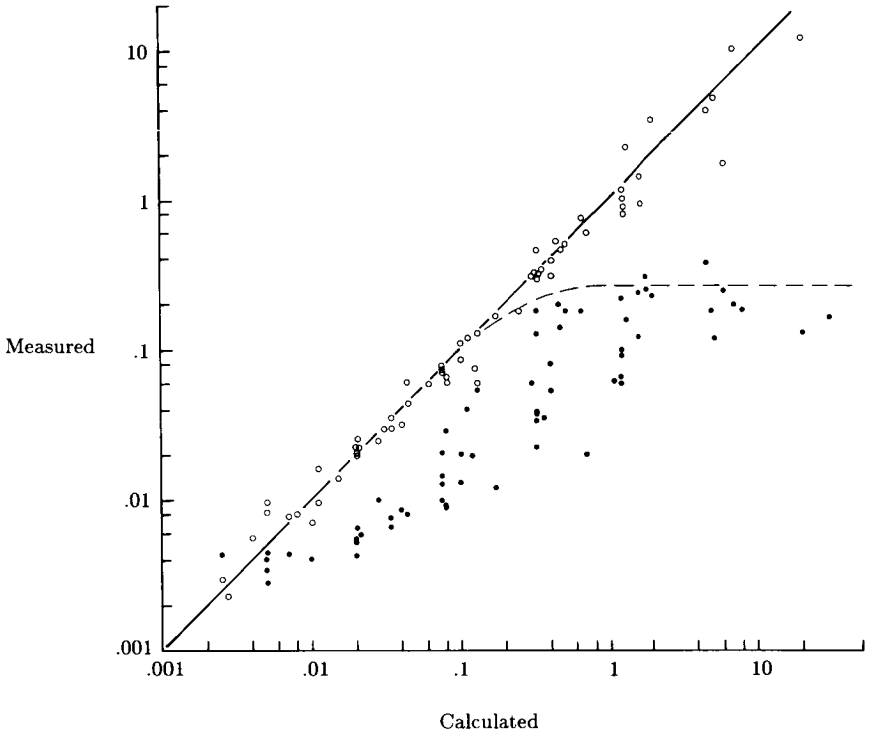

Figure 17. Measured amplitude (solid points) and phase (open points) fluctuations as a function of the corresponding calculated values. (From ref. 34.)

An effect of atmospheric turbulence, which is immediately suggested by the results shown in figure 17, is the nuisance of coping with fluctuating levels during noise measurements from relatively distant sources such as aircraft. However the saturation of the amplitude fluctuations shown in figure 17 minimizes this problem. The fluctuations in sound pressure level initially increase with increasing distance, but quickly reach a limiting value. For example when the noise from aircraft propagates under clearly line of sight conditions over distances of a few kilometers, the measured sound pressure levels fluctuate about their mean value with a standard deviation of no more than 6 dB. This is in agreement with the results of figure 17.

An effect of atmospheric turbulence which has traditionally been considered important is the direct attenuation of sound by turbulence. If the sound is in a highly directed beam, the turbulence attenuates the beam by scattering energy out of it (ref. 36). However for a spherically expanding wave this attenuation is negligible, because the scattering from turbulence is elastic and mostly in the forward direction through a small scattering angle. Therefore, in a simpleminded way, the energy scattered out from the line of sight is replaced by energy scattered back to the receiver from adjacent regions. This implies that the energy level of the root-mean-square sound pressure in an unsteady medium is the same as the level would be in the absence of turbulence. The only mechanism by which turbulence could

provide attenuation in a spherical wave field is backscattering (ref. 37). However it seems that the attenuation provided by backscattering is much smaller than the attenuation due to molecular absorption. The attenuation of sound due to scattering from a moderately directional source must lie between the two extremes of a finite-width beam and a spherical field, but has never been evaluated thoroughly. It is generally believed (ref. 3) to be negligible for most applications.

Other acoustical phenomena are most strongly and directly affected by atmospheric turbulence. For example the interference of direct and ground-reflected waves depends critically on the exact phase relationship that exists between them. The random fluctuations in phase shown in figure 17 bring into question the use of coherent acoustical theory to describe this phenomenon, as was done earlier. The points in figure 18 are excess attenuation measurements from reference 26 of jet noise propagating across a grass-covered field for various distances. (Excess attenuation is that which is over and above attenuation due to normal spreading and atmospheric absorption.) The dashed curve is calculated using the coherent acoustical theory described earlier. At frequencies below about 300 Hz, this theory adequately describes the measured values. However, above 300 Hz, the coherent theory begins to consistently overpredict the depth of the ground shadow at a distance of 100 m. The discrepancy between the measured points and the solid curve reaches about 10 dB at a distance of 1 km. The solid curves were calculated (ref. 38) by treating the atmosphere as a turbulent medium and assuming a normal distribution of phase velocities of sound having a standard deviation of about 2 parts per 1000 and some partial coherence between the direct and the reflected path. Theory (refs. 38–40) shows that the partial coherence between the two paths is very sensitive to the ratio of path separation and coherence length of the medium. A coherence length of about 1 m, typical of values measured close to the ground, was used to calculate the curves in figure 18. To assume partial, rather than complete, coherence between the interfering waves is the only simple way to obtain reasonable agreement with measurements at all frequencies and distances. Alternatives such as using a different value of ground impedance could have secured agreement at some frequencies only at the expense of worse agreement elsewhere in the spectrum or at other distances.

Another example of the degradation of an acoustical shadow region was discussed in the previous section. The measurements shown by the open symbols in figure 14 suggest that, in addition to the energy that is diffracted into the shadow region, the sound scattered by turbulence is contributing to the total level. Although there is as yet no direct quantitative calculation to support this hypothesis, it is consistent with model experiments (ref. 41) using thin barriers.

In summary, atmospheric turbulence was evoked in the past to account for decreased sound levels that did not appear to have any other explanation. However this was before the role played by many of the relevant wave propagation mechanisms had been appreciated. Now work is showing why, and to what extent, turbulence enhances the sound levels in the various types of shadow regions.

Discussion

Up to now we have discussed the consequences of the finite impedance of the ground on sound propagation outdoors in an ideal atmosphere. The discussion was then extended to a stratified atmosphere with curved ray paths, but in the absence of

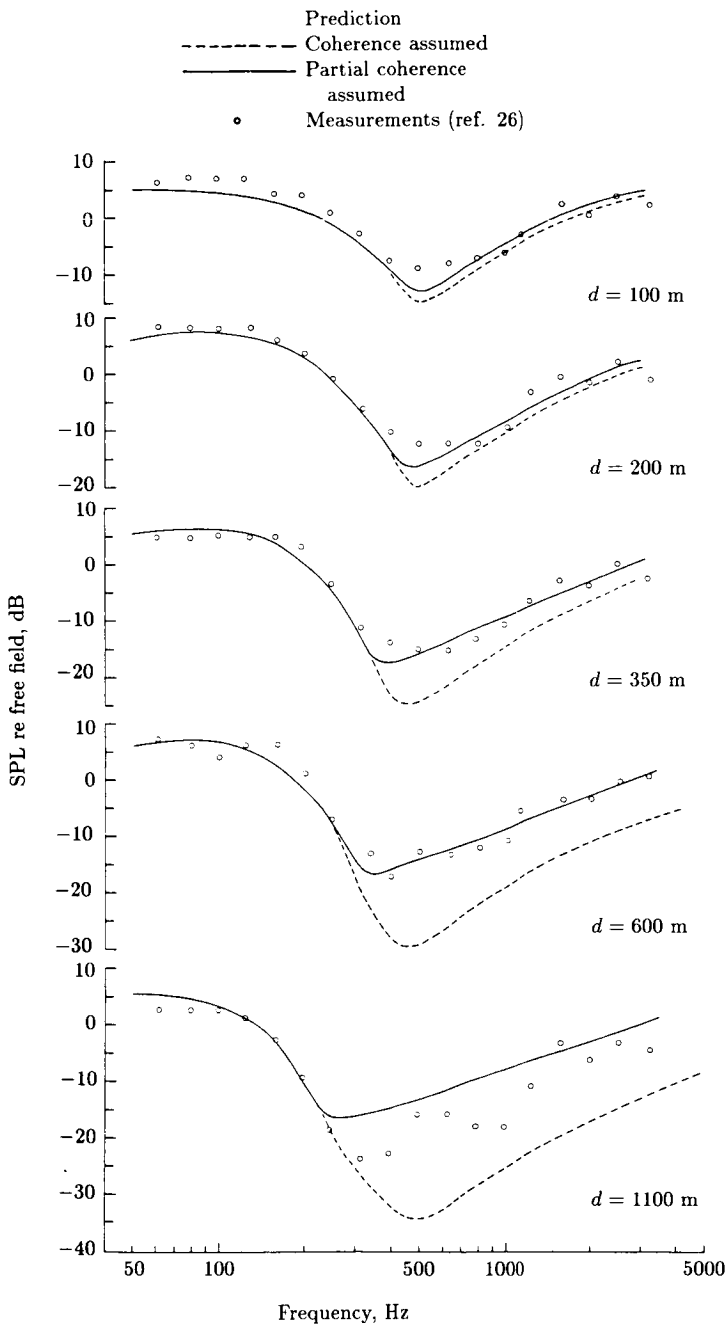

Figure 18. Comparison of measured sound levels (ref. 26) with values predicted from theory for jet noise propagating over a grass-covered field. (From ref. 38.)

turbulence, and subsequently to include the effects of the turbulent atmosphere, but for straight line propagation. It is possible, at least theoretically, to assume straight line propagation in a turbulent atmosphere. This could happen for propagation downwind on a sunny day when, fortuitously, the wind velocity gradient equals the temperature gradient in magnitude but differs in sign, to produce a zero sound speed gradient. In practice, situations do occur where the sound speed gradient is negligibly small and there is a body of theory (refs. 33 and 38–40) that accounts for partial coherence due to turbulence and which shows reasonable agreement with measurements (refs. 33 and 38).

However the idealization of a nonturbulent but stratified atmosphere may be rarely achieved in practice. The presence of strong wind and temperature gradients is usually accompanied by atmospheric turbulence. An exception could be a temperature inversion in the absence of wind. Fortunately it is not difficult to extend an existing model (ref. 27) to allow for partial coherence between the curved ray paths.

An example of such a calculation is shown in figure 19. The curves are calculated relative sound pressure levels as a function of distance for two frequencies and three atmospheric conditions. The solid curves assume propagation above grass-covered ground in a zero sound speed gradient but in the presence of atmospheric turbulence which could correspond to a Turner class (ref. 33) of 1. This calculation has been previously presented for one frequency in reference 31. At 125 Hz or any other low frequency the result is indistinguishable from theory that neglects atmospheric turbulence. However at 1.2 kHz the solid curve differs significantly from the prediction of coherent theory. This latter theory begins to predict lower sound pressure levels at a distance of about 50 m to attain −25 dB at 1 km, for a discrepancy of 15 dB between coherent theory and the solid curve.

The short-dashed curves are calculated for a slightly less turbulent atmosphere but, in addition, for a positive sound speed gradient (downward refraction). Beyond 400 m, ray theory predicts the existence of additional ray paths (see eq. (15)). At 125 Hz the results differ little from coherent theory. On the other hand at 1.2 kHz, the increased incidence angle, the additional ray paths beyond 400 m, and the loss of coherence all contribute to almost eradicating the attenuation produced by the finite impedance of the ground (at the larger distances where there are many ray paths, a simpler calculation was performed (ref. 25)).

The long-dashed curves were calculated for a slightly more turbulent atmosphere than the short-dashed curves but now for a negative sound speed gradient (upward refraction). The shadow boundary expected from ray theory occurs at 400 m. Therefore, beyond 400 m the curve is calculated using diffraction theory (ref. 31). At 125 Hz the long-dashed curve differs from the solid curve only beyond 400 m, that is, in the shadow region that exists in this case. At 1.2 kHz the long-dashed curve differs negligibly from the result that would be obtained using coherent theory up to about 400 m. This is because the reduced incidence angle of the reflected wave produces lower sound pressure levels which are then enhanced because of partial coherence between direct and reflected waves. For this particular calculation the two effects almost cancel. Beyond 400 m the levels are determined by diffraction theory up to some relative sound pressure levels shown by the shaded area. The body of available experimental data (refs. 3, 26, and 31) shows that, in practice, lower sound pressure levels are not achieved in a turbulent atmosphere. There is no

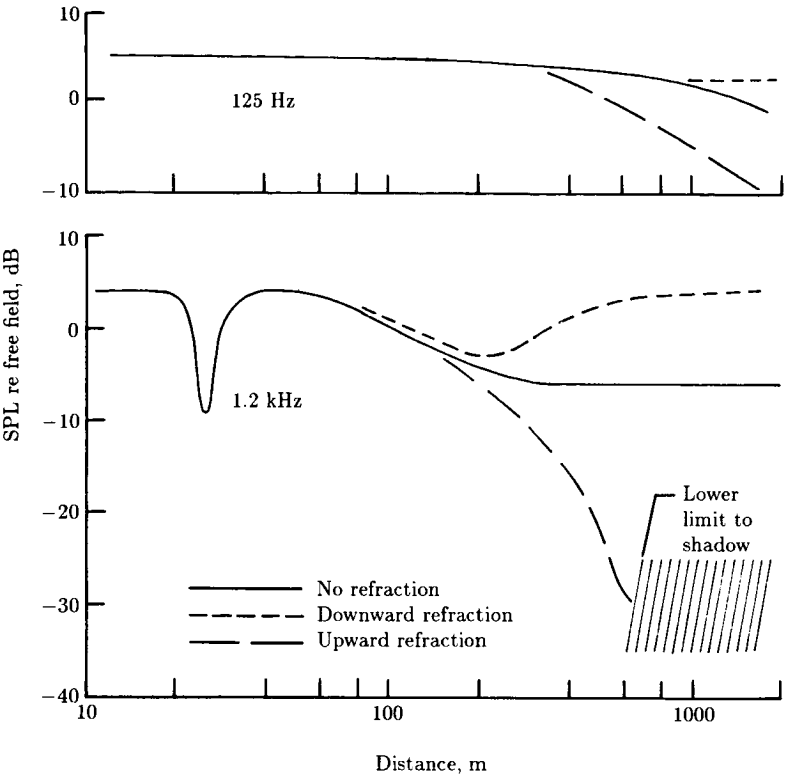

Figure 19. Comparison of predicted sound pressure levels as a function of distance for two frequencies and three atmospheric conditions. Propagation over grass in presence of atmospheric turbulence.

rigorous theory to substantiate this at present. However there is some theory (ref. 41) and experimental evidence (ref. 31) to support the explanation that scattering by turbulence is responsible for these limiting sound pressure levels.

The features shown for the 1.2-kHz calculation are also found for frequencies between 200 and 2000 Hz, but differ in detail. The results also differ in detail for different atmospheric conditions, but the main tendencies remain. The curves are examples of typical behavior justified on physical arguments and are consistent with the behavior of experimental data (see fig. 13 of ref. 31 and the data in ref. 26).

In summary, because of variations in atmospheric conditions, it is not possible to produce a unique prediction of sound pressure levels, especially for distances greater than about 50 to 100 m. The levels will not exceed those given by inverse square law and molecular absorption (unless there are sufficient multiple downward refractive paths in which case the level may be enhanced by 1 to 2 dB) but can be, and usually are, lower because of a combination of other mechanisms; the levels are rarely lower by more than −25 to −35 dB because of the turbulent atmosphere.

Diffraction

The processes of diffraction arise from the mutual interaction of neighboring elements of a wave field. They occur when the amplitude and phase of the sound

field vary spatially in ways that are incompatible with the sound wavelength at any given frequency. Far from any boundaries a sound field propagates in a relatively simple way, and one can exploit this simplicity by describing the propagation in terms of ray paths. However if a large solid body blocks the sound field, the ray theory of sound propagation predicts a shadow region behind the body with sharply defined boundaries, so in principle, on one side of the boundary there is a sound field with well-defined phase and amplitude and close by on the other side of the boundary there is essentially silence. This does not happen in practice; as the waves propagate, sound "leaks" across this sharp boundary in ways governed by the laws of wave motion and the boundary becomes less sharp. Diffraction effects are most clearly evident in the vicinity of solid boundaries, or along geometrical ray boundaries such as the limiting ray shown in figure 13.

Acoustic diffraction occurs in conjunction with a wide range of solid bodies: some such as thin solid barriers are erected alongside highways or are carefully located to shield residential communities from ground operations of aircraft; others such as buildings are often built for other purposes but fortuitously provide some beneficial shielding; yet others like undulating ground or low hills occur naturally and provide shielding at much larger distances and bring forth other manifestations of diffraction such as the creeping waves referred to earlier.

Most of the development of diffraction theory for sound waves has been adapted from optical diffraction theory (refs. 42–44). It has been applied mainly to understand and accurately predict the performance of thin barriers, including the practical situations of barriers standing on ground of finite impedance, where effects due to ground reflections and interference interact with diffraction of sound over the top of the barrier (ref. 45). Other developments have been to describe the shielding behavior of thick barriers (refs. 46 and 47), such as buildings or earth berms.

The simplest and most widely used procedure for determining the reduction of sound pressure level due to diffraction around the edge of a barrier is described in reference 48. One must first calculate the Fresnel number, which is simply the minimum increase in distance that the sound must travel around the edge of the barrier to go from source to receiver (fig. 20), divided by a half-wavelength $\lambda/2$ at the frequency of interest. The Fresnel number N is

$$N = \frac{2}{\lambda}(d_1 + d_2 - d_3) \tag{16}$$

The reduction in sound pressure level is then given as a function of Fresnel number by the curve in figure 21. This curve is obtained from diffraction theory assuming a thin knife-edge barrier and no ground and then empirically allows for the presence of the ground by reducing the loss of sound level by about 2 dB. This prediction curve is not exact because the empirical correction does not account for the frequency dependence (here, the Fresnel number dependence) of the ground-reflection interference in a specific configuration of source, barrier, and receiver heights and distances apart. The curve is correct to about ±5 dB in most cases and is the mean curve through the interference spectrum that would be measured, and can be predicted, in any specific circumstances.

In practice the reduction in sound pressure level behind a barrier rarely exceeds about 15 to 25 dB, except in extreme configurations when the diffraction angle, θ

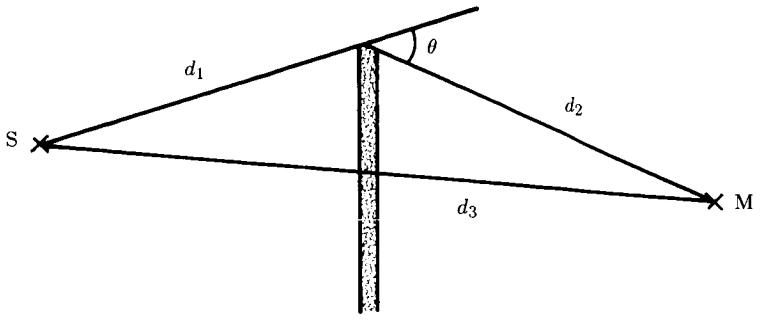

Figure 20. Schematic defining the necessary parameters for diffraction around a thin barrier.

in figure 20, is very large. More commonly the performance of a barrier is limited to these values by the effects of the turbulent atmosphere (ref. 41). As discussed previously, scattering by turbulence provides an additional mechanism by which sound energy can penetrate the shadow behind the barrier, thus resulting in an upper limit to the reduction in sound pressure level. If the barrier is not continuous, such as a row of detached houses, other empirical values are sometimes used. For example, when the gaps between houses are 30 to 50 percent of the whole, a drop of 2 to 3 dB is sometimes assumed for one row of houses, about 4 to 6 dB for two or more rows. These are obviously average values and are greater directly behind a house and much less in line with the break in the barrier.

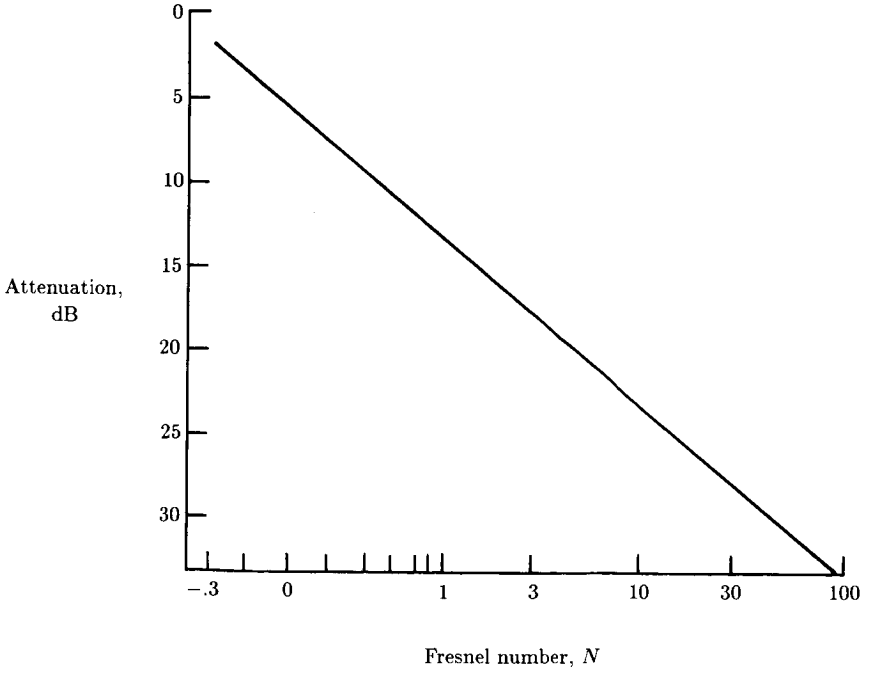

Figure 21. Reduction in sound pressure level relative to the free field without a barrier as a function of Fresnel number N. (Curve from ref. 48.)

When barriers are used specifically to reduce sound, it is good practice to locate them, when possible, as closely as possible to either the source or the receiver. A barrier of given height then results in a large value of the diffraction angle θ and a greater path lengthening $(d_1 + d_2 - d_3)$. This provides a larger insertion loss and also more protection against degradation of this insertion loss by refractive effects that, under appropriate meteorological conditions, can cause the direct sound field to curve around the edge of the barrier. It is difficult to be precise because the variables are so many, but refractive effects can often bend sound fields through a few degrees in a distance of 100 m: this suggests that the diffraction angle θ must be at least 5° for a sound barrier to provide some amount of diffractive shielding under most meteorological conditions.

At distances between source and receiver greater than a few hundred meters, it is difficult to provide man-made barriers large enough to provide any noticeable reduction in sound pressure levels. Naturally occurring topographical features such as hills can often function as barriers, blocking the line of sight between source and receiver. There has been very little systematic study of the acoustical effects of terrain shape and type at long ranges, partly because of the wide range of possible forms and the difficulties of understanding the general principles that could then be applied to other terrains and partly because dominant meteorological effects would often cast considerable uncertainty on any terrain-related results. The processes of diffraction can however assist in understanding one very simple form of ground shape, namely a spherical or cylindrical surface that curves downward. There is a close analogy between a ground surface that curves downward in conjunction with sound rays that travel in straight lines and a ground surface that is flat while sound rays curve upward because of a temperature lapse or upwind propagation. The analogy is shown in figure 22, where the reader will recognize that figure 22(b) has extracted the relevant features from figure 13 that was earlier used to describe the behavior of sound fields in upward refraction due to meteorological gradients. Measurements and relevant theory (refs. 49–52) on grass and asphalt surfaces outdoors and artificial surfaces indoors having shapes corresponding to figure 22(a) are the subject of current work. Typical results (ref. 49) for propagation around a grass-covered cylindrical mound having a radius of curvature of 25 m are shown in figure 23 for two source-to-receiver distances and three receiver heights all within the shadow region.

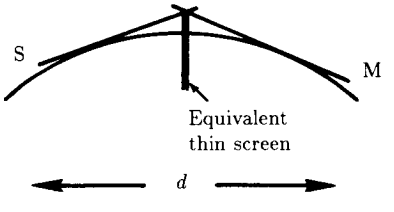

Sketch A

The short dash curves in figure 23 represent the prediction of simple diffraction theory when the curved surface is replaced by an equivalent thin barrier, with the height of the equivalent barrier being determined by line-of-sight geometry as shown in sketch A on the left. This prediction is reasonably good at low frequencies, here below about 500 Hz, but at higher frequencies it underestimates the measured shadow by as much as 20 dB. The short-long dashed line in figure 23 is the prediction for creeping-wave diffraction mechanisms assuming a surface of infinite impedance, and the lower solid line was calculated (ref. 51) assuming a grass-covered surface of finite acoustic impedance. The trend of the measured values is clear for both receiver heights and is as expected from the ground impedance values shown in figure 5—at the lower frequencies the ground impedance is higher and can be idealized as a rigid boundary;

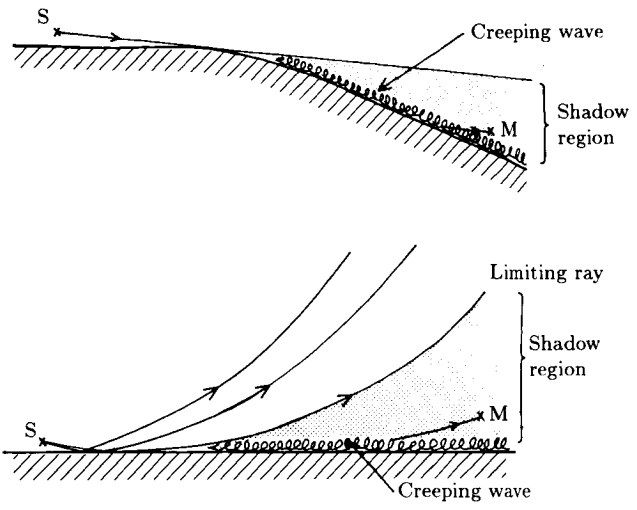

Figure 22. Analogy between sound propagation in a homogeneous, isotropic atmosphere over downwardly curving ground and sound propagation in an upwardly refractive atmosphere, above a flat ground.

as frequency increases there is a smooth transition to the predictions assuming a low acoustic impedance. The discrepancy between the measured points and the lower solid line at $d = 11$ m and $h_r = 0.25$ m is attributed to atmospheric turbulence (ref. 41).

Thus we see that diffractive mechanisms play an important part in the propagation of sound fields. These mechanisms are responsible for determining the sound pressure levels in acoustical shadow regions, whether these shadow regions are produced by solid obstacles at short or long ranges or by refractive processes causing the upward bending of sound rays.

Large-Amplitude Waves, Pulses, and Sonic Booms

The discussion of sound propagation mechanisms so far in this chapter, as in most of the acoustical literature, has assumed that sound waves propagate according to linear laws in a linear medium. It has been assumed, for example, that the speed of sound is a constant determined only by the properties of the air, principally its temperature; that the frequency and wavelength of a given sound do not change during propagation or as the sound is subjected to any of the mechanisms described so far; and that the amplitude of the sound, and its spectral content, change during these processes by the same fraction (or its sound pressure level by the same number of decibels) regardless of whether the sound initially has a high or a low sound pressure level. For many acoustical problems the assumptions of linearity, superposition of waves, and the approximations of small-amplitude acoustics are perfectly adequate.

When a sound source is sufficiently intense or when the sound field remains at a high enough level for a sufficient distance of propagation, then nonlinearity of many of the wave propagation processes becomes important, gives rise to many further phenomena, and can significantly affect the sound received by a distant observer.

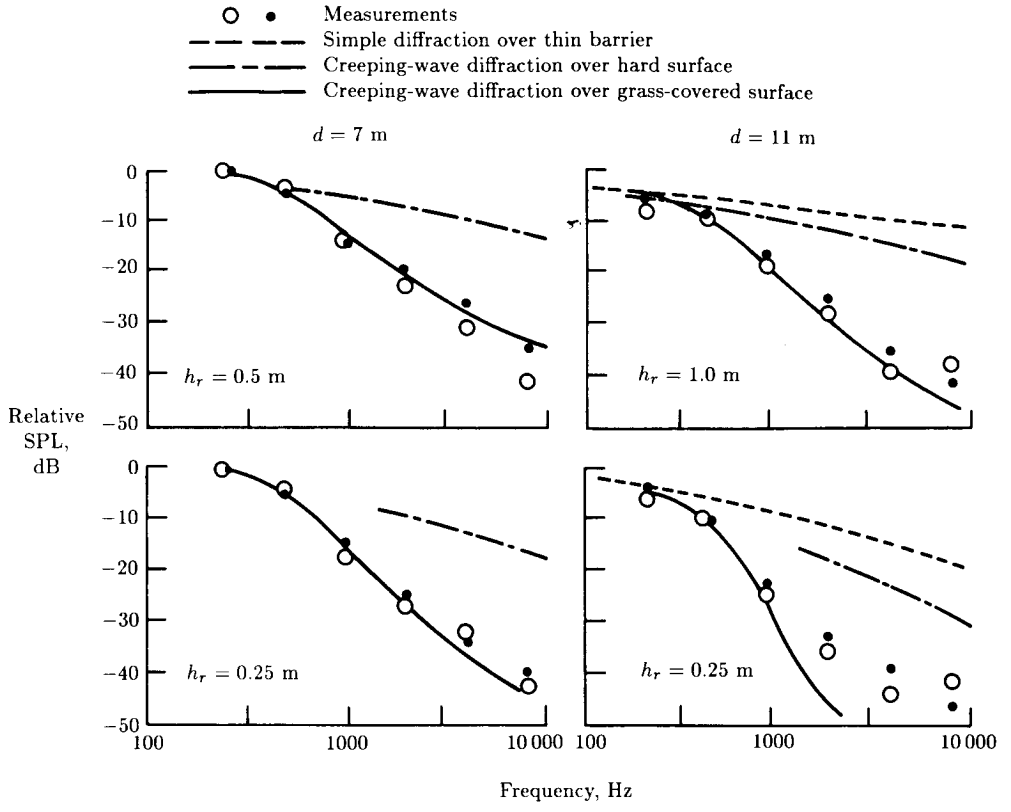

Figure 23. Sound pressure levels over a grass-covered curved ground with radius of curvature of 25 m. Source on the ground.

Here we shall focus attention on one small group of nonlinear phenomena that are all related to the fact that the propagation speed of any part of the waveform depends on its own particular particle velocity. The result is that waveforms change shape during propagation, their spectral content changes, shock waves may develop, and there is increased absorption.

Waveform Distortion

As a sound wave propagates through air, the instantaneous pressure, particle velocity, temperature, and density at any point in the waveform all vary simultaneously and are closely related. In that part of the waveform where the pressure increases, the temperature and density also increase, and the longitudinal particle velocity due to the wave is in the direction in which the wave energy is propagating. (Conversely when the pressure, temperature, and density simultaneously decrease, the particle velocity is in the opposite direction to that in which the energy is being propagated.) The zero crossings of the sound waveform travel with the "small-amplitude" speed of sound, c_o = 331.2 m/sec at 0°C, which is the speed of sound described earlier. However other parts of the waveform, which we intuitively and most commonly think of as a pressure waveform, each travel relative to the local part of the propagation medium (refs. 53 and 54). There are two distinct effects on the speed with which

individual elements of the waveform propagate. Consider an element of the wave having an instantaneous positive pressure: first the temperature is momentarily increased due to the sound wave and so the local speed of sound is increased to a value given by

$$c = c_o + \frac{\gamma - 1}{2} u \tag{17}$$

where γ is the ratio of specific heats of air ($\gamma \approx 1.4$) and u is the local particle velocity. Second the waveform travels relative to the local medium which in this region of positive pressure is traveling in the forward direction, also with the particle velocity u. The net result is that this part of the waveform travels with a velocity

$$c = c_o + \frac{\gamma - 1}{2} u + u = c_o + \frac{\gamma + 1}{2} u \tag{18}$$

Equation (18) is a general result that applies to all elements of a continuous waveform; in particular when the acoustic pressure is negative, the particle velocity is in the opposite direction and the negative half-cycle of the waveform travels in the direction of propagation more slowly than the zero crossings. Furthermore the excess velocity relative to c_o for the zero crossings is proportional to the particle velocity u (or proportional to the acoustic pressure p through the impedance relation $p/u = \rho c$ where ρ is density). Thus the positive peak of a waveform travels fastest and "catches up" to the zero crossing ahead of it, while at the same time increasing its separation from the zero crossing that follows it. The opposite process occurs for the negative peak of the waveform. The net result of these differences in propagation speed is that the waveform changes shape during propagation as illustrated in figure 24.

Figure 24 represents the pressure vs. time waveform that would be detected at successively increasing distances of propagation. The wave is assumed to be an infinitely long series of initially sinusoidal waveforms, one cycle of which is shown in figure 24(a); it propagates from right to left, and retarded time is used to reduce the corresponding zero crossings to $t = 0$ in each case. In those parts of the waveform where $\partial p/\partial t$ is positive, this gradient increases with distance of propagation; where negative, this gradient becomes less steep. At some distance the rate of change in pressure may become infinitely steep (in reality, it is finite but can take place over a distance of the order of a mean free path of the gas molecules if the pressure difference is sufficiently great) and this denotes the formation of a shock wave. In an initially symmetrical sinusoidal waveform this discontinuity occurs at those zero crossings where pressure is increasing (fig. 24(c)). As the waveform continues to propagate, the shock wave extends over a bigger change in pressure as regions of lesser pressure immediately ahead are overtaken by it, and higher pressure regions behind the shock catch up to it. A shock wave represents an abrupt change in acoustic pressure and a discontinuity in particle velocity, but once formed it travels with a velocity that is the mean of that associated with the pressures and velocities immediately ahead of and behind it. Hence, for an initially symmetrical sinusoidal waveform, the resulting shock waves remain symmetrical and travel with the small-amplitude speed of sound with the result that each cycle of the wave train remains of constant wavelength and fundamental frequency.

Once a shock wave is formed, continued use of equation (18) leads to the situation shown by the dotted waveform in figure 24(d), in which three different pressures

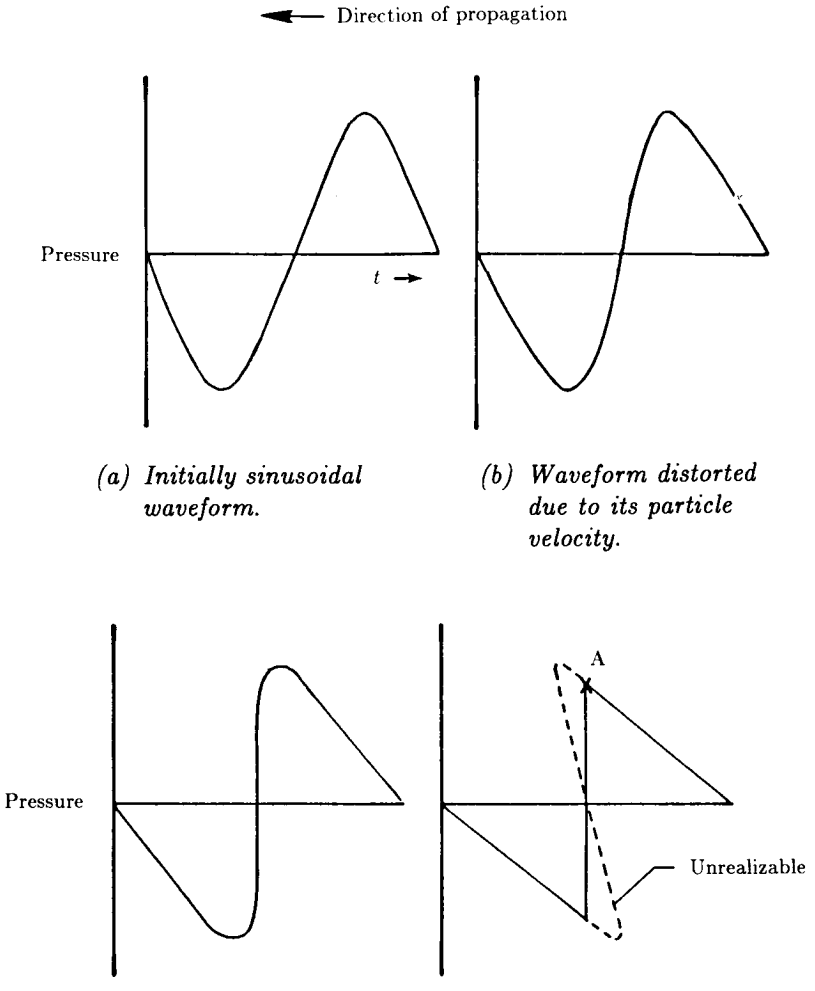

(a) Initially sinusoidal waveform.

(b) Waveform distorted due to its particle velocity.

(c) Discontinuity in pressure where $\partial p/\partial t$ was initially largest.

(d) After shock wave has formed.

Figure 24. Schematic of large-amplitude continuous waves at increasing distances of propagation, showing pressure changes as a function of time.

would coexist simultaneously at the same place—an obvious impossibility. Instead, the shock continues to propagate with an excess velocity which is nominally zero in a continuous, symmetrical waveform, and the region where $\partial p/\partial t$ is negative becomes less steep (eq. (18) still applies in this region). In particular, the element either at, or just behind, the peak marked "A" in figure 24(d), continues to propagate with a velocity given by equation (18) and so coalesces with the shock wave. Thus an element, such as point A, that has a pressure just more than the pressure in the shock wave catches up to the shock because of its greater velocity to produce a more rapid reduction in pressure amplitude than would be predicted by linear absorption

or dissipation mechanisms. Similar processes occur on the low pressure side of the shock, with the result that the magnitude of the shock is eroded from both sides simultaneously. This enhanced rate of dissipation of acoustic energy is caused by the enhanced rate of conversion of this energy into heat through thermal and viscous processes associated with the very large thermal gradients across the shock front.

We have so far in this section described the nonlinear distortion of a sound wave in terms of its waveform as a function of time. An equally valid approach is to consider the change in its spectrum. The spectrum of an initially sinusoidal wave (fig. 24(a)) is a single frequency f_1 having a wavelength λ_1 given by $\lambda_1 = c_o/f_1$. As the wave propagates and progressively distorts, in the limit into a train of triangular waveforms, as shown by the solid line waveform in figure 24(d), the initial single-frequency spectrum f_1 changes to include higher harmonics nf_1 (where n is an integer). Before shocks have formed (figs. 24(a) and (b)), the amplitude of the second harmonic in a spherically spreading wave grows at a rate given by (ref. 55)

$$\frac{dp_2}{dx} = A_2(p_1)_0^2 \left(\frac{x_0}{x}\right)^2 e^{2\alpha_1(x-x_0)} - \frac{p_2}{x} - \alpha_2 p_2 \tag{19}$$

In equation (19) the first term represents the growth of the second harmonic from the fundamental at a rate depending (ref. 56) on the square of the fundamental amplitude $(p_1)_0$ which is itself subject to geometrical spreading (x_0/x) and to a small-amplitude attenuation coefficient α_1. The second term p_2/x represents the geometrical spreading of the second harmonic with distance of propagation, and the third term its dissipative attenuation. Expressions similar to equation (19) can be developed for higher harmonics and integrated to obtain the amplitudes of each harmonic as a function of the distance of propagation. These details are beyond the scope of this summary and interested readers are referred to references 54 and 55. In equation (19) for a spherically spreading finite-amplitude wave, the rate of generation of the second harmonic decreases as x^{-2}, more rapidly than the magnitude of either the first or the second harmonic, both of which decrease as x^{-1}.

Large-Amplitude Pulses

The large-amplitude waves considered so far have been assumed to be repetitive and symmetrical. Many large-amplitude waves are, however, transient pulses such as blasts, gun shots, or sonic booms. In these waves the initial pressure disturbance, usually an increase in pressure, propagates into undisturbed air (fig. 25(a)). Subsequent parts of the disturbance can have various forms such as a decaying oscillatory waveform or after one or two half-cycles a more or less immediate return to a relatively undisturbed state.

As before, nonlinear distortion occurs due to the finite magnitude of the particle velocity u, as described by equation (18). The pulse becomes more distorted during propagation, and at some distance a shock may form in the pulse where the pressure rise time $\partial p/\partial t$ was initially steepest. For simplicity of description (and this is often the case of practice), we assume that this is at the beginning of the pressure disturbance. The zero crossings of the pressure pulse, up to this time (fig. 25(b)) travel with the small-amplitude sound speed c_o. Once a shock has formed, it propagates with a velocity that is the mean of that associated with conditions immediately ahead of and behind it. This excess velocity is in the direction of

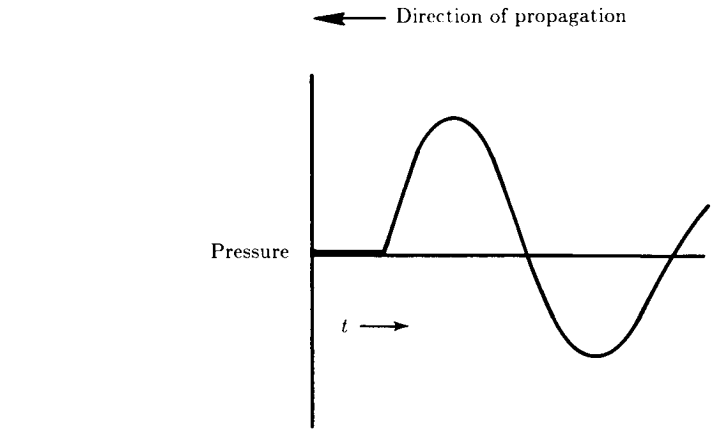

(a) Decaying sine waveform.

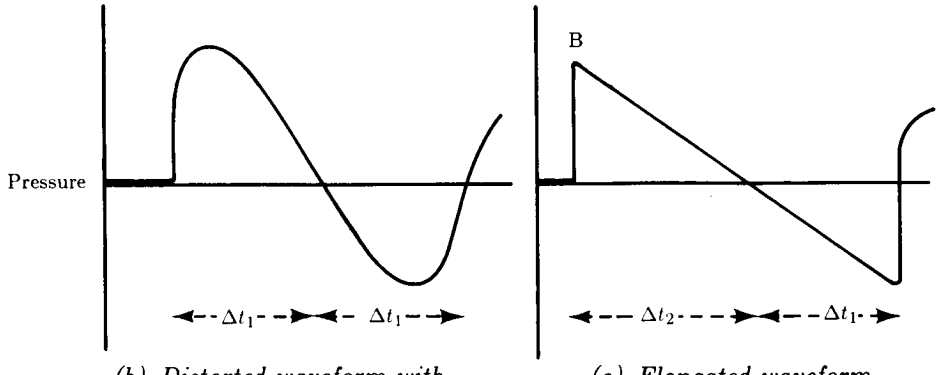

(b) Distorted waveform with shock where pressure gradient was initially steepest.

(c) Elongated waveform.

Figure 25. Schematic of a large-amplitude sound pulse at increasing distances of propagation showing pressure changes as a function of time.

propagation and causes the first half-cycle of the pulse to elongate as the pulse continues to propagate—later half-cycles of the pulse remain of constant duration Δt_1, until nonlinear distortion causes further and often unsymmetrical shocks to form in those parts of the pulse. This is illustrated in figure 25(c) where one notes that the first half-cycle has a duration Δt_2 that is longer than that of the second half-cycle of duration Δt_1. If we denote the particle velocity of the first peak of the wave, B in figure 25(c), by $u_{\max}$, then the velocity of the head shock for a pulse is given by

$$c = c_o + \frac{\gamma + 1}{4} u_{\max} \tag{20}$$

The second most likely place for a shock to form is at the end of the second half-cycle of the pulse, as shown in figure 25(c). This represents a typical N-wave, so-called because of its shape. Given the asymmetry of pressure usually associated with this tail shock, its mean velocity in the direction of propagation of the pulse is less than that of the zero crossings. Thus the head shock travels faster than c_o and the tail

shock slower, so that both contribute to the lengthening of the pulse, or equivalently an increased time duration between the head and tail shocks. The lengthening of a pulse traveling into undisturbed air is a feature that does not occur during the propagation of large-amplitude continuous waves even when shocks are present.

In terms of the spectrum of the pulse, this lengthening process represents a shift in the sound energy to lower frequencies as propagation proceeds. This is in sharp contrast to the shift in sound energy to higher frequencies as described earlier that is related to the nonlinear distortion from an initially more or less sinusoidal waveform to one having a more nearly triangular or saw-toothed shape—a process that occurs both in pulses and in continuous waves of large amplitude.

Sonic Booms

An important type of large-amplitude acoustic pulse is that caused by a body traveling faster than the local speed of sound (refs. 57 and 58). Of particular interest is the sonic boom caused by an aircraft flying supersonically. Because the aircraft is flying supersonically, pressure discontinuities (shock waves) are produced instantaneously at the source and are not produced by waveform distortion during propagation. Booms recorded on the ground from high flying aircraft are often good approximations to N-waves. If the aircraft is long or is flying sufficiently high for the N-wave to lengthen appreciably during propagation over a large distance, the head and tail shocks can be heard as two separate events between which there is a brief period of quiet. Reference 59 quotes results from several NASA Technical Notes showing that the time between head and tail shocks for a fighter aircraft increases systematically from about 50 msec to about 90 msec during propagation from 20 m to 3 km.

These authors (ref. 59) and others show that the pulse shape measured near a supersonic aircraft is not a simple N-wave but exhibits fine structure relating to the details of the aircraft's cross-sectional area and lift distribution. Each increase in cross-sectional area, such as the nose or leading edge of wing, produces its own head shock; and each decrease, such as the back end of the fuselage or wing, its own tail shock. However, following the same principles of propagation as described earlier, each head shock that starts out situated part way along the pulse, for example, that due to the leading edge of the wing, propagates faster than the local speed of sound, and makes its way forward in the pulse as the whole pulse propagates away from the aircraft. At a sufficient distance, all such intermediate head shocks coalesce with the frontmost head shock to produce a single head shock representing the beginning of the N-wave. Similarly all the intermediate tail shocks, traveling more slowly than the local speed of sound eventually coalesce into a single tail shock representing the end of the N-wave.

It is sometimes observed that sonic boom waveforms differ noticeably from well-defined N-waves. These discrepancies usually occur close to the head and tail shocks and rarely in the intermediate parts of the waveform. The peaks of the waveform may be very significantly rounded in shape; at other times the peaks appear to have sharp spikes superimposed on them. These effects are caused by propagation of the waves through turbulence and by refractive effects that can cause focusing or defocusing of the N-wave pulses at particular measuring locations. Focusing and defocusing of the waves can also be caused by aircraft maneuvers such as acceleration in straight

flight or turns. These factors have been studied by numerous workers and the reader should consult the literature for details (refs. 60–63).

Standards

The various sound propagation mechanisms described in the earlier sections of this chapter have all been studied and quantified by means of measurements. In some cases the measuring instruments used and methods of calculation or theories developed for these phenomena have been agreed upon and are now embodied in a number of national or international standards. A few of these standards are specific to noise from aircraft, but most are of more general application and relate to acoustical measurements of sound from almost any type of source. Here we can merely comment briefly on a number of these standards because standards are carefully developed precise documents, and anyone wishing to use a procedure described in a standard should refer to the standard itself.

The standard ANSI S1.13–1971 (R1986) (ref. 64) provides guidelines for the measurements of many different types of sound in various situations. A new standard is being developed to address specifically the special problems of measurement of sound pressure levels outdoors. The standards IEC 651(1979) (ref. 65) and ANSI S1.4–1983 (ref. 66) deal with the basic sound measurement system and specify frequency weighting and time constants. The standards ANSI S1.6–1984 (ref. 67), ANSI S1.8–1969 (R1974) (ref. 68) and ISO 1683–1983 (ref. 69) attempt to provide uniformity in the reporting of results. The latter two standards differ over the reference quantities to be used for vibratory velocity and acceleration. A major revision of ANSI S1.11 has been undertaken and the revised version, ANSI S1.11–1976 (R1986) (ref. 70), includes specifications for both digital and analog filters. The standard ANSI S1.26–1978 (ref. 5) relates directly to the propagation phenomenon described earlier in this chapter. It is currently undergoing revision to allow for more realistic values of attenuation at low frequencies and to include methods for calculating the attenuation of bands of noise and for calculating attenuation along a propagation path where the atmospheric properties change, for example, with altitude. Several other standards relate to specific types of aircraft operation under specific circumstances: SAE AIR-923 (ref. 71), SAE AIR-1672B (ref. 72), ISO 2249-1973 (ref. 73), and IEC 561(1976) (ref. 74).

The use of standard measurement procedures and methods of calculation has the obvious advantage of uniformity and of increasing the comparability of measurements made at different locations and times. However, in the subject of atmospheric sound propagation our collective knowledge of the several mechanisms involved and how they interact has advanced rapidly. For this reason, the discussion of some of the mechanisms in this chapter is based on new understanding that was not available at the time some of the standards were written.

References

1. Hunt, Frederick V.: *Origins in Acoustics.* Yale Univ. Press, 1978.
2. Lenihan, J. M. A.: Mersenne and Gassendi. *Acustica,* vol. 1, no. 2, 1951, pp. 96–99.
3. Piercy, J. E.; Embleton, T. F. W.; and Sutherland, L. C.: Review of Noise Propagation in the Atmosphere. *J. Acoust. Soc. America,* vol. 61, no. 6, June 1977, pp. 1403–1418.
4. Embleton, T. F. W.: Sound Propagation Outdoors—Improved Prediction Schemes for the 80's. *Noise Control Eng.,* vol. 18, no. 1, Jan.–Feb. 1982, pp. 30–39.

5. *American National Standard Method for the Calculation of the Absorption of Sound by the Atmosphere.* ANSI S1.26-1978 (ASA 23-1978), American Natl. Standards Inst., Inc., June 23, 1978.
6. Bass, H. E.; Sutherland, L. C.; Piercy, Joe; and Evans, Landon: Absorption of Sound by the Atmosphere. *Physical Acoustics, Volume XVII,* Warren P. Mason and R. N. Thurston, eds., Academic Press, Inc., 1984, pp. 145–232.
7. *Standard Values of Atmospheric Absorption as a Function of Temperature and Humidity for Use in Evaluating Aircraft Flyover Noise.* ARP 866A, Soc. Automot. Eng., Aug. 1964.
8. Zuckerwar, Allan J.; and Meredith, Roger W.: Low-Frequency Absorption of Sound in Air. *J. Acoust. Soc. America,* vol. 78, no. 3, Sept. 1985, pp. 946–955.
9. Wait, James R.: *Electromagnetic Waves in Stratified Media, Revised Edition Including Supplemented Material.* Pergamon Press Inc., c.1970.
10. Dickinson, P. J.; and Doak, P. E.: Measurements of the Normal Acoustic Impedance of Ground Surfaces. *J. Sound & Vib.,* vol. 13, no. 3, Nov. 1970, pp. 309–322.
11. Embleton, T. F. W.; Piercy, J. E.; and Olson, N.: Outdoor Sound Propagation Over Ground of Finite Impedance. *J. Acoust. Soc. America,* vol. 59, no. 2, Feb. 1976, pp. 267–277.
12. Zuckerwar, Allan J.: Acoustic Ground Impedance Meter. *J. Acoust. Soc. America,* vol. 73, no. 6, June 1983, pp. 2180–2186.
13. Allard, Jean F.; and Sieben, Benita: Measurements of Acoustic Impedance in a Free Field With Two Microphones and a Spectrum Analyzer. *J. Acoust. Soc. America,* vol. 77, no. 4, Apr. 1985, pp. 1617–1618.
14. Daigle, G. A.; and Stinson, Michael R.: Impedance of Grass-Covered Ground at Low Frequencies Measured Using a Phase Difference Technique. *J. Acoust. Soc. America,* vol. 81, no. 1, Jan. 1987, pp. 62–68.
15. Chessell, C. I.: Propagation of Noise Along a Finite Impedance Boundary. *J. Acoust. Soc. America,* vol. 62, no. 4, Oct. 1977, pp. 825–834.
16. Delany, M. E.; and Bazley, E. N.: Acoustical Properties of Fibrous Absorbent Materials. *Appl. Acoust.,* vol. 3, no. 2, Apr. 1970, pp. 105–116.
17. Embleton, T. F. W.; Piercy, J. E.; and Daigle, G. A.: Effective Flow Resistivity of Ground Surfaces Determined by Acoustical Measurements. *J. Acoust. Soc. America,* vol. 74, no. 4, Oct. 1983, pp. 1239–1244.
18. Attenborough, K.: Acoustical Impedance Models for Outdoor Ground Surfaces. *J. Sound & Vib.,* vol. 99, no. 4, Apr. 22, 1985, pp. 521–544.
19. Nicolas, J.; Berry, J.-L.; and Daigle, G. A.: Propagation of Sound Above a Finite Layer of Snow. *J. Acoust. Soc. America,* vol. 77, no. 1, Jan. 1985, pp. 67–73.
20. Naghieh, M.; and Hayek, Sabih I.: Diffraction of a Point Source by Two Impedance Covered Half-Planes. *J. Acoust. Soc. America,* vol. 69, no. 3, Mar. 1981, pp. 629–637.
21. Rasmussen, K. B.: A Note on the Calculation of Sound Propagation Over Impedance Jumps and Screens. *J. Sound & Vib.,* vol. 84, no. 4, Oct. 22, 1982, pp. 598–602.
22. De Jong, B. A.; Moerkerken, A.; and Van der Toorn, J. D.: Propagation of Sound Over Grassland and Over an Earth Barrier. *J. Sound & Vib.,* vol. 86, no. 1, Jan. 8, 1983, pp. 23–46.
23. Koers, Peter: Diffraction by an Absorbing Barrier or by an Impedance Transition. *Noise Control: The International Scene, Proceedings—Inter-Noise 83, Volume 1,* Inst. of Acoustics (Edinburgh, U.K.), c.1983, pp. 311–314.
24. Daigle, G. A.; Nicolas, J.; and Berry, J.-L.: Propagation of Noise Above Ground Having an Impedance Discontinuity. *J. Acoust. Soc. America,* vol. 77, no. 1, Jan. 1985, pp. 127–138.
25. Embleton, T. F. W.; Thiessen, G. J.; and Piercy, J. E.: Propagation in an Inversion and Reflections at the Ground. *J. Acoust. Soc. America,* vol. 59, no. 2, Feb. 1976, pp. 278–282.
26. Parkin, P. H.; and Scholes, W. E.: The Horizontal Propagation of Sound From a Jet Engine Close to the Ground, at Hatfield. *J. Sound & Vib.,* vol. 2, no. 4, Oct. 1965, pp. 353–374.
27. Hidaka, Takayuki; Kageyama, Kenji; and Masuda, Sadahiro: Sound Propagation in the Rest Atmosphere With Linear Sound Velocity Profile. *J. Acoust. Soc. Japan (E),* vol. 6, no. 2, Apr. 1985, pp. 117–125.
28. Raspet, R.; Lee, S. W.; Kuester, E.; Chang, D. C.; Richards, W. F.; Gilbert, R.; and Bong, N.: Fast-Field Program for Sound Propagation in a Layered Atmosphere Above an Impedance Ground. *J. Acoust. Soc. America,* vol. 77, no. 2, Feb. 1985, pp. 345–352.

29. Lee, S. W.; Bong, N.; Richards, W. F.; and Raspet, Richard: Impedance Formulation of the Fast Field Program for Acoustic Wave Propagation in the Atmosphere. *J. Acoust. Soc. America,* vol. 79, no. 3, Mar. 1986, pp. 628–634.
30. Pierce, Allan D.: *Acoustics—An Introduction to Its Physical Principles and Applications.* McGraw-Hill Book Co., c.1981.
31. Daigle, G. A.; Embleton, T. F. W.; and Piercy, J. E.: Propagation of Sound in the Presence of Gradients and Turbulence Near the Ground. *J. Acoust. Soc. America,* vol. 79, no. 3, Mar. 1986, pp. 613–627.
32. Tatarski, V. I. (R. A. Silverman, transl.): *Wave Propagation in a Turbulent Medium.* McGraw-Hill Book Co., Inc., 1961.
33. Johnson, Mark A.; Raspet, Richard; and Bobak, Michael T.: A Turbulence Model for Sound Propagation From an Elevated Source Above Level Ground. *J. Acoust. Soc. America,* vol. 81, no. 3, Mar. 1987, pp. 638–646.
34. Daigle, G. A.; Piercy, J. E.; and Embleton, T. F. W.: Line-of-Sight Propagation Through Atmospheric Turbulence Near the Ground. *J. Acoust. Soc. America,* vol. 74, no. 5, Nov. 1983, pp. 1505–1513.
35. Brown, Edmund H.; and Hall, Freeman F., Jr.: Advances in Atmospheric Acoustics. *Rev. Geophys. & Space Phys.,* vol. 16, no. 1, Feb. 1978, pp. 47–110.
36. Brown, E. H.; and Clifford, S. F.: On the Attenuation of Sound by Turbulence. *J. Acoust. Soc. America,* vol. 60, no. 4, Oct. 1976, pp. 788–794.
37. Wenzel, Alan R.: Radiation and Attenuation of Waves in a Random Medium. *J. Acoust. Soc. America,* vol. 71, no. 1, Jan. 1982, pp. 26–35.
38. Daigle, G. A.: Effects of Atmospheric Turbulence on the Interference of Sound Waves Above a Finite Impedance Boundary. *J. Acoust. Soc. America,* vol. 65, no. 1, Jan. 1979, pp. 45–49.
39. Clifford, Steven F.; and Lataitis, Richard J.: Turbulence Effects on Acoustic Wave Propagation Over a Smooth Surface. *J. Acoust. Soc. America,* vol. 73, no. 5, May 1983, pp. 1545–1550.
40. Hidaka, T.; Kageyama, K.; and Masuda, S.: Fluctuation of Spherical Wave Propagating Over a Ground Through Atmospheric Turbulence. *J. Acoust. Soc. Japan (E),* vol. 6, no. 2, Apr. 1985, pp. 247–256.
41. Daigle, G. A.: Diffraction of Sound by a Noise Barrier in the Presence of Atmospheric Turbulence. *J. Acoust. Soc. America,* vol. 71, no. 4, Apr. 1982, pp. 847–854.
42. Keller, Joseph B.: Geometrical Theory of Diffraction. *J. Opt. Soc. America,* vol. 52, no. 2, Feb. 1962, pp. 116–130.
43. Elmore, William C.; and Heald, Mark A.: *Physics of Waves.* McGraw-Hill Book Co., c.1969.
44. Born, Max; and Wolf, Emil: *Principles of Optics,* Fourth ed. Pergamon Press Inc., 1970.
45. Isei, T.; Embleton, T. F. W.; and Piercy, J. E.: Noise Reduction by Barriers on Finite Impedance Ground. *J. Acoust. Soc. America,* vol. 67, no. 1, Jan. 1980, pp. 46-58.
46. Pierce, Allan D.: Diffraction of Sound Around Corners and Over Wide Barriers. *J. Acoust. Soc. America,* vol. 55, no. 5, May 1974, pp. 941–955.
47. Fujiwara, K.; Ando, Y.; and Maekawa, Z.: Noise Control by Barriers—Part I: Noise Reduction by a Thick Barrier. *Appl. Acoust.,* vol. 10, no. 2, Apr. 1977, pp. 147–159.
48. Maekawa, Z.: Noise Reduction by Screens. *Appl. Acoust.,* vol. 1, no. 3, July 1968, pp. 157–173.
49. Daigle, G. A.; and Embleton, T. F. W.: Diffraction of Sound Over Curved Ground. *J. Acoust. Soc. America,* vol. 79, suppl. no. 1, Spring 1986, p. S20.
50. Pierce, Allan D.; Main, Geoffrey L.; and Kearns, James A.: Curved Surface Diffraction Theory Derived and Extended Using the Method of Matched Asymptotic Expansions. *J. Acoust. Soc. America,* vol. 79, suppl. no. 1, Spring 1986, pp. S30–S31.
51. Berry, Alain; and Daigle, G. A.: Propagation of Sound Above a Curved Surface. *J. Acoust. Soc. America,* vol. 81, suppl. no. 1, Spring 1987, p. S97.
52. Berthelot, Yves H.; Kearns, James A.; Pierce, Allan D.; and Main, Geoffrey L.: Experimental Investigation of the Diffraction of Sound by a Curved Surface of Finite Impedance. *J. Acoust. Soc. America,* vol. 81, suppl. no. 1, Spring 1987, p. S97.
53. Blackstock, David T.: Connection Between the Fay and Fubini Solutions for Plane Sound Waves of Finite Amplitude. *J. Acoust. Soc. America,* vol. 39, no. 6, June 1966, pp. 1019–1026.
54. Blackstock, David T.: Nonlinear Behavior of Sound Waves. *12th International Congress on Acoustics.* Canadian Acoustical Assoc., July 1986, Plenary 3.

55. Pernet, D. F.; and Payne, R. C.: Non-Linear Propagation of Signals in Air. *J. Sound & Vib.,* vol. 17, no. 3, Aug. 8, 1971, pp. 383–396.
56. Thuras, A. L.; Jenkins, R. T.; and O'Neil, H. T.: Extraneous Frequencies Generated in Air Carrying Intense Sound Waves. *J. Acoust. Soc. America,* vol. 6, no. 3, Jan. 1935, pp. 173–180.
57. *Proceedings of the Sonic Boom Symposium. J. Acoust. Soc. America,,* vol. 39, no. 5, pt. 2, May 1966, pp. S1–S80.
58. *Sonic Boom Symposium. J. Acoust. Soc. America,* vol. 51, no. 2, (pt. 3), Feb. 1972.
59. Carlson, Harry W.; Mack, Robert J.; and Morris, Odell A.: Sonic-Boom Pressure-Field Estimation Techniques. *J. Acoust. Soc. America,* vol. 39, no. 5, pt. 2, May 1966, pp. S10–S18.
60. Kane, E. J.: Some Effects of the Nonuniform Atmosphere on the Propagation of Sonic Booms. *J. Acoust. Soc. America,* vol. 39, no. 5, pt. 2, May 1966, pp. S26–S30.
61. Maglieri, Domenic J.: Some Effects of Airplane Operations and the Atmosphere on Sonic-Boom Signatures. *J. Acoust. Soc. America,* vol. 39, no. 5, pt. 2, May 1966, pp. S36–S42.
62. Pierce, Allan D.; and Maglieri, Domenic J.: Effects of Atmospheric Irregularities on Sonic-Boom Propagation. *J. Acoust. Soc. America,* vol. 51, no. 2, pt. 3, Feb. 1972, pp. 702–721.
63. Wanner, Jean-Claude L.; Vallee, Jacques; Vivier, Claude; and Thery, Claude: Theoretical and Experimental Studies of the Focus of Sonic Booms. *J. Acoust. Soc. America,* vol. 52, no. 1, pt. 1, July 1972, pp. 13–32.
64. *American National Standard Methods for the Measurement of Sound Pressure Levels.* ANSI S1.13-1971 (R1976) (Partial revision of S1.2-1962 (R1971)), American National Standards Inst., Inc., July 14, 1971.
65. *Sound Level Meters, First ed.* Publ. 651, International Electrotechnical Commission, 1979.
66. *American National Standard Specification for Sound Level Meters.* ANSI S1.4-1983 (Revision of S1.4-1971) (ASA 47-1983), Acoustical Soc. America, 1983.
67. *American National Standard Preferred Frequencies, Frequency Levels, and Band Numbers for Acoustical Measurements.* ANSI S1.6-1984 (Rev. of S1.6-1967 (R1976)) (ASA 53-1984), Acoustical Soc. of America, 1984.
68. *American National Standard Preferred Reference Quantities for Acoustical Levels.* ANSI S1.8-1969 (R1974) (Corrected edition), American National Standards Inst., Inc., Feb. 24, 1969.
69. *Acoustics—Preferred Reference Quantities for Acoustic Levels.* ISO 1683-1983 (E), International Organization of Standards, 1983.
70. *American National Standard Specification for Octave-Band and Fractional-Octave-Band Analog and Digital Filters.* ANSI S1.11-1986 (ASA 65-1986) (Rev. of ANSI S1.11-1966 (R1976)), Acoustical Soc. of America, 1986.
71. *Method for Calculating the Attenuation of Aircraft Ground to Ground Noise Propagation During Takeoff and Landing.* AIR 923, Soc. Automotive Engineers, Mar. 1, 1968.
72. *Practical Methods To Obtain Free-Field Sound Pressure Levels From Acoustical Measurements Over Ground Surfaces.* AIR 1672B, Soc. Automotive Engineers, Inc., June 1983.
73. *Acoustics—Description and Measurement of Physical Properties of Sonic Booms.* ISO 2249-1973 (E), International Organization of Standards, 1973.
74. *Electro-Acoustical Measuring Equipment for Aircraft Noise Certification, First ed.* Publ. 561, International Electrotechnical Commission, 1976.

13 Theoretical Models for Duct Acoustic Propagation and Radiation

Lead author

Walter Eversman
University of Missouri-Rolla
Rolla, Missouri

Introduction

In the early history of jet propulsion the principal noise source was associated with the various mechanisms in the jet itself. Only in limited regions directly ahead of the engine and over limited operating conditions were noise-generating mechanisms related to the compressor important. The development of the turbofan engine, in which a significant portion of the thrust is derived from the fan stage, led to a reduction in jet noise and an increase in fan-compressor noise, thus exposing this source as one of major importance in the overall noise signature of the engine. In high-bypass-ratio turbofan engines the fan dominates the inlet-related noise, and thus we will refer to fan-compressor noise simply as fan noise.

Figure 1 shows the various noise sources in a turbofan engine and the general direction in which they are radiated. The fan is enclosed within a duct system and propagates noise upstream to be radiated from the inlet and downstream to be radiated from the fan exhaust. The acoustic system thus consists of the fan noise source, the ducts (which may be of nonuniform geometry and which may have acoustic treatment on the walls), and the exterior of the engine to which the acoustic field is radiated. The prediction of the radiated noise, and the design of the acoustic system to minimize this noise, must consider these elements. It is the purpose of this chapter to discuss techniques for the modeling of duct propagation and radiation. The source mechanisms are discussed elsewhere.

The fan duct in a typical turbofan engine, as shown in figure 1, consists of a more or less cylindrical inlet duct (which may have a centerbody) and an annular exhaust duct. Both the inlet and the exhaust duct are contoured for aerodynamic and propulsive efficiency. In modern engines there are no inlet guide vanes ahead of the fan, but there are struts or stators or both aft of the fan. The inlet duct and the exhaust duct have a length about the same or less than the inlet diameter. For

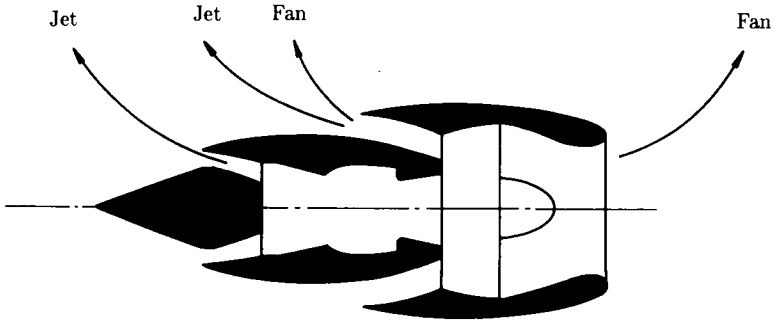

Figure 1. Major noise sources of turbofan engines.

noise suppression purposes acoustic treatment is installed on the duct walls in both the inlet and the exhaust duct, and in fact the treatment may cover most of the available surface. The aerodynamic flow through the ducts can cover a wide range of subsonic velocities, depending on the operating conditions of the engine. This flow in the ducts is nonuniform. The inlet and the exhaust duct radiate acoustic energy to free space through the nonuniform inlet aerodynamic flow field in the vicinity of the nacelle. The radiation process is coupled to the propagation process within the duct, so that in general the source and duct propagation and radiation should be considered simultaneously.

Except in the most advanced design and analysis procedures, the source model is considered to be independent of the propagation and radiation and is considered to be known, providing input to the duct propagation and radiation calculations. Furthermore, the duct propagation is generally considered independently of the radiation. Hence, in tracing the history of acoustic design and analysis methods for inlet suppression, it is found that the greatest emphasis has been on methods for the prediction of attenuation in acoustically treated ducts with a high-speed mean flow. Early work considered uniform ducts with uniform flow and was an extension of procedures developed for ducts with negligible mean flow, which had been of interest in connection with the acoustic design of air handling systems. It was soon recognized that the boundary layer in the mean flow at the duct wall can have a significant effect on the performance of acoustic treatment, so this phenomenon was added to the physical model and appropriate analysis methods developed. The question of duct nonuniformity, and the consequent nonuniformity in the mean flow, was then considered, and a substantial step in the extent of numerical analysis necessary was required.

The prediction of acoustic radiation from ducts can also be traced to investigations of air handling systems involving baffled and unbaffled pipes with negligible flow. Design and analysis requirements for turbofan engines have inspired some purely theoretical extensions of the early work by including the effect of an exhaust flow (applicable to the fan exhaust duct, although originally motivated by propagation through the jet). Approximation methods based on concepts of duct-mode propagation angles have been developed for the prediction of the direction in which peak radiation directivity occurs.

The development of computational methods in acoustics has led to the introduction of analysis and design procedures which model the turbofan inlet as a coupled

system, simultaneously modeling propagation and radiation in the presence of realistic internal and external flows. Such models are generally large, require substantial computer speed and capacity, and can be expected to be used in the final design stages, with the simpler models being used in the early design iterations.

In this chapter emphasis is given to practical modeling methods which have been applied to the acoustical design problem in turbofan engines. The mathematical model is established and the simplest case of propagation in a duct with hard walls is solved to introduce concepts and terminologies. An extensive overview is given of methods for the calculation of attenuation in uniform ducts with uniform flow and with sheared flow. Subsequent sections deal with numerical techniques which provide an integrated representation of duct propagation and near- and far-field radiation for realistic geometries and flight conditions.

A review of the status of duct acoustics in turbofan engines in reference 1 is extremely complete up to its 1975 publication date. In this chapter we unavoidably duplicate some of this discussion, with extensions representing advances since 1975. However, instead of an exhaustive review, we attempt to document specific design and analysis techniques of general utility.

The Acoustic Field Equations

In the following studies of duct acoustic propagation and radiation, modeling is based on linearization of the equations governing the isentropic motion of a nonviscous, non-heat-conducting perfect gas. The pertinent equations, in nondimensional form, are as follows:

Continuity :

$$\frac{\partial \rho^*}{\partial t} + \nabla \cdot (\rho^* \mathbf{V}^*) = 0 \tag{1}$$

Momentum :

$$\frac{\partial \mathbf{V}^*}{\partial t} + (\mathbf{V}^* \cdot \nabla)\mathbf{V}^* = -\frac{1}{\rho^*}\nabla p^* \tag{2}$$

Equation of State :

$$p^* = \frac{1}{\gamma}\rho^{*\gamma} \tag{3}$$

where the density ρ is scaled by ρ_r (a reference density), the velocity $\mathbf{V}$ is scaled by c_r (the reference speed of sound), pressure p is scaled by $\rho_r c_r^2$, time t is scaled by L/c_r (where L is a suitable reference length), and the spatial coordinates are scaled by L. In some applications a form of the energy equation is useful.

Energy :

$$\frac{\partial p^*}{\partial t} + \mathbf{V}^* \cdot \nabla p^* + \gamma p^* (\nabla \cdot \mathbf{V}^*) = 0 \tag{4}$$

The acoustic equations are obtained by considering small perturbations on a mean state ρ_o, p_o, and $\mathbf{V}_o$ so that

$$\rho^* = \rho_o + \rho$$

$$p^* = p_o + p$$

$$\mathbf{V}^* = \mathbf{V}_o + \mathbf{V}$$

The resulting acoustic field equations, after second-order and higher order terms in the small perturbations are ignored, are as follows:

Acoustic Continuity :

$$\frac{\partial \rho}{\partial t} + \nabla \cdot (\rho_o \mathbf{V} + \mathbf{V}_o \rho) = 0 \tag{5}$$

Acoustic Momentum :

$$\frac{\partial \mathbf{V}}{\partial t} + \mathbf{V}_o \cdot \nabla \mathbf{V} + \frac{1}{\rho_o} \nabla p + \mathbf{V} \cdot \nabla \mathbf{V}_o - \frac{1}{\gamma p_o \rho_o} p \nabla p_o = 0 \tag{6}$$

Acoustic Energy :

$$\frac{\partial p}{\partial t} + \mathbf{V}_o \cdot \nabla p + \mathbf{V} \cdot \nabla p_o + \gamma p_o (\nabla \cdot \mathbf{V}) + \gamma p (\nabla \cdot \mathbf{V}_o) = 0 \tag{7}$$

Acoustic Equation of State :

$$p = \gamma \frac{p_o}{\rho_o} \rho = c_o^2 \rho \tag{8}$$

In equation (8), c_o is the nondimensional local speed of sound in the mean flow.

In the acoustic radiation model the mean flow and the acoustic perturbations are taken as irrotational. In this case

$$\mathbf{V}^* = \nabla \Phi$$
$$\mathbf{V} = \nabla \phi$$
$$\mathbf{V}_o = \nabla \phi_o$$

where ϕ is the velocity potential nondimensionalized with respect to $c_r L$. The continuity and momentum equations and the equation of state are used in this case. The continuity equation follows directly from equation (5).

Acoustic Continuity Equation (Irrotational) :

$$\frac{\partial \rho}{\partial t} + \nabla \cdot (\rho_o \nabla \phi + \rho \nabla \phi_o) = 0 \tag{9}$$

In the case of the momentum equation, the implication of irrotationality is used ($\nabla \times \mathbf{V} = 0$), as is the isentropic equation of state ($dp^*/d\rho^* = (\rho^*)^{\gamma-1} = c^{*2}$), to obtain

$$\frac{\partial \mathbf{V}^*}{\partial t} + \frac{1}{2}\nabla(\mathbf{V}^* \cdot \mathbf{V}^*) + \nabla\frac{c^{*2}}{\gamma - 1} = 0$$

where c^* is the nondimensional local speed of sound. In terms of the velocity potential this can be written

$$c^{*2} = 1 - (\gamma - 1)\left[\frac{\partial \Phi}{\partial t} + \frac{1}{2}\left(\nabla\Phi \cdot \nabla\Phi - M_\infty^2\right)\right]$$

where the arbitrary function of time which arises is evaluated at infinity, where the reference conditions ρ_r and c_r are also defined. At infinity the nondimensional velocity is the Mach number M_∞. The nondimensional speed of sound c_∞^* is unity. Linearization yields the following isentropic relation for the mean flow:

$$c_o^2 = 1 - \frac{\gamma - 1}{2}\left(\nabla\phi_o \cdot \nabla\phi_o - M_\infty^2\right) \tag{10}$$

For the acoustic fluctuations, the following equation is used:

Acoustic Momentum Equation (Irrotational) :

$$\rho = -\frac{\rho_o}{c_o^2}\left(\frac{\partial \phi}{\partial t} + \nabla\phi_o \cdot \nabla\phi\right) \tag{11}$$

or

$$p = -\rho_o\left(\frac{\partial \phi}{\partial t} + \nabla\phi_o \cdot \nabla\phi\right) \tag{12}$$

In equations (11) and (12), ρ_o is the nondimensional local density and c_o is the nondimensional local speed of sound in the mean flow.

Propagation in Uniform Ducts With Hard Walls

In the case of a uniform duct with axially uniform mean flow, equations (5), (6), and (8) can be combined to yield the convected wave equation

$$\left(\frac{\partial}{\partial t} + M\frac{\partial}{\partial x}\right)^2 p = \nabla^2 p \tag{13}$$

The nondimensional velocity in this case is the local Mach number M and the nondimensional speed of sound is unity. This follows because of the nondimensionalization and because of the flow field uniformity. Equation (13) simplifies to the classic wave equation in the absence of mean flow (i.e., $M = 0$).

As shown in figure 2, attention is restricted to a duct of circular geometry with a cylindrical coordinate system (x, r, θ). For a duct with hard walls the boundary condition at $r = 1$ is that the acoustic particle velocity normal to the wall is zero.

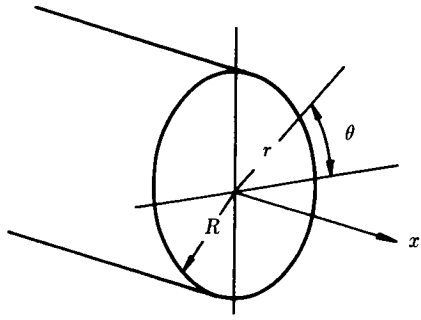

(a) Cylindrical coordinate system.

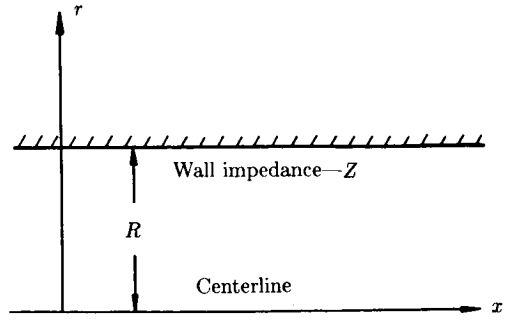

(b) Wall impedance configuration.

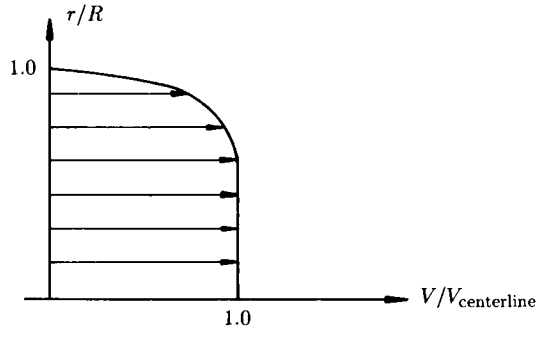

(c) Sheared velocity profile.

Figure 2. Geometrical, acoustical, and flow conditions for circular duct.

The coordinate r is scaled by the duct radius R. The acoustic momentum equation in the r direction shows that this is equivalent to the boundary condition at $r = 1$ as follows:

$$\frac{\partial p}{\partial r} = 0$$

At the duct centerline the boundary condition is that the solution should remain finite. It is assumed that an unspecified noise source introduces acoustic disturbances harmonically with time dependence $\exp(i\eta t)$, where $\eta = \omega R/c_r$, ω is the dimensional excitation frequency, and R is the duct radius. The resulting acoustic fluctuations in the duct can then be written

$$p(x, r, \theta, t) = P(x, r, \theta)\ \exp(i\eta t)$$

where $P(x, r, \theta)$ now satisfies a convected Helmholtz equation

$$(1-M^2)\frac{\partial^2 P}{\partial x^2}+\nabla_c^2 P-2i\eta M\frac{\partial P}{\partial x}+\eta^2 P=0 \tag{14}$$

with boundary condition at $r=1$ of

$$\frac{\partial P}{\partial r}=0$$

and ∇_c is the gradient operator in the polar coordinate system (r,θ) (the coordinates in the duct cross section). Solutions to equation (14) can be written in terms of traveling waves as follows:

$$P_{mn}(x,r,\theta)=P(r)\ \exp(\pm im\theta)\ \exp(-ik_{x_{mn}}x)$$

where

$$\frac{k_{x_{mn}}}{\eta}=\frac{1}{1-M^2}\left[-M\pm\sqrt{1-(1-M^2)\left(\frac{\kappa_{mn}}{\eta}\right)^2}\right] \tag{15}$$

The term $P(r)$ is then governed by the Bessel equation

$$\frac{d^2P}{dr^2}+\frac{1}{r}\frac{dP}{dr}+\left(\kappa^2-\frac{m^2}{r^2}\right)P=0$$

with boundary condition at $r=1$ of

$$\frac{dP}{dr}=0$$

The solutions to this equation, finite at the origin, are $J_m(\kappa r)$, Bessel functions of the first kind of order m. The eigenvalues κ_{mn} are defined by

$$J'_m(\kappa_{mn})=0 \tag{16}$$

A solution to equation (14) and the hard-wall boundary condition is therefore

$$p_{mn}(x,r,\theta,t)=P_{mn}J_m(\kappa_{mn}r)\ \exp[i(\eta t\pm m\theta-k_{x_{mn}}x)] \tag{17}$$

There are an infinite number of such solutions, corresponding to integer values of m and to the infinite number of values κ_{mn} defined by the eigenvalue equation (16). These solutions are referred to as modes of propagation. At a fixed x, angular traveling waves (or spinning modes) of the form

$$p\ \propto\ \exp[i(\eta t\pm m\theta)]$$

are observed, while at fixed θ axial traveling waves of the form

$$p\ \propto\ \exp[i(\eta t-k_{x_{mn}}x)]$$

are observed. A given mode of propagation is thus the combination of a spinning mode and an axial traveling wave.

The parameter k_x is referred to as the axial wave number and can be real or complex depending on values of M, κ_{mn}, and η. For

$$(1 - M^2)\left(\frac{\kappa_{mn}}{\eta}\right)^2 < 1$$

k_x is real, and for most values of M, κ_{mn}, and η in this range k_x has a positive and a negative value corresponding to axial waves propagating in the positive and negative x-directions. If $M > 0$, over the range of parameters for which

$$1 < \left(\frac{\kappa_{mn}}{\eta}\right)^2 < \frac{1}{1 - M^2}$$

there are two negative values of k_x, but an acoustic energy argument (ref. 2) can be used to show that the positive sign in equation (15) still corresponds to acoustic power transmitted in the positive x-direction and the negative sign corresponds to acoustic power transmitted in the negative x-direction. A similar result showing two positive values for k_x applies if $M < 0$.

An interesting phenomenon occurs when

$$(1 - M^2)\left(\frac{\kappa_{mn}}{\eta}\right)^2 > 1$$

and k_x becomes complex:

$$\frac{k_{x_{mn}}}{\eta} = \frac{1}{1 - M^2}\left[-M \pm i\sqrt{(1 - M^2)\left(\frac{\kappa_{mn}}{\eta}\right)^2 - 1}\right]$$

In this case the solution of equation (17) becomes

$$p_{mn}(x, r, \theta, t) = P_{mn} J_m(\kappa_{mn} r)\ \exp\left\{i[\eta t \pm m\theta - \mathrm{Re}(k_x)x \pm \mathrm{Im}(k_x)x]\right\}$$

where

$$\mathrm{Re}(k_x) = -\frac{M\eta}{1 - M^2}$$

$$\mathrm{Im}(k_x) = \frac{\eta}{1 - M^2}\sqrt{(1 - M^2)\left(\frac{\kappa_{mn}}{\eta}\right)^2 - 1}$$

are the real and imaginary parts of the complex wave number $k_{x_{mn}}$. The traveling wave is attenuated with distance, the negative sign indicating the solution in the positive x-direction and the positive sign indicating the solution in the negative x-direction. An energy argument (ref. 2) shows that no acoustic power is associated with these modes.

Acoustic duct modes which are attenuated with distance and carry no acoustic power are referred to as being "cutoff," while modes which propagate in the usual sense are said to be "cut on." Reference 3 has introduced the terminology "cutoff ratio" for the parameter

$$\beta_{mn} = \frac{\eta}{\kappa_{mn}\sqrt{1 - M^2}}$$

When the cutoff ratio exceeds unity, the frequency is high enough that the mode corresponding to κ_{mn} is cut on. Values of cutoff ratio less than unity identify modes which are cutoff.

The exact physical phenomenon occurring in cutoff modes which produces attenuation with no source of dissipation is difficult to see in the presence of flow. However, reference 4 shows that in the case without mean flow the acoustic field of a piston driver in a duct is an entirely reactive field from which no acoustic power escapes when the cutoff ratio is less than unity.

In the classic work of Tyler and Sofrin (ref. 5), it is pointed out that if the noise source is such that only modes with cutoff ratios less than unity are produced, then in principle no acoustic power is propagated from the source. This could conceivably be accomplished with an isolated rotor, in which case a judicious choice of the number of blades and the rotational speed can ensure that the cutoff ratio is less than unity. However, the inevitable presence of struts and inlet or outlet guide vanes may produce interaction tones which propagate. In addition, the finite length of the inlet and outlet ducts allows the basically reactive field to radiate some power to the far field.

Another physical picture of the propagation, which is exact in a two-dimensional duct and is approximate in a circular duct, is that of viewing the acoustic field as the result of the interference of plane waves propagating at an angle to the duct axis and therefore reflecting from the duct walls. The angle of propagation is directly related to the cutoff ratio (ref. 6). When the cutoff ratio is unity, the angle of propagation is at 90° to the duct axis and the plane-wave propagation is just across the duct, a situation in which it would not be expected that acoustic power would be propagated down the duct.

Rice (ref. 3) also used an extended concept of modal cutoff ratio to good advantage in correlating attenuation in lined ducts and in estimating the direction of the major lobe of the radiation from a duct termination. This is discussed in a subsequent section.

The modal solutions of equation (17) are solutions which can exist within the duct. Whether they are actually present depends on the source and boundary conditions (so far not specified) where the duct terminates on the x-axis. In the case of an infinite duct (i.e., one extending $-\infty < x < \infty$), only waves traveling or decaying away from the source can be present. For a source at $x = 0$, only solutions with wave numbers appropriately defined for propagation or decay for $x > 0$ exist for $x > 0$, and those defined for propagation or decay for $x < 0$ exist for $x < 0$. This makes it necessary to choose the proper sign in equation (15). We can designate the wave numbers by $k^+_{x_{mn}}$ or $k^-_{x_{mn}}$ to indicate whether they apply to solutions traveling or decaying in the positive or the negative x-direction. Thus, for $x > 0$ an appropriate solution is

$$p_{mn}(x, r, \theta, t) = P^+_{mn} J_m(\kappa_{mn} r) \ \exp[i(\eta t \pm m\theta - k^+_{x_{mn}} x)]$$

and for $x < 0$ an appropriate solution is

$$p_{mn}(x, r, \theta, t) = P^-_{mn} J_m(\kappa_{mn} r) \ \exp[i(\eta t \pm m\theta - k^-_{x_{mn}} x)]$$

In the case of a duct of finite length, boundary conditions must be specified at the terminations or the duct model must be coupled to some other description of the acoustic propagation beyond the termination. In any case, the terminations introduce reflections, and solutions corresponding to both k_x^+ and k_x^- can be present at any point in the duct.

In most cases it is not possible to write a boundary condition at a duct termination. For example, in the case of a duct terminating at free space, the acoustic response of the medium outside the duct establishes the boundary condition. Therefore the duct and radiation problems must be solved simultaneously. This matter is discussed more in a subsequent section.

Because of the difficulty with precise definition of termination conditions, two approximate ones are often introduced. At low frequencies the assumption of zero acoustic pressure for a termination at free space is reasonable. This "pressure release" boundary condition produces complete reflection of traveling waves and does not permit any acoustic power to escape from the duct. It is only useful for the study of standing waves (the interaction of waves traveling in both directions) in ducts where only the plane wave propagates.

The much more common assumption is that the termination is reflection free or that the duct is of infinite length. This assumption is difficult to justify for unlined ducts in which traveling waves are not attenuated; however, for relatively high frequencies (wavelength small relative to the duct radius) and for frequencies other than those approaching cutoff frequencies, reflections from open ends are small. For lined ducts, as shown subsequently, reflections may be even less important because the incident amplitudes are considerably reduced before reaching the termination.

General solutions to the convected wave equation for the circular duct can be given as a superposition of the eigenfunction solutions (eq. (17)) to yield

$$p(x,r,\theta,t) = \sum_{m=-\infty}^{\infty} \sum_{n=0}^{\infty} P_{mn} J_m(\kappa_{mn} r) \ \exp[i(\eta t - m\theta - k_{x_{mn}}^{\pm} x)]$$

$$p(x,r,\theta,t) = \sum_{m=-\infty}^{\infty} \sum_{n=0}^{\infty} J_m(\kappa_{mn} r) \ \exp[i(\eta t - m\theta)]$$

$$\times \left[P_{mn}^{+} \ \exp(-ik_{x_{mn}}^{+} x) + P_{mn}^{-} \ \exp(-ik_{x_{mn}}^{-} x)\right]$$

The values of the amplitude coefficients depend on the nature of the source. For example, if we were interested in acoustic propagation in the positive x-direction in an infinite duct, for which there is no reflection at the termination and therefore no waves propagating in the negative x-direction, the series would be

$$p(x,r,\theta,t) = \sum_{m=-\infty}^{\infty} \sum_{n=0}^{\infty} P_{\mu n} J_\mu(\kappa_{\mu n} r) \ \exp[imN(\Omega t - \theta)] \ \exp(-ik_{x_{\mu n}}^{+} x)$$

for a noise source consisting of a simple rotor with N blades turning at angular speed Ω. For this equation, $\mu = mN$, the $k_{x_{\mu n}}^{+}$ are limited to the proper choices for solutions with $x > 0$, and the modal amplitudes P_{mn} depend on the blade loading.

In this case the solution is spinning modes at frequency $mN\Omega$, locked in phase with the rotor. For interaction of rotor and stator or of rotor and inlet guide vanes, all modes are not spinning in the same direction and with the same angular speed as the rotor. Reference 5 gives an excellent description of the influence of the noise source on the modal character of the acoustic propagation in the duct.

Attenuation Calculations in Lined Uniform Ducts

In the previous section fundamental properties of sound propagation in uniform hard-wall ducts with uniform flow were introduced. In this section we deal with the more practically important problem of the calculation of the axial wave number, and hence the attenuation, in uniform ducts with acoustically treated walls. The ducts considered in general contain a mean flow which in the least restrictive case can have a sheared velocity profile approximating the gross effects of the viscous boundary layer.

Attenuation calculations for acoustic transmission are required in aircraft turbofan engine inlet and exhaust ducts. Problems of this type are demanding not only because of the acoustic environment involved, but also because of requirements for computational efficiency and accuracy for design studies.

The duct geometry specifically considered in this discussion is circular. Where appropriate, results are also quoted without proof for two-dimensional rectangular geometries. Most of the results can be directly extended to annular and three-dimensional rectangular ducts. Figure 2 shows the pertinent geometrical details for the circular duct.

The Physical Problem

The uniform duct carries a mean flow which is uniform axially but nonuniform radially. The mean density and pressure are assumed to be uniform. The sound transmission problem is one of modeling acoustic fluctuations on this mean flow. This representation is consistent with the developments of reference 7, which starts from the full viscous equations of compressible fluid mechanics and, with a series of approximations and assumptions, arrives at this model, which captures the important features of the refractive effects of sheared viscous flow on sound propagation.

The field equations which are appropriate are equations (5), (6), and (8), restricted to the case when ρ_o, p_o, and c_o are constant ($\rho_o = 1$, $p_o = 1$, and $c_o = 1$) and $\mathbf{V}_o = M(r)\mathbf{e}_x$:

$$\frac{\partial p}{\partial t} + M\frac{\partial p}{\partial x} + \nabla \cdot \mathbf{V} = 0 \tag{18}$$

$$\frac{\partial \mathbf{V}}{\partial t} + M\frac{\partial \mathbf{V}}{\partial x} + \nabla p + \frac{dM}{dr}v_r\mathbf{e}_x = 0 \tag{19}$$

where

$$\mathbf{V} = v_x\mathbf{e}_x + v_r\mathbf{e}_r + v_\theta\mathbf{e}_\theta$$

Equations (18) and (19) can be combined as

$$\left(\frac{\partial}{\partial t} + M\,\frac{\partial}{\partial x}\right)^3 p = \left(\frac{\partial}{\partial t} + M\,\frac{\partial}{\partial x}\right)\nabla^2 p - 2\,\frac{dM}{dr}\,\frac{\partial^2 p}{\partial x\,\partial r} \tag{20}$$

Note that if $M(r)$ is constant, $dM/dr = 0$ and equation (20) becomes

$$\left(\frac{\partial}{\partial t} + M\,\frac{\partial}{\partial x}\right)\left[\left(\frac{\partial}{\partial t} + M\,\frac{\partial}{\partial x}\right)^2 - \nabla^2\right] p = 0 \tag{21}$$

For harmonic excitation proportional to $\exp(i\eta t)$, with $\eta = \omega R/c_r = 2\pi f R/c_r$ (where $\omega = 2\pi f$ is the driving frequency), we seek solutions in the form

$$p(x, r, \theta, t) = \hat{p}(x, r, \theta)\ \exp(i\eta t)$$

The resulting equation for $p(x, r, \theta)$ is

$$\left(i\eta + M\,\frac{\partial}{\partial x}\right)^3 \hat{p} = \left(i\eta + M\,\frac{\partial}{\partial x}\right)\nabla^2 \hat{p} - 2\frac{dM}{dr}\,\frac{\partial^2 \hat{p}}{\partial x\,\partial r}$$

Traveling wave solutions in the form

$$\hat{p}(x, r, \theta) = P(r)\ \exp(\pm im\theta - ik_x x)$$

are sought. The term $P(r)$ satisfies the ordinary differential equation

$$\frac{d^2P}{dr^2} + \left[\frac{1}{r} + \frac{2(k_x/\eta)}{(1 - Mk_x/\eta)}\,\frac{dM}{dr}\right]\,\frac{dP}{dr} + \left\{\eta^2\left[\left(1 - M\frac{k_x}{\eta}\right)^2 - \left(\frac{k_x}{\eta}\right)^2\right] - \frac{m^2}{r^2}\right\} P = 0 \tag{22}$$

The boundary condition at the duct wall ($r = 1$) is based on the assumption that the lining is locally reacting and that the relationship between nondimensional pressure and nondimensional lining particle velocity v_ν is

$$\frac{p}{v_\nu} = \frac{Z}{\rho_r c_r} \tag{23}$$

where $Z/\rho_r c_r$ is the wall nondimensional specific impedance. At the duct wall the fluid particle displacement and the wall particle displacement are the same. Note that because of the convection effect of the mean flow, the fluid particle velocity is the convective, or substantial, derivative of the fluid particle displacement. When the Mach number at the wall vanishes so does this convection effect. Thus, if ζ is the particle displacement of the wall directed into the wall in the inward normal direction $\boldsymbol{\nu}$, then

$$\mathbf{V} \cdot \boldsymbol{\nu} = \left(i\eta + M\frac{\partial}{\partial x}\right)\zeta \tag{24}$$

where $\mathbf{V} \cdot \boldsymbol{\nu}$ is the fluid particle velocity in the normal direction of the wall and directed into the wall. Since the nondimensional wall particle velocity v_ν is related to the particle displacement by

$$v_\nu = i\eta\varsigma$$

equation (24) becomes

$$\mathbf{V}\cdot\boldsymbol{\nu} = \left(1 - i\frac{M}{\eta}\frac{\partial}{\partial x}\right)v_\nu \tag{25}$$

We can now replace v_ν by using equation (23) to obtain

$$\mathbf{V}\cdot\boldsymbol{\nu} = A\left(1 - i\frac{M}{\eta}\frac{\partial}{\partial x}\right)p$$

where $A = \rho_r c_r/Z$ is the wall nondimensional specific acoustic admittance.

In the case of the circular duct, $v_\nu = v_r$. The radial component of the acoustic momentum equation (19) is

$$\left(\frac{\partial}{\partial t} + M\frac{\partial}{\partial x}\right)v_r = -\frac{\partial p}{\partial r}$$

This is used to rewrite the boundary condition (eq. (25)) entirely in terms of the acoustic pressure:

$$\frac{\partial p}{\partial r} = -i\eta A\left(1 - i\frac{M}{\eta}\frac{\partial}{\partial x}\right)^2 p \tag{26}$$

Equation (26) is to be enforced on solutions of equation (22) at $r = 1$. The boundary condition at $r = 0$ is that the solution should remain finite. The field equation (22), the boundary condition equation (26), and the finiteness condition at $r = 0$ constitute an eigenvalue problem of finding values of the wave number k_x such that the homogeneous differential equation and homogeneous boundary conditions have a nontrivial solution. We now consider special cases of importance.

The Eigenvalue Problem

Sheared Flow With No-Slip Boundary Conditions

It is assumed that the sheared velocity profile is known, so that we are given $M(r)$ and dM/dr and specify $M = 0$ at the duct wall. In the circular-duct case we have shown that the field equations can be combined to yield

$$\frac{d^2P}{dr^2} + \left[\frac{1}{r} + \frac{2(k_x/\eta)}{1-(Mk_x/\eta)}\frac{dM}{dr}\right]\frac{dP}{dr} + \left\{\eta^2\left[\left(1 - M\frac{k_x}{\eta}\right)^2 - \left(\frac{k_x}{\eta}\right)^2\right] - \frac{m^2}{r^2}\right\}P = 0$$

which is equation (22). The boundary conditions at $r = 0$ and $r = 1$ are

$$\left.\begin{aligned} P(0) &= \text{Finite} \\ \frac{dP}{dr}(1) &= -i\eta AP \end{aligned}\right\} \tag{27}$$

Since many of the results in the literature are quoted for two-dimensional ducts, it is appropriate to state here the eigenvalue problem for this case with a lined wall at $y = 1$ and a hard wall at $y = 0$ as

$$\frac{d^2P}{dy^2} + \frac{2(k_x/\eta)}{1-(Mk_x/\eta)}\frac{dM}{dy}\frac{dP}{dy} + \eta^2\left[\left(1 - M\frac{k_x}{\eta}\right)^2 - \left(\frac{k_x}{\eta}\right)^2\right]P = 0 \tag{28}$$

with boundary conditions at $y = 0$ and $y = 1$ of

$$\left.\begin{aligned}\frac{dP}{dy}(0) &= 0\\ \frac{dP}{dy}(1) &= -i\eta AP\end{aligned}\right\} \tag{29}$$

where $\eta = \omega b/c_r = 2\pi f b/c_r$, where b is the duct height.

A two-dimensional duct with two symmetrically lined walls at $y = 1$ and $y = -1$ can be treated by also solving the boundary value problem with $P = 0$ at $y = 0$. The eigenfunction solutions from the boundary conditions in equations (29) are then the symmetric solutions and those generated with $P = 0$ at $y = 0$ are the antisymmetric solutions.

Uniform Mean Flow

In this case it is assumed that the mean flow Mach number is uniform across the duct. Therefore, $dM/dr = 0$. An interesting preliminary result can be obtained from equations (18), (19), and (21). In addition to equation (21), equations (18) and (19) can be combined to yield

$$\left(\frac{\partial}{\partial t} + M\frac{\partial}{\partial x}\right)\left[\left(\frac{\partial}{\partial t} + M\frac{\partial}{\partial x}\right)^2 - \nabla^2 - \nabla\times\nabla\times\right]\mathbf{V} = 0 \tag{30}$$

Equation (19) is used to show that

$$\left(\frac{\partial}{\partial t} + M\frac{\partial}{\partial x}\right)(\nabla\times\mathbf{V}) = 0 \tag{31}$$

This implies that vorticity is convected or it vanishes. In combination with equation (30) this means that the velocity field satisfies

$$\left(\frac{\partial}{\partial t} + M\frac{\partial}{\partial x}\right)^3\mathbf{V} - \nabla^2\left(\frac{\partial}{\partial t} + M\frac{\partial}{\partial t}\right)\mathbf{V} = 0 \tag{32}$$

From equation (30) or (32) it is shown that there are solutions for which

$$\left(\frac{\partial}{\partial t} + M\frac{\partial}{\partial x}\right)\mathbf{V} = 0$$

From equation (19), these solutions have $\nabla p = 0$, which implies that the perturbation pressure field vanishes, and therefore

$$\nabla \cdot \mathbf{V} = 0$$

Hence, there exists a class of velocity solutions satisfying the incompressible continuity equation, with vanishing pressure perturbations which are convected with the mean flow. For harmonic traveling waves of the form

$$\mathbf{V}(x, r, \theta, t) = \mathbf{V}(r)\ \exp(\pm im\theta)\ \exp[i(\eta t - k_x x)]$$

this means

$$(i\eta - iMk_x)\mathbf{V} = 0$$

or

$$k_x = \frac{\eta}{M} = \frac{\omega R}{V} \tag{33}$$

The traveling waves are thus of the dimensional form

$$\mathbf{V}(x, r, \theta, t) = \mathbf{V}(r)\ \exp(\pm im\theta)\ \exp\left\{i\omega[t - (x/V)]\right\}$$

This is a disturbance for which in general $\nabla \times \mathbf{V} \neq 0$ and which is propagating at the mean flow velocity. This solution with vorticity is convected with the flow. This is termed a hydrodynamic disturbance.

A second type of solution has $\nabla \times \mathbf{V} = 0$ (eq. (31)) and is therefore irrotational. These solutions satisfy

$$\left(\frac{\partial}{\partial t} + M\frac{\partial}{\partial x}\right)^2 p - \nabla^2 p = 0$$

and are the acoustic fluctuations. It is thus observed that in uniform flow hydrodynamic (rotational) disturbances and acoustic (irrotational) fluctuations can be separated.

The above observations are not generally true when the flow is sheared, and in that case acoustic disturbances are not irrotational (ref. 8). However, there are still hydrodynamic disturbances in the sheared flow. Reference 8 discusses this in the case of a linear shear profile. The main point to be made here is that the hydrodynamic solutions are contained in the field equations, even with $dM/dr = 0$, although the solutions are not generally retained in the development of the convected wave equation.

We now write the eigenvalue problem for the acoustic disturbances in the case of uniform flow. In the circular-duct case,

$$\frac{1}{r}\frac{d}{dr}\left(r\frac{dP}{dr}\right) + \left\{\eta^2\left[\left(1 - M\frac{k_x}{\eta}\right)^2 - \left(\frac{k_x}{\eta}\right)^2\right] - \frac{m^2}{r^2}\right\}P = 0 \tag{34}$$

with boundary conditions at $r = 0$ and $r = 1$ of

$$\left.\begin{aligned} P(0) &= \text{Finite} \\ \frac{dP}{dr}(1) &= -i\eta A\left(1 - M\frac{k_x}{\eta}\right)^2 P \end{aligned}\right\} \tag{35}$$

and in the two-dimensional case,

$$\frac{d^2P}{dy^2} + \eta^2 \left[\left(1 - M\frac{k_x}{k} \right)^2 - \left(\frac{k_x}{\eta} \right)^2 \right] P = 0 \tag{36}$$

with boundary conditions at $y = 0$ and $y = 1$ of

$$\left.\begin{aligned} \frac{dP}{dy}(0) &= 0 \\ \frac{dP}{dy}(1) &= -i\eta A \left(1 - M\frac{k_x}{\eta} \right)^2 P \end{aligned}\right\} \tag{37}$$

As noted previously, the boundary conditions (eqs. (37)) generate symmetric solutions for the duct spanning $-1 \leq y \leq 1$. Antisymmetric solutions arise from $P = 0$ at $y = 0$.

No Mean Flow

For no mean flow, $M = 0$. In the circular-duct case, the eigenvalue problem is given by

$$\frac{1}{r}\frac{d}{dr}\left(r\frac{dP}{dr} \right) + \left\{ \eta^2 \left[1 - \left(\frac{k_x}{\eta} \right)^2 \right] - \frac{m^2}{r^2} \right\} P = 0 \tag{38}$$

with boundary conditions at $r = 0$ and $r = 1$ of

$$\left.\begin{aligned} P(0) &= \text{Finite} \\ \frac{dP}{dr}(1) &= -i\eta AP \end{aligned}\right\} \tag{39}$$

In the two-dimensional duct,

$$\frac{d^2P}{dy^2} + \eta^2 \left[1 - \left(\frac{k_x}{\eta} \right)^2 \right] P = 0 \tag{40}$$

with boundary conditions at $y = 0$ and $y = 1$ of

$$\left.\begin{aligned} \frac{dP}{dy}(0) &= 0 \\ \frac{dP}{dy}(1) &= -i\eta AP \end{aligned}\right\} \tag{41}$$

Antisymmetric eigenfunction solutions follow from $P = 0$ at $y = 0$, as noted previously.

The boundary value problems described by equations (28) and (29) and (34) to (41) are eigenvalue problems in which we seek nontrivial solutions to the differential equation which satisfy the specified boundary conditions. The eigenvalue in each case is the axial wave number k_x/η which contains the essential attenuation information.

In each case the boundary value problem defines an infinite sequence of eigenvalues. Corresponding to each eigenvalue is a nontrivial solution, or eigenfunction, which defines a transverse pressure variation $P_{mn}(r)$ or $P_n(y)$ which propagates according to

$$p_{mn}(x, r, \theta, t) = P_{mn}(r) \ \exp[i(\eta t \pm m\theta - k_{x_{mn}} x)] \tag{42}$$

or

$$p_n(x, y, t) = P_n(y) \ \exp[i(\eta t - k_{x_n} x)] \tag{43}$$

The amplitudes of the eigenfunction are suitably normalized. Each such solution defines a mode of propagation. In general, the acoustic field in a duct is a superposition of these nodes with amplitudes dependent on the source and termination conditions

$$p(x, r, \theta, t) = \sum_{m=-\infty}^{\infty} \sum_{n=0}^{\infty} A_{mn} P_{mn}(r) \ \exp[i(\eta t \pm m\theta - k_{x_{mn}} x)] \tag{44}$$

or

$$p(x, y, t) = \sum_{n=1}^{\infty} A_n P_n(y) \ \exp[i(\eta t - k_{x_n} x)] \tag{45}$$

As previously discussed, some of the solutions correspond to propagation in the positive x-direction, while the remainder correspond to propagation in the negative x-direction.

The eigenvalue problems so described are not true Sturm-Liouville problems so that there is no general statement about orthogonality of the eigenfunctions. However, in the no-flow case it can be shown that

$$\int_0^1 r P_{mn}(r) P_{mk}(r) \, dr = M_{nn} \, \delta_{nk}$$

or

$$\int_0^1 P_n(y) P_k(r) \, dr = M_{nn} \, \delta_{nk}$$

where $\delta_{nk} = 0$ for $n \neq k, \delta_{nk} = 1$ for $n = k$, and

$$M_{nn} = \int_0^1 r P_{mn}^2 \, dr$$

or

$$M_{nn} = \int_0^1 P_n^2(y) \, dy$$

This orthogonality is not found in general when mean flow is present. The eigenfunctions are orthogonal for any uniform mean flow when the walls are hard ($A = 0$).

Calculation of Attenuation

In all the eigenvalue problems postulated we have sought solutions in the form

$$p(\mathbf{r}, x, t) = P(\mathbf{r}) \ \exp[i(\eta t - k_x x)] \tag{46}$$

Here, the harmonic time dependence is explicitly included. The term $\mathbf{r}$ is the vector of coordinates transverse to the duct axis. Attenuation is defined as the change in sound pressure level (SPL) over a specified length of duct. In the present case only ducts without end reflections are considered, so that attenuation is based only on transmitted modes. Furthermore, the attenuation is considered in each mode separately. The extension to multimode propagation is straightforward but yields a considerably complicated result. SPL is defined as

$$\text{SPL} = 20 \ \log \frac{\overline{P}}{P_o}$$

where $\overline{P}$ is the root-mean-squared acoustic pressure and P_o is a suitable reference (by convention for aeroacoustics, this is taken as $P_o = 20 \ \mu Pa$). The change in SPL over length Δx is

$$\Delta \ \text{SPL} = 20 \ \log \frac{\overline{P}_2}{\overline{P}_1} = 20 \ \log \frac{\overline{P}(x + \Delta x)}{\overline{P}(x)}$$

If $k_x = \alpha + i\beta$, it follows that

$$\frac{\overline{P}_2(x + \Delta x)}{\overline{P}_1(x)} = \exp(\beta \ \Delta x)$$

Thus,

$$\Delta \ \text{SPL} = (20 \ \log e)\beta \ \Delta x = 8.686\beta \ \Delta x \tag{47}$$

For a decaying wave, β is negative if the propagation is in the positive x-direction.

Thus, calculation of attenuation requires the solution of the eigenvalue problem for k_x.

Solution of the Eigenvalue Problem

In this section we discuss techniques for the solution of the eigenvalue problems posed in the previous section. Emphasis is on numerical techniques, although it is appropriate to refer to some methods which were developed prior to the availability of computer systems.

No Mean Flow

When the mean flow vanishes, the eigenvalue equation for the circular duct is equation (38) and the associated boundary conditions. This can be written in slightly modified form to yield

$$\frac{d^2P}{dr^2} + \frac{1}{r}\frac{dP}{dr} + \left(\kappa^2 - \frac{m^2}{r^2}\right) P = 0 \tag{48}$$

with boundary conditions (eqs. (39)) at $r = 0$ and $r = 1$ of

$$P(0) = \text{Finite}$$

$$\frac{dP}{dr}(1) = -i\eta AP$$

where

$$\kappa^2 = \eta^2 \left[1 - \left(\frac{k_x}{\eta}\right)^2\right] \tag{49}$$

Solutions to equation (48), satisfying the boundary condition at $r = 0$, are Bessel functions of the first kind of order m:

$$P = J_m(\kappa r)$$

The eigenvalue κ is determined from the boundary condition at the outer wall ($r = 1$) according to

$$\kappa \frac{J'_m(\kappa)}{J_m(\kappa)} = -i\eta A \tag{50}$$

There are an infinite number of discrete eigenvalues κ of equation (50). If these are enumerated by the angular mode number m and the radial mode number n, then from equation (49) the modal wave numbers are given by

$$\left(\frac{k_x}{\eta}\right)_{mn} = \pm\sqrt{1 - \left(\frac{\kappa_{mn}}{\eta}\right)^2} \tag{51}$$

The equivalent two-dimensional problem which follows from equation (40) leads to the eigenvalue problem

$$\kappa \tan \kappa = i\eta A \tag{52}$$

and the corresponding sequences of eigenfunction solutions

$$P_n = \cos \kappa_n y$$

These are also the symmetric solutions for $-1 \leq y \leq 1$, as previously noted. The antisymmetric solutions follow from the eigenvalue equation $\kappa \cot \kappa = -i\eta A$ and the eigenfunction solutions are $\sin \kappa_n y$. Equation (51) for the axial wave number still holds in the two-dimensional case.

The determination of the eigenvalues of equation (50) or (52) is a conceptually simple proposition. In practice it is not simple because of the topography of the complex functions of the complex variable κ the zeros of which are the eigenvalues and because of the complex arithmetic which must be performed. Because of these difficulties, early researchers were led to consider approximations. Sivian (ref. 9) and Molloy (ref. 10) arrived at essentially the same end result by different means. They used a one-dimensional propagation assumption. Sivian cast the problem as an electrical analog and Molloy used the acoustical equations directly, making his

results generally more accessible to the present generation of acousticians. Molloy also provided charts from which attenuation can be obtained directly. No restriction was placed on the shape of the duct cross section and the lining could have been circumferentially varying, provided the assumption of plane-wave propagation was adhered to. This is a low-frequency approximation consistent with the restriction to nearly plane waves and one would expect it to require relatively small wall admittance to maintain the planar approximation. This approach has the advantage of producing a direct calculation formula for the attenuation.

Perhaps one of the best known estimates of duct attenuation is presented by Sabine (ref. 11). He used the Sivian-Molloy results and his own experiments on rectangular ducts with relatively weak attenuation to establish the attenuation estimate

$$\frac{\Delta \text{ SPL}}{\Delta x} = 12.6\alpha^{-0.25} P_e/S \tag{53}$$

where Δx is the duct length in feet, α is the reverberation chamber absorption coefficient for the duct lining, P_e is the lined perimeter in inches, and S is the cross-sectional area in square inches.

The first direct attack on equation (52) for rectangular ducts appears to be presented in Morse's well-known work in references 12 and 13. Rather than attempt to solve equation (52) explicitly, Morse treated it as a conformal transformation from the κ plane to the admittance plane. He effectively picked values of κ and computed values of A. Level curves of the complex admittance were then drawn on the plane whose axes were the real and imaginary parts of κ. Morse and Ingard (ref. 13) also presented charts from which κ and hence k_x/η can be determined. They used an entirely different notation and presented the plots in a format so that the charts can be used for one or two lined walls. Great care must be exercised to fully understand the proper chart interpretation. Cremer (ref. 14) also gave a thorough discussion of the chart procedure in the rectangular-duct case. He discussed the importance of branch points of the conformal transformation in determining an optimum attenuation based on the coalescing of two modes of propagation.

In the circular-duct case, equation (50) can be rewritten through use of a recurrence relation for the Bessel function derivative to yield

$$\kappa \frac{J_{m-1}(\kappa)}{J_m(\kappa)} - m = -i\eta A \tag{54}$$

Note that if $m = 0$, $J_{-1}(\kappa) = -J_1(\kappa)$. Morse and Ingard (ref. 13) also presented charts for this case. Reference 13 presents a Morse Chart with $m = 0$ and $m = 1$, again with a different notation. Molloy and Honigman (ref. 15) also addressed the circular-duct problem and apparently first produced what is effectively a Morse Chart for the $m = 0$ case.

A feature of the Morse Charts which makes them particularly useful in applications is that only a single chart is needed for all duct configurations. Only ηA is required. This embodies the complete specification of the frequency, duct size, and lining admittance. This feature is lost when mean flow is present, as shown subsequently.

What appears to be the first attempt to produce a direct solution of equation (52) in the rectangular-duct case is presented in reference 16. The approach was to expand

the eigenvalue equation in a power series in κ and then use a standard technique to invert the power series to obtain a power series defining η.

A contribution of substantial importance for future investigators was made in reference 17. Addressed therein was the problem of axially symmetric propagation in a circular duct, for which equation (54) becomes

$$\kappa \frac{J_1(\kappa)}{J_0(\kappa)} = i\eta A \tag{55}$$

If the definitions

$$y = \frac{i\eta A}{2}$$

$$w = \left(\frac{\kappa}{2}\right)^2$$

are introduced and if equation (55) is differentiated with respect to y, through use of recurrence relations for Bessel function derivatives, the following differential equation for w results:

$$(w + y^2)\frac{dw}{dy} = w \tag{56}$$

Reference 17 sought the lowest mode eigenvalue for $m = 0$ and thus sought the solution of equation (55), which at $y = 0$ has $w = 0$. It used a power series expansion, and under the assumption that y is small, it found the solution is approximated by

$$w = 1 - \exp(-y)$$

For present applications the reference 17 result is of limited value, but Rice (ref. 18) has extended it to higher order symmetric modes by considering series solutions having initial conditions at $y = 0$, which are the hard-wall eigenvalues for any desired number of modes. He also set the problem up specifically for large admittances and used initial values corresponding to the perfectly soft-wall eigenvalues. Convergence is a problem in either case near the branch cut delineating the modal regions, and a common nonlinear equation solving routine is used when this is encountered.

Benzakein, Kraft, and Smith (ref. 19) and Zorumski and Mason (ref. 20) have extended the method to nonsymmetric eigenvalues and have used numerical integration. The differential equation derived by differentiation of equation (50) or equation (54) and the use of recurrence relations for the Bessel function derivatives is

$$\frac{d(\kappa/\eta)}{dA} = \frac{i\kappa}{(\kappa^2 - m^2) - (\eta A)^2} \tag{57}$$

This equation is integrated numerically with starting conditions corresponding to $\mathrm{Re}(A) = 0$. When $\mathrm{Re}(A) = 0$, equation (50) has only real eigenvalues which are easily found with a real search routine to yield the starting values for κ. The differential equation is then integrated along a path with $\mathrm{Im}(A) = \text{Constant}$. If $A = \mathrm{Re}(A) + i\mathrm{Im}(A)$ is the actual admittance, then the integration is along the path

$A = x + i\mathrm{Im}(A)$ $(0 \leq x \leq \mathrm{Re}(A))$, and the value of κ when $x = \mathrm{Re}(A)$ is the desired eigenvalue. Reference 20 shows some example calculations, but little is stated about the performance of the method.

Doak and Vaidya (ref. 21) have considered the nature of the eigenvalues of equation (50) in the circular-duct case and have looked at approximations of particular interest in the limit of small ηA and large A.

Perhaps the most obvious eigenvalue solution technique, the simple Newton-Raphson iteration, is notoriously unreliable as a general-purpose method for calculations involving many modes. This is because of the topography of the function for which zeros are sought. In certain instances very accurate starting values are required if convergence to a nearby root is to be achieved, and all users will attest to numerous instances when the same root is found with two different starting values or when unwanted roots are found. Christie (ref. 22) has published his approach to the use of the Newton-Raphson iteration to find the lowest order mode for a rectangular duct. He starts at low frequency. The lowest eigenvalue has $|\kappa| << 1$, where equation (52) can be written for $|\kappa| << 1$ (the lowest mode eigenvalue) as

$$\kappa^2 = i\eta A$$

The frequency is incremented and this result is used as the next starting value. This proceeds until the desired frequency is reached. This type of incrementing process minimizes the chance of unpredictable convergence. For higher order modes starting values ascending in integer multiples of π could be used. The Newton-Raphson iteration is particularly useful for refining eigenvalue estimates arrived at by other methods, such as the integration scheme of reference 20.

Other methods which have appeared in the literature to deal with the eigenvalue problem come under the general category of discretization techniques. In these methods the differential equation which governs the transverse variation of pressure in the duct (e.g., eq. (38) or (40)) is replaced by a set of algebraic equations based on a finite-difference method (FDM), a finite-element method (FEM), or a method of weighted residuals (MWR). These methods are probably too costly for circular geometries with uniform linings and rectangular geometries with uniform linings on each wall. However, they may be the only approach when the lining varies peripherally in an arbitrary way or when the duct cross section is not circular, rectangular, or some other geometry for which the Helmholtz equation has separable solutions. These methods are considered in more detail in subsequent sections. However, explicit examples of their use in the no-flow case can be found in references 23 and 24.

Uniform Mean Flow

When uniform mean flow is present, the eigenvalue problem becomes somewhat more complicated. The reduction to a transcendental eigenvalue equation follows exactly the procedure previously described. The analytic representation of the transverse pressure variation remains unchanged, but the eigenvalue equations become more complex. In the circular-duct case,

$$\kappa \frac{J'_m(\kappa)}{J_m(\kappa)} = -i\eta A \left(1 - M\frac{k_x}{\eta}\right)^2 \tag{58}$$

with

$$\frac{k_x}{\eta} = \frac{1}{1-M^2}\left[-M \pm \sqrt{1-(1-M^2)\left(\frac{\kappa}{\eta}\right)^2}\right]$$

In the two-dimensional-duct case,

$$\kappa \tan \kappa = i\eta A\left(1 - M\frac{k_x}{\eta}\right)^2 \tag{59}$$

with k_x/η as defined in the circular-duct case. Both of these eigenvalue problems can be viewed as a single, very complicated transcendental equation (if k_x/η is inserted into eq. (58) or (59) from the auxiliary equation) or as a coupled pair of equations.

The Morse method (refs. 12 and 13) becomes very unattractive for general calculations because the chart must be a conformal transformation from the κ plane to the ηA plane, with Mach number as a parameter. Thus, a separate chart for each Mach number is required. This approach has been used, but direct eigenvalue solutions are certainly of more general interest.

Reference 25 presents an interesting approximate solution technique in its study of bulk liners with an infinite backing space. This case yields a purely resistive lining, and with certain restrictions it arrived at the eigenvalue equation

$$\kappa \tan \kappa = i\eta A\left(1 - M\frac{k_x}{\eta}\right)$$

with k_x/η as previously defined in connection with equations (58) and (59). Note that the quantity $1 - M(k_x/\eta)$ appears to the first power and corresponds to a boundary condition based on continuity of particle velocity. (See the discussion of eqs. (23) and (24) regarding particle velocity and particle displacement.) This approach involved introducing an approximation for the tangent function and then obtaining a direct algebraic solution of the resulting equation.

An early direct eigenvalue solution was presented in reference 26. The method, applied to a two-dimensional duct, considered first the no-flow case. The no-flow eigenvalues were quickly estimated from a Morse Chart and used as initial estimates for a simple Newton-Raphson iteration. Eigenvalues thus determined are initial estimates for a case with a slightly incremented Mach number. Equation (59) is then solved by a combination of relaxation and Newton-Raphson iteration, the right-hand side being constructed from a previous estimate of k_x/η to form an effective admittance. At each stage of relaxation the Newton-Raphson iteration is used to calculate a new κ and k_x/η. Relaxation is carried out until convergence occurs. The Mach number is then incremented and the procedure repeated until the final Mach number is reached. The method was used for a number of calculations with little difficulty, but it has the disadvantage of requiring a solution for the no-flow problem. It is thus not a stand-alone method.

The approximation scheme developed in reference 21 for the circular duct in the no-flow case was extended to the case when flow is present. This extension first solved the problem for κ in the zero admittance case, and under the assumption of small ηA it used this solution in equation (58) to evaluate the right-hand side. This yielded a no-flow problem with an effective admittance to which the previously derived

approximation scheme for small ηA was applied. If the solutions were iterated to make successive approximations converge, the principle would have been essentially that in reference 26.

Ko (ref. 27) has made extensive calculations for the eigenvalues in a rectangular duct with two opposing walls lined. For symmetric modes the two-dimensional eigenvalue equation (59) applies, and for antisymmetric modes a second eigenvalue equation involving the cotangent applies. Ko's method of solution involves beginning with the nearly hard-wall case ($A = 0$) and using the eigenvalues so determined as initial estimates for a Newton-Raphson iteration. The driving frequency is incremented from zero to the required value, but Ko did not fully specify the manner in which the starting values are assigned with each new frequency increment. In reference 28, Ko reported the same type of method and results for a circular duct. He did not comment on the reliability of the Newton-Raphson approach, and this could be substantially affected by the incrementing and initial guess procedures.

A refinement of the Newton-Raphson iteration scheme has been used in reference 29. Instead of a Newton-Raphson iteration, a second-order method known as Bailey's method (ref. 30) was used, which is different in that it requires a second derivative but is used in exactly the same way as a Newton-Raphson iteration. In addition, a detailed study of the topography of the Morse Charts for both zero and uniform mean flow was made. In the case of mean flow, the Morse Charts are severely distorted with increasing Mach number and expand across the $\mathrm{Re}(\kappa)$ axis (at $M = 0$ all permissible solutions lie in one quadrant in the upper half-plane of κ). The starting point in the analysis is the $M = 0$ case. Based on considerable investigation, the Morse Chart (which is universal for any ηA when $M = 0$) is divided into subregions. Depending on the given value of ηA, the starting value for the Bailey iteration is chosen in a subregion near the ηA value. Convergence to the proper eigenvalue is then relatively certain. Mach number is then incremented with the previous Mach number results used for the starting values. It is reported that the result of this development is a reliable computational scheme. A modal identification scheme based on the Morse Charts has been used in reference 29 and further expanded upon in reference 31.

A worker entering the field and needing to develop a stand-alone computational scheme would probably wish to circumvent the detailed study of the topography of the eigenvalue problem if possible. With this goal in mind, Eversman (refs. 32 and 33) has developed an integration scheme to solve equation (58) for the circular-duct case or equation (59) for the two-dimensional-duct case. An integration scheme was used previously in connection with the no-flow case (refs. 17 to 20) and it was found, as demonstrated by equation (57), that the eigenvalue can be obtained as the solution of a nonlinear initial-value problem.

The initial-value-problem approach can be extended to the case when flow is present. The circular-duct case is discussed here. The eigenvalue problem

$$\kappa \frac{J'_m(\kappa)}{J_m(\kappa)} = -i\eta A \left(1 - M\frac{k_x}{\eta}\right)^2 = -i\eta A w^2 \tag{60}$$

with

$$\frac{k_x}{\eta} = \frac{1}{1-M^2}\left[-M \pm \sqrt{1-(1-M^2)\left(\frac{\kappa}{\eta}\right)^2}\right] = \frac{1}{1-M^2}\left(-M \pm v^{1/2}\right) \qquad (61)$$

can be transformed into a differential equation by differentiation of equation (60) and use of the Bessel equation to eliminate second derivatives of the Bessel functions. The result is

$$\frac{d}{d\varsigma}\left(\frac{\kappa}{\eta}\right) = \frac{-iw^2}{F(\kappa) + \kappa F'(\kappa) \pm 2iAM\left(w/v^{1/2}\right)(\kappa/\eta)} \frac{dA}{d\varsigma} \qquad (62)$$

where

$$F(\kappa) = -\frac{J'_m(\kappa)}{J_m(\kappa)}$$

and prime denotes differentiation with respect to the argument. In the derivation of equation (62), the admittance A is taken as a function of the nondimensional parameter ς (for $0 \leq \varsigma \leq 1$). If A_f is the admittance for which the eigenvalues are required, a simple choice is

$$A = \varsigma A_f$$

and

$$\frac{dA}{d\varsigma} = A_f$$

Equation (62) can be integrated from suitable initial conditions with $A = 0$ over $0 \leq \varsigma \leq 1$ to yield an eigenvalue of equations (60) and (61) corresponding to each starting value. It was previously shown (eq. (57)) that an initial-value problem not involving the calculation of Bessel functions can be generated in the no-flow case. This is appealing from an efficiency standpoint. It is also possible in the present case but has not been used because of adverse effects on the accumulation of error in the integration. This follows because when equation (62) is manipulated to eliminate the Bessel functions, equation (60) is used. Because the integration process at each step introduces slight errors, equation (60) is not actually satisfied exactly. This appears to have the effect of making equation (62) very sensitive, to the point of requiring extremely small integration steps.

The integration scheme employed is a fourth-order Runge-Kutta with variable step size. The step size is adjusted by monitoring the residual generated in equation (60) as the integration progresses. When an error bound is exceeded, the integration is halted and a Newton-Raphson iteration is performed to reinitialize the process. The step size is then reduced until the next integration step will lead to an error within the error bound. This type of self-correction is the exception rather than the rule, and a successful integration is often achieved with only 20 integration steps for $0 \leq \varsigma \leq 1$.

The choice of initial starting values for the integration process as the hard-wall eigenvalues seems obvious. However, when $\mathrm{Im}(A) > 0$ two additional starting values appear which lie at

$$\frac{\kappa}{\eta} = \frac{1 - M^2}{M^2} \frac{1}{A} \tag{63}$$

in the limit $A \to 0$. These starting values do not need to be imposed in the limit $A \to 0$, and in a practical calculation a slightly sharper estimate for the starting values is obtained which can be used to produce starting values of modest magnitude (ref. 33).

If the eigenvalues are ordered on the basis of increasing attenuation, the extra eigenvalues generally lie well down the list for parameters typical of turbofan engine applications. However, for low frequencies these eigenvalues can surface near the top. At least one of them has characteristics which have led some investigators to identify it as an instability mode. In fact, the appearance of these modes is not completely understood.

Finite-element, finite-difference, and weighted-residual methods also have applications in ducts with uniform flow, particularly in cases with cross sections which are not circular or rectangular or which have peripherally varying liners. These methods are also applicable when the flow is sheared and are discussed in the next section. The problem of uniform flow in a circular duct using the method of weighted residuals with trigonometric basis functions was specifically addressed in reference 23. The major advantage of any of the methods of discretization of the problem is that the resulting eigenvalue solution spans a complete finite subset of eigenvalues with neither omission nor duplication, provided the discretization is carried out to a high enough level of accuracy. On the disadvantage side, the accuracy of representation of mode shapes and eigenvalues is not uniform and generally decays with increasing modal complexity.

Sheared Mean Flow

When the mean flow is sheared, the eigenvalue problem is defined by equations (22) and (27) or equations (28) and (29). There does not appear to be any general method of obtaining closed form solutions to these equations. Several early investigators introduced approximate solutions. Pridmore-Brown (ref. 34) treated the two-dimensional case with a linear velocity gradient and with a 1/7 power profile by an approximate solution valid asymptotically under circumstances which in practical cases require a high-frequency restriction. In reference 35 a power series expansion was used, and in reference 36 a simple finite-difference discretization of the governing equations was used. This approach was based on a previously successful application of the finite-difference technique when flow is absent (ref. 37). These investigations were directed toward estimation of the attenuation in the fundamental mode. In reference 38 an exact solution within a linear shear profile was used to create an approximate effective impedance which could then have been used to treat the problem as one of uniform flow.

In order to obtain solutions with any degree of generality it is necessary to use methods of numerical solution of the governing differential equations and boundary conditions. In this section four such methods of numerical analysis are discussed.

These methods are all applicable to the simpler problems when the flow is uniform or when the flow vanishes. In most cases, however, they are not as efficient as analytic or semianalytic methods for the simpler problems, and their power is most fully realized in the sheared-flow case.

Reference 7 in the two-dimensional-duct case, reference 39 in the annular-duct case, and reference 40 in the circular-duct case used numerical (i.e., Runge-Kutta) integration of the governing equation. The integration is accomplished in terms of a transfer matrix relating the pressure and the pressure gradient at one wall to those at the other wall:

$$\begin{Bmatrix} P \\ P' \end{Bmatrix}_2 = \begin{bmatrix} T_{11} & T_{12} \\ T_{21} & T_{22} \end{bmatrix} \begin{Bmatrix} P \\ P' \end{Bmatrix}_1 \tag{64}$$

If the boundary conditions at walls 1 and 2 are represented by

$$P_1' = \epsilon_1 P_1$$

$$P_2' = \epsilon_2 P_2$$

we can write

$$\begin{Bmatrix} P \\ P' \end{Bmatrix}_1 = \begin{Bmatrix} 1 \\ \epsilon_1 \end{Bmatrix} P_1$$

$$[-\epsilon_2,\ 1] \begin{Bmatrix} P \\ P' \end{Bmatrix}_2 = 0$$

This leads to the eigenvalue equation

$$[-\epsilon_2,\ 1] \begin{bmatrix} T_{11} & T_{12} \\ T_{21} & T_{22} \end{bmatrix} \begin{Bmatrix} 1 \\ \epsilon_1 \end{Bmatrix} P_1 = 0$$

For nontrivial solutions,

$$F\left(\frac{k_x}{\eta}\right) = T_{21} + \epsilon_1 T_{22} - \epsilon_2 (T_{11} + \epsilon_1 T_{12}) = 0 \tag{65}$$

For sheared flow with no slip at the walls, T_{11}, T_{12}, T_{21}, and T_{22} are functions of k_x/η. For the no-slip case, ϵ_1 and ϵ_2 are not functions of k_x/η. The eigenvalue problem is to find values of k_x/η which satisfy equation (65).

Solutions to equation (65) are probably best obtained by a Newton-Raphson iteration with finite-difference derivatives. Several strategies can be employed to establish starting values. The most conservative approach begins with no-flow eigenvalues and a systematic incrementing of the Mach number. A second approach begins with eigenvalues for uniform mean flow but proceeds at some risk of nonconvergence in cases where the sheared flow substantially modifies the propagation characteristics.

A slightly different approach has been used in reference 41. This reference treated the case of rectangular-duct flow consisting of a central core of uniform flow and a

boundary-layer region of thickness δ. The solution for the central core can be written in analytic form. Equation (28) for the boundary-layer region is approximated by four finite-difference equations, and the interfaces at the duct-wall and boundary-layer uniform flow produce two additional finite-difference equations. The set of six homogeneous equations in terms of the unknown pressures at six finite-difference points in the boundary layer constitutes an eigenvalue equation for values of k_x/η. An advantage of this method is the elimination of the need to increase the number of integration steps for very thin boundary layers. The same number of integration points within the boundary layer is always used without complicating the solution in the uniform-flow region. Reference 41 elaborates no further on the eigenvalue solution technique, but presumably the strategy would be similar to that discussed in connection with the Runge-Kutta integration procedure (refs. 39 and 40). For the calculation of just a few eigenvalues these approaches can be reasonably efficient. However, for the determination of a large number of eigenvalues, certain techniques described in the following discussion may be less costly.

The method of weighted residuals (MWR) in the form of a Galerkin method has proven to be a powerful tool in extracting the eigenvalues for transmission through sheared flows. The Galerkin method begins with the assumption that the solution to the field equations (e.g., eq. (28)) can be approximated as a superposition of a subset of a complete set of functions $\phi_i(y)$ in the form

$$\hat{p}(y) = \sum_{i=1}^{N} q_i \phi_i(y) \tag{66}$$

where the number of basis functions N is chosen to produce convergence of the result based on the number of required accurate eigenvalues. In the standard application of the Galerkin method the basis functions are chosen to satisfy the boundary conditions. This poses no difficulty in the sheared-flow case with no slip at the wall since solutions to the no-flow problem serve the purpose.

The coefficients q_i in the superposition of equation (66) are determined in a way which minimizes the error of the trial solution. Equation (32) can be written in linear operator form as

$$\mathcal{L}[p] = 0$$

When the trial solution $\hat{p}$ is substituted, a residual, or error, results:

$$\mathcal{L}[\hat{p}] = R$$

The residual must vanish if it is orthogonal to every member of a complete set of functions. The set of test functions is chosen as the same subset of complete functions used as basis functions. Thus, N relations of the type

$$\int_0^1 \phi_j R \, dy = 0 \qquad (j = 1, 2, ..., N) \tag{67}$$

can be formed. This procedure leads to a set of N homogeneous algebraic equations for the N coefficients q_i. The coefficients in this equation depend on k_x/η and a nontrivial solution exists for discrete values of k_x/η. The algebraic equations can be cast as a linear eigenvalue problem:

$$\mathbf{Aq} = \lambda \mathbf{q} \tag{68}$$

where, depending on the structure of the particular problem, $\mathbf{A}$ is a matrix of coefficients, $\mathbf{q}$ is a vector related to the unknown coefficients in equation (66), and λ is the eigenvalue related to k_x/η. This type of eigenvalue problem is routinely solved by standard algorithms.

Hersh and Catton (ref. 42) were the first to use this procedure in the case of a hard-wall two-dimensional duct. They used the no-flow solutions in the form of trigonometric functions. They refined the estimates thus obtained by using them as initial values in the Runge-Kutta method previously described (refs. 39 and 40).

Savkar (ref. 43) approached the same problem using polynomial basis functions which were constructed to satisfy the boundary conditions for either a hard-wall two-dimensional duct or a two-dimensional duct with acoustically absorbing walls.

In references 44 and 45 the Galerkin method was used to study the attenuation in sheared flow in two-dimensional and three-dimensional rectangular ducts. This appears to be the first time this problem was cast as a linear algebraic eigenvalue problem and a large-scale eigenvalue solution routine was used. As a consequence of this approach eigenvalues were calculated which are clearly acoustic as well as eigenvalues which appear to be nearly hydrodynamic in nature. The Galerkin method was also used in references 46 and 23 in the uniform-flow case. This is a more difficult situation because the boundary condition at the wall involves the eigenvalue k_x/η. Rather than use basis functions which satisfy the boundary conditions, a boundary residual is introduced in addition to the field-equation residual. The modified Galerkin method is then used to obtain coefficients in equation (67) which minimize the field-equation residual and the boundary residual. A feature of this work is the use of the acoustic field equations in the form of the primitive variables p and V. This constitutes an application of the Galerkin method to a set of equations. The choice of basis functions is suggested by results in the no-flow case.

Yurkovich (ref. 47) demonstrated the power of the Galerkin method in his investigation of the acoustic transmission in circular and annular ducts carrying sheared and swirling flows.

The Galerkin method is but one of several methods by which the field equations and boundary conditions are replaced by discrete relations in the form of algebraic equations. Perhaps the most obvious way of doing this is by replacement of the differential equations with their finite-difference approximations. This was first proposed in reference 48. The appealing characteristic of this approach is the tridiagonal form of the difference equations. However, the structuring of the difference equations as a standard linear algebraic eigenvalue problem is hindered by the presence of the eigenvalue k_x/η in equation (22) or (28) in the coefficients of both P and P'. As shown in references 44 and 45, it is possible to replace the problem, which turns out to be cubic in k_x/η, with one which is linear in k_x/η but tripled in order. However, this would not preserve the tridiagonal character of the problem. In reference 48 an iterative scheme was devised to cope with this and to maintain a tridiagonal difference representation.

Dean (ref. 49) has also used a finite-difference scheme. He was primarily concerned with obtaining a simple eigenvalue procedure which takes advantage of the basically tridiagonal nature of the difference equations. Toward this end he replaced the

actual shear profile with a velocity discontinuity (similar to the boundary-layer displacement thickness concept). He was then able to put the entire effect of the boundary layer into the boundary condition and thus only slightly disrupt the very simple linear algebraic eigenvalue problem which would exist for completely uniform flow with a zero wall velocity. He used an iterative technique based on the nearly tridiagonal nature of the problem to calculate eigenvalues. The advantage of this over a standard algebraic eigenvalue routine is the ability to focus on specific modes without calculating the entire eigenvalue set. The disadvantage is the necessity of having good starting values and the resulting implication of convergence problems, which are analogous to difficulties found with other methods.

The most flexible of the methods of discretization of the field equations is the finite-element method (FEM). The major strength of FEM lies in the systematic treatment of problems with irregular boundaries and solution grids. The application of FEM to eigenvalue problems in ducts is relatively straightforward for circular and rectangular ducts because they are one dimensional (i.e., the transverse coordinate). No considerations of element geometry arise and one is concerned mainly with the question of choosing element shape functions which produce a good balance between eigenvalue solution accuracy and computational efficiency.

In general, in acoustic problems for ducts with attenuating walls and sheared mean flow, variational principles are not available. The finite-element formulation in duct acoustics is thus carried out with a Galerkin method and except for the choice of the basis functions and test functions is identical to the classic Galerkin method.

In the finite-element method the domain is divided into subdomains (or elements) in which suitable basis functions (or shape functions) are defined. A distinguishing feature of the finite-element method is that the shape functions interpolate the acoustic field within the element on the basis of the value of the acoustic field at discrete points (or nodes) within and on the boundary of the element. A second distinguishing feature is the fact that what is a global basis function in the classic Galerkin method is replaced in the finite-element method by a patchwork of local basis functions (shape functions) explicitly defined within each element. Continuity on interelement boundaries leads to a rationale for assembling the element "stiffness" matrices into a global stiffness matrix. The term stiffness matrix is used only by analogy with the more common applications of finite-element methods to structural analysis.

Finite-element analysis has become a field of applied mathematics in its own right. It is not appropriate, and in fact it is probably impossible within the constraints of space herein, to give the details of the applications in duct acoustics. Hence, we only refer to certain specific examples of application.

In the eigenvalue problem the application of the finite-element method is particularly simple since the field equation is an ordinary differential equation (e.g., eq. (28)) or perhaps the equivalent set of ordinary differential equations (derived from eqs. (18) and (19)). The main question to be answered is the achievable accuracy with various choices of element types. The element type relates to the geometrical shape of the element and the type of shape functions. In an ordinary differential equation the geometrical shape of the element is a straight line, so only the type of shape function is to be determined for the particular application.

Application of the finite-element method again leads to the linear algebraic eigenvalue problem (eq. (68)) for the axial wave numbers,

$$\mathbf{Aq} = \lambda \mathbf{q}$$

where λ is related to k_x/η. In this case the generalized coordinates in $\mathbf{q}$ are the values of the acoustic field at the finite-element nodes. Hence, the eigenvectors are the discrete analogs of continuous eigenfunctions which might arise from a solution of the boundary value problem of equations (22) and (27).

In the context of the eigenvalue problem for the uniform-flow duct with a general mean flow, the FEM has been investigated extensively in references 50 to 52. In the original formulation (refs. 50 and 51), elements with quadratic shape functions were used. These elements require a grid where nodal values of the acoustic state variables are specified. In certain instances the solution set of eigenvalues degenerates in accuracy rapidly as the modal order increases. Spurious eigenvalues occur with corresponding eigenvectors characterized by large slope discontinuities at element boundaries. The degeneration in accuracy is lessened by refining the mesh and thereby increasing the dimensionality of the problem.

A considerable improvement was achieved by the introduction of Hermitian elements (ref. 51). These elements, referred to loosely as "beam bending elements," have cubic shape functions based on specification of the acoustic states and their derivatives at the nodes (bending deflection and bending slope in the analogous structural element). Use of Hermitian elements eliminates spurious modes and improves the accuracy for a given dimensionality.

A second concept introduced in the improved version (ref. 51) is the equivalent of an eigenfunction expansion in vibration analysis. The eigenvalue problem for the case of mean flow is expanded in terms of a subset of the eigenvectors obtained when flow is absent. When flow is absent the eigenvalue problem is significantly reduced in dimensionality. The net effect of solving first the no-flow eigenvalue problem and then the flow eigenvalue problem with a reduced set of basis functions is to offer a considerable computational savings with minimal reduction of accuracy.

The FEM is not limited to simple geometries and can accommodate an arbitrary lining configuration, although at considerable cost in dimensionality. Reference 53 demonstrated the use of the FEM for the calculation of the eigenvalues for circular and rectangular ducts with a peripherally varying liner.

In many cases the boundary layer is thin in comparison with the duct transverse dimension. In this case a considerable simplification in the computation of the duct eigenvalues, and therefore the attenuation, can be achieved. References 54 to 56 used an asymptotic expansion within the boundary layer based on the small parameter δ/L, where δ is the boundary-layer thickness and L is the characteristic transverse dimension. This procedure produces an equivalent boundary condition to be enforced at the edge of the boundary layer. At the outer wall of a circular duct the boundary condition is

$$\frac{dP}{dr} = -\frac{(1 - M_o K)^2 \left(i\eta A + \epsilon \left\{ \beta \int_0^1 \left[d\xi/(1 - M_o K \phi)^2 \right] - \alpha \right\} \right)}{1 + i\epsilon\eta A \int_0^1 (1 - M_o K \phi)^2 \, d\xi} P \qquad (69)$$

where

ϵ $= \delta/R$

M_o core flow Mach number

A	wall dimensionless admittance
α	$= \eta^2 - i\eta A$
β	$= m^2 + \eta^2 k^2$
K	$= k_x/\eta$

The velocity profile in the boundary layer is given by

$$M(\xi) = M_o\phi(\xi) \qquad (0 \leq \xi \leq 1)$$

where $\xi = 1$ corresponds to the outer edge of the boundary layer. An interesting and important implication of equation (69) is the limiting case $\epsilon \to 0$, for which the boundary condition becomes identical to equation (26), thus verifying the correctness of the continuity of particle displacement assumption used in its derivation.

The boundary condition of equation (69) should be applied at the edge of the boundary layer. Since the boundary layer is assumed to be thin relative to the duct radius, it is generally adequate to apply the boundary condition at the duct wall, in which case it can legitimately be viewed as an effective admittance. Wherever applied, the effective admittance is a function of the axial wave number k_x, whereas in the usual point reacting liner boundary condition (eq. (26)) the admittance is independent of k_x (though generally dependent on η, the dimensionless frequency). In fact, the effective admittance is that of a bulk reacting boundary, that is, one that admits wave propagation.

The computation of eigenvalues can still proceed from equations (58) and (59), but the integration scheme of equations (60) to (62) is no longer directly applied. The integration scheme can be used in combination with relaxation if the eigenvalue problem is first solved with $\epsilon = 0$ (the uniform-flow case). The values of $K = k_x/\eta$ so obtained can be used to evaluate the effective admittance

$$A_{\text{eff}} = \frac{i\eta A + \epsilon\left\{\beta \int_0^1 \left[d\xi/(1 - M_o K\phi)^2\right] - \alpha\right\}}{1 + i\epsilon\eta A \int_0^1 (1 - M_o K\phi)^2 \, d\xi} \tag{70}$$

which can then be used in the integration scheme to find new values of K. This sequence proceeds to convergence of the K values. Should convergence difficulties arise, increments of ϵ can be used, but for a small ϵ this should not be necessary.

The effective admittance can be computed explicitly for linear, sinusoidal, and $1/N$ power law boundary layers. For other boundary layers the integrals may have to be computed by numerical quadrature.

Myers and Chuang (ref. 57) have improved upon the inner expansion by obtaining a uniformly valid matched asymptotic expansion which maintains accuracy for thicker boundary layers. The resulting eigenvalue problem is modified, but a similar procedure would be used to obtain eigenvalues and eigenfunctions.

General Computational Results

Design criteria for acoustic liners in turbofan inlet and exhaust ducts are considered in detail in another chapter. In this section we refer to some general results

which can be deduced. All results quoted are for tuned linings consisting of a resistive face sheet and a cavity backing. Details of lining characteristics are given in another chapter.

Rice (ref. 58) has shown that the presence of a uniform mean flow has a substantial effect on the acoustic lining impedance required to obtain maximum attenuation. For an initially planar acoustic wave introduced in a circular lined duct (constructed from the superposition of 10 nonplanar soft-wall symmetric acoustic modes), he determined the curves of equal sound power attenuation in the impedance plane, both with no flow and with an inlet flow of $M = -0.4$ (negative Mach number indicates propagation opposite to flow direction), at a nondimensional frequency $\eta = \pi$. The attenuation was computed over an axial length of 6 duct radii. The result in the impedance plane is shown in figure 3, in which it is shown that the presence of flow has a strong effect on the values of impedance which correspond to a given level of attenuation, and in particular on the impedance required to achieve optimum attenuation. He also shows that the maximum achievable level of attenuation is relatively insensitive to the mean flow. This is shown in figure 4 wherein attenuation per distance equal to duct diameter is plotted against the nondimensional frequency η. There is a substantial decrease in achievable attenuation with frequency, but very little dependence on Mach number. This result cannot necessarily be extended to other combinations of modes.

A study (ref. 26) for the two-dimensional case considered only the fundamental mode and examined the variation of the frequency at which peak attenuation occurs as a function of Mach number for specific linings. Plotted in figure 5 is the ratio of the tuning frequency f_P (frequency of peak attenuation in the fundamental mode) to the tuning frequency at zero Mach number $(f_P)_{M=0}$ as a function of Mach number. It is shown that the tuning frequency decreases in inlet flow and increases in exhaust flow. The result is relatively insensitive to the resistance of the lining.

It is found in reference 59 that modes of high spinning and radial orders (modes which are not axisymmetric) attenuate more rapidly than those of lower orders. It is concluded that some knowledge of the source is required to carry out a reasonable lining design.

The effect of the boundary layer is important in the determination of the optimum impedance. Simple considerations of ray acoustics show that for an inlet flow where the sound propagation is opposite to the mean flow, the boundary layer tends to refract acoustic rays away from the duct wall, and it might be expected that for a given lining the attenuation would be less than that calculated using a uniform mean flow. The opposite effect should occur in exhaust flows. This is supported by experiment, although a greater effect is seen in inlet flows than exhaust flows. A parametric study (ref. 60) showed that for inlet flows the optimum acoustic resistance for individual well-cut-on modes is reduced substantially with increasing boundary-layer thickness, while the boundary-layer effect on reactance is much smaller. The most significant fact found is shown in figure 6. Here the ratio of optimum attenuation with boundary layer σ to optimum attenuation with no boundary layer σ_0 is plotted against the ratio of the boundary-layer thickness δ to the wavelength λ for a given angular mode m and frequency η. For boundary layers up to 25 percent of the wavelength, the achievable attenuation is not very sensitive to the boundary-layer thickness. Hence, with proper design procedures the presence of a boundary layer need not reduce the achievable attenuation for well-cut-

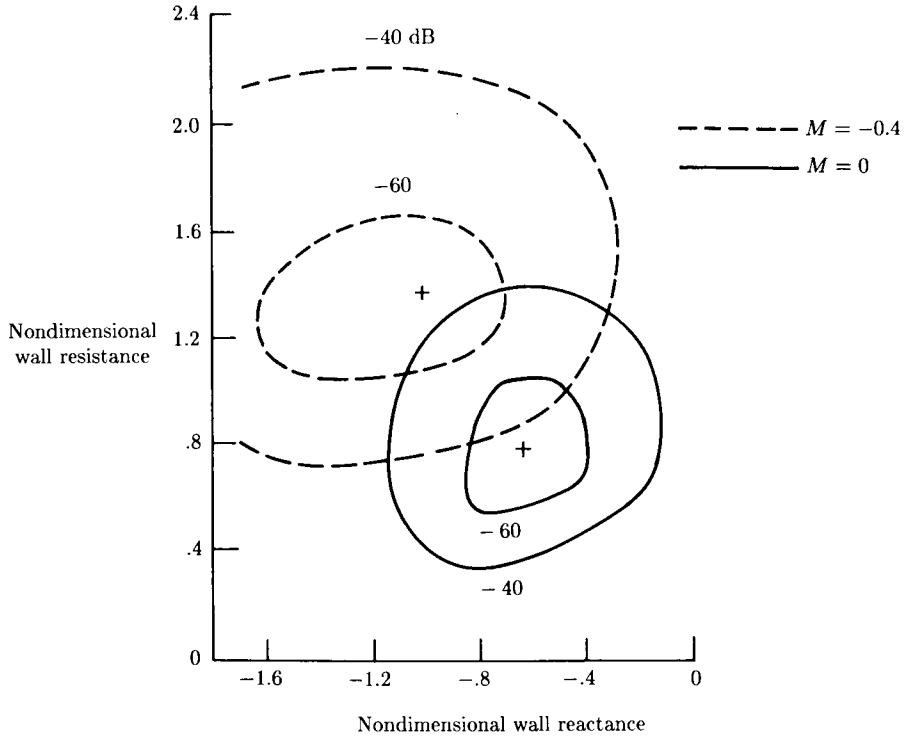

Figure 3. Contours of constant attenuation in length of 6 duct radii for circular duct. $L/D = 3; \eta = \pi$.

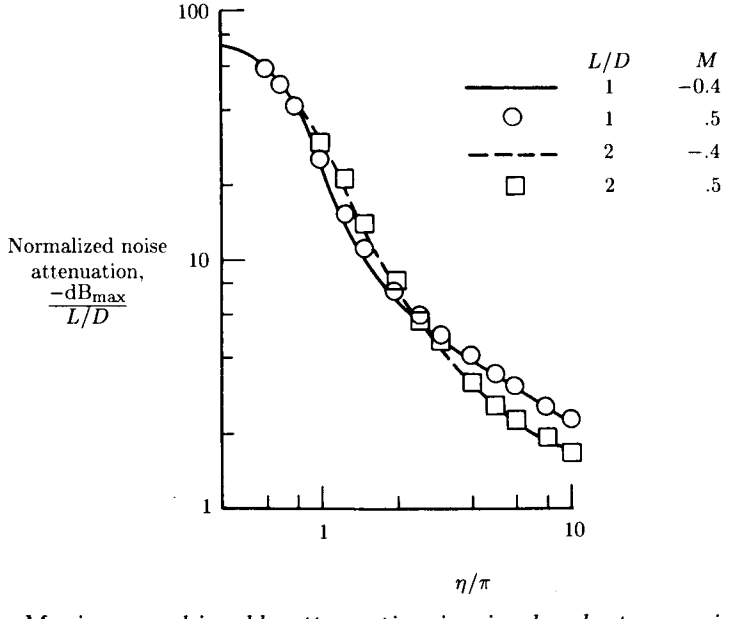

Figure 4. Maximum achievable attenuation in circular duct per axial distance equal to duct radius.

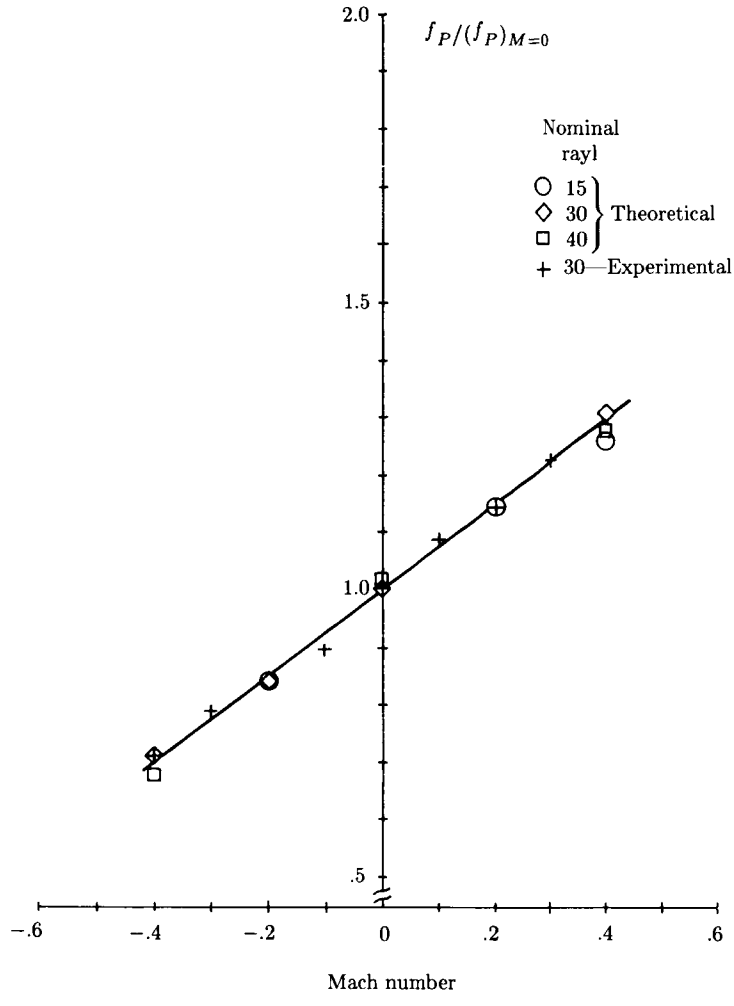

Figure 5. Comparison of theory and experiment for ratio of frequency of peak attenuation with mean flow f_P to frequency of peak attenuation without flow $(f_P)_{M=0}$ for several lining flow resistances.

on modes. This fact can be understood in the context of effective admittance. (See eq. (70).) As long as the effective admittance takes the optimal value, the attenuation is independent of boundary-layer thickness (within the limitations of the equation).

Reference 61 showed that a precise model of the boundary layer is not required to carry out practical design calculations. It showed that a boundary-layer profile which matches the shape factor (ratio of displacement thickness to momentum thickness) and the displacement thickness of the actual boundary layer produce attenuation rates essentially the same as the actual boundary layer. In particular, the 1/7 power law boundary layer can be replaced by a linear profile with slip at the wall. This observation minimizes the computational difficulties associated with sheared-flow

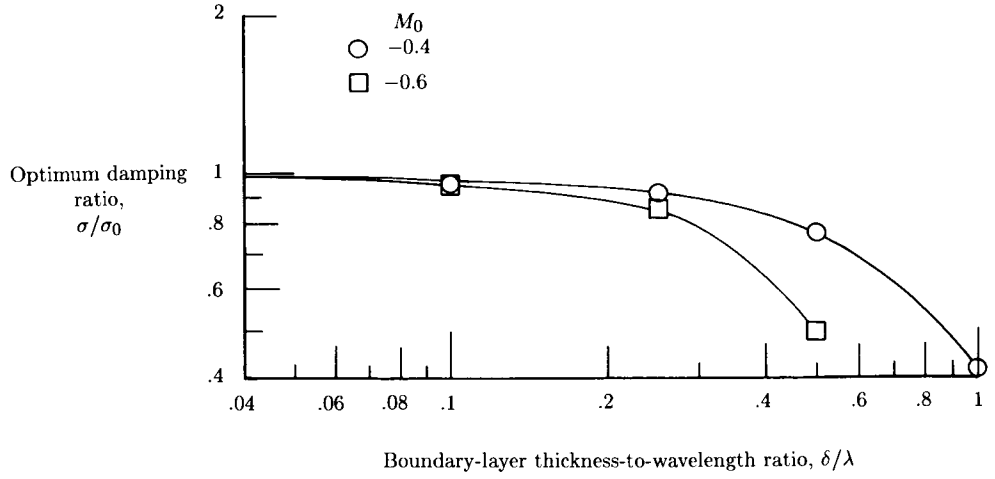

Figure 6. Effect of ratio of boundary-layer thickness to wavelength on ratio of maximum attenuation with boundary layer to maximum attenuation without boundary layer. $m = 7$ mode; $\eta = 10\pi$.

calculations. Other investigations showed that a thinner boundary layer with a linear profile but without slip can also be used to simulate the actual engine duct profiles, which are seldom of 1/7 power. If the boundary layer is not thin, care should be taken to use the actual profile.

An Alternative Calculation Scheme Based on Correlation Equations

The computation schemes introduced previously can be coupled with a suitable optimization algorithm to create a suppressor design procedure. A design iteration based on these schemes would be complicated and time-consuming and in addition may require information not available to the designer (e.g., the duct modes present). An additional complication is the large number of parameters involved, since the optimum impedance is a function of frequency, Mach number, boundary-layer thickness, and duct modes present. Furthermore, even after an optimum design is achieved (one which produces the maximum attenuation), it is necessary to consider off-design performance, which requires more analysis. In an effort to streamline this procedure, Rice (refs. 3, 59, 60, and 62 to 65) has made major contributions to the design process by identifying correlating equations from which approximate computations of suppressor performance can be made. He has found an analytic approximation for the contours of equal attenuation in the impedance plane (see fig. 3, e.g.) (refs. 62 and 63), which is a function of the optimum impedance and the optimum attenuation rate for a given mode, mean flow Mach number, boundary-layer thickness, duct geometry, and frequency. This approximation allows the rapid estimation of off-design liner performance, that is, the equal attenuation contours for linings which are not optimum.

A second major contribution to the design procedure introduced by Rice is his discovery that the optimum impedance (resistance and reactance) and the maximum

possible attenuation for a given frequency, boundary-layer thickness, and geometry are uniquely defined by the modal cutoff ratio (refs. 3 and 64). In this context, the definition of modal cutoff ratio is extended to ducts with acoustic treatment by introducing the definition

$$\beta = \frac{\eta}{R\sqrt{(1 - M^2)\ \cos\ 2\phi}} \tag{71}$$

where the axial wave number is given by

$$\frac{k_x}{\eta} = \frac{-M + \sqrt{1 - (1 - M^2)(\kappa/\eta)^2}}{1 - M^2}$$

and

$$\kappa = R\ \exp(i\phi)$$

Figure 7 shows the loci of optimum impedances for a given frequency, Mach number, and boundary-layer thickness. Numerical computations were carried out by Rice (ref. 3) to find the optimum impedance for a large number of modes with different spinning (angular) and radial mode numbers. The data symbols correspond to the angular mode m, and the location of the symbol around the curve clockwise corresponds to increasing radial mode number μ. Modal cutoff ratio decreases in the clockwise direction. Where two symbols are nearly coincident the modal cutoff ratios are nearly the same, as indicated by the identification of two symbols with cutoff ratios near $\beta = 1.2$.

Based on this observation reference 64 established a correlating equation for optimum impedance as a function of cutoff ratio for a given Mach number, boundary-layer thickness, and frequency. The success of the correlating equations is shown in figures 8 and 9 for a specific case. Optimum resistance and reactance are shown as a function of cutoff ratio with boundary-layer thickness as a parameter for a specific frequency and Mach number. The data symbols are the result of numerical computations and the curves are the result of the correlating equations.

Hence, algebraic equations, which result from extensive numerical analysis, insight into the theoretical results, and some empiricism, are available for the design process. Rice and Sawdy (ref. 66) have summarized the design procedure and an extension which also makes use of a correlation of the far-field directivity to cutoff ratio.

The results are based on analysis of ducts of infinite length; that is, there are no reflections from the duct termination. The results may be substantially modified for short ducts typical of fan engine inlets. The cutoff ratio remains a viable design parameter, but the duct L/D becomes an important additional parameter.

Acoustic Energy

One convenient measure of the effectiveness of acoustic treatment in a duct is the acoustic energy which is absorbed or reflected by the treatment. In principle this measure can be applied by computing the acoustic power or the acoustic energy flux (acoustic power per unit area) at two duct cross sections a distance Δx apart

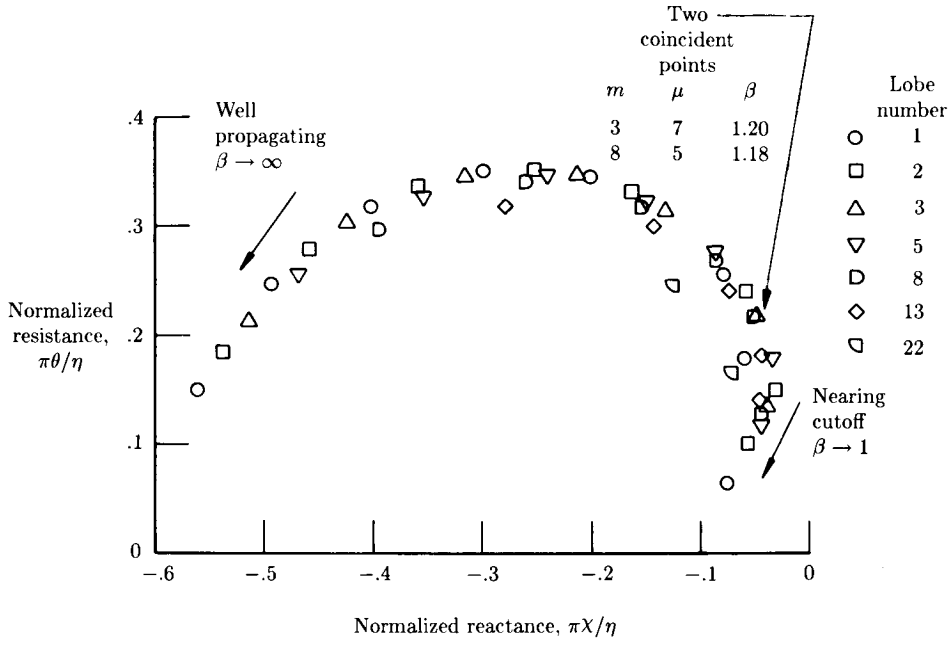

Figure 7. Loci of optimum impedance values for given frequency in circular duct with sheared mean flow. $f = 2890$ *Hz;* $\eta = 9.47\pi$; $M_0 = -0.36$; $\delta/r_0 = 0.059$.

and by then attributing the decrease in the flux to the attenuation introduced by the lining. The flux of acoustic energy can also in principle be broken down into incident, reflected, and transmitted contributions. Calculation of these components can be used to quantify the effectiveness of reactive acoustic treatment in terms of reflection and transmission coefficients.

In thermo-fluid mechanics, energy density and flux are defined in terms of products of the fluid state variables. In the acoustic case definitions of acoustic energy density and flux are to be expressed in terms of only steady-state and first-order-fluctuating acoustic perturbations. For general flows this is an elusive goal, at least in the sense of producing definitions which are appropriate for practical calculations. Morfey (ref. 67) has addressed the question of general flows, as has Möhring (refs. 68 and 69). Morfey also discussed one of two definitions of acoustic energy density and flux, which are useful for calculations in a restricted class of flows. He restricted attention to irrotational uniform entropy flow. For this case the consideration of the time-averaged flux of stagnation enthalpy across a fixed surface yields the definitions

$$E_I = \frac{1}{2\rho c^2} p^2 + \frac{1}{2}\rho V^2 + \frac{1}{c^2}(\mathbf{V}_o \cdot \mathbf{V})p \tag{72}$$

$$\mathbf{N}_I = p\mathbf{V} + \rho(\mathbf{V}_o \cdot \mathbf{V})\mathbf{V} + \frac{1}{\rho c^2}\mathbf{V}_o p^2 + \frac{1}{c^2}\mathbf{V}_o(\mathbf{V}_o \cdot \mathbf{V})p \tag{73}$$

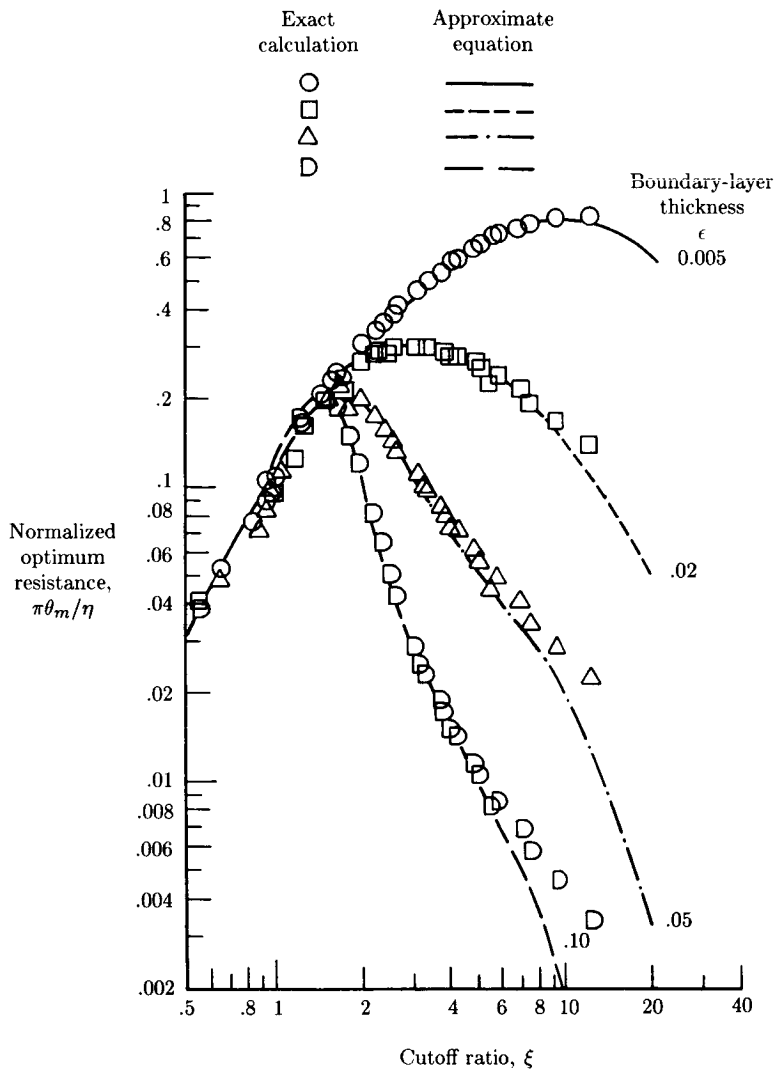

Figure 8. Comparison of correlating equation with experiment for optimum resistance for several nondimensional boundary-layer thicknesses. $\eta = 15\pi$; $M_0 = -0.4$.

where E_I is the acoustic energy density, $\mathbf{N}_\mathrm{I}$ is the acoustic energy flux, ρ is the local mean flow density, c is the local mean flow speed of sound, and $\mathbf{V}_o$ is the mean flow velocity. These definitions are given in *dimensional* form, as is almost universally the case in the literature. The equivalent nondimensional forms are easily obtained by scaling the energy density by a suitable reference value $\rho_r c_r^2$ and the flux by $\rho_r c_r^3$. It is important to note that the definitions are entirely in terms of the steady-flow

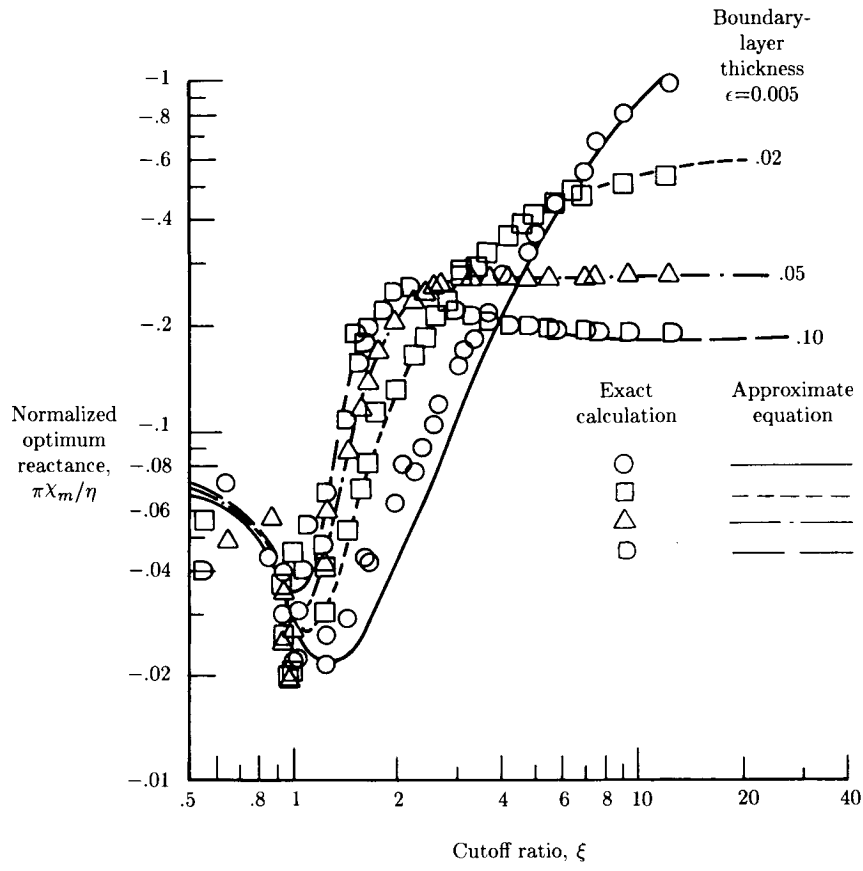

Figure 9. Comparison of correlating equation with experiment for optimum reactance for several nondimensional boundary-layer thicknesses. $\eta = 15\pi$; $M_0 = -0.4$.

state variables and second-order terms involving the first-order acoustic fluctuations p and $\mathbf{V}$.

A second approach, typified by the work in reference 70, starts directly with the thermo-fluid mechanics energy equation, expands in a perturbation series, subtracts out the steady-flow contributions, retains only second-order quantities in the acoustic fluctuations, and defines the resulting quantities as acoustic energy density and flux. If the mean flow is entirely uniform, this procedure yields the definitions

$$E_{\mathrm{II}} = \frac{1}{2\rho c^2} p^2 + \frac{1}{2}\rho V^2 \tag{74}$$

$$\mathbf{N}_{\mathrm{II}} = p\mathbf{V} + \mathbf{V}_o \left(\frac{1}{2\rho c^2}\, p^2 + \frac{1}{2}\rho V^2 \right) \tag{75}$$

These are again in terms of second-order terms involving the first-order acoustic fluctuations.

The acoustic intensity in either case is defined as the time-averaged acoustic energy flux

$$\mathbf{I} = \langle \mathbf{N} \rangle$$

The total acoustic power at a duct cross section is

$$P = \int \int_S \mathbf{I} \cdot \mathbf{n} \, dS$$

where S is the surface area over which the integral is carried out. If there are no energy sources or sinks the acoustic power is conserved between two duct cross sections Δx apart. This result is true for both definitions of acoustic energy flux.

Candel (ref. 71) has reviewed much of the literature dealing with acoustic energy principles in general and their application to ducts in particular. The classification given herein is consistent with his observations. Both forms are valid sets of definitions, but the type I energy definitions satisfy a conservation law for a wider class of flows.

Eversman (ref. 72) shows that the two forms of energy density are compatible with variational principles, from which the acoustic field equations can be derived in the case of uniform flow when both definitions satisfy a conservation law. The term E_{I} is the Hamiltonian density and E_{II} is the Lagrangian density. In general, $E_{\mathrm{I}} \neq E_{\mathrm{II}}$ and $\mathbf{N}_{\mathrm{I}} \neq \mathbf{N}_{\mathrm{II}}$. However, this is not significant; as energy-related quantities, suitable additive constants can be introduced to force equivalence. The important fact is that the change in acoustic power between two duct cross sections Δx apart is zero when no energy sources or sinks are present.

When energy sources or sinks are present, a modified form of the definition of acoustic power must be used to account for them. This has been done for a lined uniform duct with uniform flow (ref. 72). The appropriate definitions are

$$P_{\mathrm{I}} = \int \int_S \langle \mathbf{N}_{\mathrm{I}} \rangle \cdot \mathbf{n} \, dS + V \left(\langle p_b \varsigma \rangle + pV \langle u_b \varsigma \rangle \right)$$

$$P_{\mathrm{II}} = \int \int_S \langle \mathbf{N}_{\mathrm{II}} \rangle \cdot \mathbf{n} \, dS + V \int \left\langle p_b \frac{\partial \varsigma}{\partial x} \right\rangle dx$$

The surface integral terms are recognized as the power definitions for the hard-wall duct. The terms p_b and u_b are the values of the acoustic pressure and the axial component of the acoustic particle velocity at the duct wall. The term $\varsigma(x,t)$ is the wall displacement field. It is found that

$$\frac{dP_{\mathrm{I}}}{dx} = \frac{dP_{\mathrm{II}}}{dx} = -\langle r_b \varsigma_t^2 \rangle$$

where r_b is the resistive component in the lining impedance,

$$Z = \frac{P}{\varsigma_t} = r_b + i x_b$$

and ς_t is the normal component of velocity at the wall. Hence, the rate of decrease of acoustic power is the same for either definition.

Nonuniform Ducts

The duct system through which fan noise propagates and radiates is contoured for aerodynamic and propulsive efficiency. In the acoustic design sequence it may be necessary to determine the effect of the duct nonuniformity on the lining performance. Modeling of acoustic propagation in the fan inlet and exhaust ducts involves consideration of the geometric nonuniformity of the duct as well as the resultant nonuniformity in the mean flow. The problem thus becomes one of considerable complexity for which no "exact" analytical solution is generally available, as in the case of many comparable problems in uniform ducts.

As noted previously, the propagation and radiation problems are coupled and should be solved simultaneously. This is the ultimate goal of the modeling process. However, most analysis methods have approached the propagation and radiation problems separately by treating the propagation as occurring in a duct with no reflection at the termination and the radiation then proceeding from the conditions established in this manner at the termination. Even this simplification leaves the difficult problem of describing the mean flow in the duct and the acoustic propagation in the presence of this flow.

In this section we look at methods which have been used to consider the acoustic propagation in nonuniform ducts with reflection-free terminations. This challenging problem was first attacked for the case when the mean flow vanishes or can be assumed to be of negligible effect. Subsequent extensions were made to include the effect of mean flow. The discussion herein is split up in the same way and a number of techniques are reviewed.

The question of radiation to the far field is addressed in the final section of this chapter, wherein modeling methods are introduced with which the entire propagation and radiation process can be described. This section and the final one are thus closely related.

Nonuniform Ducts Without Mean Flow

Methods of modeling linear acoustic propagation in nonuniform ducts without flow can be broken down into five major categories: (1) one-dimensional or plane-wave approximations; (2) approximations for higher order acoustic modes which neglect modal coupling; (3) stepped duct approximations; (4) variational and Galerkin methods; and (5) finite-element and finite-difference methods. The last category of methods has been successfully extended to include the radiation to the far field.

At low frequencies the Webster horn equation (ref. 73) can be obtained either by directly considering one-dimensional forms of the continuity and momentum equations or by expanding the acoustic equations in terms of powers of a small parameter which is the ratio of the duct radius to the wavelength. The first-order terms are the Webster equation. The resulting theory is equivalent to the "plane-wave theory" in uniform ducts. For most problems in turbofan duct acoustics the theory is not adequate for the representation of high-frequency propagation from rotating-blade noise sources. However, the solution of Webster's equation has been used in a modern context in reference 74 in connection with studies of the acoustic properties of the contoured circular duct present in a bottle neck.

When the cross-sectional area of the duct or the acoustic lining properties vary slowly, perturbation techniques become useful. The method of multiple scales was used in reference 75 in connection with the acoustic wave equation in the case without mean flow to represent the propagation of a single mode. To this level of approximation no interaction can occur between the various acoustic modes which occur in the duct. A second approach, which arrives at essentially the same result in the case of the duct with no acoustic lining, comes from reference 76. It used a Galerkin method but neglected the modal interaction in an application of the WKB approximation for the resulting uncoupled set of ordinary differential equations with slowly varying coefficients. The result is a solution for the axial variation of amplitude of the acoustic modes in the duct, but without the effect of modal interaction.

A reasonable approach to the modeling of a nonuniform duct which includes the effects of modal interactions is the segmentation of the duct into a sequence of uniform ducts with step changes in duct cross-sectional area or lining impedance at the interfaces. It is assumed that in each segment the pressure field can be approximated by a finite (and hopefully small) number of the acoustic modes for the section, each with undetermined amplitude. Conditions of continuity of mass and axial momentum at the interfaces are enforced in that a sequence of residuals, weighted by the acoustic modes themselves, are required to be orthogonal on the cross sections of the discontinuities. For given input modal amplitudes and an assumed reflection-free termination, it is possible to set up a set of linear equations for the modal amplitudes in each segment. Acoustic pressures at any point in the duct can then be recovered by suitable postprocessing of the modal amplitudes and associated acoustic modes. In reference 77 this method was introduced for the uniform duct with an axially varying lining, and it was used in reference 78 for the case of a duct with axially varying cross-sectional area. It is appropriate to point out here that the segmentation approach has also been employed in the case of ducts with mean flow. Axially segmented linings in a uniform duct with uniform flow were considered in reference 79 and extended to shear flows in reference 80.

The first use of a Galerkin method (or, more generally, the method of weighted residuals (MWR)) in the duct acoustic propagation problem was apparently in reference 76, as previously noted. This investigation of hard-wall ducts was based on a velocity potential. The formulation admitted the effect of modal coupling, but this was subsequently neglected at the solution stage. We are interested in the more general case when modal coupling effects are retained and a locally reacting duct liner is present.

The application of the Galerkin method to propagation in nonuniform ducts is similar to the application to the eigenvalue problem described by equations (66) to (68). Figure 10 shows the general geometry of the nonuniform duct between semi-infinite uniform ducts. In the nonuniform section $0 \leq x \leq L$, the impedance $Z_B(x)$ and the area $S_B(x)$ can vary. This figure can be considered either as a two-dimensional or circular duct (θ = Constant plane in a cylindrical coordinate system).

The acoustic field is described by field equations, represented here by a linear vector operator $\mathcal{L}_F$, acting on the acoustic state variables, which may include pressure p and particle velocity $\mathbf{V}$:

$$\mathcal{L}_F[\mathbf{V}, p] = 0 \tag{76}$$

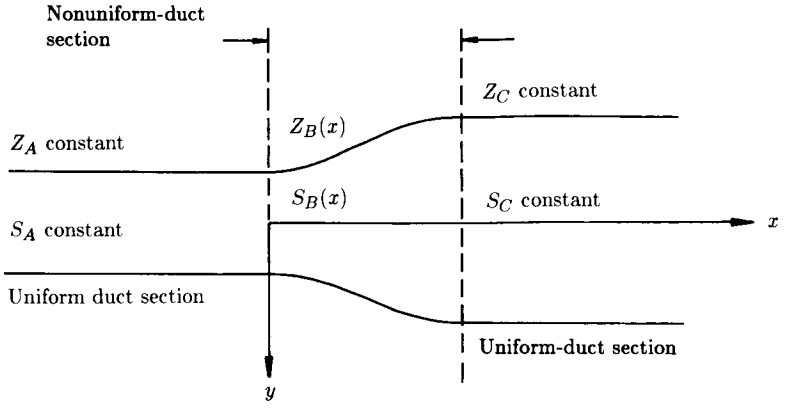

Figure 10. Geometry of nonuniform-duct segment between uniform infinite ducts.

The term $\mathcal{L}_F$ is written as a vector operator because it may represent several field equations. For example, equation (76) could be the acoustic continuity and momentum equations (eqs. (18) and (19) with $M = 0$) in the case of harmonic motion,

$$i\eta p + \nabla \cdot \mathbf{V} = 0 \tag{77}$$

$$i\eta \mathbf{V} = -\nabla p = 0 \tag{78}$$

or it could be the Helmholtz equation in pressure only:

$$\nabla^2 p + \eta^2 p = 0 \tag{79}$$

Solutions are sought in the form of a superposition of the transverse acoustic modes for a duct which is locally uniform:

$$\{P\} = [\phi]\{q\}$$

where $\{P\}$ is the vector of field variables (for example, three components of particle velocity and pressure), $[\phi]$ is a suitable modal matrix derived for a locally uniform duct, and $\{q\}$ is the vector of modal amplitudes (generalized coordinates).

The uniform-duct acoustic modes do not satisfy the boundary conditions for the nonuniform duct, and these conditions must be included as part of the problem statement. On the duct wall,

$$\mathbf{V} \cdot \boldsymbol{\nu} = \boldsymbol{A}p$$

This can be cast as the following boundary operator:

$$\mathcal{L}_B[\mathbf{V}, p] = 0 \tag{80}$$

The assumed solution $\{P\}$ is substituted in both the field equation operator and the boundary operator and produces errors, or residuals, as follows:

$$\mathbf{R}_F = \boldsymbol{\mathcal{L}}_F[\{P\}] = \boldsymbol{\mathcal{L}}_F\Big[[\phi]\{q\}\Big] \tag{81}$$

On the boundary,

$$\mathbf{R}_B = \mathcal{L}_B[\{P\}] = \mathcal{L}_B\Big[[\phi]\{q\}\Big] \tag{82}$$

For the Galerkin method (ref. 81), the residuals are required to be orthogonal to each member of a complete set, in this case the acoustic modes (basis functions) themselves, thus establishing a set of ordinary differential equations for the elements of the modal amplitude vector $\{q(x)\}$ which by implication tend to produce zero residual error. The statement of orthogonality is

$$\int_0^\sigma [\phi]^T \, \boldsymbol{\mathcal{L}}_F\Big[[\phi]\{q\}\Big] \, dy = 0 \tag{83}$$

On the boundary,

$$[\phi]^T \, \mathcal{L}_B\Big[[\phi]\{q\}\Big] = 0 \tag{84}$$

In carrying out the integration equation (83), it is found that boundary terms arise which can be eliminated with the boundary residual. This is the equivalent of natural boundary conditions in variational methods.

The set of differential equations arising from the Galerkin procedure is of the form

$$\left\{\frac{dq}{dx}\right\} = [B]\{q\} \tag{85}$$

A transfer matrix relating $\{q(0)\}$ and $\{q(L)\}$, the values of the amplitudes at $x = 0$ and $x = L$, is readily obtained by a numerical integration scheme (e.g., the Runge-Kutta scheme):

$$\{q(L)\} = [T]\{q(0)\}$$

The terms $\{q(L)\}$ and $\{q(0)\}$ can then be expressed in terms of incident and reflected acoustic modal amplitudes in the uniform sections (lined or unlined):

$$\{q(0)\} = [A(0)]\begin{Bmatrix} a^+ \\ a^- \end{Bmatrix}$$

$$\{q(L)\} = [A(L)]\begin{Bmatrix} b^+ \\ b^- \end{Bmatrix}$$

where $[A(0)]$ and $[A(L)]$ are suitable matrices for the known modal structure of incident and reflected waves at $x = 0$ and $x = L$. It is then possible to establish a transfer matrix in the form

$$\begin{Bmatrix} b^+ \\ b^- \end{Bmatrix} = [TA]\begin{Bmatrix} a^+ \\ a^- \end{Bmatrix}$$

This can be decomposed under the assumption that the incident modal amplitudes $\{a^+\}$ are known and that the duct termination is reflection free ($\{b^-\} = 0$) to define reflection and transmission coefficients. The reflection and transmission coefficients can be used in a postprocessing operation to construct the acoustic field in the nonuniform section.

The MWR was used in reference 82 for two-dimensional ducts. Reference 83 used what is essentially a MWR in connection with a "wave-envelope" representation of the acoustic state variables (in this case pressure only) to treat the same problem. The wave-envelope approach isolates the rapidly varying wave structure of the acoustic propagation from relatively slowly varying changes in the modal amplitudes in order to create a set of ordinary differential equations analogous to equations (83) and (84) but which represent the relatively slow amplitude variations. Advantages can be expected in the resolution required in the integration scheme.

The finite-element method offers a much more flexible scheme than the MWR for modeling the acoustic transmission properties of nonuniform-duct segments. As noted previously, in applications in acoustics it is generally most appropriate to base a finite-element approximation on the Galerkin method. When this is accomplished, equation (85), which is a set of ordinary differential equations for the modal amplitudes, is replaced by a set of algebraic equations for the acoustic state variables at the finite-element nodes. In a manner completely analogous to the one used in the classic Galerkin scheme, the finite-element representation in the nonuniform section can be matched to a modal representation in the semi-infinite entrance and exit ducts. The result of these operations is a large set of algebraic equations of the form

$$[K]\begin{Bmatrix} \{P\} \\ \{a^-\} \\ \{b^+\} \end{Bmatrix} = [F]\{a^+\} \tag{86}$$

where the elements of the vector $\{P\}$ are the acoustic state variables at the finite-element nodes in the nonuniform section. The term $\{a^-\}$ is a vector of reflected modal amplitudes in the inlet semi-infinite duct, $\{b^+\}$ is a vector of transmitted modal amplitudes in the exit semi-infinite duct, $\{a^+\}$ is a vector of specified incident modal amplitudes in the inlet semi-infinite duct, $[K]$ is the assembled "stiffness" matrix; and $[F]\{a^+\}$ is the generalized "force" vector. An appropriate solution of equation (86) yields the reflection and transmission matrices

$$\{a^-\} = [R]\{a^+\}$$

$$\{b^+\} = [T]\{a^+\}$$

With modern finite-element schemes the large set of equations does not actually need to be stored in active computer memory. "Frontal methods" (ref. 84) provide a systematic scheme in which the finite-element assembly process and the equation solving are integrated into an algorithm which requires only a modest active memory, almost independent of the problem size. There is a vast amount of literature on finite-element methods in general, and two particularly well-known works are references 85 and 86.

The use of the finite-element method in the absence of mean flow is discussed in references 87 to 91 in connection with the modeling of mufflers, a physical arrangement not significantly different from the fan inlet problems of interest here. Craggs' work (refs. 90 and 91) was somewhat unique in that he was interested in modeling truly three-dimensional geometries (as opposed to the more widely discussed two-dimensional or axisymmetric problems), and therefore he discusses three-dimensional elements. Tag and Akin (ref. 92) made calculations for a two-dimensional nonuniform duct. All these investigations were based on a variational formulation, requiring some manipulations which are not required when a Galerkin method is used. The chief difference in the approaches is in the specific elements used.

Reference 93 presents a comparison of the use of the method of weighted residuals and the Galerkin finite-element method for the calculation of the transmission and reflection properties of acoustically treated nonuniform ducts. The finite-element method produces virtually exactly the same results for reflection and transmission coefficients as does the standard Galerkin method. The computational cost of the finite-element method when based on the Helmholtz equation is about the same as the comparable Galerkin solution. The formulation in reference 93 is the only one which employs the matching of the finite-element solution in the nonuniformity to a modal solution in the inlet and exhaust semi-infinite ducts. This, or an equivalent approach, is essential to adequately account for inlet and exhaust boundary conditions in the finite-element solution.

Finite-difference methods have also been extensively studied for application to the duct acoustics problem. Time-dependent (transient) and harmonic steady-state formulations have been used, and implicit and explicit schemes have been tested. While good results in relatively simple test cases have been reported, the finite-difference method has not become a generally used computational scheme. The main reason is the penalty imposed on finite-difference schemes by irregular geometries. Finite-element schemes are particularly well suited for duct problems, especially when nonuniform ducts are considered and when the question of imposing meaningful forcing and termination conditions is raised. It might also be added here that the finite-element scheme is more suitable for modeling the radiation to free space when this type of boundary condition is appropriate. A complete review of finite-difference applications in duct acoustics has been made by Baumeister (ref. 94), who has also made a number of contributions in this area. Consult this review for further details.

A comparison of experiment to theory for a simple nonuniform-duct geometry was reported in reference 95. Both the finite-element theory of reference 93 and the finite-difference calculations of White (ref. 96) were found to be in good agreement with the experiments.

Nonuniform Ducts With Mean Flow

Two types of nonuniform ducts are considered. The simplest situation is that of a duct of uniform cross section but with axially varying lining impedance. In this case the mean flow is axially uniform. This problem has been of considerable interest in connection with the design of linings which are segmented axially with the two objectives of providing attenuation over a broad range of frequencies and of inducing attenuation because of the reactive effects of lining discontinuities. As previously noted the stepped duct approximation (also referred to as mode matching) is suitable

for modeling transmission in a duct with segmented linings, even in the presence of sheared mean flow. Reference 79 for ducts with uniform flow and reference 80 for sheared mean flow have used the mode matching technique.

When a duct area nonuniformity is present, we are concerned not only with the effect of the area nonuniformity on the propagation, but also with the effect of the axial and transverse flow gradients induced by the area nonuniformity. A limiting case would be the situation in which the area nonuniformity creates a sonic flow at the throat, completely cutting off upstream transmission. Experimental investigations of this attenuation mechanism in references 97 to 99 have shown that locally sonic flow conditions in an inlet can create a substantial reduction in the forward transmission of fan-generated noise, although the noise cannot be completely suppressed. Perhaps of even more interest is the observation that the mechanism appears to be at least partially effective for throat Mach numbers below sonic, perhaps as low as 0.8. An effort to determine whether linear acoustic analysis could predict this flow-induced attenuation led to a substantial effort to model propagation through high subsonic flows.

A complicated situation occurs when the duct is nonuniform in cross section. We also include the possibility that the lining is axially nonuniform. It is necessary not only to model propagation in the nonuniform geometry, but also to consider the effect of propagation through the nonuniform flow field. In general, the mean flow is computed separately and is given as data for the acoustic analysis. The model used for the mean flow has substantial influence on the complexity of the acoustic model. If no restriction is placed on the mean flow and it is allowed to be rotational (principally due to the duct-wall boundary layers), then an appropriate form for the acoustic field equations is the acoustic momentum equation and the acoustic energy equation (eqs. (6) and (7)). An alternative is the acoustic field equations derived directly from the continuity and momentum equations (1) and (2). This type of mean flow representation has to be obtained from the Euler equations or the Navier-Stokes equations. If the mean flow is irrotational, then the acoustic field equations can be obtained in the form of equations (9) and (11). This means that the mean flow must be nonviscous and that no boundary layer can be included.

The computational implications of the two representations are substantial. If the mean flow is assumed to be general, then it is necessary to work in terms of the primitive variables pressure (or density) and velocity, with four field equations for three-dimensional acoustic fields. If the mean flow is assumed to be irrotational, then the acoustic field is also irrotational and the introduction of an acoustic velocity potential leads to only one field equation for the potential. The acoustic pressure and particle velocities are obtained by postprocessing the velocity potential solution.

When there is mean flow present, the boundary condition at duct hard walls is still the requirement that the normal component of acoustic particle velocity must vanish:

$$\mathbf{V} \cdot \boldsymbol{\nu} = 0$$

When a mean flow is present in a uniform duct, it was shown in equation (26) that for a locally reacting lining within a circular duct the boundary condition is

$$\mathbf{V} \cdot \boldsymbol{\nu} = Ap - \frac{iM}{\eta} \frac{\partial}{\partial x}(Ap) \tag{87}$$

In this form the boundary condition is valid for a lining which varies axially. In the case of a nonuniform duct and nonuniform mean flow, it is shown in reference 100 that the correct boundary condition is

$$\mathbf{V} \cdot \boldsymbol{\nu} = Ap - i\frac{V_\tau}{\eta}\frac{\partial}{\partial \tau}(Ap) + i\frac{Ap}{\eta}[\boldsymbol{\nu} \cdot (\boldsymbol{\nu} \cdot \nabla)\mathbf{V}_o] \tag{88}$$

where V_τ is the tangential component of mean flow $\mathbf{V}_o$ at the duct wall. The derivative $\partial/\partial\tau$ is with respect to the curvilinear distance along the duct wall. Equation (88) is directly obtained from equation (87) by replacing the axial coordinate x with the tangential coordinate τ and adding the last term. In duct applications the extra term in equation (88) is probably extremely small, since its principal contributions are only large near a stagnation point in the mean flow. Equation (87) is therefore taken as the appropriate boundary condition.

There are fewer options available for computations of acoustic propagation in ducts with nonuniform cross sections with mean flow than for comparable problems without mean flow. They can be categorized as (1) one-dimensional or plane-wave approximations, (2) perturbation schemes for ducts with slowly varying cross sections, (3) weighted-residual methods (i.e., Galerkin), and (4) finite-element and finite-difference methods.

A particularly useful one-dimensional model for unlined ducts has been constructed in reference 101 from a one-dimensional continuity and momentum equation. Without flow the governing equations can be combined to form Webster's horn equation. In their investigation they used a shooting technique to investigate the two-point boundary value problem for wave propagation in a nonuniform duct carrying a compressible mean flow with specified driving and exit conditions. The present author has used the field equations of Davis and Johnson with a Runge-Kutta integration scheme matched to traveling wave solutions in semi-infinite uniform inlets and pipes to construct transmission and reflection equations for long-wavelength propagation. Though unpublished, this approach was used as a check on a more general Galerkin formulation to be discussed shortly. King and Karamcheti (ref. 102) obtained solutions to what is effectively the Davis and Johnson model using the method of characteristics.

Perturbation methods have been used by several investigators for studies of acoustic transmission in nonuniform ducts with mean flow. In reference 103 a ray acoustics approximation was used for the velocity potential for the lowest order mode described by a generalization of Webster's horn equation. Tam (ref. 104) used a Born approximation based on a small area variation and studied the scattering of an acoustic wave incident on a nonuniformity. His flow model was constructed from the one-dimensional gas dynamics relationships with a superposed transverse velocity to create flow tangency at the walls. References 105 and 106 extended the method of multiple scales (ref. 75) to include the case with a sheared mean flow in a lined duct.

It is difficult to draw general conclusions from these models. However it can be stated that little scattering effect is seen for acoustic waves incident upon a nonuniformity (and, hence, axial and transverse flow gradients) unless the local Mach number exceeds 0.6. For higher throat Mach numbers, scattering becomes significant (ref. 104). For propagation against the mean flow, an increase in acoustic pressure near the throat is observed, the increase being very large for high subsonic

throat Mach numbers. Even for near-sonic throat velocities no large attenuation is observed.

These analytic, or semianalytic, approximations have obvious limitations implied in the perturbation schemes. In order to relax these restrictions it is necessary to resort to the Galerkin methods or to finite-element or finite-difference schemes.

The application of a Galerkin method or a finite-element analysis to the case when a mean flow is present is formally the same as when there is no mean flow. The field equations are considerably more complex, meaning that much more time is required in the computation of the coefficient matrices in the Galerkin method and of the element "stiffness matrices" in the finite-element analysis. The actual solution of the ordinary differential equations in the Galerkin method or of the algebraic equations in the finite-element analysis is neither more time-consuming nor more storage dependent than the corresponding operations when flow is absent, provided that the same level of discretization is used. In actual computations for high subsonic mean flows, it is found that upstream of the sound source the compression of the acoustic wavelengths requires a finer discretization than in the no-flow case. Downstream of the source the opposite is true. On balance, however, it appears that a finer discretization is required when flow is present.

Acoustic transmission in nonuniform ducts with a general mean flow has been considered in references 46 and 52. In reference 46 the Galerkin method was used with basis functions derived from a uniform-duct analysis, and in reference 52 a Galerkin finite-element analysis was used. The mean flow is derived from one-dimensional compressible flow relations with a simple superposition of a transverse velocity component based on the requirement of flow tangency at the wall. This is essentially the representation of the flow used in the perturbation solution of reference 104. The techniques of references 46 and 52 give comparable results and compare well with computations based on the reference 101 formulation at low frequencies.

Reference 107 extended the wave-envelope method (ref. 83) to the case of nonuniform lined ducts carrying a compressible, sheared mean flow. As previously noted this method is basically a weighted-residual, or Galerkin, approach with the refinement that the harmonic wave character of the solution is included in the basis functions so that only the envelope of the axial variation of the acoustic modal amplitudes is numerically computed. This would appear to have some implications in the efficiency of the axial integration scheme.

The weighted-residual computational schemes have been used to shed further light on the question of attenuation in propagation through high subsonic mean flows. Results were shown in reference 46 for the transmission of initially planar two-dimensional waves through a converging-diverging nozzle at low frequency, and the results were compared with equivalent one-dimensional calculations based on the formulation in reference 101. One example was a converging-diverging hard-wall duct with propagation opposite to the flow. The duct throat height was 75 percent of the inlet and exit duct heights and the nonuniform section was 1.25 duct heights in length. Mach numbers of 0.25, 0.60, and 0.81 in the throat were considered (0.20, 0.40, and 0.48 in the uniform sections). Figure 11 is a plot of the ratio of transmitted acoustic power to incident acoustic power for nondimensional frequencies based on the duct height H_1. (This is actually half the duct height if the straight wall is construed as a centerline.)

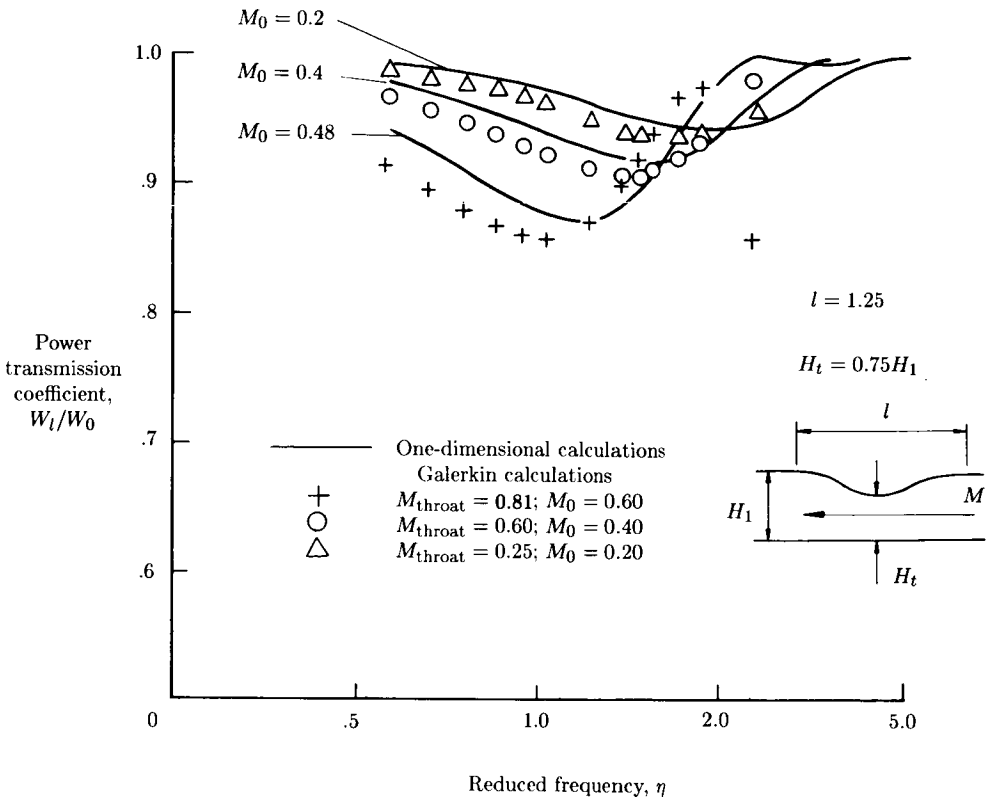

Figure 11. Ratio of transmitted power W_l to incident power W_0 in converging-diverging hard-wall duct showing comparison of one-dimensional results and Galerkin calculations.

The comparison of the one-dimensional and weighted-residual (Galerkin) results is good up to the frequency where the first higher order mode cuts on. Slight deviations occur because the weighted-residual model is inherently two dimensional, and even at low frequencies some two-dimensional effects occur. Of more interest for the present discussion is the fact that strong acoustic attenuation does not occur. What little attenuation that is shown in figure 11 is in a narrow frequency band and is the reactive attenuation of the duct nonuniformity acting as a muffler. This supports the previous observation that linear theory does not appear to predict the experimentally observed attenuation in high subsonic flows.

When the flow field can be assumed to be irrotational, the field equations become particularly simple. The continuity equation (9) and the version of the acoustic momentum equation (11) are in a form well suited for finite-element analysis. In references 108 and 109 these equations were effectively combined and a finite-element discretization was carried out based on the "wave-like" equation which results. The mean flow was generated from a boundary-element method for incompressible potential flow. A well-known compressibility correction (ref. 110) was then used to include the major effects of the compressible mean flow. Boundary conditions,

including the effect of acoustic lining, were forced on the global "stiffness" matrix. No attempt was made to match the solution in the nonuniformity region to incident- and reflected-wave structures at the terminations. The treatment of the termination conditions limits the practical application of the scheme.

When the mean flow is general and not restricted by the assumption of irrotationality, the field equations cannot be combined into a single scalar equation. Finite-element modeling schemes have been set up in references 52 and 111 for this type of flow, with the field equations in the form of equations (6) and (7) (in ref. 52) or in the form of equations (5) and (6) (in ref. 111). There are considerable differences in the details of the implementation of the Galerkin finite-element scheme. Two-dimensional flow was considered in reference 52, and natural boundary conditions were used for the duct-wall boundary conditions. A modal matching procedure was used to match the finite-element solution for the nonuniformity to the infinite inlet and exhaust ducts. This is a direct extension of the formulation for no flow (ref. 93). Reference 111 originally used forced boundary conditions, including the specification of acoustic pressure on the source plane and a modal impedance on the exit plane. In subsequent development of this scheme, modal boundary conditions were incorporated at the duct terminations. This work was directed toward the development of a very-large-scale, general-purpose duct acoustic computational scheme and was set up for axisymmetric propagation.

Finite-element methods have been shown to produce results in good agreement with results from other available computational schemes. Reference 111 shows excellent agreement with some analytic solutions. Figure 12, taken from reference 52, shows the power transmission coefficient as a function of the nondimensional frequency based on duct semiheight for the Galerkin method and for the finite-element method. The geometry is a converging two-dimensional, lined, cosine-shaped tapered-duct section with a 15-percent contraction. The propagation is against the flow, which is relatively low at $M = 0.36$ in the minimum area. The comparison of the two calculations is very good.

Finite-difference schemes, though placed on a firm foundation in reference 94, have not become generally useful. This is undoubtedly because of the simplicity with which finite-element schemes handle complicated geometries. A second consideration is the introduction of frontal solution schemes in the finite-element method which put these methods on a nearly equal footing with explicit finite-difference algorithms when computer storage is a consideration.

Radiation

It has been noted previously that duct acoustic propagation and radiation are coupled and cannot be separated in a rigorous treatment. It has also been noted that most duct propagation analysis has been carried out by ignoring the radiation aspect. The usual way to avoid it is to assume that the duct is of infinite length and that the reflection effects at the termination are unimportant. This effectively says that the radiation process proceeds on the basis of conditions established at the duct termination by propagation without reflection, and therefore the radiation process creates no reflections. For lining design this has proven to be an effective approach, since reflections are relatively unimportant except at frequencies near modal cutoff.

When the radiation pattern itself is of interest, then the problem of acoustic radiation in the infinite medium surrounding the duct exit must be addressed. In

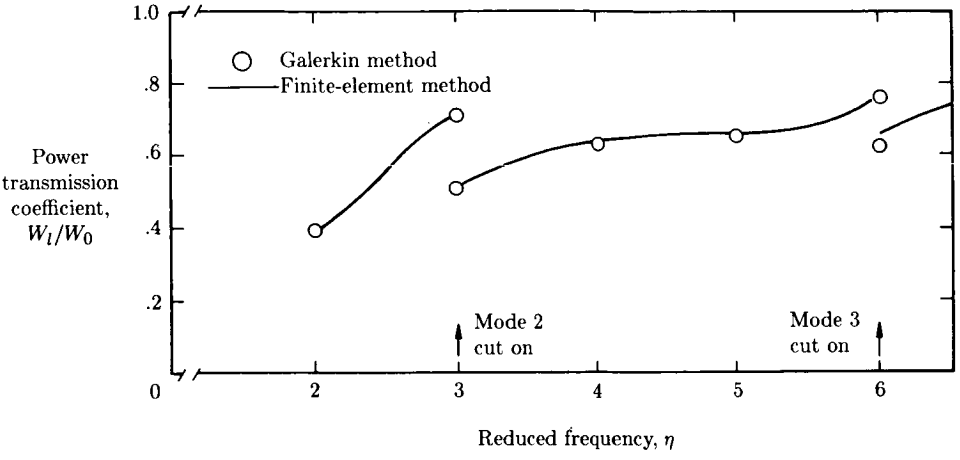

Figure 12. Variation of power transmission coefficient with frequency. $A = 0.72 + i0.42$. *(From ref. 52.)*

this discussion we limit attention entirely to the inlet radiation problem, in which propagation and radiation occur through an inlet flow field (possibly absent). We choose not to examine problems in which propagation and radiation occur through a jet, with the resulting considerations of shear layers.

Radiation from a piston in a plane wall (ref. 112) modeled using the Rayleigh integral and based on the knowledge of the velocity distribution on the piston is the classic technique for calculation of the radiation pattern of a flanged duct. At a duct termination the velocity distribution on the conceptual piston is determined by the acoustic field in the duct. In the textbook case at low frequency, the velocity distribution is assumed to be uniform and the radiation impedance is computed, providing a mechanism for connecting the duct propagation (incident and reflected plane waves) to the radiated field. Levine and Schwinger (ref. 113) considered radiation from an unbaffled open-end pipe using the Wiener-Hopf method. The duct propagation and radiation is treated as a coupled system, and both the radiation pattern and the reflection and transmission coefficients for the duct modes can be calculated. This Levine and Schwinger formulation has been widely used, but as in the case of the Rayleigh integral for the baffled termination, it is limited to the situation when no inlet flow is present.

In order to model rigorously the radiation process when an inlet flow is present, it is appropriate to use the finite-element method. This modeling method, in contrast to the finite-difference method, has the advantage of being readily adaptable to the complex geometry of a turbofan inlet.

When the finite-element method is used, propagation in the duct and radiation to the far field are included in one model. It is assumed that the inlet flow field is irrotational. The appropriate field equations are then equations (9) and (11). Equation (10) is used to compute the local speed of sound from the mean flow velocity potential. Equations (9) and (11) can be combined in a single "wave-like" equation in the acoustic velocity potential, this equation requiring as input data the

mean flow velocity potential, derivatives of the velocity potential, and the local speed of sound.

Two different finite-element models have been developed. The first to appear was developed in references 114 and 115 and is an extension of the finite-element model for duct propagation discussed in references 108 and 109. As noted previously, their field equation in the acoustic velocity potential is a direct combination of equations (9) and (11). A Galerkin method is used to formulate the problem and integration by parts is used to introduce the natural boundary conditions on the duct walls and what amounts to a radiation condition on a boundary outside the duct. The source is introduced through use of a forced boundary condition which specifies acoustic particle velocity on the source plane. The data for their field equation require first and second derivatives of the mean flow velocity potential (velocity and spatial derivatives of velocity). These data are generated by modeling the inlet flow with a boundary-element procedure.

The radiation condition is introduced by representing the acoustic field in terms of a boundary-element method in the region outside a surface exterior to the nacelle, which can be called the matching surface. The procedure is to solve the field equations interior to the matching surface using the finite-element procedure, with the radiation impedance on the matching surface assumed. This allows the computation of the acoustic potential on the matching surface. This is used to generate the exterior acoustic field and, hence, a second version of the radiation impedance. This new impedance is assumed in a new finite-element solution in the interior. The iterative procedure continues until successive finite-element and boundary-element calculations agree on the radiation impedance to some specified accuracy. After the iteration procedure, the acoustic pressure and particle velocity can be obtained by suitable processing of the acoustic velocity potential.

The second finite-element model to appear was reported in references 116 and 117. The approach used was a Galerkin formulation based on the field equations (9) and (11). The authors took advantage of the divergence term in equation (9), which in the Galerkin scheme leads (upon use of the divergence theorem) to introduction of natural boundary conditions and to the elimination of the requirement in the input data for the specification of mean flow velocity spatial derivatives. This makes it attractive to compute the mean flow field from a velocity-potential formulation with a finite-element representation on the same mesh as that used for the acoustic propagation and radiation. The source is modeled in terms of incident and reflected modes, which are matched to the finite-element solution on the source plane.

The radiation to the far field is also modeled with finite elements which have in their shape functions the wave character of the far field of a simple source. These wave-envelope elements allow the use of elements which are very large in the radial direction. With these elements the region between the near field and the far field can be spanned with a relatively small number of elements. At the far-field boundary a simple radiation condition can be imposed. The entire problem is cast in finite-element form so that no iteration is necessary. The solution is carried out with the frontal solution method of reference 84 at a modest cost in computer storage.

Examples of the success of the finite-element modeling of turbofan radiation are shown in figure 13, wherein the finite-element predictions of acoustic radiation from a turbofan engine are compared with the actual radiation patterns measured in a flight test program. The engine was modified to produce a strong tone in the $m = 13$

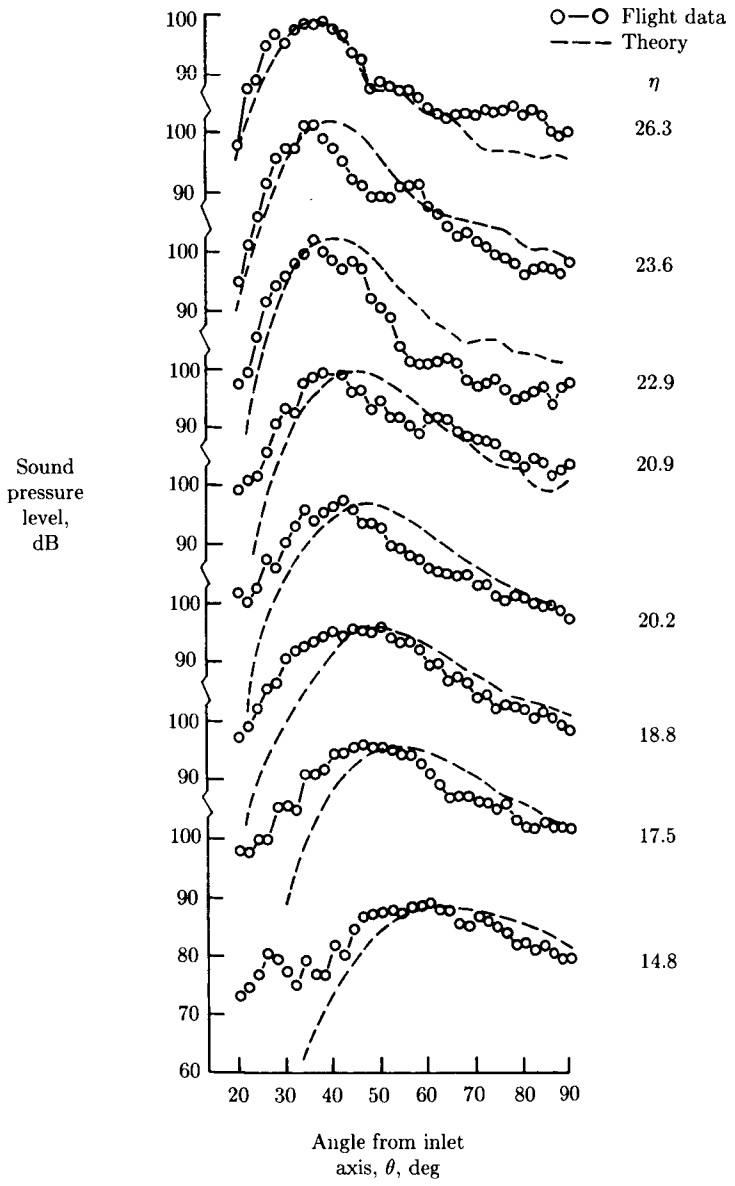

Figure 13. Experimental and computational directivity for JT15D flight inlet including flight effects.

angular mode at frequencies dependent on the engine speed. Figure 13 shows the comparison of theory and measurement for the directivity (SPL vs polar angle from the inlet centerline) for several nondimensional frequencies (based on the duct radius at the throat). The frequencies shown span the range from just barely cut on to well cut on. The agreement is remarkably good, particularly when one considers the complexities of both the modeling scheme and the flyover test procedure.

A ray acoustics model for radiation has been described in references 118 and 119. Only sparse details are available, but it is probable that the major advantage of the method is in its prediction of broadband noise radiation, as opposed to the pure tone radiation for which the finite-element procedure is particularly appropriate.

The complexity of the computation schemes which are required to compute acoustic radiation for lined ducts with interior and exterior flows has led Rice and his co-workers to extend the ideas of modal cutoff ratio to the radiation problem and to derive approximate expressions for the radiation pattern which are functions of the modal cutoff ratios for the duct modes. The starting point is the following expression derived in references 120 and 121 for the mean-square pressure as a function of the polar angle from the inlet axis ψ_o, the modal cutoff ratio β_o, and the frequency $\eta = \omega R/c$ (where R is the duct radius) for radiation from a flanged duct:

$$\overline{P}^2(\psi_o) = \frac{2\sin\psi_o\sqrt{1-1/\beta_o^2}\left(\sin\left\{\eta[\sin\psi_o - (1/\beta_o)]\right\}\right)^2}{\pi\eta[(1/\beta_o^2) - \sin^2\psi_o]^2} \tag{89}$$

This approximation is valid except for the first few radial modes of high-order angular modes. The important feature here is that the approximation to the radiation pattern depends not on the individual modal structure but instead on the cutoff ratio, an implication that all modes with the same cutoff ratio have the same radiation pattern for η being equal. Hence, just as in the suppressor design procedure (refs. 3 and 62 to 65) based on cutoff ratio, it is found that for the simple case of the flanged duct without flow the radiation pattern also depends on cutoff ratio.

Reference 121 combined this idea, the concept of a modal density function (ref. 122), and cutoff ratio biasing function to predict the directivity of broadband (multimodal) fan noise with a substantial degree of success. It was then determined (ref. 6) that the polar angle at which the peak of the radiated field occurs is a function of cutoff ratio. The functional dependence on cutoff ratio can be found for no flow, for inlet flow with no forward-flight effect, and for inlet flow with forward-flight effect. This observation led to the establishment of corrections of equation (89) for the flow effect and additionally for the unflanged duct case (ref. 66).

With this development the entire suppression design procedure can be put in an approximate but vastly simplified context in comparison with the use of the full numerical models. Such a procedure is desirable for preliminary design iterations.

Nonlinear Duct Acoustics

Nonlinear propagation phenomena in ducts present a field of study which is potentially as vast as that of the linear theory discussed to this point. In this section the intention is to address only two problems related to turbofan noise.

Under certain conditions, principally related to the presence of a shock wave system on the fan blades because of supersonic relative tip speeds, acoustic waves are propagated in the duct with a distinctive spectral content. In addition to the interaction tones of the Tyler-Sofrin theory (ref. 5), there exist multiple pure tones which are based on rotor speed rather than on blade passage frequency (refs. 123 to 126). These tones are apparently at least partly due to initially small variations in the shock wave pattern on the rotor because of nonuniformities in the blades. These initially small variations are enhanced because of nonlinear effects related to the shock structure radiated from the blades. In addition, the nonlinear shock structure produces an attenuation in the duct which is not predicted by linear theory (refs. 123 to 126) but which is related to the decay of shock strength away from the rotor face. This decay is enhanced by high subsonic inlet flows and cannot be predicted by linear acoustic theory.

It has been previously noted that in high subsonic inlet flows, the fan tones predicted by the Tyler-Sofrin theory (ref. 5) show an attenuation not predicted by linear theory. This attenuation becomes nearly complete when the inlet flow becomes sonic at the throat. It was also previously noted that linear theory does predict a large increase in the pressure amplitude for acoustic waves incident upon a throat where an approaching flow reaches high subsonic flow. This is illustrated in figure 14 (from ref. 127), wherein the pressure magnitude is plotted against the axial distance for a plane wave approaching a throat with inlet flows of $M = 0.75, 0.85$, and 0.96. The sharp pressure rise for $M = 0.96$ suggests the onset of nonlinear behavior.

A perturbation procedure was used in reference 128 to show that finite-amplitude acoustic modes show nonlinear dispersion and that the characteristic velocity of propagation of acoustic waves becomes dependent on the amplitude of the waves. Since the wave amplitude grows near the throat, as shown in figure 14, the incident waves can stop propagating before the mean flow reaches sonic velocity.

In a series of papers (refs. 129 to 131), the method of matched asymptotic expansions was used to investigate the nonlinear behavior of originally linear planar acoustic waves passing through the throat region of a duct in which the mean flow in the throat is transonic. The formation of acoustic shock waves was demonstrated and, as might be anticipated, it was shown that the nonlinear effects increase with source strength, frequency, and throat Mach number. The shock waves cause a substantial dissipation of energy and are the mechanism by which acoustic choking occurs in the one-dimensional case. The same type of behavior was found in references 132 and 133 with finite-difference solutions of the one-dimensional Euler equations, and good agreement with the matched asymptotic expansion results was also found.

In reference 134 the method of matched asymptotic expansions was extended to two-dimensional propagation. As in the one-dimensional case, shock waves develop in the acoustic field in the near-sonic mean flow in the duct throat. Coupling between acoustic modes induces the nonlinear behavior at lower Mach numbers than in the case of plane-wave propagation. Dispersion plays a major role in this case, whereas it did not in the one-dimensional case.

Much remains to be learned about nonlinear effects, particularly in complicated flows with multimodal propagation. This is a fruitful area for future research.

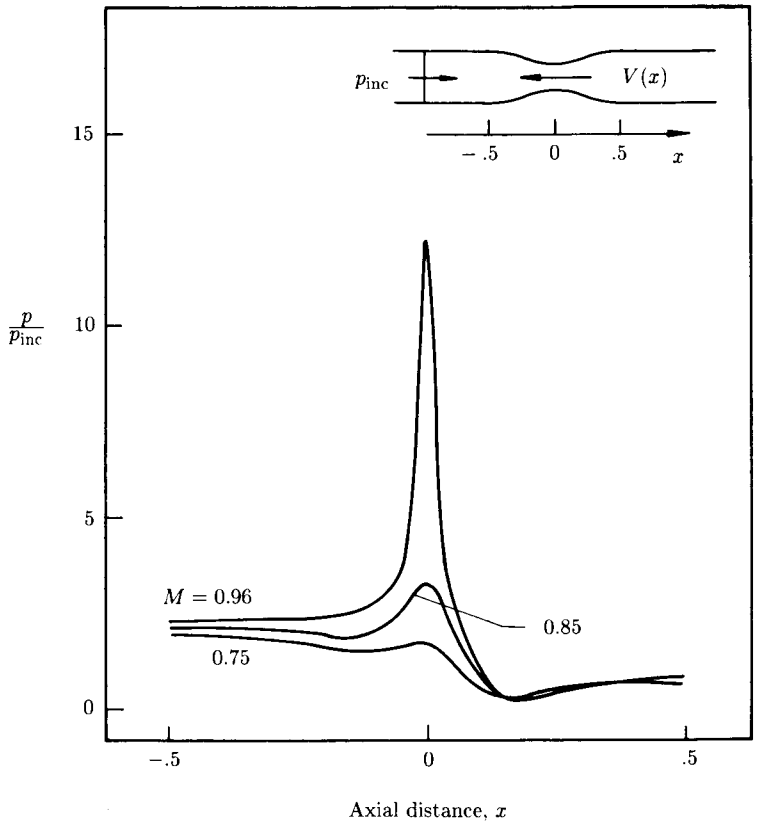

Figure 14. Pressure rise at high subsonic throat for plane wave at inlet Mach numbers of 0.75, 0.85, and 0.96. (From ref. 127.)

References

1. Nayfeh, Ali H.; Kaiser, John E.; and Telionis, Demetri P.: Acoustics of Aircraft Engine-Duct Systems. *AIAA J.*, vol. 13, no. 2, Feb. 1975, pp. 130–153.
2. Eversman, Walter: Energy Flow Criteria for Acoustic Propagation in Ducts With Flow. *J. Acoust. Soc. America*, vol. 49, no. 6, pt. 1, June 1, 1971, pp. 1717–1721.
3. Rice, Edward J.: *Acoustic Liner Optimum Impedance for Spinning Modes With Mode Cut-Off Ratio as the Design Criterion.* NASA TM X-73411, 1976.
4. Rschevkin, S. N.: *A Course of Lectures on the Theory of Sound.* MacMillan Co., 1963.
5. Tyler, J. M.; and Sofrin, T. G.: Axial Flow Compressor Noise Studies. *SAE Trans.*, vol. 70, 1962, pp. 309–332.
6. Rice, Edward J.; Heidmann, Marcus F.; and Sofrin, Thomas G.: Modal Propagation Angles in a Cylindrical Duct With Flow and Their Relation to Sound Radiation. AIAA Paper 79-0183, Jan. 1979.
7. Mungur, P.; and Gladwell, G. M. L.: Acoustic Wave Propagation in a Sheared Fluid Contained in a Duct. *J. Sound & Vib.*, vol. 9, no. 1, Jan. 1969, pp. 28–48.
8. Möhring, W.: Über Schallwellen in Scherströmungen. *Fortschritte der Akustik*, DAGA 1976, pp. 543–546.
9. Sivian, L. J.: Sound Propagation in Ducts Lined With Absorbing Materials. *J. Acoust. Soc. America*, vol. 9, no. 2, Oct. 1937, pp. 135–140.
10. Molloy, Charles T.: Propagation of Sound in Lined Ducts. *J. Acoust. Soc. America*, vol. 16, no. 1, July 1944, pp. 31–37.
11. Sabine, Hale J.: The Absorption of Noise in Ventilating Ducts. *J. Acoust. Soc. America*, vol. 12, no. 1, July 1940, pp. 53–57.
12. Morse, Philip M.: The Transmission of Sound Inside Pipes. *J. Acoust. Soc. America*, vol. 11, no. 2, Oct. 1939, pp. 205–210.
13. Morse, Philip M.; and Ingard, K. Uno: *Theoretical Acoustics.* McGraw-Hill Book Co., Inc., c.1968.
14. Cremer, Lothar: Theorie der Luftschall-Dämpfung im Rechteckkanal mit schluckender Wand und das sich dabei ergebende höchste Dämpfungsmass. *Acoustica*, vol. 3, no. 2, 1953, pp. 249–263.
15. Molloy, Charles T.; and Honigman, Esther: Attenuation of Sound in Lined Circular Ducts. *J. Acoust. Soc. America*, vol. 16, no. 4, Apr. 1945, pp. 267–272.
16. Rogers, R.: The Attenuation of Sound in Tubes. *J. Acoust. Soc. America*, vol. 11, no. 4, Apr. 1940, pp. 480–484.
17. Fisher, E.: Attenuation of Sound in Circular Ducts. *J. Acoust. Soc. America*, vol. 17, no. 2, Oct. 1945, pp. 121–122.
18. Rice, Edward J.: Attenuation of Sound in Soft-Walled Circular Ducts. *Aerodynamic Noise*, Univ. of Toronto Press, c.1969, pp. 229–249.
19. Benzakein, M. J.; Kraft, R. E.; and Smith, E. B.: Sound Attenuation in Acoustically Treated Turbomachinery Ducts. ASME Paper 69-WA/GT-11, Nov. 1969.
20. Zorumski, William E.; and Mason, Jean P.: Multiple Eigenvalues of Sound-Absorbing Circular and Annular Ducts. *J. Acoust. Soc. America*, vol. 55, no. 6, June 1974, pp. 1158–1165.
21. Doak, P. E.; and Vaidya, P. G.: Attenuation of Plane Wave and Higher Order Mode Sound Propagation in Lined Ducts. *J. Sound & Vib.*, vol. 12, no. 2, June 1970, pp. 201–224.
22. Christie, D. R. A.: Theoretical Attenuation of Sound in a Lined Duct: Some Computer Calculations. *J. Sound & Vib.*, vol. 17, no. 2, July 22, 1971, pp. 283–286.
23. Vo, P. T.; and Eversman, W.: A Method of Weighted Residuals With Trigonometric Basis Functions for Sound Transmission in Circular Ducts. *J. Sound & Vib.*, vol. 56, no. 2, Jan. 22, 1978, pp. 243–250.
24. Watson, Willie; and Lansing, Donald L.: *A Comparison of Matrix Methods for Calculating Eigenvalues in Acoustically Lined Ducts.* NASA TN D-8186, 1976.
25. Lapin, A. D.: Influence of Motion of the Medium on the Sound Attenuation in a Waveguide Lined With a Sound-Absorbing Material. *Soviet Phys.—Acoust.*, vol. 12, no. 4, Apr.–June 1967, pp. 402–404.
26. Eversman, Walter: The Effect of Mach Number on the Tuning of an Acoustic Lining in a Flow Duct. *J. Acoust. Soc. America*, vol. 48, no. 2, pt. 1, Aug. 1970, pp. 425–428.
27. Ko, Sung-Hwan: Sound Attenuation in Lined Rectangular Ducts With Flow and Its Application to the Reduction of Aircraft Engine Noise. *J. Acoust. Soc. America*, vol. 50, no. 6, pt. 1, Dec. 1971, pp. 1418–1432.

28. Ko, S.-H.: Sound Attenuation in Acoustically Lined Circular Ducts in the Presence of Uniform Flow and Shear Flow. *J. Sound & Vib.*, vol. 32, no. 2, May 22, 1972, pp. 193–210.
29. Kraft, R. E.; Motsinger, R. E.; Gauden, W. H.; and Link, J. F.: *Analysis, Design, and Test of Acoustic Treatment in a Laboratory Inlet Duct.* NASA CR-3161, 1979.
30. McCalla, Thomas Richard: *Introduction to Numerical Methods and FORTRAN Programming.* John Wiley & Sons, Inc., c.1967.
31. Bauer, A. B.; and Joshi, M. C.: Classification of Acoustic Modes in a Lined Duct. AIAA-80-1016, June 1980.
32. Eversman, W.: Computation of Axial and Transverse Wave Numbers for Uniform Two-Dimensional Ducts With Flow Using a Numerical Integration Scheme. *J. Sound & Vib.*, vol. 41, no. 2, July 22, 1975, pp. 252–255; Errata, vol. 47, no. 1, July 8, 1976, p. 125.
33. Eversman, W.: Initial Values for the Integration Scheme To Compute the Eigenvalues for Propagation in Ducts. *J. Sound & Vib.*, vol. 50, no. 1, Jan. 8, 1977, pp. 159–162; Errata, vol. 53, no. 4, Aug. 22, 1977, p. 595.
34. Pridmore-Brown, D. C.: Sound Propagation in a Fluid Flowing Through an Attenuating Duct. *J. Fluid Mech.*, vol. 4, pt. 4, Aug. 1958, pp. 393–406.
35. Tack, D. H.; and Lambert, R. F.: Influence of Shear Flow in Sound Attenuation in a Lined Duct. *J. Acoust. Soc. America*, vol. 38, Oct. 1965, pp. 655–666.
36. Kurze, Ulrich J.; and Allen, Clayton H.: Influence of Flow and High Sound Level on the Attenuation in a Lined Duct. *J. Acoust. Soc. America*, vol. 49, no. 5, pt. 2, May 1971, pp. 1643–1654.
37. Kurze, U.: Schallausbreitung im Kanal mit Periodischer Wandstruktur. *Acustica*, vol. 21, no. 2, 1969, pp. 74–85.
38. Goldstein, M.; and Rice, E.: Effect of Shear on Duct Wall Impedance. *J. Sound & Vib.*, vol. 30, no. 1, Sept. 8, 1973, pp. 79–84.
39. Mungur, P.; and Plumblee, H. E.: Propagation and Attenuation of Sound in a Soft-Walled Annular Duct Containing a Sheared Flow. *Basic Aerodynamic Noise Research*, Ira R. Schwartz, ed., NASA SP-207, 1969, pp. 305–327.
40. Eversman, Walter: Effect of Boundary Layer on the Transmission and Attenuation of Sound in an Acoustically Treated Circular Duct. *J. Acoust. Soc. America*, vol. 49, no. 5, pt. 1, May 1971, pp. 1372–1380.
41. Mariano, S.: Effect of Wall Shear Layers on the Sound Attenuation in Acoustically Lined Rectangular Ducts. *J. Sound & Vib.*, vol. 19, no. 3, Dec. 8, 1971, pp. 261–275.
42. Hersh, A. S.; and Catton, I.: Effect of Shear Flow on Sound Propagation in Rectangular Ducts. *J. Acoust. Soc. America*, vol. 50, no. 3, pt. 2, Sept. 1971, pp. 992–1003.
43. Savkar, S. D.: Propagation of Sound in Ducts With Shear Flow. *J. Sound & Vib.*, vol. 19, no. 3, Dec. 8, 1971, pp. 355–372.
44. Unruh, J. F.; and Eversman, W.: The Utility of the Galerkin Method for the Acoustic Transmission in an Attenuating Duct. *J. Sound & Vib.*, vol. 23, no. 2, July 1972, pp. 187–197.
45. Unruh, J. F.; and Eversman, W.: The Transmission of Sound in an Acoustically Treated Rectangular Duct With Boundary Layer. *J. Sound & Vib.*, vol. 25, no. 3, Dec. 1972, pp. 371–382.
46. Eversman, W.; and Astley, R. J.: Acoustic Transmission in Non-Uniform Ducts With Mean Flow. Part I: The Method of Weighted Residuals. *J. Sound & Vib.*, vol. 74, no. 1, Jan. 8, 1981, pp. 89–101.
47. Yurkovich, R. N.: Attenuation of Acoustic Modes in Circular and Annular Ducts in the Presence of Sheared Swirling Flow. AIAA Paper No. 76-498, July 1976.
48. Wynne, G. A.; and Plumblee, H. E.: Calculation of Eigenvalues of the Finite Difference Equations Describing Sound Propagation in a Duct Carrying Sheared Flow. Paper presented at the 79th Meeting of the Acoustical Society of America, Apr. 1970.
49. Dean, L. Wallace, III: Method for Computing Acoustic Mode Properties in Uniformly Treated Ducts With Sheared Flow. Paper presented at the 88th Meeting of the Acoustical Society of America (St. Louis, Missouri), Nov. 1974.
50. Astley, R. J.; and Eversman, W.: A Finite Element Formulation of the Eigenvalue Problem in Lined Ducts With Flow. *J. Sound & Vib.*, vol. 65, no. 1, July 8, 1979, pp. 61–74.
51. Astley, R. J.; and Eversman, W.: The Finite Element Duct Eigenvalue Problem: An Improved Formulation With Hermitian Elements and No-Flow Condensation. *J. Sound & Vib.*, vol. 69, no. 1, Mar. 8, 1980, pp. 13–25.
52. Astley, R. J.; and Eversman, W.: Acoustic Transmission in Non-Uniform Ducts With Mean Flow. Part II: The Finite Element Method. *J. Sound & Vib.*, vol. 74, no. 1, Jan. 8, 1981, pp. 103–121.

53. Astley, R. J.; Walkington, N. J.; and Eversman, W.: Transmission in Flow Ducts With Peripherally Varying Linings. AIAA-80-1015, June 1980.
54. Eversman, Walter; and Beckemeyer, Roy J.: Transmission of Sound in Ducts With Thin Shear Layers—Convergence to the Uniform Flow Case. *J. Acoust. Soc. America,* vol. 52, no. 1, pt. 2, July 1972, pp. 216–220.
55. Eversman, Walter: Approximation for Thin Boundary Layers in the Sheared Flow Duct Transmission Problem. *J. Acoust. Soc. America,* vol. 53, no. 5, May 1973, pp. 1346–1350.
56. Eversman, W.: Representation of a 1/N Power Law Boundary Layer in the Sheared Flow Acoustic Transmission Problem. *J. Sound & Vib.,* vol. 24, no. 4, Oct. 22, 1972, pp. 459–469.
57. Myers, M. K.; and Chuang, S. L.: Uniform Asymptotic Approximations for Duct Acoustic Modes in a Thin Boundary-Layer Flow. *AIAA J.,* vol. 22, no. 9, Sept. 1984, pp. 1234–1241.
58. Rice, Edward J.: Propagation of Waves in an Acoustically Lined Duct With a Mean Flow. *Basic Aerodynamic Noise Research,* Ira R. Schwartz, ed., NASA SP-207, 1969, pp. 345–355.
59. Rice, Edward J.: *Spinning Mode Sound Propagation in Ducts With Acoustic Treatment.* NASA TN D-7913, 1975.
60. Rice, Edward J.: *Spinning Mode Sound Propagation in Ducts With Acoustic Treatment and Sheared Flow.* NASA TM X-71672, 1975.
61. Nayfeh, A. H.; Kaiser, J. E.; and Shaker, B. S.: Effect of Mean-Velocity Profile Shapes on Sound Transmission Through Two-Dimensional Ducts. *J. Sound & Vib.,* vol. 34, no. 3, June 8, 1974, pp. 413–423.
62. Rice, Edward J.: *Attenuation of Sound in Ducts With Acoustic Treatment—A Generalized Approximate Equation.* NASA TM X-71830, 1975.
63. Rice, Edward J.; and Heidelberg, Laurence J.: Comparison of Inlet Suppressor Data With Approximate Theory Based on Cutoff Ratio. AIAA-80-0100, Jan. 1980.
64. Rice, Edward J.: Optimum Wall Impedance for Spinning Modes—A Correlation With Mode Cutoff Ratio. *J. Aircr.,* vol. 16, no. 5, May 1979, pp. 336–343.
65. Rice, Edward J.: Inlet Noise Suppressor Design Method Based Upon the Distribution of Acoustic Power With Mode Cutoff Ratio. *Advances in Engineering Science, Volume 3,* NASA CP-2001, 1976, pp. 883–894.
66. Rice, Edward J.; and Sawdy, David T.: *A Theoretical Approach to Sound Propagation and Radiation for Ducts With Suppressors.* NASA TM-82612, 1981.
67. Morfey, C. L.: Acoustic Energy in Non-Uniform Flows. *J. Sound & Vib.,* vol. 14, no. 2, Jan. 22, 1971, pp. 159–170.
68. Möhring, W.: Energy Flux in Duct Flow. *J. Sound & Vib.,* vol. 18, no. 1, Sept. 8, 1971, pp. 101–109.
69. Möhring, W.: Acoustic Energy Flux in Non-Homogeneous Ducts. AIAA Paper 77-1280, Oct. 1977.
70. Ryshov, O. S.; and Shefter, G. M.: On the Energy of Acoustic Waves Propagating in Moving Media. *J. Appl. Math. & Mech.,* vol. 26, no. 5, 1962, pp. 1293–1309.
71. Candel, S. M.: Acoustic Conservation Principles and an Application to Plane and Modal Propagation in Nozzles and Diffusers. *J. Sound & Vib.,* vol. 41, no. 2, July 22, 1975, pp. 207–232.
72. Eversman, W.: Acoustic Energy in Ducts: Further Observations. *J. Sound & Vib.,* vol. 62, no. 4, Feb. 22, 1979, pp. 517–532.
73. Webster, Arthur Gordon: Acoustical Impedance and the Theory of Horns and of the Phonograph. *Proc. Natl. Acad. Sci.,* vol. 5, no. 1, Jan. 15, 1919, pp. 275–282.
74. Cummings, A.: Acoustics of a Wine Bottle. *J. Sound & Vib.,* vol. 31, no. 3, Dec. 8, 1973, pp. 331–343.
75. Nayfeh, Ali Hasan; and Telionis, Demetri P.: Acoustic Propagation in Ducts With Varying Cross Sections. *J. Acoust. Soc. America,* vol. 54, no. 6, Dec. 1973, pp. 1654–1661.
76. Stevenson, A. F.: Exact and Approximate Equations for Wave Propagation in Acoustic Horns. *J. Appl. Phys.,* vol. 22, no. 12, Dec. 1951, pp. 1461–1463.
77. Zorumski, William E.: *Acoustic Theory of Axisymmetric Multisectioned Ducts.* NASA TR R-419, 1974.
78. Alfredson, R. J.: The Propagation of Sound in a Circular Duct of Continuously Varying Cross-Sectional Area. *J. Sound & Vib.,* vol. 23, no. 4, Aug. 22, 1972, pp. 433–442.
79. Lansing, D. L.; and Zorumski, W. E.: Effects of Wall Admittance Changes on Duct Transmission and Radiation of Sound. *J. Sound & Vib.,* vol. 27, no. 1, Mar. 8, 1973, pp. 85–100.
80. Joshi, M. C.; Kraft, R. E.; and Son, S. Y.: Analysis of Sound Propagation in Annular Ducts With Segmented Treatment and Sheared Flow. AIAA-82-0123, Jan. 1982.
81. Finlayson, Bruce A.: *The Method of Weighted Residuals and Variational Principles.* Academic Press, Inc., 1972.

82. Eversman, W.; Cook, E. L.; and Beckemeyer, R. J.: A Method of Weighted Residuals for the Investigation of Sound Transmission in Non-Uniform Ducts Without Flow. *J. Sound & Vib.*, vol. 38, no. 1, Jan. 1975, pp. 105–123.
83. Kaiser, J. E.; and Nayfeh, A. H.: A Wave-Envelope Technique for Wave Propagation in Nonuniform Ducts. AIAA Paper No. 76-496, July 1976.
84. Irons, Bruce M.: A Frontal Solution Program for Finite Element Analysis. *Int. J. Numerical Methods Eng.*, vol. 2, no. 1, Jan.-Mar. 1970, pp. 5–32.
85. Zienkiewicz, O. C.: *The Finite Element Method.* McGraw-Hill Book Co. (UK) Ltd., c.1977.
86. Bathe, Klaus-Jürgen: *Finite Element Procedures in Engineering Analysis.* Prentice-Hall, Inc., c.1982.
87. Young, Cheng-I James; and Crocker, Malcolm J.: Prediction of Transmission Loss in Mufflers by the Finite-Element Method. *J. Acoust. Soc. America,* vol. 57, no. 1, Jan. 1975, pp. 144–148.
88. Kagawa, Yukio; and Omote, Toshio: Finite-Element Simulation of Acoustic Filters of Arbitrary Profile With Circular Cross Section. *J. Acoust. Soc. America,* vol. 60, no. 5, Nov. 1976, pp. 1003–1013.
89. Kagawa, Y.; Yamabuchi, T.; and Mori, A.: Finite Element Simulation of an Axisymmetric Acoustic Transmission System With a Sound Absorbing Wall. *J. Sound & Vib.*, vol. 53, no. 3, Aug. 8, 1977, pp. 357–374.
90. Craggs, A.: A Finite Element Method for Damped Acoustic Systems: An Application To Evaluate the Performance of Reactive Mufflers. *J. Sound & Vib.*, vol. 48, no. 3, Sept. 8, 1976, pp. 377–392.
91. Craggs, A.: A Finite Element Method for Modelling Dissipative Mufflers With a Locally Reactive Lining. *J. Sound & Vib.*, vol. 54, no. 2, Sept. 22, 1977, pp. 285–296.
92. Tag, I. A.; and Akin, J. E.: Finite Element Solution of Sound Propagation in a Variable Area Duct. AIAA Paper 79-0663, Mar. 1979.
93. Astley, R. J.; and Eversman, W.: A Finite Element Method for Transmission in Non-Uniform Ducts Without Flow: Comparison With the Method of Weighted Residuals. *J. Sound & Vib.*, vol. 57, no. 3, Apr. 8, 1978, pp. 367–388.
94. Baumeister, K. J.: Numerical Techniques in Linear Duct Acoustics—A Status Report. *Trans. ASME, J. Eng. Ind.*, vol. 103, no. 3, Aug. 1981, pp. 270–281.
95. Baumeister, Kenneth J.; Eversman, W.; Astley, R. J.; and White, J. W.: Application of "Steady" State Finite Element and Transient Finite Difference Theory to Sound Propagation in a Variable Duct: A Comparison With Experiment. AIAA-81-2016, Oct. 1981.
96. White, James W.: A General Mapping Procedure for Variable Area Duct Acoustics. AIAA-81-0094, Jan. 1981.
97. Large, J. B.; Wilby, J. F.; Grande, E.; and Andersson, A. O.: The Development of Engineering Practices in Jet, Compressor, and Boundary Layer Noise. *Aerodynamic Noise,* Univ. of Toronto Press, c.1969, pp. 43–67.
98. Chestnutt, David; and Clark, Lorenzo R.: *Noise Reduction by Means of Variable-Geometry Inlet Guide Vanes in a Cascade Apparatus.* NASA TM X-2392, 1971.
99. Klujber, F.; Bosch, J. C.; Demetrick, R. W.; and Robb, W. L.: *Investigation of Noise Suppression by Sonic Inlets for Turbofan Engines. Volume I—Program Summary.* NASA CR-121126, 1973.
100. Myers, M. K.: On the Acoustic Boundary Condition in the Presence of Flow. *J. Sound & Vib.*, vol. 71, no. 3, Aug. 8, 1980, pp. 429–434.
101. Davis, Sanford S.; and Johnson, Margaret L.: Propagation of Plane Waves in a Variable Area Duct Carrying a Compressible Subsonic Flow. Paper presented at the 87th Meeting of the Acoustical Society of America (New York, New York), Apr. 1974.
102. King, L. S.; and Karamcheti, K.: Propagation of Plane Waves in Flow Through a Variable Area Duct. AIAA Paper No. 73-1009, Oct. 1973.
103. Huerre, Patrick; and Karamcheti, Krishnamurty: Propagation of Sound Through a Fluid Moving in a Duct of Varying Area. *Interagency Symposium on University Research in Transportation Noise—Proceedings, Volume II,* U.S. Dep. of Transportation, 1973, pp. 397–413.
104. Tam, C. K. W.: Transmission of Spinning Acoustic Modes in a Slightly Non-Uniform Duct. *J. Sound & Vib.*, vol. 18, no. 3, Oct. 8, 1971, pp. 339–351.
105. Nayfeh, A. H.; Telionis, D. P.; and Lekoudis, S. G.: Acoustic Propagation in Ducts With Varying Cross Sections and Sheared Mean Flow. AIAA Paper No. 73-1008, Oct. 1973.
106. Nayfeh, A. H.; Kaiser, J. E.; and Telionis, D. P.: Transmission of Sound Through Annular Ducts of Varying Cross Sections and Sheared Mean Flow. *AIAA J.*, vol. 13, no. 1, Jan. 1975, pp. 60–65.
107. Nayfeh, A. H.; Shaker, B. S.; and Kaiser, J. E.: Transmission of Sound Through Nonuniform Circular Ducts With Compressible Mean Flows. *AIAA J.*, vol. 18, no. 5, May 1980, pp. 515–525.

108. Sigman, R. K.; Majjigi, R. K.; and Zinn, B. T.: Determination of Turbofan Inlet Acoustics Using Finite Elements. *AIAA J.*, vol. 16, no. 11, Nov. 1978, pp. 1139–1145.
109. Majjigi, R. K.; Sigman, R. K.; and Zinn, B. T.: Wave Propagation in Ducts Using the Finite Element Method. AIAA Paper 79-0659, Mar. 1979.
110. Lieblein, S.; and Stockman, N. O.: Compressibility Correction for Internal Flow Solutions. *J. Aircr.*, vol. 9, no. 4, Apr. 1972, pp. 312–313.
111. Abrahamson, A. L.: A Finite Element Algorithm for Sound Propagation in Axisymmetric Ducts Containing Compressible Mean Flow. AIAA Paper 77-1301, Oct. 1977.
112. Pierce, Allan D.: *Acoustics—An Introduction to Its Physical Principles and Applications.* McGraw-Hill, Inc., c.1981.
113. Levine, Harold; and Schwinger, Julian: On the Radiation of Sound From an Unflanged Circular Pipe. *Phys. Rev.*, vol. 73, no. 4, Second ser., Feb. 15, 1948, pp. 383–406.
114. Horowitz, S. J.; Sigman, R. K.; and Zinn, B. T.: An Iterative Finite Element-Integral Technique for Predicting Sound Radiation From Turbofan Inlets. AIAA-81-1981, Oct. 1981.
115. Horowitz, S. J.; Sigman, R. K.; and Zinn, B. T.: An Iterative Finite Element-Integral Technique for Predicting Sound Radiation From Turbofan Inlets in Steady Flight. AIAA-82-0124, Jan. 1982.
116. Parrett, A. V.; and Eversman, W.: Wave Envelope and Finite Element Approximations for Turbofan Noise Radiation in Flight. *AIAA J.*, vol. 24, no. 5, May 1986, pp. 753–760.
117. Eversman, W.; Parrett, A. V.; Preisser, J. S.; and Silcox, R. J.: Contributions to the Finite Element Solution of the Fan Noise Radiation Problem. *Trans. ASME, J. Vib., Acoust., Stress & Reliab. Des.*, vol. 107, no. 2, Apr. 1985, pp. 216–223.
118. Kempton, A. J.: Ray Theory To Predict the Propagation of Broadband Fan-Noise. AIAA-80-0968, June 1980.
119. Kempton, A. J.; and Smith, M. G.: Ray-Theory Predictions of the Sound Radiated From Realistic Engine Intakes. AIAA-81-1982, Oct. 1981.
120. Saule, Arthur V.: Modal Structure Inferred From Static Far-Field Noise Directivity. AIAA Paper No. 76-574, July 1976.
121. Rice, E. J.: Multimodal Far-Field Acoustic Radiation Pattern Using Mode Cutoff Ratios. *AIAA J.*, vol. 16, no. 9, Sept. 1978, pp. 906–911.
122. Rice, E. J.: *Modal Density Function and Number of Propagating Modes in Ducts.* NASA TM X-73539, 1976.
123. Pickett, Gordon F.: Prediction of the Spectral Content of Combination Tone Noise. *J. Aircr.*, vol. 9, no. 9, Sept. 1972, pp. 658–663.
124. Morfey, C. L.; and Fisher, M. J.: Shock-Wave Radiation From a Supersonic Ducted Rotor. *Aeronaut. J.*, vol. 74, no. 715, July 1970, pp. 579–585.
125. Hawkings, D.: Multiple Tone Generation by Transonic Compressors. *J. Sound & Vib.*, vol. 17, no. 2, July 22, 1971, pp. 241–250.
126. Mathews, D. C.; and Nagel, R. T.: Inlet Geometry and Axial Mach Number Effects on Fan Noise Propagation. AIAA Paper No. 73-1022, Oct. 1973.
127. Myers, M. K.; and Callegari, A. J.: On the Singular Behavior of Linear Acoustic Theory in Near-Sonic Duct Flows. *J. Sound & Vib.*, vol. 51, no. 4, Apr. 22, 1977, pp. 517–531.
128. Tam, C. K. W.: On Finite Amplitude Spinning Acoustic Modes and Subsonic Choking. *J. Sound & Vib.*, vol. 16, no. 3, June 8, 1971, pp. 393–405.
129. Callegari, A. J.; and Myers, M. K.: Nonlinear Effects on Sound in Nearly Sonic Duct Flows. AIAA Paper 77-1296, Oct. 1977.
130. Callegari, A. J.; and Myers, M. K.: Sound Transmission in Ducts Containing Nearly Choked Flows. AIAA Paper 79-0623, Mar. 1979.
131. Myers, M. K.: Shock Development in Sound Transmitted Through a Nearly Choked Flow. AIAA-81-2012, Oct. 1981.
132. Walkington, N. J.; and Eversman, W.: A Numerical Model of Acoustic Choking. Part I: Shock Free Solutions. *J. Sound & Vib.*, vol. 90, no. 4, Oct. 22, 1983, pp. 509–526.
133. Walkington, N. J.; and Eversman, W.: A Numerical Model of Acoustic Choking. Part II: Shocked Solutions. *J. Sound & Vib.*, vol. 104, no. 1, Jan. 8, 1986, pp. 81–107.
134. Myers, M. K.; and Uenishi, K.: Two Dimensional Nonlinear Analysis of Sound Transmission Through a Near-Sonic Throat Flow. AIAA-84-0497, Jan. 1984.

14 Design and Performance of Duct Acoustic Treatment

Lead authors

R. E. Motsinger
General Electric Co.
Cincinnati, Ohio

R. E. Kraft
General Electric Co.
Cincinnati, Ohio

Orientation

This chapter discusses the procedure for designing acoustic treatment panels used to line the walls of aircraft engine ducts and for estimating the resulting suppression of turbofan engine duct noise. This procedure is intended to be used for estimating noise suppression of existing designs or for designing new acoustic treatment panels and duct configurations to achieve desired suppression levels.

Federal and local government regulations limit the level of noise that may radiate from commercial and private aircraft. Some airports impose even more severe limits, such as the Washington International Airport at night. Noise certification levels of aircraft, which are the starting point for determining the required noise suppression, are discussed in the chapter on flyover noise measurement and prediction.

In general, the noise levels generated by the source mechanisms of turbomachinery used in turbofan-powered aircraft are higher than allowed by the regulated limits. Suppression within the engine ducts, both inlet and exhaust, is necessary to meet certification levels. These noise sources normally consist of the turbofan, compressor, turbine, and combustor.

The amount of required noise suppression often establishes the length of ducting requiring treatment. Because duct lengths should be as short as possible to control weight, the designer must be concerned that the source level of each engine component is appropriately determined.

To estimate the engine contribution to aircraft flyover noise, information is needed on both suppression and the effect of the suppression on the far-field radiation pattern. Experience has shown that the required noise suppression can be predicted

reasonably well for the inlet, but the suppression required for each aft end component (fan duct, core nozzle) is not easily established.

The problem in the aft end stems from difficulty in unambiguously separating fan, turbine, jet, and combustion components contributing to the overall radiated level. The measurement of suppression of a treatment design for one of these components is difficult, particularly if the contribution of that component is 10 dB or more below the combined level of the other sources. In this case, the small decrease in the overall level of noise due to the increased suppression of the component cannot be distinguished from experimental error in the measurement.

In addition, it is important that the type of acoustic treatment panels selected have the appropriate suppression characteristics as a function of frequency. The treatment is usually designed to preferentially suppress the noise generated in those frequencies that contribute most to the aircraft noise as measured in noise certification units (perceived noise level).

Design Approach

Perspectives on Treatment Design

The panel design and associated suppression depend on the noise source characteristics defined by acoustic modes propagating within the duct, which acts as a wave guide. There are two distinct regimes, one in which the wavelength is large relative to the duct opening and the other in which it is small. Rigorous analytical techniques are necessary in the former, but ray acoustics or empirical methods are usually adequate in the latter. For the "gray" area, where large- and small-wavelength regimes overlap, a combination of the two approaches is required.

The key design parameter is the acoustic impedance of the treatment panel. The impedance is comprised of a real part, the resistance, and an imaginary part, the reactance. In practice, analytical estimation of suppression as a function of the treatment acoustic impedance forms the basis for typical designs. The results of this approach set the acoustic impedance design criteria for the treatment panels in new applications or improve performance of existing designs.

Because of limitations to the current state of the art of rigorous discrete-frequency duct propagation theory, the analytical approach is seasoned with engineering data to establish a priori estimates of the likely performance of treatment designs for new applications. Specifically, suppression is parametrically analyzed to establish the values of panel resistance and reactance that provide the closest approach to maximum suppression for the assumed engine source characteristics, within practical constraints dictated by other considerations. This analysis is performed over the frequency range of concern to establish the treatment acoustic impedance design criteria for the engine component.

The next step is to design the treatment panel to match as closely as possible the desired impedance for each frequency band of concern. Depending on the range of frequency over which suppression is required, the type of treatment is then chosen: single degree of freedom (SDOF), two degree of freedom (2DOF), or bulk absorber.

The SDOF design, shown in figure 1(a), consists of a single-layer sandwich construction with a solid backplate, porous face sheet, and cellular separator such as honeycomb. The 2DOF design, shown in figure 1(b), adds a second layer (double-layer sandwich), with a porous septum sheet, or midsheet. This concept could be

extended to multiple layers. The bulk absorber, shown in figure 1(c), has a single-layer construction in which a fibrous mat fills the panel between the porous face sheet and solid backplate.

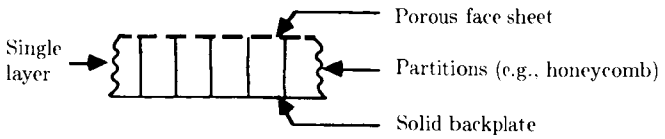

(a) Single degree of freedom (SDOF).

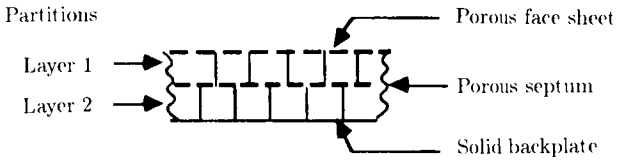

(b) Two degree of freedom (2DOF).

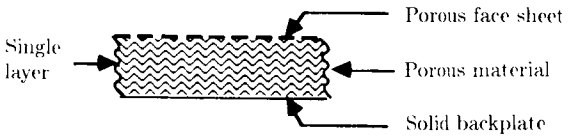

(c) Bulk absorber.

Figure 1. Conventional aircraft engine treatment panel designs.

Of the three design types, the SDOF type is effective over the narrowest range of frequencies and must be tuned to the frequency band containing the single fan tone of greatest concern. The useful bandwidth of SDOF treatment is about one octave. The 2DOF type has a wider bandwidth, being most effective for two adjacent harmonics of fan blade-passage frequency (BPF). With careful design, the useful bandwidth of 2DOF treatment can be extended to cover the BPF and its next two harmonics (about two octaves). This is generally sufficient for turbofan engine applications. The bulk absorber has the widest bandwidth, extending over three octaves in the range of concern if the panel is made sufficiently deep to be effective at the lowest frequency. Its performance at the higher frequencies then depends on the selection of fiber diameter and material density. Bulk absorber treatment has not been used in aircraft engines in commercial service because of structural design difficulties.

Note that the SDOF and 2DOF treatments are resonator panels, and their acoustic properties strongly depend on the damping that the resistance of the face sheet and midsheet provides; the acoustic properties can be either linear or nonlinear. The damping resistance of nonlinear liner face sheets and septum sheets varies with the amplitude of the acoustic wave incident on the liner, whereas the resistance of

linear face sheets and septum sheets is independent of the incident wave amplitude, at least over the range of sound pressure levels (SPL) experienced in practice. Thus, the resistance of a nonlinear treatment panel may vary along the length of the duct, as the wave amplitude is suppressed, and this variation affects its acoustic performance.

Ordinary perforate materials, typically with 1/32- to 1/16-inch-diameter holes, are in the nonlinear category. Wire-mesh materials and bulk absorbers are in the linear category except at extremely high SPL.

Generally, a more controlled treatment panel design can be obtained by using linear materials, which, to some extent, makes the treatment impedance independent of engine power setting. Since the source characteristics are known to change with engine power setting, attempting to maintain a constant treatment impedance is an oversimplification of the design problem. Conceivably, with highly sophisticated techniques, a nonlinear material could be designed with a variable impedance that used changing SPL to track optimum impedance values better than a linear material, but such an approach is beyond the scope of this discussion.

Available Design Approaches

Three design approaches are available to the acoustic engineer confronted with an engine noise suppression problem: theoretical, semiempirical, or empirical. Figure 2 illustrates graphically the acoustic treatment design approaches. The purpose of this chapter is to provide guidance to the engineer in selecting and implementing a treatment design method.

Ideal Theoretical Design Procedures

The theoretical design procedures discussed in the previous chapter represent the ideal approach for the analysis of duct acoustic propagation and radiation. These methods require knowledge of, or at least an assumption about, the source characteristics. At each problem frequency, the amplitudes and relative phases of the duct modes that are excited by the source (e.g., Tyler-Sofrin modes), or equivalent information in terms of acoustic pressure profiles, must be known for input into the analysis.

Elaborate experimental methods have been developed to measure modal content on vehicles that present unusually difficult problem tones. Successful suppression of these tones requires a closely tailored treatment design. Such theoretical design procedures represent current state of the art and have been applied in practice when the number of modes that are excited is modest. This problem arises sufficiently often to justify the significant effort required to exercise that capability.

Semiempirical and Empirical Approaches

When there is little information about the source modal characteristics, either because the particular turbomachinery is still in the early design stage and component test data are not available or because the number of duct modes carrying energy is very large (typical of high-bypass-ratio turbofan inlets), assumptions about the source characteristics usually must be made. The analytical result then becomes dependent on the modal content assumption, and experience must be a factor in providing a "best guess" assumption. To the extent that the input source characteristics are uncertain, the rigorous analysis becomes somewhat semiempirical.

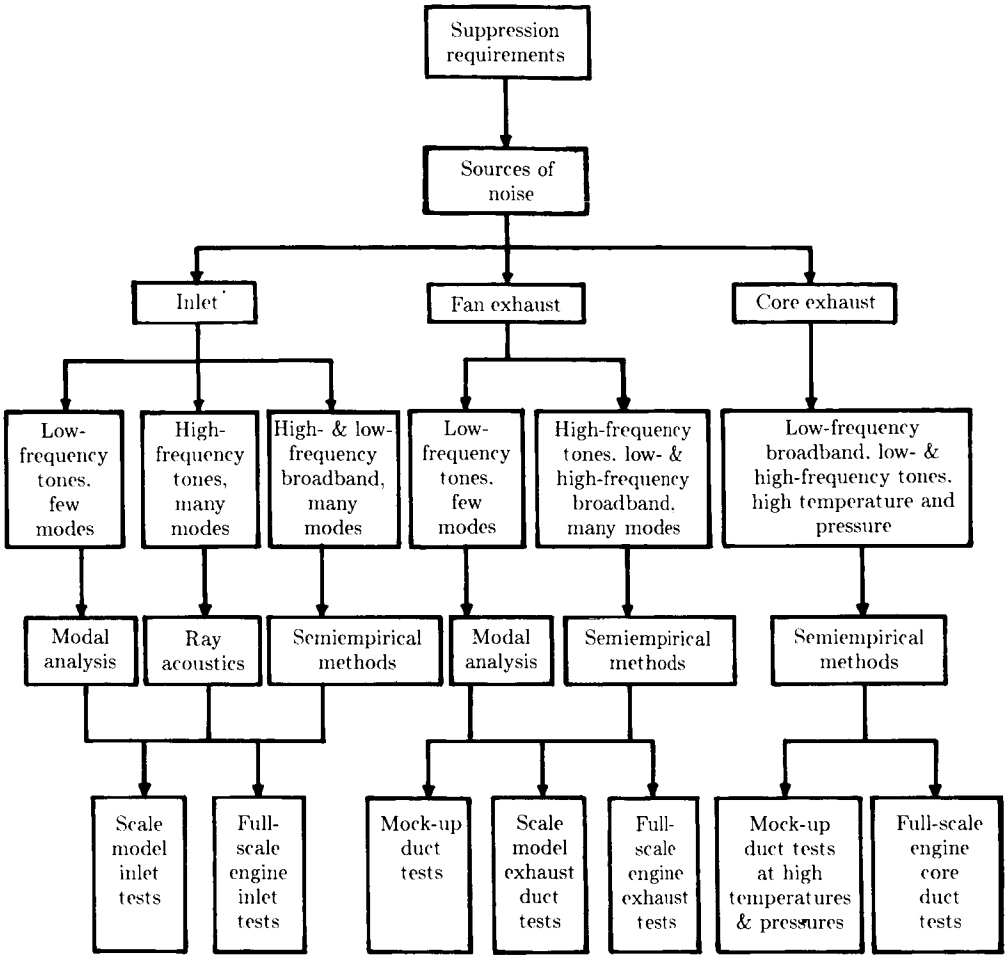

Figure 2. Schematic of engine treatment design approaches.

Progress is being made in turbomachinery source-prediction methods so that, again with experience, this prediction could reduce the uncertainty of the semi-empirical procedure. On the other hand, besides the possible uncertainty about the source, the actual conditions within engine ducts often depart significantly from the ideal. Interruptions in the treatment both circumferentially and axially, axial variations in the duct height, duct curvature, and other such departures from the ideal introduce the need to augment the theoretical approach with experimental data.

In the early years of development of acoustic treatment design for turbofan engine ducts, theoretical methods were not generally available nor sufficiently complete to permit designs by other than the purely empirical approach. The empirical approach usually consists of laboratory measurement of noise suppression, or insertion loss, when acoustic treatment is applied to the walls of a duct built to simulate the geometry of the engine duct.

The insertion loss experimental method compares the noise levels measured for a hard-walled, untreated duct with the levels measured after treatment panels have been inserted. Choices of treatment designs used for these tests are based on engineering experience, and because of the cost, the test series is seldom sufficiently exhaustive to ensure that the optimum design has been achieved. Examples of such test facilities are discussed in the subsequent section entitled "Testing for Treatment Design and Performance Measurement."

For either inlet or exhaust ducts, some of the pure empiricism can be removed by conducting an experimental test program in which SDOF treatment designs are employed. During a series of insertion loss tests the treatment panel depth and face-sheet resistance are systematically varied. The variation of panel depth controls variation of the treatment reactance, while the face-sheet resistance is varied by means of porosity if it is a perforate, or Rayl number if it is a mesh. The measured suppression can be plotted in the impedance plane, where the impedance of the panels tested has been obtained using existing methods for predicting or measuring panel impedance. Contour plots of isosuppression at each frequency then provide data on suppression in terms of impedance. Since the wall impedance is assumed to be the key parameter determining the suppression performance of the treatment panel, the isosuppression plots can be used in a semiempirical manner to predict the suppression of more complicated 2DOF or bulk absorber panels at each frequency, when the impedance for such panels is obtained by either prediction or measurement in the laboratory.

Another example of a semiempirical approach is to make geometric acoustic approximations in the analytical model used to represent the propagating sound field. For the inlet at blade-passage frequency and higher (ratio of duct diameter to wavelength greater than 10), suppression and far-field directivity of broadband noise can be closely estimated by means of simple ray acoustics, assuming equal energy distribution among the propagating modes. This semiempirical method is not adequate, however, when the noise is in a strong tone which is carried by relatively few modes excited by a source characteristic such as a vane-blade interaction. Fortunately, these exceptional cases are amenable to the rigorous analytical methods described in the previous chapter.

Design Approach Advantages and Disadvantages

The principal differences among the three approaches, and their relative advantages and disadvantages, are

1. The empirical approach requires extensive testing, which is not only time-consuming and expensive but also may not give adequate representation, or mock-up, of the conditions in the engine application. Laboratory tests can give ballpark designs, but actual engine tests are, ultimately, the most reliable way of arriving at an answer. If the design is marginal because a particular problem is unusually severe, a number of candidate designs may need to be tested.
2. The semiempirical approach by its nature entails some theoretical basis to provide coherence and understanding to the meaning of experimental data. Thus, the amount of testing required is reduced in scope and the time needed is significantly shortened. The main problem is to identify the analytical model that can be used with a limited data base to reach the objective.

3. The rigorous theoretical approach is most useful in providing understanding of the basic phenomena involved in the problem. In most cases, the rigorous model is a simplification or idealization of the actual conditions of the design application. Nevertheless, particularly when working with an actual engine development program, the theoretical approach provides such insight into cause and effect that the shortcomings of the model can be overshadowed by the gain in knowledge and understanding achieved.

Fundamentals of Duct Liner Technology

Acoustic Impedance Design Criteria

Acoustic impedance is defined as the ratio of acoustic pressure to acoustic velocity at a point on the surface of the panel and is given by the complex number

$$Z = \frac{p}{v} = R + iX \tag{1}$$

where

Z impedance, cgs rayls (g/cm^2-sec)

p acoustic pressure, dynes/cm^2

v acoustic velocity, cm/sec

R acoustic resistance, cgs rayls

X acoustic reactance, cgs rayls

i $= \sqrt{-1}$

The convention used in this chapter for time dependence of the wave solution of acoustic pressure and velocity in the duct is $e^{+i\omega t}$ (where ω is circular frequency and t is time). This leads to a positive sign for the imaginary term in the impedance, which is the usual convention. Choosing the $e^{-i\omega t}$ sign convention requires taking the complex conjugate in the definition of impedance. Further discussion of impedance (and its inverse, admittance) is given in reference 1, pp. 21–24; units and conversion factors are defined in reference 2. One of the first discussions of the impedance properties of treatment panels used in aircraft engine ducts is presented in reference 3.

Point-reacting treatment is used in aircraft engines and is the basis for the methods discussed in this chapter. To be point-reactive, the treatment panel must contain partitions that prevent propagation of the sound laterally within the panel. The point-reacting condition (which is also referred to as locally reacting) is required for the concept of impedance to be valid as a design parameter. In a non-point-reacting panel, the impedance at a point depends on the wave motion within the panel in an extended region around the point, and analysis of the design and performance of such panels must include the lateral propagation inside the panel.

As a rule of thumb, the axial extent of the partitions for resonators (SDOF, 2DOF) should be less than the depth of the panel, and partitions to block both axial

and circumferential internal propagation are desirable. In bulk absorbers, partitions with 2-inch to 4-inch axial spacing have typically been used for panels nominally 1-inch thick.

The value of impedance that provides the maximum sound absorption at a given frequency depends on the acoustic mode or ray angle of the propagating sound wave. The dependence is discussed for illustration briefly in the following paragraphs and in more detail in an elementary but clear way in reference 4, pp. 98–140. Reference 4 implicitly reveals the value of normalizing the impedance by the characteristic impedance of air ρc, such that

$$\frac{Z}{\rho c} = \varsigma = \theta + i\chi = \frac{R}{\rho c} + \frac{iX}{\rho c} \tag{2}$$

where

ς $= Z/\rho c$, the (nondimensional) impedance ratio

θ $= R/\rho c$, the (nondimensional) resistance ratio

χ $= X/\rho c$, the (nondimensional) reactance ratio

ρ density of the medium (air), g/cm^3

c speed of sound in the medium, cm/sec

One way of analyzing acoustic propagation in an idealized two-dimensional wave guide is to consider each wave to be the superposition of a series of plane waves, where each plane wave strikes the wall at a different angle and then ricochets back and forth down the duct. Reference 5, pp. 493–495, shows that in a hard-walled duct this plane-wave solution is equivalent to an acoustic mode propagating in the duct and that only certain angles of incidence to the wall (the characteristic duct modes) are allowed. This plane-wave analogy can be used to lend physical insight into the absorption process in ducts.

For the idealized case of a plane wave incident on a flat surface, the fraction of incident energy absorbed by the treatment panel is

$$\alpha = \frac{4\theta \cos\phi}{(1 + \theta\cos\phi)^2 + (\chi\cos\phi)^2} \tag{3}$$

where

α absorption coefficient

ϕ angle between the normal to the wave front and the normal to the panel, as shown in the sketch

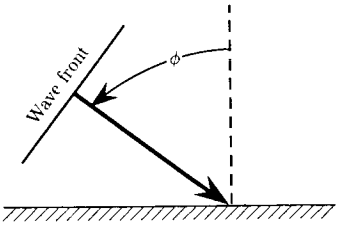

The normal-incidence absorption coefficient is the value of α when $\phi = 0$.

Equation (3) is based on the plane-wave solution to the wave equation for a reflection at a surface, assuming a semi-infinite region above the surface. This model is valid for propagation in a duct in the short wavelength (ray acoustic) limit so long as ϕ is not close to 90°. In that case, when the wave is propagating parallel to the wall, a modal analysis approach is required (see Cremer, ref. 6). For the plane-wave mode ($\phi = 90°$) without airflow, Cremer's analysis yields the optimum impedance for ducts of rectangular cross section:

$$Z_{\text{opt}}/\rho c = (0.92 - 0.77i)\eta \tag{4}$$

or

$$R/\rho c = 0.92\eta \qquad X/\rho c = -0.77\eta$$

where

η $= H/\lambda$, nondimensional frequency parameter

H height between duct walls, cm

λ wavelength of sound, cm

In contrast, the plane-wave surface reflection result indicates that the value of α is maximum when $X = 0$ and $R/\rho c = 1/\cos\phi$; that is, to obtain maximum absorption, the angle of incidence of the sound ray must be taken into account. In the event of many different ray angles, or propagating modes, the best choice of the value of R depends, then, on the amount of energy in each of the rays and on the relative attenuation rate introduced by the panel impedance selection.

Note that the plane-wave angle of incidence result for optimum modal impedance is an approximation to the exact result for a given mode. Determination of the exact optimum impedance requires solution of a complex transcendental equation derived from the duct impedance boundary condition (see the previous chapter).

If a single mode is dominant and giving trouble in the far field, the treatment may possibly be designed for it alone. The typical design problem is not that simple. Usually, there is a mix of modes with energy distributed among them in a manner that is generally unknown and, as experience to date has indicated, not easily measured. Thus an engineering assumption about the modal distribution must be introduced in order to attempt an analytical design approach. Failing an analytical approach, the designer must resort to laboratory mock-up duct testing, or even to engine testing.

The direct engine or mock-up duct testing approach has been often used, but results of laboratory mock-up duct tests for curved-duct fan reversers and engine tests for inlets suggest that a good engineering assumption for the analytical approach in these cases is to assume equal energy in all cut-on modes and random phasing among modes. At present, this provides a basis for semiempirical analytical determination of the best choices of R and X and estimation of the suppression losses caused by nonoptimum values.

In choosing the mock-up duct test approach, the designer must be aware that the source being used in laboratory testing may not closely simulate the actual engine source. Moreover, even if an engine is used as the treatment design testbed, the characteristics of certain tones produced in the presence of inflow distortion (such as

would be encountered with static engine ground testing) may be quite different from those produced in flight with cleaner inflow. When the equal energy and random phasing assumption holds, the mock-up duct procedure provides useful guidance in determining the effects of changes in duct geometry or treatment impedance, and engine static test results are improved by the provision of inlet turbulence control structures, as discussed subsequently.

Panel Configuration Design

In many cases, the desired resistance increases monotonically with frequency. Desired reactance is close to zero or even negative and becomes more negative with increasing frequency, as suggested by Cremer's (ref. 6) result (eq. (4)). These properties can be achieved over a limited range of frequency in the 2DOF construction. SDOF designs require a series of different treatment segments along the duct to achieve the same objective. Also, now that reasonably accurate impedance prediction is possible for bulk absorbers, it is understood that their previously known wide suppression bandwidth originates from inherently possessing a favorable variation of impedance (both R and X) as a function of frequency.

The properties of candidate panels and evaluations of their ability to achieve the impedance design criteria are summarized in the following sections.

Single-Degree-of-Freedom Liners

The SDOF panel (see fig. 1(a)) has a single-layer sandwich construction with a solid backplate, porous face sheet, and internal partitions as would be provided by a honeycomb. The face sheet can be a perforate with or without bonded wire mesh. The perforate is suitable for a limited range of power settings, for example, either for approach or for takeoff; if designed at one point, the other may be somewhat compromised. On the other hand, the wire mesh permits a uniform resistance property over a wide range of duct sound pressure levels and airflow velocities.

Linear face sheets maintain constant resistance with frequency because of the low-Reynolds-number viscous pressure drop for very fine screens. Nonlinear materials are effectively linearized by mean flow for typical duct Mach numbers, but may exhibit slight nonlinear resistance peaks near frequencies where the reactance approaches zero.

The reactance of single-layer panels follows a slightly modified cotangent curve, so that the optimum value can be obtained only at a single tuning frequency.

Two-Degree-of-Freedom Liners

The 2DOF panel (see fig. 1(b)) has a double-layer sandwich construction with a solid backplate, porous septum, and porous face sheet. Internal partitions such as honeycomb provide the spacing for the two layers. As with SDOF panels, the face sheet can be a perforate with or without bonded wire mesh. Even with the use of perforate only, linear properties can be approached because the septum can be made to control most of the effective acoustic resistance of the panel.

To obtain a linear property for the panel as a whole, the septum should be nearly linear. Septum linearity can be approached by using a perforate with such small holes (in the range of 5 to 10 mils) that the acoustic velocities induce only laminar orifice

flow. The closest approach to linearity identified to date, other than a bulk absorber, is to use a septum of wire mesh alone; such construction is available commercially.

The introduction of the septum has these important benefits: (1) the resistance of the panel surface is controlled by the septum rather than by the face sheet and thus the panel properties are essentially independent of duct flow effects; (2) the resistance and reactance can be tailored to approach the desired design values over a moderate range of frequencies. To achieve this benefit, the face-sheet resistance must be small. Figure 3 illustrates the degree of control of the panel properties obtainable.

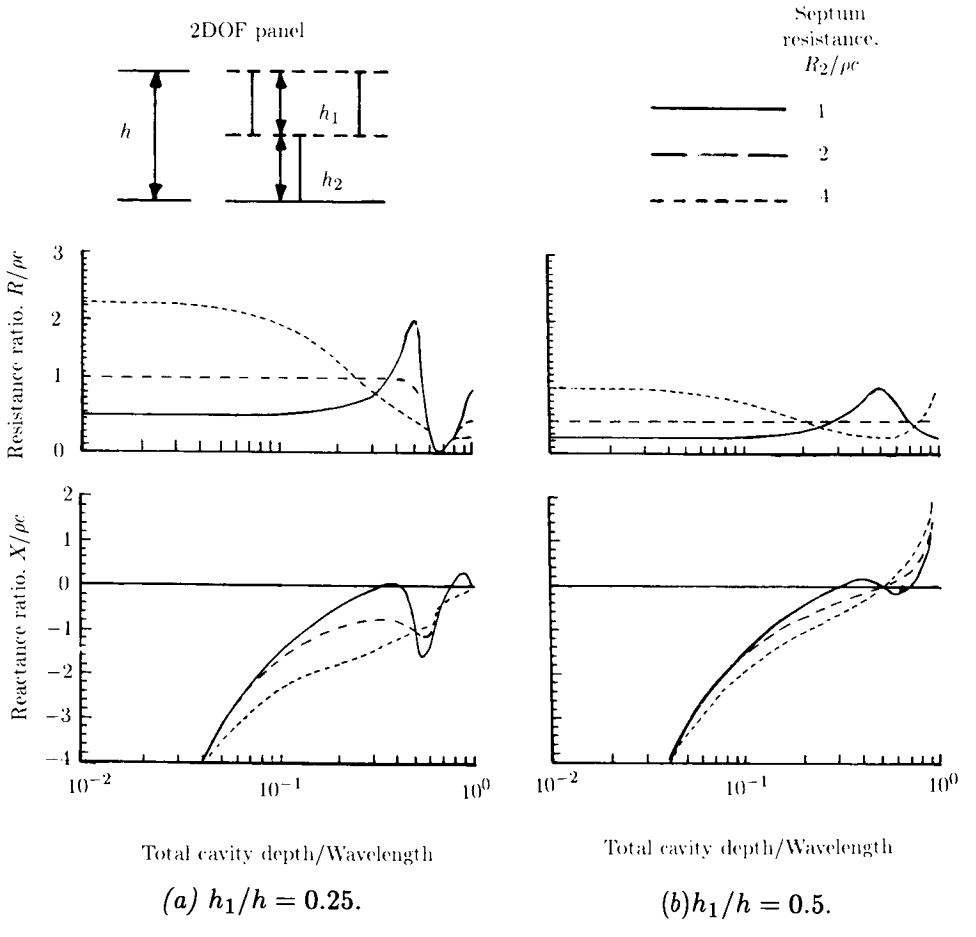

(a) $h_1/h = 0.25$. (*b*)$h_1/h = 0.5$.

Figure 3. Effect of variation of septum placement and resistance on impedance of 2DOF treatment, for face-sheet resistance of zero.

Bulk Absorber

A bulk absorber panel (see fig. 1(c)) usually consists of a single-layer construction with solid backplate and porous face sheet of negligible resistance (approximately 30-percent porosity or higher). The cavity is filled with a fibrous mat having very small air passages so that the airflow through the mat (acoustic velocity excitation) is of sufficiently low Reynolds number to be laminar throughout.

The introduction of the bulk absorber into the cavity has the same advantages as the introduction of the septum in 2DOF panels. The difference between the two is that the internal resistance of the 2DOF panel is "lumped," while that of the bulk absorber is distributed continuously over the panel depth. The 2DOF design can be tailored by varying the resistance of the septum and its location. The bulk absorber design (assuming homogeneous material) can be tailored by varying the amount of internal flow resistance (density of mat, fiber diameter, etc.).

Desired minimum tuning frequencies can be achieved with slightly thinner panel depths for bulk absorbers than for resonators, because the effective speed of sound is reduced by viscosity and heat transfer to and from the mat. The distributed resistance of bulk absorbers damps all multiples of half-wave antiresonances, whereas the 2DOF panel damps only the first one. Thus, the bulk absorber can absorb sound effectively at all frequencies above the first quarter-wave resonance, but the 2DOF panel performs well only for the range from the fan fundamental to the third harmonic.

Impedance Models

A comprehensive summary of analytical models for predicting impedance of treatment materials is given in reference 7. This report includes methods for point-reacting and distributed-reacting materials and for single- and multi-layered panels. The following discussion is specialized for the specific types of liners described in the preceding section, with emphasis on the kinds of liners that have been widely used in commercial engine ducts.

Design Parameters

By examining the mathematical models for treatment impedance for each panel type, we can readily identify the key parameters that relate the impedance to the physical construction. These physical parameters are denoted in figure 4.

The general formulas for each panel type are as follows:

For single-degree-of-freedom panels (fig. 4(a)),

$$\frac{Z}{\rho c} = \frac{R}{\rho c} + i\left(\frac{X_m}{\rho c} + \frac{X_c}{\rho c}\right) \tag{5}$$

where

$R/\rho c$ face-sheet resistance

$X_m/\rho c$ face-sheet mass reactance

$X_c/\rho c$ cavity reactance, equal to $-\cot(kh)$

h cavity depth, cm

k wave number, equal to ω/c, cm^{-1}

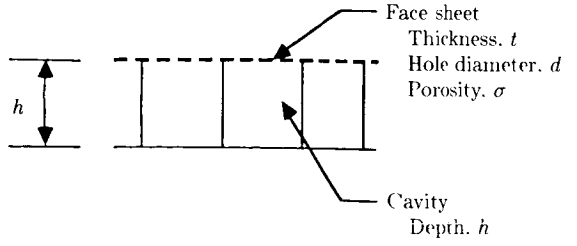

(a) Single degree of freedom.

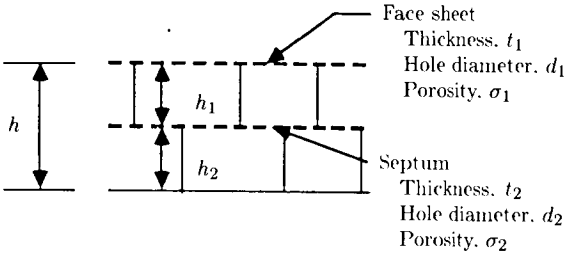

(b) Two degree of freedom.

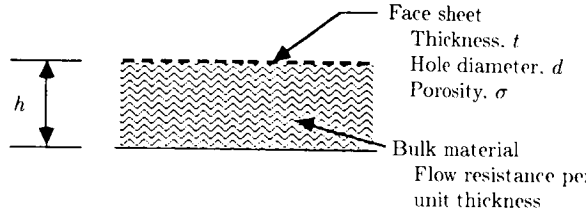

(c) Bulk absorber.

Figure 4. Treatment panel design parameters.

For two-degree-of-freedom panels (fig. 4(b)),

$$\frac{Z}{\rho c} = \frac{Z_1}{\rho c} + \frac{\frac{Z_2}{\rho c}\frac{\cos(kh_1)\sin(kh_2)}{\sin(kh)} - i\cot(kh)}{1 + i\frac{Z_2}{\rho c}\frac{\sin(kh_1)\sin(kh_2)}{\sin(kh)}} \tag{6}$$

where subscript 1 denotes the face sheet's impedance, resistance, and mass reactance and subscript 2 denotes the septum's; thus

$$\frac{Z_1}{\rho c} = \frac{R_1}{\rho c} + i\frac{X_{m1}}{\rho c}$$

$$\frac{Z_2}{\rho c} = \frac{R_2}{\rho c} + i\frac{X_{m2}}{\rho c}$$

For bulk absorber panels (fig. 4(c)),

$$\frac{Z}{\rho c} = \frac{Z_B}{\rho c} + \xi \coth(\gamma h) \tag{7}$$

where subscript B denotes the face-sheet impedance, resistance, and mass reactance, that is,

$$\frac{Z_B}{\rho c} = \frac{R_B}{\rho c} + i\frac{X_B}{\rho c}$$

and where

ξ characteristic impedance ratio of impedance of the bulk absorber to that of air

γ propagation coefficient (wave number) in the bulk absorber

The bulk absorber formulas have been adapted from reference 8. Expressions to calculate each of the parameters in these equations are given in the following discussion.

A more fundamental analytical model for bulk absorber panel impedance that should be pursued further is given in reference 9. That model, if modified to use dc flow resistance properties as input, could substantially improve the prediction of bulk absorber impedance.

Resistance: For the face sheet in the absence of grazing flow and for septum materials, the resistance term can be determined by the expression

$$\frac{R}{\rho c} = A + BV_i \tag{8}$$

where A and B are determined experimentally by dc flow resistance measurements and V_i is the velocity incident on the sample. The velocity can be taken as either the dc flow velocity or the root-mean-square of the fluctuating acoustic velocity incident on the sample. Making this identification is what relates the dc flow resistance measurement to acoustic resistance.

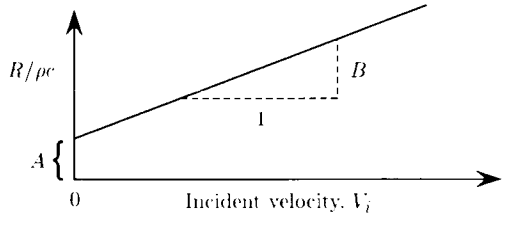

When the measurements of dc flow resistance are plotted versus incident velocity on a linear scale, the results can be described by a linear relationship (see ref. 10). The value of A is the linear component of the resistance, while B is the nonlinear

component, since the velocity-dependent term is what makes the resistance a function of the amplitude of the incident wave. In general, wire-mesh materials have both the A and the B component, while ordinary perforate materials have a significant value only for the B component.

For perforate materials, parameters determining the A and B terms can be identified from simple fluid mechanics, considering the energy loss mechanism to be caused by the pressure differential across the sample. Figure 5 illustrates the flow energy dissipation mechanisms comprising the resistance. The first term in equation (8) is the pressure loss inside the hole due to pipe-flow friction; the second term is dynamic head loss due to the turbulence associated with entrance and exit losses.

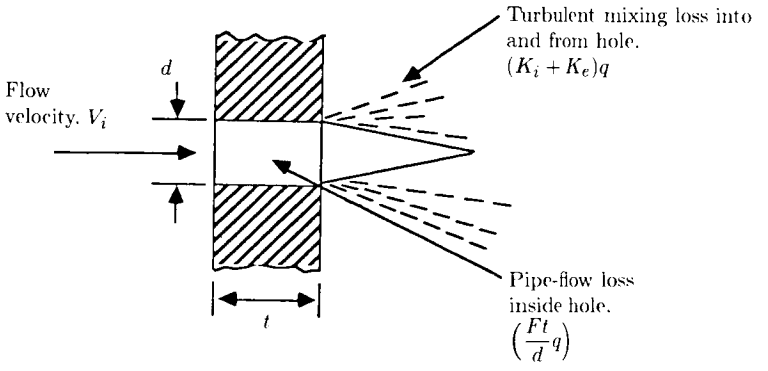

Figure 5. Flow mechanisms for dc flow resistance.

The first term is important when the diameter of the opening d is so small that the flow through the pore is laminar. This is the case for wire-mesh materials; for ordinary perforates, the flow in the hole is turbulent and the second term dominates. In the following analysis we express equation (8) in terms of acoustic resistance. This permits identification of the parameters that allow estimation of the effect of temperature and pressure on the material's resistance properties.

First, we note that for laminar flow, the friction factor is inversely proportional to Reynold's number N_{Re}:

$$F = \frac{a}{N_{\mathrm{Re}}} = \frac{a\mu}{\rho V_h d} \tag{9}$$

where

F	friction factor for pipe flow
V_h	velocity in the orifice, cm/sec
μ	fluid dynamic viscosity, dynes-sec/cm^2
d	hole diameter, cm
ρ	fluid density, g/cm^3
a	dimensionless proportionality constant, equal to 64

The ratio of pressure loss to dynamic pressure of the fluid within the hole is given by

$$\frac{\Delta p}{q} = \frac{Ft}{d} + K_i + K_e \tag{10}$$

where

Δp pressure loss, dynes/cm^2

q dynamic head, dynes/cm^2

t thickness of face sheet, cm

K_i dimensionless entrance loss

K_e dimensionless exit loss

For commercially available perforate materials, experience has shown that $K_i + K_e$ is approximately 1. The dynamic pressure in the orifice for incompressible flow is given by

$$q = \frac{1}{2}\rho V_h^2 \tag{11}$$

Note that this can be extended to compressible flow as in reference 11. The equivalent velocity through the vena contracta of the orifice is given by

$$V_h = \frac{V_i}{C_D \sigma} \tag{12}$$

where C_D is the dimensionless orifice discharge coefficient. A typical value of the discharge coefficient is $C_D \approx 0.76$. The porosity σ is given by

$$\sigma = \frac{n\pi d^2}{4} \tag{13}$$

where n is the number of holes per unit area.

Substituting equations (9), (11), and (12) into equation (10) and solving for $\Delta p/\rho c V_i$ results in

$$\frac{R}{\rho c} = \frac{\Delta p}{\rho c V_i} = \frac{a\mu t}{2\rho c(\sigma C_D)d^2} + \frac{K_i + K_e}{2c(\sigma C_D)^2} V_i \tag{14}$$

where we have inherently identified the dc flow velocity with the root-mean-square acoustic velocity. Comparing this result with equation (8), we obtain

$$A = \frac{a\mu t}{2\rho c(\sigma C_D)d^2} \tag{15}$$

$$B = \frac{K_i + K_e}{2c(\sigma C_D)^2} \tag{16}$$

Thus, A depends on both temperature (through c, μ, and ρ) and pressure of the air (through ρ) and B depends only on the temperature (through c). The values of a, C_D, and $K_i + K_e$ depend on the sheet material, whether wire mesh or simple perforate, and are most accurately determined from a dc flow resistance measurement of the actual material, which measures A and B directly.

Mass reactance: For the face-sheet and septum materials, the mass reactance term is determined by

$$\frac{X_m}{\rho c} = \frac{k(t + \epsilon d)}{\sigma} \tag{17}$$

where ϵ is the dimensionless end correction, which depends on the type of face-sheet or septum material. For perforates as in figure 5, early literature suggests $\epsilon = 0.85$; Ingard deduced a porosity effect (ref. 12):

$$\epsilon = 0.85\left(1 - 0.7\sqrt{\sigma}\right) \tag{18}$$

Note that ϵ also depends on sound pressure level and grazing flow effects (as discussed subsequently). In the septum of 2DOF panels, equation (18) is applicable because there are no grazing flow effects and the sound pressure level at the septum is relatively small. When the perforate is used over a bulk absorber, the porosity should be relatively high (greater than 25 percent), so the face sheet is acoustically transparent. For that reason, little attention has been given to this case, but, to a first approximation, the resistance term for a perforate should be valid, and the end correction on mass reactance should be about 0.3.

Bulk absorber parameters: The ratio of the characteristic impedance of the bulk absorber to that of air is given by

$$\frac{Z_B}{\rho c} = \frac{\rho_B c_B}{\rho c} = \frac{R_B}{\rho c} + i\frac{X_B}{\rho c} \tag{19}$$

where

$$R_B/\rho c = 1. + 0.05854(f\rho/P)^{-0.75}$$

$$X_B/\rho c = 0.08777(f\rho/P)^{-0.73}$$

and

$\rho_B c_B$ characteristic impedance in the bulk material

$f\rho/P$ dimensionless parameter

f frequency, Hz

P linear part of dc flow resistance per unit thickness of the material

The propagation coefficient in the bulk absorber is given by

$$\gamma = \alpha_B + \beta_B \tag{20}$$

where

$$\alpha_B = 0.19478k(f\rho/P)^{-0.59}$$

$$\beta_B = k[1. + 0.09476(f\rho/P)^{-0.7}]$$

These formulas are based on the results in reference 8.

Effects of Mean Flow on Impedance

For turbofan engines, where the mean flow is normally at Mach number M of 0.3 to 0.4, the resistance of nonlinear face-sheet materials on SDOF treatment panels is set by the grazing flow Mach number. The reactance is also affected by the end correction per equation (17), and the effect is large enough to shift the panel tuning frequency. The researcher is referred to references 7 and 13–19 for extensive discussion of this subject.

The practicing engineer who "needs a number" may find that the following relatively simple expressions for face-sheet resistance and for end correction to mass reactance are sufficiently accurate to be of practical use for typical designs in turbofan engines:

$$\frac{R}{\rho c} = \frac{0.3M}{\sigma} \tag{21}$$

$$\epsilon = 0.85\frac{(1 - 0.7\sqrt{\sigma})}{1 + 305M^3} \tag{22}$$

Equations (21) and (22) are from reference 16.

Some heretofore unpublished data, summarized in table 1, support the general validity of this approach. Also, as discussed in the derivations and interpretations in the next section, these data permit a more complete description of the combined effects of flow and SPL for real treatment materials having both linear and nonlinear properties. The table includes both measured data and predictions from the relationships derived in the following section.

Combined Effects of Mean Flow and Sound Pressure Level

For both linear and nonlinear materials, it has been generally accepted that the dc flow resistance is equal to the ac resistance of the sheet in the absence of flow, a fact verified by normal-incidence impedance measurements for pure tone excitation. The dc flow resistance parameters A and B from equation (8) provide the necessary information on the relative importance of the linear and nonlinear components. We can use these facts and the definition of impedance to derive an expression relating the panel resistance to the incident SPL and grazing flow turbulence.

Starting with the definition of impedance,

$$\frac{Z}{\rho c} = \frac{p}{\rho c V_i} = \frac{R}{\rho c} + i\frac{X}{\rho c} = \theta + i\chi$$

we multiply through by V_i, take the absolute value of both sides, and solve for V_i to obtain

$$|V_i| = \frac{|p|}{\rho c\sqrt{\theta^2 + \chi^2}} \tag{23}$$

Substituting this into equation (8) gives

$$\frac{R}{\rho c} = \theta = A + \frac{Bp}{\rho c\sqrt{\theta^2 + \chi^2}} \tag{24}$$

Normal-incidence impedance measurements have shown that equation (24) correctly handles the effect of reactance on the resistance for pure tone excitation. This equation can be rearranged in the following form:

$$(\theta - A)\sqrt{\theta^2 + \chi^2} - \frac{Bp}{\rho c} = 0 \tag{25}$$

For perforate face sheets used on turbofan engine ducts, the value of A from equation (15) is negligible, and the face sheet is essentially nonlinear. The resistance is dominated by the value of B from equation (16) and the excitation pressure p. If, further, the reactance X is zero, the resistance of the perforate is a maximum, and is given at this point by

$$\theta = \frac{R}{\rho c} = \sqrt{\frac{Bp}{\rho c}} \tag{26}$$

At other frequencies, where the reactance is not zero, the resistance for pure tone excitation is smaller, as indicated by equation (24) or (25).

For wire-mesh face sheets of very fine weave, the value of B from equation (16) can ideally be made negligible, and the face sheet is essentially linear. The resistance is dominated by the value of A, that is,

$$\theta = \frac{R}{\rho c} = A \tag{27}$$

and the resistance is constant, independent of reactance, SPL, or flow effects. Purely linear materials, of course, are not available, and the discussion in reference 20 is of interest.

For real materials, whether perforate or wire mesh, neither A nor B is zero, and all real sheet materials exhibit a combination of linear and nonlinear properties so that the excitation pressure p must be taken into account. In the absence of grazing flow, the magnitude of the pressure (in dynes/cm^2) can be obtained from the SPL of the incident wave as

$$|p| = (2 \times 10^{-4})10^{(\mathrm{SPL}/20)} \tag{28}$$

The agreement between the measured resistance values in table 1 and predictions by equations (24) and (28) is shown in figure 6. These data, for pure tone excitation, show the nonlinear effect of sound pressure level and the variation of resistance with frequency stemming from the effect of the reactance term χ in equation (24). Further

Table 1. Combined Flow and SPL Effects on Predicted and Measured Impedance for a 6.7-Percent Perforate

[Data obtained with apparatus in fig. 12
Cavity depth = 1.0 in.; Hole diameter = 0.032 in.
Face-sheet thickness = 0.032 in.; Porosity = 6.7%
$A = 1.4$; $B = 0.2336$]

Frequency, Hz	$M = 0$					$M = 0.2$				
		$R/\rho c$		$X/\rho c$			$R/\rho c$		$X/\rho c$	
	OASPL	Meas.	Pred.	Meas.	Pred.	OASPL	Meas.	Pred.	Meas.	Pred.
1100	146.9	0.37	0.39	−1.5	−1.50	146.7	0.77	0.49	−1.45	−1.51
	142.2	.24	.24	−1.49	−1.50	141.7	.69	.39	−1.45	−1.50
	137.0	.17	.13	−1.46	−1.49	136.1	.66	.34	−1.44	−1.50
	126.8	.13	.04	−1.43	−1.47					
1350	151.5	.71	.79	−1.05	−1.05	146.7	.77	.64	−1.02	−1.04
	146.5	.47	.51	−1.03	−1.04	141.2	.70	.52	−1.01	−1.04
	141.6	.31	.31	−1.02	−1.03	135.9	.65	.46	−1.00	−1.03
	136.4	.21	.18	−.98	−1.02					
	126.4	.14	.06	−.94	−.99					
1750	141.6	.44	.48	−.45	−.49	147.1	.92	.83	−.5	−.51
	136.7	.31	.33	−.48	−.47	141.7	.81	.70	−.48	−.50
	126.4	.19	.12	−.43	−.45	135.8	.75	.65	−.47	−.50
2100	139.9	.48	.52	−.13	−.12	140.8	.78	.76	−.16	−.14
	136.5	.40	.42	−.12	−.11	136.2	.74	.72	−.12	−.14
	126.7	.25	.24	−.07	−.08					
2450	141.6	.52	.56	.11	.18	141.7	.71	77	.12	.16
	136.5	.39	.41	.14	.20	136.1	.62	.72	.11	.17
	126.7	.25	.19	.21	.24					
2700	139.6	.32	.45	.39	.39	139.7	.67	.71	.3	.36
	126.8	.21	.13	.44	.44	136.0	.64	.68	.3	.37
3000	136.7	.30	.27	.66	.63	137.8	.61	.63	.46	.59
	126.7	.20	.09	.71	.68	135.9	.59	.62	.45	.59
3200	140.3	.17	.34	.83	.76	136.1	.53	.57	.67	.74
	131.5	.10	.13	.85	.81					

Table 1. Concluded

[Data obtained with apparatus in fig. 12
Cavity depth = 1.0 in.; Hole diameter = 0.032 in.
Face-sheet thickness = 0.032 in.; Porosity = 6.7%
$A = 1.4$; $B = 0.2336$]

Frequency, Hz	$M = 0.3$					$M = 0.4$				
		$R/\rho c$		$X/\rho c$			$R/\rho c$		$X/\rho c$	
	OASPL	Meas.	Pred.	Meas.	Pred.	OASPL	Meas.	Pred.	Meas.	Pred.
1100	145.4	0.92	0.73	−1.13	−1.51	146.3	0.93	1.10	−0.98	−1.52
	141.5	.86	.70	−1.14	−1.51	142.1	.68	1.08	−.98	−1.52
1350	146.9	1.04	.92	−.76	−1.05					
	141.8	.94	.86	−.72	−1.05					
1750	140.9	1.11	1.02	−.27	−.52	144.2	.95	1.38	−.13	−.53
						141.3	.86	1.37	−.13	−.53
2100	141.4	1.11	1.07	0	−.16	143.7	1.28	1.42	.33	−.18
2450	146.3	1.08	1.12	.23	.14	150.2	1.43	1.48	.37	.12
	141.4	1.02	1.08	.23	.14					
2700	140.3	.97	1.05	.33	.34	143.1	1.31	1.41	.61	.32
3000	140.1	1.01	1.00	.50	.56	142.8	1.34	1.37	.77	.54
3200						142.6	1.31	1.35	1.01	.68

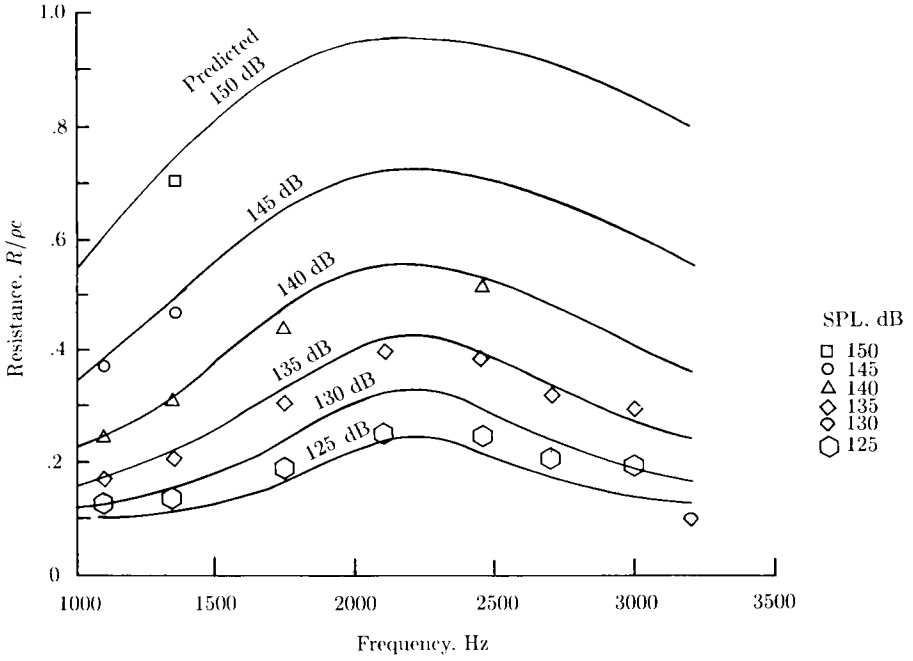

Figure 6. Effects of SPL on resistance of SDOF panel with nonlinear face sheet. Perforate properties: $A = 1.4$, $B = 0.2336$, $t = 0.032$ *in.*, $d = 0.032$ *in.*, $\sigma = 6.7$

research is needed to determine whether the effect of reactance on resistance is still present for broadband excitation.

The data in table 1 at zero flow show a systematic effect of SPL on the reactance. These data, augmented by similar data at two additional porosities, are shown in figure 7 in terms of the effect of incident velocity V_i on the end correction ϵ. Note that the data correlation indicates that the prior correlation by Ingard (eq. (18)), using porosity as a parameter, could be replaced by a relationship involving the face-sheet resistance as it affects the velocity incident on the panel; that is,

$$\epsilon = \begin{cases} 0.85 & (V_i < 0.4 \text{ cm/sec}) \\ 0.738 - 0.119 \ln V_i & (0.4 \text{ cm/sec} \leq V_i \leq 493 \text{ cm/sec}) \\ 0 & (V_i > 493 \text{ cm/sec}) \end{cases} \tag{29}$$

The value of V_i is determined by

$$V_i = \frac{p}{\rho c \sqrt{\theta^2 + \chi^2}} \tag{30}$$

The flow turbulence associated with the grazing flow results in a pressure excitation that causes the resistance to increase just as if SPL were increased. As shown by Rice, the effect of flow Mach number M is as given by equation (21).

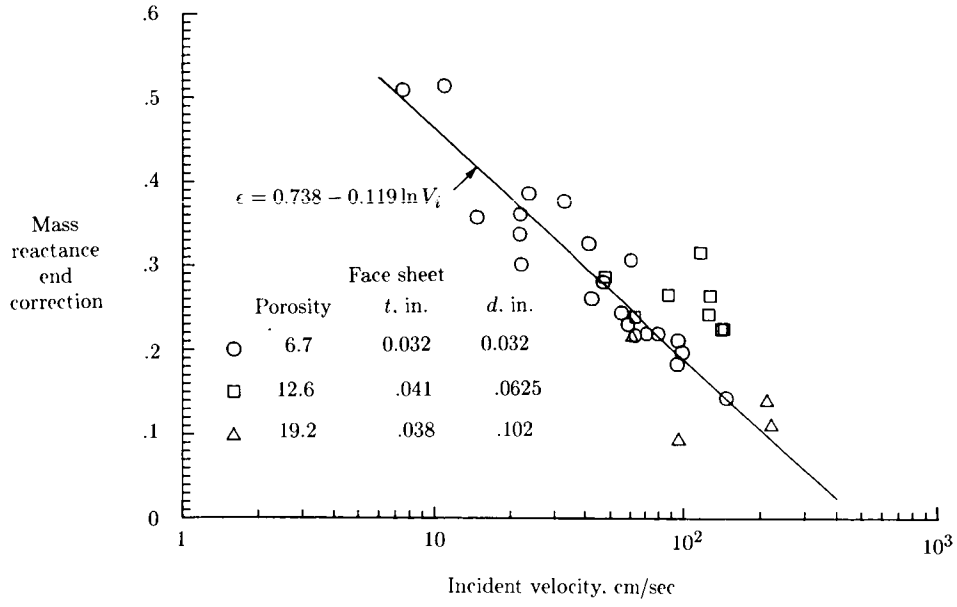

Figure 7. Effect of incident velocity on mass reactance end correction.

To further establish the effects of flow and SPL, data were obtained using the in situ impedance measurement system to be described subsequently. The experimental data for a 6.7-percent-porosity face sheet are summarized in table 1 together with results of prediction by a method to be described in the following paragraphs.

The effect of flow turbulence on the total excitation pressure p_T is assumed to add on an energy basis with that from simple acoustic excitation; that is,

$$p_T = \sqrt{p_A^2 + p_F^2} \tag{31}$$

where

p_A acoustic pressure from equation (28)

p_F flow turbulence pressure fluctuation

This is similar to the root-mean-squared velocity considered in reference 17.

The experimental data in table 1, for flow Mach numbers of 0, 0.2, 0.3, and 0.4, were used to estimate the magnitude of the turbulence effect. It was determined that a good fit was obtained between predicted and measured resistance as a function of Mach number, including the effect of SPL from equation (31), when the value of p_F was

$$p_F = 90\,000\ M^2 \tag{32}$$

As pointed out in reference 17, the value of the constant should take into account the boundary layer profile, and further research is required to improve equation (32). Nevertheless, the agreement between predicted and measured data can be seen,

in total, in table 1; the measured data show a strong increase in resistance with increasing Mach number that is reasonably well predicted, even at Mach 0.4. The additional effect of SPL as predicted by equation (31) is also demonstrated.

A more graphic demonstration of the relatively good agreement is given in figure 8 for Mach 0.3. Note that in both table 1 and figure 8 the predicted variation of resistance with frequency, and hence reactance, is reasonably well confirmed.

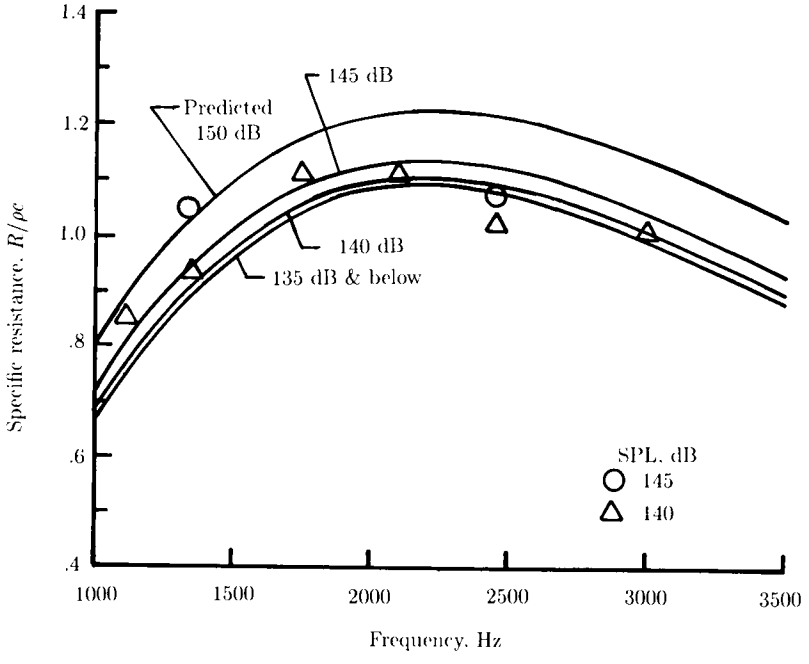

Figure 8. Predicted and measured resistance of a perforate versus frequency at Mach 0.3.

It should be noted that equation (26) can be put into the same form as equation (21) for a simple perforate using equations (16) and (32) (for the case of zero reactance) as follows:

$$\frac{R}{\rho c} = \sqrt{B\frac{p}{\rho c}} = \sqrt{\frac{(K_i + K_e)90\,000}{2cC_D^2\rho c}}\frac{M}{\sigma} \tag{33}$$

When we set $K_i + K_e = 1$, $\rho c = 41.5$ rayls, $c = 34\,380$ cm/sec, and $C_D = 0.76$, the constant factor becomes 0.24, which is within 80 percent of Rice's value of 0.3 in equation (21).

The predicted reactances in table 1 used equations (29) and (30) to determine the mass reactance end correction and used equation (31) to determine the pressure. The prediction results in a decrease in reactance with increasing Mach number; the data suggest a small increase. Further research on this aspect of flow effects is needed.

Another feature of perforate face sheets illustrated by equation (26) is that the square root permits both a positive and a negative answer:

$$\frac{R}{\rho c} = \pm\sqrt{\frac{pB}{\rho c}} \tag{34}$$

The existence of a negative square root solution implies a negative resistance, suggesting noise generation rather than absorption. For linear materials, with a significant value of A, noise generation is not a problem. Under the right conditions, noise generation has been observed experimentally many times and generally consists of a tone whose frequency is given by a dimensionless Strouhal number N_{St}

$$N_{\mathrm{St}} = \frac{fd}{V_\infty} \tag{35}$$

where V_∞ is the mean flow velocity. In reference 18, N_{St} was found to be approximately 0.2. In reference 19, the tone occurred at the resonant frequency (i.e., $X = 0$) for $N_{\mathrm{St}} = 0.26$. Extensive experimental studies of the occurrence of this phenomenon have also been reported in reference 21.

Measurement of Liner Impedance

The impedance of acoustic treatment panels can be determined experimentally in several ways: (1) by measurement of the dc flow resistance of the constituents of the panel for input to an analytical impedance model (as discussed in the preceding section), (2) by measurement of the standing wave pattern in a normal-incidence impedance tube using either a traversing probe or two (or more) fixed pressure transducers, and (3) by measuring the in situ impedance with sensors attached to the face sheet and inside the panel cavity. The first two methods are suitable when grazing airflow effects on the face sheet are of negligible concern; the last method permits impedance measurement in a duct, either in the laboratory or in the engine.

Direct Current Flow Resistance Measurement

A typical test apparatus for dc flow resistance measurement is shown in figure 9 (ref. 22). The sample panel is placed in a sample holder, which has a well-defined cross-sectional area. Then air is driven through the sample either by a pressurized line or a vacuum line, as shown, and metered by the flowmeter. The pressure drop across the sample is determined by a differential pressure measuring device. The dc flow resistance is then determined by

$$R = \frac{\Delta p}{V_i} \tag{36}$$

where Δp is the pressure drop across sample in dynes/cm^2. It is assumed that V_i has been correctly determined by accounting for the volume flow as measured in the flowmeter and the cross-sectional area of the sample.

As pointed out in reference 10, plotting R versus V_i results in a linear function of the form given in equation (8). The coefficients A and B can be determined by

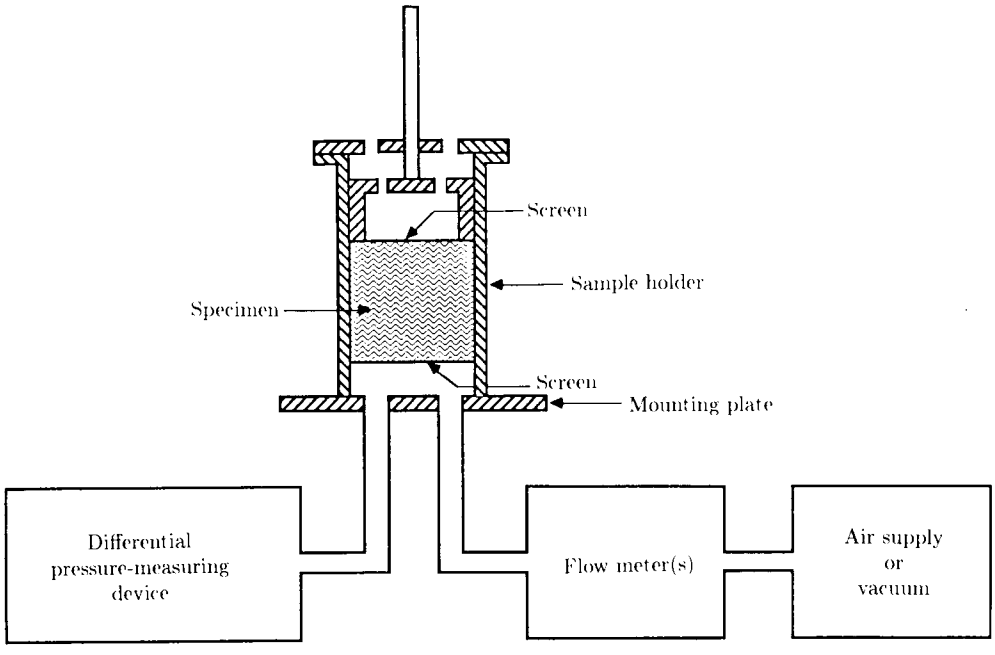

Figure 9. Apparatus for measuring flow resistance. (From ref. 22. Copyright ASTM. Reprinted with permission.)

a linear curve fit to the measured data. When the porosity of the sample is smaller than 5 to 10 percent, compressibility effects can cause an apparent departure from this simple relationship; a method for eliminating this difficulty in the measurement is described in reference 11.

Normal-Incidence Impedance Measurement

Single-sensor method: The apparatus shown in figure 10 (ref. 7) is representative of systems used for determination of impedance by reflection of normal-incidence sound waves. Sound introduced at the source end of the tube travels in a plane wave and reflects from the end containing the test sample, setting up a standing wave pattern along the length of the tube that depends on the strength and phase of the reflected wave. The traversing probe is used to measure the maximum and minimum sound pressure levels of the standing wave pattern and the distances from the face sheet of the sample to the location of the minima.

The pressure of the standing wave pattern in the tube is described by (ref. 4)

$$p(x) = \left[(A+B)^2 \cos^2\left(kx + \frac{\phi_{BA}}{2}\right) + (A-B)^2 \sin^2\left(kx + \frac{\phi_{BA}}{2}\right)\right]^{1/2} \qquad (37)$$

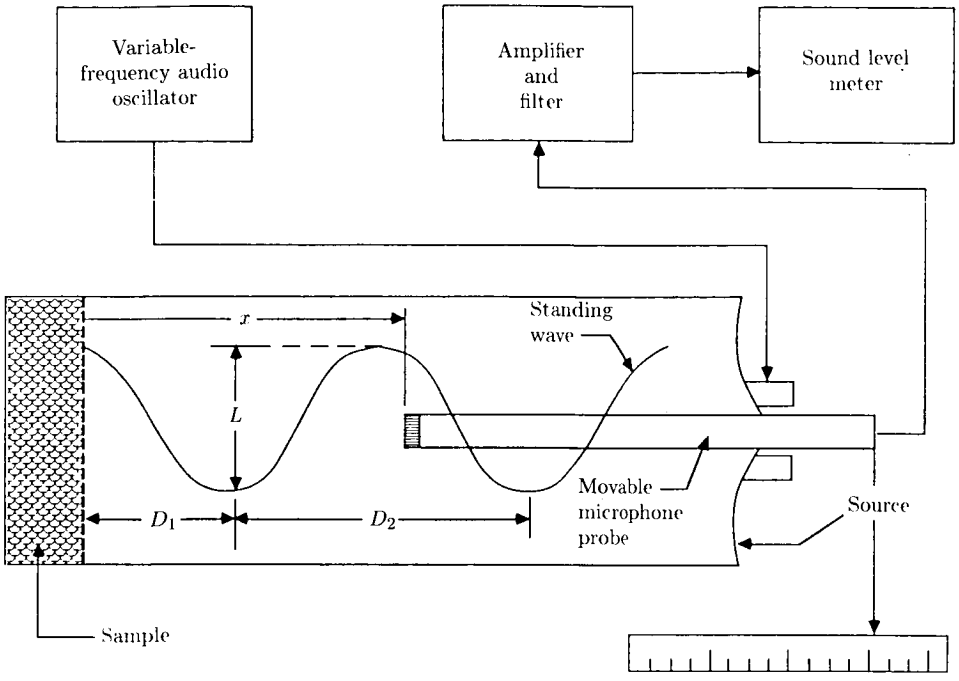

Figure 10. Normal-incidence impedance tube apparatus. (From ref. 7.)

where

p standing wave pressure amplitude, dynes/cm^2

A amplitude of incident wave, dynes/cm^2

B amplitude of reflected wave, dynes/cm^2

x distance from surface of test sample, cm

ϕ_{BA} phase angle between incident and reflected pressure waves, radians

The impedance is given by

$$\frac{Z}{\rho c} = \frac{A + Be^{i\phi_{BA}}}{A - Be^{i\phi_{BA}}} \tag{38}$$

The magnitude of B relative to A is determined from the measured standing wave ratio (SWR):

$$\text{SWR} = \frac{A + B}{A - B} \tag{39}$$

where $A+B$ is the maximum of the standing wave pattern and $A-B$ is the minimum of the standing wave pattern. Rearranging equation (39), we get

$$\frac{B}{A} = \frac{\text{SWR} - 1}{\text{SWR} + 1} \tag{40}$$

(The standing wave ratio is usually measured as the number of decibels between the peak and the null and must be converted to a ratio in pressure units for use in eq. (40).)

The phase of the reflected wave relative to the incident wave, ϕ_{BA}, is determined from the position of the first minimum, $x = D_1$ (shown in fig. 10). This first node occurs where, in equation (37)

$$kD_1 + \phi_{BA}/2 = -\pi/2$$

so that

$$\phi_{BA} = -(\pi + 2kD_1) \tag{41}$$

is the phase angle that the reflected wave leads or lags the incident wave. The results in equations (40) and (41) provide the information needed in equation (38) to determine the impedance.

Because this method depends on examining a standing wave pattern, it is limited to discrete frequencies; for that reason, in design work it has generally been discarded in favor of the dual-sensor method, described next. The data analysis and the correction for sound absorption in the tube are further discussed in references 23 and 24.

Dual-sensor method: A test setup for the dual-sensor impedance tube method is diagrammed in figure 11. A random noise signal is input from one or two speaker sources as shown in the top half of the figure. A digital thermometer is included because of the need to determine the speed of sound accurately. The bottom half of the figure shows the measurement system, which includes a fixed pressure sensor mounted flush on the wall and a translating probe-mounted sensor. The two signals are amplified and processed in a two-channel spectral analyzer that permits determination of the impedance over the full range of frequencies of interest with a single measurement. The method is discussed further in references 25, 26, and 27.

The value of impedance at a given frequency depends on the pressures at the two sensors, the phase between the two, and their separation distance and is given by

$$\frac{Z}{\rho c} = \frac{i\left[\sin(kx_1) - \dfrac{p_1 p_2 e^{i\phi_{12}}}{p_2^2}\sin(kx_2)\right]}{\dfrac{p_1 p_2 e^{i\phi_{12}}}{p_2^2}\cos(kx_2) - \cos(kx_1)} \tag{42}$$

where

x_1, x_2 distance from sample face of sensors 1 and 2, cm

p_1, p_2 pressure amplitude at sensors 1 and 2, dynes/cm^2

ϕ_{12} phase angle between pressure sensors 1 and 2, radians

The quantity $p_1 p_2 e^{i\phi_{12}}$ is the cross spectral density of the two pressure signals and p_2^2 is the auto spectral density of p_2. Many types of two-channel analyzers are available

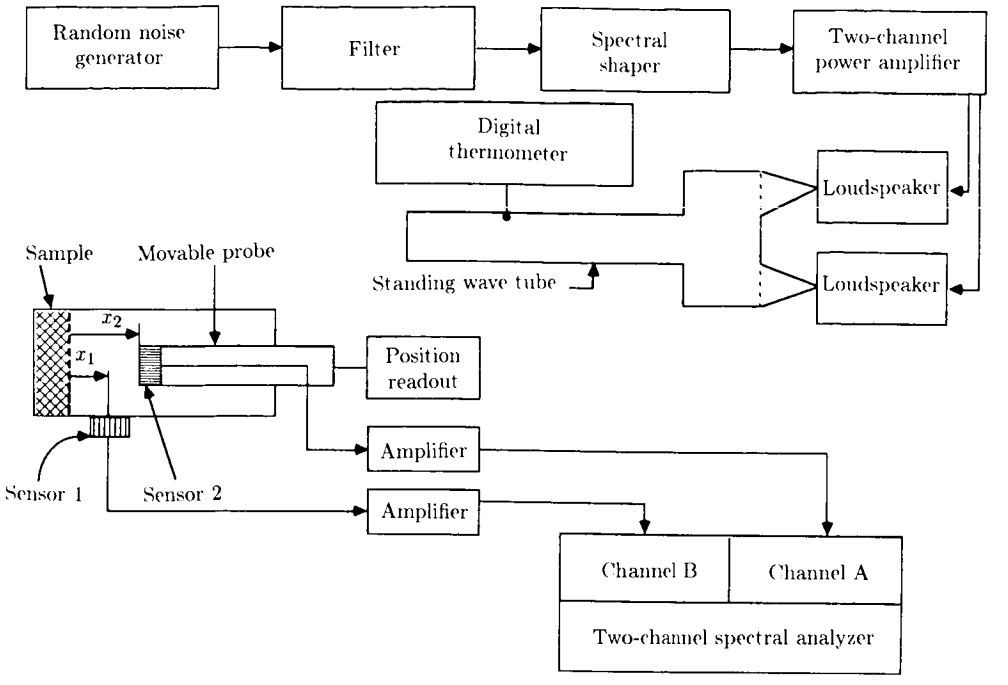

Figure 11. Dual-sensor method for normal-incidence impedance measurement.

to provide the information in equation (42), and the measurement can easily be automated using a microcomputer-based system.

Locating sensor 1 as close as practicable to the face sheet of the treatment sample gives an indication of the SPL exciting the panel and allows investigations of panel nonlinearity. Note that the measurement ideally requires only two sensors at the fixed positions x_1 and x_2. The recommendation that sensor 2 be on a movable probe, permitting variation of x_2, arises from the fact that at certain combinations of sample impedance and frequency, x_2 may fall at a null of the standing wave pattern, giving potential signal-to-noise-ratio sensitivity problems. Being able to vary x_2 avoids this problem and permits a means to verify measurement repeatability, since the results should be independent of x_2.

An inherent limitation of both single- and dual-sensor impedance tube methods is the upper frequency limit of the measurement. The measurement requires the presence of plane-wave propagation in the tube, so that the upper frequency limit is a conservative factor (roughly 0.75) times the frequency at which the first higher order mode begins to propagate. In a standard 1.0-inch-diameter tube at room temperature, the first mode above the plane wave (lowest radial mode of the first order circumferential mode) cuts on at about 8000 Hz, limiting the useful upper frequency to about 6000 Hz. The upper frequency limit can be increased by using a smaller diameter tube, but care must be taken that the treatment sample is not too small to be representative of an average panel area.

In Situ Impedance Measurement Systems

The apparatus shown in figure 12 is representative of that used for determination of impedance by the more specialized in situ method often called the two-microphone method. This method is most often used when information is required about the effects of grazing flow on the treatment impedance and can be used in a laboratory duct or on the actual engine installation. It is similar to the dual-sensor method discussed in the preceding section, but in this case both sensors are fixed within the panel itself. One sensor is mounted flush on the backplate of a chosen cavity (microphone B) and the other is inserted through the face sheet (microphone A). The sensors must be small enough to have negligible effects on the propagation within the cavity.

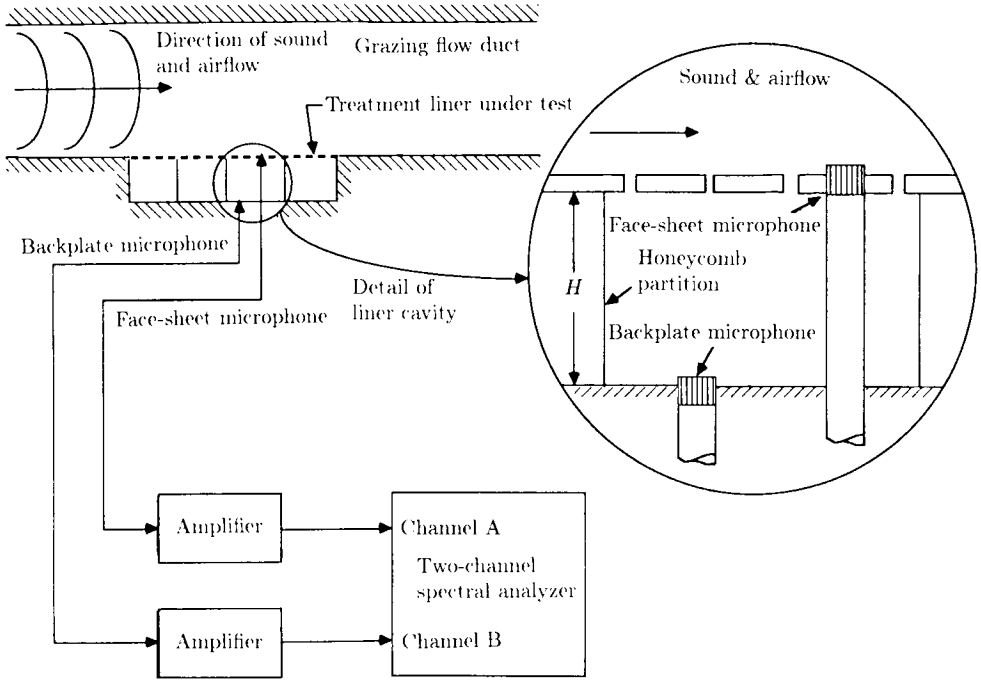

Figure 12. Measurement of grazing flow impedance by two-microphone method.

A two-channel spectral analyzer is used to obtain the amplitude and phase of the two pressure signals relative to one another. In this case the impedance for an SDOF panel is related to the measured quantities by the expression

$$\frac{Z}{\rho c} = -i\frac{p_A p_B e^{i\phi_{AB}}}{p_A^2 \sin(kh)} \tag{43}$$

where $p_A p_B e^{i\phi_{AB}}$ is the cross spectral density between microphones A and B, p_A^2 is the auto spectral density of microphone A, and h is the panel depth. Further

discussion of the method and the extension of the method to 2DOF linings is given in references 13, 14, and 28.

Empirical and Semiempirical Design Methods

Development of Design Data Bases and Charts

In the earlier section on empirical and semiempirical design approaches, the manner of evolving designs from experimental data bases was discussed. The scope of the general design problem includes the fan or compressor inlet, the fan exhaust, and the core engine exhaust. Experimental facilities for conducting these tests are discussed subsequently.

The inlet and fan exhausts are at temperatures and pressures reasonably close to ambient laboratory conditions, so that only relatively small errors are introduced if laboratory data are not corrected. In contrast, the core exhaust is always at such high temperature and, usually, elevated pressure that either tests must be conducted under the engine conditions or appropriate analytical corrections must be made to (1) the properties of the treatment and (2) the duct propagation effects.

The scaling parameter for conducting experiments at ambient or elevated conditions is the ratio of duct diameter or duct height to wavelength (D/λ or H/λ). The wavelength at a given frequency depends on the temperature in the duct.

With this in mind, contours of isosuppression can be determined to establish design data bases or design charts as described previously. An example of such a contour plot is given in figure 13, showing isosuppression contours in the impedance plane (reactance versus resistance) at a 1/3-octave band frequency of 4000 Hz and for mean flow of Mach 0.3. To generate the plot, treatment cavity depths of 0.25 inch through 1.0 inch were tested, in each case with seven wire-mesh face-sheet resistances. These variations provided data for magnitude of suppression at the intersections of the grid that were used to draw the isosuppression contours. Similar plots can be created for a range of 1/3-octave band frequencies and airflow Mach numbers. In this form, the data allow peak suppression and associated optimum resistance and reactance to be empirically determined as a function of frequency and can be used to obtain the suppression sensitivity to nonoptimum impedance.

These data can be normalized with dimensionless parameters as illustrated in figure 14, showing the ratio of peak suppression in decibels to the ratio of duct length to height as a function of duct height-to-wavelength ratio (H/λ). Figure 15 shows the optimum resistance ($R/\rho c$) versus H/λ. A similar plot can be constructed for the optimum reactance. In practice, curve fits are made for computerization of such data including the nonoptimum contours, so that by predicting the impedance of candidate treatment panel designs, the associated suppression spectrum can be quickly estimated.

Reference 29 presents an excellent summary of methods developed by Rice and others to enable analytical estimation of the peak suppression, optimum impedance, and bandwidths of suppression for particular treatment designs. These methods, when applied to inlets, lead to a "cutoff-ratio" correlating parameter that has been

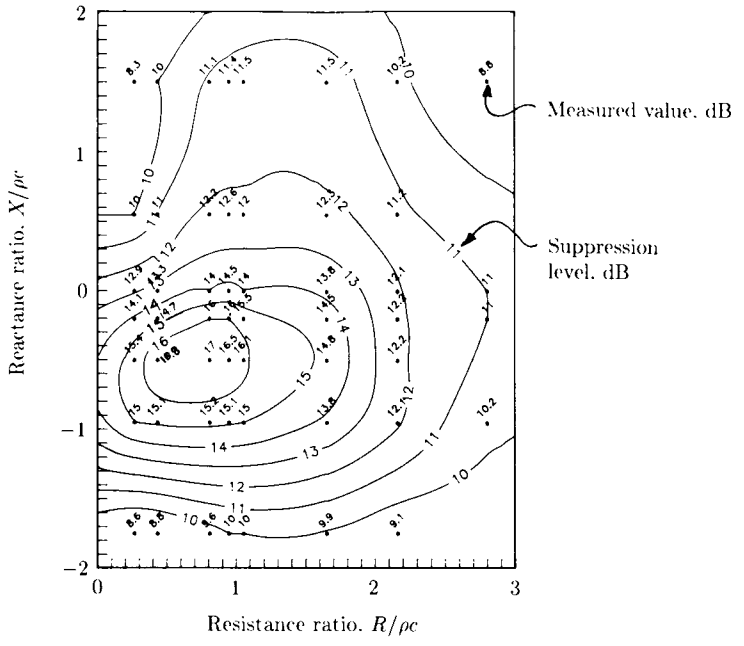

Figure 18. Example of isosuppression contours drawn in impedance plane.

recognized to be closely related to wave angles associated with the ray acoustics approach.

Reference 29 is recommended to the designer interested in closed-form solutions for suppression representing curve fits to extensive parametric study results. These studies are based on modal analysis and are correlated in terms of cutoff ratio, duct Mach number, and treatment impedance. Rice has also evaluated the effects of boundary layer thickness.

In reference 30, the ray acoustics approach was pursued for turbofan two-dimensional ducts. Such methods are in the semiempirical category, requiring an assumption about the modal energy distribution. The advantage of this approach is the reasonably good results obtained for engines, as well as the rapid computer predictions that result from this simplified calculation procedure.

Design Procedures

Choice of Suppressor Design Frequencies

Even after features have been incorporated to reduce noise at the source, turbofan engines have strong tonal content in the noise spectrum. These tones occur at the blade-passage-frequency (BPF) harmonics of the turbomachinery rotating blade rows. Problem sources are the fan itself, the booster stages feeding air into the compressor, sometimes the front stages of the compressor, and the turbine stages. When there is more than one stage in series, nonlinear effects introduce sum and difference frequencies of the tone harmonics from the individual stages.

The usual design problem, fortunately, is limited to the fan stage fundamental BPF and one or two higher harmonics. If noise at only the BPF and next higher

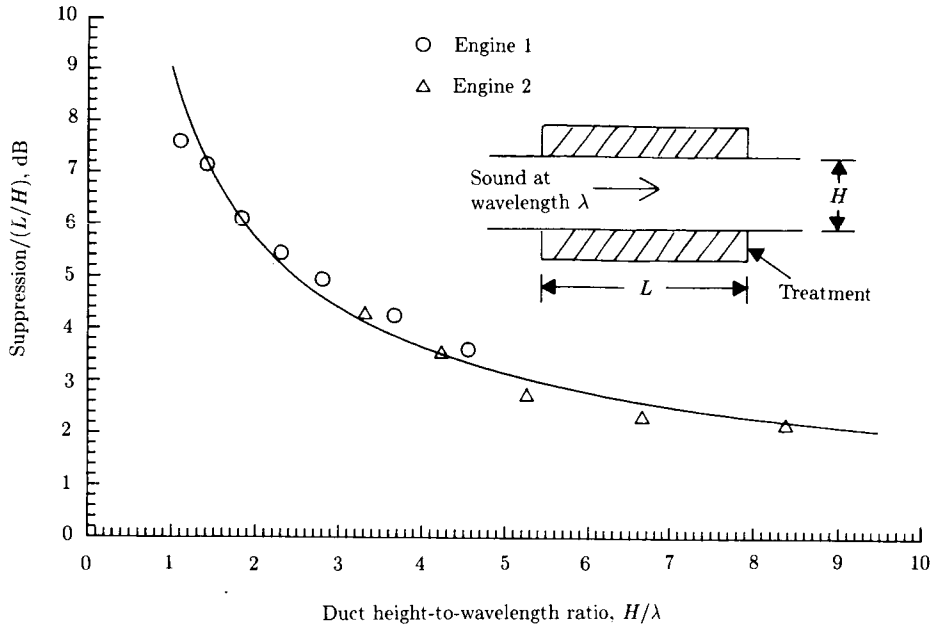

Figure 14. Ratio of maximum measured suppression to ratio of duct length to height for optimum impedance versus H/λ in fan exhaust ducts.

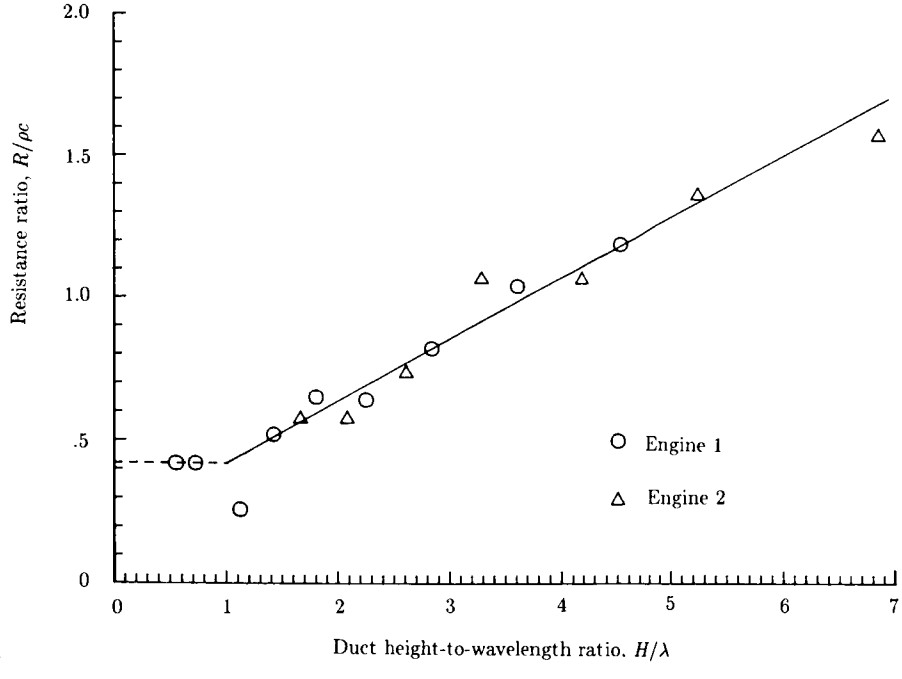

Figure 15. Optium resistance versus H/λ as measured in fan exhaust duct.

harmonic must be reduced, the single-layer SDOF panel construction is chosen. If noise at the BPF and both higher harmonics must be reduced, the dual-layer 2DOF panel construction is chosen. Broadband noise from turbomachinery is almost exclusively associated with the sideband frequencies on either side of the tone harmonics, and a design aimed at the tones is also effective for the broadband component.

Determination of Liner Design Parameters

The process to be used for selecting design values for the duct treatment acoustic impedance, both resistance and reactance, has been briefly discussed. These discussions are based on the concept of selecting the impedance parameters to achieve the largest reduction of sound within the duct itself. Actually, for turbofan engine noise, the effect of far-field directivity must also be taken into account.

When the propagating energy is comprised primarily of broadband noise in uncorrelated propagating modes (e.g., involving phase modulation by turbulent mixing layers or by unsteady inlet conditions), the angle of far-field radiation for each mode and the relative energy distribution among those modes become a primary concern. The emphasis on which modes to suppress depends on whether the inlet or the exhaust is being considered.

In the inlet, where the sound wave is propagating against the flow, the flow boundary layer tends to refract the waves toward the axis of the duct, decreasing their propagation angle and effectively converting them into lower order radial modes. In the exhaust duct, where the sound propagates with the flow, the boundary layer tends to refract waves toward the wall, increasing their propagation angle and effectively converting them into higher order modes. These phenomena affect the design philosophies for inlet and exhaust differently.

Inlet suppression: Modes that radiate from the inlet to the far field aft of about 50° from the inlet axis require more suppression than those radiating forward of that angle, because modes at higher propagation angles reach locations on the ground that receive the loudest noise levels during aircraft takeoff. Fortunately, the higher order modes, which are easier to suppress, have higher propagation angles in the duct and thus require more suppression than the lower order modes. Lower order modes and those modes refracted toward the inlet axis are less of a problem because of the long propagation distance to the ground associated with shallow radiation angles.

In reference 30, the correspondence is shown between the modal theory and the ray acoustics solution, as illustrated in figure 16. The figure shows the mean-square pressure measured on a far-field arc as a function of angle from the duct centerline. When these levels are transformed to a sideline plot (more representative of an aircraft flyover), the peak levels from the treated duct occur at 40° to 50°. As a first approximation, these angles correspond to the same angles within the duct; from simple acoustics and based on equation (3), the resistance to obtain optimum suppression at these angles should be

$$1.30 = (\sin\ 50°)^{-1} \leq R_{\text{opt}}/\rho c \leq (\sin\ 40°)^{-1} = 1.56$$

The optimum reactance should be near zero or slightly negative at the frequency of concern.

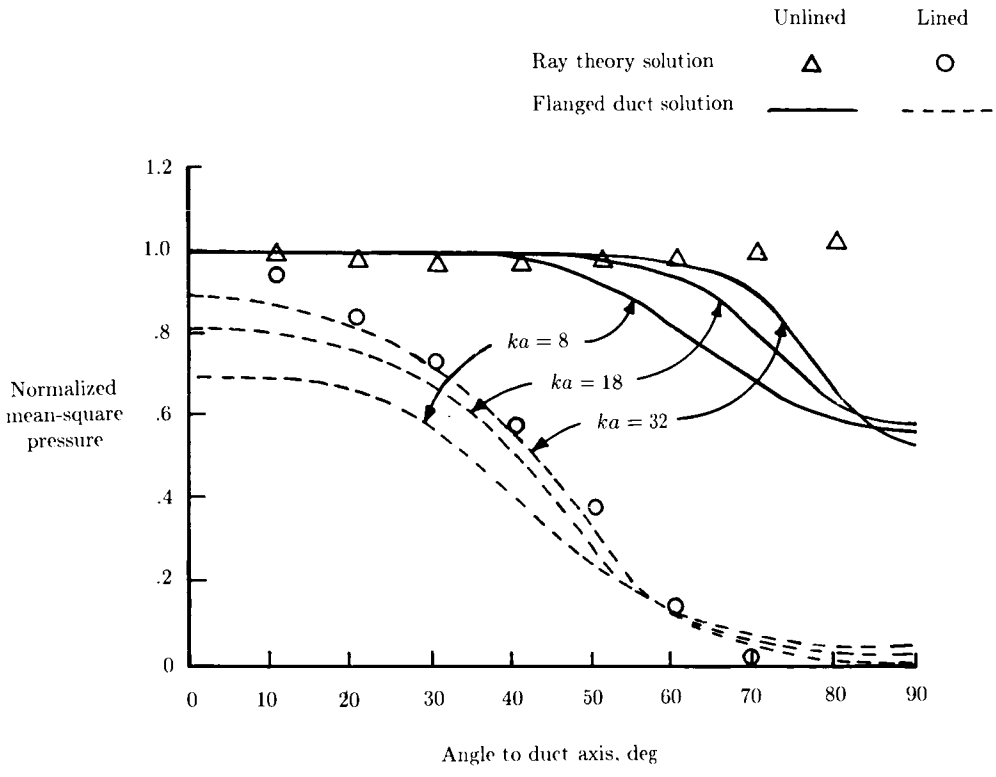

Figure 16. Comparison of ray theory and "flanged-duct" solutions for monopole sources in a cylindrical duct for various values of wave number times radius, ka. $L/a = 1$; $Z/\rho c = 0.8 + 0.4i$; mean-square pressure normalized for radius = $\lambda/4\pi\phi$. (From ref. 30. Copyright AIAA. Reprinted with permission.)

Exhaust suppression: In the exhaust, the higher order modes are refracted by the boundary layer to even higher propagation angles, increasing their attenuation rates. Therefore, the lower order modes present the greater problem, and rigorous analysis must consider modal propagation in nonuniform ducts with nonuniform flow and thus requires extensive computational capability.

The engineering solution is obtained by maximizing the suppression of noise within the duct, usually by testing a mock-up duct. This generally results in optimum suppression for the far-field radiated noise as well, excepting only very unusual problems with source mechanisms that happen to generate particularly high-amplitude higher order modes.

Total inlet or exhaust suppression: The treatment lengths needed to obtain the desired suppression are a consequence of the suppression rates achieved at the impedance values selected by the above process. To complicate this matter further, the overall suppression rates are not necessarily linear with treatment length, particularly for short treatment sections. Suppression rates may be quite high near

the beginning of a panel, as higher order modes rapidly attenuate, but gradually decrease as fewer modes contribute to the total energy. Thus, doubling the length of a short panel may not double its effectiveness.

Using Segmented Treatment Design

When two or more frequencies are so widely separated that they cannot be suppressed with either SDOF or 2DOF and when bulk absorber is not practical, use of segmented treatment in tandem is a practical approach. This might be the case in a turbine exhaust requiring suppression of both turbine tones and combustor broadband noise. Each segment of treatment must have sufficient length to achieve suppression at its design frequency. The primary deterrent to the use of segmented treatment is the normal limitation on overall duct length resulting from weight constraints.

Testing for Treatment Design and Performance Measurement

Experience has shown that treatment for fan and turbine exhaust ducts can be successfully developed by testing in the acoustic laboratory. Parametric experimental data can be obtained at a very small fraction of the cost associated with tests on an actual engine, and the results have been found to be reliable when applied to the engine, particularly if a representative sector of the exhaust duct geometry is faithfully simulated in the laboratory facility. In contrast, the inlet can be represented well enough only by testing either a scale model fan simulation or a full-scale engine.

Laboratory Testing of Exhaust Ducts

A typical test facility for the exhaust mode is shown in figure 17. The treatment is applied on the top and bottom of a small rectangular duct section, while the sides of the duct are left rigid, to simulate a circumferential segment of the exhaust annulus. The test section connects two large hard-walled plenums in which the sound levels are measured to determine the suppression provided by the treatment. Airflow is passed through the treated section to simulate engine conditions. The reverberant chambers provide a diffuse sound field, and a single microphone in each chamber is adequate for acoustic measurement; traversing the microphone assures that the data are not biased by a standing wave pattern. Suppression of a treatment design is measured by first measuring levels in the chambers with a hard-walled test section and then measuring the levels with the treatment in place. The difference in levels measured in the downstream chamber is the insertion loss of the treatment, giving rise to the term "insertion loss measurement method."

If the duct on the engine has significant curvature, disruptions of treatment, or change in duct height, higher order modes are continually regenerated. In this case, the facility test section should closely represent the duct curvature and any axial variation in duct height associated with it. Many commercial turbofan engine exhaust ducts fall into this category.

An alternative to the dual reverberation chamber method is to measure the sound pressure levels in the duct with traversing probes upstream and downstream of the

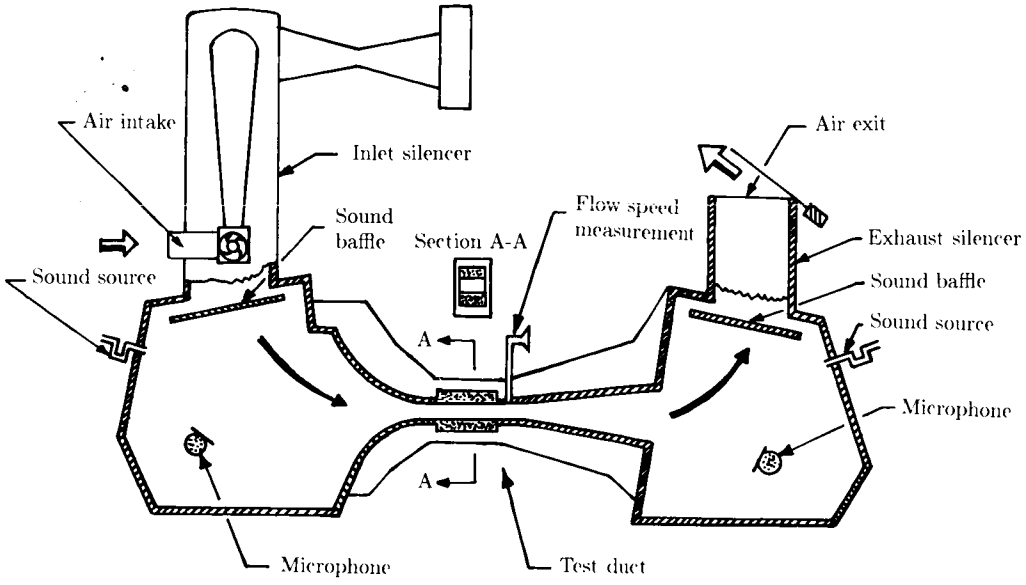

Figure 17. Typical test facility for development of exhaust duct treatment designs.

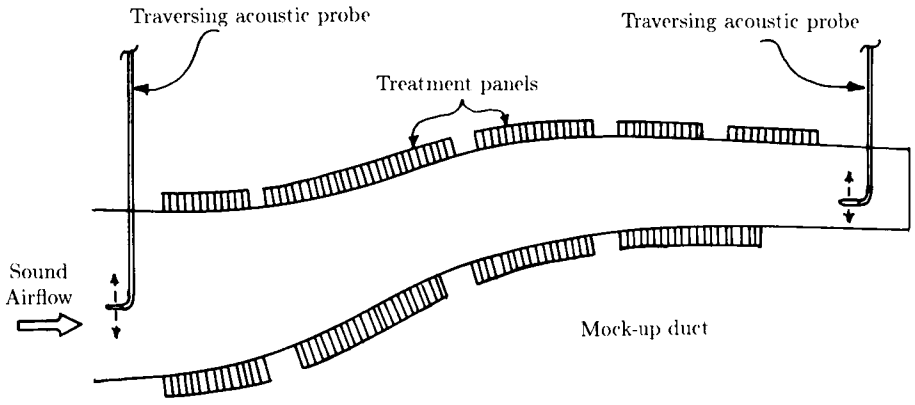

Figure 18. Typical test facility for development of treatment designs. Mock-up of curved exhaust duct.

treated section. The SPL measurement is integrated across the duct to provide estimates of the total power flux upstream and downstream of the treatment. This method is usually called the transmission loss method, as opposed to the insertion loss method described previously.

In the transmission loss method, it is assumed that backward-traveling waves have negligible effect on the measured SPL profile. Often, the transmission loss is measured in a hard-walled version of the duct at the desired flow velocity, and the transmission loss of the treated version is "corrected" by the hard-walled duct transmission loss. An example of a mock-up of such a duct is shown in figure 18.

Scale Model Test Facilities

For the inlet testing, the typical facility consists of a fan, usually a scale model, that can be motor driven, with the inlet noise radiating into an anechoic chamber. Far-field testing is essential for empirical development of inlet treatment because the wavelengths of the fan tones are small relative to the inlet diameter, and higher order modes dominate the propagating energy in the duct. In this case, actual inlet hardware, including the turbofan rotor and stator, must be closely simulated. An illustration of such a test facility is shown in figure 19. Far-field microphones are spaced along an arc to provide the essential information on the effect of the treatment on directivity.

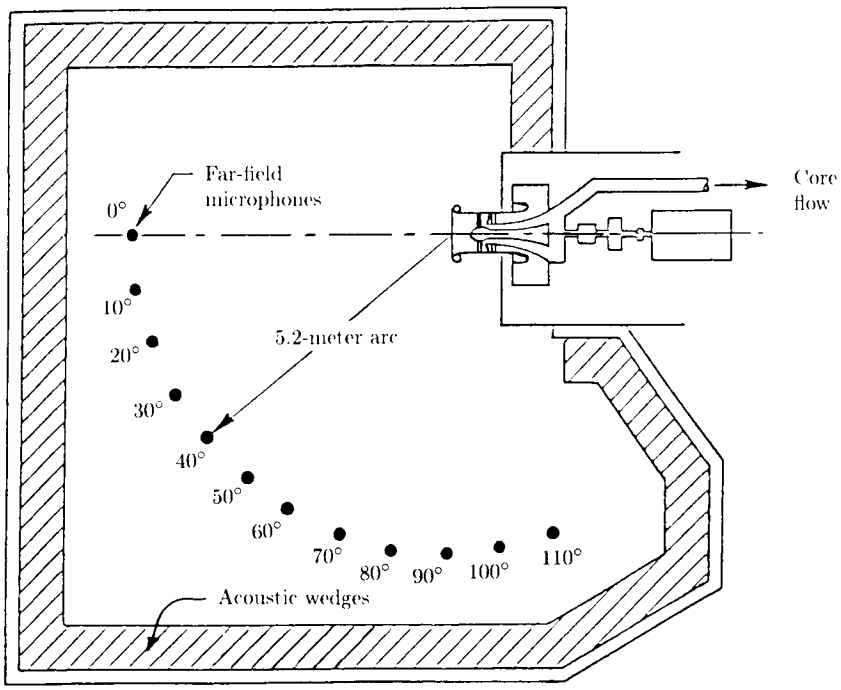

Figure 19. Typical scale model mounted in anechoic facility for development of treatment designs for inlet duct configuration.

When testing in a scale model facility in the exhaust mode, the fan inlet must have a suitably designed plenum to provide a smooth, distortion-free velocity profile into the fan, and the exhaust flow must be allowed to exit from the chamber in a way that provides good anechoic acoustics. Such an arrangement as tested in the NASA Quiet Clean Short-Haul Experimental Engine Program (ref. 31) is illustrated in figure 20.

Full-Scale Engine Tests

Full-scale engine tests for acoustic measurements are made in facilities such as in figure 21. The engine is mounted on a static test stand at the center of a far-field

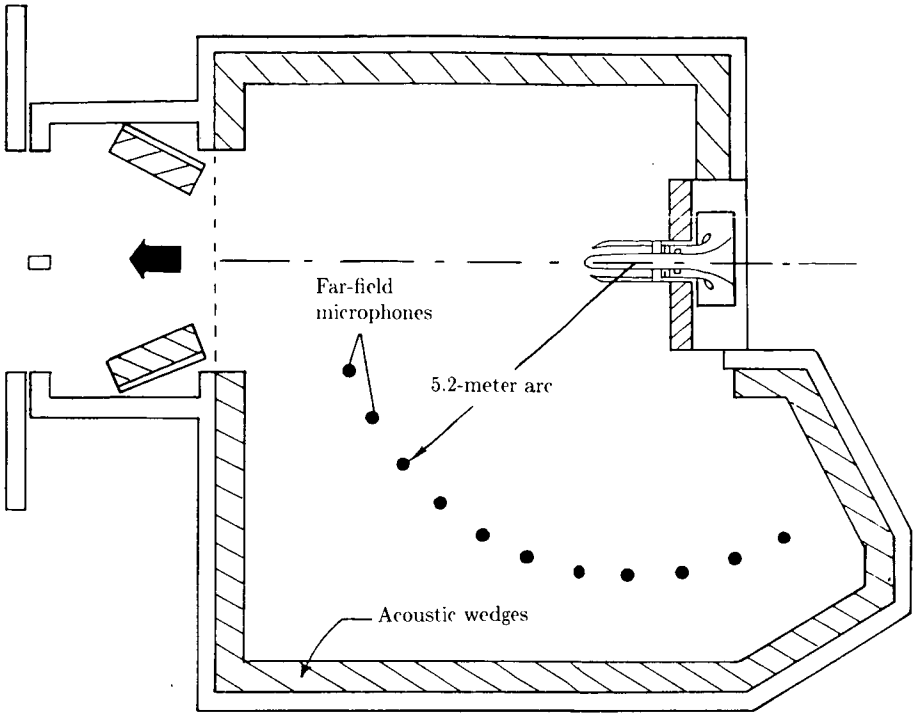

Figure 20. Typical scale model mounted in anechoic facility for development of treatment designs for exhaust duct configuration.

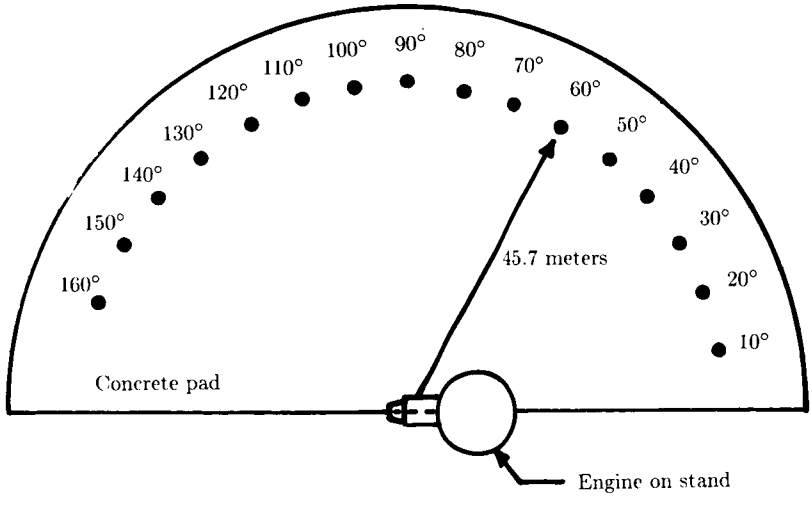

Figure 21. Test pad layout of full-scale engine test facility.

array of microphones. In the case shown, the microphone arc has a 45.7-meter radius, and a concrete pad between the engine and the microphones controls the conditions for the reflected wave.

One disadvantage of full-scale engine tests is the inability to separate the contributions from the various engine sources in the far-field measurement. The amount of suppression due to inlet treatment, for example, may be masked at certain radiation angles by the jet noise of the fan and core ducts. Several means of alleviating this problem have been proposed and investigated, including the use of barriers to shield inlet noise from exhaust noise and microphone arrays (or focusing mirrors) that focus on the noise being radiated from a particular region of space.

To obtain valid fan noise source levels representative of in-flight conditions, an "inlet turbulence control" structure, as shown in figure 22, is used. This eliminates some of the lower order modes generated by inflow distortion effects. When performing full-scale engine tests on the ground, one must choose between a bell-mouth-shaped inlet and a flight inlet. The bell-mouth inlet gives cleaner airflow with no forward motion of the engine, but changes the inlet geometry and therefore the directivity. The flight inlet gives poorer aerodynamic performance under static conditions, but has the proper geometry for duct termination radiation conditions.

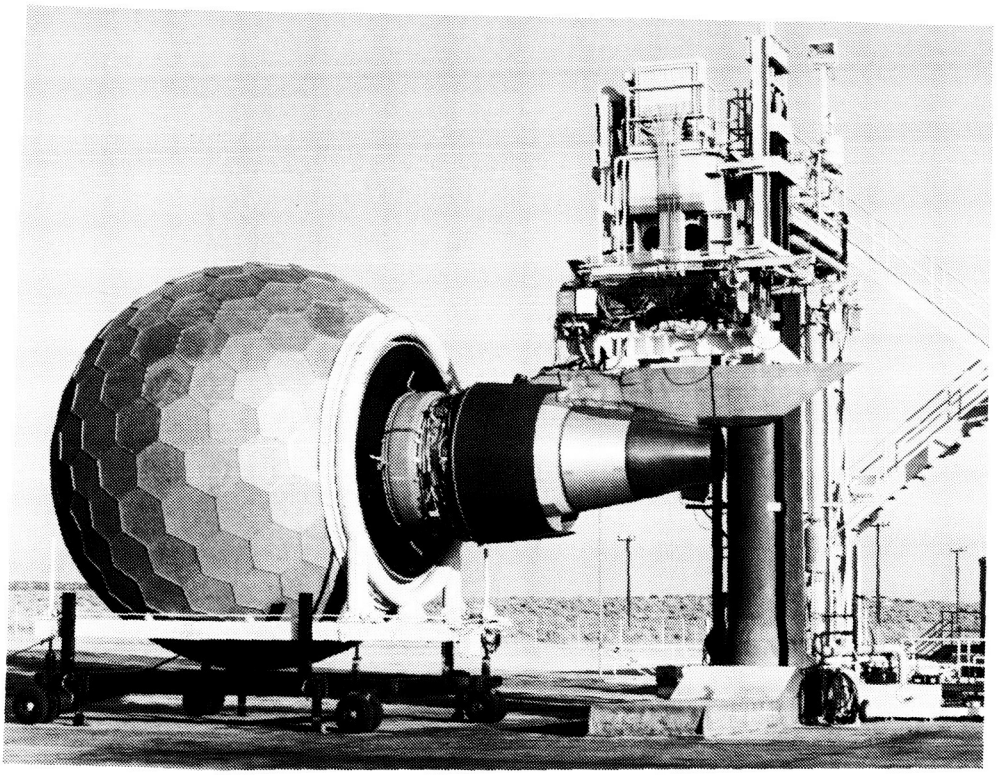

Figure 22. Full-scale engine test facility with turbulence control structure.

To measure the insertion loss of a treatment design in a full-scale inlet test, a prior test with a hard-walled inlet is necessary for comparison. Since full-scale engine

hardware and testing is so costly, this is often an unavailable luxury. Often, the most one might hope for is a comparison between the new design and the previously tested "standard" treatment design, so that the performance improvement might be determined.

Recommendations for Further Research

In the area of acoustic treatment impedance models, it has been suggested that a useful area of research might be the improvement of the impedance model for bulk absorber. Development of more practical and convenient methods to measure treatment panel impedance would be helpful.

Generally, further advancement in duct treatment design methods awaits improvements in theoretical prediction methods, either for duct propagation or turbomachinery source modal content. A useful area of innovation would be the development of more practical and efficient duct propagation prediction computer codes. Further work is needed in those areas where duct acoustics departs from ideal, axisymmetric conditions, such as ducts that are nonaxisymmetric or vary in cross-sectional area along the length of the duct. Propagation in nonuniform flow and the effects of boundary layers are important areas of research. Little research has been done into the effects of high sound pressure levels on propagation, a problem in nonlinear acoustics.

Despite the strong dependence on empirical or semiempirical methods, acoustic treatment design can be considered to be in a fairly advanced state of development. Current treatment designs are able to meet noise reduction certification requirements. Barring the possibility of a technology breakthrough, further increases in treatment effectiveness will provide marginal gains relative to development resources that must be applied. Impetus for this further research will come only if noise regulations change to the extent that new aircraft are no longer able to meet the certification requirements.

References

1. Beranek, Leo L., ed.: *Noise and Vibration Control.* McGraw-Hill Book Co., Inc., c.1971.
2. *Standard for Metric Practice.* ASTM Designation: E 380-85. Volume 14.02 of 1986 Annual Book of ASTM Standards, c.1986, pp. 339–380.
3. Groeneweg, John F.: Current Understanding of Helmholtz Resonator Arrays as Duct Boundary Conditions. *Basic Aerodynamic Noise Research,* Ira R. Schwartz, ed., NASA SP-207, 1969, pp. 357–368.
4. Kinsler, Lawrence E.; and Frey, Austin R.: *Fundamentals of Acoustics,* Second ed. John Wiley & Sons, Inc., c.1962.
5. Morse, Philip M.; and Ingard, K. Uno: *Theoretical Acoustics.* McGraw-Hill Book Co., Inc., c.1968.
6. Cremer, L.: *Theory of Attenuation of Airborne Sound in Rectangular Ducts With Absorbing Material on Their Inner Walls and the Resulting Maximum Attenuation.* BLL-NEL-TT-2590-(6075.461), British Library Lending Div., Boston Spa (England), 1973.
7. Zorumski, William E.; and Tester, Brian J.: *Prediction of the Acoustic Impedance of Duct Liners.* NASA TM X-73951, 1976.
8. Delany, M. E.; and Bazley, E. N.: Acoustical Properties of Fibrous Absorbent Materials. *Appl. Acoust.,* vol. 3, no. 2, Apr. 1970, pp. 105–116.
9. Hersh, A. S.; and Walker, B.: Acoustic Behavior of Fibrous Bulk Materials. AIAA-80-0986, June 1980.
10. Cole, Fred W.: Graphic Models for Acoustic Flow Resistance. Michigan Dynamics/AMBAC paper presented at the American Society for Metals 1969 Southern Metals Conference, Apr. 1969. (Available as Tech. Note MDD 503.)

11. Motsinger, R. E.; Syed, A. A.; and Manley, M. B.: The Measurement of the Steady Flow Resistance of Porous Materials. AIAA-83-0779, Apr. 1983.
12. Ingard, Uno: On the Theory and Design of Acoustic Resonators. *J. Acoust. Soc. America,* vol. 25, no. 6, Nov. 1953, pp. 1037–1061.
13. Kooi, J. W.; and Sarin, S. L.: An Experimental Study of the Acoustic Impedance of Helmholtz Resonator Arrays Under a Turbulent Boundary Layer. AIAA-81-1998, Oct. 1981.
14. Zandbergen, T.: On the Practical Use of a Three-Microphone Technique for In-Situ Acoustic Impedance Measurements on Double Layer Flow Duct Liners. AIAA-81-2000, Oct. 1981.
15. Rice, Edward J.: *A Theoretical Study of the Acoustic Impedance of Orifices in the Presence of a Steady Grazing Flow.* NASA TM X-71903, [1976].
16. Rice, Edward J.: *A Model for the Acoustic Impedance of a Perforated Plate Liner With Multiple Frequency Excitation.* NASA TM X-67950, 1971.
17. Rice, Edward J.: A Model for the Pressure Excitation Spectrum and Acoustic Impedance of Sound Absorbers in the Presence of Grazing Flow. AIAA Paper No. 73-995, Oct. 1973.
18. Bauer, A. B.; and Chapkis, R. L.: Noise Generated by Boundary-Layer Interaction With Perforated Acoustic Liners. *J. Aircr.,* vol. 14, no. 2, Feb. 1977, pp. 157–160.
19. Hersh, A. S.; and Walker, B.: The Acoustic Behavior of Helmholtz Resonators Exposed to High Speed Grazing Flows. AIAA Paper 76-536, July 1976.
20. Rice, Edward J.: *A Model for the Acoustic Impedance of Linear Suppressor Materials Bonded on Perforated Plate.* NASA TM-82716, 1981. (Available as AIAA-81-1999.)
21. Mechel, F.; Mertens, P.; and Schilz, W.: *Research on Sound Propagation in Sound-Absorbent Ducts With Superimposed Air Streams, Volumes I–IV.* AMRL-TDR-62-140, U.S. Air Force, 1962.
22. *Standard Test Method for Airflow Resistance of Acoustical Materials.* ASTM Designation: C 522-80. Volume 04.06 of 1986 Annual Book of ASTM Standards, c.1986, pp. 220–225.
23. *Standard Method of Test for Impedance and Absorption of Acoustical Materials by the Tube Method.* ASTM Designation: C 384-58. Part 14 of 1970 Annual Book of ASTM Standards, 1970, pp. 126–138.
24. Lippert, W. K. R.: The Practical Representation of Standing Waves in an Acoustic Impedance Tube. *Acustica,* vol. 3, no. 3, 1953, pp. 153–160.
25. Seybert, A. F.; and Ross, D. F.: Experimental Determination of Acoustic Properties Using a Two-Microphone Random-Excitation Technique. *J. Acoust. Soc. America,* vol. 61, no. 5, May 1977, pp. 1362–1370.
26. Fahy, F. J.: Rapid Method for the Measurement of Sample Acoustic Impedance in a Standing Wave Tube. *J. Sound & Vib.,* vol. 97, no. 1, Nov. 8, 1984, pp. 168–170.
27. Seybert, A. F.; and Parrott, T. L.: *Impedance Measurement Using a Two-Microphone, Random-Excitation Method.* NASA TM-78785, 1978.
28. Dean, P. D.: An In Situ Method of Wall Acoustic Impedance Measurement in Flow Ducts. *J. Sound & Vib.,* vol. 34, no. 1, May 8, 1974, pp. 97–130.
29. Rice, E. J.; and Sawdy, D. T.: *A Theoretical Approach to Sound Propagation and Radiation for Ducts With Suppressors.* NASA TM-82612, 1981.
30. Boyd, W. K.; Kempton, A. J.; and Morfey, C. L.: Ray-Theory Predictions of the Noise Radiated From Aeroengine Ducts. AIAA-84-2332, Oct. 1984.
31. Stimpert, D. L.; and McFalls, R. A.: *Demonstration of Short-Haul Aircraft Aft Noise Reduction Techniques on a Twenty Inch (50.8 cm) Diameter Fan.* NASA CR-134849, 1975.

15 Jet Noise Suppression

Lead authors

P. R. Gliebe
General Electric Co.
Cincinnati, Ohio

J. F. Brausch
General Electric Co.
Cincinnati, Ohio

R. K. Majjigi
General Electric Co.
Cincinnati, Ohio

R. Lee
General Electric Co.
Cincinnati, Ohio

Introduction

Jet noise suppression has been a technical challenge to the aeronautical engineering community since the introduction of the first-generation turbojet engines nearly 40 years ago. Extensive theoretical and experimental efforts have been expended in the United States and other countries toward solving this problem. The advent of the supersonic transport (SST, i.e., the British-French Concorde) in the late sixties and early seventies sparked a renewed interest in jet noise, particularly supersonic jet noise. Recently, interest in a high-speed civil transport (HSCT) has increased in the United States because of a projected increase in business activity between the United States and the Pacific rim countries in the nineties and beyond. Such an HSCT has to be environmentally acceptable (in terms of noise and pollution) to be a viable candidate. Significant advancements in high-velocity-jet noise reduction have been made since the introduction of the Concorde into the commercial airline service. This chapter briefly discusses the theoretical concepts of jet noise generation and suppression by utilizing a unified aerodynamic and acoustic analysis and enumerating the various jet noise suppression concepts experimentally demonstrated. It also explains the underlying physical mechanisms, so that the knowledge acquired in the past may be utilized for solving the current or future problems of jet noise suppression.

Theoretical Concepts of Jet Noise Generation and Suppression

During the past 15 years, considerable progress has been made in achieving an understanding of the noise produced by high-velocity jets. This progress is a direct

result of careful and accurate jet noise parametric testing and new theoretical developments (e.g., refs. 1 to 8). From these test results and theoretical developments, a unified theoretical model of jet noise generation and suppression has evolved, and this model has been substantiated with an extensive set of experimental data. This unified jet noise generation and suppression model is summarized in this section. Further details of the theory and the resulting prediction model can be found in references 9 to 12.

The development of the unified jet noise generation and suppression model is based on two primary assumptions: (1) the dominant noise generation mechanisms are the random momentum fluctuations of the small-scale turbulent structure in the mixing regions of the jet plume, and (2) the propagation of this noise to the far-field observer is altered significantly by the surrounding jet flow in which the turbulent eddies are embedded and convecting. This second assumption is often referred to as acoustic–mean-flow interaction. Thus, the proposed model is one in which the jet produces an intrinsic noise intensity spectrum directly relatable to the statistical aerodynamic properties of the jet (i.e., mean velocity and density distributions and local turbulent structure properties such as length scale and intensity), and this intrinsic (or "source") spectrum is modified by the acoustic–mean-flow interaction characteristics of the jet plume itself.

For jets operating at supercritical pressure ratios, one additional noise generation mechanism needs to be included in the unified theory, that is, shock-cell–turbulence interaction, commonly called shock-associated noise. This mechanism plays an important role in jet noise radiation in the forward arc portion of the directivity pattern.

The theoretical prediction method which developed from this unified theory follows the sequence of the following four basic steps:

1. Prediction of the aerodynamic characteristics (mean velocity, density, and turbulence structure properties)
2. Evaluation of the turbulent-mixing source noise spectrum with the flow properties from step 1 and the Lighthill-Ribner theory (ref. 7)
3. Construction of the far-field sound spectrum at various observer positions from the results of steps 1 and 2, with the source convection and acoustic–mean-flow interaction accounted for through use of Lilley's equation (ref. 6)
4. Computation of the shock-cell noise spectrum from the results of step 1 and the theoretical concepts in reference 13 and addition of these results to the mixing-noise spectra obtained in step 3

Jet Plume Aerodynamics

As discussed above, a prediction of the jet plume aerodynamics is required to provide the strength of the noise sources. The method selected is an extension of Reichardt's theory (ref. 14), which basically synthesizes the complex flows from nozzles of arbitrary geometry by superposition of a suitable distribution of elemental round jet flows.

Reichardt's theory is a semiempirical one, based on extensive experimental observations that the axial momentum flux profiles are bell shaped or Gaussian in the fully developed similarity region (far downstream of the exit plan) of a jet.

From these observations a hypothesis for the relation between axial and transverse momentum flux was formulated, and this hypothesis yields a governing equation for the axial momentum flux. For the similarity region of a circular jet with nozzle area A_j and exit velocity V_j, the governing equation and solution are as follows:

$$\frac{\partial}{\partial x}\langle \rho u^2 \rangle = \frac{\lambda(x)}{r}\frac{\partial}{\partial r}\left(r\frac{\partial}{\partial r}\langle \rho u^2 \rangle\right) \tag{1}$$

$$\langle \rho u^2 \rangle = \rho_j V_j^2 \frac{A_j}{\pi b_m^2} \exp[-(r/b_m)^2] \tag{2}$$

where

$$\lambda(x) = \tfrac{1}{2} b_m \, db_m/dx \tag{3}$$

u is the axial velocity component, ρ is density, the angle brackets $\langle\ \rangle$ represent the statistical time average, and $b_m(x)$ is the width of the axial momentum mixing region, taken to be proportional to the axial distance from the nozzle exit plane:

$$b_m(x) = C_m x \tag{4}$$

The jet spreading rate C_m becomes a key parameter in the theory and is determined experimentally. The coordinate system is shown in figure 1.

Because equation (1) is linear, the summation of elemental solutions (eq. (2)) is also a solution. This unique feature of Reichardt's theory allows the construction of quite complex jet flows with relatively simple mathematics. Although more rigorous (but containing just as much empiricism, albeit in different forms) theories are available for simple jets (circular and planar), there is no other technique available which offers the capability for modeling jet flows typical of aircraft engine suppressor nozzles such as multitube, lobe, and chute nozzles.

Consider a distribution of elemental jets issuing parallel to the X-axis. The jet exit areas lie in the $x = 0$ plane. Each elemental jet has an exit area $A_j = \sigma \, d\sigma \, d\alpha$ located at $(\sigma, \alpha, 0)$, as shown in figure 1. The axial momentum flux at a downstream point (r, θ, x) due to the elemental jet exhausting at $(\sigma, \alpha, 0)$ is given by (from eq. (2))

$$d\langle \rho u^2 \rangle = \rho_j V_j^2 (\sigma \, d\sigma \, d\alpha/\pi b_m^2) \exp[-(\xi/b_m)^2] \tag{5}$$

where

$$\xi^2 = r^2 + \sigma^2 - 2r\sigma\cos(\theta - \alpha)$$

Integrating equation (5) results in the following solution:

$$\langle \rho u^2 \rangle(r, \theta, x) = \frac{1}{\pi b_m^2} \int\int (\rho_j V_j^2) \exp[-(\xi/b_m)^2] \sigma \, d\sigma \, d\alpha \tag{6}$$

From the distribution of $\rho_j V_j^2$ in the exit plane, the local value of $\langle \rho u^2 \rangle$ at any point (r, θ, x) can be found from equation (6) by standard numerical integration. If we assume that the jet plume stagnation enthalpy flux H diffuses in the same manner as axial momentum, an analogous expression for stagnation enthalpy flux $\langle \rho u H \rangle$ can

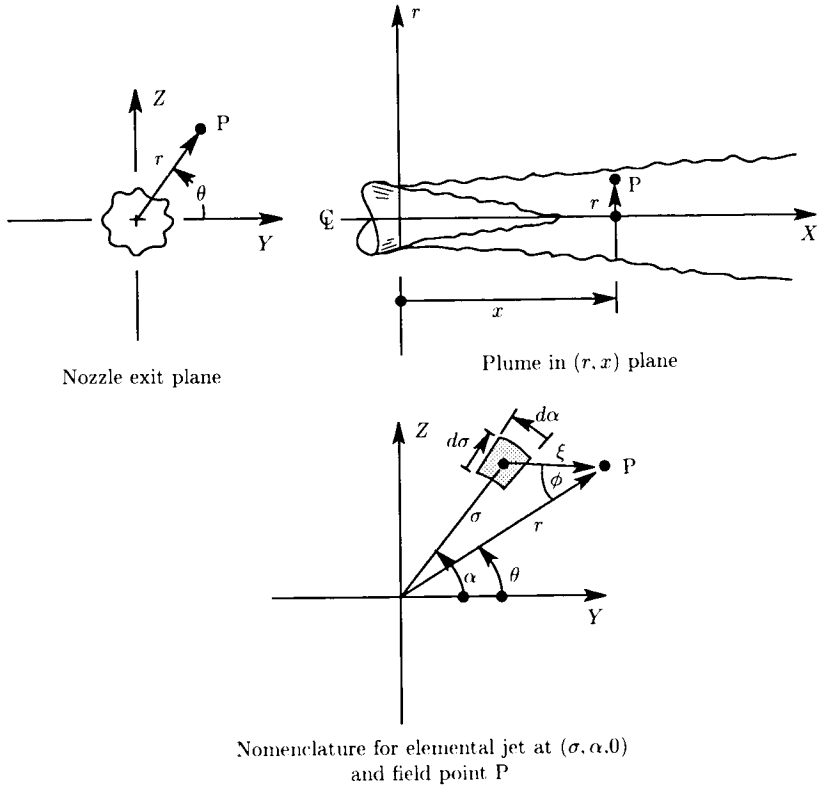

Figure 1. Jet flow coordinate system and nomenclature. (From ref. 10.)

be derived:

$$\langle \rho u H \rangle (r, \theta, x) = \frac{1}{\pi b_h^2} \int \int (\rho_j V_j H_j) \exp[-(\xi/b_h)^2] \sigma \, d\sigma \, d\alpha \tag{7}$$

where b_h is the width of the thermal shear layer, taken to be proportional to x:

$$b_h = C_h x \tag{8}$$

for constant C_h. The stagnation enthalpy is defined as $H = c_p T_j + (u^2/2) - c_p T_o$ (where c_p is specific heat at constant pressure, T_j is jet temperature, and T_o is ambient temperature), and the thermal layer spreading rate C_h also must be obtained experimentally. If we assume that the jet mixing occurs at constant static pressure equal to the ambient value, the solutions for $\langle \rho u^2 \rangle$ and $\langle \rho u H \rangle$ given by equations (6) and (7) are sufficient to determine the distributions of mean axial velocity u and temperature T_j throughout the jet plume.

In addition to the jet plume mean-flow properties, the turbulent Reynolds stress, which is assumed to be proportional to the transverse momentum flux, also can be obtained. Reichardt's hypothesis (from which eq. (1) evolved) states that the transverse momentum flux is proportional to the transverse gradient of the axial

momentum flux, the proportionality factor being $\lambda(x)$. For a simple circular jet (eqs. (2) to (4)), the Reynolds stress τ is given by

$$\tau = -\langle \rho u' v' \rangle \approx -\lambda \frac{\partial}{\partial r} \langle \rho u^2 \rangle = C_m \rho_j V_j^2 \frac{A_j}{\pi b_m^2} \frac{r}{b_m} \exp[-(r/b_m)^2] \tag{9}$$

where u' and v' are the axial and radial components of turbulent fluctuation velocity. For an elemental jet exhausting at $(\sigma, \alpha, 0)$ the shear stress at (r, θ, x) lies along a line connecting $(\sigma, \alpha, 0)$ and the projection of (r, θ, x) onto the $x = 0$ plane. This vector is at an angle ϕ to the coordinate direction r (fig. 1). The radial component of the shear stress $d\tau$ at point (r, θ, x) resulting from an elemental jet exhausting at $(\sigma, \alpha, 0)$ is then $d\tau_r = d\tau \cos\phi$. Similarly, the azimuthal component is $d\tau_\theta = d\tau \sin\phi$. If we perform the same summation and limiting process over all elemental jets, the total shear stress at (r, θ, x) is

$$\tau = (\tau_r^2 + \tau_\theta^2)^{1/2} \tag{10}$$

where

$$\tau_r(r, \theta, x) = \frac{C_m}{\pi b_m^2} \int\int \rho_j V_j^2 (\xi/b_m) \exp[-(\xi/b_m)^2] (\cos\phi) \sigma \, d\sigma \, d\alpha \tag{11}$$

The azimuthal shear stress $\tau_\theta(r, \theta, x)$ is given by a similar expression with $\cos\phi$ replaced by $\sin\phi$. The distance is again given by the expression from equation (5), and the angle ϕ is given by

$$\xi \cos\phi = r - \sigma \cos(\theta - \alpha) \tag{12}$$

Equations (5) to (12) provide the basic expressions for computation of the jet plume flow parameters T_j, u, and τ for a nozzle of arbitrary exit cross section and exit distribution of velocity and temperature. For axisymmetric nozzles, $\tau = \tau_r$ and $\tau_\theta = 0$. The basic limiting assumptions underlying this aerodynamic model for the jet plume characteristics are (1) the jet plume mixing occurs at constant static pressure, equal to the ambient value, and (2) the flow is primarily axial, with all nozzle exit elements in the same plane ($x = 0$).

Intrinsic Source Intensity Mixing-Noise Spectrum

The aerodynamic characteristics of the jet plume provide the information required to evaluate the acoustic intensity spectrum in the absence of convection and acoustic–mean-flow interaction effects. This represents the sound spectrum which would be heard if the turbulent eddies generating the sound had negligible convection speed relative to the observer and if the velocity and temperature gradients encountered by the sound as it propagated through the jet plume itself had no effect on the sound radiation. As is demonstrated, these effects are indeed powerful for high-velocity jets. The postulation herein is that the basic source strength spectrum can be developed, and the convection and acoustic–mean-flow interaction effects can then be added to this basic (intrinsic) sound spectrum.

The jet plume is first subdivided into elemental "eddy" volumes, each having its own source strength, spectrum, and flow shrouding, as illustrated in figure 2. The

jet noise generation is represented by a collection of convecting and uncorrelated quadrupole sources, each radiating noise with an intensity spectrum directly related to the local flow properties. The net radiation from each eddy is a function of the flow environment of that eddy. Each eddy volume contains a mix of quadrupoles of various orientations. By employing a model of homogeneous, isotropic turbulence in the moving-eddy reference frame and taking the azimuthal average of the resulting sound field, Ribner found that a weighted combination of the various quadrupole types contributes to the net far-field radiation (ref. 7). The amplitude of these quadrupole types is of the form

$$dI(\omega) = \frac{\rho_o l^3}{c_o^5 R^2}(u')^4 \omega^4 H(\mu)\, dV \tag{13}$$

where $dI(\omega)$ is the acoustic intensity per elemental jet volume dV, ρ_o is the ambient density, R is the source-to-observer distance, c_o is the ambient speed of sound, u' is the local turbulence intensity, $H(\mu)$ is the Fourier transform of the moving-frame space-time cross correlation of u', and μ is the ratio of emitted frequency ω to characteristic frequency ω_o. Equation (13) is used to calculate the mixing-noise amplitude and frequency content for each volume element in the jet. The characteristic turbulence frequency and length scale for each eddy volume are determined from the local mean-flow velocity, temperature, and shear stress with the empirically derived similarity relations of reference 15:

$$\left.\begin{aligned} \omega_o &\approx \partial U/\partial r \\ l &\approx u'/\omega_o \end{aligned}\right\} \tag{14}$$

where l is the characteristic turbulent eddy size and the turbulence intensity is obtained from the shear stress as follows:

$$u' \approx \sqrt{\tau/\rho}$$

Acoustic–Mean-Flow Interaction Model

The equation which describes the propagation of sound emitted by the turbulence in a jet was developed in reference 6 and is as follows:

$$\frac{1}{c^2} D_*^3 p - D_*(\Delta p)\frac{d}{dr}(\log c^2) D_* \left(\frac{\partial p}{\partial r}\right) + 2\frac{\partial u}{\partial r}\frac{\partial^2 p}{\partial \times \partial r} = S \tag{15}$$

where

$$D_* = \frac{\partial}{\partial t} + U\frac{\partial}{\partial x} \qquad \text{and} \qquad S = \rho D_* \left[\nabla \cdot \nabla \cdot (u' \cdot u')\right] \tag{16}$$

In equations (15) and (16), $U = U(r), c = c(r)$, and $\rho = \rho(r)$ are the azimuthally averaged mean-flow axial jet velocity, speed of sound, and density, respectively. The symbol Δ is the Laplacian operator, t is time, and u' is essentially the turbulent velocity fluctuation. Roughly speaking, S is the noise source strength which drives

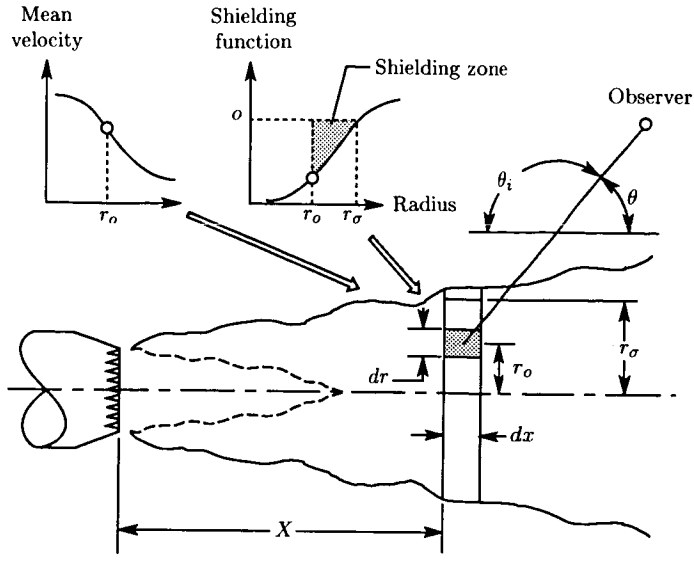

Figure 2. Generalized volume element model. (From ref. 12.)

the acoustic pressure fluctuations p. Equation (15) is a third-order wave equation for the variable p, and this equation explicitly displays the influence of mean velocity $U(r)$ and temperature (through speed of sound $c(r)$) profiles on the propagation of noise.

To solve equation (15), the profiles for $U(r), c(r)$, $\rho(r)$, and $S(r)$ must first be prescribed. These are provided by the aerodynamics calculation described in the previous section. The Green's function solution for equation (15), when convoluted with the source term S, provides the solution to Lilley's equation. From the Green's function, solutions for higher order singularities (dipoles and quadrupoles) can be obtained by differentiating the source solution with respect to source coordinates. The right-hand side of equation (15), $S(r)$, represents a mix of quadrupoles of various orientations, as discussed in the previous section. The various quadrupole contributions are added in the manner developed in reference 7, but with each quadrupole type having its own solution form representing the combined effects of convection and acoustic–mean-flow interaction.

The combined convection and interaction effects can be thought of as a multiplier of the basic source intensity spectrum given by equation (13), and this multiplier is a function of the local mean-flow properties and their radial gradients. It includes the effects of the following:

1. Convection—the effect of source motion relative to the observer, sometimes called the Doppler effect
2. Refraction—the alteration of the sound pressure and directivity as it propagates through a moving fluid with cross-stream gradients
3. Shielding—the decay of the sound as it propagates through portions of the mean-flow gradients where wave-like behavior gives way to exponential decay

Details of the acoustic–mean-flow interaction theoretical development can be found in reference 5. The details of the aerodynamic theory and source intensity spectrum model development can be found in references 9 and 14. The analytical model does take into account Mach wave radiation associated with eddies convecting at supersonic speeds (which, in turn, tends to amplify the noise levels in the region near the jet axis).

The above analytical model elements have been integrated into a unified computational procedure. The jet plume is subdivided into elemental eddy volumes (as previously mentioned), each having its own source strength, spectrum, and flow shrouding, as illustrated in figure 2. The simple closed-form acoustic pressure solutions, combined with the simple aerodynamics calculation method, permit rapid, economical computations of the entire jet plume aerodynamic and acoustic characteristics, including far-field spectra at all observer angles. The contributions from each elemental jet volume, in each frequency band, are simply added based on mean-square pressure. The shock-cell noise contribution is then computed separately and added to the mixing-noise contribution to yield the total far-field spectra.

Comparisons of Model Predictions With Experiment

Many comparisons of the predicted and measured far-field acoustic spectra of nozzles of various types have been carried out, and these results are reported in references 9 to 12. Typical examples of sound pressure level (SPL) spectra for a single-stream conical nozzle and overall sound pressure level (OASPL) for a dual-flow conventional bypass nozzle are shown in figures 3 and 4, respectively. These comparisons of prediction with experiment show that the unified aeroacoustic jet noise prediction model described above duplicates the characteristic behavior of these simple nozzles rather well. In particular, the spectrum shapes agree quite well and the trends of OASPL as a function of velocity ratio V_o/V_i and area ratio A_o/A_i predicted by the theory are consistent with the experimental results. Note that the magnitude and location of the noise minimum as a function of velocity ratio shown in figure 4 for the dual-flow coaxial jet is predicted quite well.

Comparisons of predicted noise characteristics with measured characteristics for an inverted-flow coannular nozzle are shown in figures 5 and 6 (taken from ref. 11). Note that the observed "double-peak" spectrum shape is predicted fairly well by the theory. Comparisons of predicted noise trends with measured trends for a 36-element multichute nozzle are shown in figures 7 and 8 (taken from ref. 12). The characteristic flat spectrum shape is well modeled, and the trend of noise dependence on chute area ratio (defined as annulus area divided by flow area) and jet velocity is also well predicted.

The comparison results shown in figures 3 to 8 provide reasonable verification that the unified theoretical model for predicting jet noise described herein has the necessary ingredients (i.e., the important physical mechanisms) for analyzing and diagnosing the mechanisms for controlling jet noise.

Noise Suppression Mechanisms

Conventional Bypass Versus Inverted-Flow Nozzles

Based on the reasonable successes achieved in predicting the aeroacoustic characteristics of a wide variety of nozzle types over a range of operating conditions (as

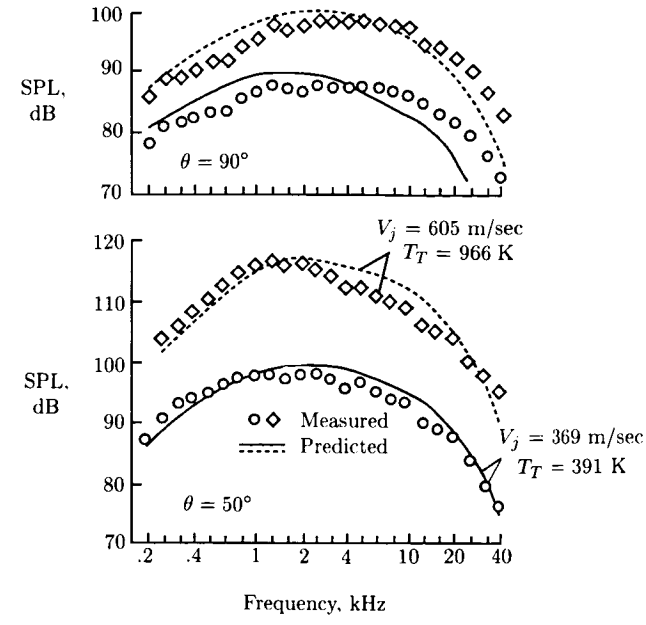

Figure 3. Conical nozzle predicted and measured SPL spectra. (From ref. 11.)

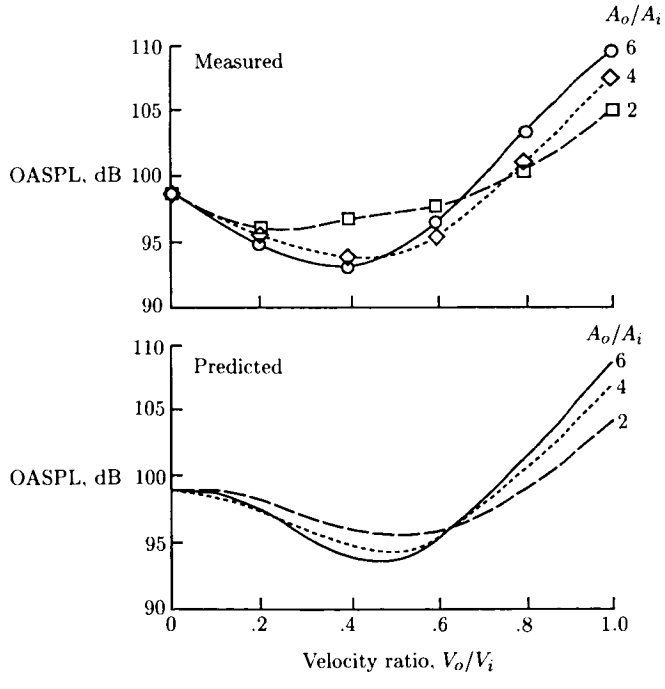

Figure 4. Influence of area ratio on conventional bypass jet OASPL. $\theta = 90°$; $V_i = 305$ m/sec; $T_{t,i} = 700$ K; $T_{T,o} = 300$ K. (From ref. 11.)

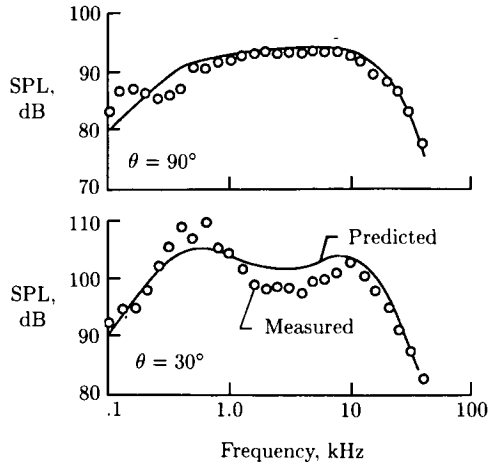

Figure 5. Measured and predicted SPL spectra for inverted-flow coannular nozzle with $A_o/A_i = 0.4; V_o/V_i = 1.5; V_i = 366$ m/sec; $V_o = 549$ m/sec; $T_{T,i} = 556$ K; $T_{T,o} = 667$ K; $R = 12.2$ m; $D_i = 11.8$ cm. (From ref. 11.)

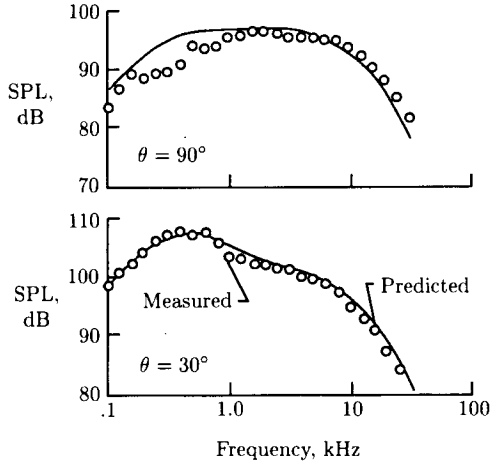

Figure 6. Measured and predicted SPL spectra for inverted-flow coannular nozzle with $A_o/A_i = 2.0; V_o/V_i = 1.5; V_i = 305$ m/sec; $V_o = 457$ m/sec; $T_{T,i} = 294$ K; $T_{T,o} = 556$ K; $R = 12.2$ m; $D_i = 11.8$ cm. (From ref. 11.)

summarized in the preceding section and detailed in refs. 9 to 12), it was deemed worthwhile to utilize the theory to analyze the noise suppression mechanisms of coannular nozzles. Of particular interest was how flow inversion (i.e., ducting the high-velocity hot stream to the outside) could provide noise reduction for dual-flow exhaust systems. Theoretical predictions were made of a conventional bypass and an inverted-flow coannular nozzle. The nozzles were sized to give the same thrust and equal primary (high-velocity) and secondary (low-velocity) flow areas. The two nozzles therefore had equivalent thrust, mass flow, primary and secondary stream

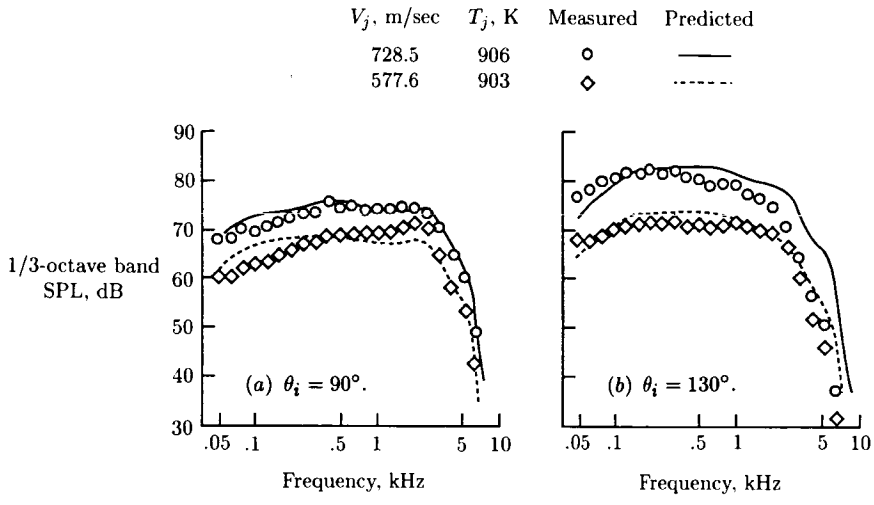

Figure 7. Predicted and measured SPL spectra for 36-chute turbojet suppressor nozzle with area ratio of 2.0. (From ref. 12.)

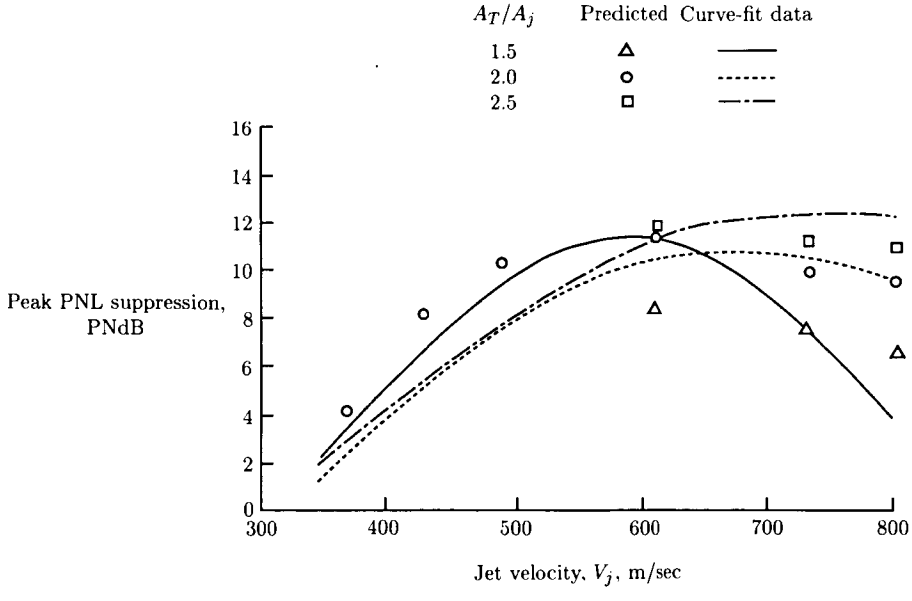

Figure 8. Predicted and measured effect of area ratio on peak PNL suppression for 36-chute turbojet suppressor nozzle. (From ref. 12.)

velocities, and temperatures; thus, the differences in noise should have been solely a function of jet plume profile development and mixing.

Aeroacoustic predictions were made for both a conventional bypass and an inverted-flow nozzle for velocity ratio $V_s/V_p = 0.7$ and area ratio $A_s/A_p = 1.0$, where subscripts p and s refer to primary and secondary streams. Figure 9 shows mean

axial velocity U profiles across the jet plume at several axial stations x/D_p along the plume. The normalized peak velocity at any axial station U_p versus downstream distance is presented in figure 10 for the two nozzle types. These results show that the flow inversion produces more rapid plume decay. Figure 11 shows axial turbulence velocity, a key ingredient in the mixing-noise source strength, at several axial stations along the plume. This figure shows the expected lower turbulence levels at small values of x/D_p for the conventional bypass jet and higher levels of turbulence at large x/D_p than the inverted-flow nozzle.

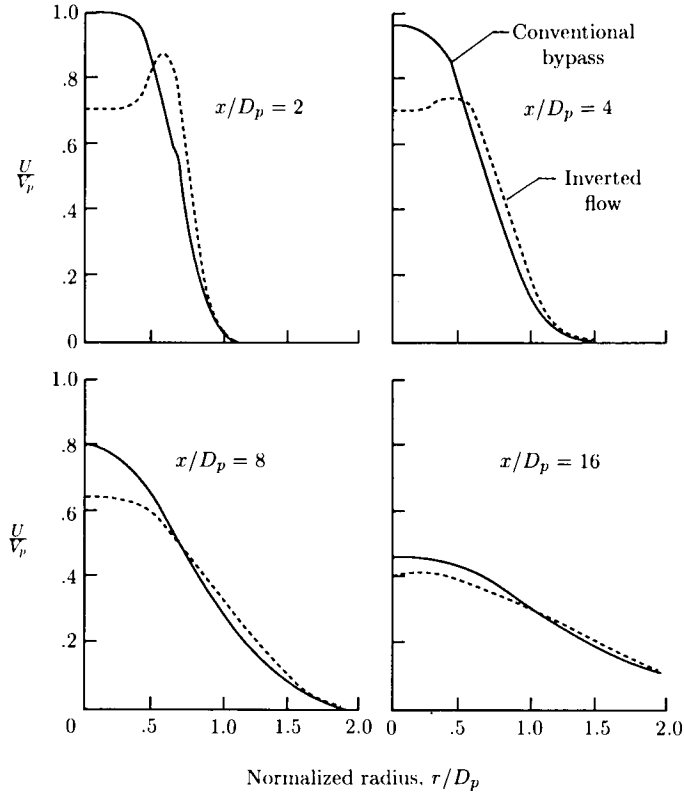

Figure 9. Inverted-flow and conventional bypass mixing mean velocity profiles. (From ref. 11.)

The corresponding far-field acoustic spectra are shown in figure 12. At $\theta = 90°$ (i.e., in the plane of the nozzle exit), the inverted-flow nozzle exhibits higher noise at high frequencies and lower noise at low frequencies than the conventional bypass nozzle. Since the high-frequency noise generally comes from regions close to the nozzle exit, the highest high-frequency noise correlates with the highest turbulence levels at small values of x/D_p shown in figure 11. Similarly, low-frequency noise is primarily from the fully developed regions far downstream, and the lowest low-frequency noise of the inverted-flow nozzle correlates with its lowest turbulence levels for large x/D_p.

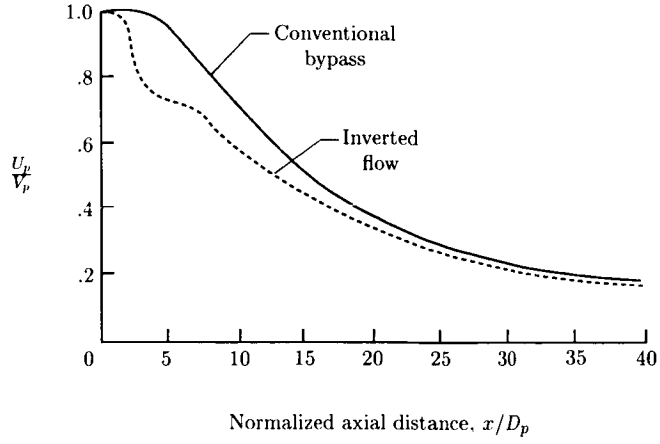

Figure 10. Inverted-flow and conventional bypass mixing peak velocity axial decay. (From ref. 11.)

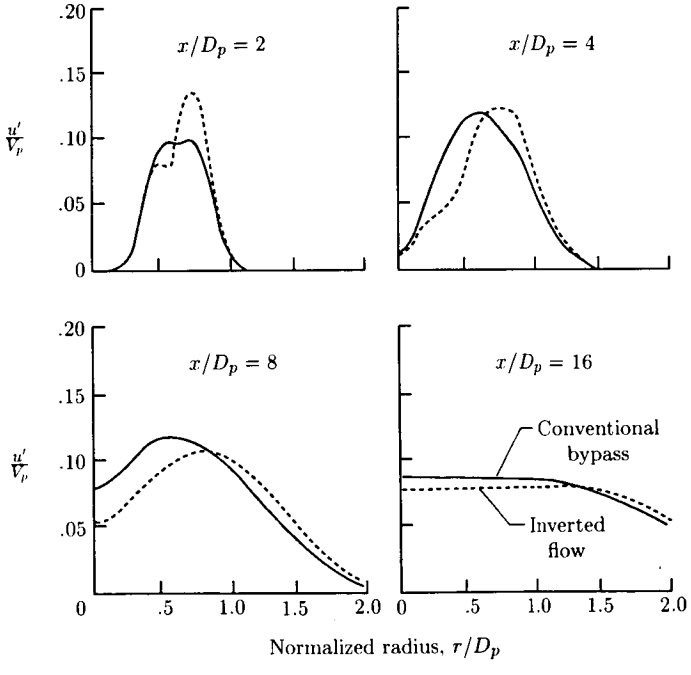

Figure 11. Inverted-flow and conventional bypass mixing turbulence intensity profiles. (From ref. 11.)

The results in figure 12 for $\theta = 50°$ (130° from the inlet axis), however, show the inverted-flow jet noise to be lower than that of the conventional bypass nozzle throughout the spectrum. This lower noise is primarily a result of reduced convective amplification, that is, lower eddy convection speeds. The eddy convection speed is proportional to the peak mean axial velocity, and the peak velocity curves shown in figure 10 imply that the inverted-flow jet exhibits lower convection speeds, and

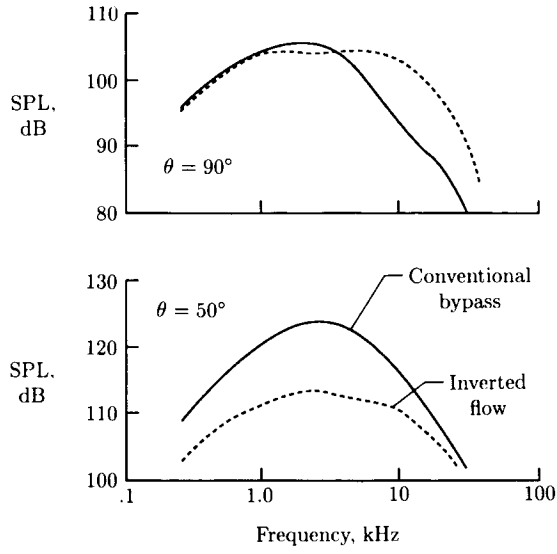

Figure 12. Inverted-flow and conventional bypass mixing SPL spectra. (From ref. 11.)

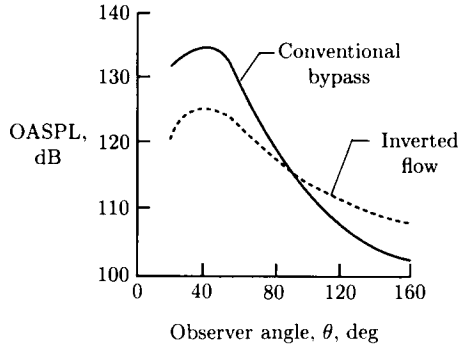

Figure 13. Inverted-flow and conventional bypass mixing OASPL directivity. (From ref. 11.)

therefore reduced convective amplification, than the conventional bypass nozzle. Figure 13 shows nozzle overall sound pressure level (OASPL) versus angle for the two nozzles. Note the shallower slope of the directivity curve for the inverted-flow nozzle, a result of reduced convective amplification.

To demonstrate the influence of flow shielding as a noise reduction mechanism, the above predictions were repeated with the shielding effects in the acoustic–mean-flow interaction model suppressed. These results are shown in figure 14 for $\theta = 30°$. First of all, flow shielding effect is less for the inverted-flow nozzle than for the conventional bypass nozzle, but the reduced convective amplification more than compensates for the loss. The main point to observe is that the shielding effect is substantial at angles

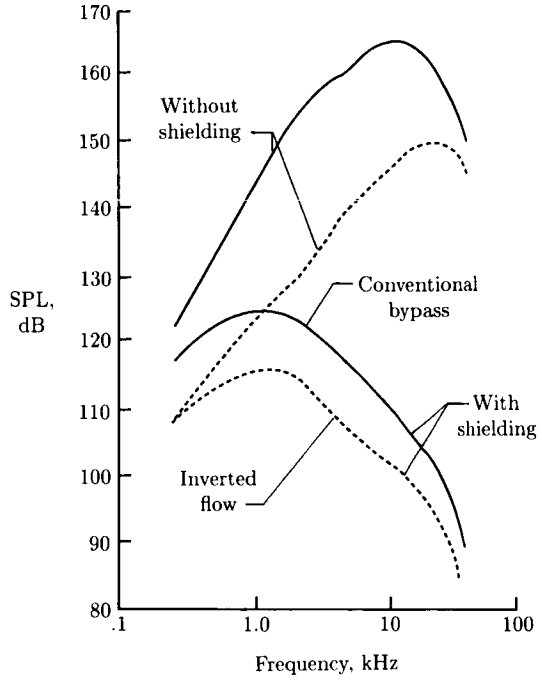

Figure 14. Influence of flow shielding on inverted-flow and conventional bypass nozzle SPL spectrum. $\theta = 30°$. (From ref. 11.)

close to the jet axis, being on the order of 30 to 40 dB at $\theta = 30°$ for these cases. The shielding effect also increases with increasing frequency, as figure 14 shows.

Multielement Nozzles

The theoretical concepts for jet noise generation and radiation discussed in the previous sections can be evaluated through use of the analytical model in selective modes. The objective is to identify the relative roles these mechanisms play in the generation and suppression of jet noise. Such a study was carried out with a multielement, 36-chute suppressor nozzle used as a representative case study (ref. 12). The basic jet noise mechanisms are as follows:

1. Turbulent-mixing-noise generation
2. Convective amplification
3. Fluid shielding
4. Shock-cell noise

It is of interest to evaluate how the individual mechanisms combine to yield the far-field result and, more importantly, how these mechanisms change due to the addition of a suppressor to a baseline nozzle.

A parametric study was performed to evaluate the relative contributions of the four mechanisms to the far-field noise for both a baseline conical nozzle and a typical high-suppression, multielement nozzle. A 36-chute turbojet suppressor with a ratio of total nozzle area A_T to flow area A_j of 2.0 was chosen for this study as representative

of a high-element-number, high-suppression (10 to 12 PNdB) exhaust system. A typical takeoff condition of $V_j = 732$ m/sec (2400 ft/sec) and $T_j = 906$ K (1630°R) was selected for evaluation. The exit area of both the baseline conical nozzle and the 36-chute suppressor nozzle was 0.218 m^2 (338 in^2). Noise characteristics were predicted for a 732-m (2400-ft) sideline distance.

The prediction computations were performed in the following four modes: (1) complete acoustic calculation; (2) as in (1), but with shock-cell noise omitted; (3) as in (2), but with fluid shielding omitted; and (4) as in (3), but with convective amplification omitted. (For the 36-chute suppressor, mode (1) was omitted since the ability to model shock-cell noise of multichute nozzles was not established at the time these computations were performed. However, Stone has evolved a semiempirical prediction method for shock-cell noise of multielement suppressor nozzles utilizing more recent data. (See ref. 16 for more details.) The difference in noise levels between modes (1) and (2) is a measure of the shock-cell noise contribution to the total jet noise signature. The difference in noise levels between modes (2) and (3) is a measure of the influence of fluid shielding on the jet noise. Finally, the difference in noise levels between modes (3) and (4) indicates the amount of convective amplification that is present in the jet.

The results of the above series of computations are summarized in figures 15 to 17. Figure 15 shows the perceived noise level (PNL) directivity patterns for the different prediction modes. Also shown for comparison are measured data from reference 12, which should be compared with mode (1) predictions (mode (2) for the 36-chute nozzle). Figures 16 and 17 show the corresponding spectrum shapes (1/3-octave SPL) at 50° and 130° relative to the inlet axis. The measured spectra are also shown for reference.

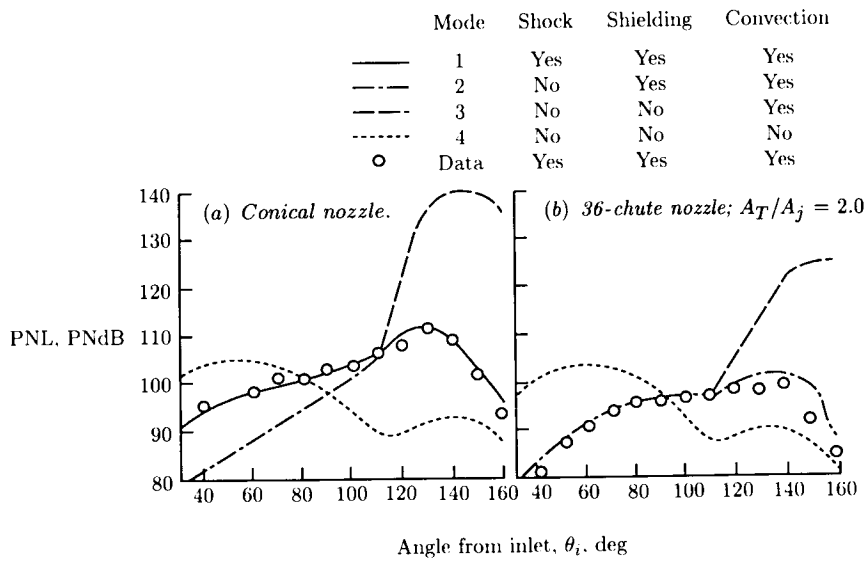

Figure 15. Relative contribution of noise mechanisms to PNL directivity at $V_j = 732$ m/sec. (From ref. 12.)

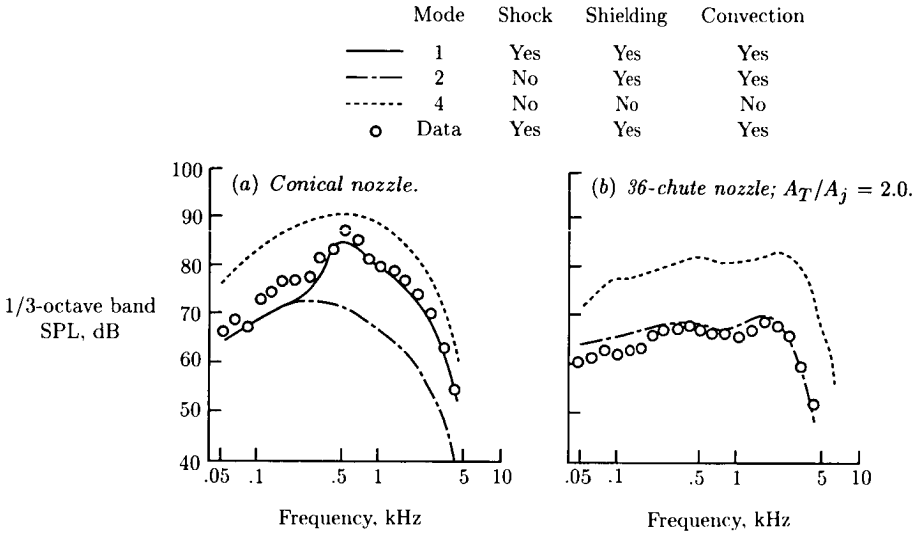

Figure 16. Relative contribution of noise mechanisms to SPL spectra at $\theta_i = 50°$ for conical nozzle and 36-chute nozzle at $V_j = 732$ m/sec. (From ref. 12.)

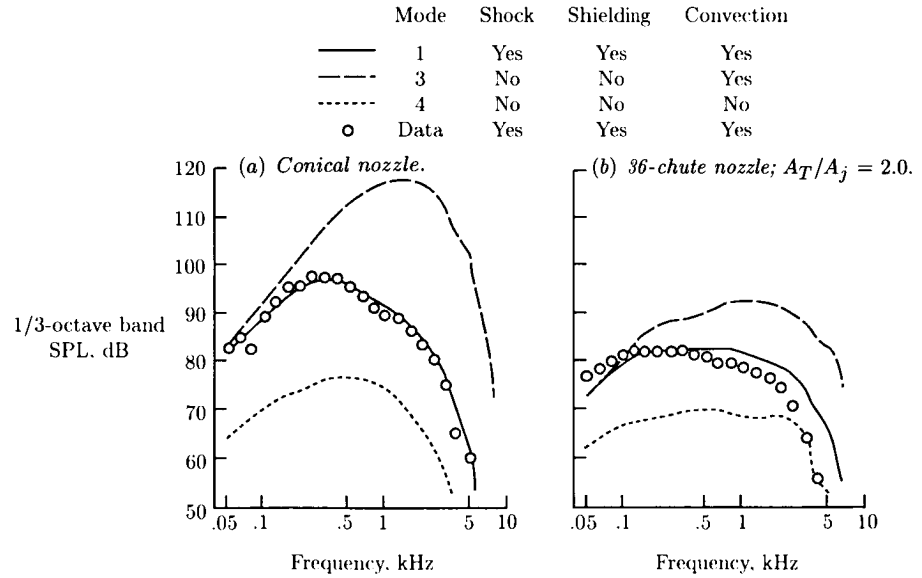

Figure 17. Relative contribution of noise mechanisms to SPL spectra at $\theta_i = 130°$ for conical nozzle and 36-chute nozzle at $V_j = 732$ m/sec. (From ref. 12.)

For the conical nozzle PNL directivity patterns (fig. 15), the shock-cell noise contributes substantially to the total noise in the forward quadrant, that is, at angles to the inlet less than 90°. This contribution can be seen in the difference between

mode (1) and (2) predictions. There is no contribution of shock-cell noise close to the jet axis (i.e., at angles greater than 120° from the inlet axis), since predictions for modes (1) and (2) are the same in this region. There is no fluid shielding for observer angles less than about 110°, based on a comparison of predictions for modes (2) and (3). For angles greater than 110°, however, shielding effects become quite substantial, on the order of 30 PNdB. Eddy-convection effects are also large; they increase the noise in the aft quadrant (angles greater than 90°). This effect is apparent from comparing predictions for modes (3) and (4).

The prediction for mode (4) shown in figure 15(a) represents the basic turbulent-mixing noise in the absence of convection and fluid-shielding effects. It possesses a basic, nonconstant directivity pattern dictated by the weighted summation of various quadrupole types composing the turbulent eddies. This basic pattern is only symmetric about 90° when the local flow Mach number is zero because the quadrupole weighting factors are a function of local Mach number and bias the radiation toward the forward quadrant.

The corresponding PNL directivity patterns for the 36-chute suppressor are shown in figure 15(b). The trends discussed above for the conical nozzle are qualitatively similar for the 36-chute nozzle, with the exception of the shock-cell noise contribution. The predictions were made with the shock-cell noise neglected (mode (2)), and yet the predictions agree well with the data, as figure 15(b) shows. This finding implies that shock-cell noise is not a significant feature of a high-element-number multichute nozzle. It also appears that neither convection effects nor fluid-shielding effects are as strong as for the conical nozzle.

The breakdown of mechanisms for a typical forward-quadrant angle of 50° is shown in figure 16. No shielding occurs at this angle; therefore, the mode (3) results are omitted, as they are identical to the mode (2) results. The conical-nozzle results (fig. 16(a)) show an interesting counteraction among the mechanisms. The basic mixing-noise spectrum (mode (4)) yields a high noise level, much higher than the measured level. The convection effect is to Doppler shift and drop this spectrum to a level significantly lower than the data (except at very low frequencies), as indicated by the mode (2) prediction. Finally, the addition of the shock-cell noise spectrum raises the spectrum back to the measured level at middle to high frequencies.

The corresponding spectrum results for the 36-chute nozzle are shown in figure 16(b). The good agreement between the spectrum prediction and the measured spectrum for mode (2) substantiates the implication from figure 15(b): shock-cell noise may not be a significant source for a high-element-number multichute suppressor. However, acoustic data for multielement suppressors employing fewer elements (e.g., 20) show evidence of shock-cell noise in the forward quadrant, particularly in flight. (See ref. 16.) Again, the effect of convection is to reduce the level and Doppler shift the spectrum to lower frequencies.

Near the peak noise angle of 130°, convection effects are significant. They produce a dramatic amplification of the mixing noise, as the results in figure 17 show. Another counteraction of mechanisms occurs at this angle and involves the competing effects of convection and fluid shielding. The basic mixing-noise spectrum (mode (4)) is much lower than the measured level, as shown in figure 17(a). The effect of convection is to increase the levels by as much as 40 to 50 dB at high frequencies. The effect of shielding, however, is to reduce the noise levels by 20 to 30 dB at high frequencies, consistent with the measured levels.

It is interesting to note that the convection effect Doppler shifts the basic mixing-noise spectrum to higher frequencies, as would be expected from classic notations of moving-source acoustics. However, the fluid-shielding effects, which increase with increasing frequency, attenuate the high-frequency portion of the convected spectrum to such a large extent that the resulting spectrum peaks at a much lower frequency, lower than even the basic unconvected spectrum peaks. This attenuation explains the observed "reverse Doppler shift" at angles close to the jet axis.

The competing influences of convection and fluid shielding are also evident in the predictions for the 36-chute nozzle shown in figure 17(b). The magnitudes of these effects are considerably smaller than those exhibited by the conical nozzle. For example, at 2000 Hz the convective amplification is 22 dB for the 36-chute nozzle, compared with 48 dB for the conical nozzle at the same frequency. Similarly, the fluid-shielding attenuation is only 12 dB at 2000 Hz for the chute nozzle, compared with 31 dB of attenuation for the conical nozzle.

The various suppression mechanisms can be isolated explicitly by examining the difference between the various prediction curves shown in figures 15 to 17. First, the total PNL suppression as a function of angle is the difference between the conical- and 36-chute-nozzle total noise PNL directivity patterns. This difference can be compared with measured PNL suppression and is shown in figure 18. The predicted total PNL suppression compares well with the measured suppression.

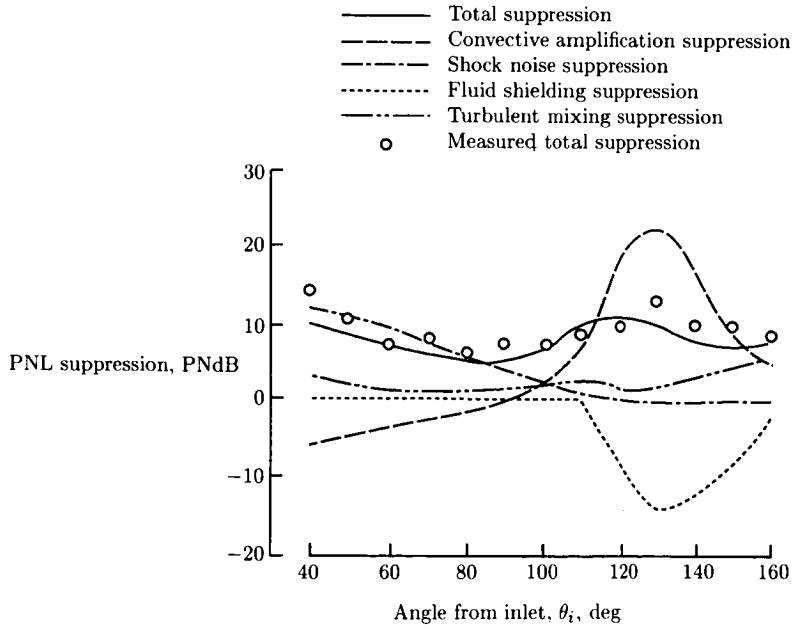

Figure 18. PNL suppression composition for 36-chute nozzle at V_j = 732 *m/sec.* $A_T/A_j = 2.0$. *(From ref. 12.)*

For the results of figures 15 to 17, it can be concluded that the high-element-number multichute nozzle almost completely suppresses the shock-cell noise and thus permits the mixing noise to dominate the forward-quadrant spectra. The shock-cell noise suppression is then approximated by the difference between mode (1) and

mode (2) conical-nozzle predictions. This estimated shock-cell noise suppression is higher than the total predicted suppression in the forward quadrant; hence, some other mechanism is providing negative suppression, that is, increasing the PNL.

The suppression due to convective amplification can be computed by first calculating the convective amplification for each nozzle (mode (3) PNL minus mode (4)) and then subtracting the 36-chute-nozzle result from the conical-nozzle result. The convective amplification suppression is shown in figure 18. Note that it is negative in the forward quadrant; this explains why the shock-cell noise suppression is greater than the total (net) suppression.

Similarly, the difference between the fluid-shielding attenuation for the 36-chute suppressor and the conical nozzle was computed from the results shown in figure 15, and this difference is also shown in figure 18. From this result, it is apparent that a multielement suppressor exhibits less fluid-shielding effects than a conical nozzle, that is, part of the beneficial effect of fluid shielding is lost by the addition of a suppressor.

The observed suppression in the aft quadrant is primarily a result of reduced convective amplification, offset somewhat by a loss in fluid shielding. This delicate balance between convection and shielding effects in the aft quadrant is very difficult to predict accurately because these two effects are large in magnitude but opposite in sign, as illustrated in figure 17.

Finally, the suppression of basic turbulent-mixing-noise generation has been evaluated by subtracting the prediction for mode (4) for the 36-chute nozzle from that for the conical nozzle, and this result is also shown in figure 18. The basic mixing-noise suppression is quite small, from 1 to 5 dB over the range of angles shown, and this result is contrary to historical conceptions of how much multielement suppressors suppress jet noise.

The multichute suppressor in fact generates approximately the same total mixing noise as the equivalent conical nozzle but redistributes the noise to higher frequencies. This is dramatically illustrated in figure 19, in which the basic mixing-noise spectra (mode (4)) for the two nozzles are presented. Also shown are these same spectra with the atmospheric air attenuation removed (i.e., the "lossless" spectra). The multichute lossless spectrum has about the same peak level as the conical-nozzle lossless spectrum, but at a much higher frequency. The ratio of 36-chute-nozzle peak-noise (lossless) frequency to conical-nozzle peak-noise (lossless) frequency is about 6:1. This is precisely the ratio of the conical-nozzle diameter to 36-chute-nozzle equivalent-area diameter.

The reduction in shock-cell noise produced by a multichute suppressor can be explained by the fact that breaking up a large, round jet into very small, discrete, rectangular jets will cause the shock-cell formation to be dissipated much more rapidly. The shock-cell spacings and cross-sectional dimensions will be much smaller, and the cells are likely to be less numerous. The resulting radiation is therefore likely to be much lower in level and higher in frequency than that for a conical nozzle.

The observation that the total generated mixing noise is not significantly different for a multichute suppressor than for a conical nozzle is explained by the fact that the multichute-nozzle mixing layer perimeter close to the nozzle exit plane is considerably larger than that of an equivalent-area conical nozzle. The high-frequency noise generated in the initial shear layers should therefore be higher by the

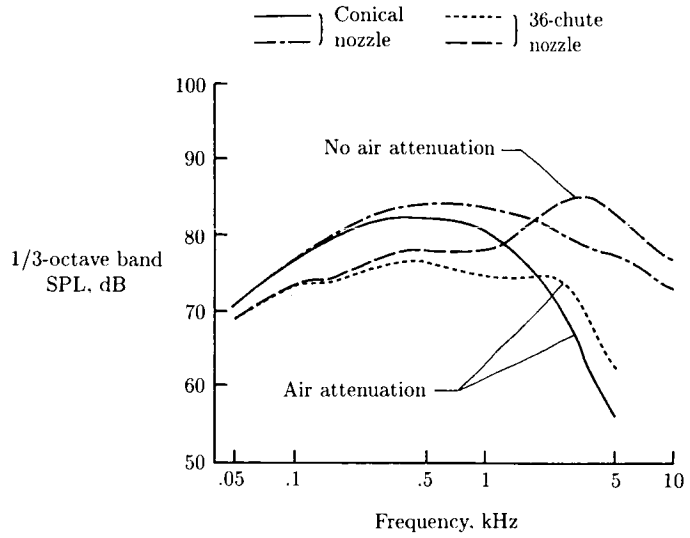

Figure 19. Predicted turbulent-mixing-noise spectra at $\theta_i = 90°$ for conical nozzle and 36-chute nozzle ($A_T/A_j = 2.0$) at $V_j = 732$ m/sec. (From ref. 12.)

ratio of perimeters, provided the premerged portions of the chute mixing layers have approximately the same turbulence characteristics. Once the chutes have merged, a large, axisymmetric jet forms which has a substantially lower velocity than the exit value; therefore, the multichute-nozzle low-frequency noise levels should be lower than the corresponding conical-nozzle levels.

The reduction in convection effects exhibited by a multichute nozzle is the result of lower eddy-convection velocities. The rapid decay of plume mean velocity exhibited by a multichute nozzle suggests that the majority of the noise-producing turbulent eddies in the plume are convecting downstream at a substantially lower velocity than in a conical nozzle.

The reduced fluid-shielding effects characteristic of a multichute nozzle can also be related to the rapid plume velocity (and temperature) decay. Fluid shielding increases with increasing plume flow velocity and temperature; therefore, the lower velocity and temperature levels resulting from the rapid chute-element mixing provide less fluid shielding than those of an equivalent-area conical nozzle.

From the preceding considerations, it can be concluded that the best suppression is achieved by producing the most rapid plume decay. Higher numbers of elements and higher area ratios give more rapid decay. Area ratio seems to control the velocity level plateau formed by the merging of the individual chute element jets into a single annular jet. Higher area ratios yield lower merged-velocity levels and hence lower convection speeds. Element number seems to control how fast the merged-velocity level is reached; higher numbers of elements give more rapid decay of the individual element jet flows to the merged-velocity level. One additional benefit of higher numbers of elements is that the initial mixing-noise generation is pushed to higher frequencies by virtue of the smaller turbulence scales associated with the smaller, individual jet elements.

Jet Noise Suppression Concepts

Various experimental studies have demonstrated the noise reduction potential of jet noise suppression concepts which essentially alter the jet plume development. All these concepts may be grouped under the following two broad categories:

1. Geometric concepts, such as multielement suppressors (e.g., chutes, spokes, and tubes) at the nozzle exit plane, ejectors surrounding the jet in the vicinity of the nozzle exit, annular plug or 2-D nozzles, and combinations of the above.

2. Aerothermodynamic concepts, such as inverted-velocity profile (i.e., a higher velocity jet surrounding a lower velocity jet), thermal acoustic shield (i.e., surrounding either fully or partially the main jet with a jet having a high static temperature and low velocity), and shock noise control by appropriate contouring of the nozzle flow path.

Some jet noise suppression concepts have employed a combination of both geometric and aerothermodynamic concepts (e.g., a dual-flow, multielement suppressor with inverted-velocity profile).

This section presents the experimental data for the above two categories collected over several years, explains the data based on physical reasoning, and evolves guidelines (where possible) for future design of jet noise suppression devices.

Geometric Concepts

Multielement Suppressors

The principal jet noise suppression mechanism underlying the multielement suppressors (such as chutes, spokes, or tubes) is the division of the large single jet into many small jets with sufficient separation between these jets to enhance mixing with the ambient air to yield a rapid decay of the jet plume. Mixing is enhanced by the increased surface area of the jet available for shear with the ambient air, a classic momentum diffusion concept. Also, since each small jet has a much smaller equivalent diameter than a circular jet, its effectiveness as a noise radiator is restricted to a much smaller physical length compared with the single large jet, as long as the separate jets do not merge. The merged jet will have a much lower jet velocity. This lower velocity results in the acoustic energy being transferred to smaller scale turbulent eddies which, by virtue of their small size, generate noise in the higher frequency ranges than the turbulent eddies of a large single jet. This higher frequency noise generation results in a suppressor spectrum which has high- and low-frequency peaks, unlike the conical nozzle, which has a low-frequency peak only. (See fig. 20, from ref. 17.) The acoustic signal suffers atmospheric absorption in reaching the far-field observer. As various data and theories have indicated (refs. 18 and 19), high-frequency acoustic waves suffer significantly more atmospheric attenuation than low-frequency waves over the same distance. Since multielement suppressors have a larger contribution of acoustic energy in the high-frequency region and that energy suffers much higher levels of atmospheric absorption, the far-field noise of these suppressors is lower than that of single conical nozzles.

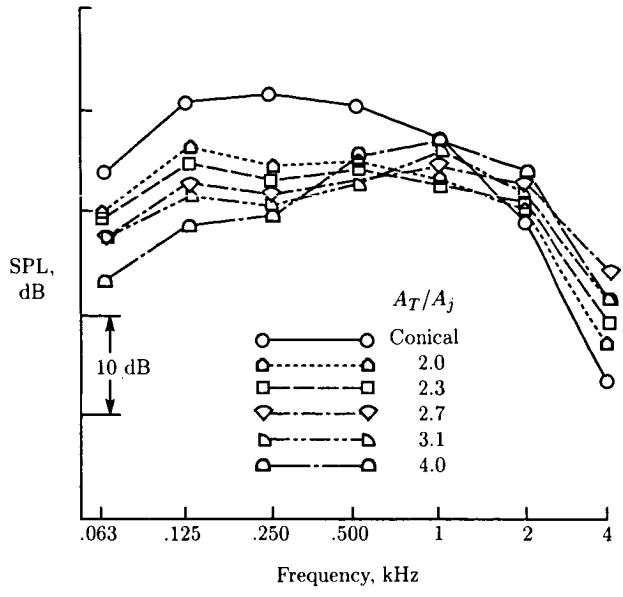

Figure 20. Spectra illustrating dual-peak characteristics of multitube nozzles. NPR ≈ 2.1; T_T ≈ 1520°R; V_j ≈ 1870 ft/sec. (From ref. 17.)

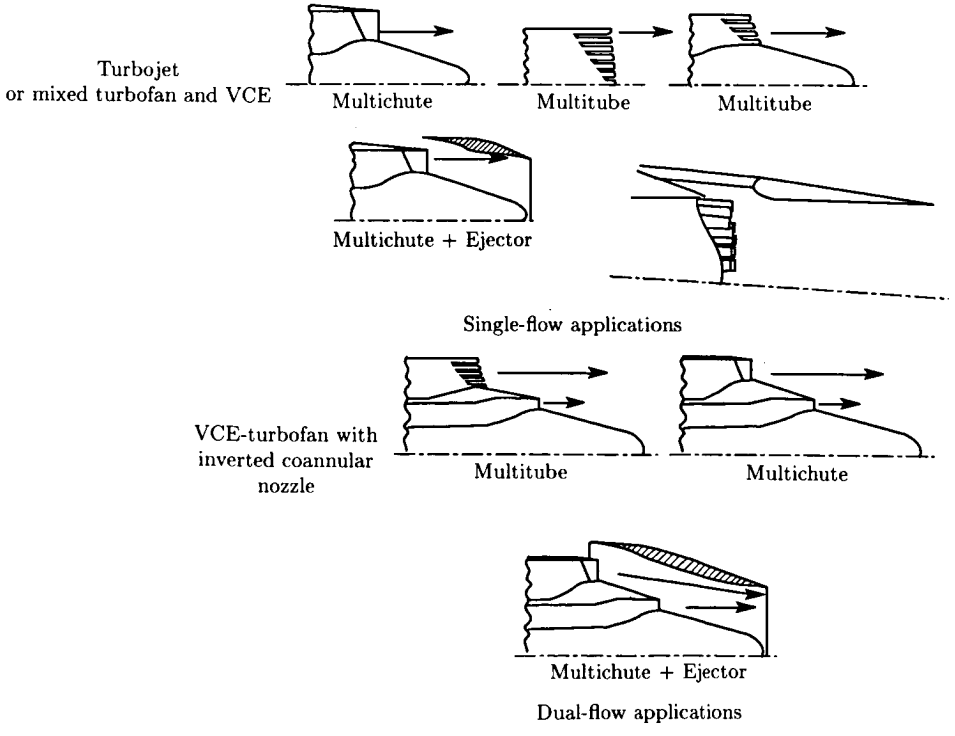

Figure 21. Examples of multielement suppressors with and without ejectors. (From ref. 20.)

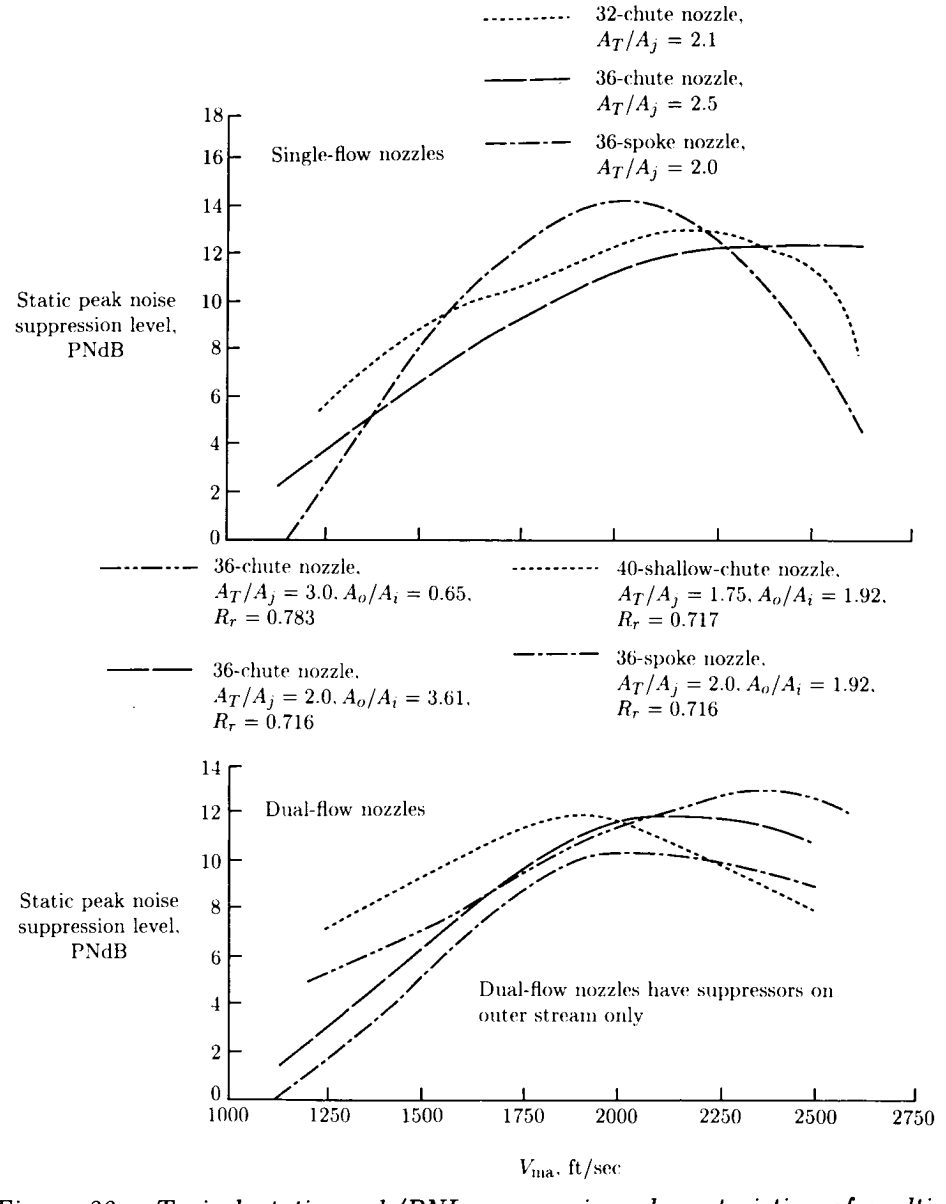

Figure 22. Typical static peak/PNL suppression characteristics of multielement suppressors. 2400-ft sideline; standard day (59°, 70 percent relative humidity); $A_T = 338$ in^2. (Based on ref. 20.)

Figure 21 shows the following two families of multielement suppressors, for which a large body of data exists (ref. 20):

1. Single-flow applications for a turbojet or mixed turbofan and variable cycle engine (VCE)
2. Dual-flow applications with a suppressor in the high-velocity stream for a turbofan and VCE with inverted-velocity profile

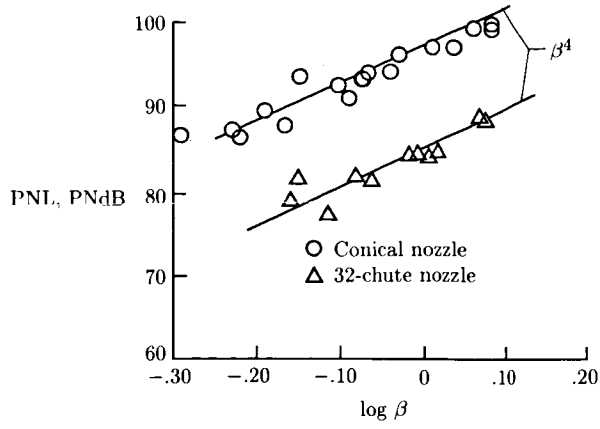

(a) PNL at $\theta_i = 50°$.

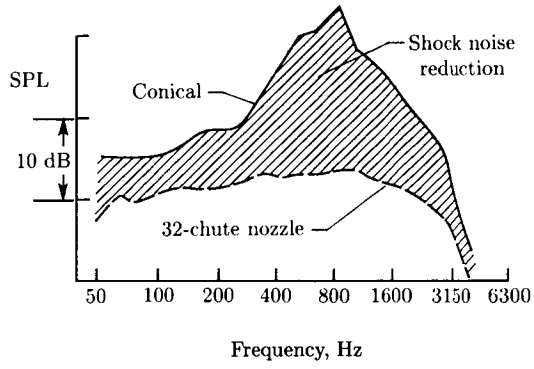

(b) SPL at $\theta_i = 50°$; 2400-ft sideline; $V_j = 2300$ ft/sec; $NPR = 3.2$; J-79 size.

Figure 23. Forward-quadrant shock noise reduction of 32-chute suppressor and conical nozzle. (From ref. 21.)

Figure 22 summarizes the suppression potential of various single- and dual-flow applications of multielement suppressor concepts in terms of static peak PNL suppression measured over the range of mass-averaged jet velocities V_{ma} covering typical takeoff, thrust cutback, and approach conditions. Single-flow applications generally exhibit slightly higher suppression than outer-stream suppressors on dual-flow systems, as the complete jet is segmented for single-flow applications. As an illustration of the potential of multielement suppressors for shock noise reduction, figure 23 (from ref. 21) shows the forward-quadrant noise reduction in terms of PNL at $\theta_i = 50°$ for a wide range of supersonic jet Mach numbers. Also shown are the spectral reductions for a 32-chute, single-stream suppressor compared with those for a conical nozzle.

Next, data trends obtained with geometric variations of multitube, multispoke, and multichute suppressors are presented. For multitube suppressors, the design variables having first order impact are

1. Suppressor area ratio (total area/flow area, A_T/A_j)
2. Number of tubes
3. Ratio of internal tube length to diameter, L_t/D_t
4. Exit plane and base plane stagger

The influence of the above four design variables on both acoustic and aerodynamic performance (in terms of pressure levels in the base region) is shown in figures 24 to 27. The following trends are indicated.

At high jet velocities, higher area ratios yield higher levels of acoustic suppression than lower area ratios yield; at low jet velocities, the inverse is true. (See fig. 24.)

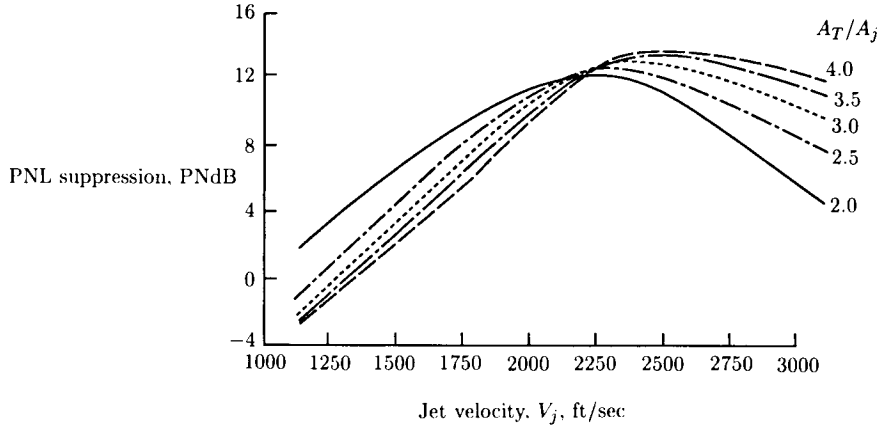

(a) PNL suppression; 1500-ft sideline; no shroud; based on data at $A_T/A_j = 2.0, 2.3, 2.7, 3.1,$ *and* 4.0 *(*2.0 *and* 4.0 *repeated).*

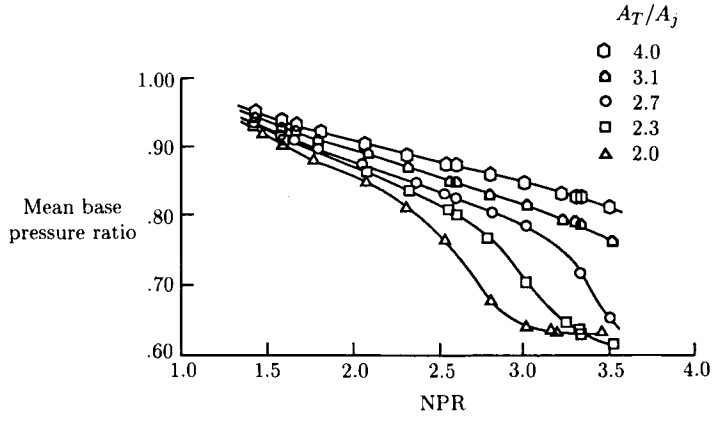

(b) Base pressure distribution; hot flow data.

Figure 24. Impact of multitube nozzle area ratio on acoustic and aerodynamic performance. $L_t/D_t = 2.2$. *(From ref. 17.)*

The designs with higher area ratios enhance ventilation of the base region to ambient air, the result being base pressures which approach the ambient pressure and thus base drag is reduced. However, increasing the area ratio requires a larger nozzle diameter and associated weight and drag penalties.

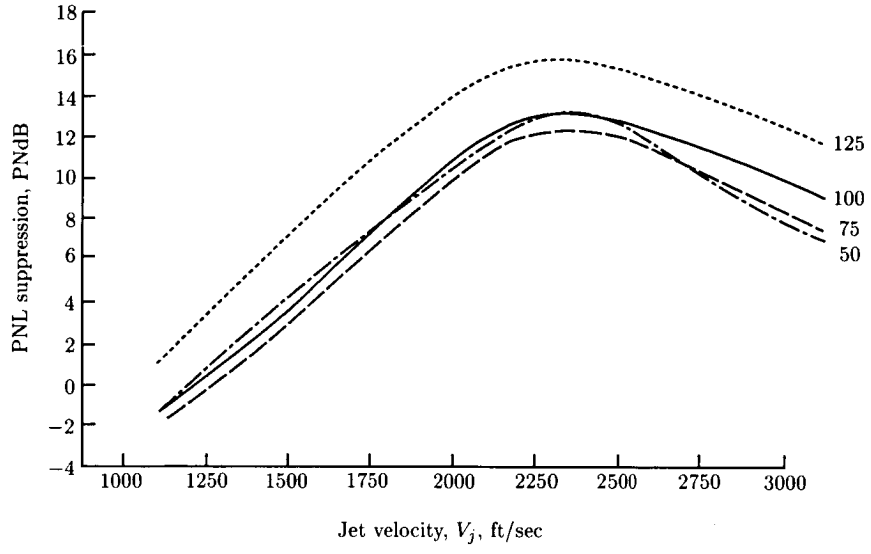

(a) Effect of number of holes; 1500-ft sideline; no shroud; based on data for 55, 85, and 121 holes (55 holes repeated).

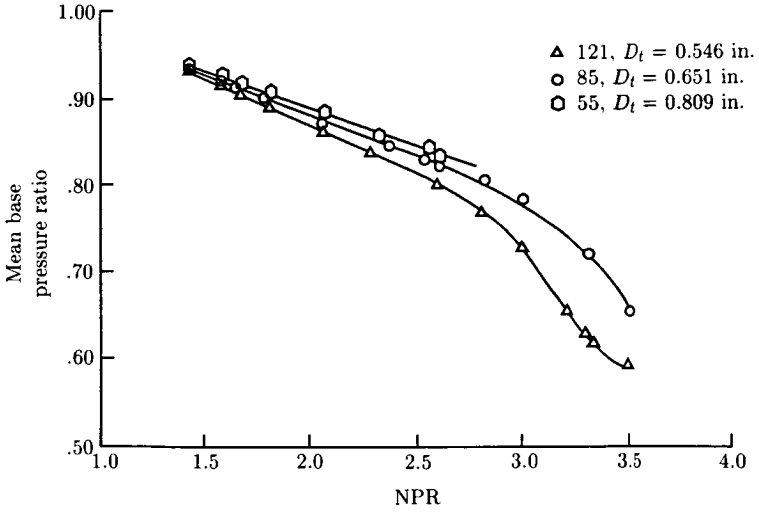

(b) Base pressure distribution; hot flow data.

Figure 25. Impact of multitube nozzle degree of segmentation on acoustic and aerodynamic performance. A_T/A_j = 2.7; L_t/D_t = 2.2. (From ref. 17.)

For a given area ratio, increasing the number of tubes results in higher levels of noise suppression because of the shift of acoustic energy into higher frequencies. However, the increase yields lower base pressure for tubes in the interior because of poor ventilation and results in high base drag. (See fig. 25.)

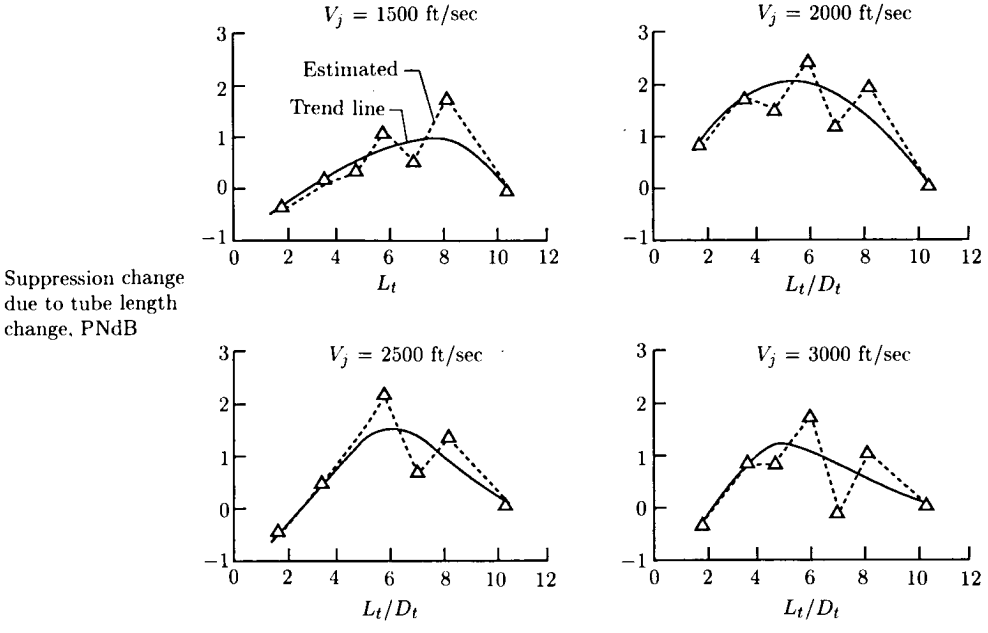

(a) Effect of tube internal length ratio on noise suppression; 300-ft sideline.

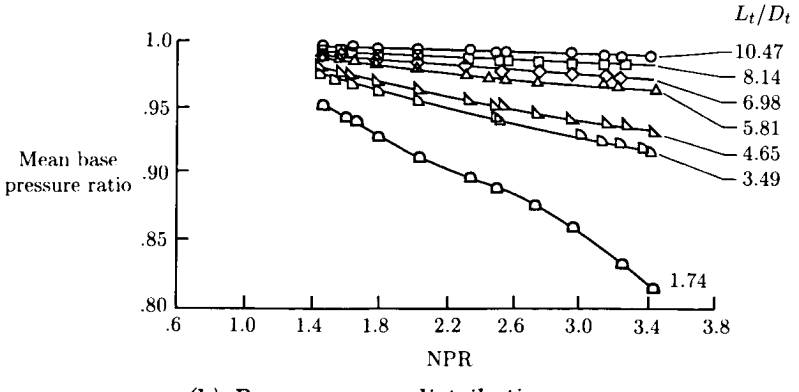

(b) Base pressure distribution.

Figure 26. Impact of multitube nozzle ratio of tube length to diameter on acoustic and aerodynamic performance. $A_T/A_j = 3.19$; 85 tubes; no shroud. (From ref. 17.)

The data for the ratio of tube length to diameter indicate optimum PNL suppression as a function of jet velocity. (See fig. 26.) Long tubes enhance base ventilation by virtue of the distance available for entrainment of ambient air. However, weight and stowing for cruise determine the upper limit for this parameter.

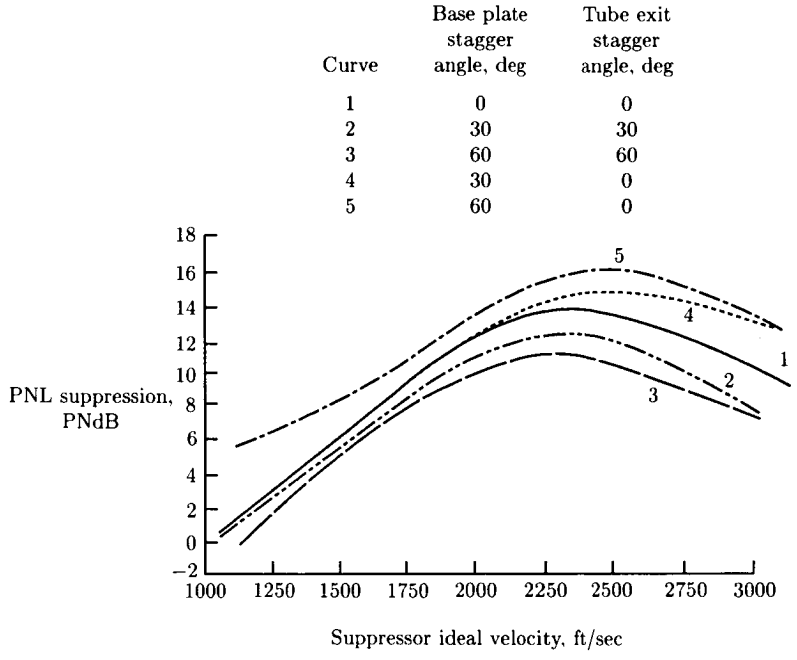

(a) Acoustic performance; 1500-ft sideline; $A_T/A_j = 2.27$.

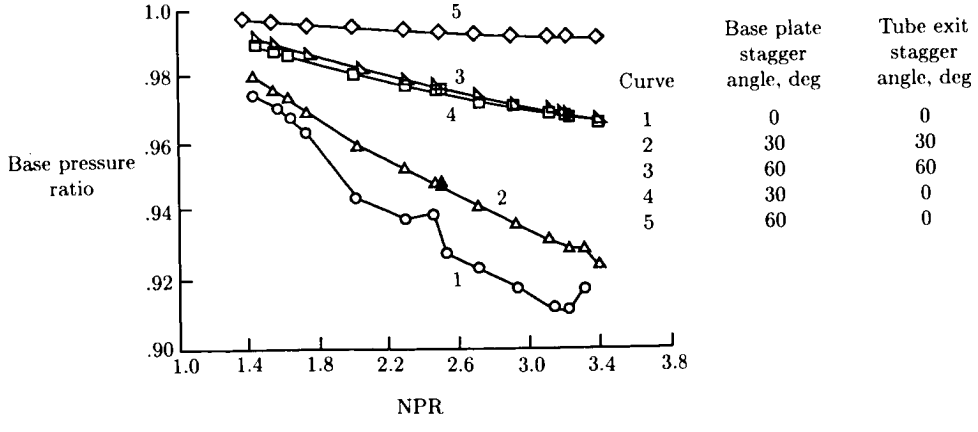

(b) Aerodynamic performance; $A_T/A_j = 2.0$.

Figure 27. Impact on multitube nozzle base and exit plane stagger on acoustic and aerodynamic performance. 72 plain tubes; no shroud. (From ref. 17.)

The data for exit plane and base plane stagger (fig. 27) indicate that jets with coplanar exits but large values of base plane stagger yield the largest levels of acoustic suppression and low values of base drag. Coplanar exits help establish a uniform coalescing of the individual jets to merge into a single jet. High values of base stagger result in adequate entrainment of ambient air for better mixing and diffusion of jets in the interior, the result being lower merged velocity and hence lower noise levels. Improved entrainment also results in lower base drag.

Chutes and spokes have similar geometric planforms, the only difference being that chutes have the capability of entraining the ambient air by means of the ventilation channel upstream of the nozzle exit plane and spokes do not. Hence, the multispoke suppressors yield lower aerodynamic performance than the multichute suppressors. Acoustic suppression potential of chutes and spokes is very similar. Figure 28 is a brief summary of the multichute and multispoke nozzle acoustic and aerodynamic performance trends with key geometric parameters, such as suppressor area ratio A_T/A_j, element number, and shape.

Chutes exhibit similar noise suppression trends with suppressor area ratio as the tubes, that is, higher area ratios yield more suppression at high jet velocities and the lower area ratios yield more suppression at lower jet velocities. (Compare figs. 28(a) and 24(a).) However, as the suppressor area ratio is increased, aerodynamic performance of chutes in terms of gross thrust coefficient[1] $C_{f,g}$ deteriorates, a trend opposite to that of tubes. The principal reason for this deterioration is that as area ratio is increased for chutes, the base area is increasing for a given area available for entrainment of ambient air through the entrainment channels. (Compare figs. 28(b) and 24(b).) Acoustic suppression is a fairly weak function of number of chutes. (See fig. 28(c).) For a given suppressor area ratio and chute depth/width ratio D/W, the aerodynamic performance of the suppressor decreases with increases in chute number. The principal reason for this decrease is that as the chute number increases for a given suppressor area ratio, the chute widths decrease. Thus for a constant chute depth/width ratio, the chute depth decreases, the result being poorer ventilation of the chute in the interior and hence an increase in base drag. (See fig. 28(b).) Acoustic suppression levels obtained with chutes and with spokes are similar (fig. 28(d)), with a slightly higher level of suppression exhibited for chutes at high jet velocities.

Exit plane angle (canting) has a noticeable impact on both acoustic and aerodynamic performance. (See fig. 28(e).) A 10° cant helps the individual jets to retain their identity for a longer distance and thus helps improve shearing of the multiple jets by the ambient air to yield higher levels of acoustic suppression. However, a 10° cant tends to separate the flow from the plug surface, the result being poor aerodynamic performance.

Planform shape of the spokes (i.e., tapered or parallel-sided) affects both acoustic and aerodynamic performance. (See fig. 28(f).) Parallel-sided spokes yield a larger flow perimeter for shearing by ambient air and thereby yield higher levels of acoustic suppression than the tapered spokes. Aerodynamic performance of parallel-sided spokes is lower than that of tapered spokes since parallel-sided spokes have larger base areas in the interior, where ambient air cannot conceivably penetrate.

[1] Gross thrust coefficient $C_{f,g}$ is defined as the ratio of actual gross thrust to ideal thrust based on isentropic expansion to ambient pressure.

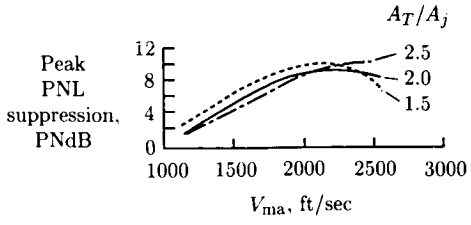

(a) Influence of 36-chute suppressor area ratio on peak PNL suppression; 2400-ft sideline; dual flow; scaled to A_T = 338 in^2.

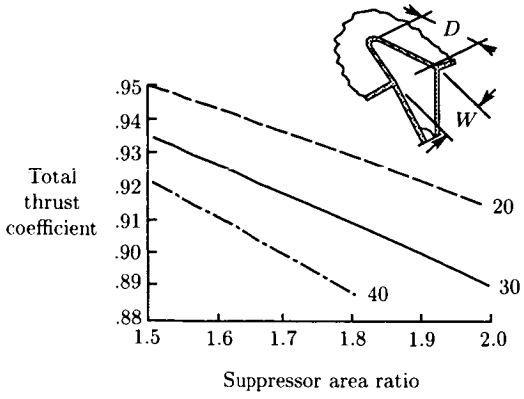

(b) Variation of total thrust coefficient with suppressor element number and area ratio; single-flow plug nozzle; D/W = 1.0; M = 0.36; 15° plug angle.

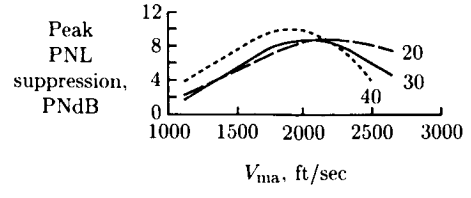

(c) Peak PNL suppression as function of suppressor element number; static; A_T/A_j = 1.75; R_r = 0.717; scaled to A_T = 338 in^2.

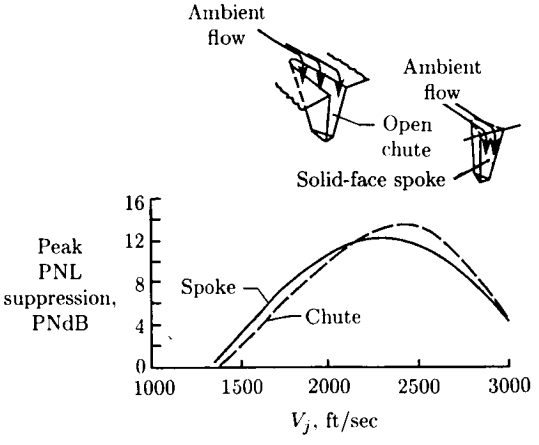

(d) Acoustic suppression of chute and spoke suppressors; 1500-ft sideline; 32 elements; A_T/A_j = 2.0; R_r = 0.498.

Figure 28. Multichute and multispoke suppressor nozzle acoustic and aerodynamic performance trends. (From ref. 20.)

Figure 29 summarizes the acoustic suppression versus thrust degradation for various tube, spoke, chute, plug, coannular, and ejector nozzles. Cruise performance

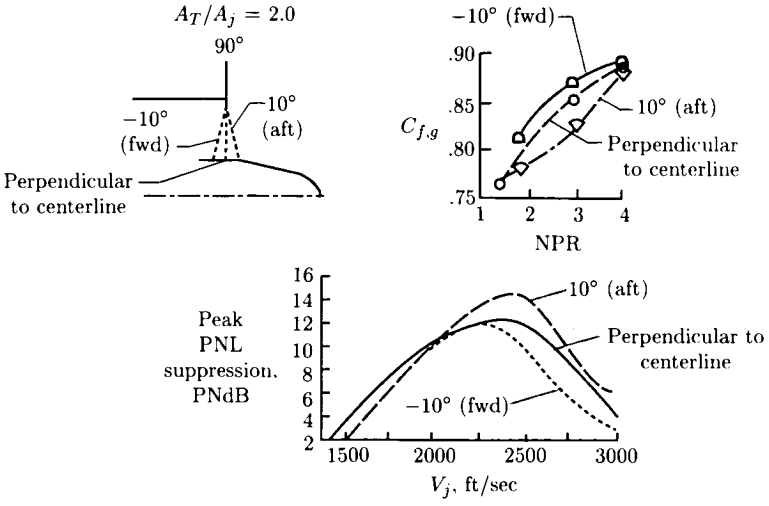

(e) Influence of element cant angle on acoustic and aerodynamic performance.

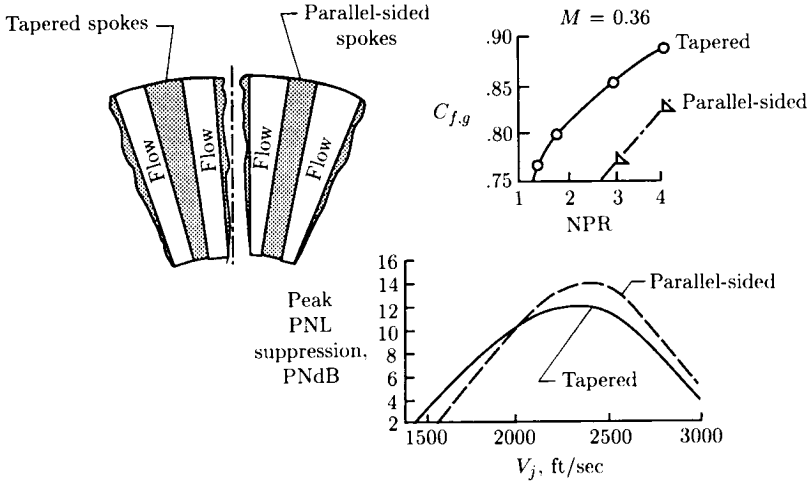

(f) Influence of element planform shape on acoustic and aerodynamic performance.

Figure 28. Concluded.

considerations certainly will require that the suppressors be stowed to minimize mission impact. Typical schemes for stowage and deployment of chutes and tubes are conceptually illustrated in figure 30.

The above discussion indicates that multielement suppressor design involves a complex interaction of acoustic suppression potential, aerodynamic performance,

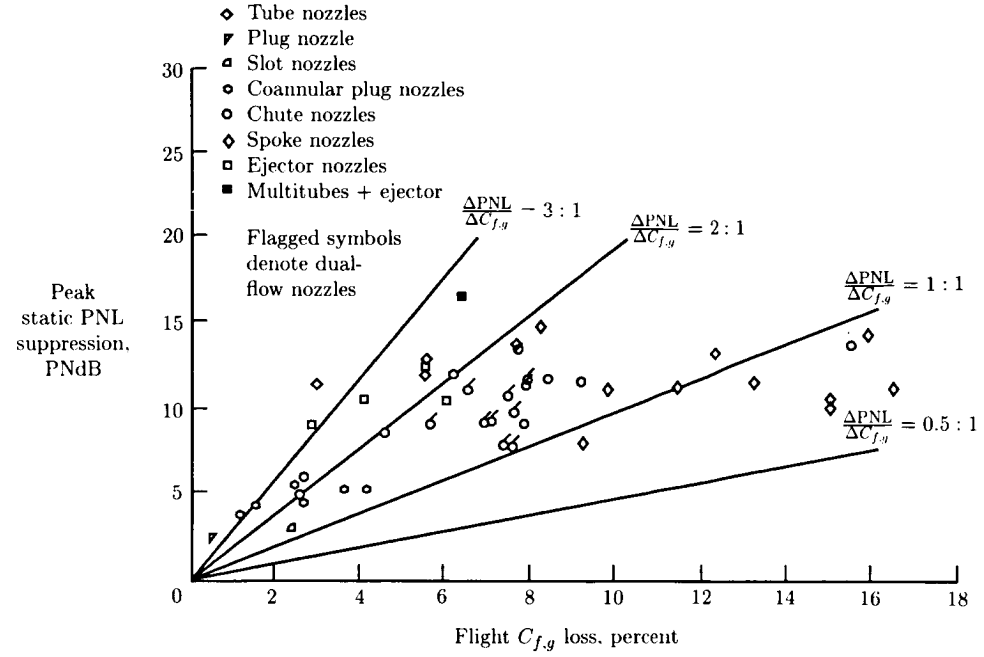

Figure 29. Generalized flight performance and static suppression levels relative to conical nozzle. Based on measured aerodynamic performance and acoustic data. Nominal conditions: single flow—$V_{ma} \approx 2400$ ft/sec and NPR ≈ 3.0; dual flow—$V_{ma} \approx 2200$ ft/sec, $NPR_o \approx 3.0$, and $NPR_i \approx 2.5 \rightarrow 3.5$. (From ref. 20.)

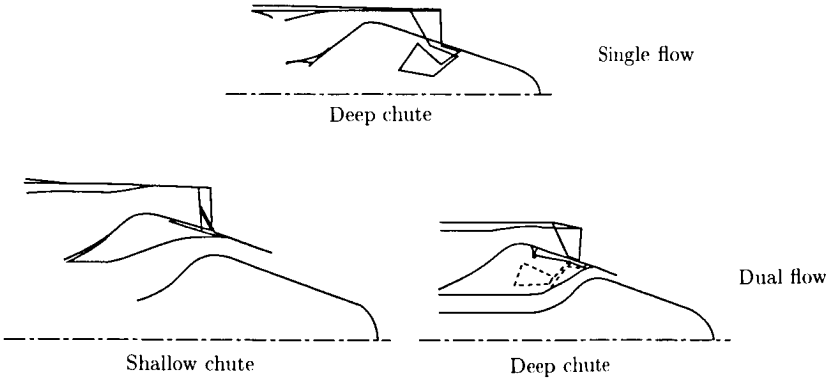

Figure 30. Installation schemes for stowed and deployed multielement suppressors. (From ref. 20.)

and mechanical feasibility (i.e., implementation, stowability, and reliability). The ultimate impact of these considerations on the mission is equally important.

Ejectors

An ejector, when designed as an integral part of the propulsive nozzle system, can yield optimum aerodynamic performance for the entire mission by providing an optimum flow expansion surface. It can also provide additional noise suppression than a nozzle system without an ejector by virtue of its capability for induction of ambient air to enhance mixing and shielding or suppression of noise sources within the ejector length. For an extensive discussion of the principles of noise reduction by mixing nozzles and ejector nozzles, see reference 22. Ejectors used in conjunction with conical nozzles or basic coannular plug nozzles have been ineffective since the dominant acoustic sources are located outside the ejector. However, for suppressor nozzles, the dominant acoustic sources are located close to the jet exit plane; hence, ejectors with acoustic treatment on the internal flow surface effectively improve the basic suppressor acoustic performance. Air induction by ejectors is also more effective, as induced air can impact mixing in the region of dominant acoustic sources.

Flight tests on a Viper turbojet engine fitted with various exhaust suppressors with and without treated ejectors are reported in reference 23. A maximum attenuation of 14 EPNdB was measured at an ideal jet exhaust velocity of 732 m/sec (2400 ft/sec) at an adjusted altitude of 152 m (500 ft).

In reference 24, researchers used a short ejector lined with bulk absorber on a 32-deep-chute primary nozzle system installed on a J-79 dry turbojet engine (nonaugmented; see fig. 31(a)). The short ejector attained a nearly uniform 2 dB more peak PNL suppression than the suppressor alone. (See fig. 31(b).) In a more extensive scale-model program sponsored by NASA Lewis Research Center (ref. 25), researchers investigated the influence of ejector geometry and acoustic treatment on acoustic and aerodynamic performance. The scale-model system employed a 20-chute outer annular suppressor with inverted-velocity profile and an ejector with or without acoustic treatment. The plug surface was both hard walled and acoustically treated.

Influence on ejector spacing S from the suppressor exit plane (normalized by the equivalent diameter based on flow area D_{eq}) on peak PNL as a function of mass-averaged jet velocity is shown in figure 32. The influence of ejector spacing on aerodynamic performance in terms of thrust loss due to chute base drag as a function of outer stream pressure ratio is shown in figure 33. Increasing the ejector spacing results in a marked improvement in the aerodynamic performance because an increased induction of ambient air into the chutes is possible with more spacing. This increased entrainment of ambient air results in improved mixing within the ejector system, and this mixing results in a lower merged velocity and hence lower noise levels.

Figures 34 and 35 show the influence of ejector length L on peak PNL and on thrust loss due to base drag. Increased ejector length yields slightly higher noise suppression at all jet velocities because of the containment of sources over a larger distance. The longer ejector shows improved aerodynamic performance as well.

Influence of acoustic treatment attached to the ejector internal surface and/or plug on acoustic characteristics is shown in figure 36. Successive treatment of the ejector and plug surfaces improves acoustic suppression. The hard-wall ejector provides the suppression by pure physical shielding and ambient air induction. Successive improvements because of the treatment are not very sensitive to treatment impedance.

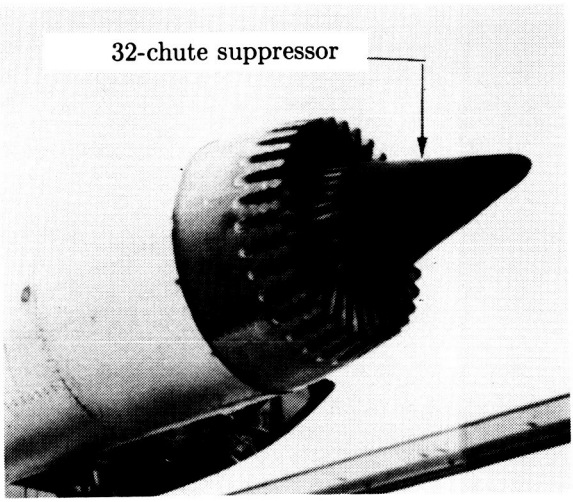

(a) Suppressor installed on J-79 engine.

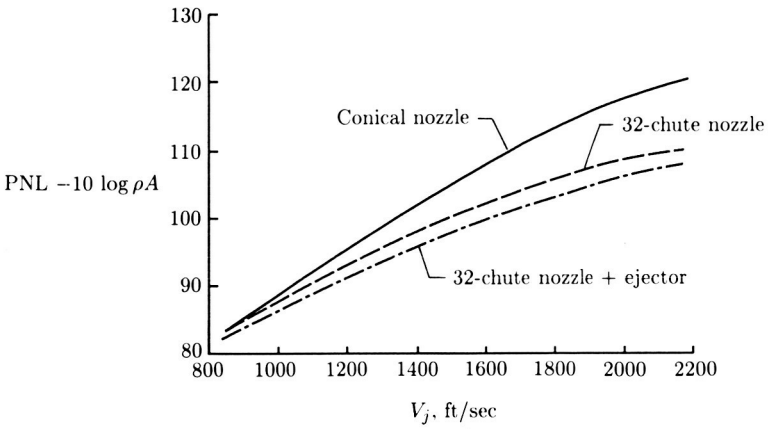

(b) Peak PNL's. 2128-ft sideline; full scale; scale factor, 2:1.

Figure 31. General Electric 32-chute annular nozzle on J-79 testbed with and without treated ejector. (From ref. 17.)

Based on these studies, the following design guidelines have evolved:

1. An increase in the axial stagger between the suppressor exit plane and the ejector improves acoustic and aerodynamic performance; however, weight and mechanical complexity increase.

2. An increase in ejector length improves noise suppression slightly.

3. Treatment of the ejector and the plug surface improves noise reduction potential, and the improvement is not sensitive to treatment impedance.

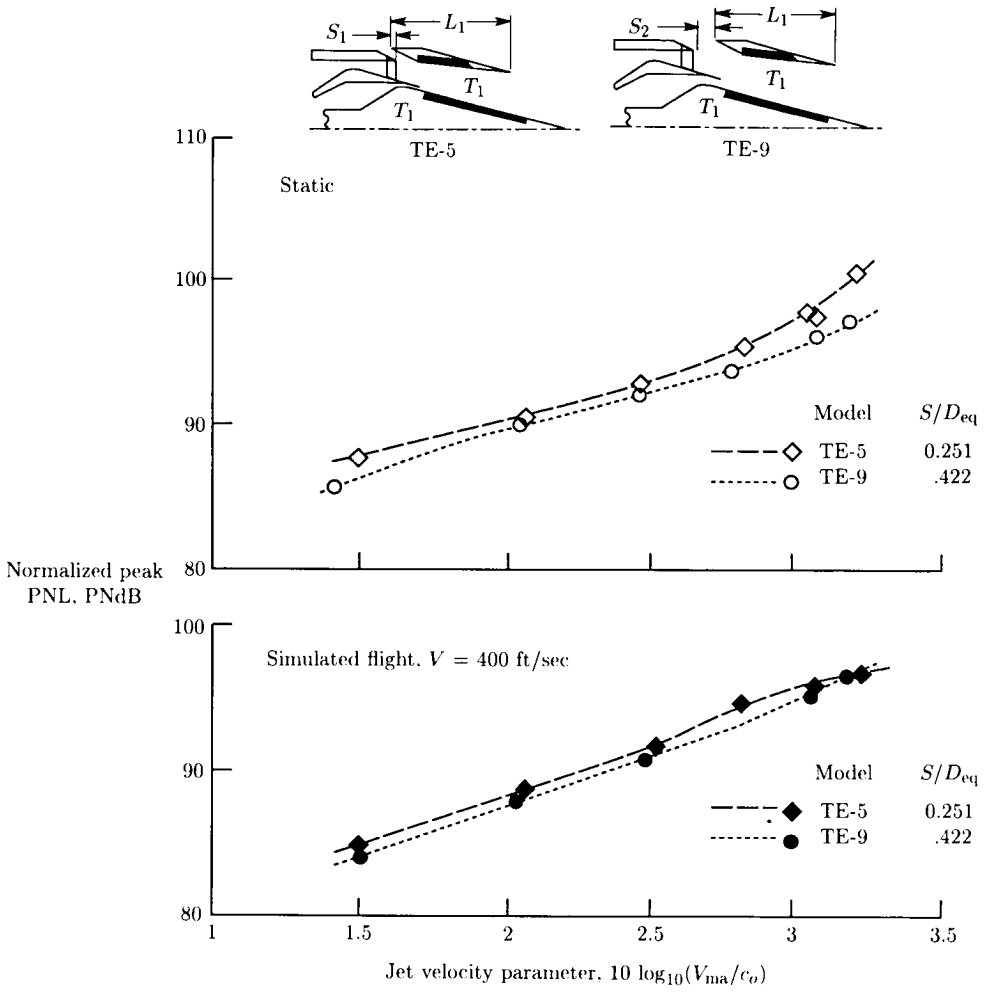

Figure 32. Influence of ejector spacing on normalized peak PNL of 20-shallow-chute suppressor nozzle (dual flow). 2400-ft sideline; A_T = 1400 in^2; standard day (59°F, 70 percent relative humidity). (Based on ref. 25.)

Annular Plug and 2-D Nozzles

Two-dimensional nozzles and plug nozzles with a high radius ratio R_r (i.e., ratio of inner radius to outer radius R_r) exhibit similar flow characteristics near the jet exit plane, since a 2-D nozzle of height h and width b can be viewed as an "unwrapped" annular nozzle of annulus height h and of circumference b. However, the flow characteristics downstream and acoustic characteristics of these two types of nozzles are quite dissimilar. They are grouped herein under one section since they both serve as the first step in departure from the simple conical nozzles to achieve jet noise suppression.

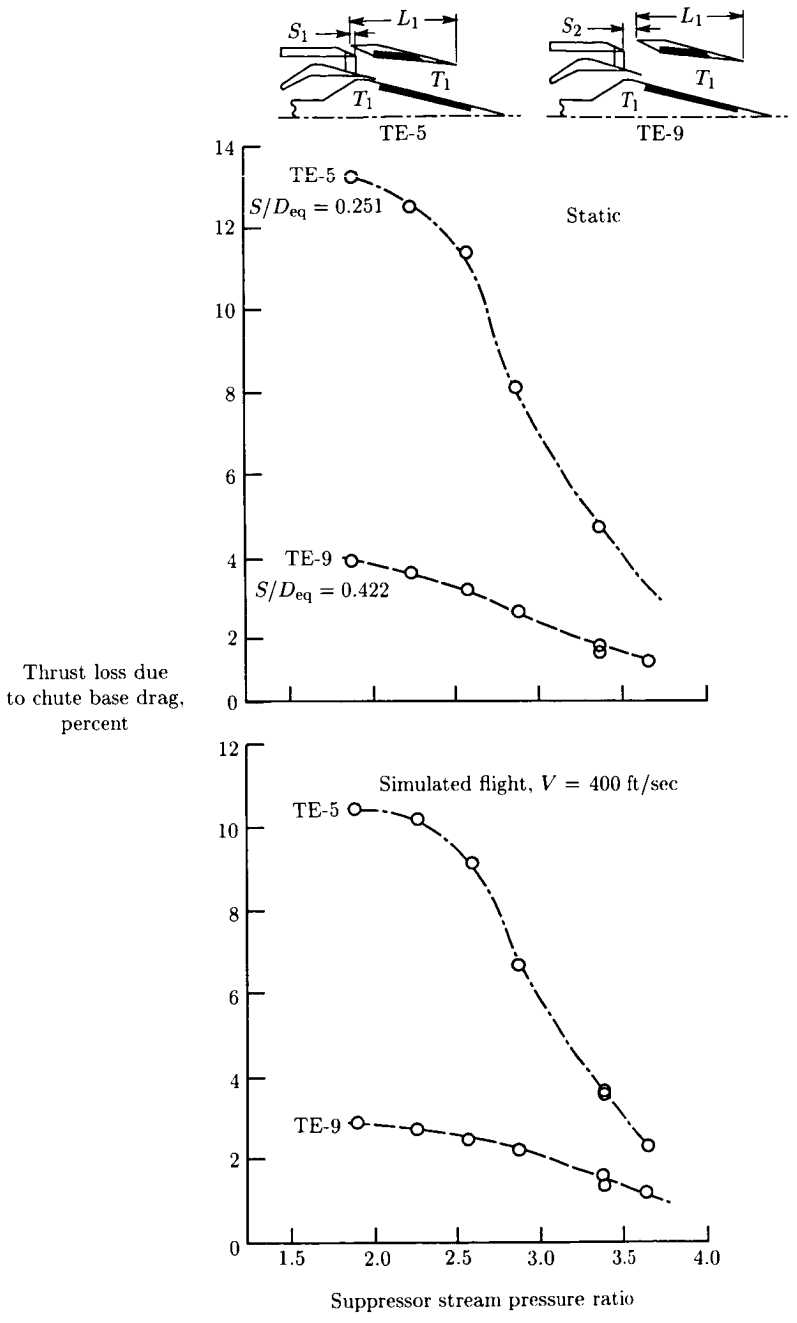

Figure 33. Influence of ejector spacing on base drag of 20-shallow-chute suppressor nozzle (dual flow). (Based on ref. 25.)

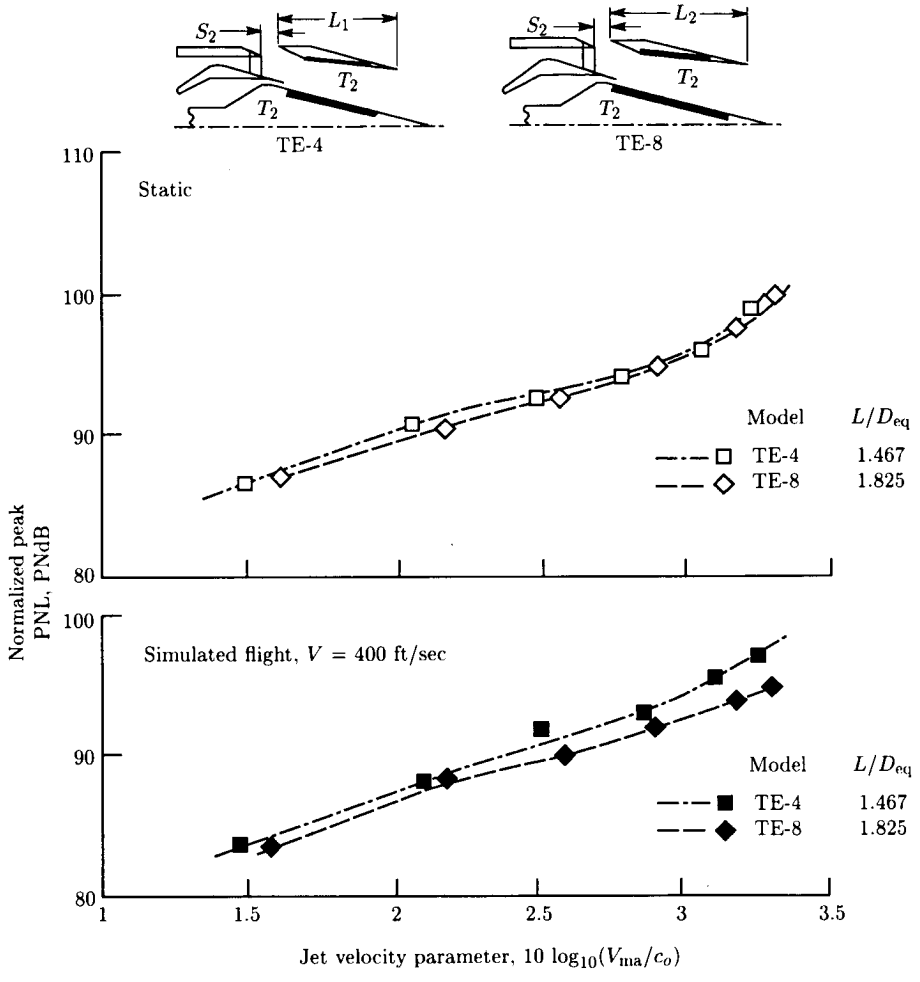

Figure 34. Influence of ejector length on normalized peak PNL of 20-shallow-chute suppressor nozzle (dual flow). 2400-ft sideline; A_T = 1400 in^2; standard day (59° F, 70 percent relative humidity). (Based on ref. 25.)

For a given flow area, as the plug nozzle radius ratio increases, annular height decreases and outer radius of nozzle increases. The noise reduction capability of plug nozzles is ascribable to the following:

1. Larger surface area is available for shear with ambient air than in the conical nozzle.
2. Additional surface (i.e., plug) is available for shearing the jet.
3. Smaller characteristic dimension (i.e., annulus height) is present in the high-jet-velocity region, and this smaller dimension implies the jet decay and shock structures are governed by annulus height rather than by the equivalent-flow-area circular nozzle diameters close to the exit plane. The annulus height being the characteristic dimension in the high-velocity region results in an acoustic power level spectrum with more high-frequency content than for

a circular nozzle. As in the case with multielement suppressors, the high-frequency acoustic content suffers larger atmospheric attenuation with plug nozzles than with circular nozzles to yield the observed noise reductions.

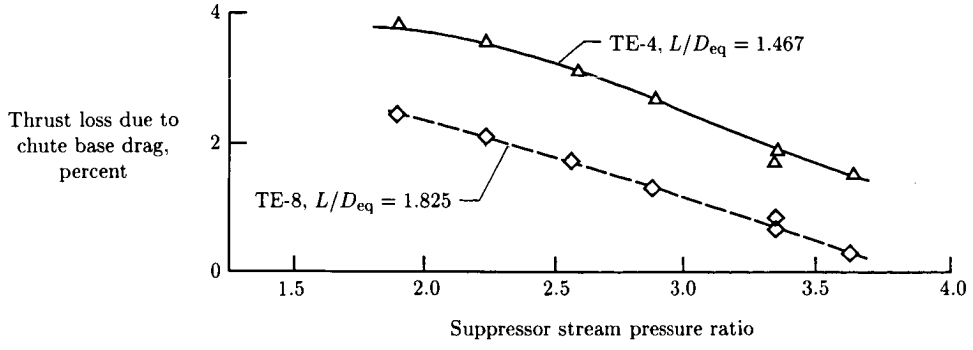

(a) Static.

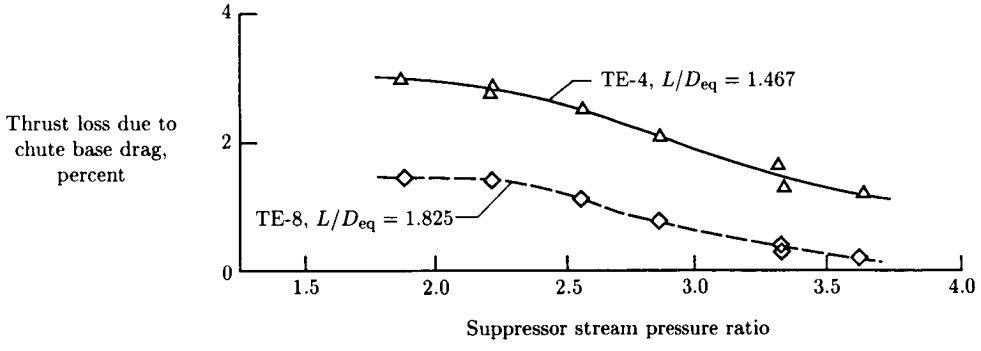

(b) Simulated flight, V = 400 ft/sec.

Figure 35. Influence of ejector length on base drag of 20-shallow-chute suppressor nozzle (dual flow). (From ref. 25.)

Figure 37 (from ref. 26) shows the noise reduction characteristics of annular plug nozzles compared with those of the conical nozzle over a range of jet velocities in the aft quadrant (shown as normalized peak OASPL), which is dominated by jet noise, and in the forward quadrant (shown as normalized 50° OASPL), which is dominated by broadband shock-cell noise. As radius ratio R_r increases, the normalized peak OASPL decreases. The trend of shock-cell noise (normalized 50° OASPL) with radius ratio is not very clear. High-radius-ratio plug nozzles which have a blunt tip tend to have two shock structures at high pressure ratios, one on

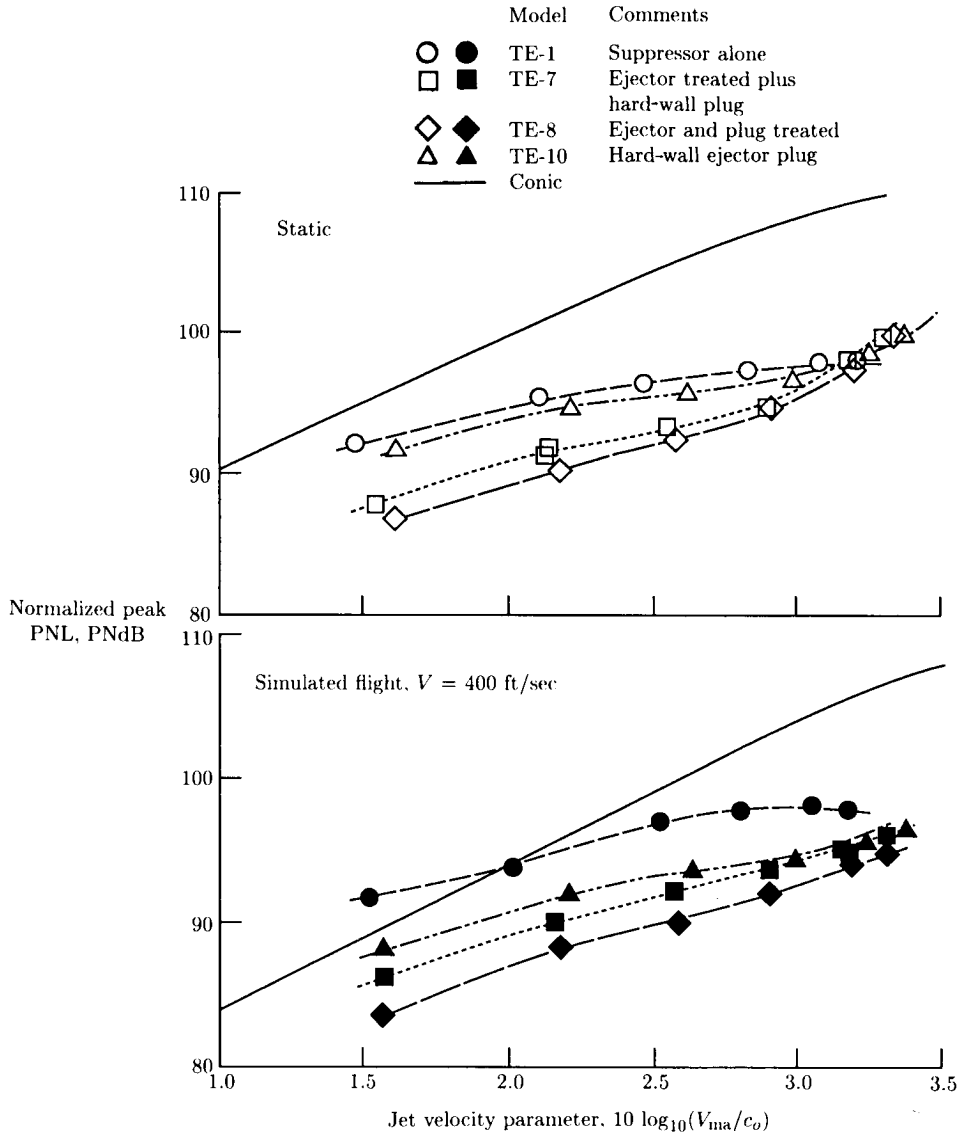

Figure 36. Influence of acoustic treatment attached to ejector and/or plug surface on peak PNL of 20-shallow-chute suppressor nozzle (dual flow). 2400-ft sideline; A_T = 1400 in^2; standard day (59°F, 70 percent relative humidity). (From ref. 25.)

the plug surface (characterized by annulus height) and another downstream of the plug surface due to a supersonic flow expansion fan around the blunt tip. When the downstream shock gets reflected from the jet shear layer it induces a train of shock-cell structures downstream of the plug. The downstream shock structure is typically characterized by the equivalent circular nozzle diameter. Thus, the shock

noise contribution observed at $\theta_i = 50°$ consists of contributions from both these two shock structures and a clear trend with radius ratio is absent.

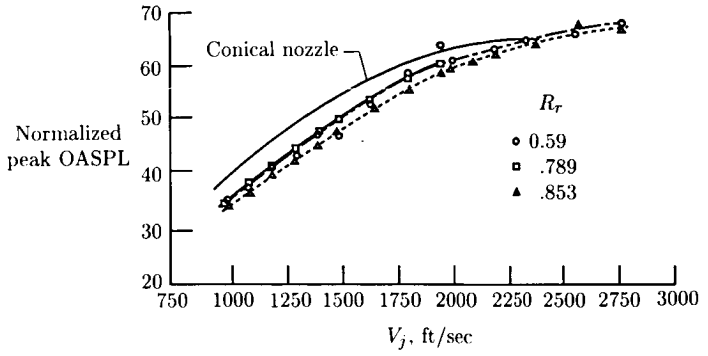

(a) Peak OASPL.

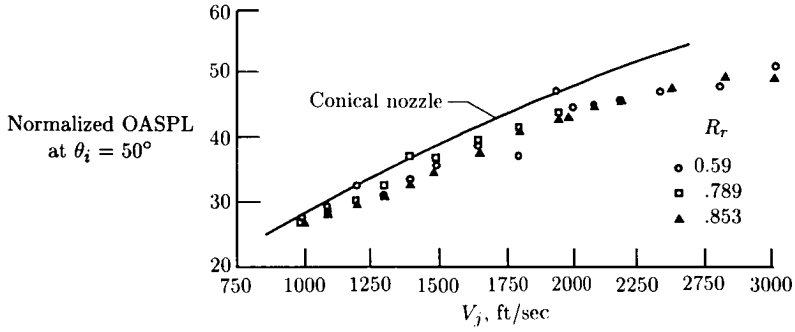

(b) OASPL at $\theta_i = 50°$.

Figure 37. Annular plug nozzle acoustic characteristics as function of radius ratio. 2400-ft sideline; $A_T = 338$ in^2. (From ref. 26.)

High-radius-ratio plug nozzles have preferred noise characteristics. However, a higher radius ratio for a given flow area dictates a larger nacelle diameter with the accompanying weight and nozzle afterbody drag penalties. A value of 0.853 is considered to be the practical limit for the radius ratio. Elimination of shock structures on the plug surface and downstream of the plug is discussed in the section entitled *Shock Noise Control.*

Two-dimensional nozzles (also called rectangular nozzles) are gaining applications in military aircraft because of their thrust-vectoring capability. Two-dimensional nozzles are characterized by their aspect ratios (defined as width/height). At sufficiently high aspect ratios (typically larger than 6), the flow near the exit plane of the jet exhibits a 2-D character. Two-dimensional nozzles tend to be generally quieter

than equivalent circular conical nozzles, essentially because of the increased surface area available for shear with the ambient air compared with that of an equivalent circular conical nozzle. Two-dimensional nozzles exhibit azimuthal variation and the plane containing the minor axis is louder than the plane containing the major axis, particularly in the high-frequency region. The 2-D jet flow loses its 2-D nature at downstream locations because of jet diffusion, and at distances sufficiently downstream the flow becomes a circular jet. Since low-frequency noise of jets is associated with large, turbulent eddies and large, turbulent eddies of 2-D nozzles are at regions where the jet is circular, low-frequency noise of 2-D jets typically does not show any azimuthal variation.

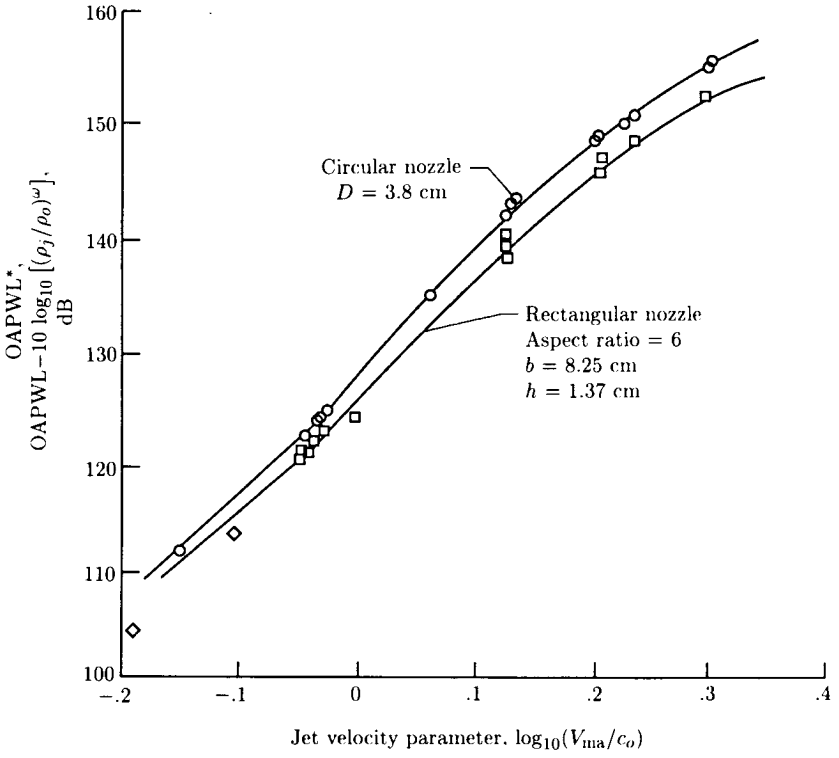

Figure 38. Overall power levels (OAPWL) of circular and rectangular nozzles. (From ref. 9.)

Scale-model tests were performed on rectangular jets (ref. 9), and some of the results are presented in figures 38 and 39 to justify the statement made above. Increasing the aspect ratio of a 2-D nozzle for a constant flow area results in the jet flow retaining its planar nature for larger distances. Also, increasing the aspect ratio for a given flow area reduces the jet height and thus results in a larger velocity gradient in the vertical direction. This larger velocity gradient in turn yields a faster decay of the jet, although the strength of the high-frequency sources (close to the jet exit plane) increases. Reduction in height also results in smaller shock cells, the structure of which extends to a smaller physical length. The smaller shock cells result in lower shock noise levels. Thus, increasing the aspect ratio of a 2-D

nozzle is beneficial acoustically. Mechanical considerations involving airframe-engine integration might limit the aspect ratio.

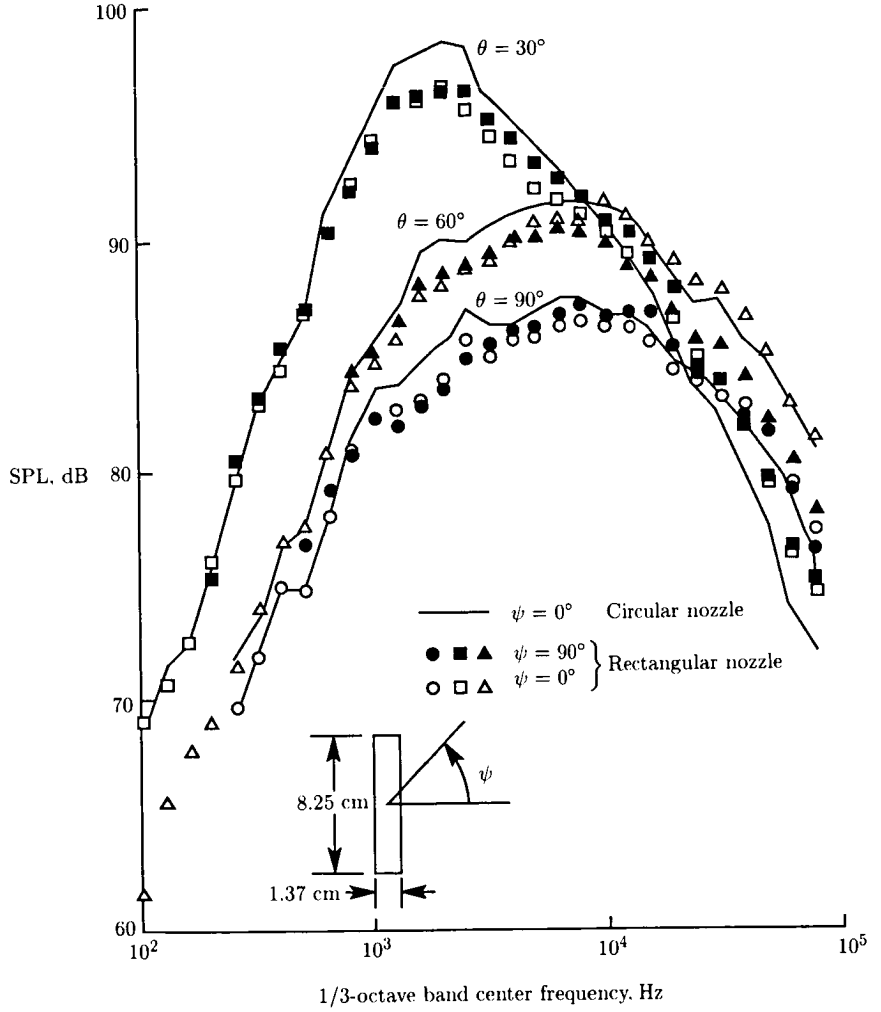

Figure 39. Spectral characteristics of circular and rectangular nozzles. V_j = 966 ft/sec; $T_o = 528°R$. (From ref. 9.)

Aerothermodynamics Concepts

Inverted Flow

The inverted-flow concept employs a nozzle system wherein the cooler, lower velocity jet is surrounded by the hotter, higher velocity jet. This arrangement is the inverse of a conventional turbofan nozzle system. By surrounding the hotter, higher velocity jet on one side by the cooler, lower velocity jet and on the other side

by the ambient airstream, one is generating a mean velocity gradient (and hence shearing stress) on both sides of the principal noise-generating jet which results in a faster decay of the jet plume. However, as noted with multielement suppressors or plug nozzles, higher shear stress in the vicinity of the jet exhaust plane results in higher acoustic source strength close to the jet exhaust plane (high-frequency content), and by virtue of atmospheric absorption this results in lower perceived noise levels in the far field. A faster decaying jet has a lower contribution to the low-frequency portion of the spectrum. The application of a high-radius-ratio plug nozzle in conjunction with an inverted-velocity profile accentuates the shifting of acoustic energy into higher frequencies.

Figure 40 presents data from reference 27. Figure 40(a) shows a design concept for obtaining an inverted-flow-velocity profile in conjunction with a high-radius-ratio plug nozzle. Figures 40(b) and 40(c) show acoustic data in the aft and forward quadrants in terms of PNL for various combinations of plug radius ratio and inner/outer area ratios A_i/A_o over a range of mass-averaged jet velocities $\left(V_{\text{ma}} = \frac{w_o v_o + w_i v_i}{w_o + w_i}\right)$ and also over a range of "averaged" shock strength parameters β. This parameter is defined as $\sqrt{M^2 - 1}$, and M is based on mass-averaged flow conditions. Substantial reductions in jet as well as shock-cell broadband noise are shown for the coannular nozzle for a wide range of plug radius ratios and area ratios.

Figures 40(d) and 40(e) show the noise reduction potential of a representative coannular nozzle ($A_i/A_o = 0.2$ and an outer stream radius of 0.853) in terms of PNL directivity and of spectral characteristics at three observer angles. Acoustic suppression in the aft quadrant and at 90° is attributable to the jet source modification by the inverted flow, whereas suppression in the forward quadrant is attributable to the modified shock structure (i.e., one set of shock cells on the plug and another set of shock cells downstream of the plug).

The inherent acoustic suppression associated with the inverted-flow concept has been demonstrated in a design wherein a duct burner in the fan stream accelerates the fan stream to a velocity higher than that of the core stream. (See ref. 28.)

Thermal Acoustic Shield

A high-temperature, low-velocity gas stream (termed a thermal acoustic shield, TAS) surrounding the principal jet yields jet noise reduction because of the acoustic wave refraction and reflection that occurs due to the impedance change at the interface between the principal jet and the TAS. Figure 41 (from ref. 29) schematically illustrates the concept of TAS wherein the high-frequency noise that is generated near the jet exit plane is either refracted away from the observer or undergoes multiple reflections within the TAS, and a weakened acoustic signal reaches the observer. Certain combinations of the velocity and speed of sound in the principal jet and the TAS yield a total internal reflection of the sound from the observer. The condition for total internal reflection is given by Snell's law as applied to the moving media.

The noise reduction potential of the TAS decreases for sources which are located far downstream from the jet exit plane since the TAS mixes with the principal jet and thereby is not able to maintain a sufficient level of discontinuity in the acoustic impedance. In other words, the TAS is not effective in reducing low-frequency noise.

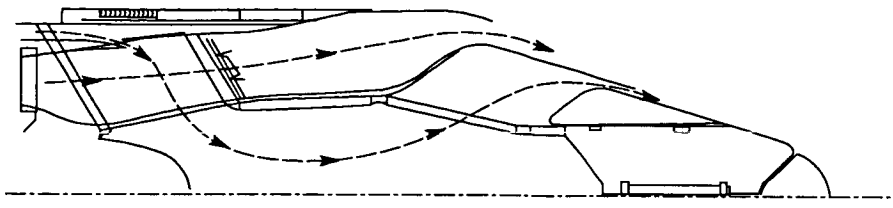

(a) Schematic.

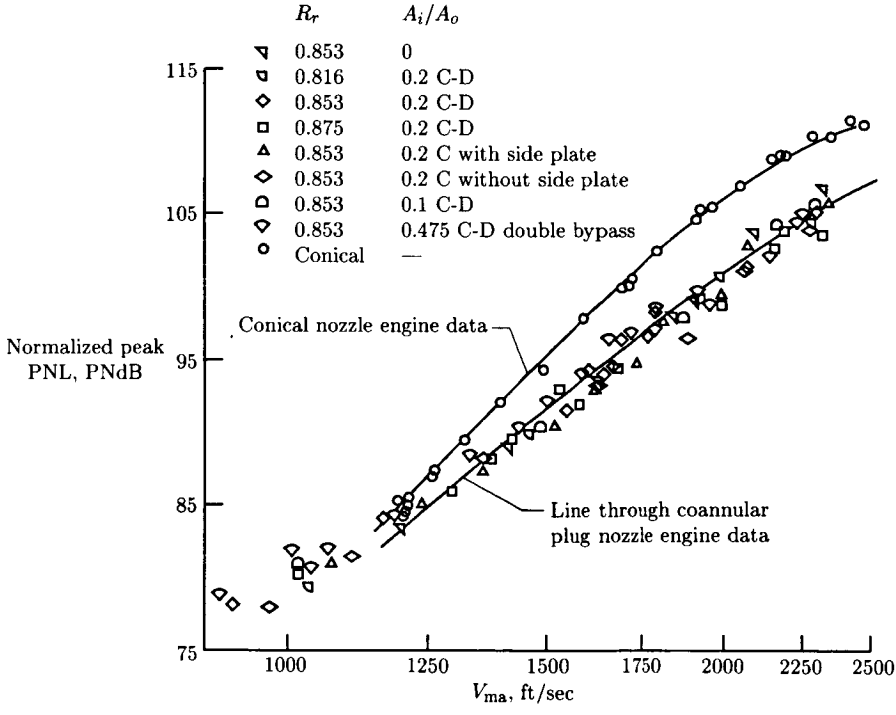

(b) Peak PNL for various radius ratios and area ratios.

Figure 40. Schematic and acoustic characteristics of coannular nozzles with inverted-velocity profile. 2400-ft sideline; $A_T = 1400$ in^2. (From ref. 27.)

Thus, the TAS concept is more effective when used in conjunction with multielement suppression concepts which have a dominant high-frequency content.

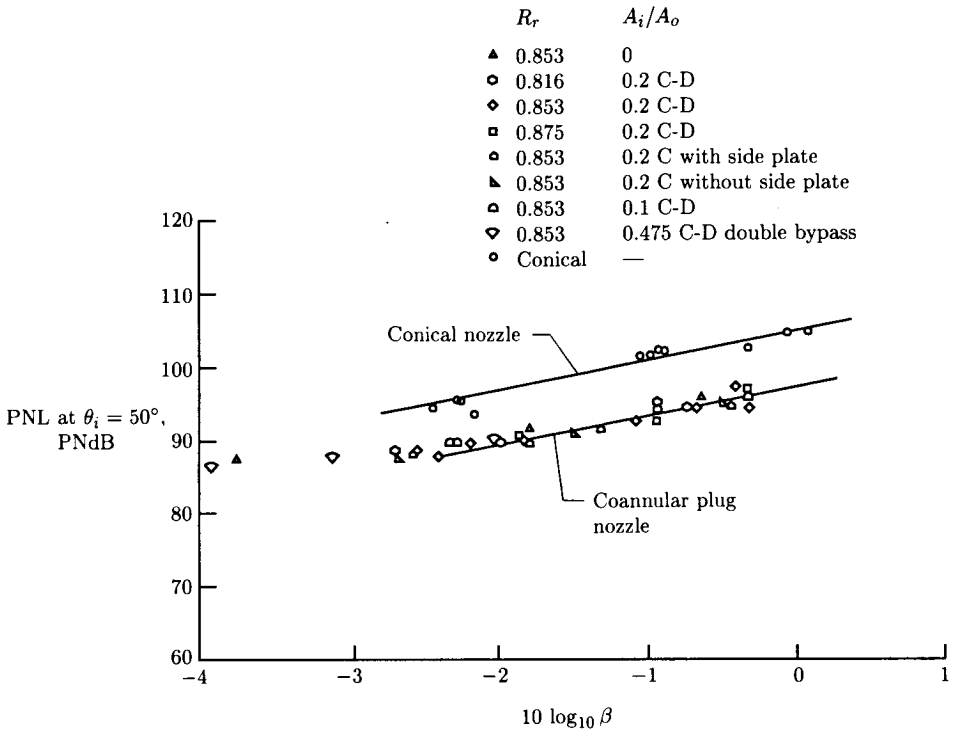

(c) PNL at $\theta_i = 50°$ for various radius ratios and area ratios.

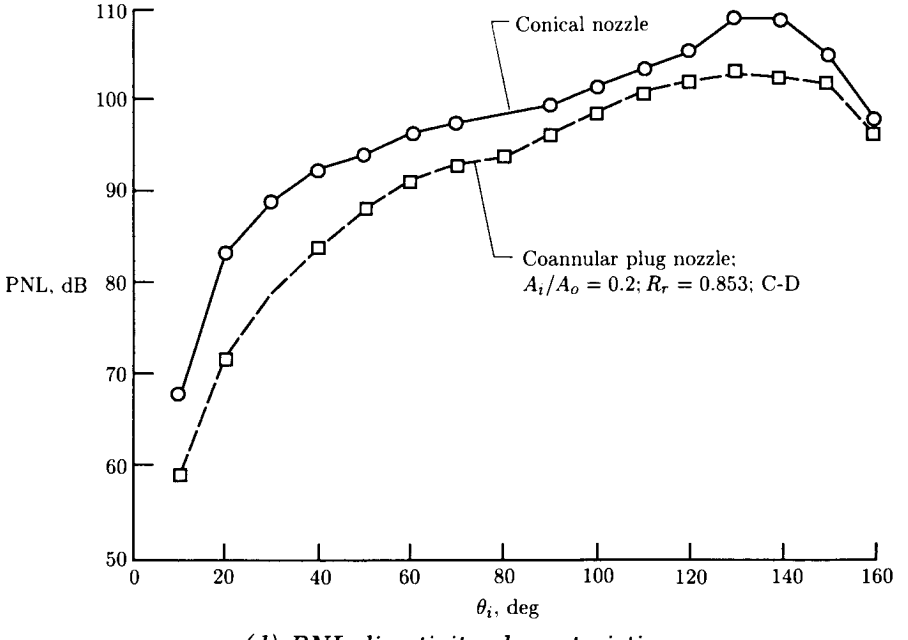

(d) PNL directivity characteristics.

Figure 40. Continued.

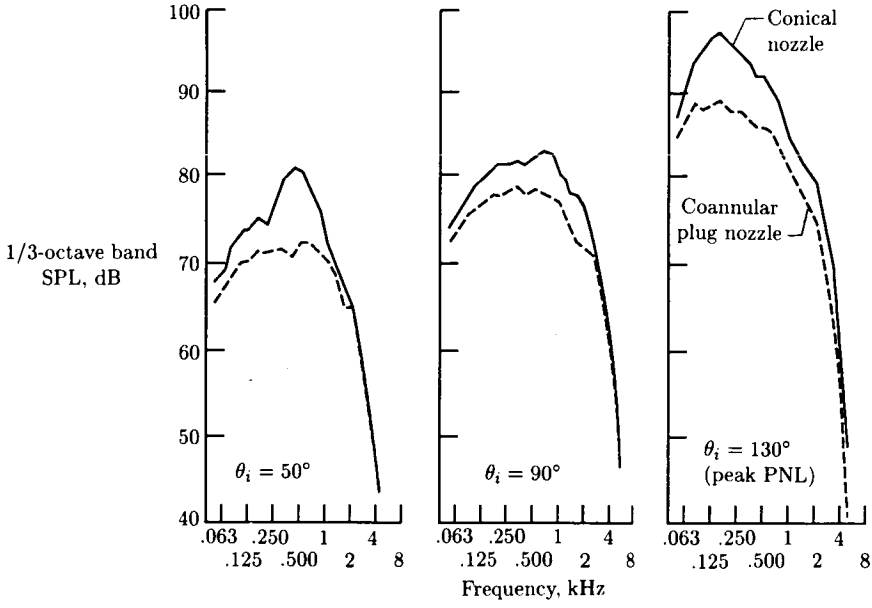

(e) Spectral characteristics.

Figure 40. Concluded.

Early experimental investigations of the TAS concept for unsuppressed nozzles (refs. 30 to 32) have shown impressive reductions in noise levels. Further detailed studies (refs. 29 and 33) involved TAS applications to single- and dual-flow nozzles with and without multichute suppression devices. Results from application of a 180° shield on an annular plug nozzle with a radius ratio of 0.85 and to a 32-chute annular plug suppressor with a suppressor radius ratio of 0.62 are shown in figure 42. The data show spectral suppression obtained by the TAS for typical advanced supersonic transport (AST) approach, cutback, and takeoff cycle conditions. Very significant suppression of high-frequency noise in the aft quadrant is shown with the 180° shield applied to both systems. The sharp increase in suppression in the aft quadrant ($\theta_i \geq 120°$) is due to a total internal reflection of the sound waves of the primary jet by the shield. Noise suppression occurs in the forward quadrant and at $\theta_i = 90°$ because velocity and temperature gradients of the core jet are reduced by the shield, thereby reducing eddy source strength close to the exit plane. The reduction in shielded velocity gradient, however, lengthens the jet plume, and this reduction in turn leads to low-frequency amplification, as particularly noted for the suppressor configuration. The TAS impacts acoustic source modification more effectively for the 32-chute suppressor than for the annular plug nozzle, as evidenced by the noise reduction due to TAS at $\theta_i = 90°$ in figure 42. This suppression is another indication that TAS is more effective on noise sources located closer to the jet exit plane. The increased effectiveness on high-frequency jet noise sources also implies a significant reduction in mean velocity gradient, and this reduction in turn results in significant growth of the plume and causes low-frequency amplification.

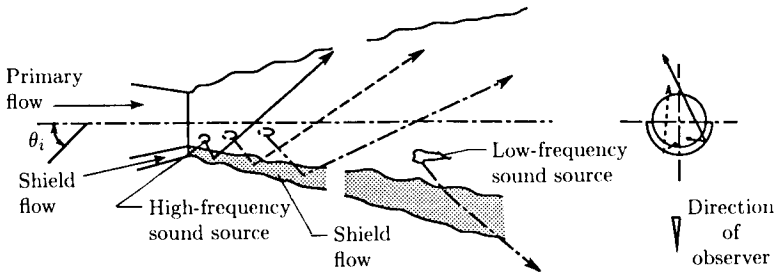

(a) Semiannular (180°) shield.

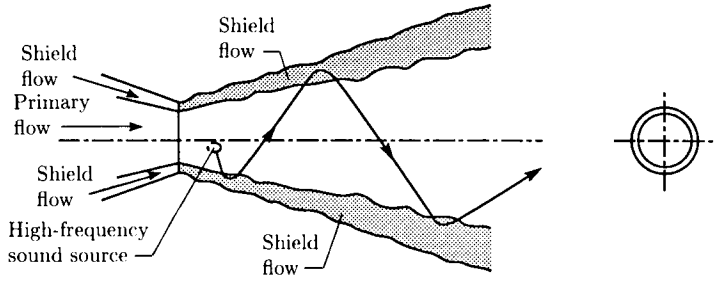

(b) Annular (360°) shield.

Figure 41. Schematics of 180° and 360° thermal acoustic shield nozzles on circular jet. (From ref. 29.)

Figure 43 shows the influence of a 180° TAS on an annular plug nozzle and on a 32-chute suppressor nozzle in terms of PNL directivity. A 2.5-dB reduction in peak PNL levels and a 4-dB reduction in PNL are shown for the front quadrant of the annular plug nozzle with the TAS. For the 32-chute suppressor nozzle with the TAS, an 8-dB reduction in peak PNL and slightly less than an 8-dB reduction in PNL for the front quadrant are shown. These reductions indicate significantly more noise suppression obtained by the TAS on multielement suppressor nozzles than on the annular plug nozzles.

General experimental trends that evolved from the TAS studies (refs. 29 and 33) are as follows:

1. Partial shields yield higher noise reduction than full shields.
2. Increasing the thickness of the shield increases the noise reduction.
3. Noise reduction potential of TAS reduces as the core jet velocity increases above 671 m/sec (2200 ft/sec) for annular plug nozzles and above 732 m/sec (2400 ft/sec) for chute suppressor nozzles.
4. The TAS yields higher PNL reductions for multielement suppressor nozzles than for annular plug nozzles.

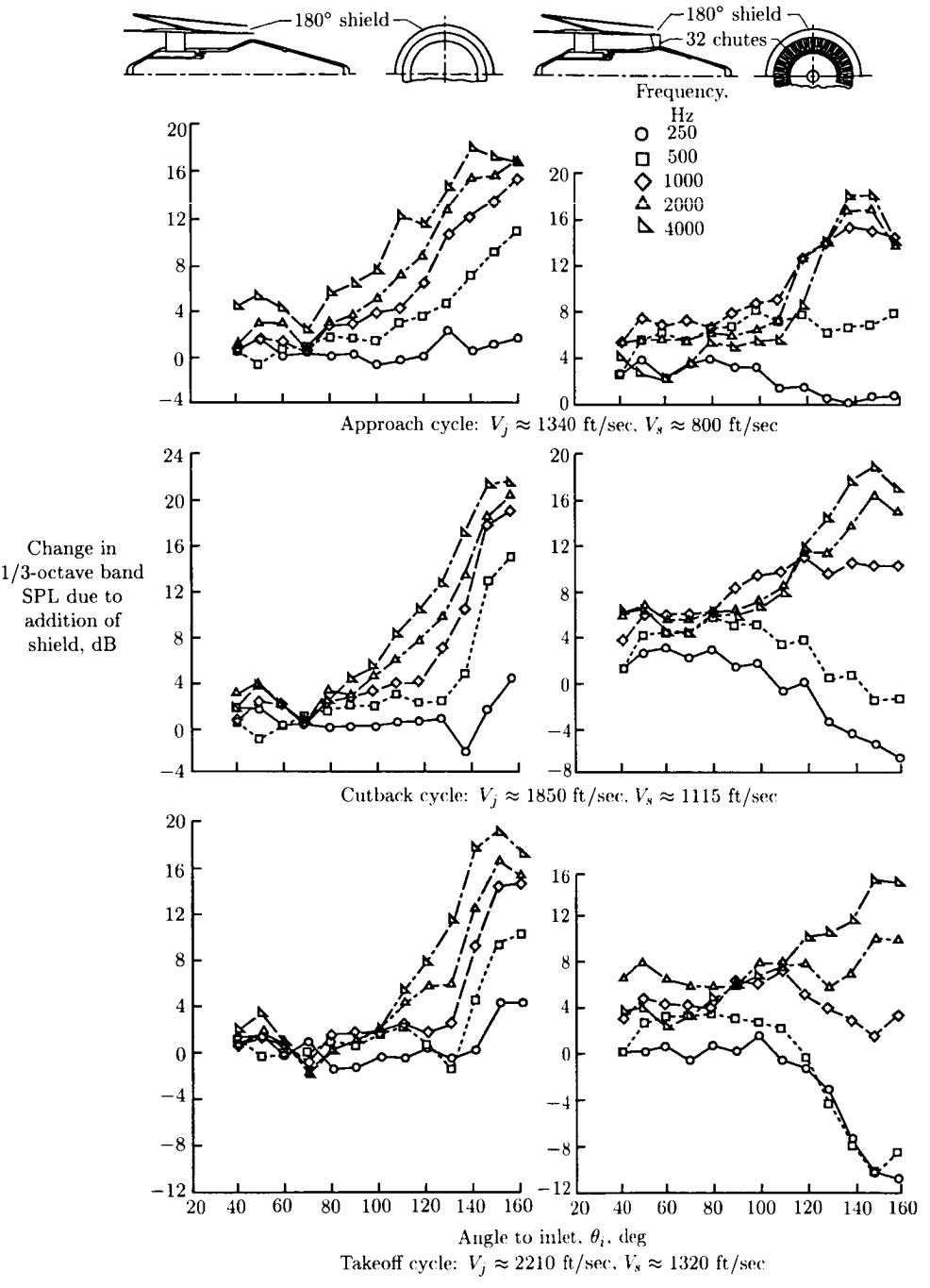

Figure 42. Influence of 180° TAS (0.97 in. thick) on directivity of various 1/3-octave bands for unsuppressed and mechanically suppressed annular plug nozzles. $A_T = 1400$ in^2; static operation. (From ref. 33.)

A TAS system can be implemented through various techniques, the end requirement being a stream of heated gas or air to surround the noisy jet. One method of implementation is to derive the TAS by bleeding the high-temperature gas from the main jet and throttling it through choke plates to reduce jet velocity and achieve a shield to the main jet velocity ratio of ≈ 0.4 to 0.6. This shield removes the energy from the main jet, so the engine throttle must be advanced to compensate for thrust loss. For AST engines this would be feasible, as they are normally sized by thrust requirements at operation points other than the takeoff condition (e.g., cruise).

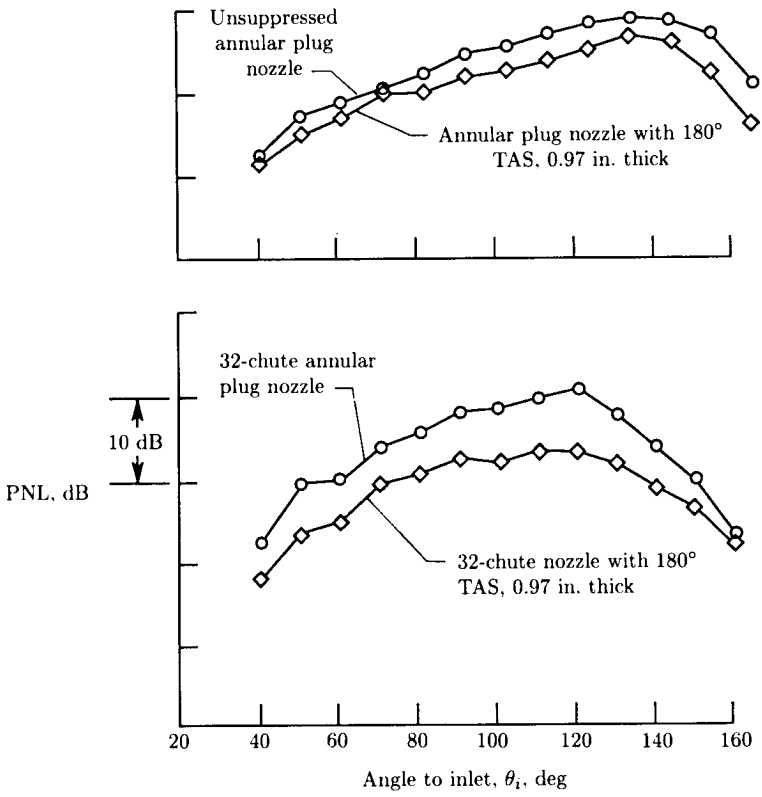

Figure 43. Influence of TAS on PNL directivity of unsuppressed annular plug and 32-chute suppressed nozzles at cutback cycle. $A_T = 1400$ in^2; 1000-ft flyover distance; static operation. (Based on ref. 33.)

Impact of a bleed-flow-type TAS was evaluated in an implementation study (ref. 33; see fig. 44). When thrust loss incurred by the bleed system is compensated for, the 180° TAS applied to the annular plug nozzle negates the benefit of the plug nozzle compared with the conical nozzle. Adding the 180° TAS to the 32-chute suppressor results in some benefit, even with the thrust loss, at lower thrust levels and results in some loss of benefit at the higher thrust levels. The study pointed out that a bleed-type system for TAS implementation would be of limited value.

An alternate method is to supply the TAS from an independent source of hot gas. This would add thrust to the overall system instead of degrading thrust by bleeding and would allow the main jet to be throttled back to a lower noise level thrust setting

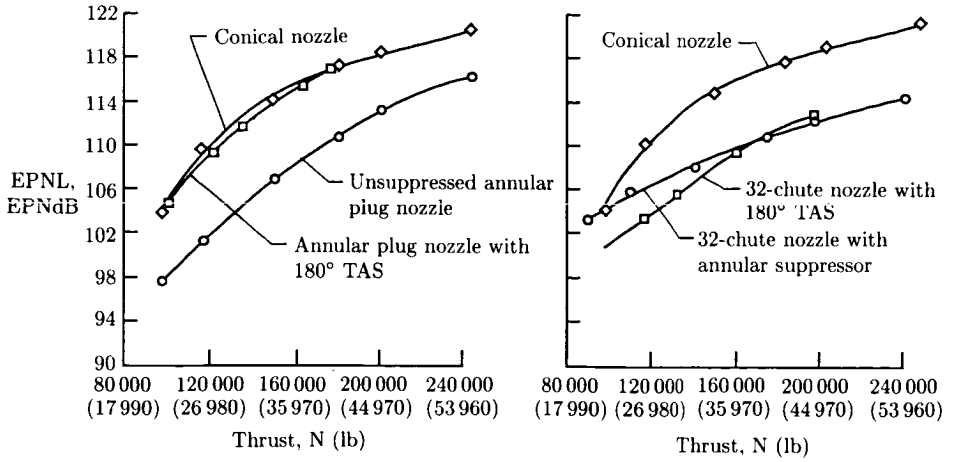

Figure 44. Integration study results of TAS implementation by bleeding. 305-m (1000-ft) level flyover at V = 122 m/sec (400 ft/sec). (From ref. 33.)

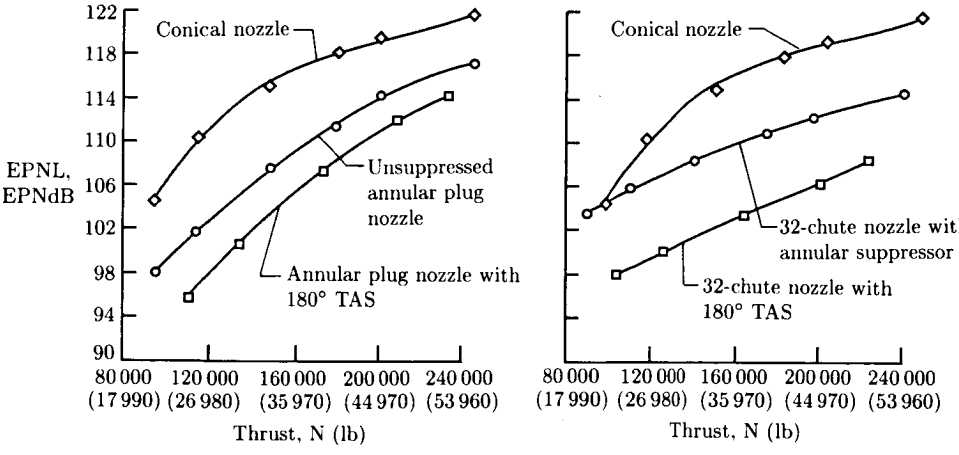

Figure 45. Integration study results of TAS implementation by independent source for shield flow. 305-m (1000-ft) level flyover at V = 122 m/sec (400 ft/sec). (From ref. 33.)

for takeoff. As noted from the results of the AST implementation study (ref. 33) presented in figure 45, this type of system has very significant advantages. For the 32-chute suppressor, jet noise levels are lowered to the point where other engine noise sources for an AST system could become the dominant noise source. A substantial effort is needed to cleverly implement an independent source of TAS that would not impose excessive weight and drag penalties.

Shock Noise Control

Shock-cell broadband noise can be a significant contributor to the total noise radiated by jets operating at supercritical pressure ratios, particularly in the forward

quadrant, where jet mixing noise is lower. Experimental observations (refs. 9, 34, and 35) indicate that the shock-cell broadband noise is amplified in the forward quadrant due to flight. Nonisentropically expanded supersonic jets contain shock-cell structures which are formed from oblique compression and expansion waves for significant lengths of the jet plume, which is the physical means by which the static pressure balance is achieved between the jet and the ambient air. Interaction of turbulent eddies of the jet with the shock-cell structure results in acoustic waves termed shock-cell broadband noise. Shock noise control is obtained essentially by either eliminating or weakening the shock-cell structure by

1. Aerodynamic design of the convergent-divergent (C-D) nozzle flow path
2. Plug structure modification for annular and dual-flow coannular plug nozzles
3. Proper choice of pressure ratios for operation of dual-flow nozzles

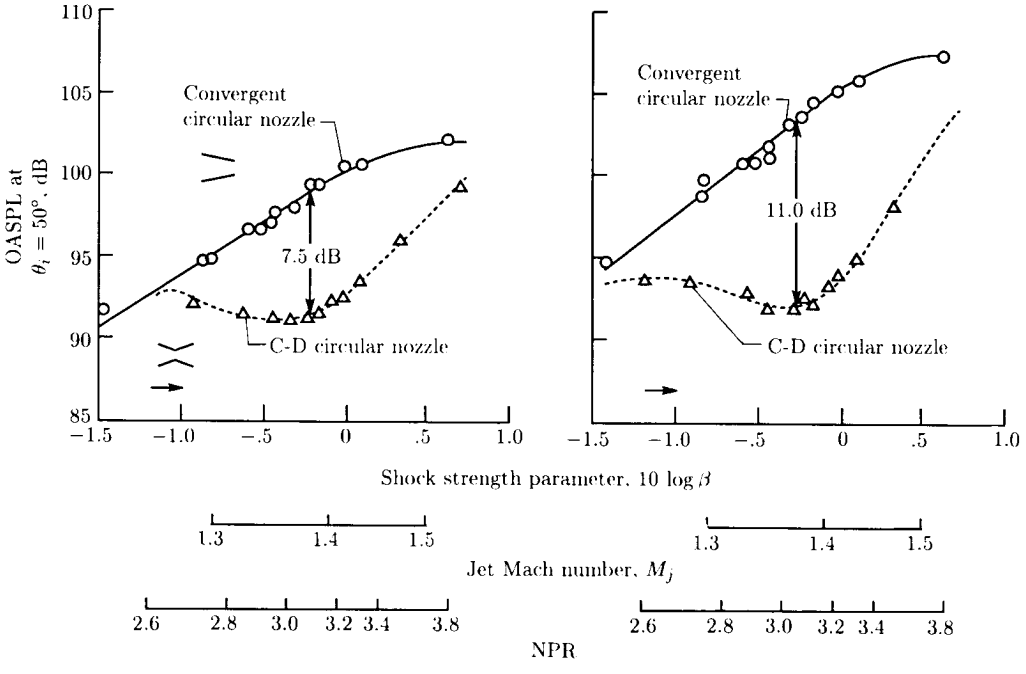

(a) Effectiveness of C-D flow path on circular nozzle in reduction of shock-cell noise. Data scaled to $A_T = 1400$ in^2 and extrapolated to 2400-ft sideline; $T_T = 1700°R$.

Figure 46. Shock-cell noise reduction of C-D nozzle and of convergent circular nozzle. (From ref. 36.)

For the simple circular nozzle, the convergent-divergent design for isentropic flow expansion can be employed to eliminate the shock-cell structure in the jet at the design Mach number and thereby obtain shock noise reduction. Figure 46(a) (from ref. 36) shows the region of effectiveness of a circular C-D nozzle and of a convergent circular nozzle in controlling shock noise at and in the vicinity of the design Mach number of 1.4 (at a ratio of total to static pressure of 3.12 and a total temperature of 944 K (1700°R)). The OASPL reductions of 7.5 and 11.0 dB for a circular C-D nozzle are shown at the design condition for static and simulated flight at $M = 0.36$. Jet plume velocity data (fig. 46(b)) measured with a laser doppler velocimeter show the absence of the shock-cell structure for the C-D circular nozzle along the nozzle centerline at the design condition, whereas the convergent circular nozzle shows significant shock-cell structure at the same condition. The OASPL directivities shown in figure 46(c) indicate significant noise reduction in the forward quadrant obtained with the C-D circular nozzle for both static and simulated flight conditions.

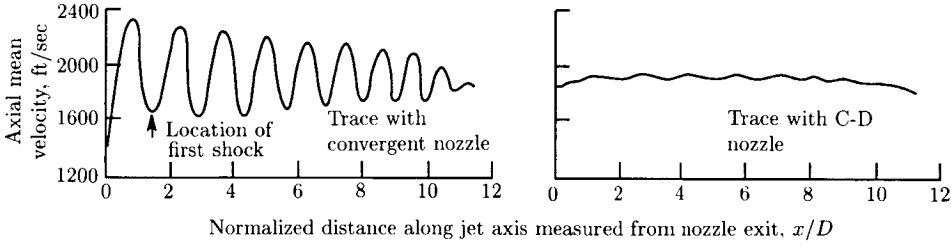

(b) Plume velocity data for conical and C-D nozzles. $V = 400$ ft/sec; $T_T = 1720°R$; $NPR = 3.12$.

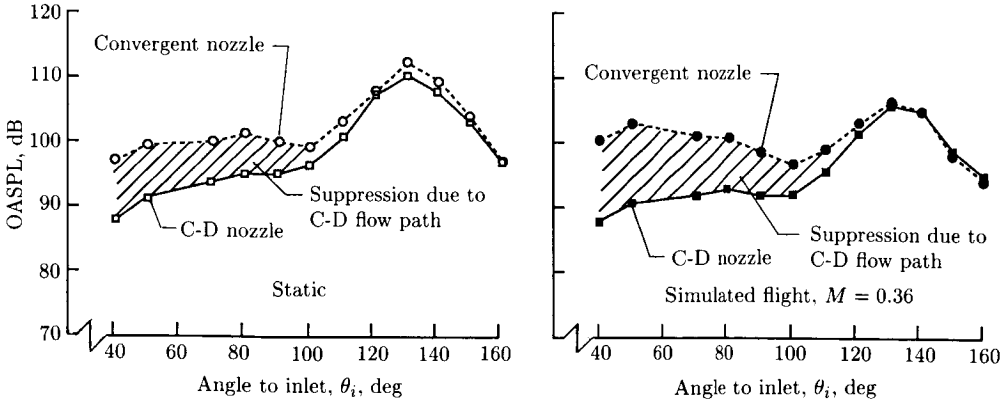

(c) OASPL directivity of convergent and C-D nozzles at C-D nozzle design conditions.

Figure 46. Concluded.

Next, the application of shock noise control techniques for annular and dual-flow coannular plug nozzles is discussed. When nozzles employing truncated plugs (i.e., plugs with a finite base area) are operated at highly underexpanded conditions, the jet plume has two shock-cell structures, one on the plug surface and one downstream of the truncated plug. The reason for two structures is that at highly underexpanded conditions, the shock-cell structure on the plug has not been able to slow the jet plume to subsonic conditions at the end of the plug. As the supersonic jet expands over the truncated plug, an expansion fan is created which reflects off the jet shear layer as an oblique shock which in turn sets up an expansion fan, and so on. This process results in another shock-cell structure downstream of the plug. Hence, shock noise control for nozzles employing plugs must address elimination or mitigation of both the shock-cell structures.

Figure 47(a) (from ref. 36) indicates the effectiveness of a C-D flow path in reducing shock noise for an annular plug nozzle with a truncated plug at or near the design Mach number of 1.44 for both static and simulated flight conditions. Jet plume velocity data both along the plug surface and downstream of the truncated

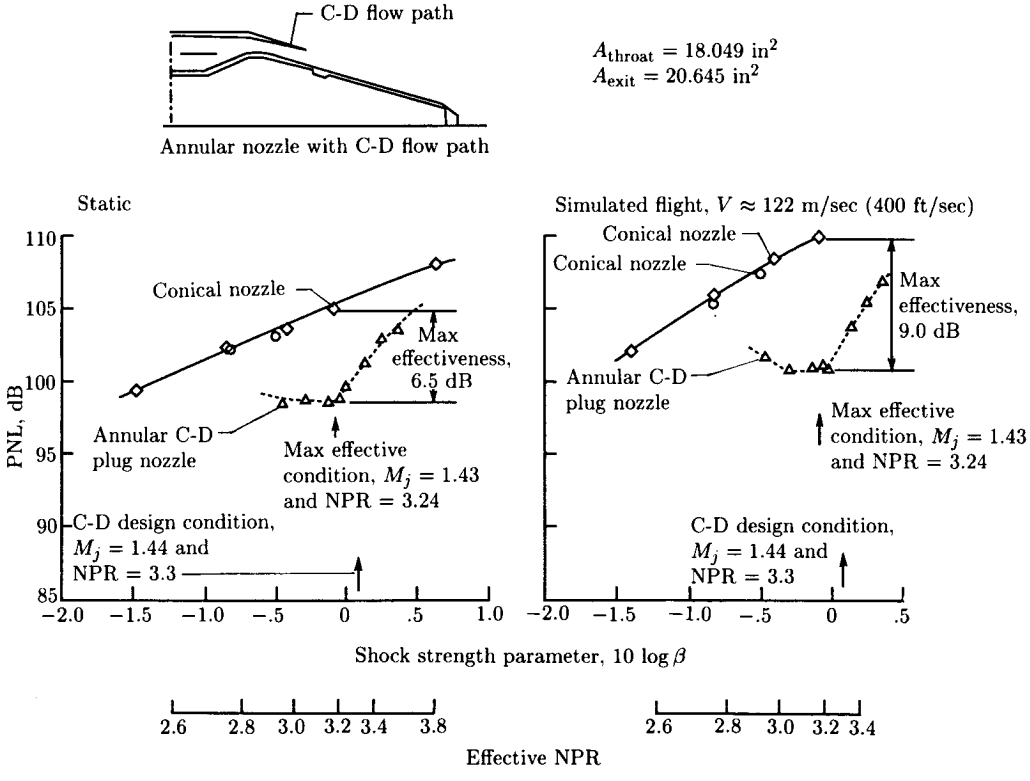

(a) Effectiveness of C-D flow path in shock noise reduction for annular plug nozzle in terms of PNL at $\theta_i = 60°$. Data scaled to $A_T = 0.903$ m^2 (1400 in^2) and 732-m (2400-ft) sideline.

Figure 47. Shock noise reduction for annular plug nozzle with C-D nozzle flow path. (From ref. 36.)

plug at the design Mach number are shown in figure 47(b). The C-D flow path for the annular passage eliminates the shock-cell structure along the plug surface, whereas both the convergent and C-D annular plug nozzles have shock-cell structures downstream of the plug. Since this design did not eliminate both the shock-cell structures, the shock noise control effectiveness of the C-D annular plug nozzle is less than that of the circular C-D nozzle (compare figs. 46(a) and 47(a)).

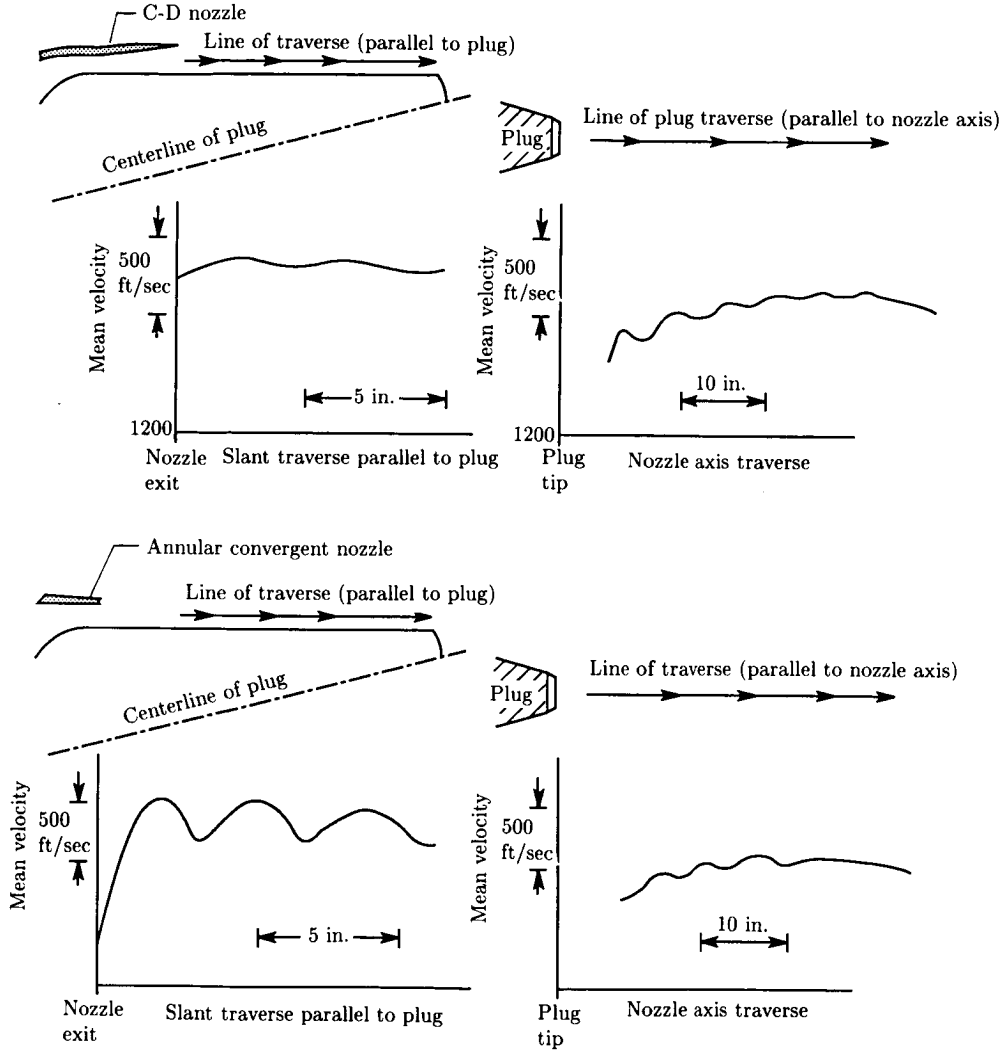

(b) Mean velocity data for C-D annular plug nozzle operating at its design condition.

Figure 47. Concluded.

Shock noise control techniques for dual-flow coannular plug nozzles with inverted velocity profiles are now examined. Figure 48 summarizes the results of shock noise control for dual-flow coannular plug nozzles with C-D flow paths for both inner and outer streams having design Mach numbers of 1.38 and 1.44, respectively. The area ratio of inner stream to outer stream is 0.2. Model 1 employs convergent flow paths

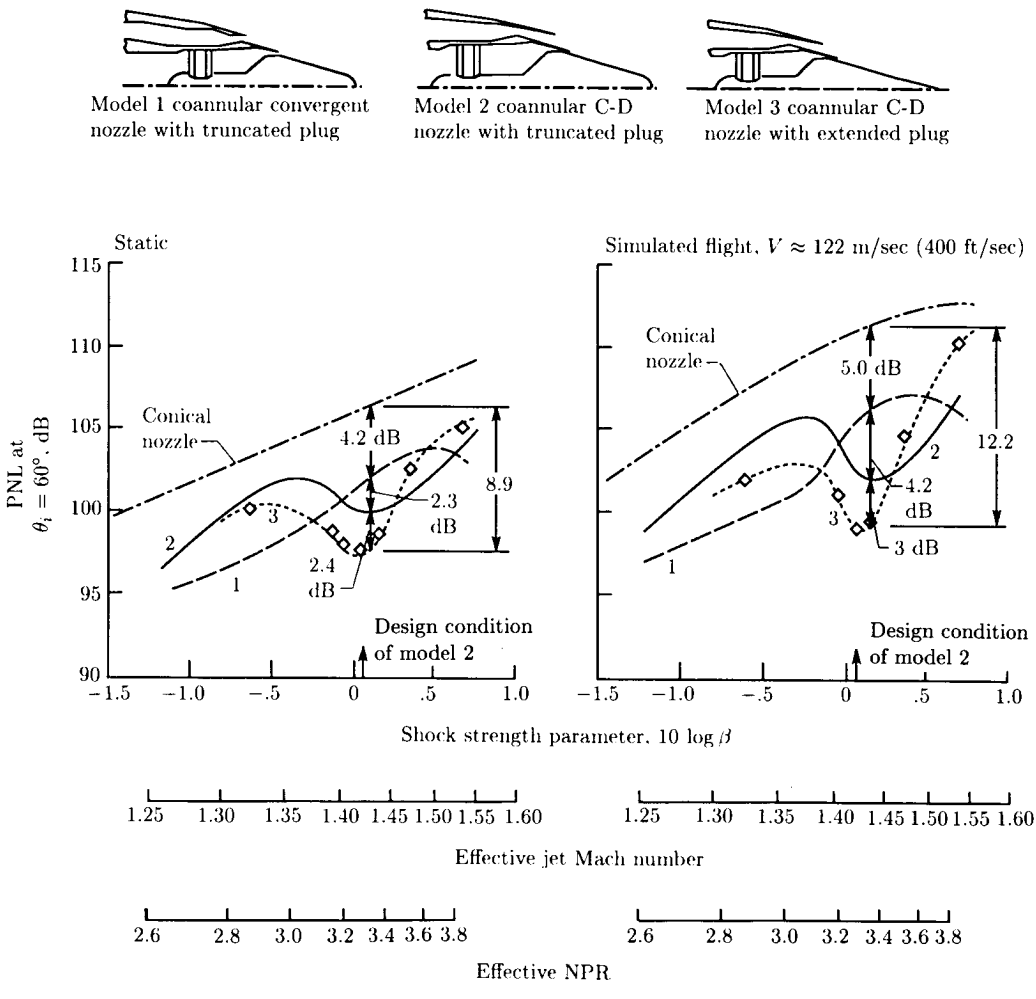

(a) Effectiveness of shock-cell noise reduction for coannular nozzles.

Figure 48. Shock noise reduction for coannular plug nozzle with C-D flow path and plug tip modification. (Based on ref. 36.)

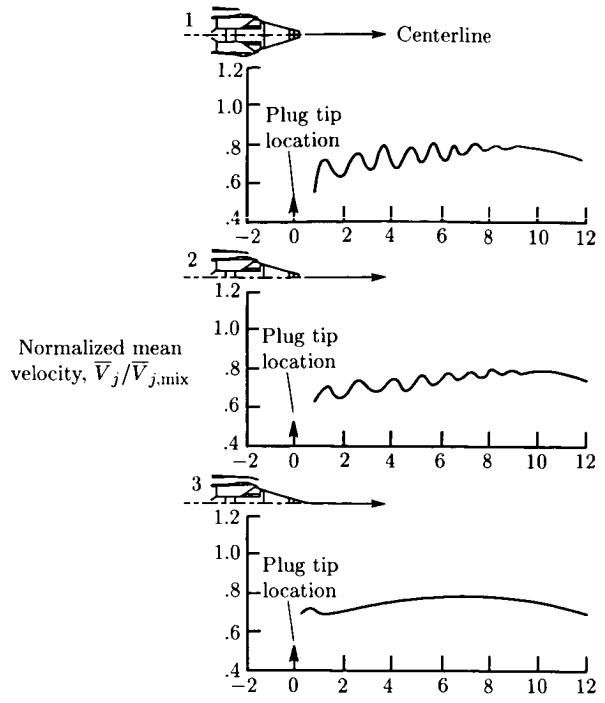

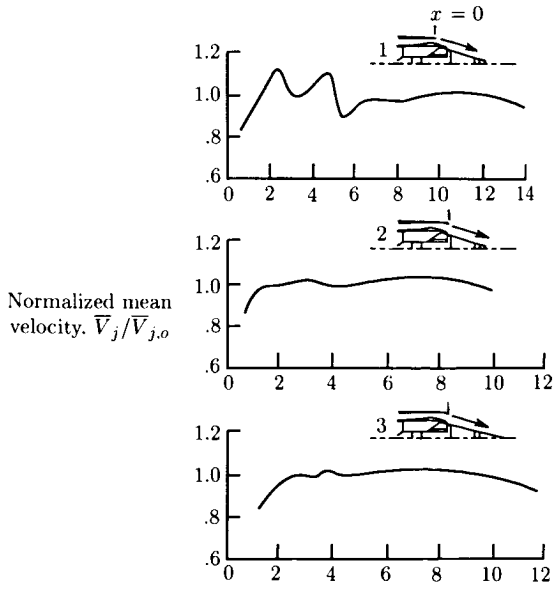

(b) Mean velocity distributions.

Figure 48. Concluded.

for both the streams and a truncated plug. Model 2 employs C-D flow paths for both the streams and a truncated plug, and Model 3 employs C-D flow paths for both the streams and a sharp-tipped plug (i.e., no base region for the plug). Application of C-D flow paths reduces the noise levels at and near the design condition. (See figure 48(a).) The application of a sharp-tipped plug reduces the shock noise further and yields about the same total effectiveness relative to the circular convergent nozzle as does the circular C-D nozzle. The jet plume traces for models 1, 2, and 3 at the design condition indicate the absence of shocks on the plug for models 2 and 3, and this absence is a direct consequence of the C-D flow path. The sharp-tipped plug eliminates shock-cell structure downstream of the plug because of the absence of the expansion fan at the plug tip. (See fig. 48(b).)

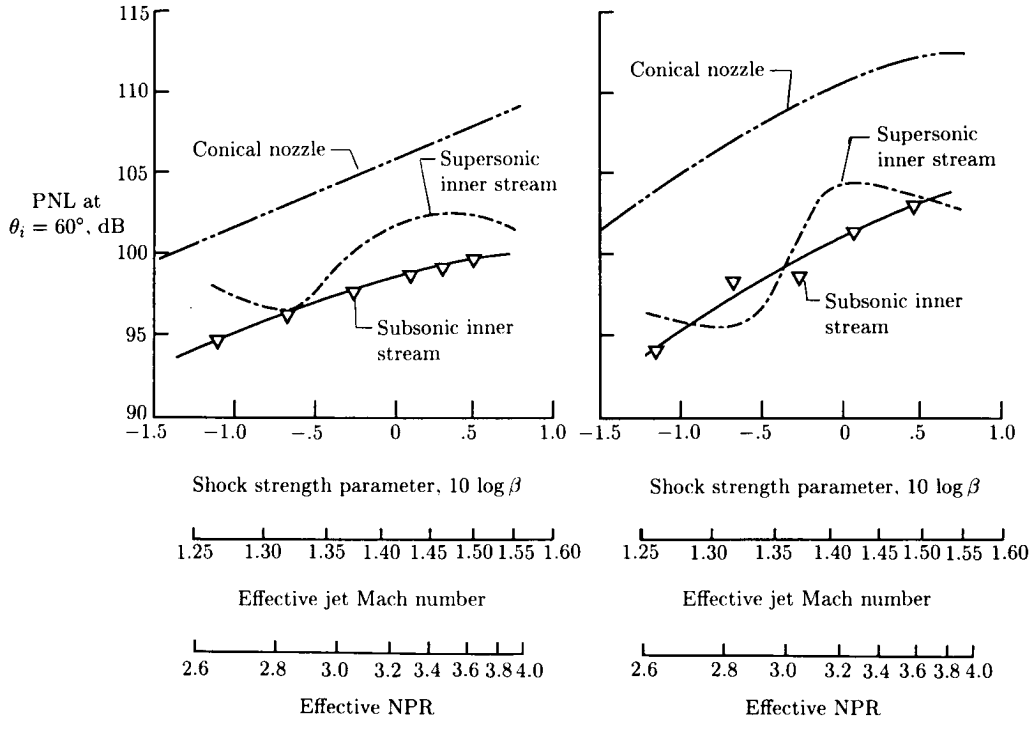

(a) Static.

(b) Simulated flight. $V_{ac} \approx 122$ m/sec (400 fps).

Figure 49. Effectiveness of subsonic inner stream operation on shock noise of coannular extended plug nozzle. Data scaled to $A_T = 0.903\ m^2$ (1400 in^2) and 732-m (2400-ft) sideline. (Based on ref. 36.)

An effective means of flow management and resultant shock structure control for the dual-flow coannular plug nozzles is obtained by operating the inner stream at subcritical pressure ratios. Figure 49 shows the shock noise characteristics obtained with the inner nozzle operated at a fixed pressure ratio of 1.80 for subsonic operation and

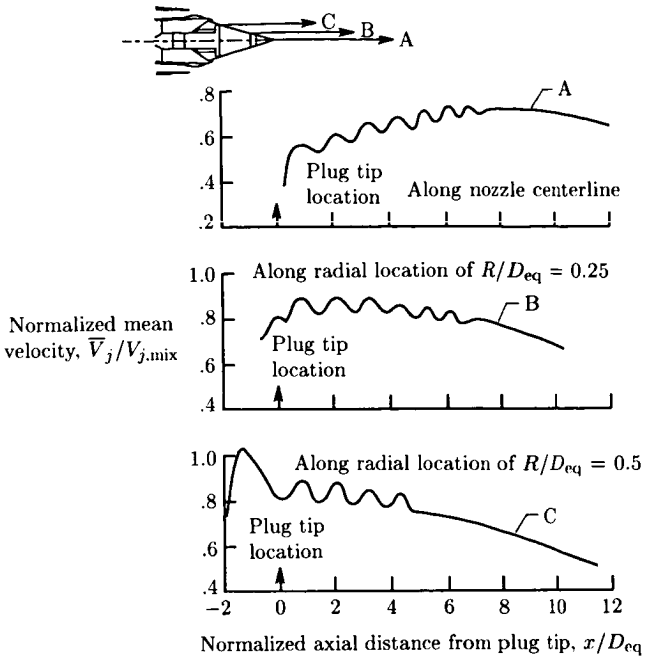

(a) Supersonic inner stream; $NPR_i = 3.14$; $NPR_o = 3.33$; $T_{T,i} = 870°R$; $T_{T,o} = 1670°R$.

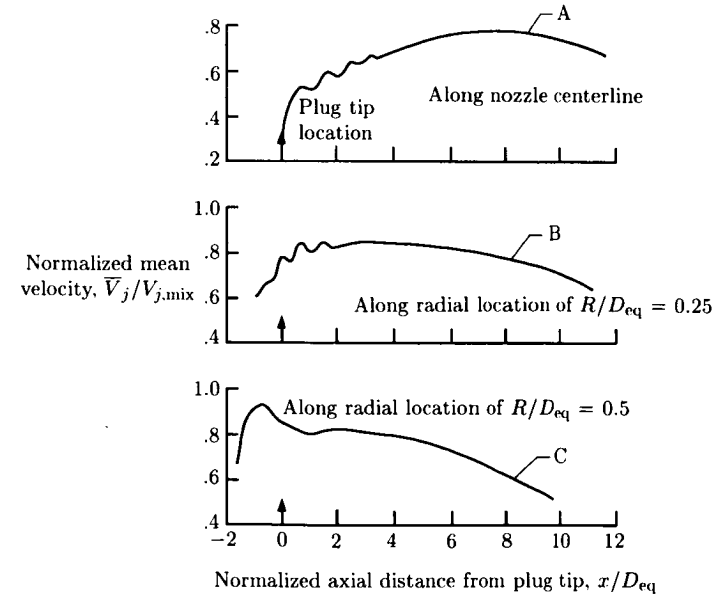

(b) Subsonic inner stream; $NPR_i = 1.80$; $NPR_o = 3.32$; $T_{T,i} = 1280°R$; $T_{T,o} = 1695°R$.

Figure 50. Axial mean velocity distribution of convergent coannular plug nozzle with supersonic and subsonic inner streams. (From ref. 36.)

3.13 for supersonic operation over a range of outer nozzle pressure ratios of 2.5 to 4.0. Significant shock noise reduction is found at *all* conditions with the subsonic inner stream. The subsonic inner stream significantly alters the shock structure downstream of the plug, as indicated by the velocity measurements shown in figure 50, which are indicative of reduced shock-cell noise.

As mentioned previously, multielement suppressors have significantly lowered shock-cell noise because of the associated rapid mixing and shock-cell structure decay and the relatively high frequencies of shock noise of individual elements, which are effectively attenuated by atmospheric absorption. However, if additional shock noise reduction is required, individual elements (such as chutes or spokes) may be designed to have C-D flow paths. (See refs. 36 and 37 for multielement suppressor nozzles with dual- and single-flow applications, respectively.)

Another approach for shock noise control is the porous plug concept, initially proposed by Maestrello (ref. 38). The application of a porous plug, either sealed or vented to the atmosphere, replaces the periodic shock-cell structure noted for nonporous plugs with a series of weak compression waves which yield shock-cell noise reduction.

Of further concern may be shock screech noise. Shock screech noise was first studied by Powell (ref. 39), who proposed the existence of a feedback mechanism between the nozzle exit and the shock cells via the upstream propagation of the acoustic wave generated at the shock cell through the subsonic mixing layer of the jet and reinforcing the feedback loop. Shock screech noise, unlike shock-cell broadband noise, has a pure tone characteristic and can lead to sonic fatigue of the nozzle hardware because of the relatively high levels. Methods employed to reduce the amplitude of shock screech noise are aimed at destroying the feedback loop by causing perturbations in the flow near the nozzle exit plane (e.g., screech tabs or nozzle exit plane roughness).

Summary

The objectives of this chapter were to review and summarize the jet noise suppression technology, to provide a physical and theoretical model to explain the measured jet noise suppression characteristics of different concepts, and to provide a set of "guidelines" for evolving jet noise suppression designs. The underlying principle for all the jet noise suppression devices is to enhance rapid mixing (i.e., diffusion) of the jet plume by geometric and aerothermodynamic means. In the case of supersonic jets, the shock-cell broadband noise reduction is effectively accomplished by the elimination or mitigation of the shock-cell structure. So far, the diffusion concepts have predominantly concentrated on jet momentum and energy (kinetic and thermal) diffusion, in that order, and have yielded better noise reduction than the simple conical nozzle.

However, these noise reductions are not large enough to guarantee compliance with noise regulations for engines being considered for high-speed applications, such as HSCT's. The current trend is toward higher jet velocities, so that engine size (and hence vehicle takeoff gross weight) will be smaller for a given sea level static thrust requirement. This trend presents tougher challenges for the scientific and technical community to reduce the jet noise at these higher jet velocities. This situation will call for innovative concepts for jet noise reduction. One avenue which has not been

vigorously pursued so far is diffusion concepts which employ concentration gradients of different species in addition to velocity and temperature gradients.

A critical technology issue that needs resolution is the effect of flight on the noise suppression potential of mechanical suppressor nozzles. Scale-model test data in simulated flight and limited flight-test data indicate that the noise suppression potential of mechanical suppressor nozzles over an equivalent conical nozzle deteriorates in flight whereas it does not in the static case. A more thorough investigation of this mechanism is necessary for the successful development and design of an acceptable noise suppression device for future HSCT's.

References

1. Lush, P. A.: Measurements of Subsonic Jet Noise and Comparison With Theory. *J. Fluid Mech.*, vol. 46, pt. 3, Apr. 1971, pp. 477–500.
2. Cocking, B. J.: *The Effect of Temperature on Subsonic Jet Noise.* R. & M. No. 3771, British Aeronautical Research Council, 1975. (Supersedes NGTE Rep. 331.)
3. Mani, R.: The Jet Density Exponent Issue for the Noise of Heated Subsonic Jets. *J. Fluid Mech.*, vol. 64, pt. 3, July 8, 1974, pp. 611–622.
4. Mani, R.: The Influence of Jet Flow on Jet Noise. *J. Fluid Mech.*, vol. 73, pt. 4, Feb. 24, 1976.
   Part 1: The Noise of Unheated Jets, pp. 753–778.
   Part 2: The Noise of Heated Jets, pp. 779–793.
5. Balsa, Thomas F.: The Far Field of High Frequency Convected Singularities in Sheared Flows, With an Application to Jet-Noise Prediction. *J. Fluid Mech.*, vol. 74, pt. 2, Mar. 23, 1976, pp. 193–208.
6. Lilley, G. M.; Morris, P.; and Tester, B. J.: On the Theory of Jet Noise and Its Applications. AIAA Paper No. 73-987, Oct. 1973.
7. Ribner, H. S.: Quadrupole Correlations Governing the Pattern of Jet Noise. *J. Fluid Mech.*, vol. 38, pt. 1, Aug. 14, 1969, pp. 1–24.
8. Goldstein, Marvin E.: *Aeroacoustics.* NASA SP-346, 1974.
9. Balsa, T. F.; Gliebe, P. R.; Kantola, R. A.; Mani, R.; Stringas, E. J.; and Wang, J. C. F.: *High Velocity Jet Noise Source Location and Reduction. Task 2—Theoretical Developments and Basic Experiments.* FAA-RD-76-79, II, May 1978. (Available from DTIC as AD A094 291.)
10. Balsa, Thomas F.; and Gliebe, Philip R.: Aerodynamics and Noise of Coaxial Jets. *AIAA J.*, vol. 15, no. 11, Nov. 1977, pp. 1550–1558.
11. Gliebe, Philip R.; and Balsa, Thomas F.: Aeroacoustics of Axisymmetric Single- and Dual-Flow Exhaust Nozzles. *J. Aircr.*, vol. 15, no. 11, Nov. 1978, pp. 743–749.
12. Gliebe, P. R.: Diagnostic Evaluation of Jet Noise Suppression Mechanisms. *J. Aircr.*, vol. 17, no. 12, Dec. 1980, pp. 837–842.
13. Harper-Bourne, M.; and Fisher, M. J.: The Noise From Shock Waves in Supersonic Jets. *Noise Mechanisms,* AGARD-CP-131, Mar. 1974, pp. 11-1–11-13.
14. Grose, R. D.; and Kendall, R. M.: Theoretical Predictions of the Sound Produced by Jets Having an Arbitrary Cross Section. *ASME Symposium on Fully Separated Flows,* 1964, pp. 58–63.
15. Davies, P. O. A. L.; Fisher, M. J.; and Barratt, M. J.: The Characteristics of the Turbulence in the Mixing Region of a Round Jet. *J. Fluid Mech.*, vol. 15, pt. 3, Mar. 1963, pp. 337–367.
16. Stone, James R.: *Supersonic Jet Shock Noise Reduction.* NASA TM-83799, 1984.
17. Brausch, J. F.; and Doyle, V. L.: *Supersonic Transport Noise Reduction Technology Summary, Phase I. Summary of GE4/SST Acoustic Suppression Research, Volume 1.* Rep. No. FAA-SS-72-42, Vol. I, Dec. 1972.

18. Shields, F. Douglas; and Bass, H. E.: *Atmospheric Absorption of High Frequency Noise and Application to Fractional-Octave Bands.* NASA CR-2760, 1977.
19. *American National Standard Method for the Calculation of the Absorption of Sound by the Atmosphere.* ANSI S1.26-1978 (ASA 23-1978), American National Standards Inst., Inc., June 23, 1978.
20. Brausch, J.; Clapper, W. S.; Gliebe, P. R.; Lee, R.; Whittaker, R.; Mani, R.; Motsinger, R. E.; Schloemer, J.; Sieckman, A.; and Stringas, E. J.: *High Velocity Jet Noise Source Location and Reduction. Task 6: Noise Abatement Nozzle Design Guide.* FAA-RD-76-79-6, Apr. 1979. (Available from DTIC as AD A103 671.)
21. Baumgardt, N.; Brausch, J.; Clapper, W. S.; Mani, R.; Stringas, E. J.; Vogt, P.; and Whittaker, R.: *High Velocity Jet Noise Source Location and Reduction. Task 5: Investigation of In-Flight Aeroacoustic Effects on Suppressed Exhausts.* FAA-RD-76-79-5, Jan. 1979. (Available from DTIC as AD A094 297.)
22. Eldred, Kenneth M.; White, Robert W.; Mann, Myron A.; and Cottis, Miltiades G.: *Suppression of Jet Noise With Emphasis on the Near Field.* ASD-TDR-62-578, U.S. Air Force, Feb. 1963.
23. Brooks, J. R.; McKinnon, R. A.; and Johnson, E. S.: Results From Flight Noise Tests on a Viper Turbojet Fitted With Ejector/Suppressor Nozzle Systems. AIAA-80-1028, June 1980.
24. Blozy, J. T.; Doyle, V. L.; Kazin, S. B.; Mishler, R. B.; Nebuda, R. L.; Stringas, E. J.; and Sieckman, A. R.: *Supersonic Transport Noise Reduction Technology Program—Phase 2.* Sept. 1975.
    Volume 1, FAA-SS-73-29-1-VOL-1. (Available from DTIC as AD B010 468L.)
    Volume 2, FAA-SS-73-29-1-VOL-2. (Available from DTIC as AD B010 469L.)
25. Brausch, J. F.; Motsinger, R. E.; and Hoerst, D. J.: *Simulated Flight Acoustic Investigation of Treated Ejector Effectiveness on Advanced Mechanical Suppressors for High Velocity Jet Noise Reduction.* NASA CR-4019, 1986.
26. Brausch, J. F.; Clapper, W. S.; Scott, P. F.; Smith, M. A.; Stringas, E. J.; and Whittaker, R. W.: *High Velocity Jet Noise Source Location and Reduction. Task 3—Experimental Investigation of Suppression Principles, Volume II—Parametric Testing and Source Measurements.* Rep. No. FAA-RD-76-79, III-II, Dec. 1978. (Available from DTIC as AD A094 294.)
27. Vdoviak, John W.; Knott, Paul R.; and Ebacker, Jon J.: *Aerodynamic/Acoustic Performance of YJ101/Double Bypass VCE With Coannular Plug Nozzle.* NASA CR-159869, 1981.
28. Kozlowski, Hilary; and Packman, Allan B.: *Aerodynamic and Acoustic Tests of Duct-Burning Turbofan Exhaust Nozzles.* NASA CR-2628, 1976.
29. Janardan, B. A.; Brausch, J. F.; and Majjigi, R. K.: *Free Jet Feasibility Study of a Thermal Acoustic Shield Concept for AST/VCE Application—Dual Stream Nozzles.* NASA CR-3867, 1985.
30. Ahuja, K. K.; and Dosanjh, D. S.: Heated Fluid Shroud as an Acoustic Shield for Noise Reduction—An Experimental Study. AIAA Paper 77-1286, Oct. 1977.
31. Goodykoontz, J.: *Effect of a Semi-Annular Thermal Acoustic Shield on Jet Exhaust Noise.* NASA TM-81615, 1980.
32. Pickup, N.; Mangiarotty, R. A.; and O'Keefe, J. V.: Tests of a Thermal Acoustic Shield With a Supersonic Jet. AIAA-81-2021, Oct. 1981.
33. Majjigi, R. K.; Brausch, J. F.; Janardan, B. A.; Balsa, T. F.; Knott, P. R.; and Pickup, N.: *Free Jet Feasibility Study of a Thermal Acoustic Shield Concept for AST/VCE Application—Single Stream Nozzles.* NASA CR-3758, 1984.
34. Sarohia, V.: Some Flight Simulation Experiments on Jet Noise From Supersonic Underexpanded Flows. *AIAA J.,* vol. 16, no. 7, July 1978, pp. 710–716.
35. Yamamoto, K.; Brausch, J. F.; Janardan, B. A.; Hoerst, D. J.; Price, A. O.; and Knott, P. R.: *Experimental Investigation of Shock-Cell Noise Reduction for Single-Stream Nozzles in Simulated Flight. Comprehensive Data Report.* 1984.
    Volume I, Test Nozzles and Acoustic Data, NASA CR-168234-VOL-I.

Volume II, Laser Velocimeter Data, NASA CR-168234-VOL-II.
Volume III, Shadowgraph Photos and Facility Description, NASA CR-168234-VOL-III.

36. Janardan, B. A.; Yamamoto, K.; Majjigi, R. K.; and Brausch, J. F.: *Experimental Investigation of Shock-Cell Noise Reduction for Dual-Stream Nozzles in Simulated Flight.* NASA CR-3846, 1984.
37. Yamamoto, K.; Brausch, J. F.; Balsa, T. F.; Janardan, B. A.; and Knott, P. R.: *Experimental Investigation of Shock-Cell Noise Reduction for Single Stream Nozzles in Simulated Flight.* NASA CR-3845, 1984.
38. Maestrello, Lucio: *Initial Results of a Porous Plug Nozzle for Supersonic Jet Noise Suppression.* NASA TM-78802, 1978.
39. Powell, A.: On the Mechanism of Choked Jet Noise. *Proc. Phys. Soc. (London),* Section B, vol. 66, pt. 12, 1953, pp. 1039–1056.

16 Interior Noise

Lead authors

John S. Mixson
NASA Langley Research Center
Hampton, Virginia

John F. Wilby
Atlantic Applied Research Corp.
Los Angeles, California

Introduction

Interior noise is an important consideration in the design and operation of virtually all aerospace flight vehicles. Noise is a natural by-product of powerful propulsion systems, high-speed aerodynamic flow over vehicle surfaces, and operation of onboard systems such as air conditioners. The noise levels produced can be intense enough to result in an unacceptable interior noise environment through effects such as passenger discomfort, interference with communication, crew fatigue, or malfunction of sensitive electronic equipment. Control of the noise environment requires substantial special effort, and the noise control measures usually result in penalties such as added structural weight, reduced cabin volume, or reduced performance. Interior noise control therefore requires a continuing search for means to reduce both the noise levels and the associated penalties, especially for new higher performance vehicles.

A variety of noise sources and transmission paths contribute to cabin noise. Sources such as propellers, inlet and exhaust systems of reciprocating or turbofan engines, turbomachinery, and turbulent airflow over the aircraft surfaces generate noise that impinges directly on the exterior of the fuselage and transmits into the cabin. This noise is referred to as "airborne noise." Sources such as engine unbalance forces transmitted through engine mounts and engine exhaust or propeller wakes impinging on wing or tail surfaces generate vibrational energy that is transmitted along the airframe structure and radiated into the cabin as acoustic noise. This noise is referred to as "structure-borne noise." Other important noise sources such as helicopter gearboxes, air-conditioning systems, and hydraulic systems used to operate landing gear or flaps are located within the fuselage of the aircraft. In general, any one of these sources can produce excessive noise; therefore all must be considered in a noise control design. Several sources may contribute about equally. Then, reducing noise from only one source to a level below that from several others has minimal effect since total acoustic power changes by only a small percentage (ref. 1, pp. 40–44). A balanced noise control treatment, therefore, would reduce the excessive noise from each source-path combination, so that all contribute about equally and the combined noise satisfies the acceptability criteria.

Interior sound levels can be controlled by reducing the noise generated by the source, by reducing the noise during transmission through airborne and

structure-borne paths, and by reducing the noise transmitted within the cabin. In some cases the interior noise sensation can be reduced, for example, by the use of ear protectors by occupants. In this chapter the emphasis is on the mechanisms of transmission through airborne and structure-borne paths and the control of cabin noise by path modification. Methods for identifying the relative contributions of the various source-path combinations are also discussed because of the need to concentrate treatment on the dominant combinations and to avoid weight penalties associated with treatment of nondominant source-path combinations. The mechanisms of source noise generation and control are discussed in other chapters of this book. However, features of the source noise that have important effects on interior noise and its control are discussed in the next section. The interior environment required for acceptability also has a major effect on the control of transmitted noise because of the penalties that have been mentioned. The effects of noise on equipment result from the vibrations that are induced; procedures are available for design and test of equipment to withstand vibrations (ref. 2). Human response to noise environments is described in detail in another chapter of this book. However, some aspects of passenger comfort of particular interest to interior noise control are described in the following paragraphs.

Noise is one of many factors that influence the comfort of passengers. Other factors include vibration, temperature, seat size and hardness, cabin air pressure, and air ventilation and quality. In spite of interactions that may occur between noise and the other factors (ref. 3), noise requirements are usually considered separately. In general, the noise level should be low enough to provide a feeling of comfort, and the noise spectrum should allow speech communication and be without excessive low-frequency "booming" or high-frequency "hissing." Noises that are annoying or alarming are undesirable, even though they may be low in level for normal operation of the aircraft. Occasionally, the noise level in the cabin may have large spatial variations that may also be undesirable. The penalties associated with noise control may be significant; therefore passenger requirements should be known accurately and the noise reduction provided should be only sufficient to satisfy those requirements.

Three parameters are in common use to quantify the subjective aspects of interior noise. The overall sound pressure level (OASPL, dB) adds most audible frequency components equally. The A-weighted sound level reduces the contributions of very low- and high-frequency components and has been found to correlate closely with the subjective response of human laboratory subjects and aircraft passengers. Speech interference level (SIL) includes only the frequencies between 350 Hz and 5623 Hz and relates to the quality of voice communication. Laboratory studies using simulated cabin noise indicate that 50 percent of the subjects reported feelings of annoyance when the A-weighted level exceeded about 82 dB or when the SIL exceeded 70 to 75 dB (ref. 4). Modern turbofan-powered aircraft having A-weighted sound levels in the range from 75 to 82 dB during cruise and associated SIL in the range from 55 to 70 dB have gained wide acceptance by travelers and are sometimes considered a standard of comparison. Values of SIL in that range are considered acceptable for large transports because nearby passengers can converse comfortably, while distant conversations that might intrude are masked. For smaller, executive class aircraft, a lower SIL is desirable so that all passengers can converse as a group. Laboratory studies have indicated that strong tones, such as those produced by propellers, tend to cause increased annoyance (ref. 5). Surveys of interior noise levels in existing

general aviation and commercial propeller and jet aircraft show that the A-weighted sound levels vary from about 67 dB to about 103 dB (ref. 4), suggesting that a range of levels is acceptable depending on the particular application. Surveys in buses, trains, and automobiles show that the A-weighted levels vary from about 60 dB to about 90 dB, so the levels in the quieter aircraft are in the same range as those in ground transportation.

The character and level of the noise differ for different aircraft and for different times during the flight. These differences affect the interior noise control efforts required. For example, the noise levels generated by full-power engine operation during takeoff and by reverse thrust during landing can exceed levels during cruise, but the takeoff and landing phases are of sufficiently short duration that the passengers can accept the additional noise without undue discomfort. Because the cruise portions of flight are of relatively long duration, the associated noise levels must be controlled for a steady state level of passenger comfort. The different durations and operating conditions for different aircraft types and flight conditions permit different noise control requirements. The most stringent requirements are usually associated with long flights that may last 12 to 16 hours. Somewhat higher noise levels are acceptable on shorter flights, but some short distance operations may involve high speeds at low altitudes which can lead to higher source noise levels and a requirement for more sound-reducing treatment. Thus, interior noise control must take account of the ultimate operational use of the aircraft, as well as the noise sources, transmission paths, and passenger comfort requirements.

Sources of Interior Noise

The source characteristics required for interior noise analysis include both magnitude and phase of the sound pressure and their distributions in frequency and space over the surface of the vehicle. These characteristics differ significantly for the different sources of interest; in some cases the sound pressures are deterministic,[1] and in other cases random. Empirical models have been developed for the pressure fields from many of the sources on an airplane (ref. 7). The different characteristics can have important effects on the noise transmitted through a fuselage, as illustrated in figure 1. These results were obtained in a theoretical study of the noise transmitted through a cylindrical aircraft fuselage of typical frame and stringer-stiffened skin construction and having a diameter of about 1.68 m (ref. 8). The source noise characteristics were carefully modeled to match available experimental data and the fuselage structure and interior were the same for both curves. For this example, fuselage noise reduction is defined as the difference between the maximum exterior SPL on the fuselage surface and the SPL transmitted through to the interior. Figure 1 shows that noise reduction is higher for the propeller source by as much as 15 dB. These differences result from the spatial distributions of source pressure magnitude and phase, which govern the total acoustic force on the fuselage and the efficiency of that force in causing motion of the fuselage structure.

[1] Deterministic pressures are those that can be described by an explicit mathematical relation, such as $\cos \omega t$ (ref. 6), where ω is circular frequency and t is time.

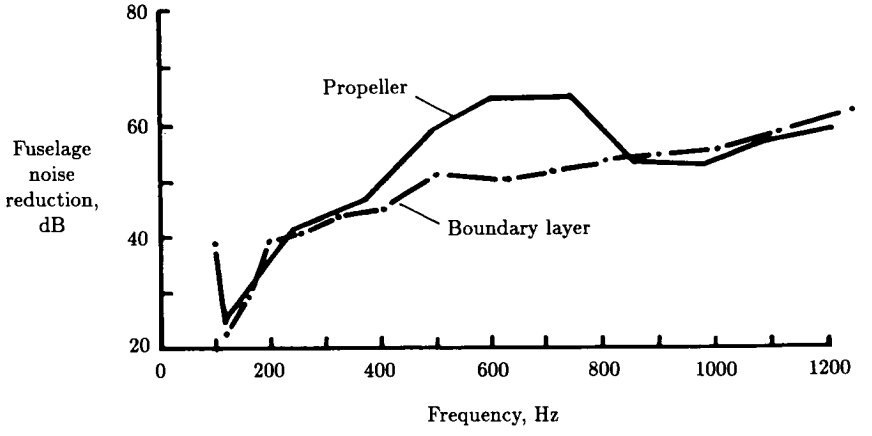

Figure 1. Predicted fuselage noise reduction for a general aviation aircraft showing effect of source character on fuselage noise transmission. (From ref. 8.)

Boundary Layer Noise

The noise generated by airflow over the aircraft surfaces is important for virtually all classes of aircraft. For the smaller aircraft with less streamlining, more exposed struts, and light structure, airflow noise is important at higher frequencies. For the larger, jet-powered, well-streamlined aircraft, high speed flows generate significant levels of turbulent boundary layer noise that usually constitutes the most important source of cabin noise during cruise. Considerable information on turbulent boundary layer pressure fluctuations is available in the literature from both wind tunnel and flight studies.

Fluctuating pressures acting on the fuselage surface beneath the boundary layer have been measured in flight of a large jet aircraft operating at speeds from 138 to 242 m/sec at an altitude of 7620 m (ref. 9). Figure 2 shows that the spectrum of the pressure is broadband and contains significant components at frequencies from below 100 Hz to above 2000 Hz. Increasing airspeed from Mach 0.45 to Mach 0.78 increases spectral density by a factor of 5, which is equivalent to about 7 dB. Since the overall root-mean-square (rms) pressure varies, approximately, as the flight dynamic pressure or the square of the flight speed, an increase of 9 to 10 dB might be expected. However, this increase is not reproduced directly in the spectrum level because the energy is distributed over a wider frequency range at the higher speed. At the aft location in figure 2, the spectral density is higher than at the forward location, but only at frequencies below about 1000 Hz. The increase is a factor of about 3.5, equivalent to 5 dB. It is due in part to a shift of energy to lower frequencies as the boundary layer thickness increases farther aft, but it also may be influenced, for the example chosen, by the presence of low-frequency jet noise contributions on the rear of the fuselage. The variations along the fuselage are large enough to influence the design of interior acoustic treatments. These flight data were used, together with

data from several laboratory studies, to develop a general empirical equation for predicting fluctuating pressure spectra (ref. 9).

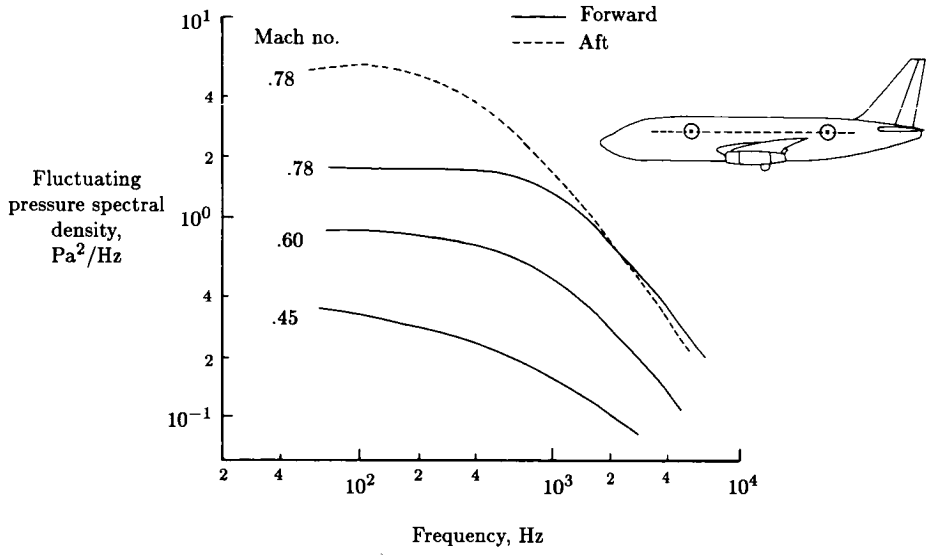

Figure 2. Spectral density of fluctuating pressure on the exterior of a large jet aircraft in flight. Boundary layer source. (From ref. 9.)

The flight data were also analyzed to determine the point-to-point correlation (in the time domain) or cross spectral density (in the frequency domain) of the pressures. Cross spectral density of a random pressure field plays an important role in determining the effective force acting on a structure, and hence, the response. Flight and wind tunnel measurements indicate that a boundary layer pressure field is convected in the direction of the flow and the coherence decreases as the separation distance between the measuring points increases. The convection speed U_c is about 70 percent of the flight speed, so that as the aircraft speed increases, there is the possibility that "hydrodynamic coincidence" will occur. When hydrodynamic coincidence occurs, the phase speed of the fluctuating pressures matches the structural bending wave speed. As a result, the structural vibration and interior sound pressure levels increase significantly. For example, figure 3 presents vibration spectra measured at the center of a fuselage skin panel on a large jet-powered airplane (ref. 10). The vibration spectral densities have been normalized with respect to the exterior boundary layer pressure spectral densities. If there were no change in correlation of the pressure field, the vibration would be expected to scale directly with exterior pressure and the two spectra in figure 3 would lie on top of each other; this is not the case. In the frequency range from 800 to 1500 Hz, the response at a flight Mach number of 0.60 is higher, by up to 7 dB, than that at a Mach number of 0.78, and at frequencies above about 2000 Hz, the converse is true. It has been shown that this effect is associated with correlation changes and coincidence conditions (ref. 10). Similar results can be seen in the sound pressures measured in the cabin. Note that, at least for subsonic flight, hydrodynamic coincidence occurs

C-4

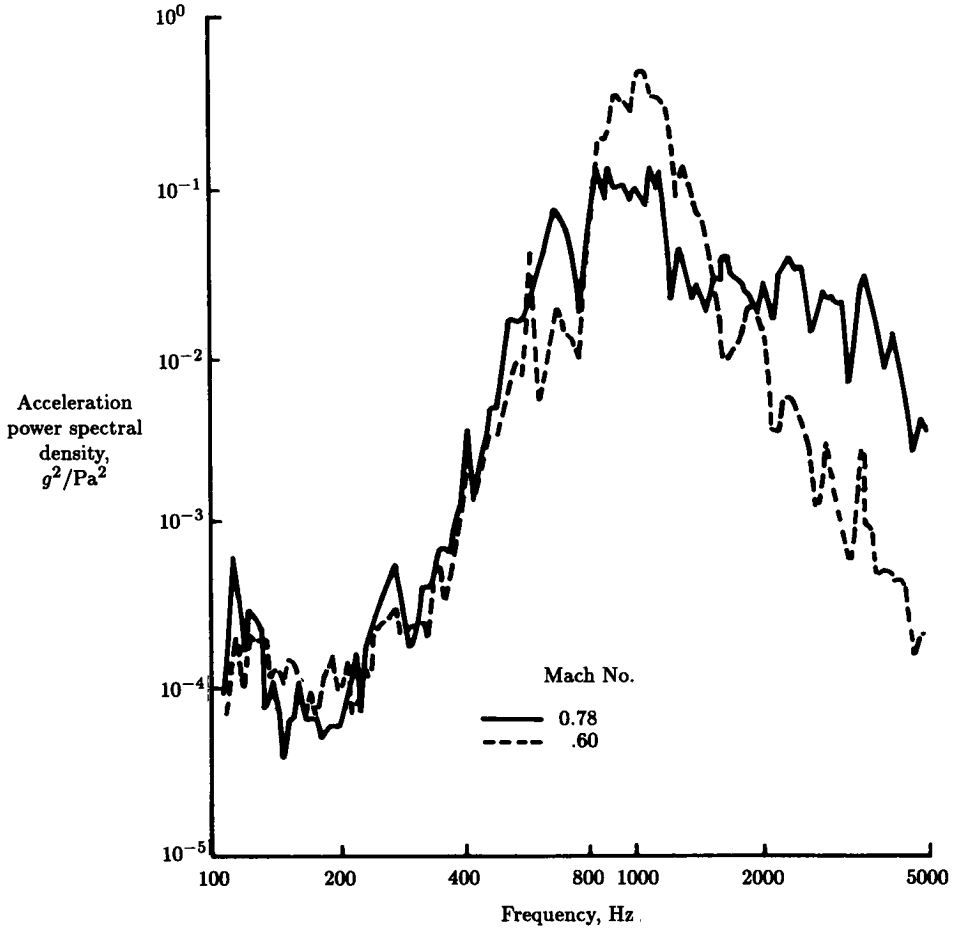

Figure 3. Fuselage panel acceleration spectra for unit excitation showing influence of pressure coherence. (From ref. 10.)

at frequencies lower than the acoustical critical frequency which, for the example shown, is about 10 000 Hz.

The correlation characteristics of turbulent boundary layer pressure fields have been incorporated into several empirical mathematical models of the pressure cross spectral density function (refs. 7 and 8). The models have been used to predict fuselage vibration (ref. 11) and airplane interior sound levels (ref. 8). The decaying and convecting nature of the pressure field is shown (in the separable form) by the cross spectral density function $S_p(\overline{x}_1, \overline{x}_2, \omega)$:

$$S_p(\overline{x}_1, \overline{x}_2, \omega) = S_p(\overline{x}, \omega) \exp(-a_x|x_2 - x_1|) \times \exp(-a_y|y_2 - y_1|) \exp[-ib\omega(x_2 - x_1)/U_c]$$

where the pressure field is taken to be homogeneous, with an auto spectral density function $S_p(\overline{x}, \omega)$. Coherence decay parameters a_x and a_y can be functions of frequency, convection velocity, and boundary layer thickness.

Propeller Noise

A single propeller generates a noise field that is highly tonal in frequency content and highly directional in spatial distribution. The noise-generating mechanisms are associated with the thickness of the blades passing through the air and with the aerodynamic pressures on the blades that produce the steady thrust and torque. As a consequence, the sound pressures are deterministic and are completely correlated at all points in the sound field. The boundary layer turbulence in the airflow over the blade surfaces also generates a broadband random noise, but this source is generally low level. The noise level generated by a propeller is influenced by factors such as power produced, tip speed (rotational and forward), number of blades, blade shape, and distance from the propeller. The effects of these factors have been studied experimentally (ref. 12). Also, nonuniformity of the airflow into the propeller can generate increased noise. Nonuniform inflow occurs when a propeller is operated at nonzero angle of attack, in the wake from a wing or strut, or at near-zero forward speed. Theoretical methods are available to predict test results with good accuracy and to include complicating factors such as nonuniform inflow and interaction with a fuselage (refs. 13 and 14).

The spectrum of exterior noise on a twin-engine aircraft is illustrated in figure 4. These results were measured in flight using a flush-mounted microphone on the port side of the aircraft (ref. 15). Each engine was run at a different rpm, so the contribution from each propeller can be seen. The tone at the blade-passage frequency of about 75 Hz has the highest level; succeeding tones decrease at a rate of about 3 dB per harmonic. The first few tones greatly affect passenger comfort and are difficult to control by sidewall treatment, especially at the lower frequencies. Blade-passage frequencies fall in the range from 75 to 125 Hz for light aircraft and in the range from 160 to 250 Hz for the new high-speed turboprops. The overall level and falloff rate vary with operating condition, altitude (ref. 15), and propeller tip speed (ref. 13). The propeller tones decrease with frequency faster than the boundary layer noise; therefore at high frequency the boundary layer noise is dominant.

Propeller directional characteristics are illustrated in figure 5. These results were obtained for a model of a blade designed for operation at Mach 0.8 (ref. 16). Design helical tip speed is slightly greater than Mach 1.0. The test results were obtained in flight with the model propeller mounted on a pylon atop a jet-powered aircraft and with microphones flush-mounted in the skin of the aircraft. The figure shows that the OASPL is highest near the plane of rotation of the propeller and decreases rapidly in both forward and aft directions. This directivity pattern suggests that fuselage noise control treatment (ref. 15) is required primarily near the region of highest noise. For a transport aircraft concept designed for 155 passengers, the propeller noise is estimated to require extra treatment over about 28 percent of the cabin length (ref. 17). For smaller general aviation aircraft (see fig. 4), treatment may be required over a greater percentage of the cabin length. The noise distribution pattern can be expected to be broader for larger propeller diameter and for greater clearance between the propeller and the fuselage. In addition, the directional characteristics

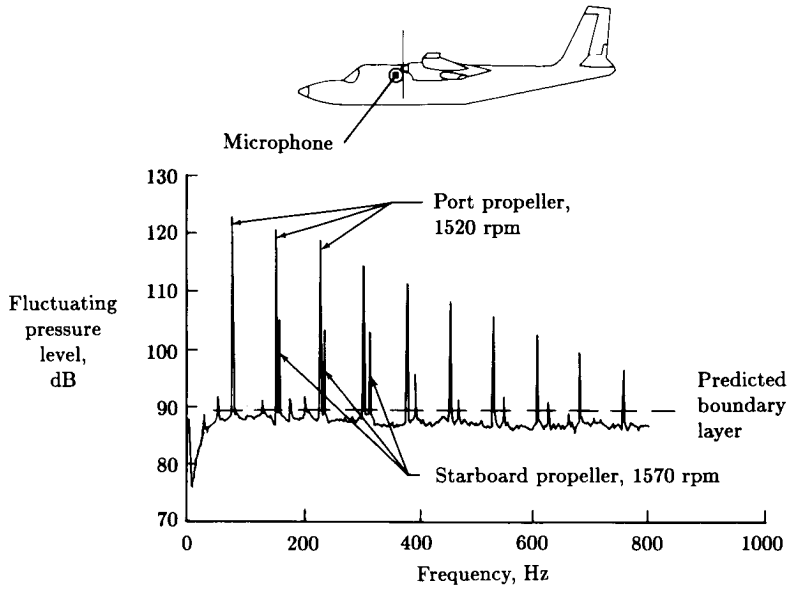

Figure 4. Spectrum of fluctuating pressure on exterior of a light twin-engine aircraft in flight. Altitude = 9100 m; Speed = 154 m/sec. (From ref. 15.)

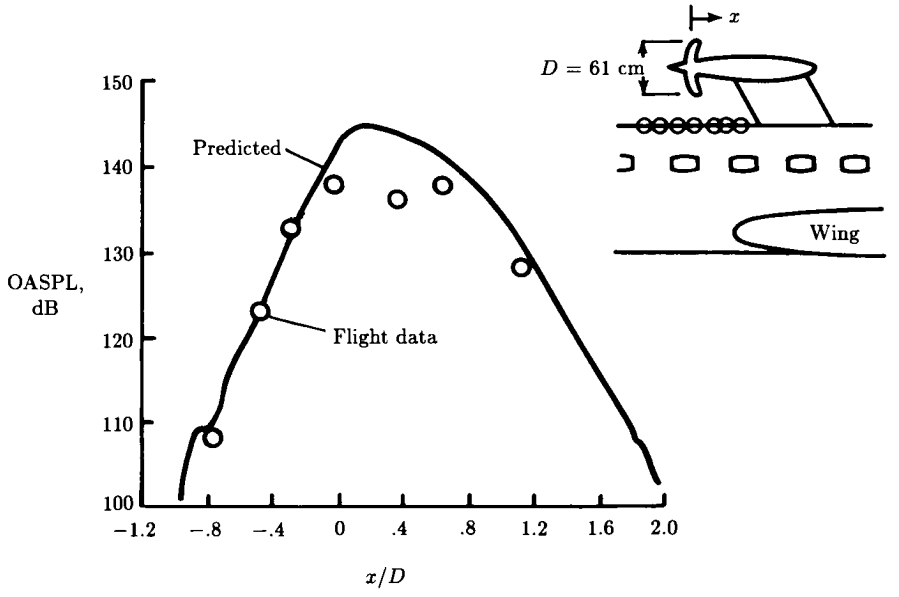

Figure 5. Overall sound pressure level generated by scale model of high-speed propeller. Measured on carrier aircraft at Mach 0.8. (From ref. 16.)

may be affected by operational factors such as flight speed, by interactions with the fuselage flow field, and by interaction with a second propeller in a counterrotating configuration. For a propeller of a light aircraft the higher frequency harmonics were found to decrease faster with distance than the lower frequency harmonics (ref. 18). In the circumferential direction the noise level also decreases rapidly, and in general the noise level on the opposite side of the aircraft is lower by a large amount (fig. 4 indicates about 15 dB).

Phase characteristics are illustrated in figure 6 for the same high-speed propeller model studied in figure 5. The results of figure 6 apply to tests carried out in an acoustic wind tunnel with a massive steel cylinder to simulate a fuselage (ref. 19). Tunnel airflow was carefully managed to minimize turbulence flowing into the propeller, and propeller rotational speed was increased to produce the correct supersonic helical tip speed since the tunnel flow speed was less than design flight speed. The figure shows that large variations in phase angle occur on the cylinder. Such phase variations could have an important effect on the fuselage response and resultant noise transmission. The propeller of figure 6 was located with a tip clearance of 0.8 propeller diameter from the cylinder. For general aviation aircraft, tip clearance is often much less and may be of the order of 0.1 propeller diameter. The measured phase characteristics of one such configuration were found to describe a traveling wave field, rotating in the circumferential direction at a speed approximately equal to the propeller tip speed (ref. 20).

Cabin noise characteristics can be affected in an important way by interactions between the noise fields of several propellers and by interactions of a propeller noise field with the fuselage. For example, when two propellers are operated at slightly different rpm values, beating interference between the two sources occurs, and the noise level in the cabin rises and falls in a manner that is easily detectable and possibly annoying (ref. 21). Many aircraft are equipped with an electromechanical phasing device that is intended to control rpm and phase in an attempt to reduce these fluctuations. It has been proposed that the phase be adjusted to minimize the cabin noise, with the thought that acoustic interference might be used to obtain a noise level below that which results from each propeller separately. The interaction of the propeller noise with the fuselage dynamics is not well understood but is being studied (ref. 22). The noise reduction that may be possible has been estimated in a flight study of a large four-engine aircraft (ref. 23). Some of the results are illustrated in figure 7. Interior noise levels were measured at six longitudinal positions for a flight where the four propellers were controlled only by a mechanical governor that allowed slow angular drift of the relative propeller positions. The data were analyzed to determine the cabin noise levels associated with 5832 combinations of relative phase positions of the four (four-bladed) propellers at 5° angular steps for each propeller. The lowest space-averaged acoustic pressure level was 94 dB and the highest was 103 dB. Larger differences are observed in figure 7 at some fuselage locations. The combination giving the 94-dB average, referred to as "optimum phase," also resulted in noise levels well below the maxima at most of the individual locations. These results indicate that substantial benefits can be obtained throughout the cabin when the propeller phase angles can be accurately controlled.

The interaction of a single propeller with the fuselage has been studied for a twin-engine commuter class aircraft (ref. 24). Interior noise levels were obtained in flight and ground tests with each engine at a different rpm to identify the contribution

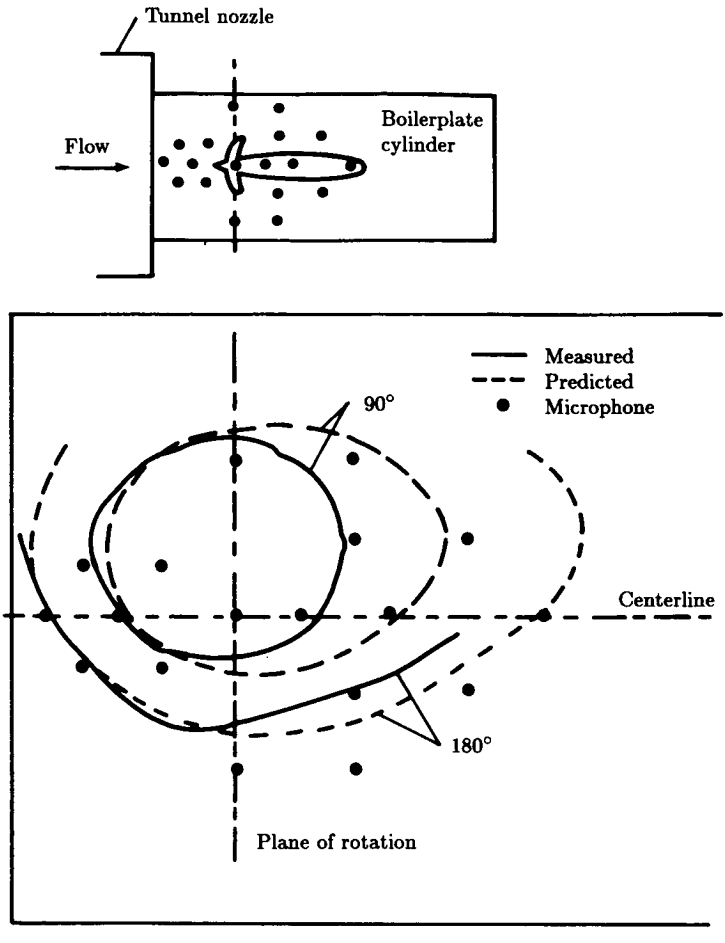

Figure 6. Phase angle distribution of blade-passage harmonic of scale model of high-speed propeller. (Based on ref. 19.)

from each propeller. As the aircraft was configured, the right propeller tip was moving upward as it passed near the fuselage while the left propeller tip was moving downward. Interior levels, obtained by averaging the microphones at left and right seat positions just aft of the propeller plane, indicated that the up-sweeping propeller produced as much as 10 dB less cabin noise in individual blade-passage harmonics than did the down-sweeping propeller. This effect is thought to be associated with nonsymmetries of the fuselage structure and the propeller noise field with respect to the fuselage upper and lower halves. Nonuniform inflow and installation effects may also contribute (ref. 25). These measured cabin noise reductions are significant, but the mechanisms involved are not well understood.

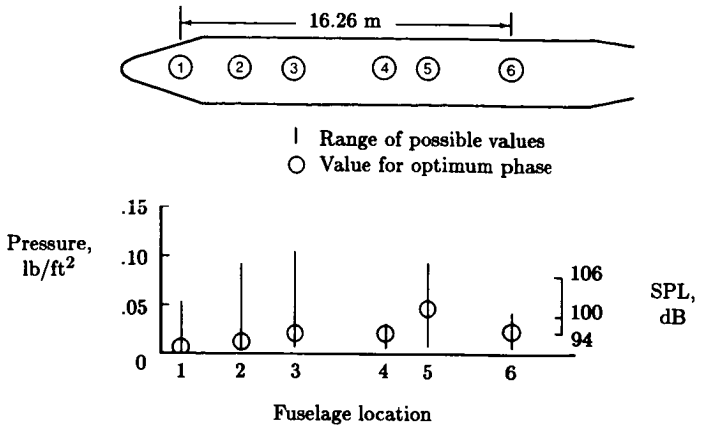

Figure 7. Variation of interior noise level with propeller phase angle for four-engine aircraft. Calculated for blade-passage frequency of 68 Hz. (From ref. 23. Copyright AIAA; reprinted with permission.)

Other Sources of Cabin Noise

The noise radiated by the exhaust from a jet engine has been studied extensively and methods are available for predicting the acoustic near field on an airframe (ref. 7). The impact of jet noise on the cabin environment is reduced greatly by the use of high-bypass engines with low-velocity exhaust and by locating the engines at outboard or aft positions. The influence of jet noise on the fuselage of an airplane with wing-mounted jet engines has been investigated in reference 26. A related phenomenon is associated with the noise from rocket exhausts on space vehicles, such as the Space Shuttle at lift-off (ref. 11). For jet and rocket exhaust noise, the acoustic field on the airframe is random and has a trace velocity in some direction over the structure. Thus, the cross spectral density function can be represented analytically in a manner similar to that used for turbulent boundary layers, but with different values for the coherence decay parameters and convection velocity. Because of the differences in the cross spectral density function, jet noise is often a more efficient exciter of structural vibration at low frequencies than is a subsonic turbulent boundary layer. Acoustic loadings associated with powered-lift configurations have been investigated for STOL (short takeoff and landing) aircraft applications in reference 27. Reciprocating engine exhaust noise and forward-radiated noise from a jet engine fan inlet can sometimes influence cabin noise.

Engine unbalance forces and other sources of engine vibration are known to cause cabin noise (refs. 28 and 29), but information for modeling these sources for cabin noise prediction is not available. It has been postulated that the wake of a propeller striking a wing (or empennage) could be a source of structural vibration with subsequent noise transmission into the airplane cabin. Wind tunnel measurements have been made of the fluctuating pressures produced by a high-speed propeller model on a simulated wing surface placed in the propeller wake (ref. 30). The pressure spectrum was found to be rich in blade-passage harmonics and the pressure levels were found to exceed by more than 15 dB the maximum direct noise which

would strike the fuselage. The mechanisms of acoustic transmission through wing structures have not yet been clearly defined.

Sources of cabin noise in a large helicopter are indicated in figure 8 (ref. 31). The main and tail rotors are located outside the fuselage and can generate significant cabin noise. Main-rotor noise extends into the very low-frequency range. For this helicopter, the main gearbox generates intense tones at frequencies of about 1350 Hz and 2750 Hz, where the human ear is quite sensitive and passenger annoyance may result. Other internal equipment, such as pumps and drive shafts, also contributes to the cabin noise.

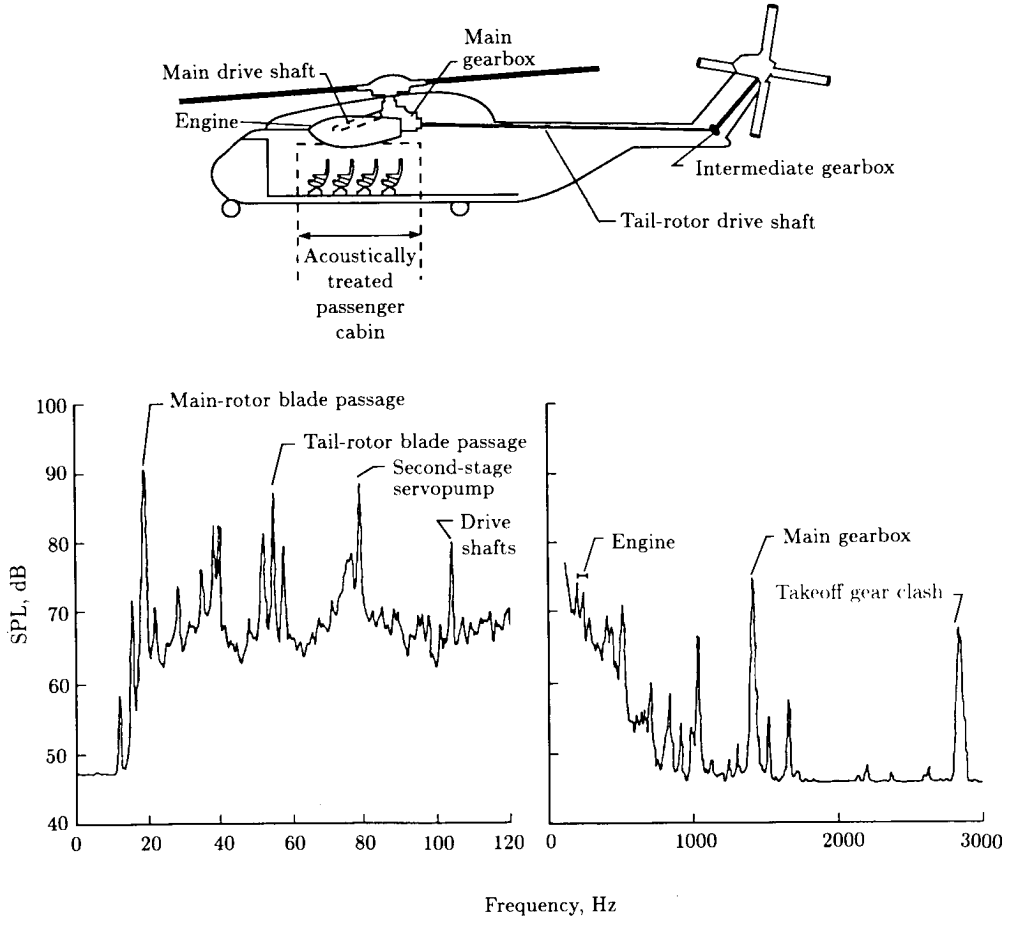

Figure 8. Sources of interior noise in a large helicopter. (From ref. 31.)

Airborne Noise

Airborne noise is defined as that part of the cabin noise that is transmitted through the fuselage sidewall from sources that exert pressures directly on the exterior of the fuselage. Such noise is a major contributor to the cabin noise in

virtually all aircraft and consequently has been studied extensively. The elements to be considered include the source noise characteristics, the noise transmission through the fuselage structure and attached acoustic treatment (or "trim"), and the distribution and absorption of the noise within the cabin. Aircraft noise sources and their effect on sidewall transmission were described in the previous section on sources. This section focuses on noise transmission into the cabin, with emphasis on aircraft structural characteristics, theoretical methods for understanding and predicting airborne noise, and approaches for controlling it. The actual application of these noise control approaches to aircraft is discussed in a later section of this chapter.

Aircraft Sidewall Transmission

Cabin Noise in Flight

Some effects of the sidewall transmission characteristics are evident in the measured cabin noise shown in figure 9 (ref. 15). Both the propeller tones and the boundary layer noise appear in the cabin, with the propeller harmonics dominating, as they do in the exterior noise shown in figure 4. The largest magnitudes occur at the first two propeller tones; these tones occur at low frequencies where noise control is difficult. The appearance of an engine tone in the cabin sound levels but not in the exterior noise suggests the presence of structure-borne noise for this source. Both the propeller tones and the boundary layer noise levels inside the cabin vary in an irregular manner with frequency, in contrast to the smoother variations exhibited by the exterior noise levels. These variations are evidence of the frequency-dependent transmission characteristics of the fuselage, probably associated with fuselage shell and panel modal activity. The levels in the cabin are significantly lower than the levels on the exterior, indicating that the sidewall provides substantial noise reduction. While the boundary layer noise is much less than the propeller noise in the low-frequency range shown in figure 9, at the higher frequencies, which contribute to speech interference, the boundary layer noise may make a major contribution, even for a propeller-driven aircraft (ref. 32).

Sidewall Noise Reduction

The noise transmission properties of aircraft sidewalls have been studied in flight and ground tests. Transmission is characterized in terms of noise reduction which is defined for this chapter as the difference between two noise levels measured simultaneously at positions inside and outside the aircraft.[2] For the results shown in figure 10, the measurements were made in the plane of the propellers, where

[2] The use of transmission loss (TL), as is customary in architectural acoustics, is not appropriate to characterize aircraft sidewall noise transmission in flight for several reasons. The incident and transmitted acoustic powers required by the definition of TL (ref. 1) cannot be determined in general for aircraft noise sources. The source noise implied by the use of TL is a diffuse, reverberant field (ref. 33). As indicated in figure 1, source characteristics have an important effect on the transmitted noise, and so the transmission of reverberant sound can be expected to differ from the transmission of aircraft sources. Finally, TL does not include the effects of the receiving space (the aircraft cabin) on the transmitted noise. These effects can be significant.

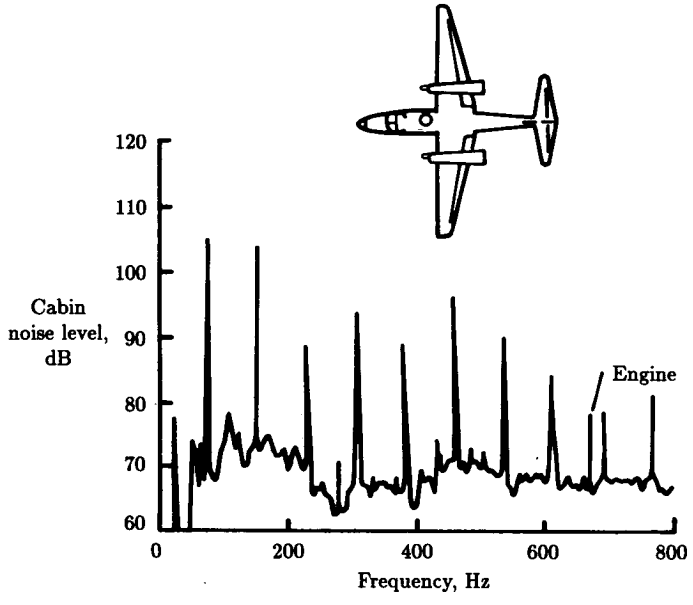

Figure 9. Cabin noise spectrum in flight of a light twin-engine aircraft. No cabin noise control treatment. (From ref. 15.)

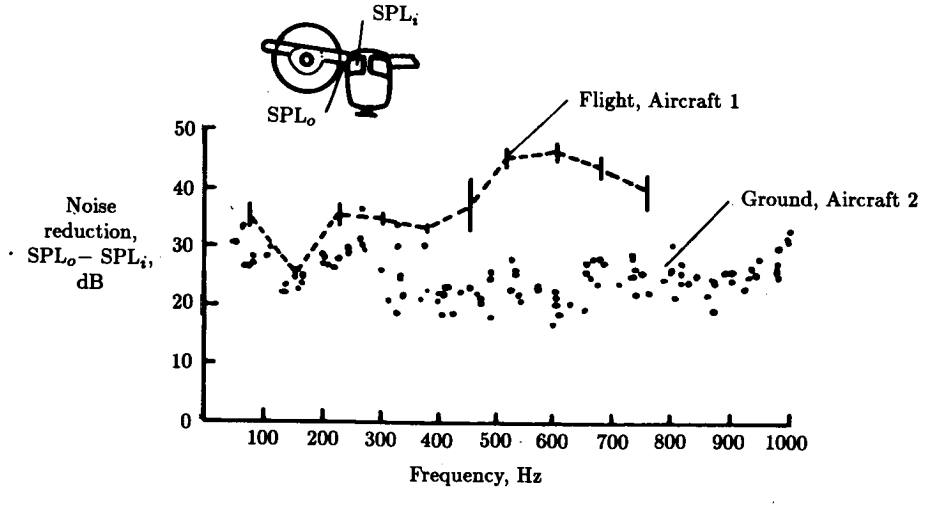

Figure 10. Reduction in propeller noise transmitted through light aircraft sidewalls. Aircraft 1: Weight of 5079 kg, pressurized, no interior treatment (ref. 15). Aircraft 2: Weight of 3175 kg, unpressurized, fiberglass treatment (ref. 34).

both outside and inside noise levels are expected to be maximum with respect to other locations. The two aircraft in the study had similar configurations as shown in figure 10, but differed somewhat in size and weight. The exterior noise was measured by a microphone mounted flush with the surface at about mid-window height, and the interior noise was measured at about ear height for a passenger seat on the side of the aircraft near the window.

The vertical bars in figure 10 indicate data measured in flight on aircraft 1 (ref. 15). The engines of this aircraft operated at (virtually) a single rpm, so results are shown only at the propeller blade-passage frequency and at its harmonics. The height of the bars indicates the range of noise reduction values measured at the various flight conditions. Altitude varied from 3000 m to 8500 m, and cabin pressure, flight speed, and engine power differed somewhat at different altitudes.

Measurements made with aircraft 2 stationary on a runway (ref. 34) are also shown in figure 10. Noise reduction was calculated at each of approximately 10 propeller tones. Operation of the (reciprocating) engine at several different rpm values resulted in the almost continuous distribution of data points.

For the ground tests the noise reduction has a minimum value of about 20 dB in the range from 300 to 600 Hz and increases for lower and higher frequencies. Noise reduction measured in flight is slightly higher than ground measurements for frequencies below 400 Hz and is substantially higher (about 20 dB) at higher frequencies. For both ground and flight tests, the noise reductions at low frequency (below 300 Hz) are significantly higher than the value of about 10 dB that would be expected from architectural experience (i.e., from transmission loss). The trend and magnitude of the noise reductions shown in figure 10 are thought to be strongly influenced by the highly directional nature of the propeller noise field (illustrated in fig. 5) and by interaction with the dynamic wave properties of the sidewall structure (ref. 35). Other variables that may also affect the noise reduction include pressurization, transmission loss and absorption by fiberglass or other treatment, and the position where the interior noise is measured.

Mass and Stiffness Effects

Changes in sidewall noise reduction due to addition of mass or stiffness to the sidewall structure are illustrated in figure 11, from a laboratory test of a light aircraft fuselage using a horn to simulate propeller noise (ref. 36). Skin stiffness was increased by bonding aluminum honeycomb panels to the inner side of the fuselage skin. The stiffness treatment provided more noise reduction than an equal weight of mass treatment in most of the frequency range shown. The increase in noise reduction due to addition of mass can be estimated from (ref. 37)

$$\Delta \mathrm{NR} = 20 \log(1 + m_t/m_s) \tag{1}$$

where m_t is the added treatment mass and m_s is the original skin mass, provided that the sidewall is sufficiently massive that $(\pi m_s f/\rho c)^2 >> 1$, where f is frequency and ρc is the characteristic acoustic impedance. For the aircraft of figure 11 with 2 kg/m^2 of added mass, the noise reduction estimate is about 5.4 dB for frequencies above about 200 Hz, which is in approximate agreement with the results presented. The effect of added stiffness has been shown to be beneficial in some, but not all,

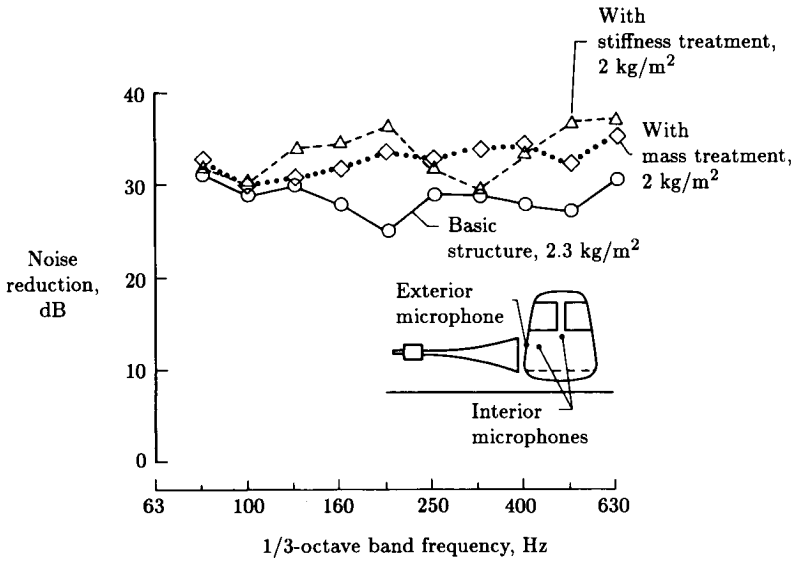

Figure 11. Measured noise reduction due to mass and stiffness treatments for cabin noise control. Mass and stiffness added to fuselage sidewall structure. (From ref. 36.)

laboratory studies, but no flight test results are documented to demonstrate the benefits. Addition of stringers and ring frames is another method of adding stiffness.

Add-On Treatment

The effect on cabin noise level of add-on acoustic treatment is illustrated in figure 12 (ref. 32). Add-on treatments consist primarily of fiberglass wool and impervious layers, which may vary from lightweight to heavy, and are usually installed so that they have minimum contact with the fuselage skin and ring frames. Their acoustic function is to provide an additional barrier to the noise, rather than to modify the sidewall structural behavior as the mass and stiffness treatments do (fig. 11). The fiberglass also provides thermal insulation and the innermost impervious mass layer usually serves as the decorative panel that gives the passenger cabin a finished appearance. These treatments are characterized in terms of insertion loss, defined as the reduction in cabin noise that results from the installation of the treatment. This approach is used because cabin noise levels can be measured conveniently in flight, but exterior noise levels required for noise reduction measurements usually are difficult to measure, especially in an aircraft to be delivered to a customer. Insertion loss is determined from two flights, one with and one without the treatment; therefore flight conditions must be repeatable so that only the change in treatment affects the noise level. Such repeatability of flight conditions can be difficult to obtain (ref. 15), and the best results have been obtained when special flights are dedicated to the noise study.

Fiberglass provides little insertion loss at low frequencies, but is quite effective at high frequencies; its light weight is a great advantage. Cabin absorption is an

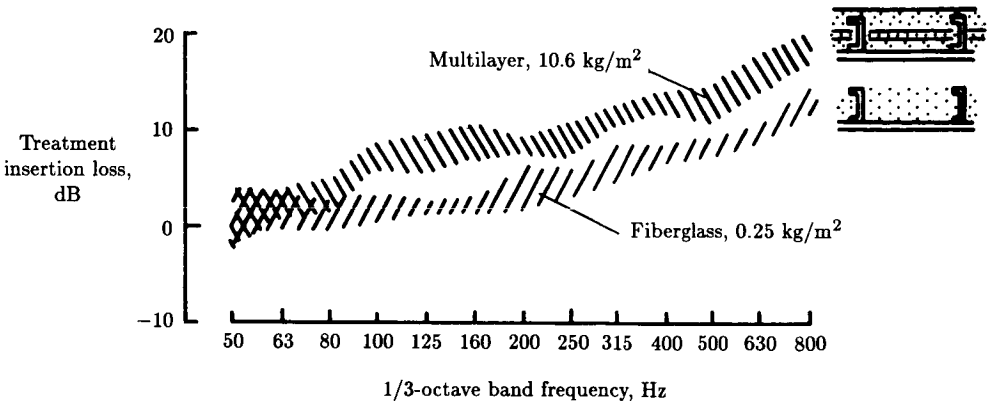

Figure 12. Insertion loss of add-on sidewall treatment for cabin noise control measured in flight of a light twin-engine propeller aircraft (ref. 32). Insertion loss equals SPL before treatment minus SPL after treatment.

important factor in the results shown in figure 12. The multilayer treatment weighs significantly more than the fiberglass, but the extra insertion loss provided, about 5 dB, can be important to cabin comfort. The insertion loss values of figure 12 were found to be approximately predictable from values of sidewall noise transmission and absorption measured under laboratory conditions (ref. 32).

The insertion loss provided by a treatment depends not only on the treatment itself but also on the fuselage configuration (including other treatments) to which the treatment is added (ref. 38). Development of lightweight and effective add-on treatments is of major importance in aircraft cabin noise control.

General Modal Theory

Modal analysis forms the basis of many of the theoretical methods that have been used for the prediction of aircraft interior noise. The basic principles, developed in general without specifying a particular aircraft (ref. 39), are described in the following sections for the cabin and structure.

General Modal Analysis of Cabin Acoustics

Let the aircraft cabin occupy a volume V and be surrounded by a wall surface, of which the portion with area A_F is flexible while the remainder of area A_R is rigid; neither surface provides much absorption. If the air within the cabin is at rest prior to motion of the wall, the acoustic pressure p satisfies the wave equation and associated boundary conditions:

$$\nabla^2 p - \ddot{p}/c_o^2 = 0 \tag{2}$$

$$\partial p/\partial n = \left\{ \begin{matrix} -\rho_o \ddot{w} & (\text{On } A_F) \\ 0 & (\text{On } A_R) \end{matrix} \right\} \tag{3}$$

The dot denotes differentiation with respect to time t, ρ_o and c_o are the equilibrium density and acoustic velocity within the cabin, and w is the displacement of the

flexible portion of the wall in the normal direction. The acoustic pressure is expressed in the modal series

$$p(\bar{x}, t) = \rho_o c_o^2 \sum_n P_n(t) F_n(\bar{x}) / M_{an} \tag{4}$$

where $\bar{x}$ is the position coordinate vector, P_n are generalized coordinates, F_n are the acoustic mode shapes of the volume when all the walls are rigid, and M_{an} are the generalized masses of the acoustic modes.[3] The wave equation (2) can be transformed into a set of ordinary differential equations in time by using Green's theorem, the modal series equation (4), and the orthogonality properties of the acoustic mode functions $F_n(\bar{x})$. The result for the undamped nth acoustic mode is

$$\ddot{P}_n(t) + \omega_{an}^2 P_n(t) = \frac{-1}{V} \int_{A_F} F_n(\bar{x}) \ddot{w}(\bar{x}, t)\, dA \tag{5}$$

where ω_{an} is the natural frequency of the nth acoustic mode. Solution of equation (5) for each mode produces the coefficients P_n that enter equation (4) along with the mode functions F_n to give the cabin acoustic pressure. In general the acoustic response is coupled with the structural motion $\ddot{w}(\bar{x}, t)$ through the structural equations of motion, to be discussed subsequently. Solution of these coupled structural-acoustic equations is quite complex; therefore solutions have been found for only a few systems (ref. 39). Fortunately the effects of the acoustic pressure on the structural motion are small for most aircraft applications, so the structural equations can be solved uncoupled from the acoustics. The resulting structural motions $\ddot{w}(\bar{x}, t)$ can then be inserted as known quantities into the right side of equation (5), which can then be solved directly using known methods for single-degree-of-freedom undamped systems with a known forcing function.

The effects of acoustic damping can be included in several ways. When one of the walls of the cabin is highly absorbent, it is often characterized by a simple point-impedance model which states that

$$p = Z_A \dot{w}_A \qquad (\text{On } A_A) \tag{6}$$

where the subscript A is used to refer to the absorbent wall characteristics; that is, w_A is the absorbent wall displacement and Z_A is the absorbent wall impedance. The boundary condition equation (6) can be combined with equation (3) to obtain the boundary condition for the absorbing wall:

$$\partial p / \partial n = -\rho_o \dot{p} / Z_A \qquad (\text{On } A_A) \tag{7}$$

This boundary condition can be used instead of equation (3) in the Green's theorem derivation to obtain a damping term proportional to $\dot{P}_n$ that adds to the left side of equation (5). The resulting equation has been used to study the relation between wall impedance Z_A, acoustic damping, and reverberation time (ref. 41). The damping

[3] Since the normal modes F_n satisfy the homogeneous boundary condition (eq. (3)) on the entire wall surface, the normal derivative of pressure (eq. (4)) does not converge uniformly on the flexible portion of the wall surface. Equation (4), is suitable, however, for calculating the pressure itself throughout the cavity and everywhere on the wall surface, including the flexible portion (ref. 40).

term couples all the acoustic modes[4] and increases the complexity of the solution; therefore this approach is not often used in practice. An alternative approach is simply to add to the left side of equation (5) a modal damping term that combines the coordinate velocity $\dot{P}_n$ with a modal damping coefficient that is to be determined experimentally (ref. 42). The exact form of this damping term is determined by analogy with a damped single-degree-of-freedom system. The acoustic modes remain uncoupled and the solution is straightforward.

Prediction of Acoustic Modes

Clearly, acoustic modes and their prediction are important in predicting interior noise using modal theory. As illustrated in figure 13, acoustic mode predictions are accurate for the lower frequency modes of rectangular parallelepiped enclosures having hard, nonabsorbing walls and geometries that are not too complicated. The results of figure 13 were obtained using a subspace mode coupling method (ref. 39), which was also found to predict test results for a variety of other enclosure shapes.[5] Finite element analysis has also been shown to predict hard-wall acoustic modes accurately for three-dimensional analysis (ref. 43) of a large reverberant chamber, a very irregularly shaped model of an automobile compartment (ref. 44), and a model of a general aviation aircraft cabin (ref. 45). Reasonable predictions of acoustic modes have also been obtained using finite element analysis for an enclosure and a light aircraft fuselage having flexible walls (refs. 45 and 46).

Other methods have been used to predict acoustic modes in volumes of various shapes in aerospace vehicles. A perturbation method was applied to the closed-form analysis of rectangular parallelepiped volumes in order to describe the acoustic characteristics of the Space Shuttle payload bay (ref. 47), closed-form solutions have been obtained for cylindrical cavities, and the finite difference method was used to predict acoustic modes in a cylindrical fuselage with a floor (ref. 48). The mode shape shown in figure 14 was calculated with the finite difference method and shows the distortion of the modal node pattern caused by the presence of the floor.

Addition of acoustic damping in the form of absorption material on the walls greatly affects the acoustic character of the enclosure. As illustrated in figure 15, the addition of fiberglass lining all but eliminates the resonant response peaks of the acoustic modes (ref. 49). A simplified analysis for this situation has been proposed. There are few reports in the literature on acoustic characteristics of furnished aircraft cabins, but occasionally evidence of standing waves has been found (refs. 50 and 51). Mathematically, the addition of damping on the walls can cause the modes to be complex (having real and imaginary components) and greatly increase the difficulty of the solution. Theoretical analysis of a cylindrical enclosure indicates that wall damping equivalent to a Sabine acoustic absorption coefficient of 25 percent is sufficient to suppress the acoustic mode resonances (ref. 52). Absorption coefficient values of such magnitude have been reported for furnished aircraft cabins (ref. 4).

[4] Conditions that allow neglect of the modal coupling due to damping have been defined (refs. 39–41). A method for estimating acoustic damping from wall impedance is also described.

[5] The experimental studies revealed a sound suppression effect by which sound levels in a large enclosure can be reduced by constructing a smaller enclosure around the moving portion of the wall so that the smaller enclosure resonates at the frequency at which the wall is moving.

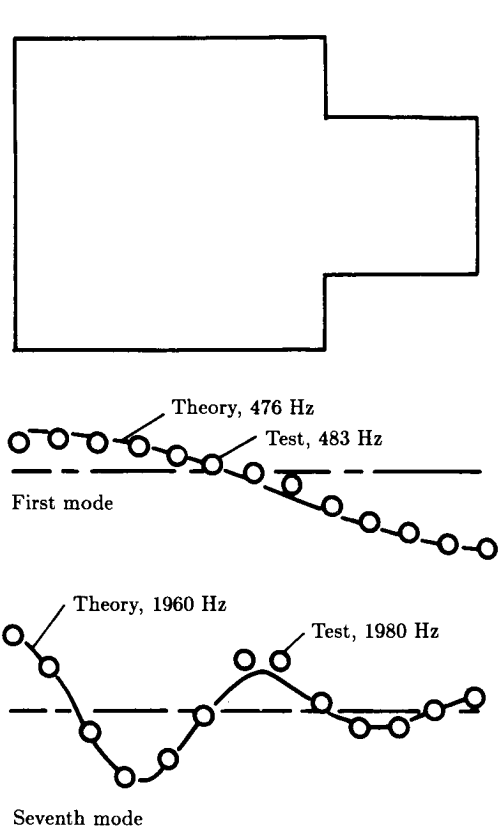

Figure 13. Longitudinal pressure distribution for acoustic modes in a hard-wall enclosure. (From ref. 39.)

General Modal Analysis of Structural Response

When the structure is represented by a linear mathematical model, the structural response, including acoustic interaction, may be analyzed in a straightforward way (ref. 39). Let the structure be represented by a linear, partial differential equation:

$$S(w) + c\dot{w} + m\ddot{w} = p - p_s \tag{8}$$

where S is a linear differential operator representing structural stiffness. For example, for an isotropic flat plate, $S = D\nabla^4$, where D is bending stiffness and ∇^4 is the biharmonic operator. The second term on the left side of equation (8) represents a damping contribution, c being the viscous damping coefficient, and the third term is the structural inertia, m being structural mass per unit area. On the right side are two pressure loadings, the first due to the cabin acoustics and the second due to some specified external noise source. For a modal solution, the structural deflection $w(\bar{x}, t)$ is taken as the series:

$$w(\bar{x}, t) = \sum_m q_m(t)\Psi_m(\bar{x}) \tag{9}$$

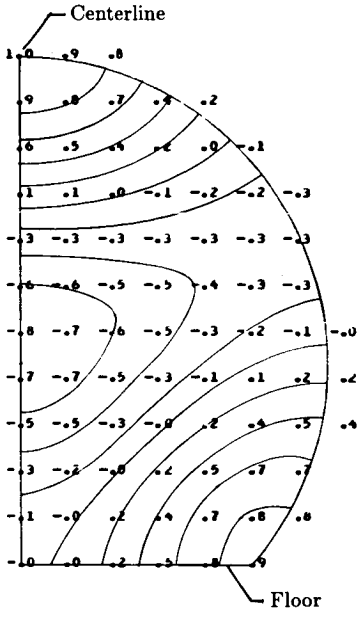

Figure 14. Acoustic mode shape of a cylindrical fuselage with an integral floor, calculated using finite difference method (ref. 48). Numbers are modal amplitudes.

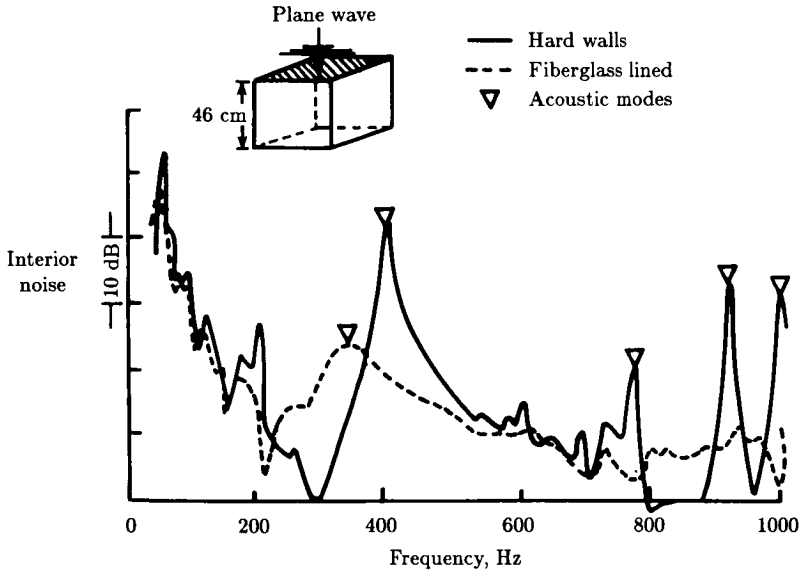

Figure 15. Effect of fiberglass sound-absorbing material on noise transmitted into an enclosure through a 0.32-cm-thick rubber panel (ref. 49).

where q_m are the structural generalized modal coordinates. The mode functions Ψ_m are defined on the flexible region of the enclosure wall and satisfy the eigenvalue equation obtained by setting the right side of equation (8) to zero. Solution of equation (8) is obtained by substituting the structural modal series (eq. (9)) and the acoustic modal series (eq. (4)) and making use of the orthogonality properties of the structural modes. The result is

$$M_m\ddot{q}_m + c_m\dot{q}_m + M_m\omega_m^2 q_m - \rho_o c_o^2 \sum_n C_{mn}P_n = Q_{ms} \tag{10}$$

In this equation M_m, c_m, and ω_m are the generalized mass, damping, and frequency of the structural modes. The coefficients C_{mn} couple the structural and acoustic responses and are given by

$$C_{mn} = \int_{A_F} F_n \Psi_m \, dA/M_{an} \tag{11}$$

The term Q_{ms} is the generalized force acting on the mth structural mode due to the known external source and is given by

$$Q_{ms} = -\int_{A_F} p_s(\bar{x}, t)\Psi_m(\bar{x}) \, dA \tag{12}$$

Equations (10) and (5) form a set of coupled differential equations in time to be solved for the structural and acoustic mode coefficients q_m and P_n due to the action of known acoustic forces $Q_{ms}(t)$. The complete coupled equations have been solved in only a few cases for simple configurations. Coupling was found to be important in a case where the forcing frequency was equal to the resonance frequency of an acoustic mode in the enclosure (ref. 39). The effect of the coupling was to limit the magnitude of the acoustic pressure in the enclosure to a value that did not exceed the exterior source pressure. The acoustic mode acted, in effect, as a vibration absorber and caused the structural panel deflection to approach zero. Coupled equations have also been used to analyze a cylindrical shell model with dimensions appropriate for a light aircraft (ref. 53). The effect of acoustic coupling was found to be small. In most analyses of the vibration of aircraft fuselage structures the coupling terms in equation (10) are dropped. The structural motions can then be determined in a straightforward way without acoustic effects, and the structural motions can then be used as known quantities to solve equation (5), as has been described previously.

Calculation of noise transmitted into an idealized enclosure using modal methods (ref. 54) is illustrated in figure 16. Test results were obtained using a sinusoidal acoustic wave applied at normal incidence at 100 dB onto a thin aluminum panel. The panel was attached to a specially constructed box that allowed noise transmission only through the panel. The panel was flat with uniform properties and the enclosure was rectangular with hard walls so that accurate modes could be obtained by closed-form analysis. The modal behavior of the system is clearly shown by the sharp resonance peaks. The noise levels at the acoustic modes do not exceed the source level of 100 dB, as described by the theory. The interior levels at structural modes, however, exceed the exterior source levels by as much as about 18 dB, a phenomenon

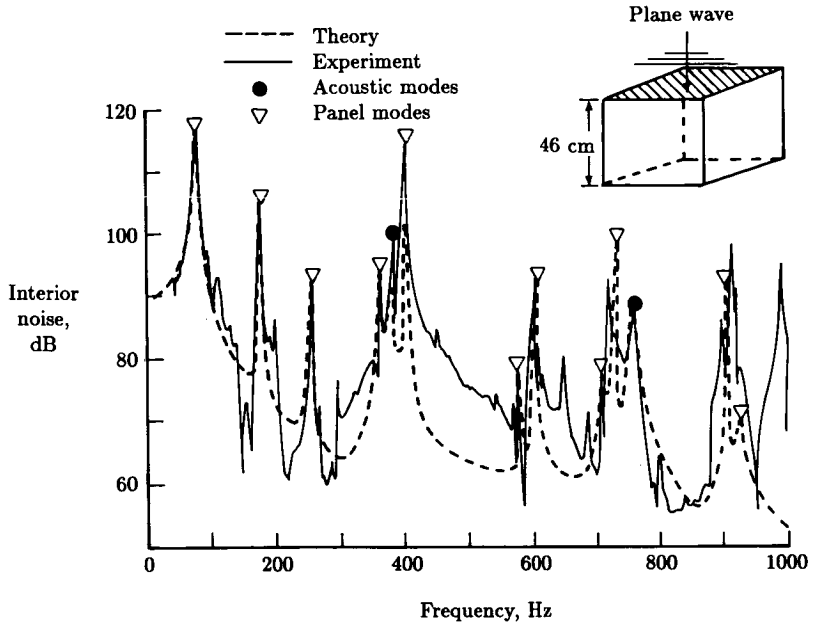

Figure 16. Noise transmitted into a hard-wall enclosure through a 0.08-cm aluminum panel. Source level = 100 dB. (From ref. 54.)

also described by the theory. The agreement between theory and test is good, indicating that modal analysis is a useful solution method.

The frequency range and number of modes shown in figure 16 are in the range of values of practical importance for many full-scale aircraft applications. For aircraft, however, the configurations of the structure and cabin geometry, as well as the presence of absorption on the walls, add sufficient complication that major efforts are required to determine the mode shapes and frequencies. Thus it is now appropriate to consider the practical applications of airborne noise transmission analysis.

Simplification of Analysis Methods

In applying theoretical principles to the calculation of aircraft cabin noise, simplifications are usually made to reduce the numerical processing to a manageable level. The essential features of the noise transmission process must be retained, however, for accurate predictions. Simplified and rapid procedures also are advantageous for displaying trends, for generating insight into noise level variations with system parameters, and for use in design or noise control. Assumptions made in a particular theoretical method tend to reduce its range of application, but a number of methods have been developed covering most of the aircraft situations of interest. The representations of the source and cabin acoustics differ for each method to be discussed in later sections of this chapter. The structural models and approach to treatment, however, are similar.

Representation of Fuselage Structure

As indicated in figure 17, a typical aircraft fuselage consists of longitudinal and circumferential stiffeners that support a thin skin. The stiffeners are normally closely spaced compared with the overall fuselage dimension. Detailed mathematical modeling of each skin panel and stiffener element for calculations throughout the acoustic frequency range is beyond current capabilities. However, it is feasible to apply different simplified models to different frequency ranges (ref. 55). Measurements on the aircraft illustrated in figure 17 have shown that at low frequencies the skin and stiffeners tend to vibrate with about the same magnitude (ref. 36) and the modal wavelengths are long compared with the stiffener spacing (ref. 56). This behavior leads to a low-frequency orthotropic model wherein the actual structural properties are averaged over a large sidewall area. At high frequencies the stiffener motions tend to become small compared with the panel motions and the modal wavelengths become short. This leads to a high-frequency panel model wherein the stiffeners are assumed motionless and all noise is transmitted only through the vibrating skin panels. At intermediate frequencies, both panel and stiffener motions have to be modeled. These models are more difficult to analyze, and results for the mid-frequency region are occasionally obtained by interpolating results obtained from low- and high-frequency models. The frequency range where each model is applicable depends on the particular aircraft being considered.

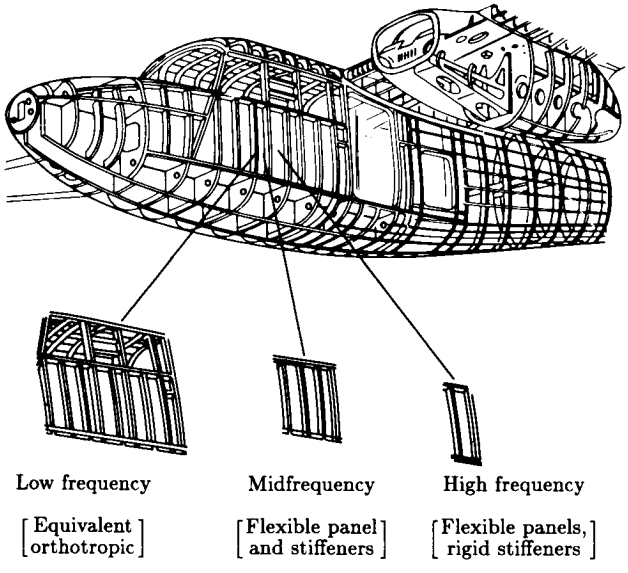

Figure 17. Simplified mathematical models of aircraft fuselage structure for interior noise prediction.

A simple illustration of this structural modeling approach can be found in acoustic transmission loss measurements (fig. 18) made on a flat, aircraft-type panel in a laboratory transmission loss facility (ref. 38). The panel was 1.22 m by 1.52 m and was stiffened by 4 frame stiffeners and 10 stringers. The panel was full-scale in

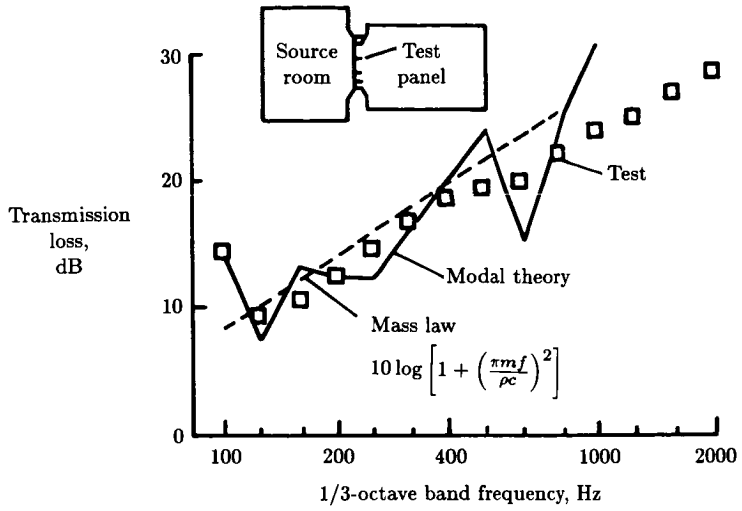

Figure 18. Noise transmission loss of an aircraft-type panel for a diffuse reverberant source noise in a laboratory transmission loss facility. Skin and stiffener mass $m = 5.5$ kg/m^2. (From ref. 38.)

that the material thicknesses and stiffener spacings are representative of full-scale general-aviation-class aircraft.

Test results give transmission losses (TL) at frequencies between 125 and 400 Hz that are only slightly less than mass law predictions using the total mass of skin and stiffeners. The results, along with measured panel mode shapes, suggest that significant motion of both skin and stiffeners is taking place and that panel wavelengths are large compared with stringer spacing. Such behavior is appropriately modeled with the low-frequency, equivalent orthotropic model used in the modal theory results shown in the figure. While the mass law is somewhat closer to the test data, the modal theory is close enough to establish its validity, and it also has the advantage of sufficient flexibility to handle configurations not treatable with the mass law approach.

At frequencies higher than 400 Hz the test results fall below the mass law curve shown. This indicates that the stiffener motion has become small and that the transmission is being controlled by the skin motion. The high-frequency panel model (fig. 17) would be more appropriate in this frequency region.

The panel considered in figure 18 has mass and structural values that are quite similar to the values for aircraft 2 in figure 10. Figure 18 indicates a TL of about 10 dB at frequencies below 200 Hz, whereas figure 10 indicates noise reduction of more than 20 dB at these frequencies. This difference in transmission is thought to be due primarily to differences in the excitation pressure fields; however, differences in structure, structural support conditions, or backing cavity may also contribute. Laboratory TL testing is useful for evaluating theories, because of the controlled test conditions, and for comparing treatment effects, but results should be used with caution because the TL values may not be representative of sidewall noise transmission behavior in an actual aircraft in flight.

Representation of Sidewall Treatment

The elements of importance to interior noise transmission include the fuselage structure and the acoustic treatment in the cabin. A calculation procedure that can rigorously handle these elements and their interactions is not yet available. Therefore approximate methods are required, such as that illustrated in figure 19, which was developed for a particular calculation procedure (ref. 57). Similar approaches are used in other methods. The approach is to calculate the noise transmission through each element separately and then combine the results additively. Thus, noise transmission through the cylindrical structure is calculated without treatment or absorption. Transmission through a skin panel with treatment is calculated separately using methods developed for an incident plane wave and a flat panel of infinite extent (ref. 58). The increment in transmission loss provided to the panel by the treatment is then added to the loss provided by the untreated cylinder, to obtain a combined treated cylinder noise reduction (NR). This NR is then combined with the cabin average absorption coefficient (α) to obtain the noise reduction of the treated fuselage with cabin absorption. The equation used to include absorption is obtained from diffuse room acoustics considerations, and when TL is large, the equation can be written as

$$\mathrm{NR} = \mathrm{TL} + 10\log(\alpha \mathrm{A}_\alpha / \mathrm{A}_t) \tag{13}$$

where A_α and A_t are the areas of absorbing and transmitting surfaces, respectively. These areas may differ in an aircraft due to the presence of floors, bulkheads, seats, and baggage compartments. This equation has been used with reasonable accuracy to relate treatment TL and α measured using laboratory methods (ref. 33) to treatment insertion loss measured in light aircraft cabins (refs. 32 and 59).

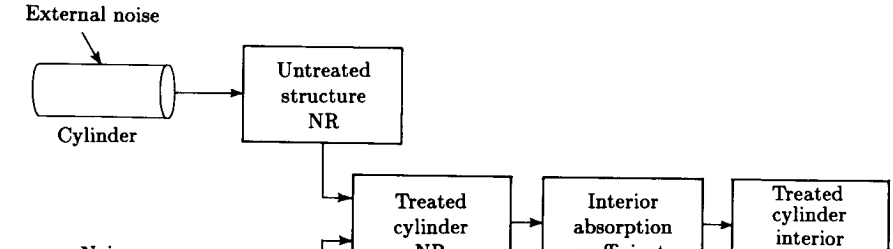

Figure 19. Approach for combining structure, treatment, and cabin absorption for theoretical prediction of aircraft interior noise (ref. 57).

Laboratory TL testing of add-on acoustic treatments has the advantages that test conditions can be accurately controlled, many treatment configurations can be tested at relatively low cost, and treatment effects can be studied separately from other factors (such as structure-borne noise) that can affect cabin noise. TL testing

is commonly used, therefore, for evaluating aircraft cabin noise control treatments (refs. 57, 60, and 61). Figure 20 illustrates treatment insertion loss obtained from TL tests and from theoretical predictions (ref. 38). The structural panel was the one used for figure 18. The treatment consisted of fiberglass and a trim panel located at a distance from the skin just large enough to avoid hard contact with the 7.6-cm-deep frames. Both test results and theory indicate that the insertion loss is negative at frequencies just above 100 Hz, meaning that the treatment increases the noise transmitted compared with the noise transmitted by the untreated panel. This phenomenon is caused by a resonance of the double-panel system. The frequency of this resonance can be predicted, approximately, by modeling the panels as having only mass with surface densities m_1 and m_2 separated by an air gap of thickness d. The resonance frequency is

$$f_d = \frac{1}{2\pi \cos\theta}\left[\frac{\rho_o c_o^2 (m_1 + m_2)}{d m_1 m_2}\right]^{1/2} \tag{14}$$

where θ is the angle of incidence of the acoustic wave. This negative effect can be a disadvantage in practice if significant noise levels exist at frequencies near the double-panel resonance.

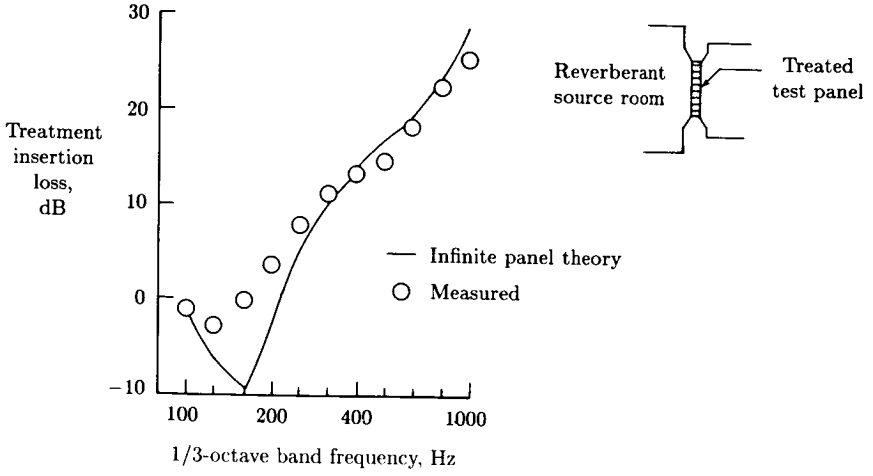

Figure 20. Insertion loss of fiberglass batt and trim panel treatment added to an aircraft panel. Laboratory TL test. (From ref. 38.)

At frequencies above 200 Hz the insertion loss rises rapidly with increasing frequency and quickly exceeds the insertion loss that would be obtained by adding the treatment mass directly to the structure. Thus, a double-wall treatment may have a weight advantage if the negative effects of the double-wall resonance can be avoided and if sufficient cabin absorption can be added to compensate for the usually low absorption characteristics of trim panels. Trade-off analysis is required to determine the best combination of treatments for a particular application (ref. 38).

The theoretically predicted insertion loss is much lower than test results at frequencies between 100 Hz and 200 Hz, where the double-wall resonance is important.

This difference is thought to be caused by the infinite representation of the treatment used in the theory. Theoretically, acoustic waves are allowed to travel parallel to the skin surface, whereas in the aircraft panel the frames form a barrier that prevents such parallel travel. Improvements to the theory have been examined (refs. 38 and 62), but they increase the difficulty of the solution. A rigorous (and manageable) analysis of double-wall treatment has not yet been developed, so most analysis methods use the infinite-panel theory. As shown in figure 20, the theory agrees well with test data at frequencies well above the double-wall resonance, where design attention should be focused anyway because of the double-wall advantage.

Acoustic Power Flow Into an Enclosure

The overall analysis of noise transmission into an airplane fuselage can be considered in terms of acoustic power flow. This approach is quite general and allows different analysis methods to be combined to cover an extensive frequency range. For example, finite element analysis can be performed at low frequencies and statistical energy analysis at high frequencies. Acoustic power flow has been used in varying forms, including the prediction of rocket noise transmission into the payload bay of the Space Shuttle orbiter (ref. 47) and propeller noise transmission into high-speed (ref. 63) and general aviation (ref. 48) aircraft.

The basic concept of the acoustic power flow approach is that of power balance; power flow into a system must be balanced by power flow out of the system and power absorbed within. Thus,

$$P_{\text{in}} = P_{\text{diss}} \tag{15}$$

where P_{in} is the net, time-averaged power flow into the structure and receiving volume, and P_{diss} is the net, time-averaged power dissipated in the structure and on the interior walls. Since P_{in} is the *net* inflow of power, it takes into account any acoustic power that flows back from the fuselage interior to the exterior. In principle, acoustic energy can be stored only in resonant modes, but it has been shown that nonresonant response can also be considered in the analysis (ref. 64).

Statistical Energy Analysis

Statistical energy analysis (SEA) was first developed in 1959 (ref. 65); the original theory was presented with considerable generality so that it would be applicable to a wide variety of physical problems (ref. 66). A number of early applications involved spacecraft launch vehicles, and since about 1974 (ref. 67), the method has been applied to the prediction of noise transmission into aircraft. Certain assumptions inherent in the method mean that SEA is valid only at high frequencies, although the definition of "high" frequency is fairly flexible and varies from one application to another. However, because of this restriction, SEA is often used in conjunction with other methods, particularly modal methods which can be used at low frequencies. This joint application of SEA and modal methods is particularly suitable when the modal approach involves the concept of acoustic power flow. SEA depends explicitly on the concept of power or energy flow in the derivation of the analytical model.

General Concepts of SEA

SEA views a particular system, such as a specific aircraft cabin, as a sample drawn from a statistical population with random parameters. Statistical estimates of

average response parameters, such as acoustic pressure averaged over time and space (e.g., cabin volume), are derived starting with modal equations such as equation (10). The advantage of this approach can be seen by considering the calculation of the response of a complex structure such as that shown in figure 17 at high frequencies using the classical modal methods described in previous sections. As previously mentioned, it takes great effort to calculate the large number of modes that may be required to describe response to a broadband input. In some cases computing capacity and cost limit the number of modes that can be accurately computed (ref. 46). Manufacturing tolerances and variations in material properties may also affect the high-frequency modes; such variations would be impractical to define. The SEA approach is to avoid consideration of the detailed structural characteristics and, instead, focus attention on the use of energy conservation principles to develop relations between acoustic and structural responses that depend on average modal properties over a frequency band.[6] This procedure leads to comparatively simple solutions that depend on structural and acoustic parameters (such as modal density, radiation resistance, and coupling loss factors) that are unique to SEA (refs. 65 and 69). In some problems the answers are independent of many structural details. Major activities in a typical SEA calculation are modeling the system and evaluating the SEA parameters for the system (ref. 70). If the analysis is initiated early in the development of a vehicle, successive improvements to the model and parameter values can lead to good predictions of interior noise for quite complex vehicles (ref. 47).

SEA of Aircraft Sidewall

The first step in an SEA calculation is the synthesis of a model (ref. 70). A model used for an aircraft interior noise analysis (ref. 67) is shown in figure 21. The elements of an SEA model consist of interacting energy storage systems composed of resonant modes. In figure 21 each box represents a single physical element of the sidewall, but this correspondence is not necessary. For example, the torsional and flexural modes of a beam might be represented in separate boxes if they interact differently with neighboring elements. Transmission by nonresonant modes that do not store appreciable energy is represented only by the dashed lines in figure 21. The synthesis of an SEA model might be suggested by previous work, but judgment is required for reliable modeling of each new system.

Energy balance relations are then written for each element of the model. For the fuselage skin, the energy balance is

$$P_{s,e} + P_{s,d} + P_{s,w} + P_{s,f} = 0 \tag{16}$$

where

$P_{s,e}$	power flow from skin to exterior
$P_{s,d}$	power dissipated within skin
$P_{s,w}$	power flow from skin to wall cavity
$P_{s,f}$	power flow from skin to frame

[6] Dowell and Kubota (ref. 68) have developed a new high-frequency approach utilizing asymptotic analysis.

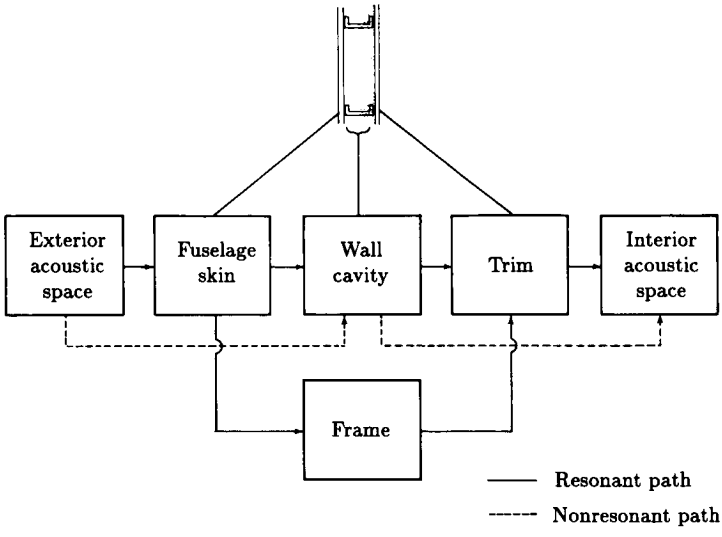

Figure 21. Model of sidewall noise transmission used in statistical energy and power flow theories for aircraft interior noise prediction. (From ref. 67.)

Expressions similar to equation (16) are written for each box in figure 21 and form a set of linear algebraic equations that must be solved simultaneously, in general. For simplified analysis the skin response is determined assuming no power flow to the wall cavity or frame.

Analysis of modal energy shows that the power dissipated in the structure is proportional to the total mean square energy E_s by the relation

$$P_{s,d} = 2\pi f \eta_s E_s \tag{17}$$

where η_s is the damping loss factor. The power flow from the exterior to the skin is found to be proportional to the difference between the energy of the two systems[7]

$$P_{s,e} = 2\pi f n_s \eta_{s,e} \left(\frac{E_s}{n_s} - \frac{E_e}{n_e} \right) \tag{18}$$

where

n_s	modal density of the skin
$\eta_{s,e}$	coupling loss factor defining the power flow from skin to exterior
E_e	energy in exterior field
n_e	modal density of exterior field

[7] The similarity of this equation to the equations for heat and electrical flow leads to the use of thermal and electrical analogies in the development of SEA results (ref. 66).

The energies in the exterior field (modeled as reverberant) and the skin are given by

$$E_e = \frac{V_e}{\rho_o c_o^2} < p_e^2 > \tag{19}$$

$$E_s = \frac{\rho_s V_s}{(2\pi f)^2} < a_s^2 > \tag{20}$$

where

$< p_e^2 >$	space-time mean-square pressure in reverberant field
$< a_s^2 >$	space-time mean-square skin acceleration
V_e, V_s	volumes
ρ_o, ρ_s	density of acoustic medium and skin

Substitution of equations (17) to (20) into equation (16), with $P_{s,w} = P_{s,f} = 0$, leads to the expression for skin acceleration resulting from the exterior pressure:

$$< a_s^2 > = \left[\frac{(2\pi f)^2 V_e}{\rho_s V_s \rho_o c_o^2}\right] \left(\frac{n_s}{n_e}\right) \left(\frac{\eta_{s,e}}{\eta_{s,e} + \eta_s}\right) < p_e^2 > \tag{21}$$

Further solution of equation (21) requires evaluation of the modal densities n_s and n_e and the loss factors η_s and $\eta_{s,e}$. Evaluation of these parameters is a major area of effort in SEA calculations. For simple physical systems such as uniform flat plates or cylinders, modal densities can be accurately calculated using theoretical methods. For complex systems (fig. 17) direct theoretical calculation would be impractical; therefore modal densities are usually estimated from known results for simple configurations. Catalogs of modal densities of many types of systems have been compiled for such estimation purposes (ref. 71). Damping loss factors η_s involve internal dissipation and usually must be measured or estimated from available test results from similar structures. Coupling loss factors $\eta_{s,e}$ can be calculated with reasonable accuracy using theoretical methods for simple configurations, but may have to be estimated or measured for complex systems. Coupling of mechanical systems (plates and shells) with acoustic media can be expressed in the relation

$$\eta_{s,e} = \frac{\rho_o c_o}{2\pi f \rho_s h} \sigma_{s,e} \tag{22}$$

where h is skin thickness, and $\sigma_{s,e}$, known as radiation efficiency, is the ratio of the actual power radiated to the power radiated by an infinite flat plate (with the same mean-square velocity) generating a plane wave. Extensive calculations have been carried out to determine radiation efficiencies of common practical structures (ref. 72).

Solution of the power balance equations for each element in the model of figure 21 leads to an expression for mean-square cabin pressure as a function of exterior pressure and the parameters of each system element. SEA has been applied in

various forms to a number of aircraft and aircraft model configurations (refs. 4, 8, 47, 48, 63, 67, 73, and 74) and found to give results that agree with other analytical methods and with test results.

Analysis of Rectangular Fuselage

A number of aerospace vehicles are characterized by fuselage sidewalls having large areas with little or no curvature and nearly rectangular fuselage cross sections. Many of the vehicles consist of aircraft driven by propellers that generate the major part of the cabin noise by transmission through the sidewall, but the category also includes the Space Shuttle orbiter where the sources of noise in the payload bay at lift-off are the rocket exhausts.

Propeller-Driven Aircraft

The sketches in figures 9 and 10 show a configuration associated with propeller-driven aircraft. Modal theory has been applied to the prediction of cabin noise in these aircraft (ref. 42). The sidewall is modeled as flat, the structural models indicated in figure 17 are used, and the cabin is modeled as rectangular with equivalent modal damping of the acoustic modes. Effects of add-on acoustic treatments are included using an approach like the one illustrated in figure 19 and using infinite-panel theory to calculate treatment effects. Variations of propeller noise over the surface of the sidewall are accounted for by averaging the propeller noise level over each panel and then assuming in the analysis that the average level acts uniformly over that panel.

At midfrequencies the theory considers the sidewall to consist of an array of stiffened panels (fig. 17). In one application of modal theory, three skin panels and four flexible stiffeners are analyzed together as one stiffened panel (ref. 75). The modes of such a stiffened panel are complicated and require considerable effort to calculate accurately (ref. 76). The exterior noise is assumed to act uniformly over each stiffened panel. The cabin noise at any position is obtained by summation on an rms basis of the contribution from each stiffened panel (this assumes that the contributions are area-related). Predictions using this theory have been compared with test results, as illustrated in figure 22 (ref. 77). The exterior noise was directed onto one stiffened panel at a time using an "acoustic guide." For the example shown in the figure, agreement between test and theory is excellent at frequencies below about 250 Hz.

Study of a complete aircraft fuselage in the laboratory has advantages over TL or flight testing. The panel area under study can interact with the noise source, adjacent structure, and cabin acoustics in a realistic manner, but test conditions can be carefully controlled and a variety of tests can be performed at relatively low cost (ref. 78). For example, tests such as that illustrated in figure 22 showed that different stiffened panels transmitted different amounts of noise, and this result was then used to tailor the distribution of treatment over the sidewall to provide a minimum-weight treatment (ref. 75). The acoustic guide has been used to isolate the transmission of noise through a window, thus providing data to support theory for double-pane windows (ref. 77).

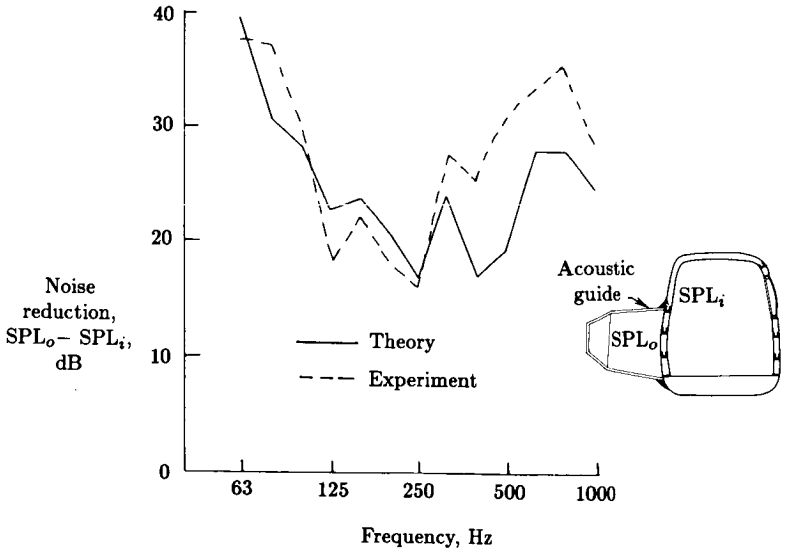

Figure 22. Noise reduction through a light aircraft fuselage using a localized source noise. Laboratory test. (From ref. 77.)

Comparison With Flight Measurements

Measured and predicted interior noise for flight conditions is compared in figure 23 (ref. 5). The aircraft is a twin-engine turboprop weighing about 5080 kg and was operated at an altitude of about 9000 m with a pressurized cabin and nominal cruise engine power settings. The cabin contained seats for pilot, copilot, and test engineer but no other furnishings. Several sidewall treatments were tested; the results shown are for an experimental configuration having several layers of mass-loaded vinyl septa and fiberglass blankets. The analysis (ref. 75) used experimental information for propeller and boundary layer source noise to establish levels on 12 stiffened panel areas of the sidewall. Structural vibration modes of these 12 panels, 6 of which were windows, were determined using detailed finite element strip methods and/or transfer matrix methods. The cabin was modeled as a rectangular enclosure with absorption included as "equivalent" damping of the acoustic modes. The effects of sidewall treatment were included by adding insertion loss values determined from infinite-panel theory, as discussed previously. Figure 23 shows that the theory predicts the overall trend of the flight data quite well. In making a detailed comparison of measured and predicted levels at individual frequencies, one must consider both theoretical approximations and measurement precision, either of which could account for the differences shown.

Treatment Design for Airplane Cabin

The modal methods described above have been used to search for optimum combinations of structural and add-on treatments that satisfy a target interior noise level with the least added weight (refs. 42 and 75). Structural modifications considered included increased skin thickness, addition of stiffeners, addition of mass

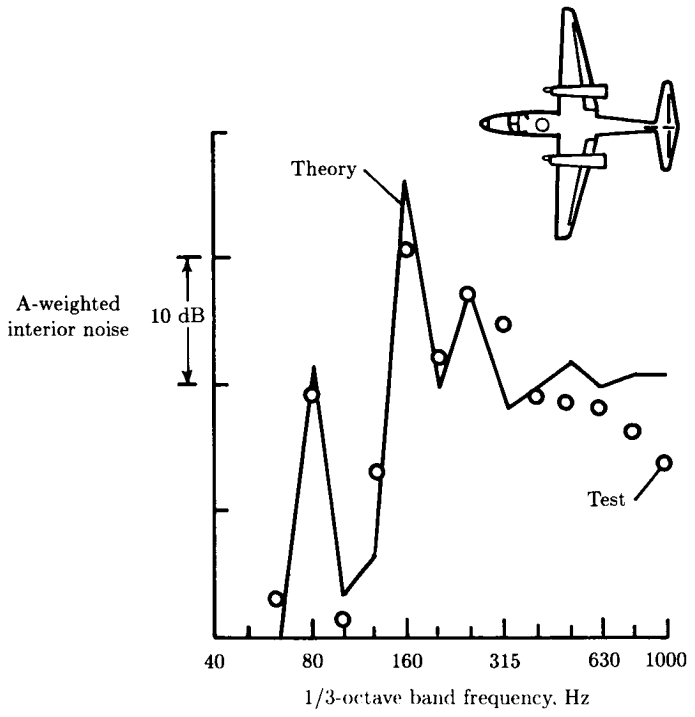

Figure 23. Predicted and measured interior noise in a light aircraft in flight. (From ref. 5.)

or damping layers to the skin, and addition of honeycomb stiffening panels to the skin. Add-on treatments considered included fiberglass blankets, lead-vinyl septa, and trim panels in numerous combinations. Treatment designs were studied for two twin-engine propeller-driven aircraft, one of which was flight tested to obtain the results shown in figure 23.

An example of parameter studies conducted for structural treatments is shown in figure 24 (ref. 79). The interior noise level at zero added weight is the calculated value for an untreated interior. The figure shows that different treatments provide different amounts of reduction in interior noise for a given value of added weight, indicating that there is substantial benefit potential in optimum choice of treatment. For each treatment the curve tends to flatten as weight increases, so that benefits tend to diminish as greater weight of treatment is added. In such a case the alternative to a large weight penalty is to use some other treatment. In the example shown in figure 24 the treatment labeled "damping" would be the best, for that particular noise spectrum and structure, because it provides the lowest noise level for a given weight.

Parameter studies such as that shown in figure 24 have been conducted for a variety of treatments, and several candidate configurations have been developed (ref. 75). Laboratory TL tests of several of these configurations (ref. 80) tend to confirm the ability of the theory to represent the contribution of the treatment elements and to identify a superior treatment combination.

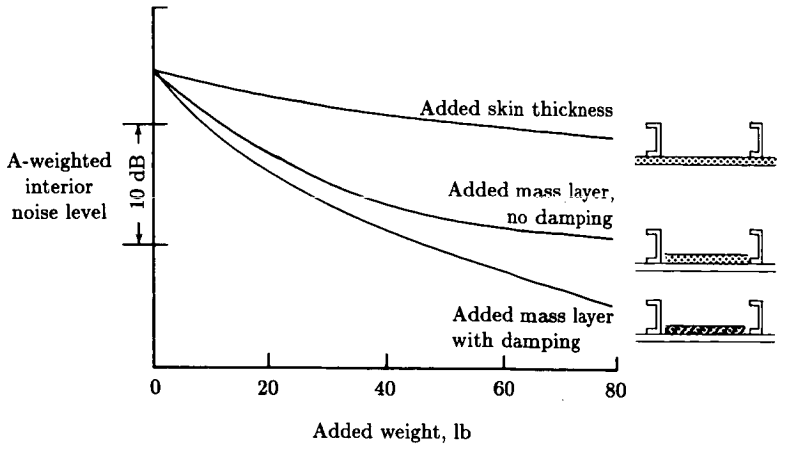

Figure 24. Reduction in aircraft interior noise predicted by modal theory (ref. 79) for three structural treatments.

Space Shuttle Payload Bay

The payload bay of the Space Shuttle orbiter consists of flat sidewalls and bulkheads (forward and aft) and slightly curved bottom structure and bay doors (fig. 25). Thus, the analytical model developed to predict noise transmission into the payload bay envisaged the transmitting structure as an array of flat panels (ref. 47). At low frequencies, below about 60 Hz, the modal characteristics of the structure were predicted using finite element methods. Then, at higher frequencies, where the large number of modes made use of finite element methods very time-consuming, the structure was modeled as equivalent single orthotropic panels. In this case, mass and stiffness of the frames and stringers were averaged over the panel surface to give the structure orthotropic characteristics, and closed-form equations were developed to represent the motion of the panels. The orthotropic model included both frames and stringers until the frequencies exceeded the lowest resonance frequencies of individual panels of a given structural region. At higher frequencies, mass and stiffness of the frames were often excluded from the model.

The coupling between the structure and the excitation field generated by rocket exhaust noise was determined (refs. 11 and 47) by use of the joint acceptance function $j_r^2(\omega)$ for mode of order r. The joint acceptance function is defined by

$$j_r^2(\omega) = \int_{\bar{x}_1} \int_{\bar{x}_2} \frac{S_p(\bar{x}_1, \bar{x}_2; \omega) \Psi_r(\bar{x}_1) \Psi_r(\bar{x}_2)\, d\bar{x}_1\, d\bar{x}_2}{A^2 S_p(\bar{x}_o, \omega)} \tag{23}$$

where

$S_p(\bar{x}_1, \bar{x}_2; \omega)$ the cross spectral density of the "blocked pressure" (ref. 69) on the exterior of the fuselage

Ψ_r eigenfunction (mode shape) of the rth mode of the structure

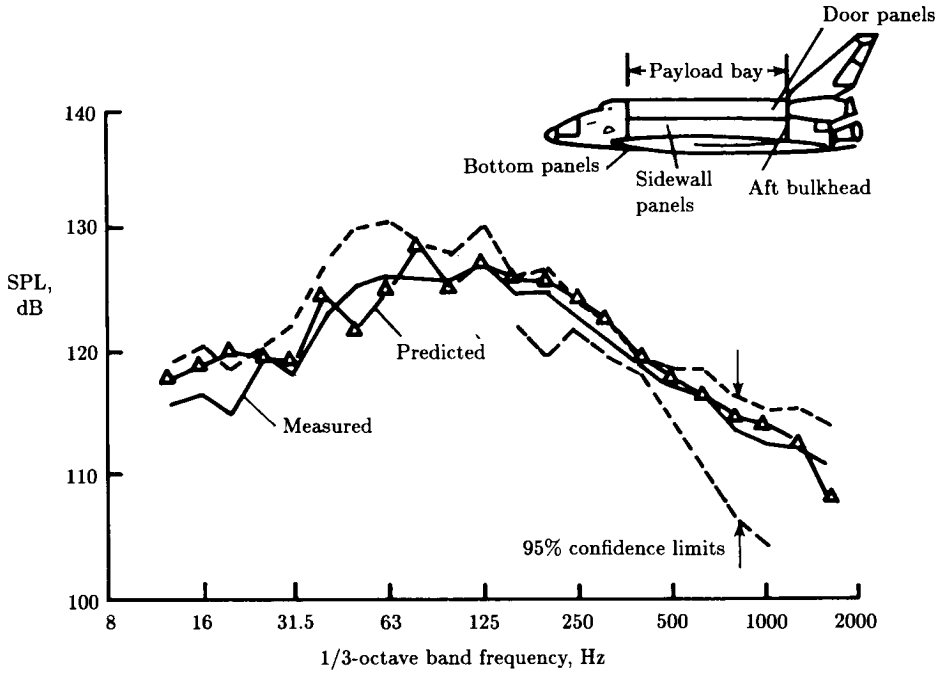

Figure 25. Measured and predicted space-average sound pressure level in the payload bay of the Space Shuttle orbiter (ref. 47).

A	structure area
$S_p(\bar{x}_o, \omega)$	reference value of power spectral density of blocked pressure

The cross spectral density functions of the excitation pressures were obtained from model-scale test data. The pressure field was represented as a convected field with exponential decay of the correlation (ref. 47). In a similar manner, the response of the structure to the acoustic pressure field in the payload bay was predicted from the joint acceptance function with the pressure field assumed to be reverberant. The same approach could be used to predict the response of the payload bay structure to boundary layer excitation during high dynamic pressure conditions on ascent (ref. 11).

Acoustic response of the payload bay was calculated from the coupling of the modes of the structure and the volume. The acoustic modes were predicted for a slightly deformed parallelepiped volume, but at higher frequencies, SEA methods were used. Dissipation of acoustic power in the volume resulted from the absorption of sound by the thermal control material covering the walls of the bay.

During development of the analytical model, ground test and, eventually, launch data were used to evaluate some of the assumptions. This resulted in an analytical model (ref. 81) which could predict the payload bay sound levels with reasonable accuracy, as is shown in figure 25. The model was then used to predict the effect of the presence of a payload on the sound levels in the payload bay.

Analysis of Cylindrical Fuselage

For a large class of aircraft, the fuselage is nearly circular and analysis methods have been developed that consider the transmission of noise into these circular fuselages. The methods differ in the manner in which the fuselage structure is represented and in the analytical model used for the exterior pressure field. In one case, the fuselage is assumed to be infinitely long, since the fuselage length is large relative to both the fuselage diameter and the acoustic wavelength in the frequency range of interest. Furthermore, the exterior pressure field is represented by acoustic plane waves. In another case, the fuselage is assumed to be finite and the excitation pressure field is a detailed representation of that generated by a propeller.

Infinite-Cylinder Analysis

Theories have been developed for analysis of sound transmission into infinitely long cylinders, with the exterior sound field modeled as a plane wave incident to the axis of the cylinder at an angle θ (ref. 82). Because of the geometry of the infinite cylinder, coupling of the shell with the exterior and interior acoustic dynamics, as represented in equation (10) by the C_{mn} terms, can be included without undue difficulty. The effects of external airflow, representing aircraft forward speed, and cabin static pressurization are included in the analysis,[8] and several models of the shell structural dynamics and cabin acoustics have been analyzed.

A theoretical model consisting of an infinite skin that is stiffened at periodic intervals in the direction of a traveling wave has also been applied to aircraft fuselage vibration and noise transmission analysis (ref. 83). The structure behaves as a bandpass filter, responding very efficiently in certain frequency bands (pass bands) but not so efficiently in other frequency bands (stop bands). The model allows a detailed study of the interaction between the skin and stiffener dynamics. Application of this theory to aircraft configurations (ref. 84) has led to development of noise and vibration control concepts involving "intrinsic structural tuning" and damping applied to stringers and frames. Flight test data tend to support the theoretical conclusions, and several operational control devices have been developed and used.

Plane-Wave Transmission Into Cylinder

Figure 26 illustrates cylinder noise transmission as measured and predicted by infinite-cylinder theory (ref. 57). A cylinder of 0.508-m diameter and 1.98-m length was subjected to loudspeaker-generated noise in an anechoic chamber. The skin was unstiffened and the interior contained a core of sound-absorbing foam to simulate the theoretical model of an interior containing only radially inward-traveling waves.[9]

[8] Results have been calculated for a typical narrow-body aircraft with fuselage diameter of 3.66 m, at an altitude of 10 660 m. The results show that forward speed provides a small increase in TL in the mass law region and interacts strongly with the cylinder resonances at lower frequencies. Internal pressure decreases TL slightly, and the acoustic mismatch between external and internal properties increases TL.

[9] The shell interior has also been modeled using acoustic modes (ref. 52).

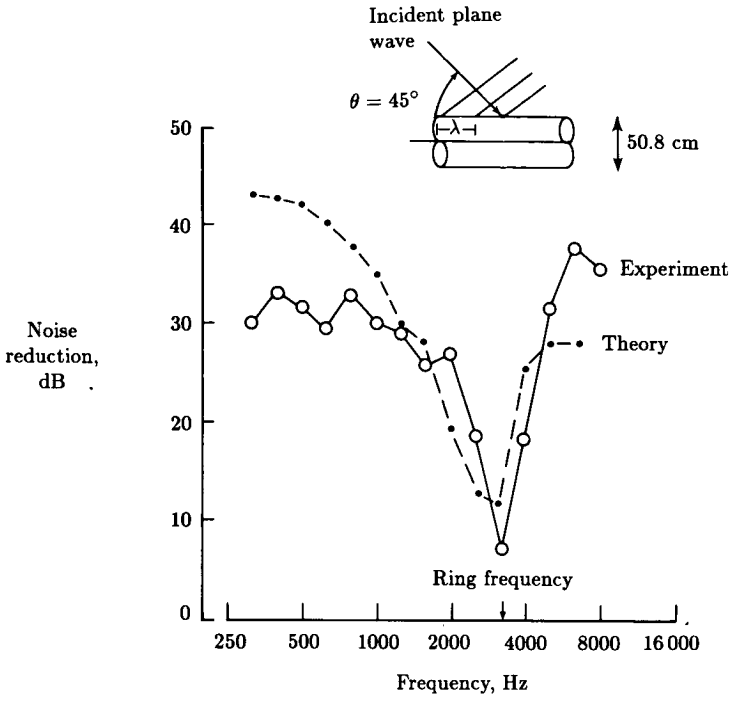

Figure 26. Transmission of sound incident at 45° into an unstiffened cylindrical shell. (From ref. 57.)

Both theory and test show a large decrease in noise reduction at frequencies near the ring frequency for the particular incident angle illustrated. Ring frequency f_r is given by the relation

$$f_r = C_L/\pi D \approx 1700/D \tag{24}$$

where C_L is the longitudinal wave speed in the shell material, D is the cylinder diameter, and the approximate relation applies to aluminum when D is expressed in meters (ref. 85). The mechanism of noise transmission near the ring frequency has been analyzed using statistical methods showing a large concentration of structural modes (ref. 86). Furthermore, some of the structural modes at, and just below, the ring frequency have high acoustic radiation efficiencies. For aircraft, the effects of ring frequency are often not as large as shown in figure 26, probably because of the effects of structural complexities such as stiffeners, floor, or add-on acoustic treatment.

It may be noted that this infinite-cylinder theory is based on incident and transmitted acoustic power and full coupling of acoustic and structural dynamics, in much the same manner as the classical analysis of noise transmission through an infinite flat panel used for architectural TL studies. The effects of curvature have been investigated in comparison with flat panels (ref. 87). The equations presented provide a means of quantitatively estimating curvature effects that may account in part for differences between laboratory TL results and flight results.

Structural Models for Infinite Cylinder

Orthotropic-panel and discrete stiffener structural models have been incorporated in the infinite-cylinder theory (refs. 88 and 89) to explore the influence of these realistic factors on predicted transmission loss. These studies show that the added structural complexity leads to transmission loss characteristics with new features which probably would not have been foreseen based on previous experience and which have not yet been fully explained. The results must therefore be considered preliminary. However, the importance of realistic modeling of ring- and stringer-stiffened aircraft structures and the possible use of fiber-reinforced composites for structural tailoring for noise control make the results of considerable interest.

As an example, the transmission loss (TL) of an orthotropic cylinder is shown in figure 27 for three values of ratio E_ϕ/E_x, where E_ϕ and E_x are Young's moduli in the circumferential and axial directions, respectively. For these calculations, parametric values typical of a narrow-body aircraft fuselage were used, and the ring frequency f_r (and consequently the circumferential stiffness E_ϕ) was held constant at 445 Hz. In this case variations of the ratio E_ϕ/E_x result only from variations of E_x, and E_x is important because it influences the axial bending wave of wavelength λ induced in the cylinder by the incident sound wave.

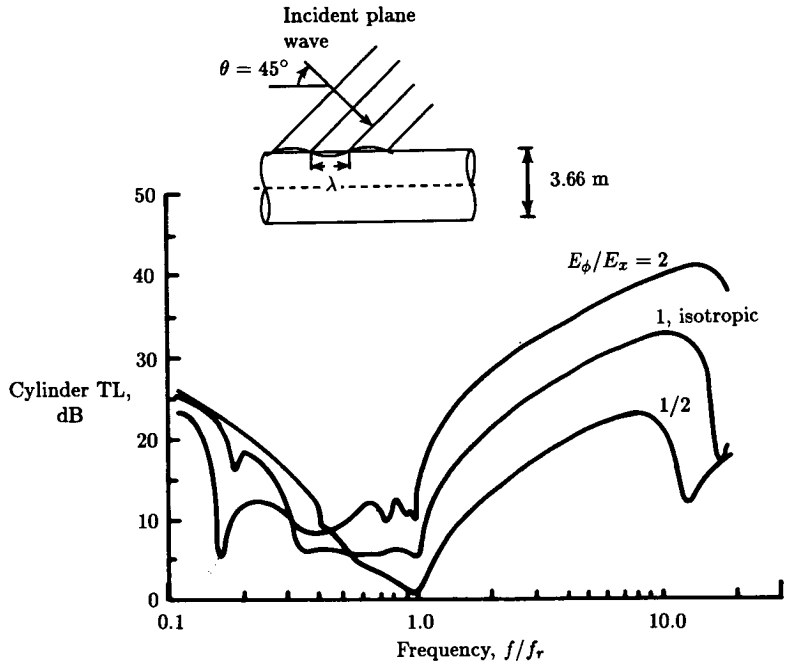

Figure 27. Calculated effect of modulus ratio on transmission loss of a cylindrical shell. (From ref. 88.)

Careful examination of figure 27 reveals the following TL characteristics that are consistent with general experience with flat panels. At low frequencies (in the

stiffness controlled region) the TL increases with decreasing f/f_r at a rate of about 6 dB/octave, and for f/f_r between 1.0 and 10 (often considered the mass controlled region) the TL increases at about 6 dB/octave. The TL dips at the ring frequency, $f/f_r = 1$, and at the coincidence frequency, $f/f_r = 12$ to 20. Increasing the axial stiffness (increasing E_x corresponds to decreasing E_ϕ/E_x) increases the TL at low frequency and reduces the coincidence frequency.

However, the figure also shows other, new features, the main one being the large variation of TL with E_ϕ/E_x for $f/f_r = 1$ to 10. In this frequency region the predicted TL increases by 6 to 8 dB for a doubling of E_ϕ/E_x, indicating that panel mass is not the only controlling parameter. While the analysis of the cylindrical shell (refs. 88 and 89) does not provide a ready explanation of the phenomenon, analysis of an infinite flat plate (ref. 35) shows explicitly that mass and stiffness are coupled and that TL can vary significantly with stiffness. Possibly, the predicted TL for the cylindrical shell involves both resonant and nonresonant (mass law) transmission, and the changes in the acoustic radiation efficiency of the shell associated with change in shell stiffness influence the acoustic transmission.

The choice of orthotropic properties for optimum noise control would have to depend on both the directional and the frequency characteristics of the important noise sources. The calculated results show complex changes in the TL curves with incidence angle (ref. 88). For realistic ring frequencies, important noise sources can be expected to occur at frequencies both above and below f_r. Therefore a detailed analysis of the particular configuration of interest would be required to determine appropriate values of the orthotropic moduli for minimum noise transmission.

Analysis of Aircraft Cabin Treatment

The infinite-panel theory has been combined with add-on treatment and cabin absorption analysis in a manner indicated in the diagram of figure 19. The resulting prediction method has been used to design cabin noise control treatment for high-speed propeller-driven aircraft of three sizes (ref. 57). To handle the propeller source noise having a nonuniform distribution, the fuselage was divided longitudinally into several segments. The average sound pressure level and a range of incidence angles were determined for each segment from estimated propeller characteristics and locations indicated in figure 28. Then sound transmission calculations were performed for several angles of incidence within the range for each segment and an average sound transmission was determined.

The treatment design approach was to estimate the exterior noise generated by a high-speed propeller and then to design a minimum-weight sidewall configuration that would provide an A-weighted cabin sound level of 80 dB. Extensive parametric studies varied sidewall and trim panel weights, configurations, and materials (ref. 57). Results are illustrated in figure 28. As shown by the various shadings in the figure, the treatment varied in several steps along the fuselage length, but was uniform circumferentially except that no treatment was applied below the floor. It was concluded that conventional treatment could provide the required noise reduction provided that sufficient weight was added. The weight required differed for the executive class, narrow-body, and wide-body aircraft studied.

The detailed analysis confirmed weight estimates made earlier using more simplified prediction methods (ref. 90). It was estimated that cabin noise control treatments with added weights up to 2.3 percent of aircraft gross weight, even though

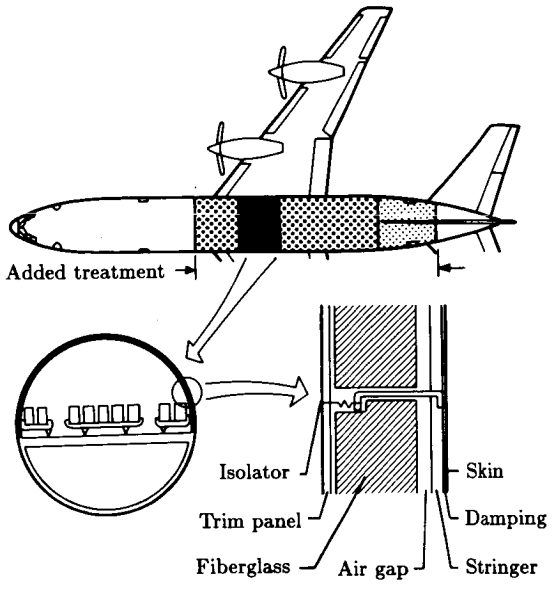

Figure 28. Cabin noise control treatment for a transport aircraft powered by propellers with supersonic tip speed. Weight of treatment required to control propeller noise is 0.75 to 2.3 percent of aircraft gross weight. (From ref. 57.)

much heavier than the more usual value of about 1 percent of gross weight, were not large enough to reduce significantly the advantage in fuel used and direct operating cost obtained by the use of advanced propellers. However the sidewall treatment weights are large enough that worthwhile reductions in fuel consumption would result if treatment weight were reduced. Efforts have been conducted in a search for lighter weight treatment concepts specially suited to the tonal noise spectrum characteristic of propellers (ref. 91).

The detailed analysis also provided an engineering description of the sidewall configurations required. An experimental program was carried out to validate the theoretical prediction methods, to evaluate the sidewall designs developed by the analysis, and to provide experience with the very heavy sidewalls that the theory indicated were necessary for high-speed turboprop application (ref. 92). The test fuselage was a segment taken from an operational commuter aircraft to obtain a realistic structure. The fuselage, a specially designed floor, and the sidewall treatment were designed to be a 43-percent scale model of the narrow-body aircraft design of the theoretical study. Test results were obtained for several sidewall and treatment configurations to obtain trends with weight. Noise reduction results are shown in figure 29 for the configuration representing the design point resulting from the analytical study. The figure indicates that the theory predicts slightly less noise reduction than is measured, suggesting that the weight estimates (ref. 57) are conservative. Test and theory do not agree as well for the other sidewalls, especially at lower frequencies for the lighter weight configurations. Improved representations

of the sidewall structure, the propeller source noise distribution, and the interior acoustics may be required for improvement of the theoretical predictions.

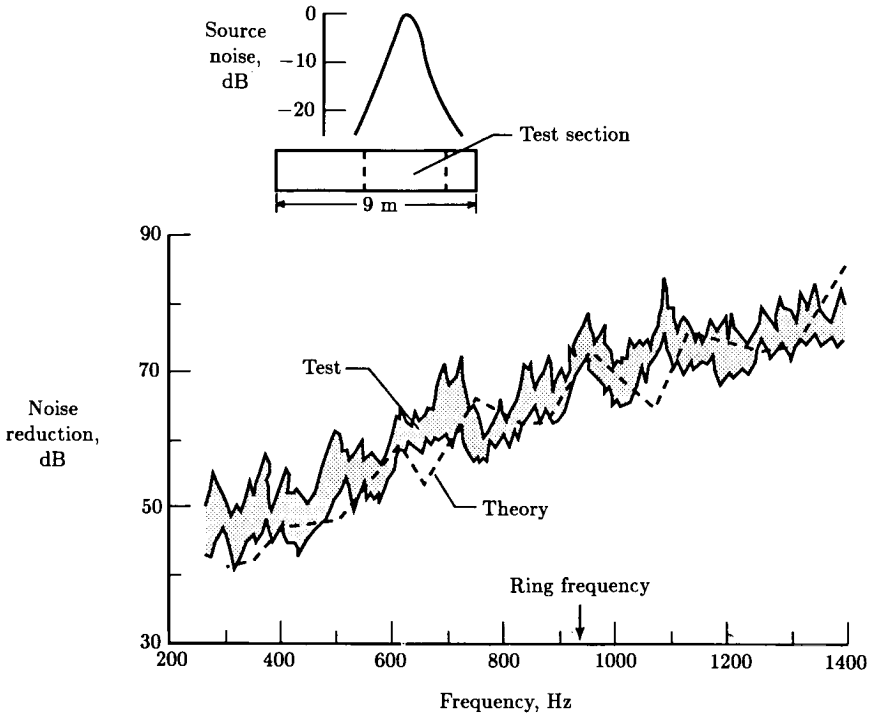

Figure 29. Noise reduction of a 168-cm-diameter aircraft fuselage with double-wall noise treatment (ref. 92). Propeller source noise simulated with a horn. Mass of outer wall was 9.47 kg/m^2; inner wall, 7.13 kg/m^2.

Testing of realistic fuselage and treatments entails substantial cost and time. The theory clearly showed its value in this program by providing candidate treatment configurations at much less cost than would have been required by experimental approaches alone.

Finite-Cylinder Analysis

It is not necessary to model cylindrical fuselages as having infinite length; analyses have been performed wherein the fuselage was considered to have finite length. Those analyses included both model and full-scale situations, and the excitation field was represented as either random or deterministic.

In one approach, transmission of propeller noise into a cylindrical fuselage of finite length has been analyzed using the general method developed for noise transmission into the Space Shuttle payload bay (ref. 63). The fuselage structure was idealized as a series of curved, orthotropic panels with frames and stringers included at low frequencies but not at high frequencies. The fluctuating pressure generated by the propeller was represented as a random, convected pressure field,

but since the pressure field is inhomogeneous, modifications had to be introduced into the analytical model developed initially for the more homogeneous case. The modifications allowed calculation of a joint acceptance function that depends on the distance of a particular panel from the location of maximum excitation pressure. Division of the fuselage structure into several panels allowed calculation of noise transmission through different regions of the cabin and determination of noise control treatments that varied in composition along the length of the cabin. The sidewall treatment was modeled in this approach as an independent module of the analytical procedure.

Transmission of random noise was also considered in another analytical model (refs. 48 and 73), but an important contribution of that study was the detailed representation of propeller acoustic pressures as a deterministic field. Measurements on general aviation aircraft indicate that the harmonic components of propeller noise are essentially deterministic. Furthermore, analytical methods are becoming available to predict the magnitude and phase of each harmonic component. This detailed representation of a propeller acoustic field has been used to calculate the deterministic forcing function on a cylindrical fuselage (ref. 48). In this approach, the region of the fuselage exposed to the acoustic pressure is represented by a grid of points, with the harmonic pressure and phase defined at each point. The grid shown in figure 30 has 160 points on the upper quadrant of the fuselage. The pressure field for the lower quadrant is determined from that of the upper quadrant, with a phase shift introduced to account for the rotational speed imposed by the propeller.

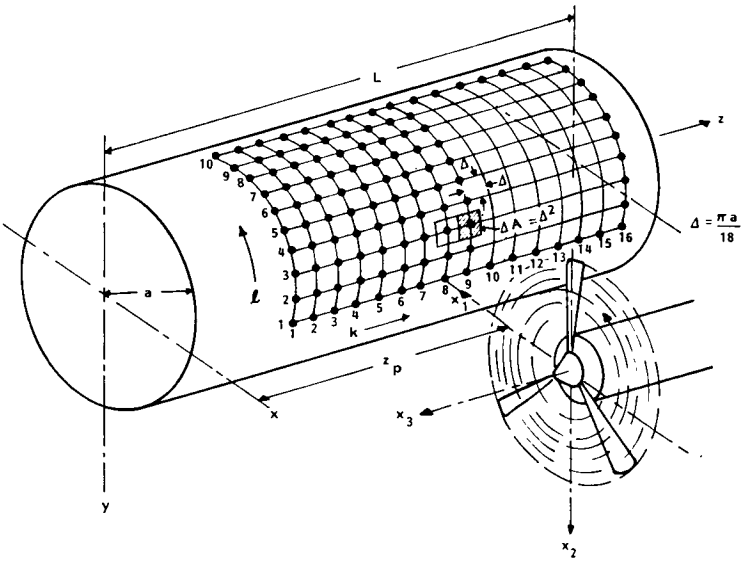

Figure 30. Grid used to couple ANOPP theoretical propeller noise model with cylinder noise transmission in the propeller aircraft interior noise prediction program (ref. 73).

Other important aspects of the analytical model are the representation of the cabin floor as a longitudinal partition and the first attempt to integrate the sidewall treatment into the noise transmission model (ref. 48). The presence of the cabin

floor can strongly influence the dynamic characteristics of the structure and interior volume. For example, the acoustic mode shapes of the cabin may differ from those of a cylindrical volume, as can be seen from figure 14. The floor and shell of the structure can be modeled as an integral unit. Mode shapes can be calculated for such a configuration (refs. 48 and 93), a typical mode shape being shown in figure 31.

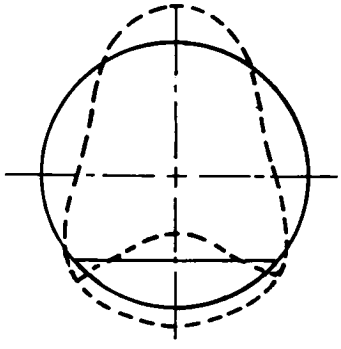

Figure 31. Calculated structural mode of a cylindrical shell with an integral floor. (From ref. 48.)

The analytical model was developed in conjunction with a series of laboratory experiments on test cylinders with diameters of 50.8 to 66 cm and a variety of configurations of circumferential and longitudinal stiffeners, floor structures, and interior acoustic treatments. These cylinders were exposed to broadband random noise and to acoustic pressures generated by a model-scale propeller. As an illustration, figure 32 compares measured and predicted noise transmission spectra for random noise excitation (ref. 73). The agreement between test and theory is good at frequencies below 500 Hz, but deteriorates at high frequencies. In the experiment the treatment consisted of a layer of fiberglass and vinyl about 1.3 cm thick that was attached to the interior of the cylinder wall. The stringer web, however, was 2.5 cm high and, therefore, extended through the treatment into the interior of the cylinder. In the analysis it was possible, using a high-frequency approximation, to estimate the acoustic power flowing through the stringer webs. It was found that at high frequencies the fiberglass-vinyl treatment was very effective and transmitted little noise and that the exposed stringers transmitted the major part of the interior noise. The predicted noise reduction is therefore reduced greatly, as shown in figure 32. In the frequency region between about 500 and 2000 Hz, neither of the theories agrees very well with the test results. However, it can be concluded that relatively small areas of exposed stringer (or ring frame) can be significant noise transmission paths when the skin areas are covered with effective treatment.

The analytical model has also been used to predict sound levels inside a general aviation airplane, for comparison with measured levels (ref. 74). The measurements were performed using a space-averaging technique that was designed to provide space-averaged levels suitable for comparison with the predictions. As shown in figure 33, the predicted sound levels agree closely with the measured results for three of the five harmonic components.

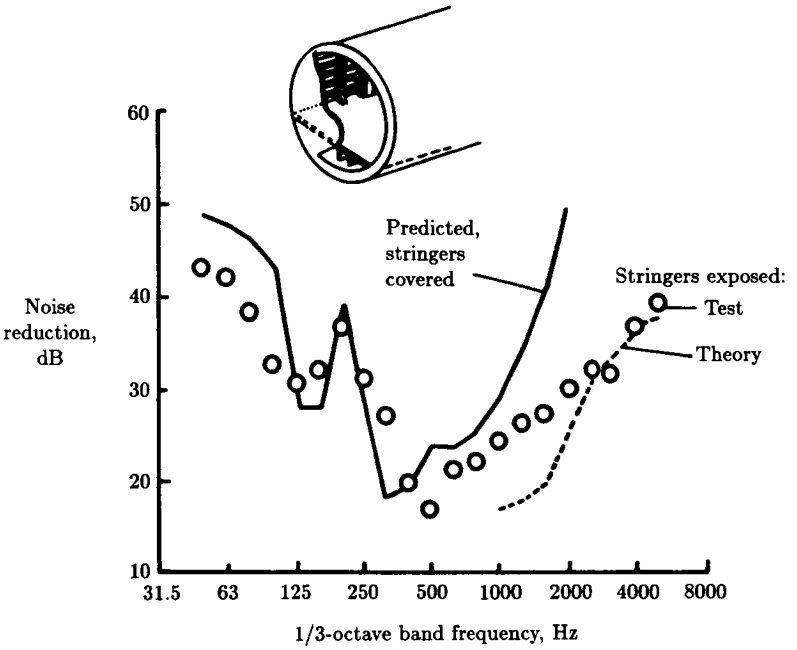

Figure 32. Predicted noise reduction of a stiffened cylinder with acoustic treatment and an integral floor. Power flow theory (ref. 73).

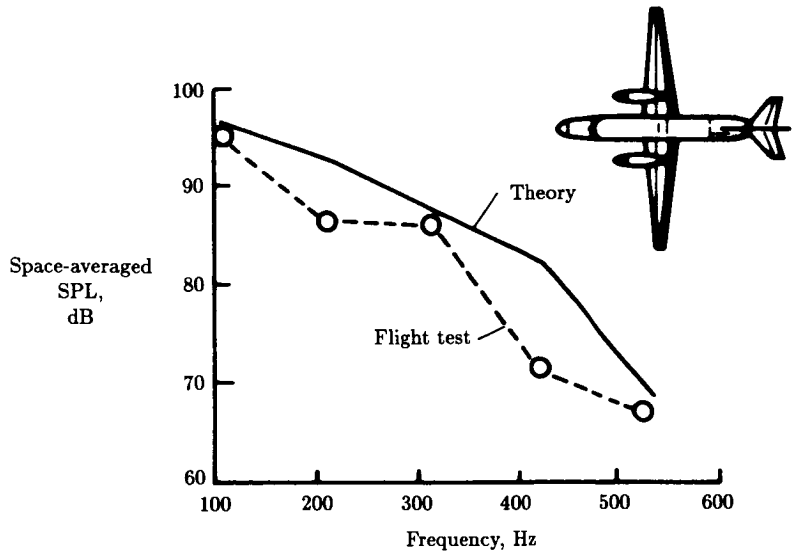

Figure 33. Prediction of cabin noise at propeller tones in flight of a light twin-engine aircraft. Power flow theory (ref. 74).

Structure-Borne Noise

Not all the sound in an aircraft interior is associated with airborne transmission. Some components of the interior acoustic field are the result of mechanical forces or aerodynamic pressures acting on distant regions of the airframe. The resulting vibrational energy is transmitted through the structure and then radiated into the fuselage interior as sound. These components of the interior sound field are referred to as "structure-borne sound."

It has long been recognized that structure-borne sound transmission could contribute to interior sound levels in certain types of aircraft. Bruderline (ref. 94) in 1937 and Rudmose and Beranek (ref. 95) in 1947 observed that structure-borne vibration from wing-mounted reciprocating engines contributed to interior sound levels. Thus, Bruderline noted that on the DC-4, "rubber supports" were to be provided for the engines, and all controls and conduits were to be flexible between the nacelles and engines. However, in both references, discussion of structure-borne sound transmission is only qualitative, Rudmose and Beranek noting that no scheme existed at that time for estimating quantitatively the amount of structure-borne vibration in an aircraft fuselage.

The situation has changed, with an improved understanding of structure-borne sound transmission in aircraft, ground vehicles, ships, and buildings. These activities have been the subject of several review papers (refs. 96 and 97) which provide numerous references associated with a wide range of aerospace and nonaerospace applications. The discussion in this section is directed specifically to the topic of structure-borne sound in aircraft, an application that is probably not as well developed as in some other fields.

Structure-Borne Sound in Aircraft

In general, structure-borne sound in aircraft is associated with discrete frequency components. This does not mean that broadband structure-borne sound is not present; however, if it is present, it has not been identified, probably because of masking by broadband airborne noise. The occurrence of structure-borne sound is not limited to propeller-driven aircraft with reciprocating engines; the sources could be turboprop, turbojet, or turbofan engines, air-conditioning systems, hydraulic pumps, and other rotating or reciprocating equipment.

One of the best documented studies of structure-borne sound in an airplane with turbofan engines is that of the DC-9 (refs. 28 and 98), but the phenomenon has been observed on other aircraft that have turbojet or turbofan engines mounted on the rear of the fuselage. For example, figure 34 shows a narrow-band sound pressure level spectrum that was measured in the cabin of a business jet airplane powered by two twin-spool turbofan engines (with geared fan) mounted on the rear of the fuselage (ref. 29). The spectrum contains a number of discrete frequency components that can be associated with the rotational frequencies of the fan, low-pressure compressor and turbine, and high-pressure compressor and turbine. These discrete frequency components are associated with structure-borne sound, whereas the broadband components result from airborne transmission, mainly due to the turbulent boundary layer on the exterior of the fuselage. Various tests have been performed to demonstrate that the discrete frequency components are definitely associated with structure-borne transmission. The tests have included ground

experiments with engines disconnected and changes to engine mounts for repeated flight tests. Also, external acoustic measurements and analysis show that acoustic radiation from the engine inlet would not generate sufficiently high sound pressure levels to be the dominant source. Structure-borne sound is present also in aircraft with wing-mounted turbojet or turbofan engines, but the sound pressure levels may not be significant except in some aircraft with large turbofan engines.

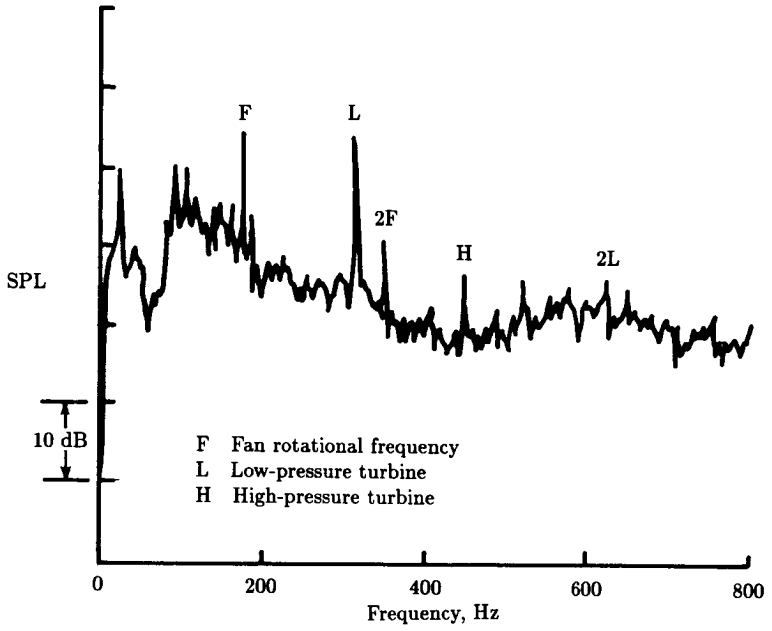

Figure 34. Discrete frequency structure-borne components in sound levels in the cabin of a business jet airplane. (From ref. 29. Copyright 1982 SAE, Inc.; reprinted with permission.)

Structure-borne sound can be a major contributor to the sound pressure levels in the cabin of a helicopter (refs. 99 and 100). For example, an investigation of the noise sources contributing to the acoustic environment in an eight-seat helicopter indicated that structure-borne noise from the engine and gearbox dominated cabin sound levels at frequencies above about 3000 Hz, as shown in figure 35. In this respect the helicopter differs from the fixed wing airplane. Structure-borne sound in helicopters is mainly high frequency, whereas it is usually low frequency in fixed wing airplanes. This difference can influence the choice of analysis method and noise control procedure used for each type of aircraft.

The preceding discussion has been concerned with the direct transmission of mechanical vibration from the engine and associated machinery into the airframe. A second path may also be present, although its importance has not yet been established. This path involves impingement of a propeller wake on the surface of a wing or empennage, with subsequent transmission of vibration energy into the cabin. Such a structure-borne path is difficult to identify, even under ground test conditions. Measurements on a twin-engine general-aviation airplane with a high

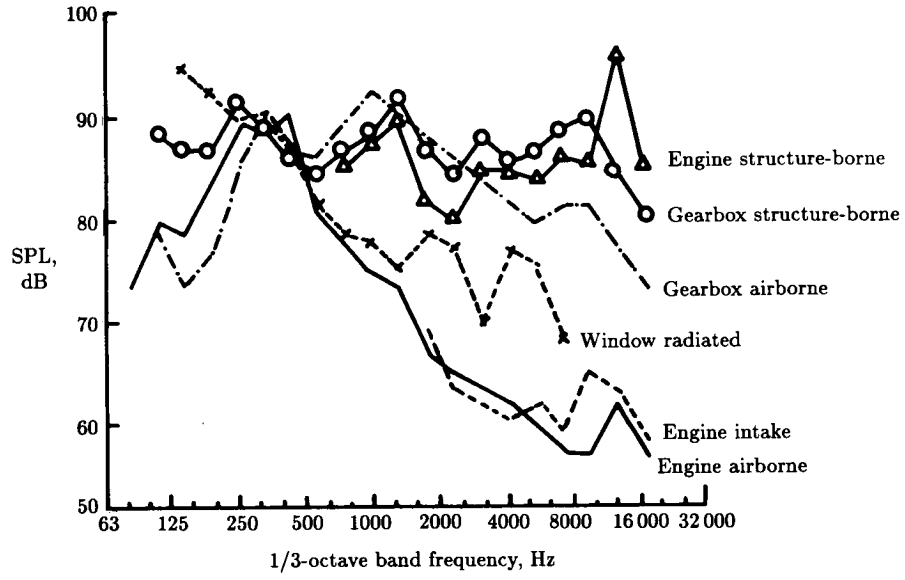

Figure 35. Noise source contributions to sound pressure levels in a helicopter cabin. (From ref. 100.)

wing (ref. 101) suggest that, at least under ground test conditions, the importance of the propeller wake as a noise source could be significant at high propeller torque (fig. 36).

Although most examples of structure-borne sound are associated with the main propulsion system of an airplane, other examples exist, although they are often of short duration. Air cycle machines in air-conditioning systems can transmit discrete frequency vibration which radiates sound into the cabin. Also, vibration can be transmitted from hydraulic pumps into the fuselage structure, with eventual radiation as sound into the cabin.

Usually, structure-borne sound components cannot be measured directly and have to be deduced from other measurements. Exceptions to this general rule occur if the airborne components can be removed (ref. 101), but it is often only the structure-borne path that can be broken and, then, only in ground tests (ref. 102). There still remains the problem of determining the structure-borne components during flight conditions.

Analysis of Structure-Borne Sound Transmission

An analysis of structure-borne sound in aircraft can be divided into three main parts: excitation, transmission, and acoustic radiation. The precise role played by each part depends on the particular aircraft configuration, but the general approach can be discussed using the example of an airplane with wing-mounted turboprop engines and propellers (fig. 37). The main components associated with structure-borne sound transmission are identified in figure 38. For this aircraft the excitation is in two forms: a mechanical component that is associated with out-of-balance forces in

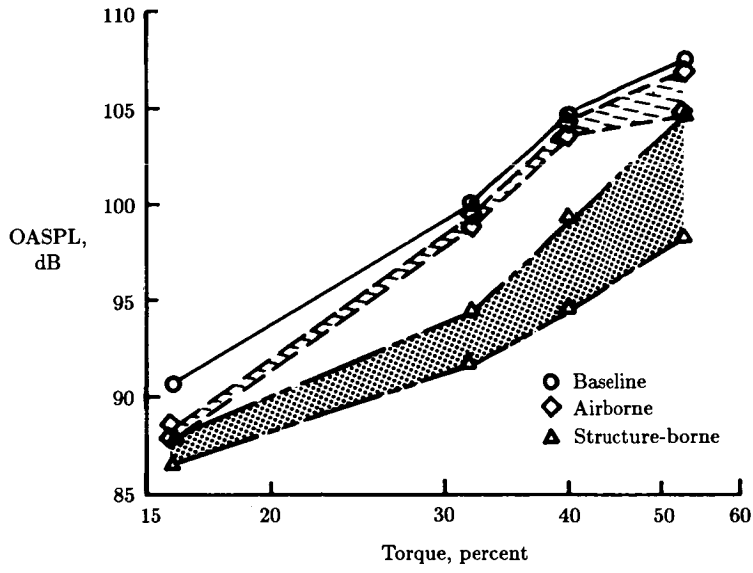

Figure 36. Airborne and structure-borne sound levels deduced from measurements in passenger compartment of a twin-engine, propeller-driven airplane. (From ref. 101.)

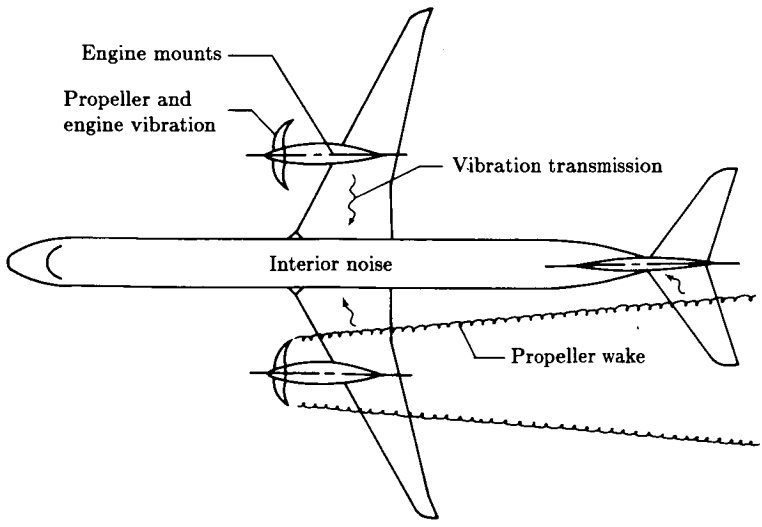

Figure 37. Sources and paths of structure-borne sound in twin-engine, propeller-driven airplane.

the engine and propeller and an aerodynamic component generated by the propeller wake on the wing. The out-of-balance forces are transmitted through the engine mounts (which may be rigid or include vibration isolators) into the wing structure, whereas the aerodynamic pressures act directly on the wing skin. Structure-borne transmission along the wing occurs in the spars and skin, although it is possible that different paths are important for different frequency components.

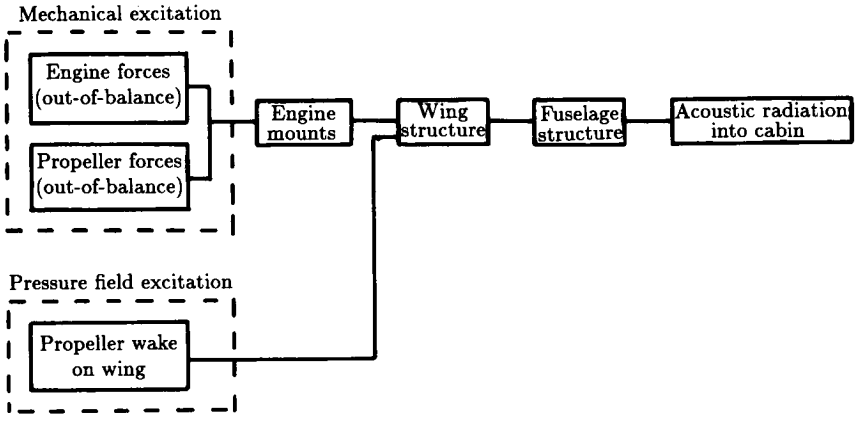

Figure 38. Main components of structure-borne sound transmission path for twin-engine airplane.

Excitation

When the excitation is generated by mechanical forces, the vibrational power P flowing into the airframe structure can be estimated by use of the impedances of the various structural components (ref. 98). Thus, typically,

$$P = \mathrm{Re}\{FV^*\} = \frac{|Z_s|^2}{|Z_s + Z_f|^2}\mathrm{Re}\{Z_f\}V_s^2 \tag{25}$$

where F and V are, respectively, the force and velocity at the connection between the source and the structure, an asterisk denotes the complex conjugate, Z_s is the impedance looking into the source, Z_f is the impedance looking into the airframe, and V_s is the "free velocity" of the source (i.e., the engine vibratory velocity for the hypothetical case when the engine is not constrained).

When an isolator is introduced, the power flow equation becomes more complicated. For the simplest case of a massless isolator with impedance Z_i,

$$P = \frac{|Z_s|^2|Z_i|^2}{|Z_iZ_f + Z_fZ_s + Z_sZ_i|^2}\mathrm{Re}\{Z_f\}V_s^2 \tag{26}$$

The value of V_s cannot be measured directly, but a practical approach is to measure the velocities on an engine or on an airframe during engine operation

when no vibration isolators are present (ref. 98). Impedances can be obtained from measurements (ref. 103) or calculations (ref. 104).

If the excitation is a pressure field, such as the wake generated by the propeller, the loading on the structure can be estimated if the characteristics of the pressure field and the excited structure are known (ref. 105). This can be accomplished using techniques similar to those used to predict the response of fuselage structures to acoustic or aerodynamic excitation, as discussed earlier.

Energy Transmission

The transmission of vibrational energy in a structure involves the participation of several types of waves (ref. 106)—flexural, longitudinal, and transverse (plane and torsional). Thus the analysis is more complicated than for transmission through air. Longitudinal and transverse waves are nondispersive, their propagation speed being independent of frequency; flexural waves are dispersive, the phase speed being proportional to the square root of frequency. A complete estimate of energy transmission has to include contributions from all wave types. The situation is further complicated because at any discontinuity in the structure, such as a frame or stiffener, energy can be transferred from one wave type to another. For example, when a flexural wave in a plate is incident on an unsymmetrically attached mass, the resulting wave system includes transmitted and reflected flexural waves and transmitted and reflected longitudinal waves (ref. 107).

Various analytical approaches can be used to predict structure-borne transmission, but the choice may depend to some extent on the frequency range of interest. At high frequencies, where the vibrational wavelengths are small relative to the structural dimensions, statistical energy analysis methods have been used (refs. 99 and 107) since the requirement of high modal density is satisfied. An alternative approach has used the theory of waveguides (ref. 105). At low frequencies, where the wavelengths of the vibration are long relative to local structural dimensions and the modal density is very small, SEA methods are no longer valid. However, it is then practical to use finite element or other methods (refs. 108 and 109).

In some cases it is appropriate to apply empirical or semiempirical methods to supplement the analysis. For example, empirical methods were applied in the determination of transfer functions relating the forces induced by engine vibration to sound pressure in the cabin of a small, single-engine airplane (ref. 102). Also, experimental techniques have been used to determine transmission paths by disconnecting the engine from the fuselage structure (ref. 102) or by replacing vibration isolation mounts with rigid connections (ref. 110). To some extent, these experimental methods are more correctly considered as source-path identification methods, to be discussed later.

Acoustic Radiation

The final component in the determination of structure-borne sound in aircraft is the radiation of acoustic energy into the receiving volume. This is equivalent to airborne sound transmission except that in structure-borne transmission the structural response is only resonant, whereas in airborne transmission the response can include nonresonant contributions (which may be the major contributions). As was true for the analysis of vibration transmission, different analytical methods may

be applicable for different frequency ranges. SEA methods have been used where the acoustic modal densities in the receiving volume were high (ref. 99), and finite element methods where the acoustic modal densities were low (refs. 45 and 108). One example of the latter situation is the analysis of engine-induced noise in small general aviation airplanes.

Source-Path Identification

Aircraft cabin noise is generated by a variety of sources, such as turbulent boundary layers, jet exhaust, propellers, and engine unbalance forces. Noise from different engines or different locations, such as turbulent boundary layers on forward and aft regions, can be considered separate sources. Transmission can be airborne or structure-borne, but either can propagate along a variety of paths. For example, airborne noise can enter through windows, side panels, or ceiling panels, and structure-borne noise from a propeller wake can enter through excitation of wing panels or horizontal tail surfaces.

The need to minimize the weight of noise control devices requires that the contributions from various sources and paths be known in some detail. Then the cabin noise and structural weight limits may be satisfied by controlling only the dominant source-path combinations, by locating treatments where several sources or paths are affected, or by locating treatments at a position in the path where maximum noise reduction can be obtained with minimum treatment weight.

No single identification method is available that satisfies all situations. A number of methods have been developed, however, and it is usual that several are needed for any particular noise control application. Many identification methods have been developed originally for architectural and surface vehicle applications, and there is extensive literature available (refs. 111 and 112). Identification methods and results for aircraft applications are described in the following sections.

In-Place Measurement Methods

Identification measurements made with an aircraft in an operational flight condition are potentially the most reliable and accurate because all noise sources are present and are interacting in the actual manner to be controlled. Flight tests are expensive, however, and the interactions may not allow separation of the various sources and paths. Development of new measurement techniques and equipment that can operate without interference but in conjunction with other required testing is important for reduction of cost.

Frequency Separation

When the spectral characteristics of the dominant sources are distinctly different, their contributions can be identified from a spectrum of the cabin noise. This is illustrated in figure 9. The principal noise generated by the propeller occurs at the tones, whose frequencies can be obtained from the propeller rpm and number of blades. For this aircraft it is known that no other source produces this spectral characteristic, so the tones are identified as of propeller origin. The propeller broadband noise levels are low, so the broadband spectrum at about 70 dB is associated with the aerodynamic boundary layer. The measurement

of instrumentation noise floor and exterior sound levels on the fuselage (fig. 4) supports this conclusion. The appearance of a tone in the cabin at about 670 Hz associated only with an engine turbine speed suggests the presence of engine-generated structure-borne noise (ref. 4). The spectrum does not separate the contribution from the two propellers, however. For aircraft with piston engines the tone spectra from the propeller and pulsating exhaust usually overlap. Then, exhaust and propeller contributions can be separated only if the propeller is geared to operate at an rpm different from that of the engine (ref. 21) or if some engine tones occur at frequencies between the propeller tones (refs. 110 and 113).

Correlation

Where several sources are present having broadband or overlapping tonal spectra, the contributions can sometimes be separated by correlating the characteristics of the cabin noise with those of the sources.[10] The method requires simultaneous measurement of cabin noise and source noise so that a measured signal can be obtained for each source that contains information for only that one source. Extensive statistical theory has been developed for the separation of the source contributions (ref. 6), and methods of this type have been evaluated for surface-radiated noise (ref. 114), gas turbine combustion noise (ref. 115), and aircraft cabin noise (refs. 116 and 117). Use of coherent output power methods enabled separation of contributions from the right and left propellers, as they occurred at slightly different frequencies (ref. 117). The separation of the contributions from five fuselage panels was only a limited success (ref. 116). Only 35 percent of the sound energy at the copilot's position was attributed to the five panels, and this 35 percent resulted from the coherent motion of the panels, rather than from their independent motions. More extensive evaluation of the fuselage vibration might have been obtained through measurements at additional locations.

These methods require an understanding of fairly sophisticated statistical concepts and the use of a digital computer for processing of the data. Modern self-contained, portable, special purpose hardware for fast Fourier transform (FFT) analysis greatly facilitates such data handling.

Intensity

The distribution of sound radiated into the cabin by the enclosing walls is of interest for laying out the sidewall treatment distribution and for locating "hot spots" that indicate acoustic leaks in a finished cabin. Occasionally a trained observer can identify such hot spots simply by listening or with the aid of a microphone. Recent advances in instrumentation, however, have made possible the measurement of acoustic intensity for identifying the distribution of sound radiated from a vibrating surface (ref. 118).

Acoustic intensity measurements make use of a pair of carefully matched and calibrated microphones that are mechanically held at a fixed distance apart (ref. 119), as shown in figure 39. The pair is then sensitive to intensity flowing along the line joining the microphones and is much less sensitive to intensity flowing in

[10] Two deterministic, discrete frequency sources of precisely the same frequency will always be completely correlated so that this approach is not useful.

other directions. The signals from the microphones are summed to obtain pressure and subtracted to obtain velocity (from the slope of pressure). The complex product yields acoustic intensity. Such measurements are only widely practical through the use of special purpose FFT analysis hardware. The availability of such instrumentation has stimulated a surge in research on intensity methods (ref. 120) and has led to development of special equipment and procedures for measurements on aircraft in flight (ref. 121). Intensity methods have been applied to aircraft panels (ref. 122) and a complete aircraft fuselage in laboratory studies (ref. 123).

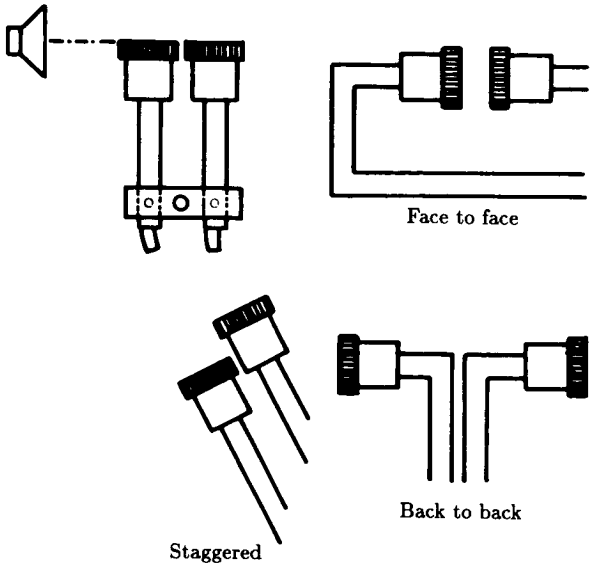

Figure 39. Microphone arrangements for acoustic intensity measurement. (From ref. 119.)

Measurement of sidewall noise transmission (ref. 123) is illustrated in figure 40. A fuselage of a light aircraft was suspended in a semianechoic chamber and a pneumatic driver with a rectangular horn was used to simulate the localized sound field of a wing-mounted propeller. Total acoustic power transmitted through each of four panel areas was measured by sweeping the two-microphone probe over the interior of the panel while the instrument system integrated the instantaneous intensity signal. Incident power was obtained using the same two-microphone technique with the fuselage removed and sweeping over the area previously occupied by the panel. For some tests, measurement results were improved by installing fiberglass absorption blocks in the fuselage when measuring power transmitted. Transmission loss obtained from incident and transmitted power for a window area is shown in figure 40. The measured TL of the plastic window agrees with infinite-panel mass law, and the technique is shown to detect changes in TL due to addition of a window shade such as might be used for noise control purposes. At low frequencies the measurements showed differences from the mass law, as would be expected from the finite nature of the window area. Special efforts have been directed toward design of two-microphone

systems for use in the low-frequency region of importance to propeller aircraft. It was shown that the TL values for the four panel areas could be used to obtain the sound pressure level in the cabin and that changes in SPL due to changes in TL of one panel area could be reasonably well predicted.

The two-microphone method can be expected to cause minimal change in the vibration and acoustic behavior of the fuselage and therefore should produce accurate results.

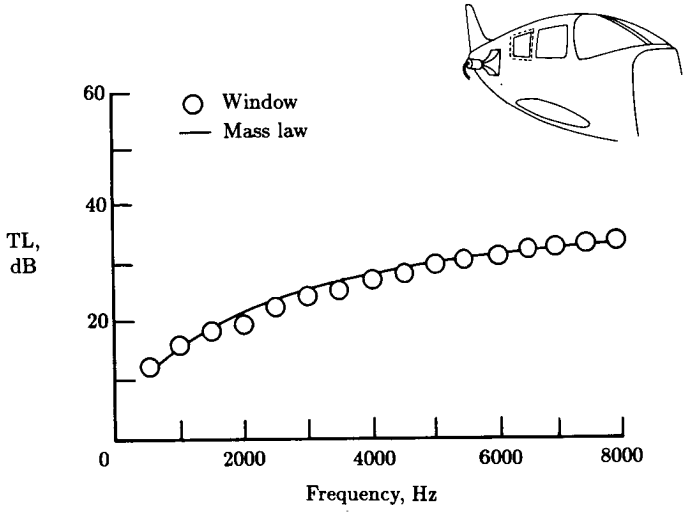

Figure 40. In-place measurement (ref. 123) of aircraft window noise transmission loss using acoustic intensity.

Holography

Near-field acoustic holography (NAH) is a new technique for studying the sound radiation of vibrating surfaces (ref. 124). The technique is quite similar to conventional acoustical holography and is based on the same principles. There are differences, however, that allow NAH to provide significantly more information. Measurements are made as close as possible to the vibrating surface to detect both the radiating and the nonradiating pressure components. For example, one system uses a 16×16 plane array of 256 inexpensive electret microphones located just a few centimeters from the vibrating surface (fig. 41). Processing these data using FFT algorithms to evaluate Rayleigh's integral formulas (ref. 125) allows calculation of the pressure, the velocity, and the vector intensity at any point in the acoustic field. The method has been used to study sound radiation from flat plates (fig. 41) and displays unique "source" and "sink" features of the intensity field.

System Modification Methods

Information on sources and paths can be obtained by modification of some feature of the aircraft operation or configuration. For example, changing the rpm of one engine (when both are normally operated at the same rpm) separates the tones in

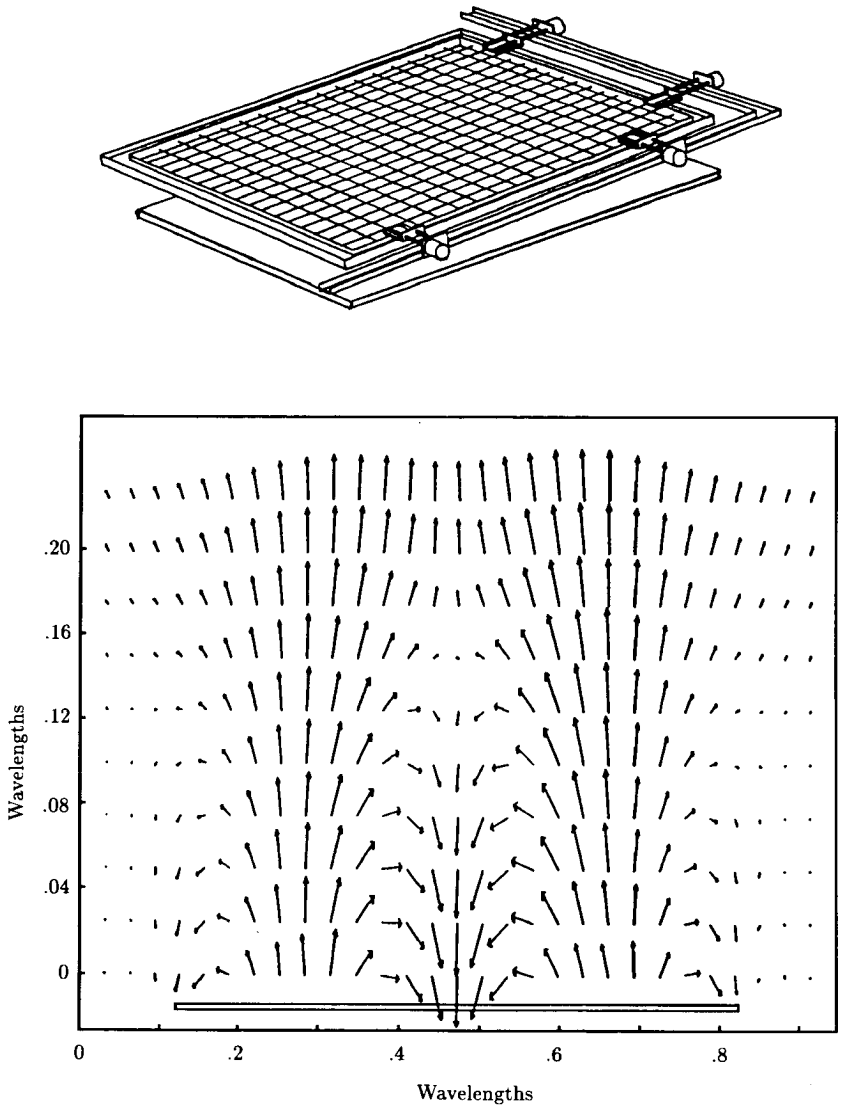

Figure 41. Vector acoustic intensity field of a vibrating plate using near-field acoustic holography. (From ref. 124.)

the frequency spectrum so that the contribution of each engine can be identified, as shown in figure 4. For the analysis to be rigorous, it should be shown that the modification does not change the source strength, the path characteristics, or their interactions. For the rpm change (fig. 4), a number of rpm values for both engines could be investigated to determine the effect of rpm changes. In most cases, however, the effect of the modification cannot be rigorously determined, so the results must be considered only estimates.

The precision obtainable by source-path modification is suggested by figure 42 (ref. 110). A variety of identification techniques, including modification methods, were used to determine the cabin noise contributions from various sources and paths (fig. 42(a)). The component contributions were added to obtain a computed cabin noise level. This is compared with the actual measured noise level in figure 42(b). The overall shape of the spectrum is predicted quite well, but differences of several decibels appear at many frequencies.

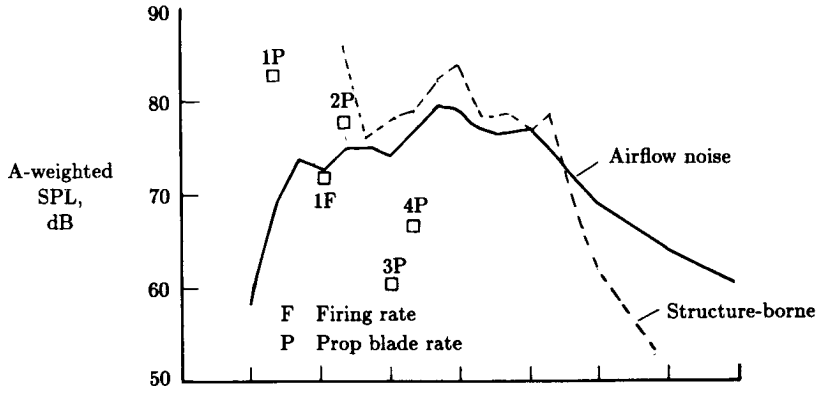

(a) Component contributions.

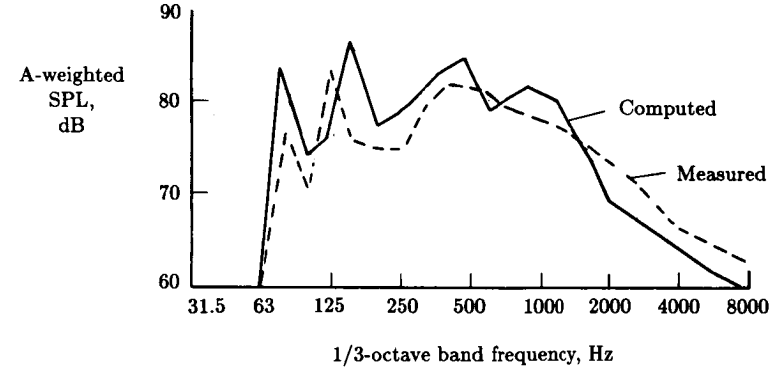

(b) Summation.

Figure 42. Cabin noise contributions for a twin-engine light aircraft in cruise flight. (From ref. 110.)

Turning Off Sources

If one of the noise sources can be turned off, then the reduction in cabin noise that occurs can be considered the contribution of that source. This is true provided

that turning off a source does not change the output of the remaining sources. For example, turning off one engine of a twin-engine aircraft can be expected to reduce airspeed and thus reduce both the aerodynamic noise and the noise of the remaining engine and propeller. These effects can be evaluated either by special tests or by theoretical considerations.

When a source is turned off, it sometimes happens that the cabin noise level is not reduced; it may increase. Such results can occur when two sources have a phase relation that results in cancellation, so that the two sources together make less noise than either one alone. Synchrophasing of multiple propellers and active noise control are intended to reduce cabin noise by such cancellation.

The strength of aerodynamic sources of cabin noise in several light aircraft has been estimated by operating in flight with the engines partly or completely shut down (ref. 110) and some results are shown in figures 43 and 44. As reported by the authors,

> Similar dive tests were carried out with several twin-engine aircraft, on which propellers and engines could be brought completely to a stop without creating unusual propeller wakes which would excite the fuselage in an uncharacteristic manner. In most cases, the dive speed did not reach the cruise velocity. Therefore, a scaling relationship was needed to extrapolate nonpropulsion noise measured at a low speed to the cruise velocity for comparison with "all sources." ... [Figure 43] shows the results of one such scaling test, where data taken at 110 kt is scaled to closely match the 150 kt data using a V^4 relationship [where V is velocity], which is normally associated with the scaling of mean-square pressures in a turbulent boundary layer, wake, or jet when the turbulence structure remains basically unchanged over the speed (and Reynolds number) range of interest .... These 150 kt data are then scaled to the 178 kt cruise condition by a V^4 relationship; the comparison with "engine on" noise levels is shown in ... [figure 44.] Again, the nonpropulsion contribution to the broadband spectral levels is found to be substantial. In this case, the only major uncertainty is whether or not the flow field over the aircraft was identical between the dive and cruise conditions.

Path Blocking

If a transmission path can be blocked, or cut, so that it transmits little or no noise or vibration, then the resulting reduction in cabin noise can be attributed to that path.[11]

Structure-borne noise from engine vibration has been investigated (ref. 102) by detaching the engine from the fuselage in ground tests (fig. 45). The engine support frames were in place for both tests so that the aerodynamic flow noise would be the same, and the tires were partly deflated to minimize any vibration transmission through the ground. When the engine was detached from the fuselage, both engine and cowl were moved forward about 5 cm so that there would be no mechanical connection. All engine loads were then carried by the support frames. The space between the cowl and fuselage at the detachment line was covered with soft adhesive tape that would maintain the aerodynamic lines of flow but not transmit structural

[11] Note the cautions described above that other sources and paths should not be altered and that acoustic cancellation may occur.

vibrations. The reduction of 3 dB for the overall cabin noise (fig. 45) indicates that the noise transmitted through the engine attachments was equal to the noise from all other sources in that test setup. Larger reductions in some 1/3-octave bands indicate that the proportion is larger at those frequencies, and significant structure-borne noise is evident throughout the frequency range.

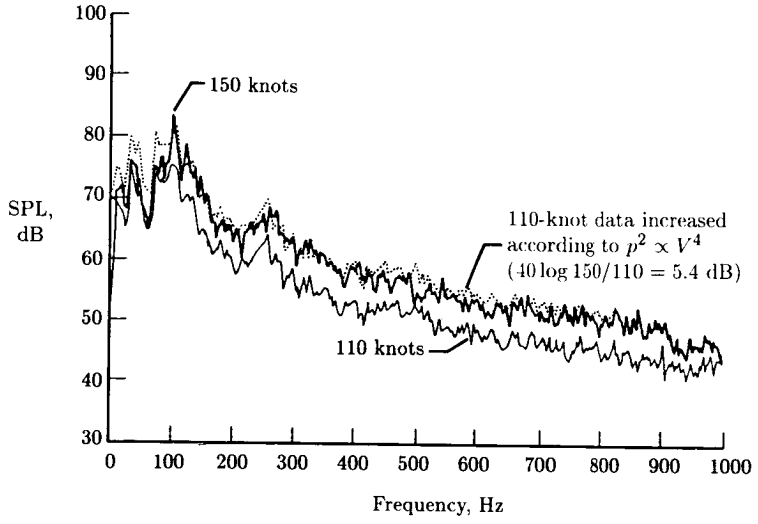

Figure 43. Estimation and scaling of cabin noise due to airflow using engine-off dive tests of a large twin-engine light aircraft. (From ref. 110.)

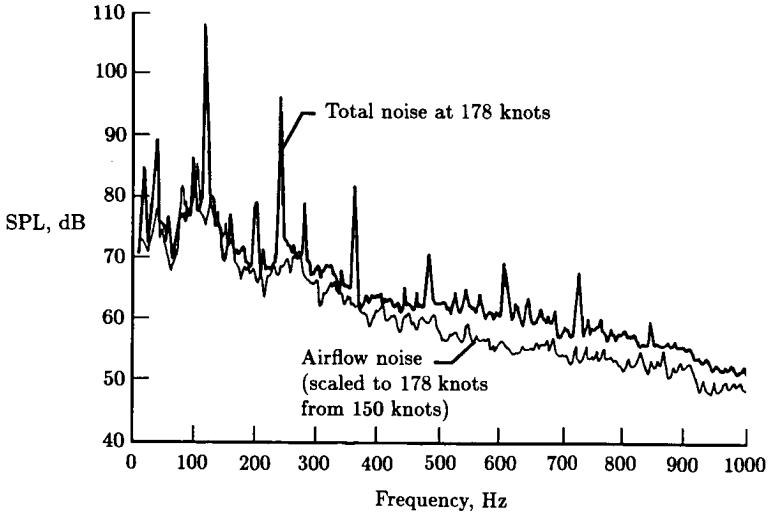

Figure 44. Airflow noise relative to total noise in the cabin of a large twin-engine light aircraft. (From ref. 110.)

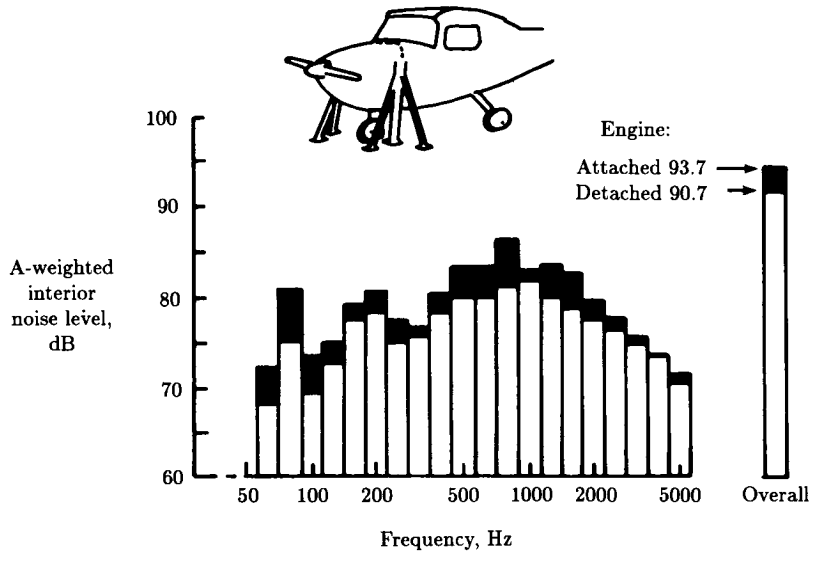

Figure 45. Determination of structure-borne noise by engine detachment method. (From ref. 102.)

Airborne paths are often studied using a heavy mass-loaded vinyl material to cover the surface (fig. 46). Vinyl sheets of 5 to 10 kg/m^2 have been used with soft foam or fiberglass between the vinyl and the surface to minimize the effects on the dynamics of the fuselage structure. Transmission through windows was studied in a reverberation room (ref. 126) by testing with windows uncovered and then covered, as illustrated in figure 46(a). The objective of covering the windows was to eliminate the sound transmission. The results showed that the covering effect depended on frequency; at some frequencies the interior noise was higher with the windows covered, but the overall sound level decreased by 3 dB with the windows covered. Transmission through the fuselage sidewall and the wing structure was studied in ground tests of a light aircraft with engines running (ref. 101). The covered areas are sketched in figure 46(b). The fuselage and wing coverings consisted of one or two layers of foam and septum material weighing 3.08 kg/m^2 each. The entire wing surface was covered from the fuselage to a position outboard of the region where the propeller wake impinged on the wing. By testing with a variety of combinations of fuselage and wing coverings, it was concluded that the propeller wake interaction with the wing surface was a significant structure-borne noise source in the cabin.

Surface covering is an often used and seemingly straightforward approach to path identification. However, unexpected results are sometimes observed, for example the increase in noise level when windows were covered in reverberation room tests (ref. 126), and the reduction in cabin noise level when a window was opened in a propeller aircraft ground test (ref. 127). Explanation of these effects of path changes would require a more in-depth analysis than has been applied yet.

Acoustic enclosures of several kinds can be used to limit the area on the exterior of the fuselage over which the source noise impinges or to limit the sidewall area on

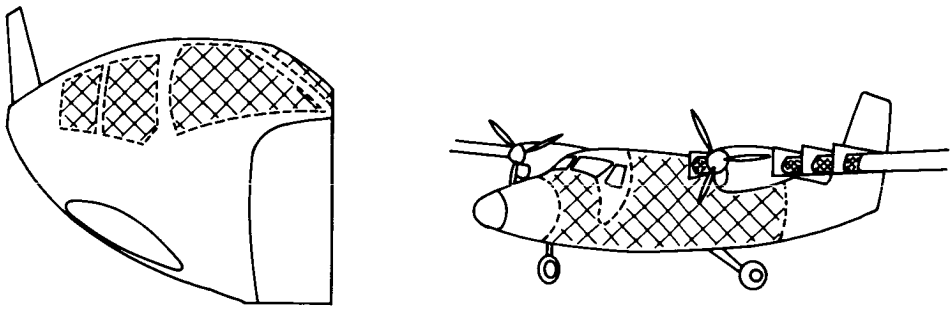

(a) Windows covered. *(b) Fuselage and wing covered.*

Figure 46. Surface covering for path identification by the path blocking method (refs. 101 and 126).

the interior of the aircraft from which the radiated noise is measured. The use of an exterior acoustic guide to measure the noise transmitted through an aircraft window (ref. 77) is illustrated in figure 47. The acoustic guide is constructed of plywood and mass-loaded vinyl walls so that noise generated by the speaker in the enclosure is directed only onto the window. A soft material is applied where the guide walls meet the fuselage surface to provide an acoustic seal but to minimize the effect on vibration behavior. Test results showed that the noise level outside the enclosure was 30 dB less than the level inside. The test results indicate good agreement between the measured and predicted transmission through the window. Location of the acoustic guide at various positions on the fuselage exterior, on the wings, or on tail surfaces would provide information on the relative sensitivity of cabin noise to source noise position.

Parameter Variation

When a transmission path cannot be completely blocked, either by disconnecting structure or by adding mass, then a change in transmission properties may alter the transmitted noise enough to infer the importance of the path. As an example, the structure-borne noise in a single-engine light aircraft has been studied using this technique (ref. 110). The aircraft engine was run on the ground in two test configurations, one using the standard soft rubber engine isolation mounts and the second using solid metal blocks in place of the soft isolators. Cabin noise and acceleration at the four mount locations were measured. For one frequency band the test results obtained were

	Average mount acceleration, dB (re $1g$)	Cabin noise level, dB (re 20 μPa)
Hard mounts	10	88
Soft mounts	−3	84

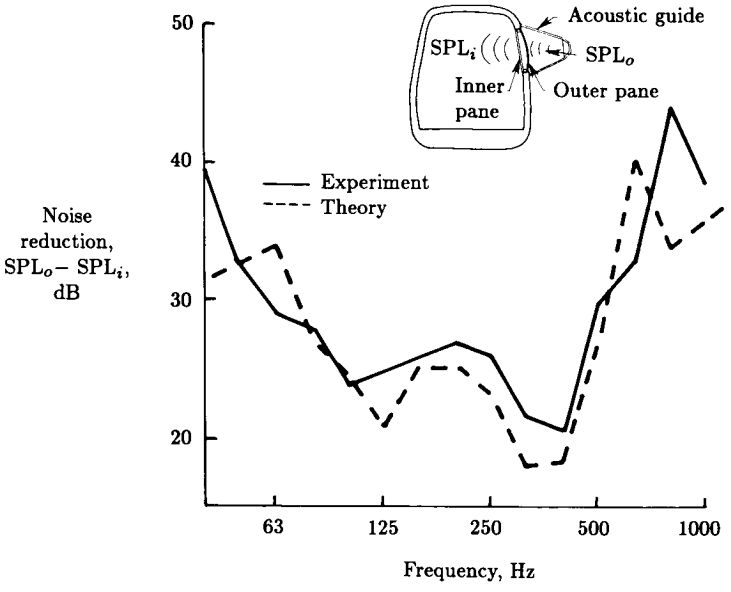

Figure 47. Identification of window noise transmission using an acoustic guide. (From ref. 77.)

Airborne and structure-borne noise were assumed to be independent and therefore to add in the cabin according to the relation,

$$< p^2 >_{\text{total}} = < p^2 >_{\text{air}} + < p^2 >_{\text{struct}} \tag{27}$$

where

$< p^2 >_{\text{total}}$ mean square total acoustic pressure

$< p^2 >_{\text{air}}$ mean square airborne component

$< p^2 >_{\text{struct}}$ mean square structure-borne component

The structure-borne component is then assumed to be proportional to the average acceleration $< a >$ at the engine mounts:

$$< p^2 >_{\text{struct}} = < (ka)^2 > \tag{28}$$

The measured mount accelerations and cabin noise were then used in these expressions to obtain two equations that were solved to obtain the following result for the sound pressure contributions in the frequency band:

	Airborne noise level, dB	Structure-borne noise level, dB
Hard mounts	83.7	86
Soft mounts	83.7	73

The structure-borne noise is seen to be considerably greater with the hard mounts, as would be expected.

Transfer Function Methods

Transfer function methods for source-path identification consist of three steps. First the transfer function between the cabin noise and the source of interest is obtained. Measurements usually are done in a nonoperational environment where no other sources are present and input and cabin noise can be accurately measured. Theoretical methods may also be used (refs. 99 and 110). The second step is to measure the source noise in the operational flight condition. Finally, the product of the transfer function and the flight input noise gives an estimate of the interior noise in flight due to the source of interest.

The structure-borne noise measurements described in the previous section may be considered as an example. The factor k in equation (28) that multiplies mount acceleration to give structure-borne cabin noise is the transfer function for the engine vibration source. The simultaneous equations obtained by using the ground-measured data for hard and soft mounts can be solved for the transfer function k (as well as the airborne component). The use of flight-measured mount accelerations along with k would then yield the estimate of cabin noise in flight due to engine vibration sources.

Radiation Efficiency

Another method developed for separating airborne and structure-borne noise is based on their differing radiation characteristics and relies on the ability to measure radiated intensity (ref. 128). In certain frequency ranges, structure-borne noise and airborne noise have different associated radiation efficiencies because they generate differing types of structural vibration. The first step in the method therefore is to measure the radiation efficiencies, σ_a and σ_s, defined as

$$\sigma_a = \frac{|\mathbf{I}_a|}{\rho c < v_a^2 >} \tag{29}$$

for airborne noise and

$$\sigma_s = \frac{|\mathbf{I}_s|}{\rho c < v_s^2 >} \tag{30}$$

for structure-borne noise. As indicated in figure 48, the radiation efficiency of a skin panel or window is measured with an intensity probe to determine average radiated intensity $|\mathbf{I}|$ and an array of accelerometers to determine mean-square panel velocity $< v^2 >$. Airborne radiation efficiency σ_a is measured with only the speaker in operation, and structure-borne radiation efficiency is measured with only the shaker in operation. When both sources are in operation, the total panel velocity $< v^2 >$ and radiated intensity $|\mathbf{I}|$ are measured and the components of radiated power P are determined using the relations

$$P_a = \rho c A \sigma_a \frac{\sigma_s < v^2 > - |\mathbf{I}|/\rho c}{\sigma_s - \sigma_a} \tag{31}$$

for airborne power P_a and

$$P_s = \rho c A \sigma_s \frac{\sigma_a < v^2 > - |\mathbf{I}|/\rho c}{\sigma_a - \sigma_s} \tag{32}$$

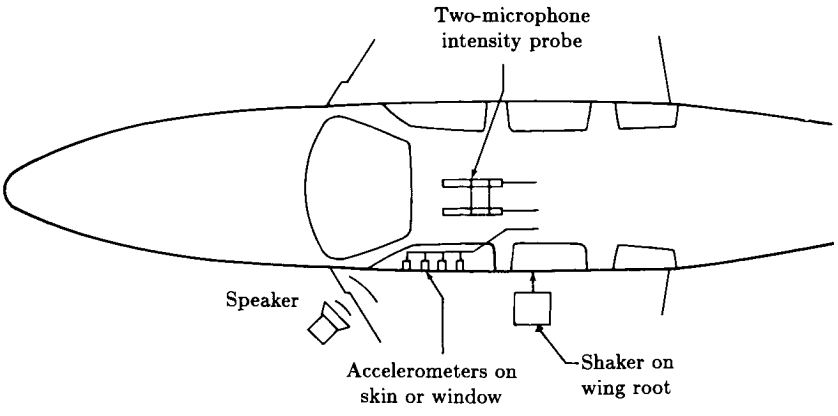

Figure 48. Setup for separating airborne and structure-borne noise using radiation efficiency method (ref. 128).

for structure-borne power P_s, where A is panel area, and certain simplifying assumptions are valid (ref. 128).

The method has been investigated using a number of aircraft panels in a transmission loss setup and using an aircraft fuselage with laboratory sources, as indicated in figure 48. Both coherent and incoherent sources were used. In general the method successfully separated airborne and structure-borne components and determined the proportions of radiated acoustic power. Limitations of the method were identified as (1) a requirement that the radiation efficiencies σ_a and σ_s differ, (2) some unexplained overestimation of the airborne contribution at some frequencies, (3) possible difficulties in determining the separate radiation efficiencies σ_a and σ_s for complex aircraft sources in flight, and (4) a restriction to low frequencies because, above the coincidence frequency of the panel, σ_a and σ_s are expected to be equal. This low-frequency limitation may not be serious because in many aircraft configurations the coincidence frequency can be expected to be well above the frequency of important noise sources. Several significant advantages of the method were also identified. No changes in the aircraft structure or operation are required, in contrast to the system modification methods. The studies indicate that the method is quick and inexpensive and that it works for a variety of stiffened-skin structures. The method was successful when the acoustic and vibrational sources were fully coherent, in contrast to the previously discussed correlation methods, which may not be able to separate contributions from several highly coherent sources. Finally, there are no limitations in principle to the use of this method in flight.

Reciprocity

Application of reciprocity principles to aircraft cabin noise transmission has been explored with the objective of identifying noise sources and transmission paths (ref. 129). The reciprocity principle envisions two configurations of the aircraft, as illustrated in figure 49. The first configuration represents the operational situation for which results are sought. In figure 49(a) the cabin noise due to external sources, represented as speakers, is the information desired. In the second configuration,

referred to here as the "reciprocal configuration" (fig. 49(b)), the positions of speakers and microphones are interchanged, and the exterior noise due to a speaker in the cabin is measured. The principle of reciprocity states that the transfer functions obtained in the two configurations are equal. In mathematical terms,

$$(\mathrm{SPL}_{\mathrm{in}} - Q_{\mathrm{out}})_a = (\mathrm{SPL}_{\mathrm{out}} - Q_{\mathrm{in}})_b \tag{33}$$

where Q is the volume-acceleration level of the speaker output and subscripts in and out indicate measurements inside and outside. The subscripts a and b refer to configurations shown in figure 49. Similar reciprocal relations have been developed for the cabin noise due to a mechanical excitation on the exterior of the fuselage (ref. 129). The advantage of using the reciprocal configuration is that the measurements may be more convenient or more feasible to make. For example, the configuration of figure 49(b) may be required so as to limit the noise levels radiated to nearby test activities. In the case of mechanical forces, a typical engine compartment does not have room for bulky shakers, but accelerometers can usually fit in.

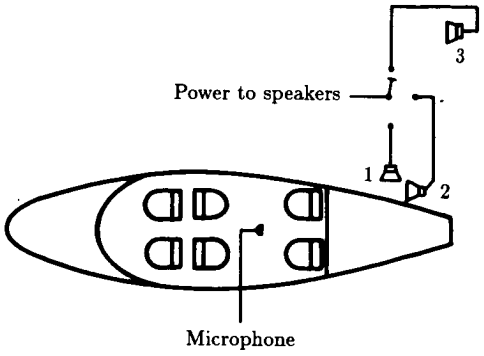

(a) Operating configuration.

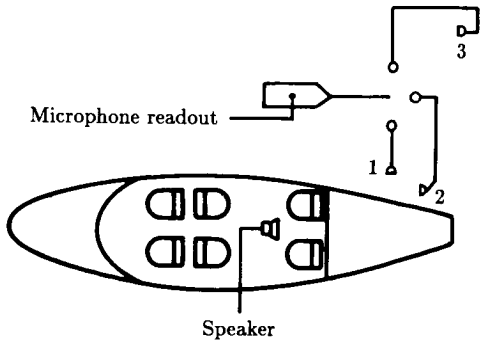

(b) Reciprocal configuration.

Figure 49. System configurations for reciprocity measurements (ref. 129).

Investigations completed using a light aircraft fuselage and special omnidirectional speakers in laboratory tests (ref. 129) have verified the validity of reciprocal transfer functions when applied to the complex structure, damping treatments, sound-absorbing material, and cabin furnishings of the aircraft interior. These results suggest that the assumptions of reciprocity, such as the requirement that the system be linear and time invariant, are satisfied for the fuselage. These results were valid for both single inputs of mechanical or acoustic type and multiple correlated mechanical inputs acting simultaneously.

Theoretical Methods

Some theoretical methods for interior noise prediction are formulated in a manner that provides information on transmission path sensitivity (refs. 45, 79, and 130). As an example, figure 50 illustrates interior noise prediction for an aircraft fuselage. In this method the fuselage sidewall is divided into a number of units, each consisting of one to three skin panels and up to two internal stiffeners. The horizontal edges are simply supported and the vertical edges of each panel unit are supported by flexible stiffeners. The cabin noise is calculated separately for each panel unit, and the contributions from all panel units are added to obtain the total interior noise. As shown in the figure, the noise transmitted through the different panel units varies considerably in the baseline configuration. The addition of damping tape to the skin panels reduces the noise transmitted through all panel units except number 9, so that with damping tape the contributions of all units are more nearly equal. Such information could be useful in identifying which sidewall areas most need additional treatment or in determining the sensitivity of transmitted noise to the addition of various types of treatment to different sidewall regions.

Noise Control Application

General Approach

Interior noise levels can be reduced by noise control at the source or by attenuation during transmission. In principle, noise control at the source is the most desirable approach, but it may be extremely difficult or expensive unless the techniques are incorporated in the basic design of the airplane. Consequently, noise attenuation in the transmission path is also required in most aircraft.

The methods used to reduce noise generation depend on the nature of the source. For propeller noise, the methods could include increasing the clearance between the propeller tip and the fuselage, lowering the propeller rotational speed, locating the propeller plane away from the occupied region of the fuselage, synchrophasing the propellers, and changing the direction of rotation of the propeller (ref. 131). The first three methods involve the basic design of the airplane, although there may be some benefit in retrofitting different engines and propellers. Propeller synchronization involves accurate control of the propeller speed in multiengine configurations. In turbojet and turbofan aircraft, structure-borne noise can be controlled by reducing the out-of-balance forces generated by the rotating components; and airborne noise can be controlled by locating jet exhausts well away from the fuselage. Turbulent boundary layer pressure fluctuations can be reduced by avoiding flow separation,

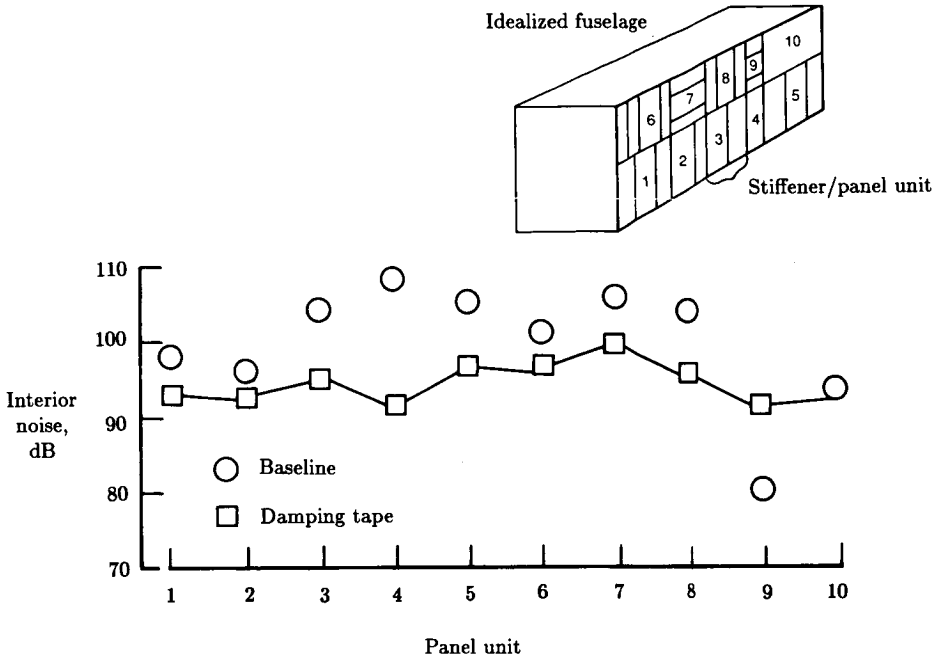

Figure 50. Interior noise contributions of panel areas of a fuselage as determined by theoretical analysis (ref. 79).

but the main reductions can be achieved only by removing the turbulent boundary layer itself, a solution that has not yet been accomplished. With the exception of propeller synchronization and direction of rotation, reduction at source is not considered further in this chapter.

Descriptions of noise control methods applied to aircraft of various configurations (refs. 28, 61, 100, and 132–141) show that the most common approach is to utilize cabin sidewall treatments that reduce interior sound pressure levels to the desired values. A typical sidewall treatment, from a large modern jet aircraft, is shown in cross section in figure 51. The sidewall is a multielement system with fiberglass blankets, impervious septa, an interior decorative trim, and multipane windows. Damping materials are applied to the fuselage skin. This type of treatment reduces both airborne (transmission through the fuselage skin) and structure-borne (radiated by the skin) noise, although the effectiveness may differ for the two components. Dynamic vibration absorbers are used in several cases to reduce structure-borne noise from turbofan engines (ref. 28) or airborne propeller noise (refs. 136 and 142). Various noise control methods are reviewed in the following sections.

Multielement Sidewall

The sidewall treatment has to satisfy both thermal and acoustic requirements, although adequate thermal insulation can usually be achieved with less treatment than is needed for noise control. In addition, the acoustical treatment has to have minimum weight and volume, should not readily absorb moisture, should be resistant

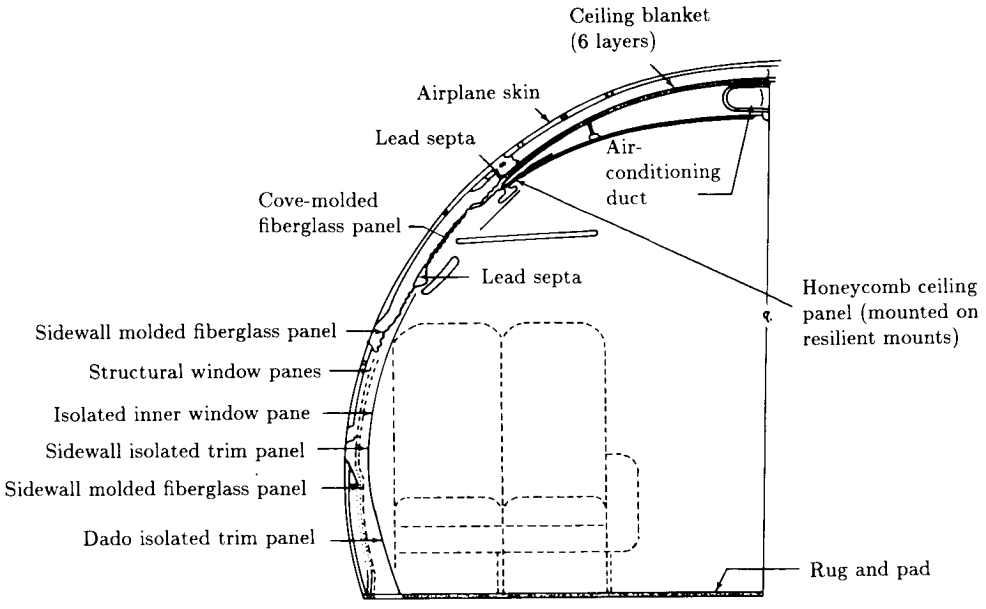

Figure 51. Typical sidewall cross section of a large passenger transport aircraft. (From ref. 133. Copyright AIAA; reprinted with permission.)

to flame, and should not give off smoke or toxic fumes. Laboratory measurements have shown that fiberglass blankets satisfy these criteria and are more effective than other materials in terms of noise reduction per unit weight. The fiberglass is available in various densities, such as 6.4, 8, and 24 kg/m^3, and the lowest density material is preferred unless there is a very stringent space limitation. Typically, the fibers have diameters of about 0.00013 cm and are bonded together by a resin material that constitutes about 15 percent of the total weight of the blanket. The fiberglass material is enclosed in very thin impervious sheets to protect it from moisture.

Typical examples of multielement sidewalls in large commercial airplanes are shown in figure 52, which compares sections through sidewall treatments for standard-body (3.6-m-diam) and wide-body (5.8-m-diam) (ref. 135) airplanes. The standard-body treatment consists of a fiberglass blanket filling the depth of the ring frame stiffener and a relatively thin blanket between the cap of the ring frame and the interior trim panel. Attachment of the interior panel to the frame causes compression of the thin blanket and thereby degrades the acoustic insulation of the sidewall. The wide-body treatment uses the same type of low-density glass fiber but provides a thicker blanket between the frame and the interior trim panel and an air gap between the two blankets.

The acoustic design of the sidewall treatments has undergone extensive experimental and analytical study over a number of years to optimize the configuration (e.g., refs. 36, 38, 57–60, 62, 63, 92, 95, 132, and 143–146). The studies have investigated not only the use of the fiberglass material, but also the insertion of heavy impervious septa. This is particularly true with respect to the advanced turboprop airplane (refs. 63 and 92) where greater transmission losses are required at low frequencies than are provided by current production sidewall treatments.

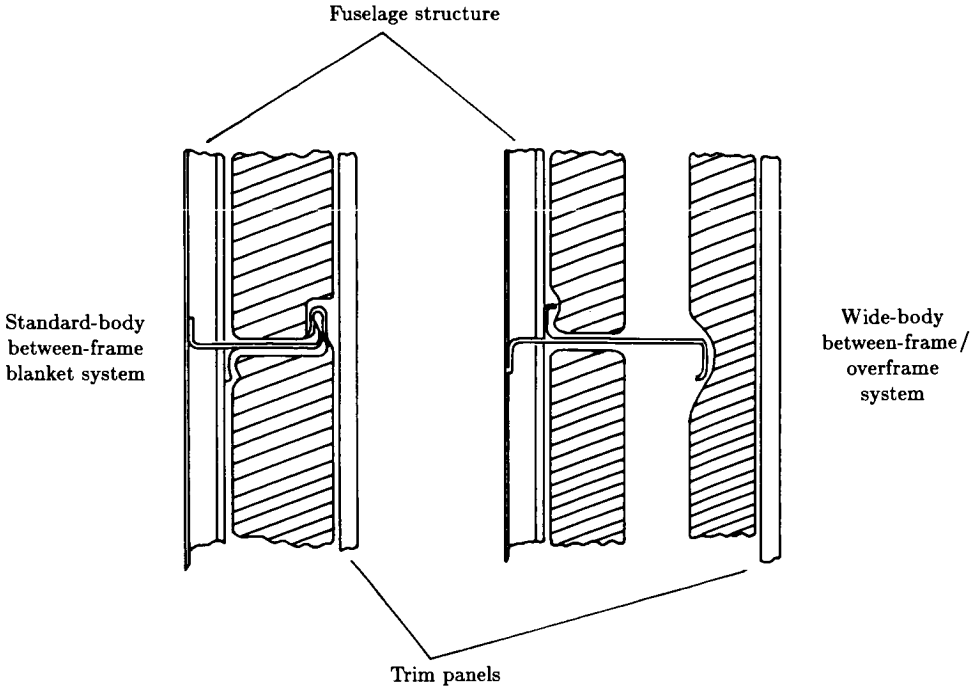

Figure 52. Sections through sidewall treatments used on large passenger aircraft. (From ref. 135.)

Transmission loss characteristics of an idealized double-wall treatment are shown in figure 53, which presents predicted increases in transmission loss relative to the untreated fuselage (ref. 63). Transmission loss spectra are plotted for cases with and without porous material between the two walls. When there is no material in the air gap, the spectra clearly show the predicted decrease in transmission loss at the double-wall (mass-spring-mass) and air gap acoustic resonance frequencies. It is possible that, at some frequencies in the neighborhood of the resonances, the transmission loss for the double-wall system can be less than the original single panel. As the surface mass density m_2 of the inner trim panel increases, the frequency of the double-wall resonance f_d decreases but the air gap acoustic resonance frequency is unchanged. When porous materials are introduced, the effects of the double-wall and acoustic resonances are reduced significantly. Test data show the presence of the double-wall resonance, but the magnitude of the effect can vary considerably. The results in figure 53 refer to a sidewall that is 13 cm thick, thicker than that usually found in a general aviation airplane but typical of larger commercial aircraft. Increasing the distance between the sidewall panels reduces both the mass-spring-mass and the air gap resonance frequencies, a factor that can be important when designing for low-frequency noise control.

The analysis assumes that the trim panel is limp, since all the components of the multielement sidewall are assumed to be locally reacting. In practice, trim panels are usually stiff, such as 2.08-mm-thick aluminum panels, 6.35-mm-thick honeycomb, or 2.03-mm-thick crushed-core honeycomb (ref. 61). Thus, the assumption of limpness

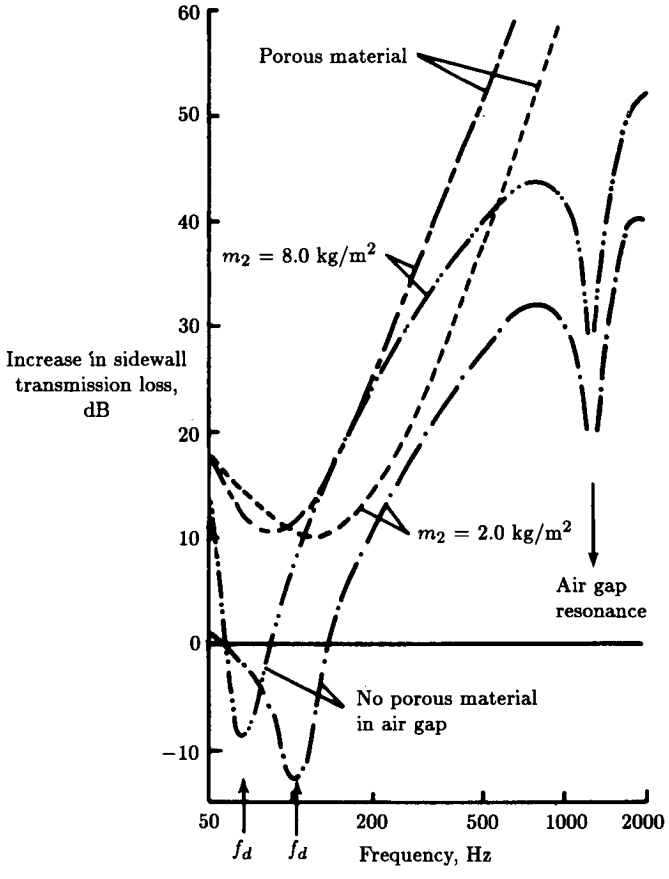

Figure 53. Predicted increase in sidewall transmission loss due to addition of a trim panel or fiberglass treatment. (From ref. 63.)

is not necessarily valid. However, an approximation to a limp panel can be achieved by addition of damping material to the trim panel (ref. 134). Alternatively, a mass-loaded septum, such as vinyl impregnated with lead or iron oxide, can be inserted between the fiberglass blankets and trim panel (refs. 61 and 133).

Mass-loaded septa can also be inserted between the various layers of fiberglass blankets in an attempt to optimize transmission loss and weight (refs. 50 and 144). However, when using multiple layers it is necessary to avoid multiple mass-spring-mass resonances that can degrade the transmission loss in the frequency range of concern.

Experimental and analytical studies of the transmission loss provided by multi-element treatments assume that the interior trim panel is mounted so that no structure-borne path for noise transmission exists. Any such path would degrade the acoustic insulation provided by the treatment. In practice, the conventional trim panel has to be mounted to the fuselage structure in such a manner that the attachment will not collapse under shock loading yet will be soft enough to provide insulation at low frequencies. These opposing requirements could be satisfied by

using mounts with snubbers, provided that the snubbers are not activated by the normal static loads. The attachment of the trim panel to the fuselage structure usually occurs at fuselage ring frames; figure 54 shows an example of a trim panel vibration isolation mount used to attach a trim panel to the cap of a ring frame (ref. 61). The vibration and acoustic performance of typical trim mounts is illustrated in figures 55 and 56. In one case, the vibration reduction provided by two mounts was measured in the laboratory when each mount was subjected to a static load of 0.45 kg (ref. 29). Figure 55 shows that at low frequencies neither mount provides isolation (there may even be an increase in the transmitted vibration at the resonance frequency of the mount), and at high frequencies the stiffer the mount, the lower the vibration isolation. Figure 56 illustrates acoustic performance in terms of the noise reduction through a double-wall system with the panels connected by mounts of various stiffnesses (ref. 61). Stiff mounts provide little improvement over a rigid connection, whereas soft mounts can provide a good simulation of the completely uncoupled system, at least for high frequencies.

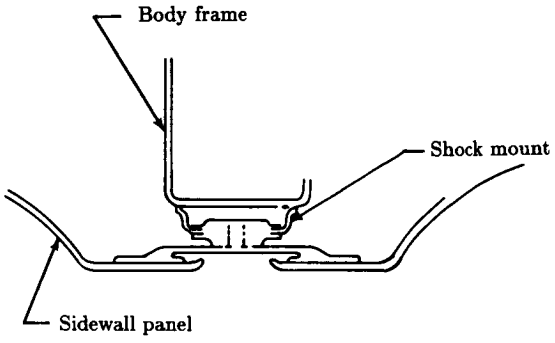

Figure 54. Vibration isolation mount for sidewall trim panel in large passenger aircraft. (From ref. 61. Copyright 1981, SAE, Inc.; reprinted with permission.)

Since there is a practical limit to the vibration isolation that trim panel mounts can provide at low frequencies, it may sometimes be necessary to consider the installation of an interior trim panel that is a self-supporting structure with a minimal number of attachment points to the fuselage (ref. 134). Examples of possible applications are cases where significant noise reductions are required at low frequencies (50 to 200 Hz) associated with propeller noise or structure-borne noise from engine out-of-balance forces. Finally, any discussion of multielement sidewall treatments should include mention of items such as windows and doors that can be weak links in a noise control approach. Windows are typically multipane systems so that an adequate transmission loss can be achieved, the innermost pane being part of the trim panel. Doors have low transmission loss because the presence of opening and closing mechanisms limits the space available for acoustic treatment and acoustic leaks can occur around the door seals. One solution is to provide sound-absorbing panels in entry areas (refs. 61 and 133).

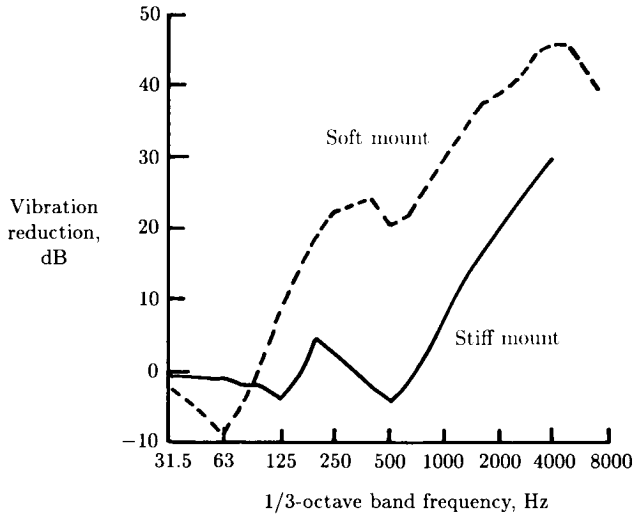

Figure 55. Vibration attenuation provided by two trim panel mounts. Static load of 0.45 kg. (From ref. 29. Copyright 1983, SAE, Inc.; reprinted with permission.)

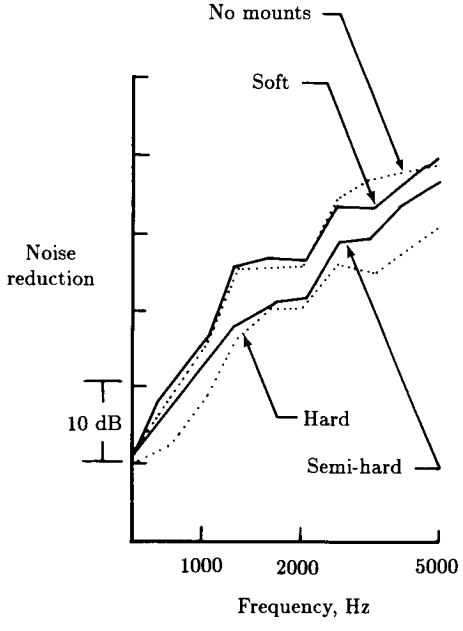

Figure 56. Noise reduction across a double-wall sidewall with several mount configurations. (From ref. 61. Copyright 1981, SAE, Inc.; reprinted with permission.)

Additions to Structure

In addition to the use of sidewall treatments, the noise transmission and acoustic radiation characteristics of the fuselage structure can be modified by the addition of mass, damping, or stiffness. Of the three alternatives, damping is the method most commonly used in production aircraft; mass and stiffness changes have been investigated mainly on an experimental basis.

The addition of damping material to the skin can significantly reduce cabin noise levels if the sound transmission or radiation is controlled by resonant response of the structure and the existing damping is not high. Below the fundamental frequency of the skin panel the response of an individual panel is stiffness controlled so that increasing the damping of the panel has a negligible effect on sound transmission.[12] Also, damping is not very effective for mass-law-controlled transmission except near the critical frequency, which is often above the frequency range of interest for airplane interior noise.

Damping material has been used in production turbojet (refs. 134, 140, and 141) and turboprop (ref. 136) aircraft, and experimental installations can be found in a variety of airplanes and helicopters (refs. 147–150). In many examples the damping material is aluminum-backed tape, the aluminum foil acting as a constraining layer to generate the damping through shear strain within the viscoelastic material, which also provides the adhesive. In some cases the tape includes a thin layer of foam between the viscoelastic material and the aluminum foil. The foam displaces the foil away from the viscoelastic material and thereby augments its constraining action. In other examples the damping material is unconstrained tiles. The damping material is applied only to the skin in all the preceding examples, usually covering only part (roughly 80 percent) of the skin area.

Measurements on a large, modern jet aircraft (ref. 148) showed that the addition of damping tape reduced interior sound pressure levels by 3 to 8 dB at frequencies above about 800 Hz (fig. 57). It was estimated that the addition of the damping material would increase the total damping factor of the panels from about 0.01 to about 0.05. In this application, the sound pressure levels were associated with external turbulent boundary layer excitation, and the skin structural response was resonant. The presence of the damping tape would also have some effect on the stiffness-controlled response because of the weight of the tape; it was estimated that the frequency of the fundamental mode of the panel was reduced from 625 Hz to 595 Hz. The effectiveness of damping tape could, perhaps, be extended to lower frequencies by application to stringers and ring frames (ref. 84) as well as to the skin panels. Damping material can also attenuate structure-borne sound, when resonant bending modes dominate radiation (ref. 100). Analysis of a helicopter structure indicated that panel loss factors could be increased from about 0.01 to about 0.07, resulting in noise reduction of approximately 7 dB.

One important parameter affecting the acoustic performance of a given damping material is the damping coefficient at low temperatures; fuselage skin temperatures during cruise conditions can be −29°C (ref. 15) or lower. Many damping materials are most efficient at room temperatures, so that suitable materials must be selected carefully.

[12] This assumes that the panel weight is small compared with average sidewall weight and that damping is increased without adding weight.

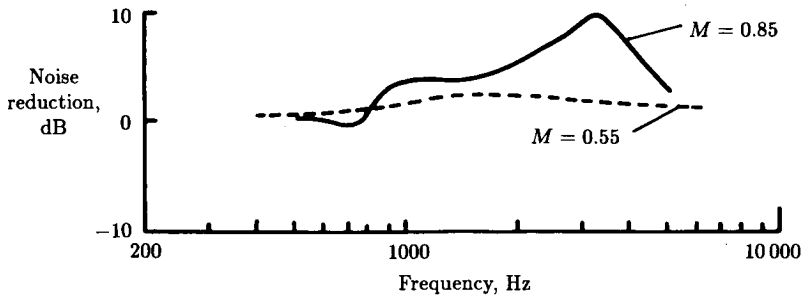

Figure 57. Noise reduction provided by damping tape on fuselage skin. Boundary layer excitation, flight test. (From ref. 149.)

The use of damping material need not be restricted to the fuselage skin and stiffeners. It can be applied to other structures if sound transmission or radiation is dominated by resonant response of those structures. For example, damping material has been applied in a recent installation (ref. 134) to the sidewall trim panel as well as the fuselage skin. Also, additional damping has proven effective in reducing acoustic radiation from gearboxes in helicopters (ref. 149).

Increasing the basic stiffness of a fuselage structure may appear to be an attractive way of decreasing low-frequency sound transmission. However, several factors must be considered. First, the overall low-frequency response of the fuselage structure should be understood, so that the frequency range associated with stiffness response can be determined. Second, if the fuselage is pressurized during flight, the effective stiffness of the structure is already much higher than that of the unpressurized fuselage. Third, increasing the stiffness with only a negligible weight increase lowers the critical frequency. Consequently, the decreased transmission loss associated with coincidence occurs at lower frequencies.

The main application of structural stiffness in noise control has been concerned with the modification of existing structures by the addition of honeycomb material to the skin (refs. 36, 79, 149, and 151). In practice, the honeycomb material can be applied only in relatively small panels, because of the obstructions presented by longitudinal and circumferential stiffeners on the fuselage. Since the honeycomb panel can reduce vibration (and, hence, noise) only when the flexural wavelengths in the fuselage skin are small relative to the planform dimensions of the honeycomb panel, the method is effective only at relatively high frequencies. This is illustrated in figure 58, which contains data from an experimental installation on a pressurized cylindrical fuselage under cruise conditions (ref. 149). At low frequencies, where the dimensions of the honeycomb panel are small relative to the flexural wavelengths, the honeycomb material acts mainly as additional mass and has little or no noise control capability.

In figure 58 the honeycomb panels provide essentially no vibration reduction at frequencies below about 400 Hz. Vibration and noise reductions at lower frequencies were obtained in ground tests of a general aviation airplane (refs. 36 and 151), but in that case the fuselage panels were flat rather than curved and the fuselage was unpressurized during the tests. The panel fundamental frequency was 69 Hz compared with a corresponding frequency of about 400 Hz for the untreated skin panels associated with the data in figure 58. Noise reductions of up to 10 dB were

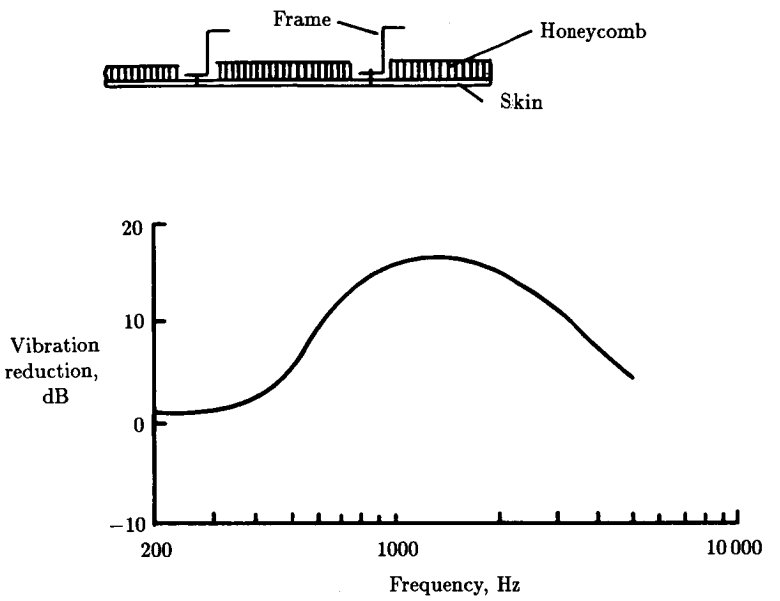

Figure 58. Vibration reduction provided by honeycomb panels attached to skin. Honeycomb thickness = 1.9 cm, Weight = 1.2 kg/m^2. (From ref. 149.)

measured in the frequency range from 100 to 600 Hz during ground tests (refs. 36 and 151), even though it is possible that the data were contaminated by noise transmission through flanking paths (no flight tests were performed).

Dynamic Absorbers

Dynamic vibration absorbers can alter the vibration characteristics of a system, particularly at frequencies in the neighborhood of the resonance frequency of the absorber. However, devices of this type are useful only when the vibration to be controlled is dominated by a single constant frequency. The absorber is tuned to this frequency by adjusting the absorber mass and stiffness until the resonance frequency of the absorber equals the frequency to be attenuated. The vibration of the system at the attachment point of the absorber can then be reduced significantly, since the absorber provides a force that acts against the vibration of the system.

Dynamic absorbers have been used to attenuate structure-borne and airborne sound associated with engines operating at constant speed during cruise conditions. For a jet airplane with rear-mounted engines (ref. 28), dynamic absorbers were attached to the fuselage structure close to the turbofan engine mounts to reduce structure-borne sound transmission. Two sets of absorbers were tuned to the rotational frequencies of the low- and high-pressure compressors of the turbofan engine, 120 and 180 Hz, respectively. Noise was reduced by 5 to 10 dB in flight tests.

Propeller noise has been controlled in turboprop aircraft by installing dynamic absorbers on the ring frames of the fuselage (refs. 136 and 142) and by attaching absorbers to cabin trim panels (ref. 136). Absorbers were tuned to the fundamental, first harmonic, or second harmonic of the propeller blade-passage frequency. For

a twin-engine aircraft (ref. 136), absorbers tuned to the blade-passage frequency of 88 Hz were attached to the ring frames to reduce noise by about 10 dB for a weight penalty of 30 kg. Also, three sets of absorbers tuned to frequencies of 88, 176, and 264 Hz and attached to the interior trim panels reduced the A-weighted sound level by about 2 dB for a weight penalty of 25 kg.

Vibration Isolators

Vibration isolators are widely used in engine mounting systems to attenuate structure-borne sound associated with engine out-of-balance forces. This is particularly true for reciprocating engines where significant levels of vibration can be transmitted into the fuselage structure, but it is also true for turboprop and turbofan installations. Vibration isolators are constructed from elastomeric material or metal, the choice being influenced to some extent by the thermal conditions to which the mounts will be exposed. Isolators usually have nonlinear characteristics and the system stiffness has to be chosen so that the required vibration reduction is achieved under the normal static load conditions. The static loads are imposed by engine thrust and weight and by aircraft maneuvers; snubbers are provided for extreme load conditions. The operating stiffness range is chosen so that there is adequate attenuation at the frequencies of concern.

Design of vibration isolators involves a large number of factors in addition to the vibration and acoustic transmission characteristics (ref. 152). An engine has several mounts, each having to provide vibration isolation in more than one direction. Furthermore, the overall isolation performance of the mounting system is no better than the performance of the least effective isolator. The vibration isolation of engine mounts has been investigated for a single-engine propeller-driven airplane with reciprocating engine (ref. 153). It was found that isolator stiffness is a strong parameter in controlling noise transmission while isolator damping is a much weaker parameter. Interior noise level was reduced by up to 10 dB by using experimental isolators in laboratory tests.

Acoustic Absorption

Noise control methods are successful only if an adequate amount of acoustic absorption exists within the airplane cabin. The absorption can be provided on the interior surfaces of the cabin—sidewall, bulkheads, and floor—or within the volume by, for example, the seats. If there is little or no absorption, the space-averaged sound pressure levels are high and there are strong spatial variations (ref. 50). However, the benefits of increased absorption soon reach a stage of diminishing returns. For example, increasing absorption coefficient from 0.80 to 0.95 reduces noise, on the average, by less than 1 dB, whereas the same change of 0.15 in coefficient from 0.20 to 0.35 would reduce noise by about 2.5 dB. Thus, it is useful in some cases to add sound-absorbing material only in local areas such as close to the heads of passengers.

The design of a sidewall trim panel is usually dictated by factors other than high acoustic absorption. The trim panels are selected for resistance to mechanical damage and ease of cleaning as well as appearance and acoustic performance. This often results in a surface that has a low acoustic absorption coefficient, except perhaps at low frequencies where there may be some absorption due to membrane action of the panel. However, there are several surface areas that can be designed with acoustic

absorption in mind. These include ceiling panels, bulkheads, closet doors, and areas of the overhead baggage containers. A typical sound-absorbing panel (refs. 61, 133, and 135) consists of a perforated surface that is exposed to the interior of the cabin, a flow-resistive screen or cloth, a honeycomb core, and an impervious backing sheet (fig. 59). The honeycomb core can be in different thicknesses depending on the space available or the frequency range of interest. The thicker the core, the greater the absorption at low frequencies, but there may be an associated reduction in absorption at higher frequencies. The absorption at high frequencies can be increased by placing low-density fiberglass in the honeycomb core.

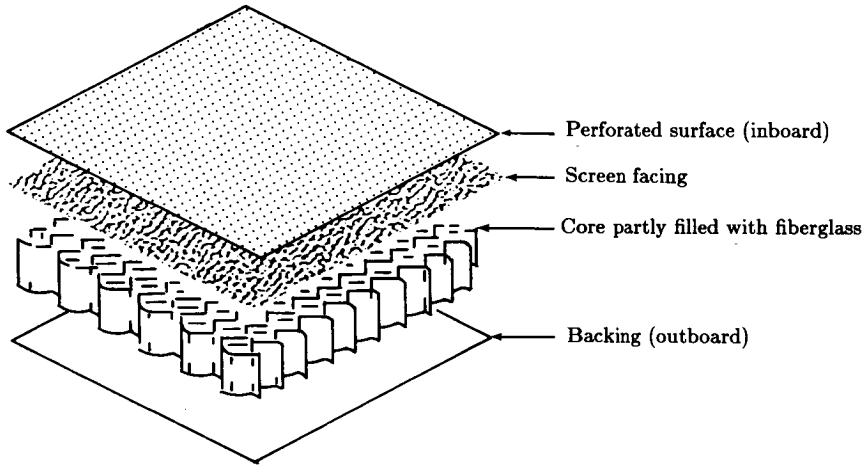

Figure 59. Components of sound-absorbing panel for airplane interior. (From ref. 135.)

In most designs the contributions of transmission loss and absorption have to be considered together and optimized to achieve the maximum noise reduction within the restrictions of space and weight. Sometimes an impervious trim with relatively low absorption may be more desirable than a perforated surface with high absorption but relatively low transmission loss (ref. 132).

Exploratory Concepts

Various methods or designs for interior noise control have been studied on an exploratory basis but not applied to production aircraft. The main objective of the studies has been to further reduce noise transmission through the sidewall without additional weight penalties, particular emphasis being given to the low-frequency regime associated with propeller noise. In general, the proposed methods have been restricted to laboratory measurements or analytical studies, but some have been used in flight tests. The methods include the basic design of the fuselage structure, nonstructural additions to the fuselage skin panels, and new concepts for the sidewall treatment.

Proposed modifications to the fuselage structure include the design of integrally stiffened panels with stiffeners forming a triangular array similar to the isotropic

panels currently used in space vehicle structures (ref. 154). Other approaches involve fuselage structures constructed from honeycomb panels, the use of closely spaced stiffeners, or the use of stiffeners made from composite materials (ref. 155). Also, it has been proposed that fuselage structures can be designed in such a manner that certain frequencies are filtered out during acoustic transmission (ref. 84). This approach is based on analytical studies which show that periodic structures have frequency bands where there is no transmission of flexural waves.

Novel additions to the fuselage skin panels are the bonding of rubber wedges to the panel boundaries (ref. 148) or the use of waveguide absorbers to provide broadband damping (ref. 156). In the first case the wedges were installed in a large jet airplane in a region of the fuselage where the dominant excitation is the external turbulent boundary layer. Multiple blocking masses have been investigated as an alternative to a single mass in the control of structure-borne sound in helicopters (ref. 157). This approach was not a realistic concept for panel-stringer configurations but may have application in parts of the structure, such as the main frames, where the modal density is lower. Sidewall treatments containing resonators located between the fuselage skin and the trim panel have been tested in laboratory conditions (ref. 91) and found to have promise for improved noise transmission with minimum increase in weight.

Active noise control is an electronic means of reducing noise by the cancellation, or partial cancellation, of the noise of interest. The method has been demonstrated successfully in duct acoustics and in certain other environments with a relatively compact source. In potential aircraft applications, two general approaches are being pursued. One method provides local control for each occupant of the cabin by providing headsets for the flight crew of a helicopter (ref. 158) or by providing loudspeakers in the headrest of the seat of each occupant (ref. 159). The second method is directed toward reduction of the general noise levels in the cabin by the judicious placement of noise-cancelling sources (refs. 160 and 161).

References

1. Beranek, Leo L., ed.: *Noise and Vibration Control.* McGraw-Hill Book Co., Inc., c.1971.
2. Harris, Cyril M.; and Crede, Charles E., eds.: *Shock and Vibration Handbook,* Second ed. McGraw-Hill Book Co., c.1976.
3. Leatherwood, Jack D.; Clevenson, Sherman A.; and Hollenbaugh, Daniel D.: *Evaluation of Ride Quality Prediction Methods for Helicopter Interior Noise and Vibration Environments.* NASA TP-2261, AVSCOM TR 84-D-2, 1984.
4. Wilby, John F.: Propeller Aircraft Interior Noise. *Propeller Performance and Noise, Volume 2,* VKI-LS-1982-08-VOL-2, Von Karman Inst. for Fluid Dynamics, 1982.
5. Mixson, John S.; and Powell, Clemans A.: Review of Recent Research on Interior Noise of Propeller Aircraft. *J. Aircr.,* vol. 22, no. 11, Nov. 1985, pp. 931–949.
6. Bendat, Julius S.; and Piersol, Allan G.: *Random Data: Analysis and Measurement Procedures.* John Wiley & Sons, Inc., c.1971.
7. Ungar, E. E.; Wilby, J. F.; Bliss, D. B.; Pinkel, B.; and Galaitsis, A.: *A Guide for Estimation of Aeroacoustic Loads on Flight Vehicle Surfaces—Volume 1.* AFFDL-TR-76-91-Vol. 1, U.S. Air Force, Feb. 1977. (Available from DTIC as AD A041 198.)
8. Wilby, E. G.; and Wilby, J. F.: *Application of Stiffened Cylinder Analysis to ATP Interior Noise Studies.* NASA CR-172384, 1984.

9. Bhat, W. V.: Flight Test Measurement of Exterior Turbulent Boundary Layer Pressure Fluctuations on Boeing Model 737 Airplane. *J. Sound & Vibration,* vol. 14, no. 4, Feb. 22, 1971, pp. 439–457.
10. Wilby, J. F.; and Gloyna, F. L.: Vibration Measurements of an Airplane Fuselage Structure: I. Turbulent Boundary Layer Excitation. *J. Sound & Vibration,* vol. 23, no. 4, Aug. 22, 1972, pp. 443–466.
11. Wilby, J. F.; and Piersol, A. G.: Analytical Prediction of Aerospace Vehicle Vibration Environments. ASME Paper 81-DET-29, Sept. 1981.
12. Hubbard, Harvey H.; and Houbolt, John C.: Vibration Induced by Acoustic Waves. *Engineering Design and Environmental Conditions, Volume 3* of *Shock and Vibration Handbook,* Cyril M. Harris and Charles E. Crede, eds., McGraw-Hill Book Co., Inc., c.1961, pp. 48-1–48-57.
13. Farassat, F.; and Succi, G. P.: A Review of Propeller Discrete Frequency Noise Prediction Technology With Emphasis on Two Current Methods for Time Domain Calculations. *J. Sound & Vibration,* vol. 71, no. 3, Aug. 8, 1980, pp. 399–419.
14. Hanson, D. B.; and Magliozzi, B.: Propagation of Propeller Tone Noise Through a Fuselage Boundary Layer. AIAA-84-0248, Jan. 1984.
15. Wilby, J. F.; McDaniel, C. D.; and Wilby, E. G.: *In-Flight Acoustic Measurements on a Light Twin-Engined Turboprop Airplane.* NASA CR-178004, 1985.
16. Zorumski, William E.: *Propeller Noise Prediction.* NASA TM-85636, 1983.
17. Goldsmith, I. M.: *A Study To Define the Research and Technology Requirements for Advanced Turbo/Propfan Transport Aircraft.* NASA CR-166138, 1981.
18. Šulc, J.; Hofr, J.; and Benda, L.: Exterior Noise on the Fuselage of Light Propeller Driven Aircraft in Flight. *J. Sound & Vibration,* vol. 84, no. 1, Sept. 8, 1982, pp. 105–120.
19. Magliozzi, B.: Acoustic Pressures on a Prop-Fan Aircraft Fuselage Surface. AIAA-80-1002, June 1980.
20. Barton, C. Kearney; and Mixson, John S.: Characteristics of Propeller Noise on an Aircraft Fuselage. *J. Aircr.,* vol. 18, no. 3, Mar. 1981, pp. 200–205.
21. Mixson, John S.; Barton, C. Kearney; and Vaicaitis, Rimas: Investigation of Interior Noise in a Twin-Engine Light Aircraft. *J. Aircr.,* vol. 15, no. 4, Apr. 1978, pp. 227–233.
22. Fuller, C. R.: *Analytical Investigation of Synchrophasing as a Means of Reducing Aircraft Interior Noise.* NASA CR-3823, 1984.
23. Johnston, J. F.; Donham, R. E.; and Guinn, W. A.: Propeller Signatures and Their Use. AIAA-80-1035, June 1980.
24. Willis, Conrad M.; Mayes, William H.; and Daniels, Edward F.: *Effects of Propeller Rotation Direction on Airplane Interior Noise Levels.* NASA TP-2444, 1985.
25. Wilby, J. F.; and Wilby, E. G.: *Analysis of In-Flight Acoustic Data for a Twin-Engined Turboprop Airplane.* NASA CR-178389, 1988.
26. Wilby, J. F.; and Gloyna, F. L.: Vibration Measurements of an Airplane Fuselage Structure: II. Jet Noise Excitation. *J. Sound & Vibration,* vol. 23, no. 4, Aug. 22, 1972, pp. 467–486.
27. Schoenster, James A.; Willis, Conrad M.; Schroeder, James C.; and Mixson, John S.: Acoustic-Loads Research for Powered-Lift Configurations. *Powered-Lift Aerodynamics and Acoustics,* NASA SP-406, 1976, pp. 429–443.
28. Van Dyke, J. D., Jr.; Schendel, J. W.; Gunderson, C. O.; and Ballard, M. R.: Cabin Noise Reduction in the DC-9. AIAA Paper No. 67-401, June 1967.
29. Wilby, John F.: Interior Noise of General Aviation Aircraft. *SAE Trans.,* sect. 3, vol. 91, 1982, pp. 3133–3144. (Available as SAE Paper 820961.)
30. Miller, Brent A.; Dittmar, James H.; and Jeracki, Robert J.: *The Propeller Tip Vortex—A Possible Contributor to Aircraft Cabin Noise.* NASA TM-81768, 1981.
31. Howlett, James T.; Clevenson, Sherman A.; Rupf, John A.; and Snyder, William J.: *Interior Noise Reduction in a Large Civil Helicopter.* NASA TN D-8477, 1977.

32. Mixson, John S.; O'Neal, Robert L.; and Grosveld, Ferdinand W.: *Investigation of Fuselage Acoustic Treatment for a Twin-Engine Turboprop Aircraft in Flight and Laboratory Tests.* NASA TM-85722, 1984.
33. Standard Method for Laboratory Measurement of Airborne Sound Transmission Loss of Building Partitions. ASTM Designation: E 90-85. *Volume 04.06 of 1986 Annual Book of ASTM Standards,* c.1986, pp. 764–775.
34. Piersol, A. G.; Wilby, E. G.; and Wilby, J. F.: *Evaluation of Aero Commander Propeller Acoustic Data: Taxi Operations.* NASA CR-159124, 1979.
35. Mixson, John S.; and Roussos, Louis A.: *Consideration of Some Factors Affecting Low-Frequency Fuselage Noise Transmission for Propeller Aircraft.* NASA TP-2552, 1986.
36. Barton, C. K.; and Mixson, J. S.: Noise Transmission and Control for a Light Twin-Engine Aircraft. *J. Aircr.,* vol. 18, no. 7, July 1981, pp. 570–575.
37. Heitman, Karen E.; and Mixson, John S.: Laboratory Study of the Effects of Sidewall Treatment, Source Directivity and Temperature on the Interior Noise of a Light Aircraft Fuselage. AIAA-86-0390, Jan. 1986.
38. Mixson, John S.; Roussos, Louis A.; Barton, C. Kearney; Vaicaitis, Rimas; and Slazak, Mario: Laboratory Study of Add-On Treatments for Interior Noise Control in Light Aircraft. *J. Aircr.,* vol. 20, no. 6, June 1983, pp. 516–522.
39. Dowell, E. H.; Gorman, G. F., III; and Smith, D. A.: Acoustoelasticity: General Theory, Acoustic Natural Modes and Forced Response to Sinusoidal Excitation, Including Comparisons With Experiment. *J. Sound & Vibration,* vol. 52, no. 4, June 22, 1977, pp. 519–542.
40. Dowell, E. H.: *Aeroelasticity of Plates and Shells.* Noordhoff International Publ. (Leyden, Netherlands), c.1975.
41. Dowell, E. H.: Reverberation Time, Absorption, and Impedance. *J. Acoust. Soc. America,* vol. 64, no. 1, July 1978, pp. 181–191.
42. Vaicaitis, R.: Noise Transmission Into a Light Aircraft. *J. Aircr.,* vol. 17, no. 2, Feb. 1980, pp. 81–86.
43. Van Nieuwland, J. M.; and Weber, C.: Eigenmodes in Nonrectangular Reverberation Rooms. *Noise Control Eng.,* vol. 13, no. 3, Nov./Dec. 1979, pp. 112–121.
44. Wolf, J. A., Jr.; and Nefske, D. J.: NASTRAN Modeling and Analysis of Rigid and Flexible Walled Acoustic Cavities. *NASTRAN: User's Experiences,* NASA TM X-3278, 1975, pp. 615–631.
45. Unruh, J. F.: Finite Element Subvolume Technique for Structural-Borne Interior Noise Prediction. *J. Aircr.,* vol. 17, no. 6, June 1980, pp. 434–441.
46. Unruh, J. F.: Structure-Borne Noise Prediction for a Single-Engine General Aviation Aircraft. *J. Aircr.,* vol. 18, no. 8, Aug. 1981, pp. 687–694.
47. Wilby, John F.; and Pope, Larry D.: Prediction of the Acoustic Environment in the Space Shuttle Payload Bay. *J. Spacecr. & Rockets,* vol. 17, no. 3, May–June 1980, pp. 232–239.
48. Pope, L. D.; Wilby, E. G.; and Wilby, J. F.: *Propeller Aircraft Interior Noise Model.* NASA CR-3813, 1984.
49. Barton, C. Kearney; and Daniels, Edward F.: *Noise Transmission Through Flat Rectangular Panels Into a Closed Cavity.* NASA TP-1321, 1978.
50. Wilby, John F.; O'Neal, Robert L.; and Mixson, John S.: Flight Investigation of Cabin Noise Control Treatments for a Light Turboprop Aircraft. *SAE Trans.,* sect. 4, vol. 94, 1985, pp. 4.614–4.624. (Available as SAE Paper 850876.)
51. Beranek, Leo L.; Nichols, Rudolph H., Jr.; Rudmose, H. Wayne; Sleeper, Harvey P., Jr.; Wallace, Robert L., Jr.; and Ericson, Harold L.: *Principles of Sound Control in Airplanes.* OSRD No. 1543, National Defense Research Committee, 1944.
52. Koval, L. R.: Effects of Cavity Resonances on Sound Transmission Into a Thin Cylindrical Shell. *J. Sound & Vibration,* vol. 59, no. 1, July 8, 1978, pp. 23–33.
53. Howlett, James T.; and Morales, David A.: *Prediction of Light Aircraft Interior Noise.* NASA TM X-72838, 1976.

54. Mixson, John S.; Barton, C. Kearney; and Vaicaitis, Rimas: Interior Noise Analysis and Control for Light Aircraft. SAE Paper 770445, Mar.–Apr. 1977.
55. Cockburn, J. A.; and Jolly, A. C.: *Structural-Acoustic Response Noise Transmission Losses and Interior Noise Levels of an Aircraft Fuselage Excited by Random Pressure Fields.* Tech. Rep. AFFDL-TR-68-2, U.S. Air Force, Aug. 1968.
56. Geisler, D. L.: *Experimental Modal Analysis of an Aero Commander Aircraft.* NASA CR-165750, 1981.
57. Revell, J. D.; Balena, F. J.; and Koval, L. R.: *Analytical Study of Interior Noise Control by Fuselage Design Techniques on High-Speed, Propeller-Driven Aircraft.* NASA CR-159222, 1980.
58. Beranek, Leo L.; and Work, George A.: Sound Transmission Through Multiple Structures Containing Flexible Blankets. *J. Acoust. Soc. America,* vol. 21, no. 4, July 1949, pp. 419–428.
59. Heitman, Karen E.; and Mixson, John S.: Laboratory Study of Cabin Acoustic Treatments Installed in an Aircraft Fuselage. *J. Aircr.,* vol. 23, no. 1, Jan. 1986, pp. 32–38.
60. Grosveld, Ferdinand W.: Noise Transmission Through Sidewall Treatments Applicable to Twin-Engine Turboprop Aircraft. AIAA-83-0695, Apr. 1983.
61. Tate, R. B.; and Langhout, E. K. O.: Aircraft Noise Control Practices Related to Ground Transport Vehicles. *SAE Trans.,* sect. 3, vol. 90, 1981, pp. 2648–2666. (Available as SAE Paper 810853.)
62. Grosveld, Ferdinand W.: Field-Incidence Noise Transmission Loss of General Aviation Aircraft Double-Wall Configurations. *J. Aircr.,* vol. 22, no. 2, Feb. 1985, pp. 117–123.
63. Rennison, D. C.; Wilby, J. F.; Marsh, A. H.; and Wilby, E. G.: *Interior Noise Control Prediction Study for High-Speed Propeller-Driven Aircraft.* NASA CR-159200, 1979.
64. Pope, L. D.; and Wilby, J. F.: Band-Limited Power Flow Into Enclosures. *J. Acoust. Soc. America:*
    Part I. vol. 62, no. 4, Oct. 1977, pp. 906–911.
    Part II. vol. 67, no. 3, Mar. 1980, pp. 823–826.
65. Lyon, Richard H.: Analysis of Sound-Structural Interaction by Theory and Experiment. *Noise and Vibration Control Engineering,* Malcolm J. Crocker, ed., Purdue Univ., c.1972, pp. 182–192.
66. Lyon, Richard H.; and Maidanik, Gideon: Power Flow Between Linearly Coupled Oscillators. *J. Acoust. Soc. America,* vol. 34, no. 5, May 1962, pp. 623–639.
67. Wilby, J. F.; and Scharton, T. D.: *Acoustic Transmission Through a Fuselage Sidewall.* NASA CR-132602, 1975.
68. Dowell, E. H.; and Kubota, Y.: Asymptotic Modal Analysis and Statistical Energy Analysis of Dynamical Systems. *J. Appl. Mech.,* vol. 52, no. 4, Dec. 1985, pp. 949–957.
69. Smith, P. W., Jr.: Response and Radiation of Structural Modes Excited by Sound. *J. Acoust. Soc. America,* vol. 34, no. 5, May 1962, pp. 640–647.
70. Lyon, Richard H.: What Good is Statistical Energy Analysis, Anyway? *Shock and Vibration Dig.,* 1970, pp. 2–10.
71. Hart, F. D.; and Shah, K. C.: *Compendium of Modal Densities for Structures.* NASA CR-1773, 1971.
72. Runkle, Charles J.; and Hart, Franklin D.: *The Radiation Resistance of Cylindrical Shells.* NASA CR-1437, 1969.
73. Pope, L. D.; and Wilby, E. G.: *Analytical Prediction of the Interior Noise for Cylindrical Models of Aircraft Fuselages for Prescribed Exterior Noise Fields. Phase II: Models for Sidewall Trim, Stiffened Structures, and Cabin Acoustics With Floor Partition.* NASA CR-165869, 1982.
74. Beyer, T. B.; Powell, C. A.; Daniels, E. F.; and Pope, L. D.: Effects of Acoustic Treatment on the Interior Noise of a Twin-Engine Propeller Airplane. *J. Aircr.,* vol. 22, no. 9, Sept. 1985, pp. 784–788.

75. Vaicaitis, R.; and Mixson, J. S.: Theoretical Design of Acoustic Treatment for Noise Control in a Turboprop Aircraft. *J. Aircr.*, vol. 22, no. 4, Apr. 1985, pp. 318–324.
76. Vaicaitis, R.; and Slazak, M.: Noise Transmission Through Stiffened Panels. *J. Sound & Vibration,* vol. 70, no. 3, June 8, 1980, pp. 413–426.
77. Vaicaitis, R.; Grosveld, F. W.; and Mixson, J. S.: Noise Transmission Through Aircraft Panels. *J. Aircr.*, vol. 22, no. 4, Apr. 1985, pp. 303–310.
78. Vaicaitis, R.; Bofilios, D. A.; and Eisler, R.: *Experimental Study of Noise Transmission Into a General Aviation Aircraft.* NASA CR-172357, 1984.
79. Vaicaitis, R.; and Slazak, M.: *Cabin Noise Control for Twin Engine General Aviation Aircraft.* NASA CR-165833, 1982.
80. Grosveld, Ferdinand W.; and Mixson, John S.: Noise Transmission Through an Acoustically Treated and Honeycomb-Stiffened Aircraft Sidewall. *J. Aircr.*, vol. 22, no. 5, May 1985, pp. 434–440.
81. Wilby, John F.; Piersol, Allan G.; and Wilby, Emma G.: A Comparison of Space Shuttle Payload Bay Sound Levels Predicted by PACES and Measured at Lift-Off. *Proceedings of the Shuttle Payload Dynamic Environments and Loads Prediction Workshop, Volume I,* JPL D-1347, California Inst. of Technology, Jan. 1984, pp. 113–134.
82. Koval, L. R.: On Sound Transmission Into a Thin Cylindrical Shell Under "Flight Conditions." *J. Sound & Vibration,* vol. 48, no. 2, Sept. 22, 1976, pp. 265–275.
83. SenGupta, G.: Current Developments in Interior Noise and Sonic Fatigue Research. *Shock & Vibration Dig.*, vol. 7, no. 10, Oct. 1975, pp. 3–20.
84. SenGupta, G.; and Nijim, H. H.: Control of Cabin Noise in a Prop-Fan Aircraft by Structural Filtering. AIAA-79-0583, Mar. 1979.
85. Lyon, Richard H.: *Lectures in Transportation Noise.* Grozier Publ. Inc., c.1973.
86. White, Pritchard H.: Sound Transmission Through a Finite, Closed, Cylindrical Shell. *J. Acoust. Soc. America,* vol. 40, no. 5, Nov. 1966, pp. 1124–1130.
87. Koval, Leslie R.: Effects of Air Flow, Panel Curvature, and Internal Pressurization on Field-Incidence Transmission Loss. *J. Acoust. Soc. America,* vol. 59, no. 6, June 1976, pp. 1379–1385.
88. Koval, L. R.: On Sound Transmission Into an Orthotropic Shell. *J. Sound & Vibration,* vol. 63, no. 1, Mar. 8, 1979, pp. 51–59.
89. Koval, L. R.: On Sound Transmission Into a Stiffened Cylindrical Shell With Rings and Stringers Treated as Discrete Elements. *J. Sound & Vibration,* vol. 71, no. 4, Aug. 22, 1980, pp. 511–521.
90. Revell, J. D.; and Tullis, R. H.: *Fuel Conservation Merits of Advanced Turboprop Transport Aircraft.* NASA CR-152096, 1977.
91. May, D. N.; Plotkin, K. J.; Selden, R. G.; and Sharp, B. H.: *Lightweight Sidewalls for Aircraft Interior Noise Control.* NASA CR-172490, 1985.
92. Prydz, R. A.; Revell, J. D.; Balena, F. J.; and Hayward, J. L.: Evaluation of Interior Noise Control Treatments for High-Speed Propfan-Powered Aircraft. AIAA-83-0693, Apr. 1983.
93. Peterson, M. R.; and Boyd, D. E.: Free Vibrations of Circular Cylinders With Longitudinal, Interior Partitions. *J. Sound & Vibration,* vol. 60, no. 1, Sept. 8, 1978, pp. 45–62.
94. Bruderline, Henry H.: Developments in Aircraft Sound Control. *J. Acoust. Soc. America,* vol. 8, no. 3, Jan. 1937, pp. 181–184.
95. Rudmose, H. Wayne; and Beranek, Leo L.: Noise Reduction in Aircraft. *J. Aeronaut. Sci.,* vol. 14, no. 2, Feb. 1947, pp. 79–96.
96. Vaicaitis, Rimas; and Mixson, John S.: Review of Research on Structureborne Noise. *A Collection of Technical Papers, Part 2—AIAA/ASME/ASCE/AHS 26th Structures, Structural Dynamics and Materials Conference,* Apr. 1985, pp. 587–601. (Available as AIAA-85-0786.)
97. Lyon, R. H.; and Slack, J. W.: A Review of Structural Noise Transmission. *Shock & Vibration Dig.,* vol. 14, no. 8, Aug. 1982, pp. 3–11.
98. Rubin, S.; and Biehl, F. A.: Mechanical Impedance Approach to Engine Vibration Transmission Into an Aircraft Fuselage. *SAE Trans.,* vol. 76, 1967, pp. 2711–2719. (Available as SAE Paper 670873.)

99. Yoerkie, C. A.; Moore, J. A.; and Manning, J. E.: *Development of Rotorcraft Interior Noise Control Concepts, Phase 1: Definition Study.* NASA CR-166101, 1983.
100. Bellavita, Paolo; and Smullin, Joseph: Cabin Noise Reduction for the Agusta A-109 Helicopter. *Proceedings of Fourth European Rotorcraft and Powered Lift Aircraft Forum, Volume 2,* Associazione Italiano di Aeronautica ed Astronautica and Associazione Industrie Aerospaziali (Gallarate, Italy), Sept. 1978, pp. 61-0–61-29.
101. Metcalf, Vern L.; and Mayes, William H.: Structureborne Contribution to Interior Noise of Propeller Aircraft. *SAE Trans.,* sect. 3, vol. 92, 1983, pp. 3.69–3.74. (Available as SAE Paper 830735.)
102. Unruh, James F.; Scheidt, Dennis C.; and Pomerening, Daniel J.: *Engine Induced Structural-Borne Noise in a General Aviation Aircraft.* NASA CR-159099, 1979. (Available as SAE Paper 790626.)
103. Ewins, D. J.; and Silva, J. M. M.: Measurements of Structural Mobility on Helicopter Structures. *Proceedings of Symposium on Internal Noise in Helicopters,* Univ. of Southampton (England), 1980, pp. D1 1–D1 19.
104. Eichelberger, E. C.: Point Admittance of Cylindrical Shells With and Without Ring Stiffening. ASME Paper 80-WA/NC-5, Nov. 1980.
105. Junger, M. C.; Garrelick, J. M.; Martinez, R.; and Cole, J. E., III: *Analytical Model of the Structureborne Interior Noise Induced by a Propeller Wake.* NASA CR-172381, 1984.
106. Cremer, L.; and Heckl, M. (E. E. Ungar, transl.): *Structure-Borne Sound.* Springer-Verlag, 1973.
107. Ungar, Eric E.: Transmission of Plate Flexural Waves Through Reinforcing Beams; Dynamic Stress Concentrations. *J. Acoust. Soc. America,* vol. 33, no. 5, May 1961, pp. 633–639.
108. SenGupta, G.; Landmann, A. E.; Mera, A.; and Yantis, T. F.: Prediction of Structure-Borne Noise, Based on the Finite Element Method. AIAA-86-1861, July 1986.
109. Eversman, W.; Ramakrishnan, J. V.; and Koval, L. R.: A Comparison of the Structureborne and Airborne Paths for Propfan Interior Noise. AIAA-86-1863, July 1986.
110. Hayden, R. E.; Murray, B. S.; and Theobald, M. A.: *A Study of Interior Noise Levels, Noise Sources and Transmission Paths in Light Aircraft.* NASA CR-172152, 1983.
111. Royster, Larry H.; Hart, Franklin D.; and Stewart, Noral D., eds.: *NOISE-CON 81 Proceedings—Applied Noise Control Technology.* Noise Control Found., c.1981.
112. Crocker, Malcolm J.: Identification of Noise From Machinery, Review and Novel Methods. *INTER-NOISE 77 Proceedings, Noise Control: The Engineer's Responsibility,* Eric J. Rathe, ed., International Inst. of Noise Control Engineering (Switzerland), c.1977, pp. A 201–A 211.
113. Jha, S. K.; and Catherines, J. J.: Interior Noise Studies for General Aviation Types of Aircraft, Part I: Field Studies. *J. Sound & Vibration,* vol. 58, no. 3, June 8, 1978, pp. 375–390.
114. Kumar, Sudhir; and Srivastava, Narayan S.: Investigation of Noise Due to Structural Vibrations Using a Cross-Correlation Technique. *J. Acoust. Soc. of America,* vol. 57, no. 4, Apr. 1975, pp. 769–772.
115. Strahle, Warren C.; Muthukrishnan, M.; and Neale, Douglas H.: Coherence Between Internal and External Noise Generated by Gas Turbine Combustors. AIAA-77-20, Jan. 1977.
116. Keefe, Laurence: Interior Noise Path Identification in Light Aircraft Using Multivariate Spectral Analysis. AIAA-79-0644, Mar. 1979.
117. Piersol, A. G.; Wilby, E. G.; and Wilby, J. F.: *Evaluation of Aero Commander Sidewall Vibration and Interior Acoustic Data: Static Operations.* NASA CR-159290, 1980.
118. Forssen, Bjorn Henry: Determination of Transmission Loss, Acoustic Velocity, Surface Velocity and Radiation Efficiency by Use of Two Microphone Techniques. Ph.D. Thesis, Purdue Univ., Aug. 1983.
119. Atwal, Mahabir; and Bernhard, Robert: *Noise Path Identification Using Face-to-Face and Side-by-Side Microphone Arrangements.* NASA CR-173708, 1984.

120. Crocker, Malcolm J.; Forssen, Bjorn; Raju, P. K.; and Wang, Yiren S.: Application of Acoustic Intensity Measurement for the Evaluation of Transmission Loss of Structures. Purdue Univ. paper presented at the International Congres on Recent Developments in Acoustic Intensity Measurement (Senlis, France), Sept. 30–Oct. 2, 1981.
121. Dalan, G. A.; and Cohen, R. L.: Acoustic Intensity Techniques for Airplane Cabin Applications. *J. Aircr.*, vol. 22, no. 10, Oct. 1985, pp. 910–914.
122. McGary, Michael C.: *Noise Transmission Loss of Aircraft Panels Using Acoustic Intensity Methods.* NASA TP-2046, 1982.
123. Crocker, M. J.; Heitman, K. E.; and Wang, Y. S.: Evaluation of the Acoustic Intensity Approach To Identify Transmission Paths in Aircraft Structures. *SAE Trans.*, sect. 3, vol. 92, 1983, pp. 3.59–3.68. (Available as SAE Paper 830734.)
124. Maynard, J. D.; Williams, E. G.; and Lee, Y.: Nearfield Acoustic Holography: I. Theory of Generalized Holography and the Development of NAH. *J. Acoust. Soc. America,* vol. 78, no. 4, Oct. 1985, pp. 1395–1413.
125. Williams, Earl G.: Numerical Evaluation of the Radiation From Unbaffled, Finite Plates Using the FFT. *J. Acoust. Soc. America,* vol. 74, no. 1, July 1983, pp. 343–347.
126. Jha, S. K.; and Catherines, J. J.: Interior Noise Studies for General Aviation Types of Aircraft, Part II: Laboratory Studies. *J. Sound & Vibration,* vol. 58, no. 3, June 8, 1978, pp. 391–406.
127. Howlett, James T.; and Schoenster, James A.: An Experimental Study of Propeller-Induced Structural Vibration and Interior Noise. SAE Paper 790625, Apr. 1979.
128. McGary, Michael C.; and Mayes, William H.: A New Measurement Method for Separating Airborne and Structureborne Aircraft Interior Noise. *Noise Control Eng. J.*, vol. 20, no. 1, Jan.–Feb. 1983, pp. 21–30.
129. Ver, Istvan L.: Some Uses of Reciprocity in Acoustic Measurements and Diagnosis. *Inter-Noise 85, Proceedings 1985 International Conference on Noise Control Engineering, Volume II,* Tagungsbericht—Tb Nr. 39, Federal Inst. for Occupational Safety (Munich), Sept. 1985, pp. 1311–1314.
130. Bernhard, R. J.; Gardner, B. K.; Mollo, C. G.; and Kipp, C. R.: Prediction of Sound Fields in Cavities Using Boundary Element Methods. AIAA-86-1864, July 1986.
131. Metzger, Frederick B.: Strategies for Aircraft Interior Noise Reduction in Existing and Future Propeller Aircraft. SAE Paper 810560, Apr. 1981.
132. Goss, Russell P.: Acoustics Program for the Grumman Gulfstream II. AIAA-71-783, July 1971.
133. Gebhardt, George T.: Acoustical Design Features of Boeing Model 727. *J. Aircr.*, vol. 2, no. 4, July–Aug. 1965, pp. 272–277.
134. Holmer, Curtis I.: Approach to Interior Noise Control. *J. Aircr.:*
Part I: Damped Trim Panels, vol. 22, no. 7, July 1985, pp. 618–623.
Part II: Self-Supporting Damped Interior Shell, vol. 22, no. 8, Aug. 1985, pp. 729–733.
135. Marsh, Alan H.: Noise Control Features of the DC-10. *Noise Control Eng.,* vol. 4, no. 3, May–June 1975, pp. 130–139.
136. Waterman, E. H.; Kaptein, D.; and Sarin, S. L.: Fokker's Activities in Cabin Noise Control for Propeller Aircraft. SAE Paper 830736, Apr. 1983.
137. Hunter, Gertrude S.: Sound Reduction Program for Convair-Liner 340. *Noise Control,* vol. 2, no. 1, Jan. 1956, pp. 27–32.
138. Sternfeld, Harry, Jr.: New Techniques in Helicopter Noise Reduction. *Noise Control,* vol. 7, no. 3, May–June 1961, pp. 4–10.
139. Leverton, J. W.; and Pollard, J. S.: Helicopter Internal Noise—An Overview. *Proceedings of Symposium on Internal Noise in Helicopters,* Univ. of Southampton (England), 1980, pp. A4 1–A4 22.
140. Forth, Karl D.: Quiet Interiors. *Aviation Equip. Maint.*, vol. 5, no. 9, Sept. 1986, pp. 30–35.
141. Large, J. B.; Wilby, J. F.; Grande, E.; and Andersson, A. O.: The Development of Engineering Practices in Jet, Compressor, and Boundary Layer Noise. *Aerodynamic Noise,* Univ. of Toronto Press, c.1969, pp. 43–67.

142. Olcott, John W.; Larson, George C.; and Aarons, Richard N.: B/CA Analysis: Gulfstream 1000. *Bus. & Commer. Aviation,* vol. 49, no. 2, Aug. 1981, pp. 49–52.
143. Nichols, R. H., Jr.; Sleeper, H. P., Jr.; Wallace, R. L., Jr.; and Ericson, H. L.: Acoustical Materials and Acoustical Treatments for Aircraft. *J. Acoust. Soc. America,* vol. 19, no. 3, May 1947, pp. 428–443.
144. Mangiarotty, R. A.: An Isolator-Membrane for Soundproofing Aircraft Cabins Exposed to High Noise Levels. *J. Sound & Vibration,* vol. 3, no. 3, May 1966, pp. 467–475.
145. Balena, F. J.; and Prydz, R. A.: Experimental and Predicted Noise Reduction of Stiffened and Unstiffened Cylinders With and Without a Limp Inner Wall. AIAA-81-1968, Oct. 1981.
146. Vaicaitis, R.; and Mixson, J. S.: Theoretical Design of Acoustic Treatment for Cabin Noise Control of a Light Aircraft. AIAA-84-2328, Oct. 1984.
147. Howlett, James T.; and Clevenson, Sherman A.: *A Study of Helicopter Interior Noise Reduction.* NASA TM X-72655, 1975.
148. Bhat, W. V.; and Wilby, J. F.: Interior Noise Radiated by an Airplane Fuselage Subjected to Turbulent Boundary Layer Excitation and Evaluation of Noise Reduction Treatments. *J. Sound & Vibration,* vol. 18, no. 4, Oct. 22, 1971, pp. 449–464.
149. Wilby, J. F.; and Smullin, J. I.: Interior Noise of STOL Aircraft and Helicopters. *Noise Control Eng.,* vol. 12, no. 3, May–June 1979, pp. 100–110.
150. Henderson, John P.; and Nashif, Ahid D.: Reduction of Interior Cabin Noise Levels in a Helicopter Through Additive Damping. *Shock & Vibration Bull.,* Bull. 44, Pt. 5, U.S. Dep. of Defense, Aug. 1974, pp. 13–22.
151. Barton, C. K.: Structural Stiffening as an Interior Noise Control Technique for Light Twin-Engine Aircraft. Ph.D. Thesis, North Carolina State Univ., 1979.
152. Hrycko, G. O.: Design of the Low Vibration Turboprop Powerplant Suspension System for the DASH 7 Aircraft. *SAE Trans.,* sect. 3, vol. 92, 1983, pp. 3.133–3.145. (Available as SAE Paper 830755.)
153. Unruh, J. F.: Specification, Design and Test of Aircraft Engine Isolators for Reduced Interior Noise. *J. Aircr.,* vol. 21, no. 6, June 1984, pp. 389–396.
154. Lorch, D. R.: Noise-Reduction Measurements of Integrally Stiffened Fuselage Panels. AIAA-80-1033, June 1980.
155. Getline, G. L.: *Low-Frequency Noise Reduction of Lightweight Airframe Structures.* NASA CR-145104, 1976.
156. Ungar, Eric E.; and Kurzweil, Leonard G.: *Preliminary Evaluation of Waveguide Vibration Absorbers.* AFWAL-TR-83-3125, U.S. Air Force, Jan. 1984. (Available from DTIC as AD A140 743.)
157. Ellen, C. H.: *A Study of the Use of Blocking Masses in Reducing Helicopter Cabin Noise.* Tech. Memo Aero 1838, Royal Aircraft Establ., Mar. 1980.
158. Wheeler, P. D.; Rawlinson, R. D.; Pelc, S. F.; and Dorey, A. P.: The Development and Testing of an Active Noise Reduction System for Use in Ear Defenders. *INTER-NOISE 78, Designing for Noise Control,* William W. Lang, ed., Noise Control Found., c.1978, pp. 977–982.
159. Keith, S. E.; and Scholaert, H. S. B.: *A Study of the Performance of an Olson-Type Active Noise Controller and the Possibility of the Reduction of Cabin Noise.* UTIAS Tech. Note No. 228, Inst. for Aerospace Studies, Univ. of Toronto, Mar. 1981.
160. Silcox, R. J.; Fuller, C. R.; and Lester, H. C.: Mechanisms of Active Control in Cylindrical Fuselage Structures. AIAA-87-2703, Oct. 1987.
161. Salikuddin, M.; Tanna, H. K.; Burrin, R. H.; and Carter, W. E.: Application of Active Noise Control to Model Propeller Noise. AIAA-84-2344, Oct. 1984.

17 Flyover-Noise Measurement and Prediction

Lead author

Noel A. Peart
The Boeing Co.
Seattle, Washington

Contributing authors

Boeing Noise Engineering Organization
The Boeing Co.
Seattle, Washington

Introduction

Community noise in the vicinity of major airports around the world is an obstacle to the natural growth of airline traffic. During the almost 30 years since the advent of commercial jet transports in the late 1950's, flyover noise levels of individual aircraft have been dramatically reduced. This reduction in noise was brought about by a combination of market forces—for example, competition, Federal and international regulations, engine efficiency and cycle improvements, and noise reduction technology development. In the same time period, however, there has been only a slight increase in the number of airports, despite the tremendous growth in airport operations—especially since deregulation of U.S. airlines went into effect. These factors have combined to make airport noise a potential deterrent to the otherwise orderly growth of the world's air transportation system.

Details are presented in this chapter for the measurement and prediction of aircraft flyover noise to be used for certification, research and development, community noise surveys, airport monitors, and pass-fail criteria. Test details presented are applicable to all types of aircraft, both large and small, and the use of Federal Aviation Regulations (FAR) Part 36 (ref. 1) is emphasized. The test procedures described in FAR Part 36 are considered the best for all types of aircraft-noise testing. Accuracy of noise measurements is important. Thus, a pass-fail criterion should be used for all noise measurements. Finally, factors which influence the sound propagation and noise prediction procedures, such as atmospheric and ground effects, are also presented.

Measurement of Noise Produced by Airplanes Powered by Turbofan Engines

Purpose and Objectives for Conducting Tests

A long-term goal of the aircraft manufacturing industry is to achieve community compatibility by phasing out the older, noisier airplanes and replacing them with newer, quieter designs. Improved flight operational procedures, land acquisition, and land usage are other methods being used to help reduce airplane-noise exposure. The imposition of local airport noise regulations and operating restrictions is becoming more prevalent as a means of improving airport compatibility with the community. In addition, some older jet transports have been modified to quieter versions by refitting them with higher-bypass-ratio turbofan engines or by adding sound-absorbing material to the nacelles. These events have resulted in the increased need for in-flight measurements together with the need to follow strict guidelines when acquiring flyover-noise measurements.

Certification

Flight-testing for aircraft-noise certification must be tightly controlled and rigorously specified in order to assure validity and credibility. In the United States, Federal standards intended to control aircraft noise began with the adoption of Federal Aviation Regulations (FAR) Part 36 in 1969. This regulation initially applied only to new designs of turbojet and transport category airplanes and required that they be markedly quieter than the earlier airplanes of these types. Since the adoption of FAR Part 36, the Federal Aviation Administration (FAA) has amended this regulation 15 times to cover all categories of aircraft, including helicopters. (See Amendment 15, ref. 1.)

A parallel set of aircraft-noise requirements was adopted by the International Civil Aviation Organization (ICAO) in 1971 as Annex 16 to the Convention on International Civil Aviation. As with FAR Part 36, Annex 16 has been continually reviewed and revised, with the latest change being Amendment 5, applicable on November 26, 1981 (ref. 2).

Research and Development

The major airframe and engine companies involved in the production of large commercial jet airplanes made extensive use of airplane flyover-noise measurements for research and development during the 1960's and 1970's. The prime purposes of those tests were to define the noise characteristics and to develop modified engines and/or nacelles that would reduce flyover-noise levels. Data from such flight tests have led to the development of analytical tools that enable noise measurements obtained during static engine operation to be projected to flight conditions for those airplanes. The result of these developments is that a large portion of turbofan engine noise research and development programs now rely heavily on static engine measurements, with some supplemental flight test data acquired usually in conjunction with a noise certification flight test.

Community Noise Surveys

An aircraft and airport community noise survey may be conducted for a variety of reasons:

1. Assessment of land use suitability
2. Comparison with local noise ordinances
3. Identification and quantification of major noise sources
4. Determination of sound exposure at particular locations
5. Determination of trend in sound exposure levels
6. Determination of need for new or additional noise control measures

Outdoor community noise measurements are generally made during a noise survey. The purpose of each survey plays a major role in deciding the extent, type, and quantity of equipment required to measure aircraft flyover noise.

Airport Noise Monitors

Aircraft-noise monitoring systems are usually set up at fixed locations in the vicinity of airports and are activated when the A-weighted sound level of an aircraft flyover exceeds a given threshold level. The monitor normally provides a printout that includes time of day, maximum A-weighted sound level in decibels, and A-weighted sound exposure level (SEL) in decibels.

Many airports throughout the world have round-the-clock monitoring of aircraft traffic. Some airports, such as Los Angeles and San Jose, California, have a public display located in the terminal where on-line readouts of each monitor microphone are visible to the general public.

Test Requirements

The objective of any flight test is to acquire noise levels that are representative of the flight conditions desired and that are from a sufficient number of flights of a particular aircraft to derive a subjective noise measure (e.g., effective perceived noise level (EPNL) as discussed in appendix B of ref. 1) for takeoff, sideline, and approach conditions.

Test Site Terrain

Tests to show compliance with aircraft-noise-level standards consist of a series of actual or simulated takeoffs and approaches during which measurements are taken at noise measuring stations located at reference points such as those shown in figure 1. For each actual or simulated takeoff, simultaneous measurements are made at the sideline noise measuring stations on each side of the runway and also at the takeoff noise measuring station. Each noise measuring station should be surrounded by relatively flat terrain having no excessive sound absorption characteristics, such as those which might be caused by thick, matted, or tall grass, shrubs, or wooded areas.

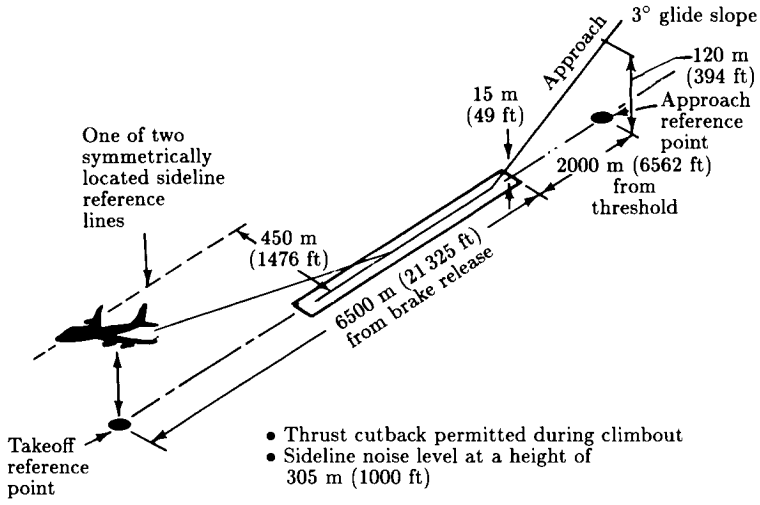

Figure 1. Noise certification measurement locations for new designs.

During the period when the flyover-noise time record is of interest, no obstruction should exist that would significantly influence the sound field from the aircraft.

Aircraft Testing Procedures

The aircraft height and lateral position relative to the extended centerline of the runway should be determined by a method which is independent of normal flight instruments, such as radar tracking, theodolite triangulation, or laser trajectography. Photographic scaling techniques have also been used.

Aircraft position along the flight path should be synchronized to the noise recorded at the noise measuring stations with time code signals. Also, the position of the aircraft should be recorded during the entire time period in which the acoustic signal is recorded for analysis.

Microphone Array

To acquire data consistent with the requirements of FAR Part 36 or ICAO Annex 16 (refs. 1 and 2), each microphone should be mounted with the center of the sensing element 1.2 m (4.0 ft) above the local ground surface. Each microphone should be oriented to provide a known angle of sound incidence at all times of interest throughout the significant duration of each flyover-noise measurement. To avoid ambiguity, most flyover-noise measurements are made with a windscreen around each microphone at all times. Correction for any insertion loss produced by the windscreen should be applied to the measured data.

The microphone array should consist of at least three microphones, one directly under the flight path and two to measure maximum sideline noise. Each sideline microphone should be placed symmetrically with respect to the one on the opposite sideline so that the maximum noise on either side of the airplane is measured.

Flight Path Intercepts

Simulated takeoffs and approaches consisting of flight path intercepts are often used in lieu of actual takeoffs and landings at an airport. For takeoff and sideline noise measurements, the procedure consists of intercepting and following the desired climb profile. To perform the approach intercepts, a normal approach path is maintained over the microphone array, the test condition being ended prior to landing with power being reapplied and a go-around initiated. Aircraft weights and configurations should be selected carefully in order to maintain near-constant indicated airspeed during each test condition.

The benefits of using flight path intercepts are that they permit much greater test site selection flexibility and they permit target altitude over the centerline microphone to be chosen to optimize the signal-to-noise ratio. Shorter test times and lower test costs are further benefits.

Measurement of Aircraft Noise

All noise measurements should be made with instruments meeting the specifications of FAR Part 36 (ref. 1).

Weather Restrictions

There should be no rain or other precipitation during the testing. Also, the ambient air temperature should be between 2.2°C and 35°C (36°F and 95°F), inclusive, over that portion of the sound propagation path between the aircraft and a point 10.0 m (32.8 ft) above the ground at the noise measuring station. The lower temperature will avoid freezing and the upper temperature will avoid takeoff power settings that result in lower than the flat temperature-rated takeoff power settings as well as highly absorptive atmospheric conditions. Relative humidity and ambient temperature over that portion of the sound propagation path between the aircraft and a point 10.0 m above the ground at the noise measuring station should be such that the sound attenuation in the 1/3-octave band centered at 8000 Hz is not greater than 12 dB/100 m (3.66 dB/100 ft) and the relative humidity should be between 20 and 95 percent, inclusive. A graphical representation of the foregoing weather restrictions is provided in figure 2.

Wind Limits

Tests may be conducted when (1) the wind speed over the noise measurement period does not exceed an average of 12 knots or a maximum value of 15 knots and (2) the crosswind component over the noise measurement period does not exceed an average of 7 knots or a maximum value of 10 knots. An averaging period less than or equal to 30 sec may be used to define wind speed. Wind measurements should be made 10.0 m (32.8 ft) above the ground in the vicinity of the microphones. No anomalous wind conditions (including turbulence) which will significantly affect the noise level of the aircraft when the noise is recorded at each noise measuring station should exist during any test.

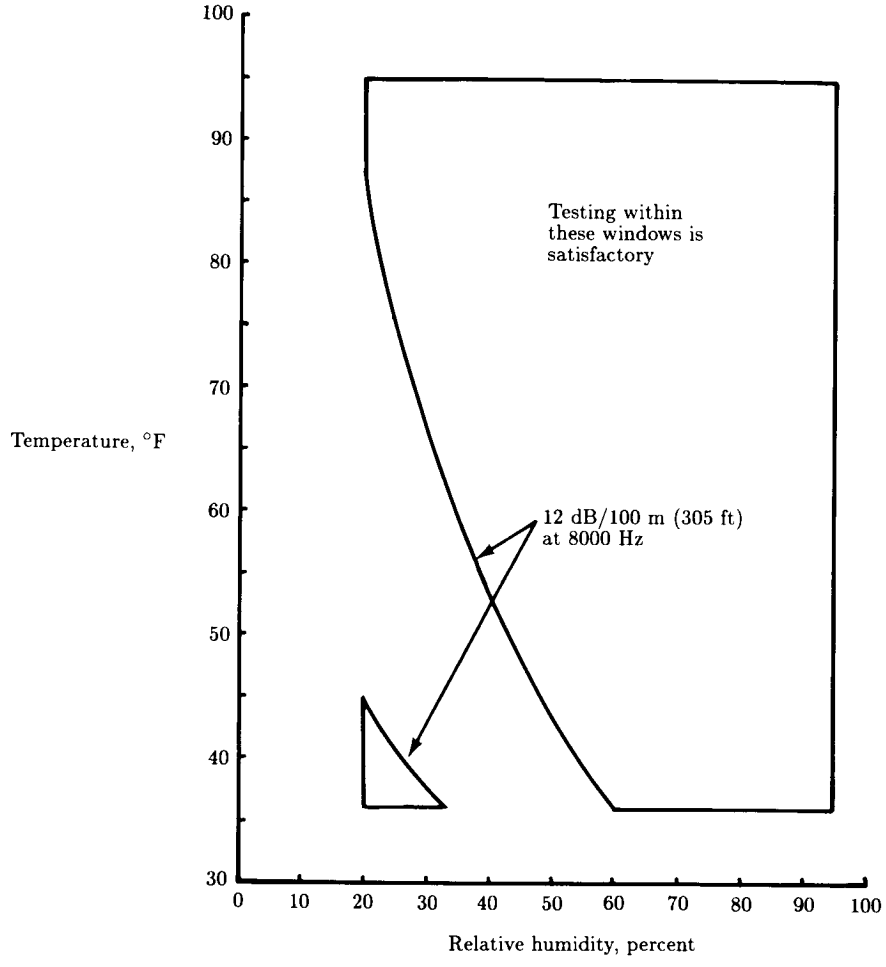

Figure 2. Test weather windows from 10.0 m (32.8 ft) to airplane height.

Reference Conditions

Aircraft position, performance data, and noise measurements should be adjusted to the following noise reference atmospheric conditions:

1. Sea level pressure of 101.3 kPa (1 atm)
2. Ambient temperature of 25°C (77°F)
3. Relative humidity of 70 percent
4. Zero wind

The above reference conditions provide near-minimum atmospheric absorption, that is, maximum aircraft flyover-noise levels.

Determination of a Subjective Measure

Noise Floor Corrections

Aircraft sound pressure levels within the 10-dB down times should exceed the mean background sound pressure levels by at least 3 dB in each 1/3-octave band to be included in the calculation of a subjective measure for a given aircraft flyover. In the case where the aircraft acoustic signal is greater than the background acoustic level, the true aircraft signal may be determined by subtracting the background mean-square sound pressure levels from the indicated mean-square aircraft-noise sound pressure levels.

When a 1/3-octave band sound pressure level from an aircraft-noise recording is not more than 3 dB greater than the corresponding 1/3-octave band sound pressure level of the background noise, the aircraft's signal in that 1/3-octave band is defined as being masked. When masking occurs, levels for the masked bands may be estimated by applying one or more of the correction procedures described in reference 3.

Pseudotone Identification

Aircraft-noise measurements obtained from microphones located 1.2 m (4.0 ft) above the ground are susceptible to spectral irregularities caused by ground plane reflections or introduced by data processing techniques that account for background noise contamination. Tone corrections to perceived noise levels are only intended to account for the subjective response due to the presence of pronounced spectral irregularities from aircraft-noise sources.

Any spectral irregularities not related to aircraft-noise sources are termed *pseudotones,* or fictitious tones, and may be excluded from the calculation of effective perceived noise levels. Methods to detect and identify pseudotones are discussed in reference 3.

Test Condition Acceptance and On-Line Systems

Test Condition Acceptance Criteria

Each acceptable aircraft-noise flyover measurement should comply with all the following criteria. The weather window between the aircraft and 10.0 m (32.8 ft) above the noise measuring station should consider temperature, relative humidity, and atmospheric absorption at 8000 Hz. The wind limits should consider average wind, maximum wind, and crosswind. Aircraft performance should consider lateral offset from the target flight path, overhead height, airspeed, and engine power setting.

On-Line Data Acquisition and Reduction

Most major airframe manufacturers have developed systems which enable an assessment of the quality of the test data and an initial determination of final noise levels to be made "on-line" and "on-site." The systems use digital computation to determine the test aircraft position in real time, integrate that information with airplane performance data, and telemeter the data to a ground-based test coordination

and control station. One such system is described in detail in reference 4. In this particular example a ground station performs an acceptance check on the telemetered data by comparison with predetermined positioning and performance limits. Data from a particular run are accepted and recorded if aircraft, engine, acoustical, and meteorological parameters are all within established tolerance limits.

The entire process takes place while the test aircraft flies a continual traffic pattern circuit. If the test site is free of other aircraft traffic, the typical time of 6 minutes between tests is interrupted only by the vertical soundings of the meteorological airplane.

Validity of Results

The sample size should be large enough to establish statistically a 90-percent confidence limit not to exceed ±1.5 dB. No test result should be omitted from the final values of effective perceived noise level in calculating this value. From each sample compute the arithmetic average of the effective perceived noise level for all valid test runs at the takeoff, approach, and sideline measuring stations. If more than one noise measurement system is used at any single measuring station, the resulting data for each test run (after correction) should be averaged as a single measurement. If more than one test site or noise measuring station location is used, each valid test run should be included in the computation of the average values and their confidence limits.

The minimum sample size for each of the three measurements (takeoff, approach, and sideline) should be six. For tests designed to determine the variation of effective perceived noise level as a function of engine power setting (for constant height and airspeed), there should be at least six valid data points over the power setting range of interest. The number of samples should be large enough to establish statistically for each of the three average noise levels a 90-percent confidence limit which does not exceed ±1.5 dB. No test result should be omitted from the averaging process.

Measurement of Helicopter Noise

Measurement of helicopter noise in flight has many requirements in common with that of airplane noise. However, there are several significant differences that make the planning and conducting of a noise test for helicopters somewhat unique. A major reason for the differences is that with helicopters, the primary noise sources are the rotor systems while the engines are usually secondary sources.

Because of the importance of the aerodynamic environment, helicopter noise tends to be more sensitive to flight conditions than to power or weight. For example, rotor noise in partial power descent tends to be higher than that during full power takeoff because rotor blades are closer to tip vortices shed from preceding blades in descent than in climb. Furthermore, noise during landing may be very sensitive to operating conditions such as combinations of airspeed and rate of descent.

Test Design

In general, there are three types of testing conducted to measure the external noise of helicopters. They are as follows:

1. Certification testing
2. Evaluation of flight procedures and measurement of noncertification test procedures
3. Rotor noise research

Most noise testing procedures are based on ICAO Annex 16 (ref. 2). That document contains information regarding all aspects of helicopter noise measurement, instruments, and analysis. Specifics of flight conditions, microphone locations, data analysis, and corrections, however, are rather narrowly defined and are applicable primarily to noise certification.

In many cases, it is desirable to include in the test program conditions that are more representative of the way helicopters are actually operated than those that are reflected by noise certification testing. For example, the approach condition for certification is a constant 6° approach angle at a constant indicated airspeed. In practice, however, many approaches are made by continuously varying both the airspeed and the rate of descent such that neither is held constant.

Test programs that are research oriented may often be designed to investigate a particular phenomenon, such as impulsive noise at high rotor tip speeds or blade vortex interaction in descent. In these cases, appropriate prediction analyses should be employed to define the range of operating parameters of interest.

When designing a helicopter noise test, keep in mind that the sound field around a helicopter is usually not symmetrical with respect to the aircraft centerline. This is because the main rotor advances on one side of the aircraft and retreats on the other side and because the tail rotor is usually located to one side of the aircraft. For these reasons it is important to make acoustical measurements on both sides of the flight path. Measurements obtained by placing a microphone on one side only and flying reciprocal headings to gather data should be restricted to extremely low wind conditions.

Configuration and Operation

The most important parts of the helicopter, with respect to external noise generation, are the rotor blades. The blades should be "tracked" to within manufacturer's specifications (i.e., the out-of-tolerance amount permitted by the manufacturer when the blades are hand turned) prior to testing.

It is recommended that testing be limited to gross weights not less than 90 percent of maximum and that the helicopter be refueled when this condition is reached. This range of weights represents the typical operating condition of a helicopter.

The following operating conditions should be considered and selection made as applicable to a specific test: ground idle with rotors not turning, flight idle with rotors turning, hover in ground effect, hover with wheels about 1.5 m (5 ft) from ground, takeoff at maximum continuous power, flyovers at various airspeeds up to the maximum, and approaches at various airspeeds and rates of descent. Most helicopters have a permissible range of rotor speed selection. Testing should always be conducted

at 100 percent of design rotor speed and at other rotor speeds applicable to the test objectives.

Some helicopters have special control features that are designed to perform certain functions, such as maintaining the fuselage at a level attitude. Some of these controls (for example, longitudinal differential cyclic trim on tandem rotor helicopters) can have a major influence on noise. The test should include operation of these devices over their permissible range.

Most helicopters do not include engine-noise suppression devices as standard equipment. In some cases, such as critical rotor noise research, it may be desirable to equip the test helicopter with engine-noise suppression devices to further enhance a measurement of rotor noise.

Test Site

When selecting a site for hover noise tests, keep in mind that rotor downwash can cause local velocities in excess of 26.8 m/sec (60.0 mph). Loose articles that could be blown about and cause potential damage or injury should be secured or removed. Whenever possible, the area should be cleared of debris such as loose vegetation and gravel. In all other aspects the test site requirements should be the same as those for large airplanes.

Hover noise measurements should be made at a horizontal distance of at least two rotor diameters to avoid the acoustic "near field." Many researchers use 61.0 and 152.4 m (200 and 500 ft) as preferred distances since they are in the "far field" of the low-frequency rotor noise and yet are close enough to give a satisfactory signal-to-noise ratio.

Hover noise measurements should be made at several locations around the azimuth because of the directional nature of the acoustic field. Increments of 30° are adequate for general purposes, although smaller increments might be required for special purposes. Hover noise should be recorded for at least 30 sec to allow sufficient time to average what are often rather unsteady sound signals.

Flyover noise should be measured on both sides of the helicopter. The sideline distance on approach and departure depends on the specific helicopter; however, in general, valid data can be acquired from the time when the helicopter is about 1524 m (5000 ft) in horizontal ground distance on the approach side (approximately 152.4 m (500 ft) height) of the microphones to a distance of approximately 914.4 m (3000 ft) on the departure side.

Instruments

A typical acoustical spectrum of a helicopter is presented in figure 3. Examination of this spectrum reveals two important elements. First of all, the dominant spectral components are harmonic, and second, the highest amplitudes tend to occur at the main rotor passage frequency, which is of the order of 10 to 15 Hz. In order to properly measure such acoustic signals, the instrumentation system, from microphone through recorder, must be selected with these low-frequency requirements in mind. Many helicopter researchers use 1-in. microphones and FM recording to preserve the rotor noise signal. If the purpose of the test is more general,

such as measurement of the peak level (e.g., maximum A-weighted sound pressure levels and maximum perceived noise level), simpler systems may suffice.

Although microphones located above the ground level may be used for many measurements and are required for certification, ground-level microphones may be preferred for research in order to minimize distortion of the measured sound spectrum due to the reflected ground wave. Figure 4 illustrates the difference in sound pressure levels as sensed by a ground-level microphone and by an elevated microphone located near a rotor. In figure 4 the slope above 400 Hz is correct for the ground-level microphone.

In some flight conditions, the sound of a helicopter can become quite impulsive. A pressure-time history of such an event is illustrated in figure 5. In such situations, the high ratio of peak to root-mean-square sound pressure effectively eliminates noise measurement systems that include exponential time weighting (i.e., slow, fast, or impulse). Recording levels should be carefully selected to avoid overloading input amplifiers.

For many applications, such as noise certification and research (e.g., comparison with prediction), it is necessary to know the helicopter location with respect to the microphones and to have this information coordinated with the acoustical records. Several methods, including radar tracking, laser tracking, and photo-optical tracking, may be employed. When conducting precise research, it may also be important to instrument the helicopter for measurement of parameters such as fuselage attitude, rotor blade motions, and hub motions and to have these measurements coordinated with the acoustical data by use of time codes or telemetering.

Factors Influencing Sound Propagation (Full-Scale Static and Flight Testing)

Atmospheric Effects

Beyond the immediate vicinity (near field) of a sound source, the acoustic energy spreads out spherically, resulting in a level reduction described by the inverse-square law. The acoustic energy is also subject to absorption (by molecular resonance and thermal conduction), change of direction, focusing, impedance changes, scattering (by turbulent eddies), and Doppler shifts. Some of these effects are more significant than others, and in some cases the current technology is not adequate to correct for them.

The most important effect is certainly atmospheric absorption. It is a strong function of temperature and humidity (see fig. 6, from ref. 5) and can change sound levels substantially. Indeed, it is not uncommon for absorption at high frequencies to reduce sound levels below the test site background sound level, making it impossible to conduct a flight test until the weather conditions improve. Currently there are two standard methods for predicting absorption, the Society of Automotive Engineers (SAE, ref. 5) and the American National Standards Institute (ANSI, ref. 6) standards. Both methods calculate absorption as a continuous function of frequency. Absorption is such a strong function of frequency that it is difficult to generate accurate values for use in a 1/3-octave band. As an approximation, for aircraft noise spectra the SAE method specifies the use of absorption at 1/3-octave band center frequencies for bands of 4000 Hz and below and at 1/3-octave band lower

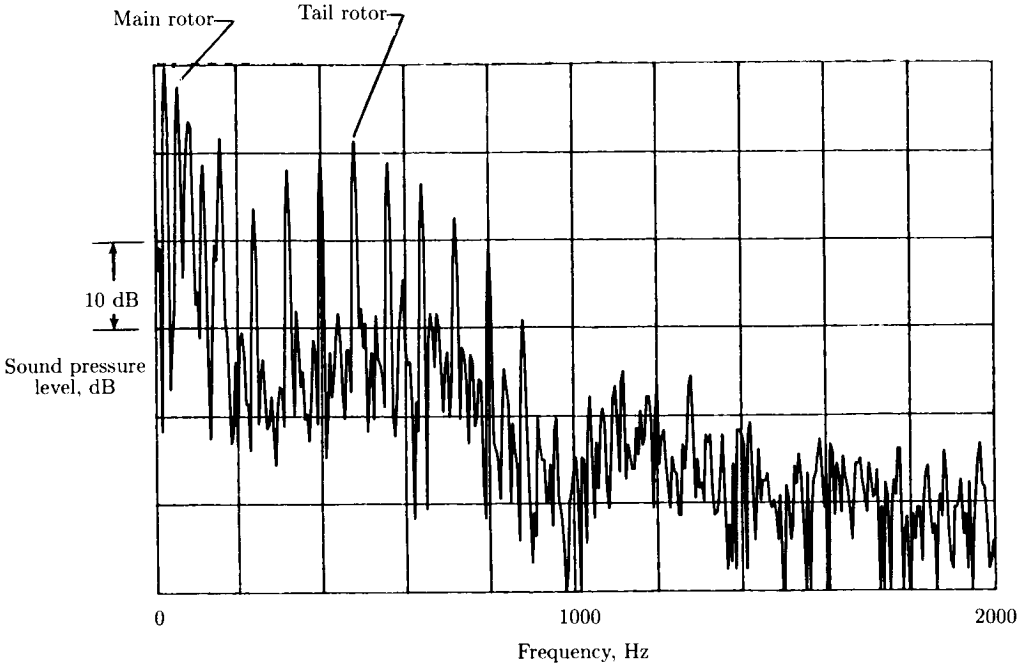

Figure 3. Spectrum of recorded noise generated by helicopter in forward flight.

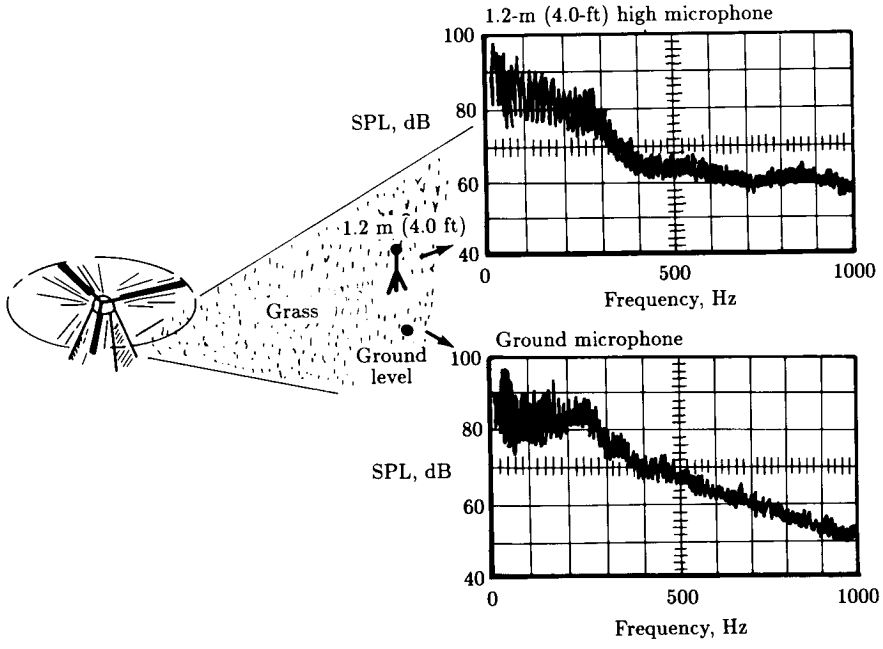

Figure 4. Effect of microphone height on spectrum of sound from helicopter rotor.

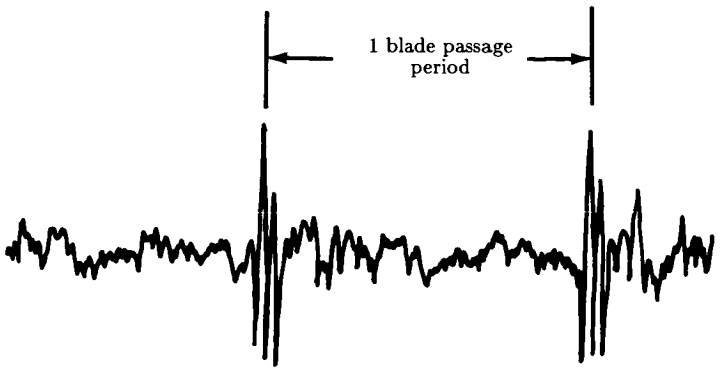

Figure 5. Example of impulsive helicopter rotor sound.

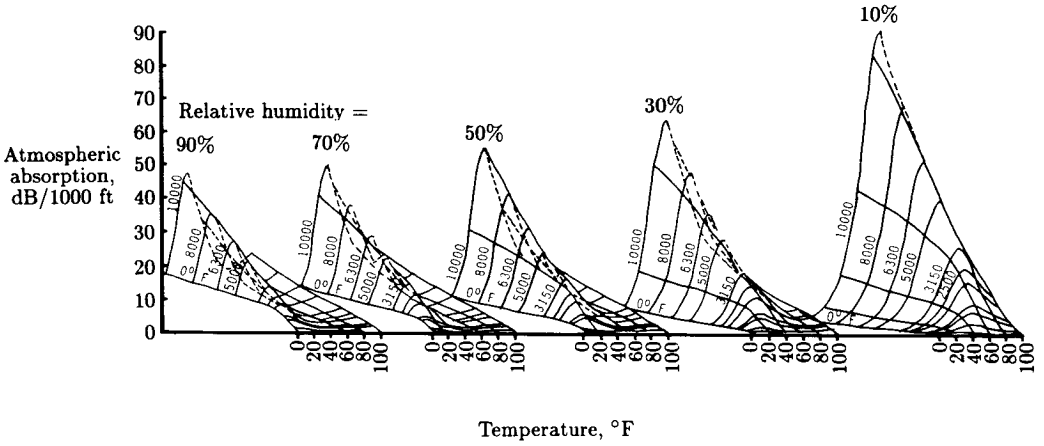

Figure 6. Atmospheric absorption coefficients for 1/3-octave bands of noise as function of temperature and humidity. (From ref. 5. Reprinted with permission, copyright 1975, SAE, Inc.)

edge frequencies for bands above 4000 Hz. The current ANSI procedure does not specify a method to use with 1/3-octave spectra. For flight testing, it is important to acquire an accurate profile of the temperature and relative humidity between the ground and the aircraft, since the absorption can vary widely along the path.

For the presence of wind, accurate absorption calculations should be done in a frame of reference moving with the wind. The path length is then distorted and the frequencies are Doppler shifted from what they would be in a calm atmosphere. These effects combine to increase the levels for sound propagating downwind and decrease them for sound propagating upwind. In addition, wind and temperature gradients cause sound rays to curve and, especially at shallow angles to the ground, there can be focusing effects. As there are no standards for predicting these effects,

it is best simply to avoid testing in the presence of strong winds or temperature gradients.

Atmospheric pressure affects source noise. Sound pressure is directly proportional to atmospheric pressure for most noise sources important to aeroacoustics, so aircraft altitude may be an important consideration. In addition, as sound travels along a ray tube through moderate gradients of acoustic impedance it conserves power (except for absorption), but the sound pressure may vary. This variation results in a correction to the acoustic pressure, which is proportional to the square root of acoustic impedance and which typically partially cancels the ambient pressure effect on source level. Impedance gradients strong enough to cause significant reflections are unlikely in the atmosphere.

Doppler frequency shift in the case of a uniform stationary atmosphere is a well-known effect usually accounted for by the equation

$$f_o = \frac{f_s}{1 - M \cos \theta}$$

where f_o is observed frequency, f_s is source frequency, M is Mach number, and θ is the angle between the flight path and the ray direction. The frequency shift does change in the case of a windy atmosphere; it can be calculated (ref. 7) and basically depends on the aircraft speed relative to the air and the sound ray angle. The finite integration time of the measurement system may cause Doppler-shifted tones to appear to be spread out in frequency.

The presence of turbulence in the atmosphere causes scattering, but there are no good quantitative predictions of this effect available yet. For noise sources having narrow beams of sound, the peak is reduced and the beam is broadened, but aircraft-noise sources tend to be more nearly omnidirectional and are not likely to exhibit this effect. Turbulence may have a more significant effect on ground-reflection patterns near the ground.

It is common practice to restrict flight testing to those weather conditions within which atmospheric and propagation effects are either insignificant or calculable.

Ground Effects

Sound propagation near the ground is somewhat different from propagation through the atmosphere. Reflections from the ground affect the sound received by a microphone; turbulence may also play a role. Wind and temperature gradients may become steep enough near the ground to create "shadow zones" for shallow angle propagation.

Ground-reflection problems occur when a ray reflected off the ground combines with a direct ray at the microphone. The two rays may reinforce or cancel each other (depending on their relative phase), resulting in a spectrum modified by "ground dips" of as much as 15 dB. This effect can be ignored if the microphone installation and flight path of the normalized conditions are close enough to those of the measured conditions, but it is important if static data or predictions are to be extrapolated to flight. Propeller airplanes or other types with dominant low-frequency tones can produce noise which is extremely sensitive to the exact location in frequency of the ground dips, and even slight differences in flight path may need to be corrected.

Though there are no universally accepted standard methods for calculating ground-reflection effects, the work of Chessell (ref. 8) and others, especially as summarized in reference 9, is widely used. The situation is most difficult when shallow angles are involved, such as in static engine testing. When more repeatable results are needed, the microphone must be placed very near the ground on a hard surface. This method gives a microphone signal 6 dB above free field, at least up to 10 kHz; it is frequently used for static testing and occasionally for flight testing. Elevated microphones over natural terrain are subject to significant variations because of ground impedance variations, turbulent scattering of phase relations, and changes in ray arrival angle due to ray curvature; all these sources of variation are extremely difficult to predict. Occasionally, microphones are placed very high (10.0 m (32.8 ft) is common); they then have ground dips so closely spaced that the 1/3-octave band spectrum appears smooth, at least if there are no dominant low-frequency tones. For flight testing, note that ground dips can be spread out over frequency by the measurement system integration time in the same manner as Doppler-shifted tones.

When the wind or temperature gradients are such that the ray from the source to the microphone curves up, it is possible that the microphone will be in a shadow zone into which no direct ray penetrates. This is most likely in static testing when the ground surface is hot from solar heating and the ray is propagating upwind. This shadow zone problem is difficult to treat theoretically, and it is usually handled by using empirically derived wind and temperature limits or by using extra microphones to detect shadowing effects (because they show up most strongly at high frequencies).

Turbulence effects are more likely to be visible when sound is propagating near the ground. When ground reflections are involved, different turbulence in the two paths causes a randomization of phase and reduces the peaks and dips. This shows up first at high frequencies, where wavelengths are short, and is quite visible in narrow-band data. Turbulence also smooths out a shadow zone boundary, and scattering of eddies is responsible for what little sound does penetrate deep into shadow zones. Quantitative predictions of these effects are not yet available.

It has been common to lump the foregoing ground effects together as "lateral attenuation" or "extra ground attenuation (EGA)," using an empirically derived extra attenuation for shallow angle propagation. Although it is widely agreed that EGA is mostly ground-reflection effect, with some effects due to inaccurate atmospheric absorption used when the curves and source nonaxisymmetry are derived, the standard used for aircraft-noise prediction is that provided in reference 10.

Prediction of Noise for Airplanes Powered by Turbofan Engines

Noise Prediction Capability

In order to receive approval for production and operation in a particular country, essentially all aircraft must now satisfy that government's noise standards. In the United States, these standards are contained in FAR Part 36 (ref. 1), while most other countries have adopted the standards of ICAO Annex 16 (ref. 2). For turbojet and transport airplanes, noise limits are defined for approach, sideline, and takeoff locations, and are dependent on maximum certificated takeoff gross weight (mass). For the takeoff location, the noise limits are also dependent on the number of engines

mounted on the airplane. The unit of measurement is the effective perceived noise level (EPNL) in decibels. This unit takes into account the duration of the noise event and penalizes any discrete frequencies or tones which have been found to be more annoying than broadband noise of the same intensity.

The elements of a successful aircraft-noise prediction include a reliable definition of the aircraft performance, a confident prediction of the noise characteristics of the power plant (as a function of power setting, altitude, and flight speed), and, in some flight conditions, the noise of the airframe. When there are substantial measured noise data to support a new airplane-engine configuration, they can be projected to the new flight conditions through fairly clearly defined procedures. For example, if the new airplane incorporates power plants which are not very different from versions already in service, flight-test data can be transposed to the new conditions. Or, where the measured information is obtained from static engine tests during the development program prior to airplane flight, there are methods for transposing these data to the flight conditions (ref. 11). The least predictable mode of operation embraces the totally new airplane-engine configuration and, under such circumstances, it is necessary to rely on accumulated past experience in the form of component-based prediction procedures. These procedures have to embrace not only noise but also aircraft performance.

Figure 7 outlines the minimum elements necessary to provide a credible estimate of the noise of a given airframe–power-plant combination. The main features are expanded in the following sections.

Power-Plant Design Details and Performance Characteristics

At the very minimum, there should be either a design scheme for the power plant in question and a knowledge of how the individual noise-producing component areas perform or a credible extrapolation/interpolation of both noise and performance data from a similar power plant. If the latter exists then the detailed component noise prediction procedures described below may become unnecessary.

Component Noise Prediction Procedures

Component noise prediction procedures are required which allow all the significant noise sources to be related to leading engine performance parameters and to be integrated to reflect the noise of the total system, including any noise reductions resulting from specific noise control actions. The depth of detail and breadth of coverage of the component procedures necessary are related directly to the type of power-plant–propulsion system and the aims of the prediction exercise. For example, prediction of certification noise levels demands a knowledge of all the sources that lie within 10 dB of the peak level throughout the total noise-time history (see fig. 8), whereas a prediction of levels at large distances is controlled by low-frequency sources and thus it may be possible to limit the breadth of the coverage.

Normally, it is the propulsion system noise that controls the overall aircraft noise, and there are three fundamental types of "jet" propulsion system. (See fig. 9.) These types are the single shaft, single-flow-duct "pure" jet, or turbojet engine; the two-shaft, double-flow-duct low-bypass-ratio engine; and the two- or three-shaft, double-flow-duct turbofan engine. The total noise is illustrated in figure 8.

C-5

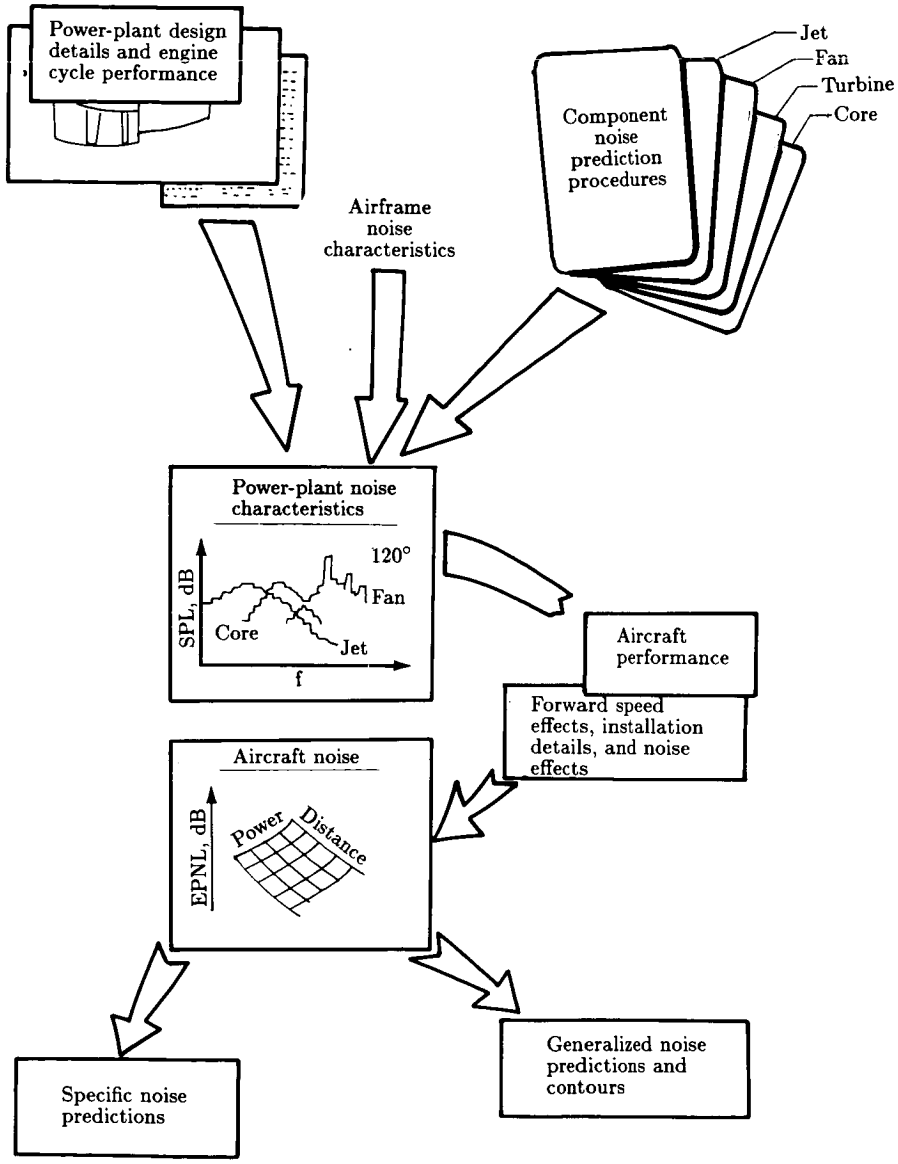

Figure 7. Elements necessary for noise prediction.

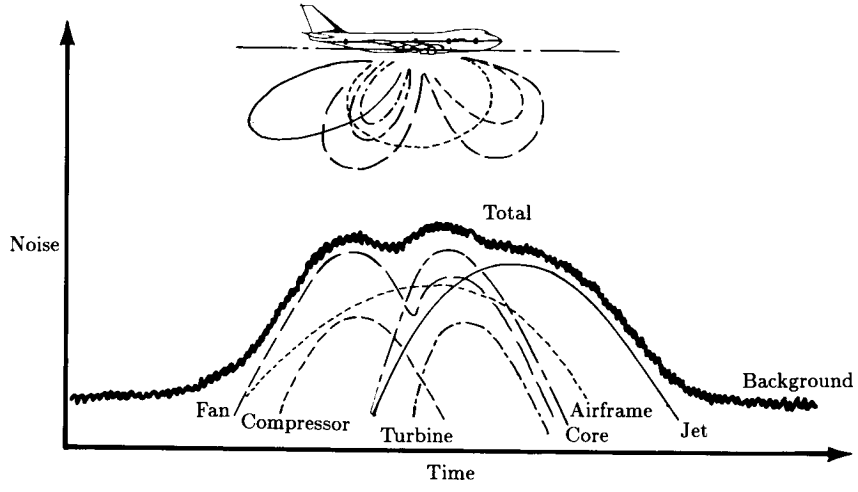

Figure 8. Contribution of major components to total noise.

Turbojet
Single shaft

Applications

1950's designs:
Comet, Caravelle,
Early B-707 and DC-8,
Business jets (Concorde uses pure jet with afterburning)

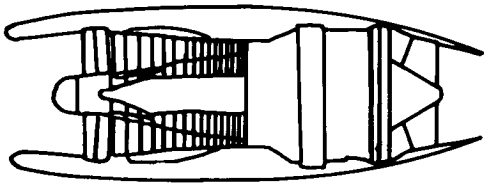

Bypass
2 shafts

1960's designs:
B-707, DC-8, VC-10,
B-727, B-737-100/200,
DC-9, BAC 111,
Trident, F-28,
Business jets

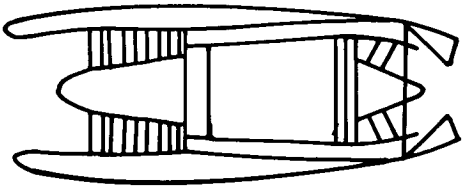

Turbofan
2 or 3 shafts

1960's designs (1-, 2-stage fan):
B-707, DC-8, Military,
Early B-747

1970's and 1980's designs (1-stage fan):
B-737-300, B-747, B-757, B-767,
L-1011, DC-10, A300,
MD-80, BAe 146,
A320, F-100, Business jets

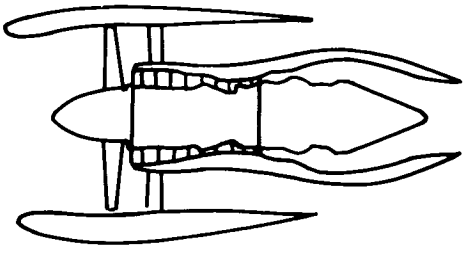

Figure 9. Three types of jet propulsion system.

Sources of Noise

Noise sources vary according to the engine cycle and are located both internally and externally. They may be summarized as follows:

1. In all cases, the exhaust-jet mixing process with the atmosphere produces broadband noise. Additionally, where the exhaust flow is supersonic (in zero- or low-bypass-ratio engines), there are other noise sources associated with the expansion-shock structure.
2. In all cases, compressor-generated tonal and broadband noise radiates through the engine air intake and, in all but the pure jet, may propagate down the bypass duct to radiate with the compressor exhaust stream.
3. In all cases, tonal noise from the turbine and broadband noise from this component and the "core" combustor propagate from the final nozzle in the hot core flow.
4. In a turbofan, tonal and broadband fan noise radiates both forward and rearward from the engine.
5. Other minor noise sources, peculiar to the engine design, may be present (e.g., bleed valves, flow mixers, and support struts).

Available Component Prediction Models

The following published component noise prediction procedures are available:

1. For single-stream exhaust flow conditions, SAE ARP 876C (ref. 12) provides the most widely used method of jet noise prediction. Based on normally available jet flow parameters, it provides both mixing and shock-associated spectral levels over a wide range of pressures, velocities, temperatures, and radiation angles.
2. For dual-stream flows there is no widely accepted method, but SAE AIR 1905 (ref. 13) describes three methods that could be used, one being a simple extension of the single-stream method of SAE ARP 876C.
3. For multistage compressor noise, the sensitivity of commercial organizations to compressor design details and noise data has meant that there is no method of the same acceptance level as that in procedure 1 for jet noise. However, the methods of House and Smith (ref. 14) and of Heidmann (ref. 15) are well-known and demand only the use of compressor performance parameters that are usually available.
4. For fan noise, it almost goes without saying that commercial sensitivity has the greatest effect on the availability of published data or prediction methodology. The method of Heidmann is the only freely available procedure.
5. For turbine noise, the same problem of commercial sensitivity exists, but the method of Matta, Sandusky, and Doyle (ref. 16) is available.
6. For combustor noise, the method of SAE ARP 876C (ref. 12) is the most widely accepted procedure.
7. Since most engines now incorporate noise-absorbent linings in the major air and flow ducts, a method is needed for computing duct attenuation as it affects fan, core compressor, turbine, and combustor noise. The method of Kershaw and House (ref. 17) is available.

Airframe Noise Characteristics

The above procedures allow predictions to be made of the component spectral levels in the far field at any given angle to the power plant. Unless it is a requirement to maintain spectral information in fine detail throughout the noise-time history of an aircraft flyover, it is normal to sum the noise energy to produce a single numerical expression of the noise of a single flight event at a given power setting, either in terms of peak level (e.g., peak PNL or peak A-weighted sound level) or time-integrated energy (EPNL or SEL). However, before this process can be conducted, it is important to consider the inclusion of one further source, which is most relevant at approach conditions.

The airframe noise varies with flight speed, mass of the airplane, and configuration. The most important feature is deployment of the wing flaps and landing gear. A procedure which provides the spectral information necessary to allow this source to be integrated into the total flyover level (in the same way as the engine components) is provided by Fink (ref. 18).

Total Airplane Noise

Having compiled a set of component noise predictions for the power plant and the airframe, we can construct a "carpet" of noise as a function of engine power and distance for the relevant flight speeds. For example, takeoff flight speeds are usually at Mach numbers of 0.25 to 0.30 and approach flight speeds are at Mach numbers of 0.20 to 0.25. Hence, for all the component sources, it is necessary to make appropriate corrections for changes in flight speed between the takeoff and approach conditions.

Even with these corrections, at this stage any noise-power-distance carpet that is constructed will apply only to the isolated power plant in the "overflight" condition, and it is necessary to make further adjustments for several other factors. For example, the effects of having more than one engine on the aircraft need to be accounted for. Equally, it may be that there are some special amplifying installation effects which can be computed from previous observations, or there may be some shielding of the noise because of the installation. Examples of these are the amplifying interaction between the jet and the wing flaps on the one hand and the shielding effect of a center engine installation of a trijet on the other hand. For a trijet, noise from the inlet is not heard by an observer beneath the airplane, but it becomes progressively audible as the observer moves to the side of the flight track.

There are no readily available methods for computing these effects, but generally noise from engines mounted under the wing is amplified whereas that from engines mounted at the rear of the fuselage is shielded, both beneath and to the side of the aircraft flight track. All these effects are normally no greater than 3 dB, except when the aircraft subtends a very small angle of elevation to the receiver.

Similarly, the effects of the ground plane (in the form of over-ground and airborne "lateral" attenuation) together with the effects of the measurement position (ground reflection) also have to be taken into account before the noise from the airplane can be presented (either instantaneously or integrated into a single-number index) from the observer's standpoint. These effects may be accounted for either in the manner presented by ESDU (ref. 9) or, more simply, in the manner of SAE AIR 1751 (ref. 10).

Prediction Methods Generally Available

The methods already referenced represent the latest available. In some cases there are no generally accepted procedures. There is only one comprehensive aircraft noise prediction method freely available, the Aircraft Noise Prediction Program (ANOPP) (ref. 19). This method utilizes many of the procedures referenced herein.

Accuracy

The component noise prediction procedures have variable accuracies, those associated with turbomachinery being the least reliable. Those procedures associated with zero- and low-bypass-ratio powered aircraft were studied in the 1970's and found to be sufficiently accurate to be utilized in a major study of supersonic transport noise by ICAO (ref. 20). No other comprehensive studies have been undertaken other than those conducted for NASA in validating ANOPP.

Prediction of Noise for Airplanes Powered by Propellers or Propfans

Components of Interest

Propeller and propfan noise is dominated by low-frequency tones. These tones consist of a fundamental, the frequency of which is given by the propeller or propfan rotation rate in revolutions per second times the number of blades, and integer multiples of the fundamental frequency (i.e., harmonics). For propellers, the fundamental frequency is typically 60 to 150 Hz. Propfans have fundamental frequencies from 125 to 300 Hz. Although it is possible to identify individual harmonics by use of narrow-band frequency analyses, the 1/3-octave band analyses performed for noise certification purposes allow the identification of the fundamental through the third harmonic. Higher harmonics are more closely spaced in frequency than the bandwidth of the 1/3-octave bands so that several harmonics fall within a band. The higher frequencies may thus appear as broadband noise, but really they are not.

Another component of propeller and propfan noise is broadband noise. This component is currently considered insignificant for normal operation in flight. During static and very-low-speed operating conditions, turbulence ingestion noise occurs. This noise has some characteristics of tones and broadband noise. However, it becomes insignificant during normal flight conditions. Finally, a propeller or propfan powered airplane may have contributions from other sources of noise such as that from the engines and the airframe. In this section only the dominant propeller and propfan tones are described, as the other components are insignificant during normal flight or are covered in another section.

Component Noise Prediction Models

Types of Noise Prediction Models

Propeller and propfan noise prediction models come in basically two types: empirical and theoretical. Empirical models are based on regression analyses of

test data. Theoretical models are based on mathematical modeling of the physical processes of propeller and propfan noise generation.

Empirical models for predicting propeller noise have been reasonably successful and work well for fairly conventional designs that operate over a reasonable range of tip speeds and power loading (power divided by propeller disk area). Empirical models have generally not been successful for propfan noise prediction.

The most commonly used empirical propeller noise prediction method is that of reference 21. This method allows calculation of propeller noise based on only five parameters: tip speed, diameter, number of blades, flight speed, and distance. Because it is based on a collection of measured data, mostly from turboprops, the method intrinsically contains most other sources of noise, such as installation effects, engine noise, and airframe noise.

Many theoretical models exist. These relate the radiated noise to the forces imparted to the air by the physical volume of the blades and the pressure distribution on the blade surfaces. Theoretical propeller noise prediction models consist of two parts: an acoustic radiation model, which "converts" the forces on the blades to noise, and an aerodynamic model, which allows the calculation of the forces on the blades. Both are needed, along with detailed definition of the propeller geometry, to perform noise predictions.

Relationship of Static to Flight Effects

As previously mentioned, under static conditions a significant amount of noise due to inflow turbulence ingestion occurs. This is a source of noise which disappears in flight. Figure 10, from reference 22, illustrates the influence of forward flight on propeller noise. Under static conditions, the noise spectrum is dominated by intense higher harmonics. In flight, the levels of these upper harmonics are greatly reduced. Figure 11 shows the effect as measured on the airplane and on the ground during static operation and during a flyover. The middle 1/3-octave bands show high levels during static operation while the flight data show much lower levels. The measured differences are greater than 10 dB.

It is thus apparent that static propeller noise data projected to flight generally result in significant overpredictions. Static propeller noise data are thus of little value. Even *trends* in noise under static conditions are suspect.

Installation Effects

Installation effects result in additional noise sources which generally raise propeller and propfan noise levels. These effects are due to distortions in the inflow which are caused by angle of attack, engine nacelle blockage, wing upwash, pylon wakes, etc., and which are unavoidable in the installation of a propeller or propfan on an airplane. The additional noise is caused by unsteady-loading noise, which results from the periodic loading variation on the blades as they pass through the flow distortion. Unsteady-loading noise is a source usually included in the theoretical noise prediction methods. For such calculations a means for calculating the flow field is required. Empirical noise prediction methods include some form of installation effects by default, as they are included in the data.

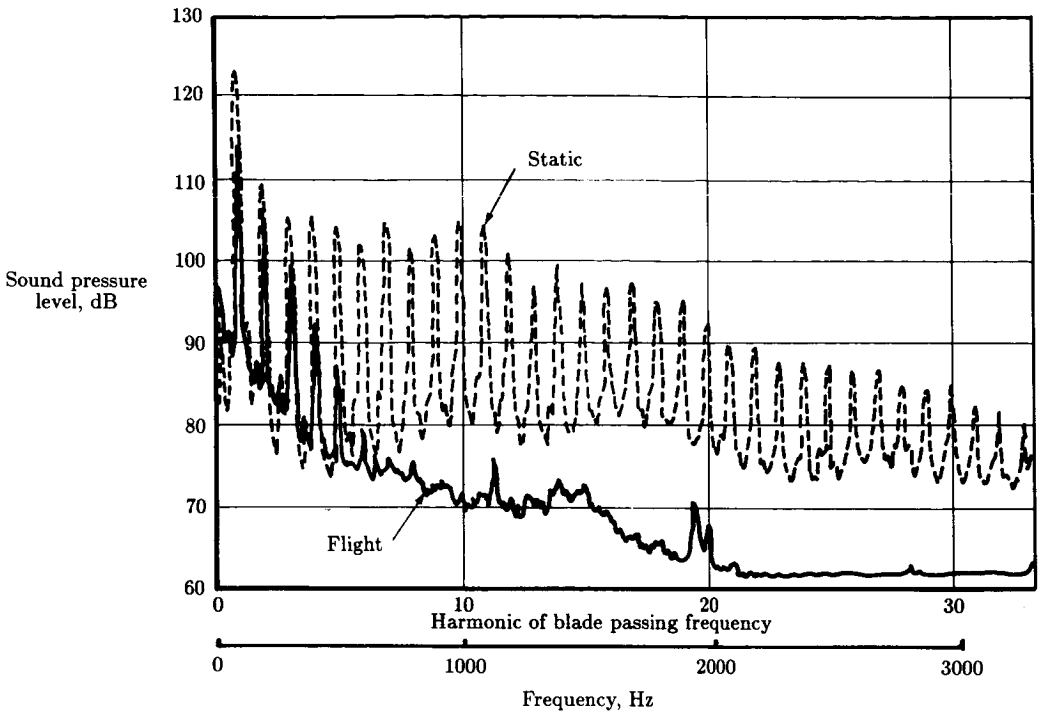

Figure 10. Comparison of static and flight propeller noise narrow-band spectra. (From ref. 22.)

Accuracy of Prediction

It is difficult to make a precise assessment of propeller and propfan noise prediction accuracy because of the types of methods available and the degree of detail which can be applied. In general, the accuracy of empirical noise prediction methods is about ±3 dB, providing that the noise of the configuration being estimated does not fall too far outside the data base inherent in the prediction method. It is not surprising to find errors of ±10 dB for unusual configurations.

The accuracy of theoretical noise prediction methods includes the accuracy of the actual noise radiation model, how well the blade geometry can be defined (propfan blades can have very complicated shapes), and how well the blade loading in both the chordwise and the spanwise direction can be defined. It is expected that a carefully calculated noise prediction in terms of effective perceived noise level or A-weighted overall noise would have an accuracy of about ±1.5 dB. Other variables, such as ground reflection effects, atmospheric absorption, and tilt of the propeller axis relative to the flight path, can introduce additional errors.

Future Developments

It is generally agreed that existing propeller and propfan noise radiation models are complete and detailed enough to provide good predictions. The prediction

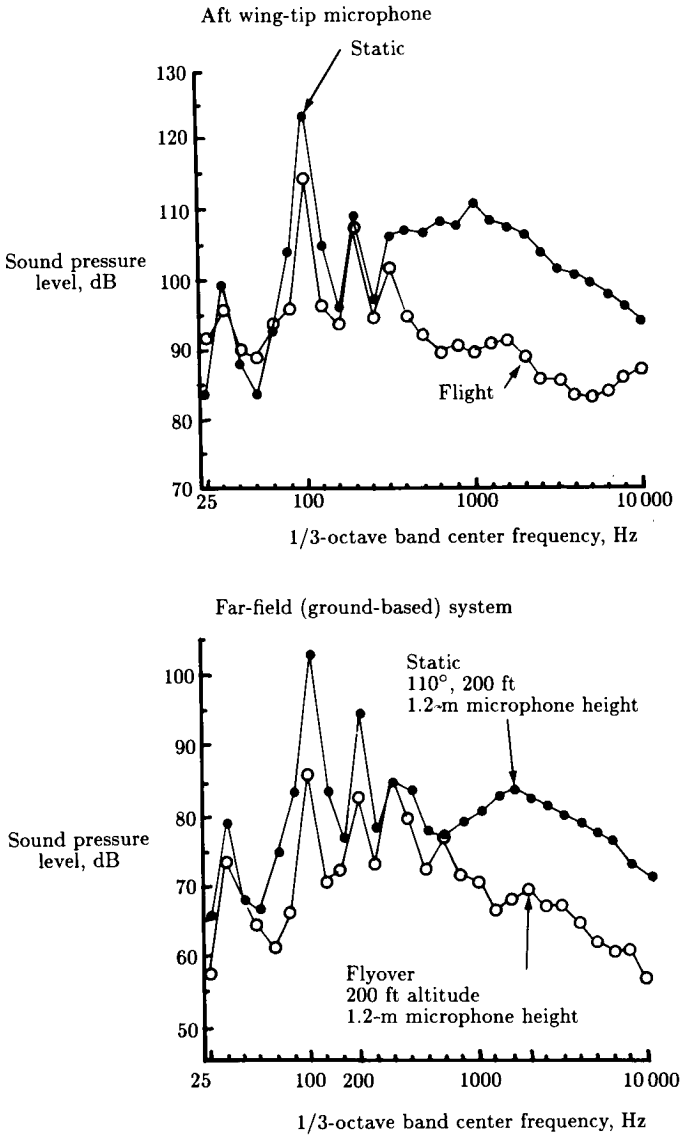

Figure 11. Comparison of static and flight propeller noise 1/3-octave band spectra. (From ref. 22.)

limitations appear to be in the aerodynamic codes required to define the inflow to the propeller and to define the steady and, especially, the unsteady blade loading. It is expected that improvements in propeller and propfan noise predictions will come from improved aerodynamic codes.

Other Prediction Methods

It is feasible to scale model propeller and propfan tone noise data to full scale. The scale limitation is not an acoustic one but rather one imposed by aerodynamics

(i.e., Reynolds number effects) and the ability to manufacture an accurate model preserving airfoil contours. From an acoustic standpoint a model propeller has the same harmonic spectrum as a full-scale propeller at the same blade angle, tip rotational Mach number, and flight Mach number. The tone frequencies are inversely proportional to the diameter ratio. Model broadband noise does not scale geometrically.

Experience has indicated that models in the 0.61-m (2-ft) diameter range (approximately 1/5 scale) or larger scale very well. It should be apparent from the foregoing discussion that the accuracy of scaling model data depends on how well the model simulates the actual installation. For accurate results, one should consider including a simulation of the flow field of the propeller. It is strongly cautioned that there is no means for acquiring propeller noise under static conditions that can be used for flight simulation.

References

1. Standards Governing the Noise Certification of Aircraft. *Fed. Regist.*, vol. 53, no. 88, May 6, 1988, pp. 16360–16372.
2. *Environmental Protection—Annex 16 to the Convention on International Civil Aviation. Volume I—Aircraft Noise, First ed.* International Civil Aviation Organization, Nov. 26, 1981. (As amended Nov. 21, 1985.)
3. *Noise Certification Handbook.* AC No. 36-4B, Federal Aviation Adm., Mar. 23, 1988.
4. Borfitz, Michael H.; and Glover, Billy M.: Community Noise Testing—New Techniques and Equipment. *Flight Testing Today: Innovative Management and Technology—14th Annual Symposium Proceedings,* Soc. of Flight Test Engineers, 1983, pp. 4.3-1–4.3-8.
5. *Standard Values of Atmospheric Absorption as a Function of Temperature and Humidity.* ARP 866A, Soc. of Automotive Engineers, Mar. 15, 1975.
6. *American National Standard Method for the Calculation of the Absorption of Sound by the Atmosphere.* ANSI S1.26-1978 (ASA 23-1978), American National Standards Inst., Inc., June 23, 1978.
7. Roy, Dipankar: Doppler Frequency Shift in a Refractive Atmosphere. *J. Aircr.*, vol. 24, no. 9, Sept. 1987, pp. 577–586.
8. Chessell, C. I.: Propagation of Noise Along a Finite Impedance Boundary. *J. Acoust. Soc. America,* vol. 62 , no. 4, Oct. 1977, pp. 825–834.
9. *The Correction of Measured Noise Spectra for the Effects of Ground Reflection.* ESDU Item Number 80038 (With Amendments A and B), Engineering Sciences Data Unit (London, England), Nov. 1984.
10. *Prediction Method for Lateral Attenuation of Airplane Noise During Takeoff and Landing.* AIR 1751, Soc. of Automotive Engineers, Inc., Mar. 30, 1981.
11. *Environmental Technical Manual on the Use of Procedures in the Noise Certification of Aircraft, First ed.* Doc. 9501-AN/929, International Civil Aviation Organization, 1988.
12. *Gas Turbine Jet Exhaust Noise Prediction.* ARP 876C, Soc. of Automotive Engineers, Inc., Sept. 1982. (Supersedes ARP 876B.)
13. *Gas Turbine Coaxial Exhaust Flow Noise Prediction.* AIR 1905, Soc. of Automotive Engineers, Inc., Dec. 1985.
14. House, M. E.; and Smith, M. J. T.: Internally Generated Noise From Gas Turbine Engines—Measurement and Prediction. ASME Paper 66-GT/N-43, Mar. 1966.
15. Heidmann, M. F.: *Interim Prediction Method for Fan and Compressor Source Noise.* NASA TM X-71763, 1975.
16. Matta, R. K.; Sandusky, G. T.; and Doyle, V. L.: *GE Core Engine Noise Investigation, Low Emission Engines.* FAA-RD-77-4, Feb. 1977. (Available from DTIC as AD A048 590.)

17. Kershaw, R. J.; and House, M. E.: Sound-Absorbent Duct Design. *Noise and Vibration,* R. G. White and J. G. Walker, eds., John Wiley & Sons, c.1982, pp. 477–495.
18. Fink, Martin R.: *Airframe Noise Prediction Method.* FAA-RD-77-29, Mar. 1977. (Available from DTIC as AD A039 664.)
19. Zorumski, William E.: *Aircraft Noise Prediction Program Theoretical Manual.* NASA TM-83199, Parts 1 and 2, 1982.
20. *Committee on Aircraft Noise, Seventh Meeting.* Doc. 9419, CAN/7, International Civil Aviation Organization, May 1983.
21. *Prediction Procedure for Near-Field and Far-Field Propeller Noise.* AIR 1407, Soc. of Automotive Engineers, Inc., May 1977.
22. Magliozzi, B.: *The Influence of Forward Flight on Propeller Noise.* NASA CR-145105, 1977.

18 Quiet Aircraft Design and Operational Characteristics

Lead author

Charles G. Hodge
The Boeing Co.
Seattle, Washington

Scope

In contrast to the preceding chapters, which have dealt largely with the physics of the generation and suppression of specific noise sources, this chapter deals with the application of aircraft noise technology to the design and operation of aircraft. Areas of discussion include the setting of target airplane noise levels, major design considerations in achieving these levels, operational considerations and their effect on noise, and the sequencing and timing of the design and development process. Primary emphasis is placed on commercial transport aircraft of the type operated by major airlines. The final sections of the chapter include brief comments regarding the noise control engineering of other types of aircraft.

Airplane Noise Level Design Requirements and Objectives

The adoption of the target levels for the community, interior, and ramp noise of an airplane includes consideration of regulatory requirements, customer guarantees, risk assessment, and design margins.

Regulatory Requirements for Community Noise

Regulatory requirements for commercial aircraft include national regulations, international standards, and local airport requirements.

FAA Regulations

In the United States, the Federal Aviation Administration (FAA) requires transport aircraft to comply with the noise requirements of Federal Aviation Regulations

(FAR) Part 36 (ref. 1) as one condition for the issuance of a type certificate (for a model) or an airworthiness certificate (for an individual airplane). Maximum noise levels for individual flights are specified under standardized test conditions at three locations: (1) during takeoff, directly under the flight path at a distance of 6500 meters (approximately 4.0 statute miles) from brake release; (2) at the point of maximum noise during takeoff along a sideline 450 meters (approximately 0.28 mile) from and parallel to the (extended) runway centerline; and (3) during approach, directly under the flight path at a distance of 2000 meters (approximately 1.25 miles) from the runway threshold. These locations are illustrated in figure 1.

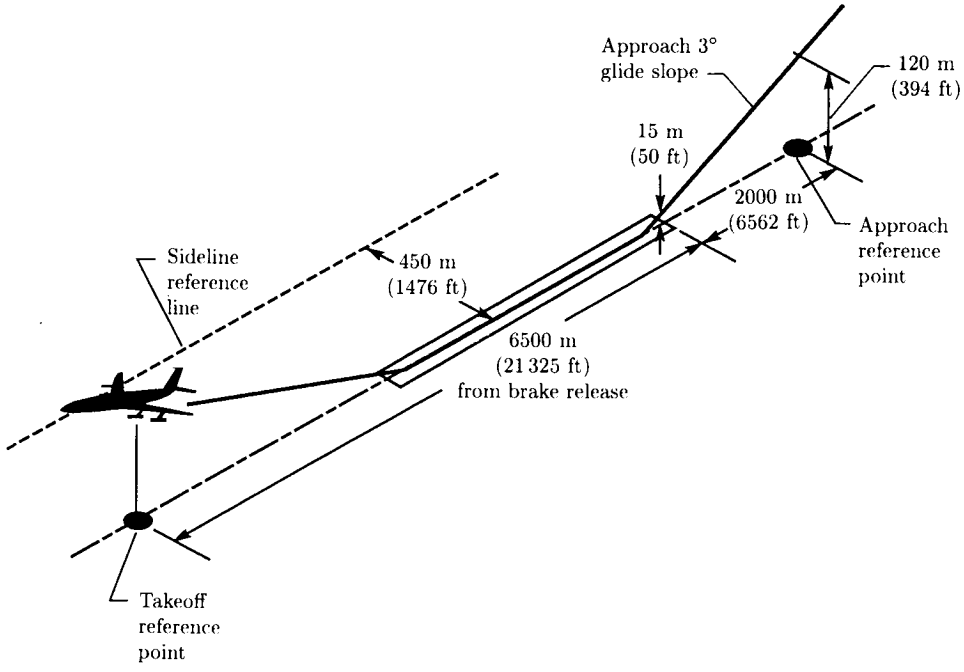

Figure 1. FAR Part 36 noise certification conditions.

The allowable noise levels are specified in terms of effective perceived noise level (EPNL) in decibels and depend on the maximum certificated takeoff gross weight of the airplane. These limits are illustrated in figure 2. The more stringent limits are known as the stage 3 requirements and apply to airplanes for which applications for type certifications were made on or after November 5, 1975 (which roughly corresponds to commercial transports certified after 1978). Between December 1, 1969, and November 5, 1975, the applicable requirements were the stage 2 limits, which were not as stringent as the current stage 3 rules. Airplanes for which application for type certificates were made prior to December 1, 1969, are defined as stage 1 airplanes and were not required to meet noise regulations. In issuing aircraft noise standards and regulations, the FAA must consider whether such requirements are "economically reasonable, technologically practicable, and appropriate for the particular type of aircraft" (ref. 1). Thus as noise reduction technology has developed, requirements have become more stringent.

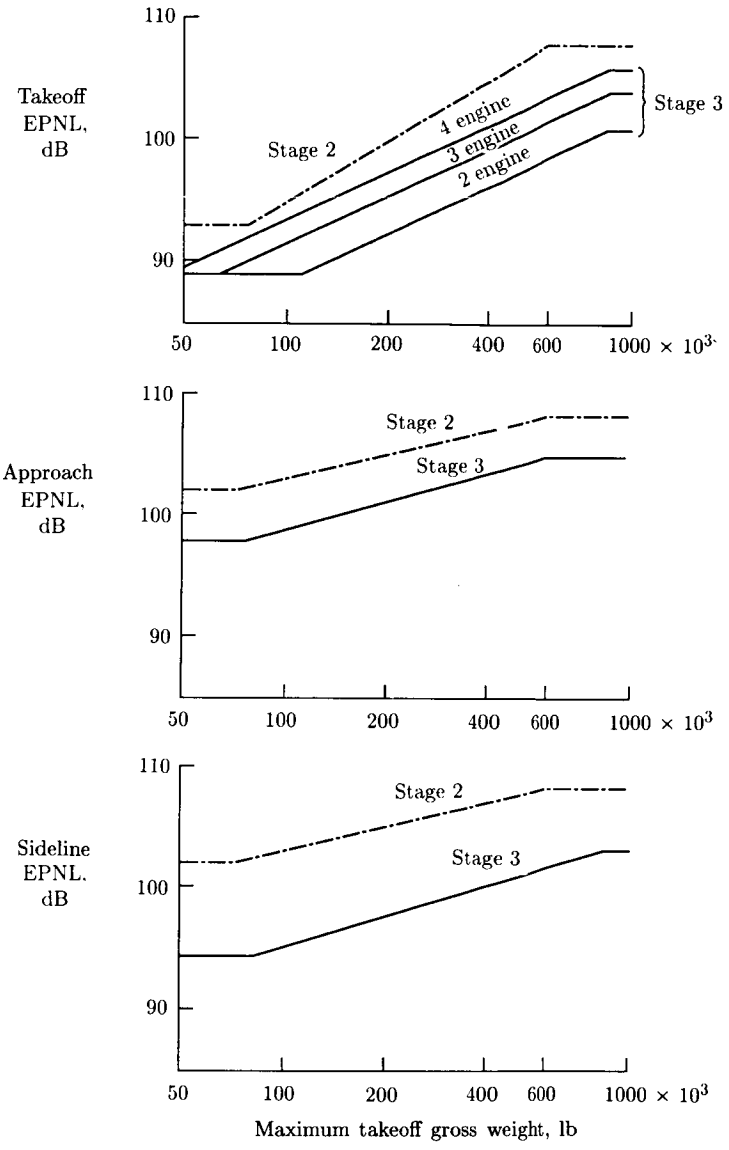

Figure 2. FAR Part 36 certification noise rules.

Unlike the approach and sideline requirements, the stage 3 takeoff limits depend on the number of engines, for the following reasons. Safety considerations require that an airplane have enough thrust to meet its critical takeoff performance requirement with one engine inoperative. Consequently, during normal takeoff with all engines operating, a two-engine airplane is 100 percent overpowered, a three-engine airplane 50 percent overpowered, and a four-engine airplane 33.3 percent overpowered. Therefore, with all engines operating, an airplane with fewer engines can take off from a shorter field length at a steeper climb angle and thus achieve a higher altitude

over the takeoff measurement point under the flight path. The noise regulations, which invoke a policy of equal stringency (i.e., demanding the same noise control technology irrespective of the number of engines on the aircraft), require the airplane with fewer engines to meet a lower noise requirement. In this manner, the regulations recognize the noise implications of the engine-out safety requirement and the need to be technologically practicable and appropriate for the particular type of aircraft.

An additional important feature of the FAR Part 36 noise requirement is the trade-off provision: an aircraft may exceed the nominal EPNL limit by a maximum of 2 dB at a single point and by a maximum of 3 dB collectively at two points provided that there are compensating margins at the other point(s). That is, the sum of the exceedances over the respective nominal requirements at the three points does not exceed zero. This "3-2 trade" provision is illustrated graphically in figure 3, in which the region inside the geometric figure corresponds to compliance with FAR Part 36.

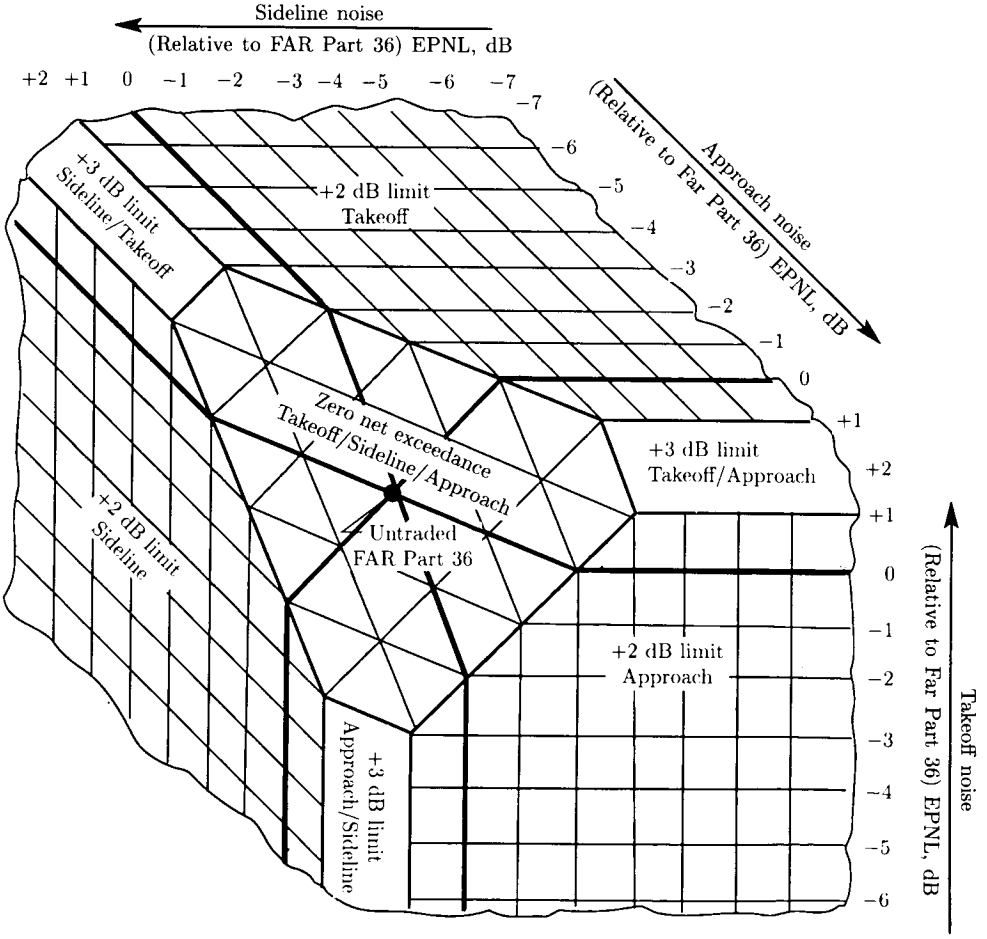

Figure 3. Three-dimensional illustration of possible combinations that ensure compliance with FAR Part 36 requirements.

In addition to requirements for new type designs, there are also noise limitations on both continuing production (FAR Part 36) and operation of previously certified aircraft (FAR Part 91, ref. 2). These rules are designed to phase out the operation of older, noisier airplanes in the United States. Figure 4 shows the effective dates of each of the three types of requirements.

ICAO Requirements

Similar to the FAA requirements, the International Civil Aviation Organization (ICAO), consisting of representatives of most governments throughout the world, makes recommendations to its member countries for noise requirements for aircraft to operate in these countries. The requirements are recommended for both domestically registered aircraft and for those aircraft from other countries. Most countries, including the European countries, Japan, and Australia, require compliance with the ICAO guidelines, known as Annex 16 (ref. 3), which have evolved to the point of being essentially equivalent to the FAA requirements. There has typically been a time lag between the adoption of the FAA stage 2 and stage 3 requirements and the corresponding ICAO Chapter 2 and Chapter 3 guidelines, as illustrated in figure 4.

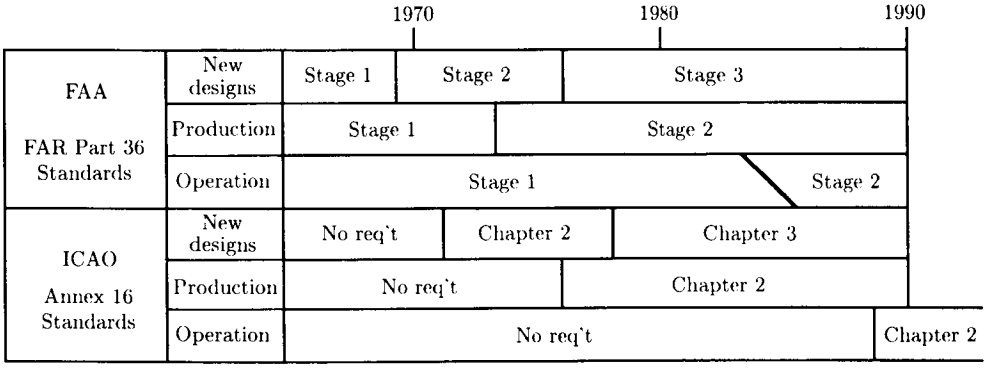

Figure 4. Noise rule progression.

Local Airport Regulations

In addition to the FAR Part 36 and ICAO Annex 16 requirements, commercial aircraft are often required to meet local noise restrictions at specific noise-sensitive airports. These restrictions may take the form of curfews, noise-dependent usage fees, noise level requirements based on various noise metrics, integrated fleet noise level restrictions on individual operators, etc. They include a multitude of noise units. The most prominent and restrictive of these local regulations are at Washington National Airport, John Wayne Airport (Orange County) and other California airports, and European airports. The widespread nature of these local regulations in the United States is illustrated in figure 5, from an FAA document (ref. 4). Each black dot represents an airport which has local noise regulations. These requirements significantly influence airplane sales competitions for individual customers and increase the complexity of design-goal development.

Figure 5. Extent of local actions to control airport noise. (From ref. 4.)

Compliance Demonstration

Initial compliance of an airplane model with an FAA (or ICAO) certification requirement is demonstrated by flight test and is described in detail in a previous chapter of this book. The history of a given airplane model, however, is typified by numerous design changes, some of which may affect community noise. Common examples of major changes are (1) changes in maximum takeoff or landing weight associated with airplane growth or (2) alternative engine offerings on the same airplane, in which the noise may differ from that with the parent engine. In this latter certification, what has become known as the "family plan" is often invoked. In a family plan certification, the effect of the engine change is based on comparative ground tests of the original and the new engine designs. First the noise increment δ between flight and ground tests of the parent aircraft (aircraft 1) is determined:

$$\delta = \mathrm{EPNL}_{\mathrm{flight},1} - \mathrm{EPNL}_{\mathrm{ground},1}$$

This noise increment is then superimposed on the ground test results for the new engine to determine the flight noise of this follow-on aircraft (aircraft 2):

$$\mathrm{EPNL}_{\mathrm{flight},2} = \mathrm{EPNL}_{\mathrm{ground},2} + \delta$$

Use of the family plan method can greatly reduce the cost and time of the certification program and has been shown to provide adequate technical accuracy. Smaller design changes, for example, modification of a small area of acoustic treatment of an engine duct, can sometimes be certificated by analysis alone, without additional testing.

Local airport compliance is typically monitored in service by the airport authorities themselves.

Airline Customer Guarantees

As part of the business arrangement in which an airline purchases a commercial airliner, the airframe manufacturer is typically required to guarantee that the airplane will meet certain maximum allowable community, interior, and ramp noise levels.

Community Noise

As a minimum, the manufacturer will be required to comply with the appropriate noise certification standards for the airplane in the countries in which the airline will operate it. For a domestic airline, this requirement would be the appropriate stage of FAR Part 36; for an international airline, the appropriate chapter of the ICAO guidelines is typical.

In addition to the certification requirements, an airline may request or demand compliance with the requirements at one or more specific local airports at which the airline expects to operate the airplane. Such guarantees are often very important in the competition among airplane (and engine) manufacturers for an airline order.

Interior Noise

Although there are currently no certification requirements on interior (passenger cabin or flight deck) noise, airlines still require that the manufacturer guarantee noise levels in the passenger cabin. As a minimum, the guarantee is specified at the passenger seats. Often, flight deck, galley, and/or lavatory noise levels are also specified. Typical guarantees are written for the cruise condition in terms of both overall sound pressure level (OASPL) and speech interference level (SIL). OASPL includes the entire audible spectrum and is typically dominated by low-frequency fuselage-boundary-layer noise; SIL includes the three octave bands centered on 500, 1000, and 2000 Hz and typically includes contributions from both the boundary layer and the cabin air-conditioning system.

Ramp Noise

In addition to airport community and interior noise guarantees, the manufacturer typically also guarantees that ramp noise—that is, the noise exposure to the airline maintenance crew when servicing the airplane or to passengers when boarding or deplaning via outdoor stairways—will not exceed certain limits. The most important sources of ramp noise are usually the auxiliary power unit (APU) and the air cycle machines (ACM's).

Contractual Arrangements

Standard noise guarantees that are offered to all customers are typically cited in the airplane specification document, which describes the airplane and the various

aspects of its performance. Exceptions to these standard guarantees may be included in jointly signed side letters. The airplane contract cites the specification and/or the appropriate side letters.

Guarantee levels and tolerances: Noise guarantees are often expressed as a nominal value, together with an allowable demonstration tolerance to cover measurement uncertainties during compliance demonstration. In some cases, however, the guarantee is written simply as a not-to-exceed value, which exceeds the nominal value by the demonstration tolerance. These concepts are illustrated in figure 6.

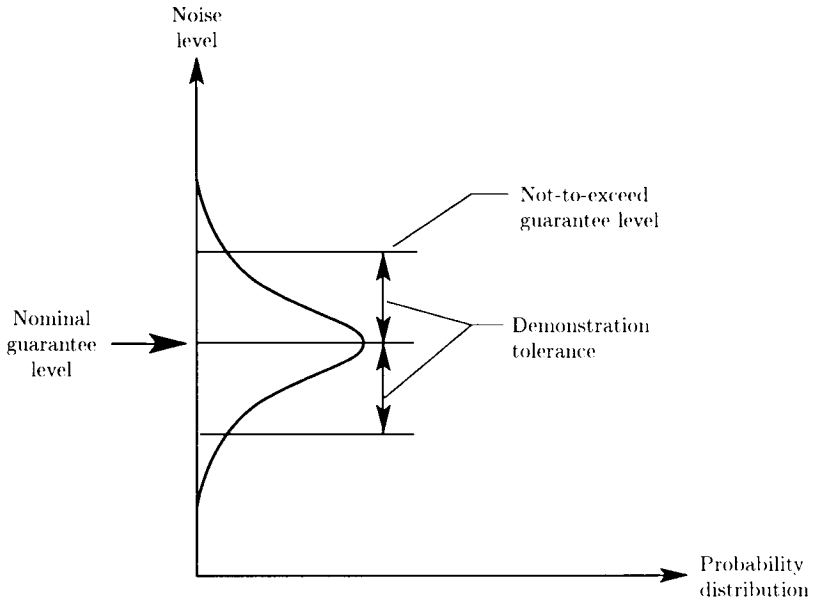

Figure 6. Airline customer guarantee nomenclature.

Compliance demonstration: As part of the contractual arrangement between the airplane manufacturer and airline customer, compliance with noise guarantees is normally demonstrated by tests performed by the manufacturer. When the guarantee is identical to a certification requirement, the certification test itself suffices. Compliance with local airport rules is demonstrated by different means—sometimes by testing at the airport itself, sometimes by analysis based on the certification test data. Interior noise guarantee compliance tests are typically performed on the customer's airplane—sometimes for the first airplane of a group of airplanes of a given design, sometimes on each airplane delivered.

Nominal Noise Estimates, Uncertainty Analysis, and Risk Assessment

During the design of an airplane, expected noise levels are estimated for community, interior, and ramp noise. These estimates are made for various configuration options during the preliminary design of the airplane; they are then refined as test

data are obtained, design details frozen, and estimating methods improved as a result of ongoing noise research. Closely related to these estimates is the uncertainty in the estimates themselves and the resulting confidence level of compliance with various requirements.

Nominal Noise Level Estimates

The nominal noise level estimates are the noise engineer's most accurate estimates of the airplane noise, for example, a FAR Part 36 approach EPNL of 97.3 dB or an OASPL in the last aisle seat in the first-class cabin of 85 dB. The engineer does not inject any deliberate conservatism or optimism into these estimates. These estimates are, therefore, those levels which the airplane has a 50-percent chance of achieving. For community noise, they are typically based on a 1/3-octave band synthesis of the expected contributions from each (suppressed) noise source at each directivity angle, as explained previously in this book.

Uncertainty Analysis

The process of noise level assessment also includes an uncertainty analysis—that is, a determination of the degree of uncertainty in the nominal estimates, or determination of the probability that the actual levels will deviate from the estimates by a particular amount when the compliance demonstrations are performed. The possible range of noise levels is typically assumed to be normally distributed about the nominal estimate, with the distribution characterized by its standard deviation, as illustrated by figure 7(a). The standard deviation itself is an engineer's best estimate, aided by a comparison of estimated and realized noise levels for similar circumstances in the past. The standard deviation representing the uncertainty in a noise estimate is comprised of two parts: the prediction uncertainty and the measurement uncertainty. Several definitions are helpful in understanding this concept:

True noise level: The true noise level is defined as that level that would be measured by a (hypothetical) perfect experiment or the average level that would be obtained from a large number of repeated measurements of the airplane noise level.

Measurement uncertainty: The measurement uncertainty is the uncertainty in the ability of an individual test (e.g., the compliance demonstration test) to represent the true value of the noise level, as illustrated in figure 7(b). Factors that contribute to the measurement uncertainty include test site variations, variations in atmospheric conditions (together with imperfect correction methods), instrumentation inaccuracies and imprecision, truncation (or round-off) errors, pilot or instrumentation operator variability, and variations (among airplanes of the same design) associated with manufacturing variability.

Prediction uncertainty: The prediction uncertainty is the uncertainty in the ability of the nominal estimate to represent the true noise level, as shown in figure 7(c). It includes any imperfections in analytical or empirical methods (based on other similar airplanes or engines) used to predict source noise levels, together with the measurement uncertainties in any "anchor point" measurements on which the predicted nominal estimate is based.

Overall uncertainty: The relevant uncertainty in the noise-estimating process is the uncertainty in the future measurement relative to the predicted value. Simplified

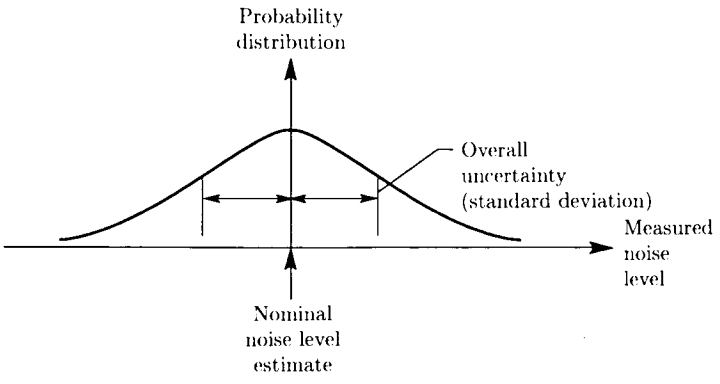

(a) Overall uncertainty.

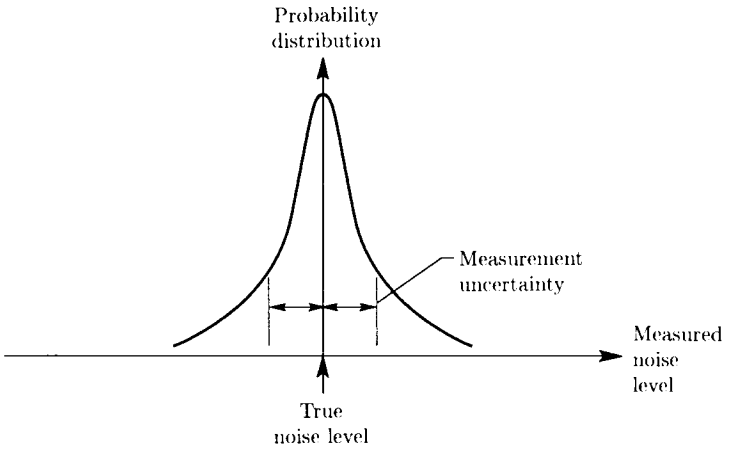

(b) Measurement uncertainty.

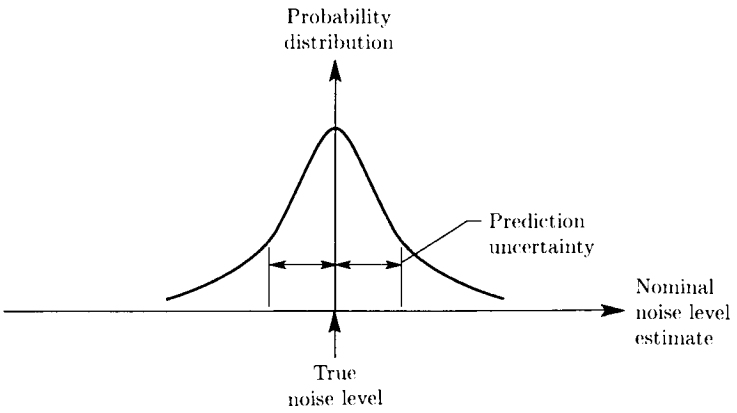

(c) Prediction uncertainty.

Figure 7. Uncertainty analysis.

statistical theory shows that this overall uncertainty, depicted in figure 7(a), is the root sum square of the measurement and prediction uncertainties. This total uncertainty in EPNL typically corresponds to a standard deviation of 1 to 4 dB at a specific flight condition, depending on the basis for the predictions and measurements. As an aircraft program proceeds from the preliminary design, through developmental testing, to the certification flight-test phase, this uncertainty is reduced. For a small design change that can be demonstrated using carefully controlled incremental testing anchored to an existing flight-test data base, the uncertainty may be quite low. However, for a completely new engine and new airplane design, decisions on airplane go-ahead and customer guarantee offerings typically must be made when uncertainties are reasonably high.

Risk Assessment

The confidence of complying with a certification requirement or customer guarantee level—or, alternately, the risk of not complying—is calculated from the nominal noise level estimate, the overall uncertainty, and the compliance requirement, as shown in figure 8. For a single point guarantee, if the nominal estimate is equal to the compliance requirement, the compliance risk is 50 percent, characteristically an unacceptable situation. If the nominal estimate is one standard deviation (sigma) below the requirement, the risk of noncompliance is approximately 16 percent—or, alternately, the compliance confidence is about 84 percent.

For assessments involving more than one compliance point, the risk assessment calculation is more complicated. For example, in a FAR Part 36 certification, there are compliance requirements at three different flight conditions—approach, takeoff, and sideline—and limited exceedances are permitted at one or two points provided that there are compensating margins at the other conditions(s). (This situation is pictured graphically in figure 3, in which the three axes represent the noise at the three flight conditions, and the region inside the beveled geometric figure represents situations of compliance, and that outside the figure noncompliance.) The risk assessment calculation involves calculating the probability that the result will comply with the requirement (i.e., it will lie within the beveled geometric figure). The result depends on the relationship between the three nominal noise level estimates and their respective certification requirements, together with the overall uncertainties at the three conditions and the assumed degree of dependence of these uncertainties on one another.

Design Requirements, Objectives, Margins, and Risk

As can be deduced from the previous discussion, the imperfections in noise prediction and measurement processes make it imperative that the design targets for an airplane's noise levels be below the levels that the airplane is expected to meet. During the initial stages of a preliminary design, the design requirements and objectives are established, resulting in tolerances appropriate to the situation.

Design Requirements and Objectives

A design requirement is just that—a criterion that an airplane design must satisfy prior to go-ahead. Examples of design requirements are that the airplane be designed

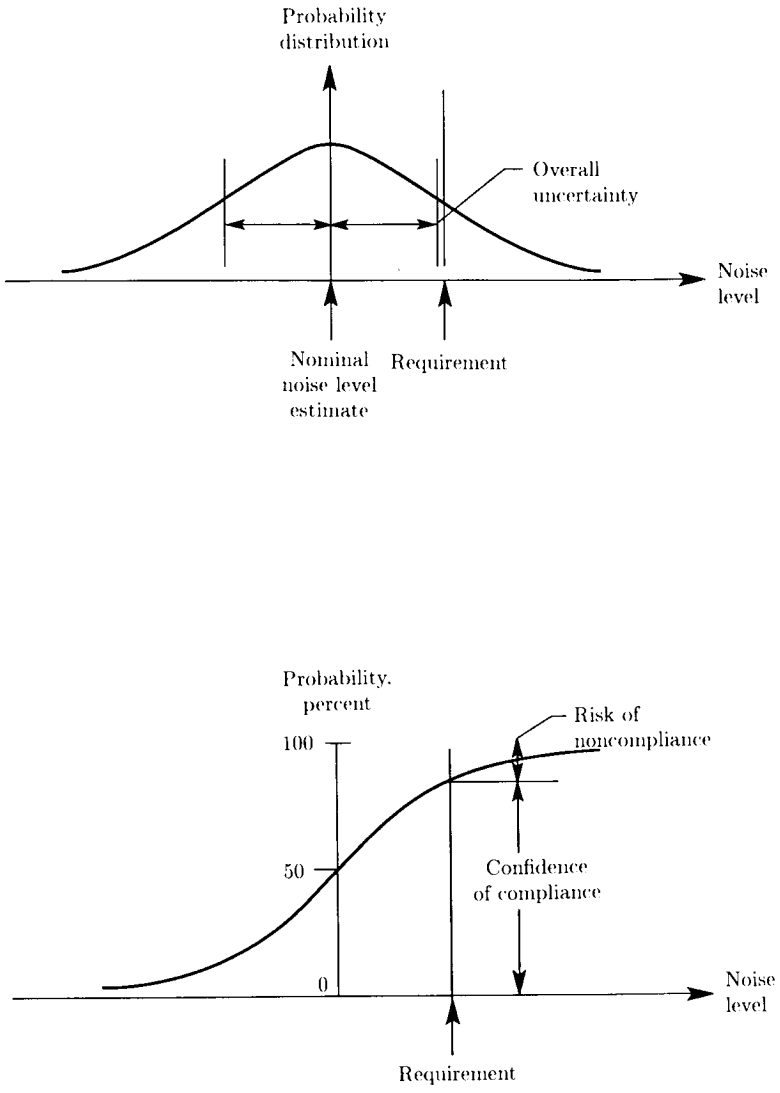

Figure 8. Risk assessment.

to meet FAR Part 36 with 90-percent confidence, that the airplane be designed to be nominally quieter than a competitor's airplane at a certain airport for a certain critical mission, or that the speech interference level in the first-class cabin not exceed a certain value with 80-percent confidence. If the airplane does not meet a requirement, it is unacceptable and must be redesigned, and the redesigned airplane must be re-evaluated.

A design objective is a less stringent goal than a design requirement. An objective is expected to be met, but does not constitute an absolute requirement for the design to proceed to production go-ahead. Design objectives, nevertheless, are intended to make the airplane more marketable and more profitable for the airline customer.

Design Margins

As can be seen from the above discussion, for an airplane to meet a requirement with greater than 50-percent confidence (or equivalently a risk below 50 percent), it must be designed to have nominal noise level estimates below the nominal requirement. These required margins, as depicted in figure 9, are derived from the uncertainty analysis described above. The larger the uncertainty and/or the lower the acceptable design risk, the larger the margins must be. The prediction and measurement uncertainties give rise to design and demonstration tolerances, respectively.

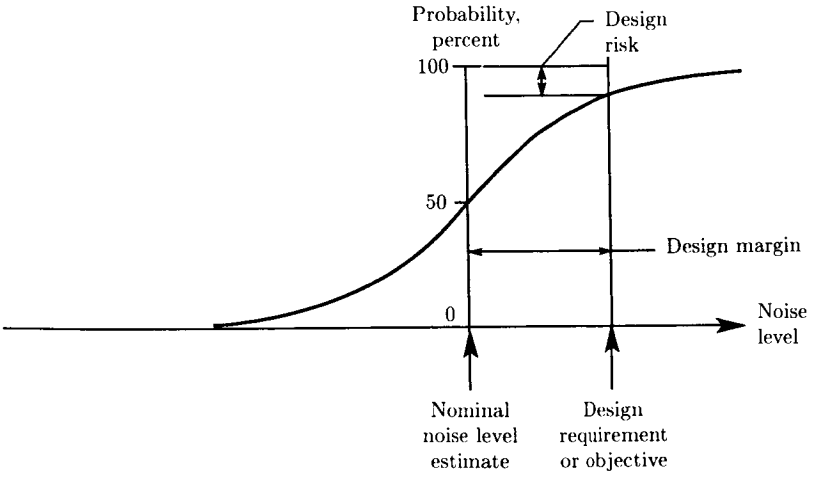

Figure 9. Design margin and risk.

Design Risk

From the concepts of uncertainty analysis, it is not difficult to see that a finite risk is associated with any finite design margin. A key element of airplane (and engine) design, therefore, is determination of the appropriate risk for a given situation. A number of factors affect this choice: the marketability of the airplane; the feasibility and cost of a redesign, retrofit, and other consequences in the event of noncompliance; the performance and cost penalties associated with designing for lower noise; the profit potential of the program; the development cost of the program; and others. For example, if the development costs of an airplane (or engine) are very high and the possibility of subsequent successful redesign and retrofit very remote, the program manager would require a very low risk of noncompliance (high confidence of compliance) with a certification requirement and therefore a relatively high design margin. If, on the other hand, the development costs are low, subsequent redesign and retrofit quite feasible, and the goal applicable to very few customers for very limited situations, a reasonably high risk would be appropriate. Certification risk typically ranges from 5 percent to an absolute maximum of 20 percent.

Major Design Considerations

Having discussed the adoption of airplane design requirements, we now discuss the major aspects of an airplane design which affect the ability to meet these objectives, the penalties associated with a low-noise design, and the engineering of derivative airplanes.

Engine Acquisition

The major source of community noise, and often a significant contributor to the interior noise of an airplane, is the propulsion system, exemplified by figure 10. The propulsion system includes both the basic gas generator—which includes the fan (or propeller), the compressor, combustor, and turbine—and the nacelle—which includes the inlet, exhaust nozzles, and thrust reverser. The basic gas generator and (in recent years) often the nacelle are supplied by an engine company. The engineering of the installed propulsion system is a cooperative effort among the engine company, the airplane manufacturer, and (in some cases) a nacelle manufacturer. This engineering effort is very critical to the airplane noise and warrants special discussion.

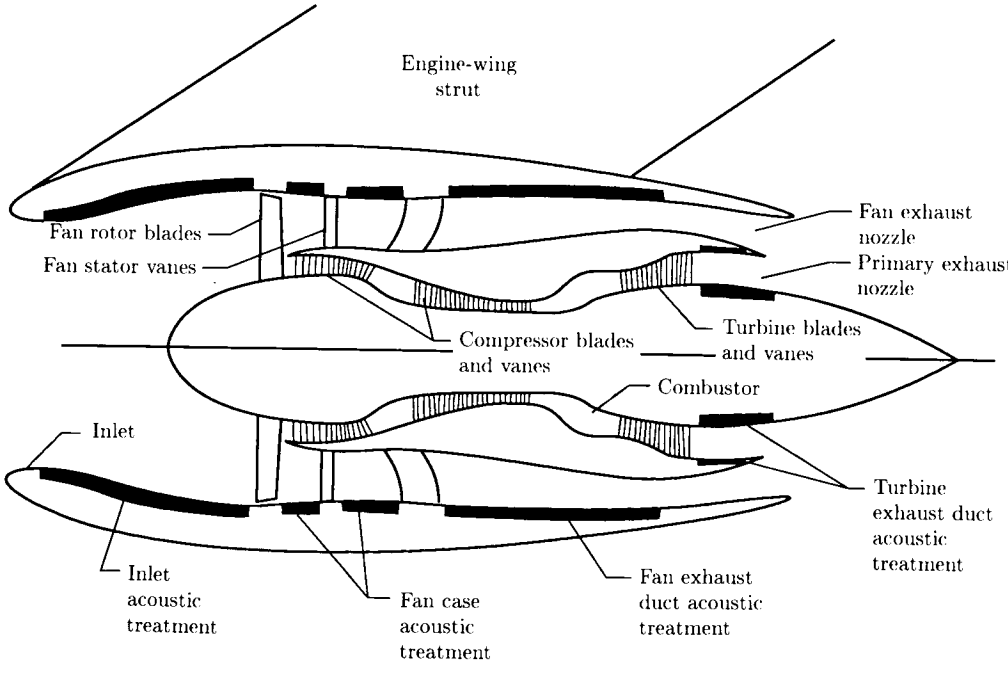

Figure 10. High-bypass-ratio engine and nacelle.

Engine Specification and Guaranteed Noise Levels

An engine specification is a description of the engine and other parts of the propulsion system that the engine company supplies. It normally includes noise guarantees, that is, noise levels that the engine is required to meet. As in the airplane

specification, these may be expressed in terms of nominal levels and tolerances, not-to-exceed levels (that have the tolerance already incorporated), or merely the guarantee to comply with certain regulatory levels. Typically, the engine company must guarantee the flight noise levels.

The engine company is frequently required to meet certain noise levels during ground static operation. The engine company also may commit to provide ground static test data during the development program and to carry out a recovery program if certain noise levels are exceeded. The purpose of these ground test requirements is to obtain an early assessment and resolution of any potential noise problems and therefore avoid an unsatisfactory airplane and/or an expensive retrofit.

Compliance Demonstration

An engine noise compliance demonstration can be of different forms. Usually it is tied to the method by which the airplane is certified; if possible, the engine compliance demonstration and the airplane compliance demonstration are accomplished with the same test and the same basic data. This philosophy avoids the necessity to compound demonstration tolerances for two different tests and motivates the engine and airplane manufacturers to work together toward a common goal: a quiet airplane that meets its noise requirements and objectives. In effect, the airplane certification risk is shared by the engine company and the airplane manufacturer.

If the engine is the first to be introduced on a model, the engine and airplane compliance test is usually the FAR Part 36 certification flight test. In addition to the primary test, the airplane is flown at very low power to demonstrate the airframe noise levels and at various power settings and altitudes in level flight to provide a comprehensive data base for future interpolation and family plan analyses.

If the engine is not the first to be introduced on a model and the family plan concept is used to certify the airplane, then the engine noise compliance test is often a ground static test of a single representative engine on a test stand with a turbulence inflow control structure, shown in figure 11. The turbulence inflow control structure reduces the inflow turbulence to the fan, which is typically much higher statically than in flight, so that the resulting fan noise generation is representative of the flight situation. As explained previously, the results of this test, together with results of a previous engine ground test and airplane flight test with the original engine, are used to calculate the certified noise levels of the airplane.

Major Design Parameters for Community Noise

During the preliminary design of an airplane, a number of key decisions are made which significantly affect the community noise of an airplane. In addition to their noise implications, these decisions affect safety, performance, manufacturing cost, and maintainability of the airplane and/or engine.

Number of Engines

The number of engines on an airplane can significantly affect the airplane noise, particularly at takeoff. As explained previously, for a given total (engine-out) thrust requirement, an airplane with fewer engines tends to have (with all engines operating) higher total takeoff thrust, and hence higher maximum sideline noise levels. On the

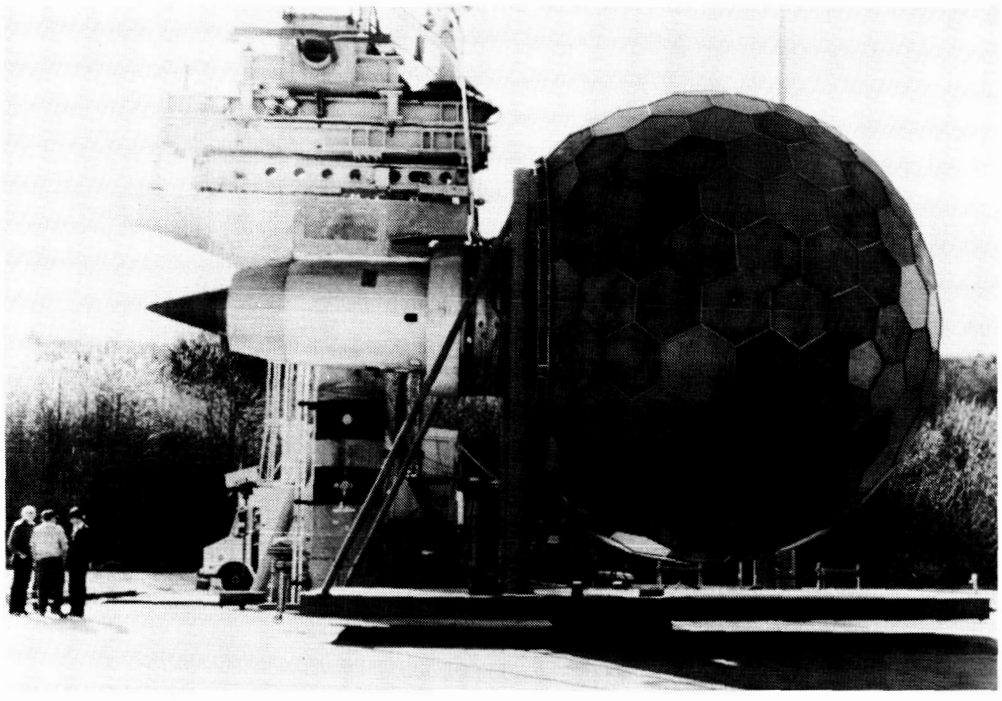

Figure 11. Fan flight noise simulation full-scale testing.

other hand, the same airplane has superior climbout performance and lower noise at the takeoff certification point and other points beneath the flight track. The effect of higher altitude is usually stronger than the effect of higher thrust. Thus, on balance, for the same takeoff gross weight, an airplane with fewer engines tends to have lower noise on takeoff.

Engine Design

The power plant type and performance cycle have a major influence on the community noise of an airplane. The evolution of the turbojet and turbofan engine has significantly affected noise. There has been a continuing trend toward higher engine bypass ratios, starting with the turbojet (with no bypass flow), to the low-bypass-ratio engine, to the high-bypass-ratio engine. Engine cycle analysis studies show that turbine materials and cooling improvements, coupled with improved fan aerodynamics, make possible significant fuel consumption advantages with higher bypass ratios. A higher bypass ratio results in a larger mass flow of air being accelerated to a lower exhaust velocity (to develop a given amount of thrust) and/or greater power extraction from the turbine reducing the primary jet velocity. A major community noise implication of this trend is reduced jet noise associated with the reduced turbulence intensity of the jet efflux. This historical trend is illustrated in figure 12.

This trend toward higher bypass ratios, larger diameter engines, and reduced jet noise has resulted in greater relative importance of fan noise and other internal

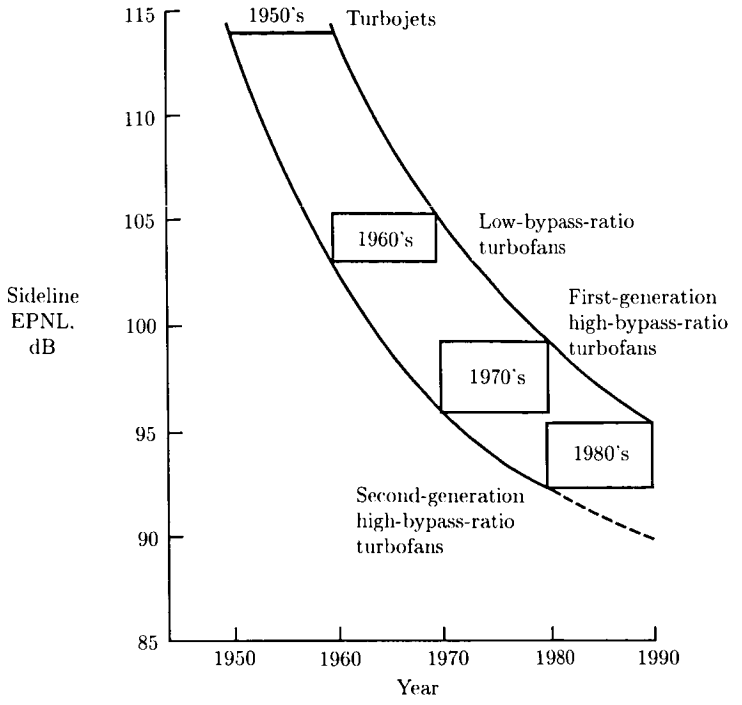

Figure 12. Noise reduction with engine evolution. Total airplane sea level static thrust is 100 000 lb. (From ref. 5.)

sources, which stimulated the development of sound-absorbing duct lining and low-noise fan blade design techniques. The noise from airplanes powered by high-bypass-ratio engines is typically quite well balanced between fan and jet noise.

Power Plant Location

The engines on a subsonic commercial airliner are typically either mounted on struts attached near the leading edge of the wing or closely coupled to the fuselage at the rear of the airplane. Three-engine airplanes have the center engine integrated into the tail cone and/or empennage. The community noise is affected by this configuration choice. Exhaust flows from wing-mounted engines often interact with the wing flaps to cause jet-flap interaction noise. Improvements in engine installation aerodynamics have made possible more closely coupled engines, resulting in a greater need to consider not only this jet-flap interaction noise, but also jet-wing interaction noise. Rear-mounted engines can benefit from shielding of fan noise by the fuselage, wings, flaps, and wing wake.

Thrust-to-Weight Ratio

Another parameter that affects community noise is the thrust-to-weight ratio of the airplane. A higher thrust-to-weight ratio results not only from selection of fewer engines but also from selection of a larger engine to obtain greater cruise thrust, greater climb thrust, or shorter takeoff field length. Again the sideline noise tends

to be controlled by the thrust level, while the takeoff noise is strongly affected by the climbout performance.

Flap Systems

The design of the flap system of an airplane has several noise implications. A more sophisticated flap system can mean a more efficient airplane on takeoff, resulting in higher altitudes and lower noise on the ground under the flight path. The design of the approach flap system can significantly affect not only the thrust required on approach but also the airframe noise and jet-flap interaction noise.

Engine Nacelle

The design of the engine nacelle, particularly the quality and extent of the acoustic treatment in the inlet and fan exhaust, can significantly affect fan noise (and other internal noise sources).

Penalties for Noise Reduction

The previous chapters of this book have dealt in considerable depth with the physics of noise generation and suppression; and the initial impression of the reader might be that noise reduction technology is readily available to achieve low noise levels without serious penalties to the airplane. This is not the case. To the contrary, each noise reduction feature of an airplane must be assessed carefully to determine the impact on airplane thrust, installed thrust-specific fuel consumption, weight and balance, drag, manufacturing cost, maintenance cost, safety, and dispatch reliability.

Cost-Benefit Law of Diminishing Returns

Noise reduction, like many other environmental benefits, can often be represented by a cost-benefit curve of a typical qualitative shape, as represented in figure 13. The cost axis may represent a parameter such as block fuel or direct operating cost for a given payload and range. The benefit axis may be noise reduction at one of the FAR Part 36 certification locations, average design margin at the three flight points, certification confidence level, reduction in footprint contour area, reduction in speech interference level or OASPL in the passenger cabin, or any other noise benefit.

Each point on the curve represents a point design, in particular, that design which results in the minimum penalty for that particular noise level. All other designs corresponding to that noise level lie above the cost-benefit curve. In other words, optimum designs for a given noise level or for a given amount of penalty lie on the curve, and all other designs lie to the left and above the curve.

It is important to observe the shape of the cost-benefit curve. Initial increments of noise reduction have a relatively low cost compared with further increments of benefit. Eventually, the curve has a vertical slope, which represents the maximum possible noise reduction, in most cases at a prohibitive penalty. If the noise reduction is expressed in terms of a FAR Part 36 noise level, the term "technologically practicable" refers to the limit imposed by the vertical asymptote of the line, and the term "economically reasonable" is related to the slope of the line at the required level of noise reduction.

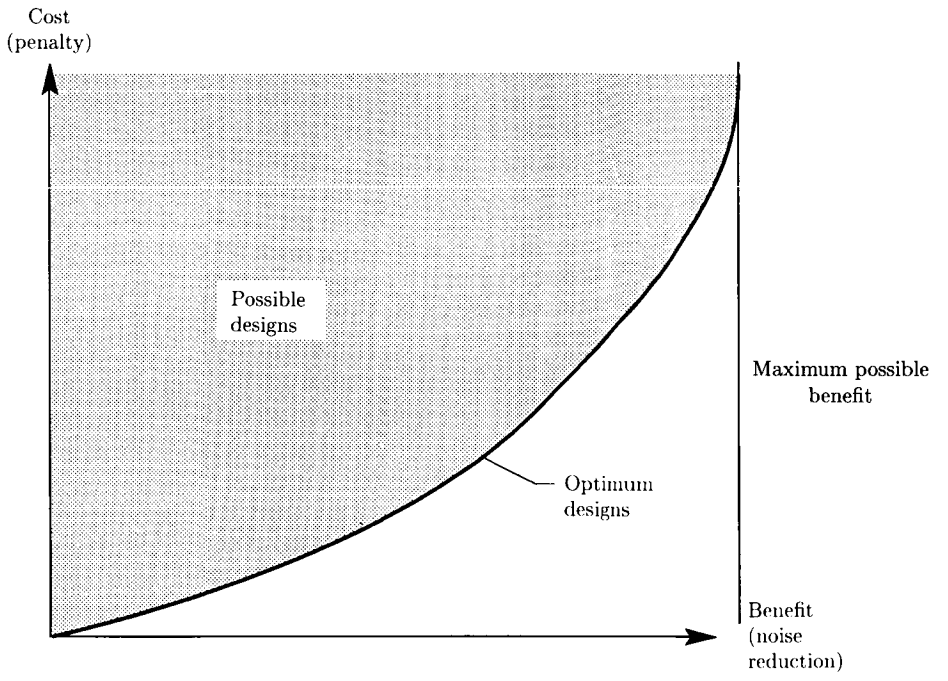

Figure 13. Cost-benefit law of diminishing returns.

Community Noise Example

An example of a cost-benefit curve is represented by figure 14, from reference 5. The curve was actually developed to assess the penalties associated with various hypothetical requirements during the Boeing evaluation of the FAR Part 36 stage 3 noise levels when they were first proposed. Each point on the line corresponds to a different degree of acoustic treatment. The penalty is the additional fuel consumption of the airplane corresponding to the additional weight and drag of the heavier and larger nacelles. The benefit is the reduction in the noise level (relative to the stage 2 requirement that was applicable at the time of the evaluation). It can be seen that, for this particular airplane and mission, the requirement to satisfy the FAR Part 36 stage 3 EPNL (which is 3.5 dB below the stage 2 EPNL) resulted in a penalty of approximately 3 percent in fuel consumption when design margins are included in the assessment.

Interior Noise Example

A second example of a cost-benefit curve is illustrated by figure 15. In this particular case, a number of sidewall treatment options were evaluated, and the weight penalty associated with each option was estimated by the designers. This display enabled the designers to eliminate some designs as being heavier than others for the same noise reduction, or less effective, from a noise reduction standpoint than others at the same weight.

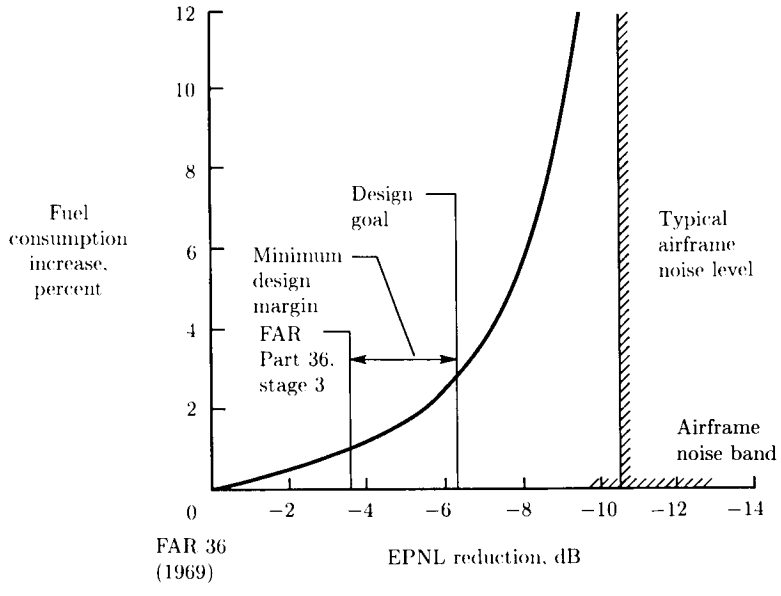

Figure 14. Noise reduction penalties. Approach power; engine treatment only. (From ref. 5.)

Effect of Technology Improvement

The effect of technology improvements on the cost-benefit curve is worthy of some discussion. The cost-benefit curve represents a given level of technology or state of the art in designing airplanes. Technology improvements resulting from research programs in noise (and in other technologies) can shift the cost-benefit curve down and to the right, as indicated in figure 16. In other words, additional noise reduction can be obtained at the same penalty, and/or the same noise reduction can be obtained at a less severe penalty.

Returning to the example of figure 14, an improvement in the acoustic technology involved in treatment design would result in additional noise reduction within a given nacelle and hence shift the line to the right. On the other hand, an improvement in materials technology that would make possible a lighter nacelle of the same shape and size would shift the curve downward.

It is seen from the above example that improvements in noise technology and in technologies that affect the penalties associated with the noise reduction together make lower noise levels more economically reasonable and more technologically practicable.

Derivative Airplanes

The previous section discussed the typical steps in developing the first design of a particular model, for example, a Boeing 747-100. A derivative airplane, for example, a Boeing 747-200, is based on a design derived from the first of the model or parent airplane. The noise engineering relies as much as possible on knowledge of the noise

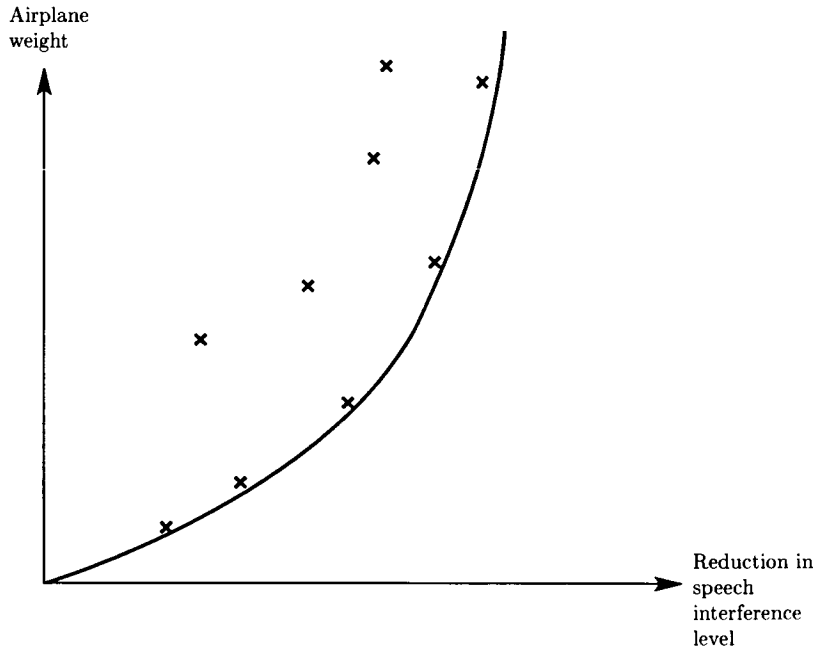

Figure 15. Weight penalty for interior noise reduction.

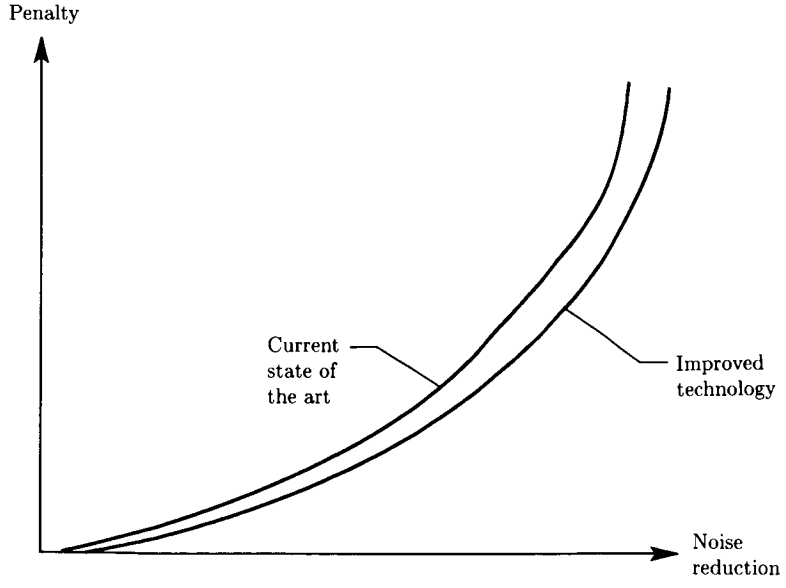

Figure 16. Effect of technology improvement on cost-benefit curve.

aspects of the parent airplane. Analyses are performed incrementally relative to the established noise levels of the parent airplane.

Growth Airplanes

Many derivative airplanes simply represent growth versions of the parent airplane. There are two typical types of growth: (1) growth in payload, usually accompanied by a lengthening of the fuselage, and (2) growth in range, usually accompanied by higher takeoff thrust and gross weight, together with an increase in fuel capacity, and perhaps a reduction in fuselage length and passenger capacity. Growth airplanes are the natural evolution that results from (1) improvements in technology, (2) engineering development and refinement based on operating experience with the airplane, and (3) the requirements of the air transportation system for airplanes with a variety of payload and range characteristics—without incurring the incremental maintenance, training, and engineering costs associated with introducing a completely new model into the operating fleet. The potential for growth must be preserved during the design of the parent airplane, including the provision for adequate noise design margins to accommodate the typical increases in noise with growth.

Alternative Engines

In some cases, derivative airplanes result from alternative engines becoming available and being installed. For example, the airplane manufacturer may wish to generate a more competitive supplier situation by means of introducing a second engine supplier with a very similar engine. Another situation comes from installing a significantly improved engine from a fuel and/or noise standpoint, for example, the introduction of the high-bypass-ratio SNECMA/GE CFM56 on the Boeing 737-300 airplane and the refanned Pratt & Whitney JT8D engine on the McDonnell-Douglas MD-80.

Major Operational Considerations

The previous sections of this chapter have dealt with design considerations of an airplane. This section deals with the effects on noise levels of the manner in which an airplane is operated. These operational considerations are closely related to the design itself and are considered during the design process.

The major determinant of the noise level of an airplane is the design of the airplane itself. There is some ability, however, to vary operational procedures to affect the certification noise levels of the airplane, its ability to meet local airport requirements, or its environmental impact in certain communities.

Takeoff Operational Procedures

For a given airplane design, the noise under the flight path (and to the sideline) during takeoff is determined by the thrust, flap, rotation, and landing gear schedules. These factors, in turn, control the altitude and flight speed, which, together with the power setting itself, determine the noise for a given (flap and landing gear) configuration. An example of the wide variety of noise signatures associated with different schedules is shown in figure 17 (from ref. 6) which describes different operational procedures and the resulting noise under the flight path. Comparison of

the noise aspects of different takeoff flight procedures usually results in lower noise levels for one procedure at some points in the community, accompanied by higher noise levels at other points.

When noise in proximity to an airport is not important, the normal procedure is to maintain full takeoff thrust rating until reaching a given altitude, after which the thrust is reduced to climb thrust.

Noise-Abatement Cutback

A takeoff procedure that is sometimes used over noise-sensitive communities involves reducing the power to a lower, but safe, level to reduce the noise exposure to the community near the airport. This results in a shallower climbout and tends to increase the noise over parts of the community farther from the airport, as seen from figure 17. A particular special case of a noise-abatement thrust cutback is that permitted by FAR Part 36 (ref. 1) and ICAO Annex 16 (ref. 3) for noise certification under the takeoff flight path.

The safety of thrust cutback during in-service operations is, of course, paramount and can be enhanced by automated features in the flight guidance and control system which provide for automatic rapid thrust increases in the remaining engines in the event of an engine failure.

Reduced-Power Takeoff

When the takeoff field length is not critical, an airplane is sometimes operated at takeoff thrust below the maximum rating; this option tends to extend engine life and lower maintenance costs. In this case, the sideline noise is lower than with full takeoff power; however the liftoff point is delayed, initial climb rate is reduced, and thus the noise benefits under the flight path are reduced or eliminated.

Rotation Point and Overspeed

Another flight procedure that can be invoked when takeoff field length is not critical is to delay rotation, resulting in overspeeding the airplane compared with its typical rotation velocity. This tends to reduce sideline noise, increase noise under the flight path at liftoff, but permit lower takeoff flap settings, more favorable lift-to-drag ratio, and higher climb rates—resulting in lower noise farther from liftoff.

Flight Track Selection and Variation

In addition to variations in thrust, flaps, landing gear, and rotation schedules, the takeoff noise in the community can be affected by the choice of flight tracks. Routing airplanes over large bodies of water, industrial areas, or sparsely populated areas instead of over densely populated residential areas can significantly reduce complaints. An example of such a strategy is that developed in the 1970's for the Seattle-Tacoma International Airport; eastbound flights taking off to the north were routed over the industrial area and Puget Sound before turning east over the residential areas of Seattle and its eastern suburbs. As a result, the airplanes were at much higher altitude over these residential areas, and community exposure was reduced.

Consistency Versus Special Procedures

The many possibilities of flight procedures might be misconstrued to imply that a given airline should fly the same airplane in a different manner at each different

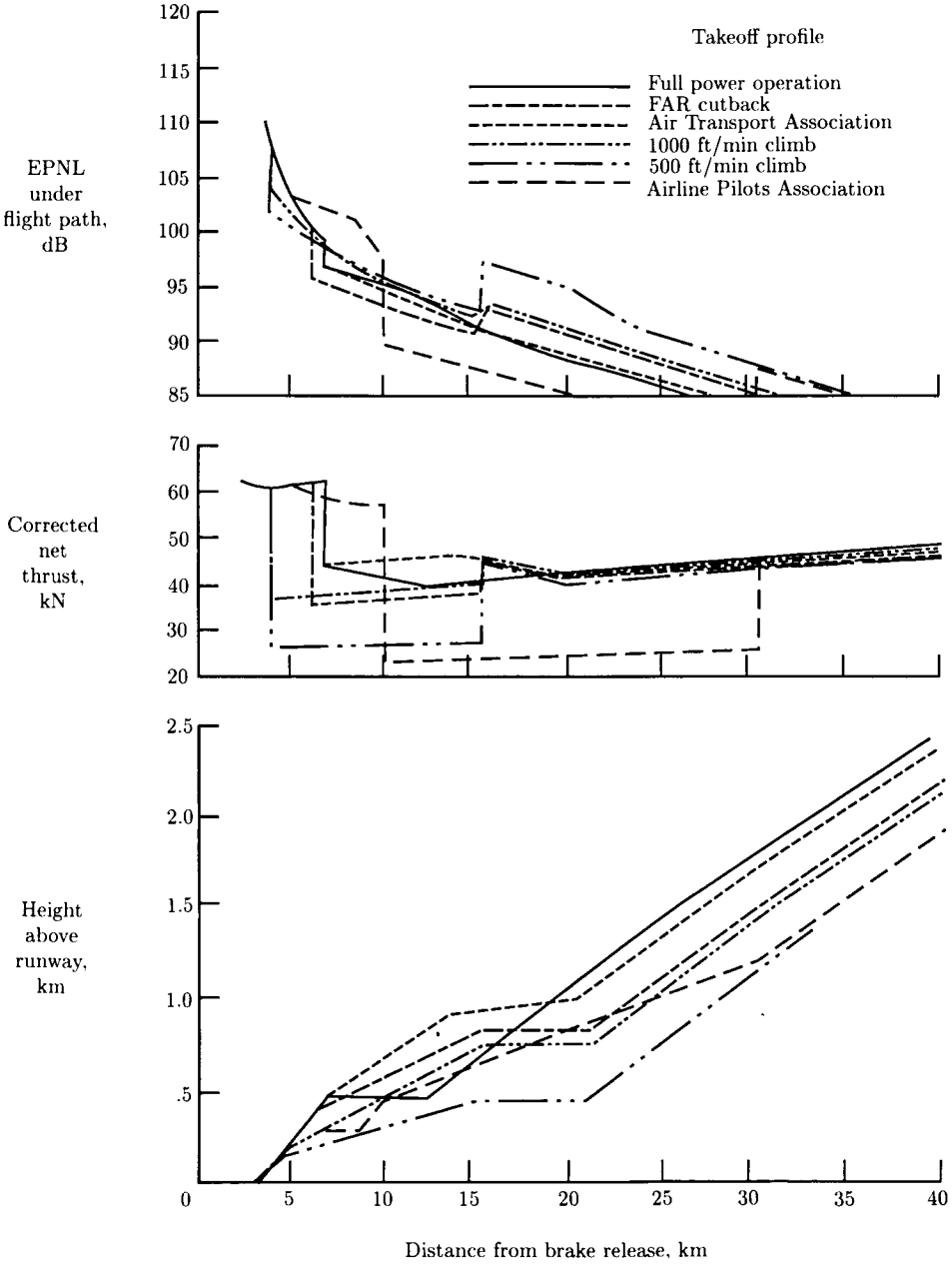

Figure 17. Takeoff noise variations with flight procedures. Airplane is 727 refan with flaps deflected 5°; temperature, 77°F; relative humidity, 70 percent. (From ref. 6.)

airport or that each airplane at a given airport can fly an optimum procedure independent of the procedure being used by other airplanes taking off and landing in the same community. Either of these hypothetical situations can cause confusion and/or increase workload on the part of the pilot, which can have safety implications. Therefore special procedures are not used as extensively as if noise abatement were the predominant objective. Safety remains the first priority in selecting takeoff procedures and flight tracks.

Landing Operational Procedures

As with takeoff, landing operational procedures can be varied somewhat to affect the certificability of the airplane, its ability to meet local airport requirements, or its environmental impact on certain communities.

Similar to the takeoff situation, for a given airplane design, the noise under the approach flight path (and to the sideline) is determined by the thrust, flap, and landing gear schedules. For the typical landing situation, the gross weight and approach speed determine the required lift coefficient. The flap setting and required lift coefficient determine the angle of attack. The flap setting, landing gear position, and angle of attack determine the drag coefficient, which, together with the glide slope, determines the thrust required. The altitude is determined by the glide slope and the distance from threshold. Thus, the noise-determining parameters (thrust, altitude, and flight Mach number) are fixed by approach speed, flap setting, and glide slope.

The normal landing approach follows a 3° glide slope and the flap setting corresponds to the minimum safe landing speed. This results in a reasonably high landing thrust requirement and typically corresponds to higher than minimum noise on approach.

Decelerating Approach

In a decelerating approach, as the airplane proceeds down the glide slope, the flight speed is progressively reduced to the final landing speed, with a corresponding increasing angle of attack and increasing thrust until the final approach thrust is reached. The decreased thrust reduces the noise levels during the initial phases of final approach.

Reduced Flap Settings

Approach noise may also be decreased by reducing the flap setting, retaining the lift by increasing the landing speed, and hence reducing the drag and the required thrust. The result is reduced noise at the expense of longer landing field length and additional tire and brake wear.

Multisegment Approach

In a multisegment approach procedure, the initial segments are carried out at a steeper glide slope. These segments require lower approach thrust, which, together with the higher altitude, reduces approach noise. The overall effect is usually small, since approach noise in the community remote from the airport is not typically as important on landing as on takeoff.

Consistency Versus Special Procedures

The same comments made previously regarding takeoff procedures also apply to landing procedures. Safety is again the paramount consideration.

The Design and Development Process

The noise engineering aspects of an airplane are a part of a very complex design process that has many engineering and economic factors and can require as much as 5 years to complete. This section outlines typical phases and milestones for a new airplane model.

The Preliminary Design Phase

The preliminary design phase of an airplane includes the determination of customer airline needs, together with enough depth in the airplane and major subsystem design to assure that the airplane can meet these needs.

Initial Preliminary Design and Airline Discussions

The initial preliminary design of an airplane involves developing an understanding of the airline customers' needs in terms of payload, range, economics, community and interior noise, airplane price, and other parameters. These needs are translated into an airplane design, including layout drawings that incorporate the major aspects of the configuration.

Initial discussions with engine suppliers result in selection of candidate engines, together with installation concepts and acoustic treatment designs. For these airplanes and installed propulsion systems, the spectra and directivity of each (treated) propulsion and airframe noise source are estimated, summed, and projected to points in the community at which flight noise time histories are constructed. These time histories are then used to estimate flight noise levels, which are compared with design requirements and objectives at specific locations and also to estimate certification confidence. If the engine model is already in operation on another airplane type, available flight data are used in the analysis. If the engine is in the initial development phase, ground test data may be available for these analyses.

During this same phase of the development process, the corresponding work for interior noise, including preliminary treatment designs, is carried out. The airplane design effort and the airline discussions are iterative and interactive. During this period, the design requirements and objectives are adopted, including those for noise.

Initial Application for Type Certificate

As the airplane begins to take shape, preliminary application is made to one or more certifying authorities, for example, the FAA, for a type certificate. Associated with this application are discussions regarding the plan for noise certification of the airplane. For example, if the airplane is the first of a model, a certification flight test is required. If it is a derivative airplane with a new engine, family plan certification may be proposed. The result of this phase is a specific plan for noise certification.

Preliminary Design Review

At the culmination of the preliminary design effort, a preliminary design review is conducted to scrutinize the design that has evolved. A team of experts reviews the

design to develop an independent opinion of its quality and appropriateness. This review is often accompanied by audits of different aspects of the design, including noise. Noise levels and risk assessments are reviewed in detail. Major design changes beyond this time period can seriously affect program cost and schedule.

Configuration Freeze

Following the preliminary design review, the configuration is usually "frozen." In effect the freeze applies to the major aspects of the design. Detailed design has not yet been accomplished, but there is high confidence that the major aspects will be amenable to successful detailed design.

Airplane and Engine Specifications

The process of preliminary design of the airplane and engine includes the formulation of airplane and engine specifications, both of which include noise level estimates and guarantees. These specifications are the basis for contractual commitments by the airplane manufacturer and engine supplier, respectively.

The Firm Commitment Phase

After the preliminary design phase, the airplane development moves into the firm commitment phase—firm commitments on the part of the airline customers, the engine suppliers, and the airplane manufacturer.

Firm Proposals to Airline Customers

When the preliminary design and airplane and engine specifications have been completed, the next step in airplane development process is that of making firm proposals to the airline customers. These proposals include guarantees for community, interior, and ramp noise. The guarantees may vary for different customers, depending on specific needs in terms of local airport regulations, route structures, and interior noise configurations and desires.

Engineering Go-Ahead

At engineering go-ahead, detailed design of the airplane begins, with the goal of supporting a given production schedule with an airplane that meets the specification. In order to protect the delivery date of the first airplane, engineering go-ahead may be authorized before the steps necessary for a production go-ahead have been completed.

Initial Orders and Production Go-Ahead

An airplane manufacturer requires a certain number of airplane purchase commitments by the airline customers prior to a production go-ahead. Once the required number of orders is obtained, a full production go-ahead is made, and the engine contracts are signed. This go-ahead includes a commitment to incur the immense costs of hard tooling for manufacturing.

The Final Design and Fabrication Phase

After firm commitments have been made, the next phase of the airplane development process is the detailed design and initiation of manufacturing, which culminates in rollout of the prototype airplane.

Detailed Design

The detailed design of the airplane includes the design of the hardware that influences community, interior, and ramp noise. The noise engineer works very closely with hardware designers, manufacturing people, and engine company engineers to develop the optimum design. Details of acoustic treatment, structural damping, and interior trim panels are among the decisions that are made during this phase. Often, developmental testing of selected hardware elements is conducted to assure the desired acoustic performance.

Manufacturing and Rollout

The design phase dovetails into the manufacturing phase. The fabrication of the first parts and major subassemblies, delivery of the first engines, and final assembly of the first airplane are, of course, major steps in the development process.

A key event for the first airplane is the rollout, in which the first airplane of the model leaves the final assembly building, usually accompanied by considerable publicity.

The Flight-Test and Certification Phase

After rollout, the airplane enters the flight-test and certification phase, which culminates in the first delivery to a customer.

After several weeks or months of taxi tests, the first flight of the airplane is performed by the flight-test organization. Initial flight noise measurements are often made at this time to identify any unforeseen noise level characteristics as early as possible.

The certification flight-test program for a new type of airplane typically includes a noise certification flight test, witnessed by the certificating authority, to demonstrate compliance with FAR Part 36 (ref. 1) and the ICAO Annex 16 (ref. 3) requirements. Detailed documentation of the test is submitted as evidence of compliance.

In addition to the certification flight test, additional testing is typically performed to demonstrate compliance with guarantees to airline customers. Additional community noise testing may be required; as a minimum, interior and ramp noise compliance must be demonstrated.

The culmination of the engineering process is the initial delivery of the airplane to the customer.

Product Improvement and Derivative Phase

The noise engineering does not end with delivery of the first airplane. Product improvements (to the engine and/or airframe) and/or major derivatives require effort until the delivery of the last airplane of a model.

Product Improvements

After the design and delivery of the prototype airplane, an airplane model is continually improved throughout its production life. The design is modified to improve performance, enhance passenger and airline appeal, and reduce cost. Each design modification is checked for noise implications. For any change that has noise

implications, the manufacturer must submit evidence to the FAA (and/or other certification agencies) that the resulting certification levels still comply with the applicable regulatory requirements. This step is often done by analysis; sometimes engine ground testing or flight testing may be necessary.

Derivative Airplanes

The previous discussion focused on the typical steps in developing the first design of a particular model. The same basic steps are performed for a derivative airplane as for the first of a model; however the central idea is to use as much of the design of the original airplane as possible, in order to significantly reduce cost and flow time from that required for the parent design. Correspondingly, the noise engineering relies as much as possible on knowledge of the noise aspects of the parent airplane (and engine). Analyses are performed incrementally relative to the established noise levels of the parent; designs of various noise aspects are identical or similar within the limitation that they still meet the design requirements and objectives of the derivative.

The certification of a derivative airplane is also based on that of the parent airplane to the greatest degree possible. In some cases, the noise changes can be shown by analysis to be negligible, for example, if the same engine is used and the gross weight increase is very small. In other cases, a supplemental flight test is needed to extend the data into a higher gross weight range. For a new engine, the family plan certification scheme described previously is often used, in which ground test increments are superimposed on the flight-test data base of the parent.

Noise Engineering of Other Flight Vehicles

The previous discussion has centered upon the engineering of subsonic commercial airliners powered by conventional turbojet or turbofan engines, which represent the largest share of the noise engineering and certification to this point in time. The basic ideas and philosophies of applying noise engineering principles to other flight vehicles are similar, with differences in emphasis resulting from differences in the function of the vehicle and the applicable regulatory climate.

Propeller Airplanes

The propeller airplanes that preceded the turbojets as the mainstay of the commercial fleet were certificated prior to the age of noise regulations. Smaller (less than 12 500 lb takeoff gross weight) propeller-driven airplanes are subject to FAR Part 36 (ref. 1, appendix F) requirements, which are specified in terms of maximum A-weighted sound level for level flyovers at 1000 ft.

Recent aerodynamic developments have resulted in renewed interest in advanced high-speed propellers as a propulsion system with the potential for significant fuel savings compared with the turbofan. These ultrahigh-bypass-ratio engines will have no inlet or fan duct available for acoustic treatment and will have low-frequency propeller tones that must be recognized and controlled in both the community and the interior noise engineering process. Also, in the absence of inlets to control and direct the flow upstream of the propeller, forward speed simulation, as is available with wind tunnel testing, will be required for valid simulation of flight noise during isolated tests of engines or propellers.

Military Airplanes

In military airplane design, noise is not as important as in the design of commercial airplanes, partly because their utility is not typically in proximity to populated communities and partly because of the paramount performance requirements of a military airplane. FAA and ICAO noise requirements apply specifically only to civil aircraft, and military requirements are typically less stringent. However, some military procurement contracts require compliance with FAR Part 36 unless serious losses in performance would result.

The near-field noise of high-performance closely coupled power plants has sonic fatigue implications that are important in service life design.

Supersonic Transports

Noise is a major consideration in supersonic transport design. Supersonic cruise performance considerations tend to promote low-diameter, high-pressure-ratio, low-bypass-ratio engine designs, which in turn result in much higher jet noise than a high-bypass-ratio engine. Noise considerations may drive the propulsion system design to a variable-cycle engine, having higher bypass ratios and lower noise on takeoff, and lower bypass ratios at cruise for superior supersonic cruise performance.

An additional important consideration is the en route noise associated with sonic booms caused by shock waves fixed with the airframe extending to the ground. FAR Part 91 (ref. 2) prohibits supersonic flight over U.S. land, and thus prevents sonic booms (reaching the ground) from civil aircraft. This requirement plays a significant role in the design of a supersonic transport.

Boundary-layer noise at supersonic cruise Mach numbers is critical to the passenger acceptance of a supersonic transport airplane.

Business Jets

Business jets are subject to the same FAR Part 36 noise regulations as commercial airliners. Because of their small size, most business jet airplanes meet FAR Part 36 standards, particularly those being produced with high-bypass-ratio engines. However, business jets make frequent use of small airports, at which stringent local airport regulations often apply. Consequently there are pressures toward low-noise designs.

Rotorcraft

Helicopters are subject to FAR Part 36 (ref. 1, appendix H) and ICAO Annex 16 (ref. 3, chapter 8) certification requirements for noise. Helicopters face severe constraints because they operate close to populated areas, both at heliports and en route. Rotor noise, particularly from the main rotor(s), is the most prevalent source. Interior noise and vibration due to both the rotor(s) and the gearbox are also very important design considerations.

References

1. *Noise Standards: Aircraft Type and Airworthiness Certification.* FAR, Pt. 36, Federal Aviation Adm., June 1974. (Consolidated Reprint Aug. 12, 1985.)
2. *General Operating and Flight Rules.* FAR, Pt. 91, Federal Aviation Adm., Mar. 1974. (Consolidated Reprint With Changes 1 through 67 as of May 1, 1986.)
3. *Annex 16—Environmental Protection.* International Civil Aviation Organization, Oct. 1981.
4. *Report to Congress—Alternatives Available to Accelerate Commercial Aircraft Fleet Modernization.* Federal Aviation Adm., Apr. 11, 1986.
5. Russell, Richard E.; and Peart, N. A.: Aircraft Noise Reduction Progress. Boeing paper presented at AAAE Conference and Airport Equipment Exposition (Phoenix, Arizona), May 1982.
6. *Phase II Program on Ground Test of Refanned JT8D Turbofan Engines and Nacelles for the 727 Airplane—Final Report. Volume IV, Airplane Evaluation and Analysis.* NASA CR-134800, 1975.

Glossary of Terms

Absorption coefficient—The ratio of sound energy absorbed by a surface to the sound energy incident upon the surface.

Acoustic power level (PWL)—Ten times the logarithm to the base 10 of the ratio of the acoustic power of a sound source to a reference power:

$$\text{PWL} = 10 \log_{10} \frac{W}{W_{\text{ref}}}, \text{dB}$$

where, in this text, $W_{\text{ref}} = 10^{-12}$ W and W is the radiated acoustic power corresponding to a particular frequency bandwidth.

Acoustic shadow region—A region in which sound pressure levels decrease rapidly as distance increases. It exists at distances larger than those for which the limiting rays refracted upward just miss the ground.

Active noise control—The use (by electronic means) of auxiliary sound sources to cancel or partially cancel the original sound field.

Airborne noise—Noise generated by aeroacoustic sources such as propellers and jet exhausts. It impinges directly on the external aircraft surfaces and is then transmitted into the cabin.

Atmospheric refraction—Varying conditions of wind and temperature with height in the atmosphere result in a varying speed of sound which causes sound waves to propagate along curved paths. For upwind propagation, the sound speed generally decreases with height and ray paths curve upward. In a temperature inversion or for propagation downwind, the ray paths curve downward.

A-weighted sound pressure level (SLA)—Sound pressure level that has been weighted to approximate the response of the human ear. It is measured with a standard sound level meter equipped with an "A" weighting network.

Bulk absorber acoustic duct liner—Consists of a single-layer construction with a solid backplate and a porous face sheet of negligible resistance. The cavity

between the backplate and face sheet is filled with a fibrous mat having very small air passages.

Cabin insertion loss—Loss determined by subtracting cabin sound pressure levels measured after the acoustic treatment is in place from levels measured before treatment installation. Treatment may sometimes increase the sound pressure level; therefore, insertion loss can be negative.

Cutoff, cut-on modes—Acoustic duct modes which are attenuated with distance and carry no acoustic power are referred to as being "cutoff," while modes which propagate in the usual sense are said to be "cut on."

Decelerating approach—A noise abatement procedure that may be used to achieve lower noise exposures under the approach path during the initial phases of final approach. The airplane flight speed is progressively reduced to the final landing speed, with a corresponding increased angle of attack and increased thrust until final approach thrust is reached.

Derivative airplanes—Growth versions of the parent airplane which arise as a result of operational experience, improvements in technology, or customer demands. Growth in payload and/or range is usually accompanied by higher takeoff thrust and gross weight and associated higher noise levels.

Diffraction—The amplitude and phase distortion of a sound field due to the presence of a barrier or other solid body.

Dispersive waves—Those waves whose propagation speed is proportional to the square root of frequency. For instance, bending waves in a plate are dispersive.

Duct insertion loss—Loss determined by subtracting the sound pressure levels measured for a hard-wall, untreated duct from those levels measured after treatment panels have been inserted.

D-weighted sound level (SLD)—Sound pressure level that has been weighted to reduce the effects of low-frequency noise and to increase the effects of high-frequency noise. It is measured with a standard sound level meter equipped with a "D" weighting network.

Eddy convection speed—The speed at which an eddy embedded in the flow is transported by the flow. Convection speeds are typically 0.5 to 0.7 times the free-stream value.

Effective perceived noise level (EPNL)—Derived from perceived noise level (PNL), but includes correction terms for the duration of an aircraft flyover and the presence of audible pure-tone components.

Equivalent continuous sound level (LEQ)—Calculated from A-level noise measurements to provide an equivalent steady-state value.

E-weighted sound level (SLE)—Sound pressure level weighted to approximate the perceived level of a sound. It is measured with a standard sound level meter equipped with an "E" weighting network.

Excess attenuation—That attenuation which is over and above that due to normal geometrical spreading and atmospheric absorption.

Geometrical spreading—The spreading out of acoustical energy as it propagates away from a source. For the special case of a point source, the corresponding decrease in sound pressure level is 6 dB per doubling of distance for all frequencies.

Hydrodynamic coincidence—Occurs when the convection speed of the boundary-layer fluctuating pressure field (about 70 percent of flight speed) equals the flexural wave speed of the skin structure.

Loudness—The perceived intensity of a sound.

Molecular (classical) absorption—The absorption of sound in the atmosphere due to the direct transfer of acoustic energy into heat energy through processes involving viscosity and heat conduction and due to molecular relaxation which is redistributed into rotational and vibrational modes of the molecules through binary collisions.

Multisegment approach—A noise abatement procedure that may be used to achieve lower noise exposures under the approach path during the initial phases of final approach. The initial segments are carried out at a higher altitude, at a steeper glide slope, and at a lower approach thrust.

Noise—Sound that produces adverse effects.

Noise abatement cutback—A noise abatement takeoff procedure that is sometimes used and involves reducing the engine power for a short time to a lower, but safe, level to reduce noise exposures over a certain area. This results in a shallower climbout angle and tends to increase the noise exposures over other parts of the community farther from the airport after normal climbout power is reapplied.

Noise certification of aircraft—Usually a requirement for operation of certain aircraft, particularly for commercial purposes. Certification rules are set by Federal and/or international authorities and specify maximum noise levels allowable during landing approach operations, during takeoff-climbout operations, and in some cases during en route operations.

Noise exposure forecast (NEF)—Used to determine the relative noise impact of aircraft noise near an airport. It is expressed as the total summation (on an energy basis) over a 24-hour period, weighted for the time of day, of the effective perceived noise level (EPNL) minus the constant 88 dB.

Noisiness—That characteristic or attribute of a sound which makes it unwanted, unacceptable, disturbing, objectionable, or annoying and which may be distinguishable from loudness, which is also a subjective quantity.

Nondispersive waves—Those waves whose propagation speed is independent of frequency. For instance, longitudinal and transverse waves are nondispersive.

Normal full-power takeoff—At airports for which noise in proximity to the airport is not a concern, the normal procedure is to maintain full takeoff rating until reaching a given altitude, after which the thrust is reduced to climb thrust.

Normal landing approach—Approach which follows a 3° glide slope and the flap setting corresponding to the minimum safe landing speed. This results in a relatively high landing thrust requirement and in higher noise levels on approach.

Overall sound pressure level (OASPL)—A physical measure which gives equal weight to all frequencies. This is not standardized but is generally considered to extend from 20 to 20 000 Hz, a range which corresponds to human hearing.

Overspeed takeoff—A noise abatement procedure that may be used to achieve lower noise exposures along the sideline and far from the airport. Provided field length is not critical, rotation can be delayed to higher speeds, thus permitting lower flap settings, more favorable lift-drag ratios, and higher climb rates.

Perceived noise level (PNL)—Calculated from broadband noise measurements to provide a rating of noisiness for sounds which have similar time durations and which do not contain strong discrete frequency components.

Reduced flap settings—A noise abatement procedure that may be used to achieve generally lower noise exposures under the approach path. The lift is maintained by increased landing speed; hence, the drag and the required thrust are reduced, but with the requirement of greater field length.

Reduced-power takeoff—A noise abatement procedure that may be used where takeoff field length is not critical. This results in lower sideline noise levels than with full takeoff power; however, the liftoff point is delayed and initial climb rate is reduced, thus eliminating noise benefits under the flight path.

Single-degree-of-freedom acoustic duct liner— Consists of a single-layer sandwich construction with a solid backplate. A porous face sheet and internal partitions are used, as would be provided by honeycomb separator material.

Sound exposure level (SEL)— A duration-corrected noise metric used to predict the annoyance of a single noise event such as an aircraft flyover. It is time-integrated A-level noise and is expressed by the level of an equivalent 1-sec-duration reference signal.

Sound pressure level (SPL)— Equal to 20 times the logarithm to the base 10 of the ratio of the sound pressure to a reference pressure:

$$\text{SPL} = 20 \log_{10} \frac{p}{p_{\text{ref}}}, \text{dB}$$

where, in this text, $p_{\text{ref}} = 2 \times 10^{-5}$ Pa and p is the sound pressure corresponding to a particular frequency bandwidth.

Speech interference level (SIL)— Developed to evaluate the effects of aircraft noise on passenger communications. It is calculated from the arithmetic average of the sound pressure levels of four octave bands having center frequencies of 500, 1000, 2000, and 4000 Hz.

Structure-borne noise— Noise generated by mechanical means, such as engine unbalance, transmitted along the airframe structure, and then radiated into the cabin.

Turbulent scattering—Occurs due to local variations in wind velocity and temperature which induce fluctuations in phases and amplitudes of the sound waves as they propagate through an inhomogeneous medium. There is a tendency for high frequencies to be affected more than low frequencies.

Two-degree-of-freedom acoustic duct liner—Consists of a double-layer sandwich construction with a porous septum sheet or midsheet and a porous face sheet. Internal partitions from material such as honeycomb provide spacings for the two layers.

Index

NASA
National Aeronautics and Space Administration

Report Documentation Page

1. Report No.	2. Government Accession No.	3. Recipient's Catalog No.
NASA RP-1258, Vol. 2 WRDC Tech Rep 90-3052		

4. Title and Subtitle	5. Report Date
Aeroacoustics of Flight Vehicles: Theory and Practice Volume 2: Noise Control	August 1991
	6. Performing Organization Code
7. Author(s)	
H. H. Hubbard, Editor	8. Performing Organization Report No.
	L-16926
9. Performing Organization Name and Address	10. Work Unit No.
NASA Langley Research Center Hampton, VA 23665-5225	535-03-11-03
12. Sponsoring Agency Name and Address	11. Contract or Grant No.
National Aeronautics and Space Administration Washington, DC 20546-0001 Department of the Air Force Wright Research and Development Center Wright-Patterson Air Force Base, OH 45433-6553 U.S. Army Aviation Systems Command Moffett Field, CA 94035	13. Type of Report and Period Covered Reference Publication 14. Sponsoring Agency Code

15. Supplementary Notes

This is a joint NASA, U.S. Air Force, and U.S. Army project. H. H. Hubbard is supported under U.S. Air Force Contract No. F33615-84-C-3202.

16. Abstract

This document is oriented toward flight vehicles and emphasizes the underlying concepts of noise generation, propagation, prediction, and control. Authors are from government, industry, and academia in the United States, England, and Canada. This volume includes those chapters that relate to flight vehicle noise control and operations: Human Response to Aircraft Noise; Atmospheric Propagation; Theoretical Models for Duct Acoustic Propagation and Radiation; Design and Performance of Duct Acoustic Treatment; Jet Noise Suppression; Interior Noise; Flyover-Noise Measurement and Prediction; and Quiet Aircraft Design and Operational Characteristics.

17. Key Words (Suggested by Author(s))	18. Distribution Statement
Flight vehicle acoustics Noise sources Noise control	Unclassified--Unlimited Subject Category 71

19. Security Classif. (of this report)	20. Security Classif. (of this page)	21. No. of Pages	22. Price
Unclassified	Unclassified	446	A19

NASA FORM 1626 OCT 86

NASA-Langley, 1991

For sale by the National Technical Information Service, Springfield, Virginia 22161-2171